BPS Black Holes and Donaldson–Thomas Invariants

Rishi Raj

A dissertation submitted to Sorbonne Université
and the École Doctorale de Physique en Île-de-France (EDPIF)
in partial fulfillment of the requirements for the degree of
Doctor of Philosophy in Physics.

September 2026

Defended on June 10, 2026, before a jury composed of:

Cyril Closset	External reviewer
Veronica Fantini	Examiner
Amir-Kian Kashani-Poor	Examiner
Ruben Minasian	Jury Chair
Sameer Murthy	External reviewer
Boris Pioline	Thesis advisor

© 2026 Rishi Raj



Except where otherwise noted, this work is licensed under the **Creative Commons Attribution 4.0 International** (CC BY 4.0). To view a copy of this license, visit:

`https://creativecommons.org/licenses/by/4.0/`

You are free to share and adapt this work for any purpose, including commercially, provided appropriate attribution is given.

Abstract

In type II string theory on Calabi–Yau threefolds, BPS black holes are realized at weak coupling as bound states of D-branes, and can be counted robustly by protected BPS indices, also known in mathematics as generalized Donaldson–Thomas (DT) invariants. These invariants and their refined counterparts depend on the choice of Bridgeland stability condition and jump across walls of marginal stability. To determine BPS spectra in concrete examples and their reorganization across stability space, this thesis employs the framework of "BPS dendroscopy." By anchoring the spectrum to initial rays associated with massless spherical objects at the boundary of stability space, dendroscopy reconstructs DT invariants via attractor flow trees.

The first part develops BPS dendroscopy for the total spaces of the canonical bundles over $\mathbb{F}_0 = \mathbb{P}^1 \times \mathbb{P}^1$ and $\mathbb{F}_1$. For local $\mathbb{F}_0$, it constructs scattering diagrams near the orbifold point, on the large-volume slice, and along the physical Π-stability slice. After extending the large-volume diagram below the natural parabola, the infinite families of boundary rays are shown to arise from scattering of finitely many pure D4–anti-D4 rays with Dirac pairing ± 2. On the physical slice, ramification points and branch cuts are present for generic values of the mass parameter, namely the 5d gauge coupling, so stability space becomes an infinite cover of the upper half-plane with sheets labelled by $\mathbb{Z}^4$. The resulting diagram is determined by its large-volume and orbifold limits together with monodromy invariance, and carries an action of a $\mathbb{Z}^4$ extension of $\Gamma_0(4)$.

For local $\mathbb{F}_1$, the existence of an effective curve of negative self-intersection prevents line bundles from being everywhere stable on the large-volume slice. Nevertheless, after extending the diagram below the parabola, the initial rays reorganize into pure D4–anti-D4 pairs associated with a geometric helix of invertible sheaves. On the mirror side, the family of elliptic curves has generic ramification type $I_8 + 4I_1$, and no modular parametrization by a subgroup of $\mathrm{PSL}(2,\mathbb{Z})$ exists in general. Using a rational parametrization of the nodal mirror curve at the conifold locus, the conifold periods are expressed in closed form in terms of the Bloch–Wigner dilogarithm. At the special value of the mass parameter, $\ell = -27/256$, two I_1 fibers collide to produce an Argyres–Douglas point of type H_0; the monodromy group then reduces to an extension of a genus-zero non-congruence subgroup $\Gamma \subset \mathrm{PSL}(2,\mathbb{Z})$ of index 10, yielding a modular parametrization of the Coulomb branch and a Γ-invariant scattering diagram without branch cuts.

The second part studies the modular completion of generating series of D4-D2-D0 invariants. When the D4-charge splits into n irreducible constituents, S-duality predicts mock modular forms of depth $n-1$ with non-holomorphic completion governed by generalized error functions. The thesis derives these terms from the supersymmetric quantum mechanics of multi-centered BPS black holes. Using localization, it reduces the total refined Witten index to a finite-dimensional integral over time-independent configurations. This is rewritten as the product of an integral over the $(2n-2)$-dimensional phase space of multi-centered solutions and an integral over the $n-1$ transverse directions associated with the dynamical Fayet–Iliopoulos parameters. The latter produces the generalized error functions governing the non-holomorphic completion, identifying the modular anomaly with the spectral asymmetry of the continuum of scattering states.

Together, these results provide tools for analyzing BPS spectra in string theory, and clarify how wall-crossing, multi-centered dynamics, and modularity enter the description of supersymmetric black holes and D-brane bound states.

Acknowledgements

No thesis is written in isolation. Although only one name appears on the title page, any PhD is in truth the product of a much wider web of generosity: of teachers and collaborators, of institutions and communities, of friends and loved ones who sustain both the work and the person carrying it. It is a pleasure to acknowledge here some of the people and places without whom this thesis would not have taken shape.

First and foremost, I would like to express my deepest gratitude to my supervisor, Boris Pioline. I have benefited immensely from his guidance, encouragement, and demanding scientific standards throughout this PhD. His insight, breadth of knowledge, and ability to identify the right questions have shaped this work in countless ways. I am especially grateful for his mentorship, for many useful discussions, and for consistently pushing me to do better while giving me the freedom to grow into my own way of doing research.

I would also like to thank all the members of my thesis jury: Cyril Closset and Sameer Murthy as reviewers, and Veronica Fantini and Amir-Kian Kashani-Poor as examiners, along with Boris for their careful reading of this work and for the time and effort they invested in evaluating it.

I am very grateful to Bruno Le Floch for insightful discussions and for the collaboration that led to our work on local $\mathbb{F}_0$. I would also like to thank Marcos Mariño for the opportunity for a short collaboration and for several illuminating discussions. More broadly, I am thankful to Mark Goodsell, Ayan Mukhopadhyay, and Vishnu Jejjala for valuable conversations, guidance, and encouragement on side projects and related directions. I am also grateful to Sergey Alexandrov for useful discussions and comments on early work, and to Sameer Murthy for helpful comments on a draft. My thanks also go to Pierrick Bousseau, Andrea Brini, Cyril Closset, Pierre Descombes, Horia Magureanu, Jack Huizenga, Heeyeon Kim, Jan Manschot, Thorsten Schimannek, David Berghaus, Pierre Lairez, and Marc Mezzarobba for helpful discussions or correspondence connected to different parts of this thesis.

I would like to thank LPTHE for being such a stimulating and welcoming place to work. I am particularly grateful to Michela Petrini, the lab director, and to Marco Pico for their support and for handling so many practical matters that make daily research life possible. I also warmly thank my labmates, and especially Greivin Alfaro, for his kindness and for helping me find my footing with administrative matters when I first joined the lab. My sincere thanks go to Grégory Schehr and Amir-Kian Kashani-Poor for serving on my thesis monitoring committee during my first two years, and to Michael Joyce from the doctoral school for very useful career advice early on. I am also grateful to Boris and to all those involved in organising the scientific life of the Paris high-energy theory community: the Rencontres théoriciennes, the Séminaire Darboux, and the mathematical physics seminars at LPTHE which made these years intellectually alive.

I gratefully acknowledge EDPIF for funding my PhD, COST for travel support, and the support of Boris' grants, which funded several research trips. I also thank Sorbonne Université, ENS, UniGE, as well as CERN, for schools, workshops, and stimulating scientific environments that played an important role in my formation. In particular, I would like to thank Troels Petersen for organizing the Summer School on Machine Learning in Physics in Copenhagen, which was

both scientifically valuable and personally memorable.

Life outside research matters just as much as research itself, and I have been very fortunate in the people around me. I owe the most to my parents, Ashok Kumar and Poonam, for their unwavering support, encouragement, and constant concern for my well-being. I am equally grateful to my extended family for their affection and belief in me. My deepest personal thanks go to my closest friend, Ananya Shetty, for extraordinary emotional support and for always being there for me, and to my partner, Tejeswini Jayakumar, whom I met during my initial training at CERN, for her love, steadiness, and the joy she has brought into my life. I also warmly thank Natasha for making the PhD years feel more bearable and more normal, Susmitha and Prasanth for unforgettable weekend trips and adventures in and around Paris, Harsh, Sakshi, and Nishtha for making the New Year holidays away from home so magical, and my childhood friends Chakshu and Lakshya for the unlikely and wonderful reunion in Paris. I am also grateful to my cousin Rohit, Vishno, and Vedika for the joyful time spent with them in Munich.

Finally, I would like to acknowledge the places that quietly shaped these years. CIUP and Maison de l'Inde gave me a beautiful home in Paris, and I am grateful to my floormates there for their warmth and friendliness. Some of my happiest moments during this PhD were tied to movement and travel, and to the simple pleasure of discovering new places. I remain grateful for those journeys, which made these years fuller than work alone ever could have.

Contents

Abstract iii

Acknowledgements v

1 Introduction 1
- 1.1 Protected BPS Spectra in Supersymmetric Theories . . . 2
- 1.2 Local Calabi–Yau Geometry, Stability, and Wall-Crossing . . . 2
- 1.3 Methods and Main Results . . . 3
- 1.4 Outline of the Thesis . . . 5

2 BPS Spectrum in Calabi–Yau compactifications 7
- 2.1 Supersymmetric Black Holes in $\mathcal{N} = 2$ Supergravity . . . 7
- 2.2 Multicentered Black Holes and the Denef Formalism . . . 11
- 2.3 BPS States and Protected Indices . . . 14
- 2.4 Refined and Rational Indices . . . 16
- 2.5 Wall-Crossing and Chamber Structure . . . 18
- 2.6 The Split Attractor Flow Conjecture . . . 20
- 2.7 Coulomb Branch Formula . . . 26
- 2.8 Quiver Quantum Mechanics . . . 30
- 2.9 Coherent Sheaves and Gieseker Stability . . . 36
- 2.10 Derived Categories and Bridgeland Stability Conditions . . . 43
- 2.11 Generalized Donaldson–Thomas Invariants . . . 49

3 BPS Spectrum in Local Calabi–Yau Models 57
- 3.1 Non-compact toric Calabi-Yau models . . . 57
- 3.2 Exceptional collections and quivers on local surfaces . . . 62
- 3.3 Scattering diagrams . . . 70
- 3.4 Local mirror symmetry and Pi-Stability . . . 77

4 BPS Dendroscopy on Local $\mathbb{P}^1 \times \mathbb{P}^1$ 87
- 4.1 Introduction . . . 87
- 4.2 Generalities . . . 98
- 4.3 Quiver scattering diagram . . . 112
- 4.4 Large volume scattering diagram . . . 121
- 4.5 Scattering diagram in the Π-stability slice . . . 127
- 4.6 Appendix: Central charge as Eichler Integrals . . . 138

5 BPS Dendroscopy on Local $\mathbb{F}_1$ 161
- 5.1 Introduction . . . 161
- 5.2 Generalities . . . 163
- 5.3 Quiver descriptions . . . 168
- 5.4 Large volume Scattering diagram . . . 172

5.5 Π-stability slice . . . 178
5.6 The Non-congruence subgroup $\Gamma(10;0,3,0,1;8)$ . . . 195
5.7 Conifold periods from dilogarithms . . . 198

6 Black Hole Quantum Mechanics and Generalized Error Functions 203
6.1 Introduction . . . 203
6.2 Modular completions and generalized error functions . . . 205
6.3 Witten index from localization . . . 212
6.4 Comparison with modular predictions . . . 226
6.5 Discussion . . . 230
6.6 Appendix: The master integral identity . . . 231

7 Conclusions and Outlook 235
7.1 Summary of the thesis . . . 235
7.2 Lessons from dendroscopy . . . 236
7.3 Lessons from quantum mechanics and modularity . . . 238
7.4 Broader perspective . . . 239

A Modular Forms and Theta Series 243
A.1 Classical modular forms for $SL(2,\mathbb{Z})$ . . . 243
A.2 Congruence subgroups and modular forms of level N . . . 246
A.3 Quasimodular forms . . . 248
A.4 Jacobi forms and positive-definite theta series . . . 250
A.5 Mock modular forms and harmonic Maass forms . . . 251
A.6 Modular forms on noncongruence subgroups . . . 254
A.7 Vignéras' theorem and indefinite theta series . . . 256

References 270

List of Figures 275

List of Tables 277

Résumé en français 279

1
Introduction

"It is comforting to see how mathematics has been able to absorb so much of the intuitive, often imprecise reasoning of quantum physics and string theory, and to transform many of these ideas into rigorous statements and proofs."

— Robbert Dijkgraaf
The Power of Mirror Symmetry

The quantum structure of black holes remains one of the most compelling windows into fundamental physics. A consistent theory of quantum gravity must explain how gravitational thermodynamics emerges from microscopic degrees of freedom, how apparently smooth spacetime geometry is encoded in quantum states, and how exact observables survive across regimes that are usually separated by strong coupling. String theory offers a concrete setting in which these demands can be made precise. In supersymmetric compactifications with enough control, black holes admit a microscopic description as bound states of D-branes, and their degeneracies are captured by protected indices that remain under computational control even when other quantities do not.

These indices have turned out to occupy a central position in modern mathematical physics, well beyond their original application to black hole counting. They govern the spectra of BPS particles and bound states in supersymmetric gauge theories, encode the chamber structure of moduli spaces, and are reformulated in the mathematics literature as Donaldson–Thomas (DT) invariants associated with derived categories of sheaves. Their generating series transform under dualities as modular or mock modular forms, and their discontinuities across walls of marginal stability are governed by precise algebraic identities. BPS counting thus provides a meeting point for questions that originate in quantum gravity, supersymmetric field theory, algebraic geometry, and mirror symmetry — and progress in one area has repeatedly fed back into the others.

The non-compact, or local, Calabi–Yau setting plays a privileged role in developing these ideas. Removing gravity from the picture isolates the gauge-theoretic and geometric content of BPS counting and makes the dependence on stability conditions accessible to explicit computation. The quiver descriptions that arise near special boundary points in moduli space, the scattering diagrams that encode global wall-crossing data, and the mirror-symmetric descriptions of the moduli space all become tractable simultaneously. The local setting is therefore not merely a simplification of the compact problem: it is a context in which one can formulate precise, answerable questions about global BPS spectra in genuinely non-trivial examples.

This thesis is concerned with exactly these questions, in two related directions. The first is the global organization of BPS spectra for D-brane configurations on local toric Calabi–Yau threefolds, specifically the canonical bundles $K_{\mathbb{F}_0}$ and $K_{\mathbb{F}_1}$ over the first two Hirzebruch surfaces. The central problem is to understand how these spectra depend on stability data, how they reorganize across walls of marginal stability, and whether they can be reconstructed efficiently

from data at the boundary of stability space. The second direction concerns a complementary problem: the modular properties of generating series of $D4$–$D2$–$D0$ invariants, and the physical origin of the generalized error functions that appear in their non-holomorphic completion.

1.1 Protected BPS Spectra in Supersymmetric Theories

In any supersymmetric theory admitting a central charge, BPS states are those that saturate the mass bound

$$M = |Z(\gamma)|\,,$$

for charge γ. Their degeneracies are encoded in protected indices $\Omega(\gamma; z)$, which depend on the charge and on the vacuum parameters z. These indices are insensitive to most continuous deformations, and remain well-defined even when interpolating between weakly and strongly coupled regimes. They are not, however, constant functions of z. Across codimension-one loci in parameter space where the phases of two central charges align, bound states can form or decay, and the indices jump discontinuously. Understanding this wall-crossing is the fundamental problem.

The problem recurs across several physical settings that, on the surface, appear quite distinct. In four-dimensional $\mathcal{N} = 2$ field theories, BPS particles appear on the Coulomb branch and their spectrum undergoes Seiberg–Witten-type wall-crossing as one moves through moduli space. In five-dimensional theories compactified on a circle, analogous states encode instanton particles, monopole strings, and their composites. In type IIA string theory on a Calabi–Yau threefold, the same charges are realized geometrically by D-branes wrapping internal cycles, and in the compact case with dynamical gravity, the stable bound states are supersymmetric black holes. The formalism of protected indices and wall-crossing applies uniformly across all of these settings, and insight gained in one context has repeatedly transferred to the others.

The jumps of $\Omega(\gamma; z)$ across walls are governed by the Kontsevich–Soibelman wall-crossing formulae, which express the change in the spectrum entirely in terms of the spectra of the constituent charges. In favorable cases, this means the full spectrum at any point in moduli space can be reconstructed from data specified once near the boundary. A particularly powerful organizing principle, and one central to this thesis, is that multi-particle and multi-centered bound states can be classified by rooted trees encoding their successive decay channels. In the supergravity context this is the split attractor flow picture; in the scattering diagram context, it is the successive scattering of rays. In both cases, classifying bound states by their possible nested decompositions provides both physical intuition and a concrete computational strategy.

The perspective adopted in this thesis is therefore to regard the BPS index as a structured object over stability space, one whose global properties, chamber-structure, and boundary behaviour are all part of what must be understood.

1.2 Local Calabi–Yau Geometry, Stability, and Wall-Crossing

The geometric setting in the first part of the thesis is provided by non-compact toric Calabi–Yau threefolds of the form $X = K_S$, the total space of the canonical bundle over a compact toric surface S. These geometries are simple enough to permit complete computations yet complex enough to exhibit genuinely non-trivial phenomena: rich chamber structures, infinite families of BPS rays generated from finite initial data, derived autoequivalences, non-trivial monodromy on the physical slice of stability conditions, and mirror-symmetric descriptions. They form a natural

bridge between the algebraic geometry of derived categories and sheaves, the physics of D-brane bound states, and the enumerative geometry of DT invariants.

From the string-theoretic viewpoint, compactifying type IIA on X engineers a four-dimensional $\mathcal{N} = 2$ theory in which gravity is absent, so the BPS sector can be studied without the complications of dynamical gravity. The relevant invariants are generalized DT invariants counting semistable objects in the derived category $D_c^b(X)$ of compactly supported coherent sheaves on X, and their dependence on the vacuum moduli, encoded through a choice of Bridgeland stability condition, is the central question. Stability determines which objects contribute to the spectrum, and wall-crossing describes how that determination changes as one moves through moduli space.

The natural language for organizing this dependence is provided by scattering diagrams in spaces of stability conditions. One associates "rays" to charges admitting semistable objects of fixed central charge phase, and imposes the consistency conditions that arise when rays intersect. The result is a global combinatorial object that encodes all wall-crossing data simultaneously. For the local toric geometries considered here, this picture is tightly connected to attractor flow trees on the physical side and to quiver descriptions near the orbifold points in moduli space.

The two geometries studied in this thesis, $K_{\mathbb{F}_0}$ and $K_{\mathbb{F}_1}$, are among the simplest local models with a compact effective divisor, yet each already displays the full range of phenomena that make the subject interesting. Local $\mathbb{F}_0$ has a two-dimensional Kähler moduli space and a relatively tractable large-volume limit. Local $\mathbb{F}_1$ is more subtle: the presence of an effective curve of negative self-intersection on $\mathbb{F}_1$ destabilizes line bundles on part of the large-volume slice, and the physical slice carries a monodromy structure with no global modular description, except at special values of the mass parameter. This makes local $\mathbb{F}_1$ not merely harder than local $\mathbb{F}_0$, but qualitatively different, and a more demanding test of any general method.

1.3 Methods and Main Results

The overarching methodological framework of this thesis is *BPS dendroscopy*. The central observation is that the BPS spectrum at a generic point in stability space need not be enumerated chamber by chamber; rather, it can be systematically reconstructed from a controlled set of initial data attached to distinguished loci on the boundary of stability space, where certain elementary objects become massless or acquire self-stability. Propagating this data through the interior via wall-crossing, or equivalently, via the associated scattering diagram or attractor flow trees, yields the global spectrum. The emphasis throughout is therefore on reconstruction from boundary data, rather than on direct enumeration.

Part I: BPS Dendroscopy on Local Surfaces

The first part of the thesis develops this programme for the canonical bundles over the Hirzebruch surfaces $\mathbb{F}_0 = \mathbb{P}^1 \times \mathbb{P}^1$ and $\mathbb{F}_1$.

For local $\mathbb{F}_0$, scattering diagrams are constructed in three complementary regimes: near the orbifold point, on the large-volume slice, and along the physical slice of Π-stability conditions. A central structural result is that, upon extending the large-volume diagram below the natural parabola in affine coordinates, the infinite families of boundary rays are generated by scattering from finitely many pure $D4$–$\overline{D4}$ rays with Dirac pairing ± 2. On the physical Π-stability slice, the picture is more intricate: ramification points and branch cuts are present for generic values of the mass parameter (the five-dimensional gauge coupling), so that stability space becomes an infinite cover of the upper half-plane with sheets labelled by $\mathbb{Z}^4$. The full scattering diagram is

thereby determined by its large-volume and orbifold limits together with monodromy invariance, and carries an action of a $\mathbb{Z}^4$ extension of $\Gamma_0(4)$.

For local $\mathbb{F}_1$, the same strategy leads to a substantially richer and more delicate structure. The existence of an effective curve of negative self-intersection on $\mathbb{F}_1$ prevents line bundles from being everywhere stable on the large-volume slice, so the initial data cannot be read off by the same procedure as in the $\mathbb{F}_0$ case. Nevertheless, after extending the diagram below the parabola, the boundary rays reorganize into pure $D4$–$\overline{D4}$ pairs associated with a geometric helix of invertible sheaves. On the mirror side, the family of elliptic curves has generic ramification type $I_8 + 4I_1$, and admits no modular parametrization by a subgroup of $\mathrm{PSL}(2,\mathbb{Z})$ in general. The conifold periods are expressed in closed form in terms of the Bloch–Wigner dilogarithm, using a rational parametrization of the nodal mirror curve at the conifold locus. At the special value of the mass parameter $\ell = -27/256$, two I_1 fibres collide to produce an Argyres–Douglas point of type H_0; the monodromy group then reduces to an extension of a genus-zero non-congruence subgroup $\Gamma \subset \mathrm{PSL}(2,\mathbb{Z})$ of index 10, yielding a modular parametrization of the Coulomb branch and a Γ-invariant scattering diagram free of branch cuts. These features make local $\mathbb{F}_1$ a particularly stringent test of the dendroscopic approach.

Part II: Modular Completions of D4–D2–D0 Generating Series

The second part addresses the modular properties of generating series of $D4$–$D2$–$D0$ Donaldson–Thomas invariants. When the $D4$-charge decomposes into n irreducible constituents, S-duality predicts that the holomorphic generating series is a mock modular form of depth $n-1$, whose non-holomorphic completion is governed by generalized error functions. The thesis derives these completions from first principles, within the supersymmetric quantum mechanics of multi-centred BPS black holes. By applying localization, the total refined Witten index is reduced to a finite-dimensional integral over the moduli space of time-independent configurations. This integral factorizes into a contribution from the $(2n-2)$-dimensional phase space of multi-centred solutions and a contribution from the $n-1$ transverse directions associated with the dynamical Fayet–Iliopoulos parameters; the latter yields precisely the generalized error functions governing the non-holomorphic completion. The modular anomaly thus acquires a transparent physical interpretation: it reflects the spectral asymmetry in the continuum of scattering states of n BPS dyons with mutually non-local charges.

Collectively, these results establish that scattering diagrams, attractor indices, wall-crossing formulae, and modular completions are not independent structures, but rather distinct facets of a unified problem: the global organization of protected BPS spectra in compactifications of string theory with $\mathcal{N} = 2$ supersymmetry.

Publications The research undertaken during this doctoral programme has resulted in the following publications.

1. B Le Floch, B Pioline, and R Raj. "BPS Dendroscopy on Local $\mathbb{P}^1 \times \mathbb{P}^1$". In: *Annales Henri Poincaré* (2026). DOI: 10.1007/s00023-026-01666-3. arXiv: 2412.07680 [hep-th]

2. B Pioline and R Raj. "Black hole quantum mechanics and generalized error functions". In: *JHEP* 03 (2026), p. 179. DOI: 10.1007/JHEP03(2026)179. arXiv: 2507.08551 [hep-th]

3. B Pioline and R Raj. "BPS Dendroscopy on local $\mathbb{F}_1$". Manuscript in preparation. 2026

4. V Jejjala, S Mondkar, A Mukhopadhyay, and R Raj. "Learning holographic horizons". In: *Phys. Rev. D* 111.2 (2025), p. 026016. DOI: 10.1103/PhysRevD.111.026016. arXiv: 2312.08442 [hep-th]

This thesis is based on publications 1, 2, and 3.

1.4 Outline of the Thesis

Chapter 2 constitutes the first of two background review chapters, providing a self-contained account of the physical and mathematical structures underlying BPS state counting in Calabi–Yau compactifications. Topics covered include supersymmetric black holes and multi-centred solutions in $\mathcal{N} = 2$ supergravity, protected and refined indices, wall-crossing phenomena, attractor flow trees, quiver quantum mechanics, coherent sheaves, Bridgeland stability conditions, and generalised Donaldson–Thomas invariants.

Chapter 3 introduces the complementary background on BPS state counting on local (non-compact) Calabi–Yau threefolds. Local Calabi–Yau geometries are presented as a tractable arena for engineering sophisticated supersymmetric gauge theories with rich BPS spectra. The chapter establishes a correspondence between the derived category of compactly supported D-branes and the category of representations of quivers arising from exceptional collections of fractional BPS-branes. It proceeds to define the notion of scattering diagrams, a central tool in the analysis of the subsequent chapters, and concludes with a discussion of local mirror symmetry, Π-stability, and the structure of the Coulomb branch of the associated supersymmetric field theories.

Chapter 4 is based on the paper *BPS Dendroscopy on Local* $\mathbb{P}^1 \times \mathbb{P}^1$. It develops the dendroscopic framework for the local $\mathbb{F}_0$ geometry and constructs the associated scattering diagram in several complementary regimes: at large volume, in the vicinity of the orbifold point, and in full generality within the Π-stability slice.

Chapter 5 is based on ongoing work on local $\mathbb{F}_1$. It extends the analysis of Chapter 4 to a geometry in which the negative self-intersection of curve classes on $\mathbb{F}_1$ renders the wall-crossing structure substantially more intricate. The chapter employs Bloch–Wigner dilogarithms to express the periods at conifold points, establishes a modular presentation of the Coulomb branch at special values of the mass parameter, and constructs the large-volume scattering diagram for local $\mathbb{F}_1$ from elementary $D4$–$\overline{D4}$ pairs associated to a geometric helix of invertible sheaves.

Chapter 6 is based on the paper *Black Hole Quantum Mechanics and Generalised Error Functions*. It derives the generalised error functions governing the modular completion of generating series of $D4$–$D2$–$D0$ Donaldson–Thomas invariants via localisation of the Witten index in the supersymmetric quantum mechanics of multi-centred bound states. The modular completion is given a transparent physical interpretation in terms of the spectral asymmetry of the quantum-mechanical system.

2

BPS Spectrum in Calabi–Yau compactifications

This chapter reviews the physical and mathematical structures that underlie the study of BPS states in Calabi–Yau compactifications of type II string theory. It provides the background for the later chapters, where these ideas will be specialized to the non-compact geometries relevant for BPS dendroscopy. We first review supersymmetric black holes and multicentered solutions in four-dimensional $\mathcal{N} = 2$ supergravity, together with protected BPS indices and their wall-crossing behaviour across moduli space. We then discuss the split attractor flow picture, the Coulomb branch and quiver descriptions of BPS bound states, and finally the sheaf-theoretic framework of stability conditions and Donaldson–Thomas invariants.

The chapter is organized as follows. Sections 2.1 and 2.2 review single-centered and multicentered BPS black hole solutions. Sections 2.3, 2.4, and 2.5 introduce protected indices and wall-crossing. Section 2.6 discusses split attractor flows, and Section 2.7 reviews the Coulomb branch formula. Section 2.8 discusses quiver quantum mechanics. Finally, Sections 2.9, 2.10, and 2.11 review coherent sheaves, Bridgeland stability, and generalized Donaldson–Thomas invariants.

2.1 Supersymmetric Black Holes in $\mathcal{N} = 2$ Supergravity

The low-energy effective action of Type IIB string theory compactified on a Calabi-Yau threefold X yields a four-dimensional $\mathcal{N} = 2$ supergravity theory coupled to $n_V = h^{1,2}(X)$ massless abelian vector multiplets and $n_H = h^{1,1}(X) + 1$ massless hypermultiplets. In the two-derivative description of stationary BPS black holes, the hypermultiplet scalars may be taken to be constant, so the relevant dynamics is governed by the vector multiplet sector. The complex scalars of the vector multiplets, corresponding to the complex structure moduli of X, parametrize a special Kähler manifold $\mathcal{M}$ of complex dimension n_V. We denote local holomorphic coordinates on $\mathcal{M}$ by z^a, with $a = 1, \ldots, n_V$. We now recall the basic ingredients needed in the description of BPS black hole solutions: the symplectic charge lattice, the special geometry of $\mathcal{M}$, and the central charge. This section is based primarily on the classic literature on supersymmetric black holes and the attractor mechanism, especially [58, 72, 90, 91, 174].

The underlying mathematical structure of $\mathcal{M}$ is dictated by special geometry. The fundamental objects in special geometry are constructed from the $2n_V + 2$ dimensional symplectic vector space V, naturally identified with the middle cohomology $H^3(X, \mathbb{R})$. Electric and magnetic charges of the black holes are quantized and take values in the lattice $H^3(X, \mathbb{Z})$. The charge of a state is represented by a symplectic vector $\Gamma = (P^\Lambda, Q_\Lambda)$ with $\Lambda = 0, 1, \ldots, n_V$, corresponding to the magnetic and electric charges, respectively. The antisymmetric bilinear form on this vector space

is given by,

$$\langle \Gamma_1, \Gamma_2 \rangle = \int_X \Gamma_1 \wedge \Gamma_2 = P_1^\Lambda Q_{2,\Lambda} - Q_{1,\Lambda} P_2^\Lambda, \tag{2.1}$$

which is a topological, moduli-independent invariant representing the Dirac–Schwinger–Zwanziger (DSZ) symplectic product.

The geometry of $\mathcal{M}$ is encoded in a holomorphic symplectic section of an $\mathrm{Sp}(2n_V + 2, \mathbb{R})$ bundle over moduli space. Locally, in a suitable symplectic frame, this section can be described in terms of a holomorphic prepotential $F(X)$, which is a homogeneous function of degree two. The coordinates of the section are given by the (holomorphic) period vector $\Pi(z) = (X^\Lambda(z), F_\Lambda(z))$ with $\Lambda = 0, 1, \ldots, n_V$, where $F_\Lambda = \partial F(X)/\partial X^\Lambda$. On the Calabi-Yau threefold X, this holomorphic data is determined by the unique holomorphic 3-form $\Omega_{3,0}$.

The Kähler potential $\mathcal{K}(z, \bar{z})$ determining the metric $g_{a\bar{b}} = \partial_a \bar{\partial}_{\bar{b}} \mathcal{K}$ on the vector multiplet moduli space $\mathcal{M}$ is defined by the symplectic inner product of the holomorphic section with its complex conjugate :

$$e^{-\mathcal{K}(z,\bar{z})} = i\langle \Pi, \bar{\Pi} \rangle = i\left(\bar{X}^\Lambda F_\Lambda - X^\Lambda \bar{F}_\Lambda\right). \tag{2.2}$$

Because the moduli space metric encodes the kinetic terms for the scalar fields, the special Kähler geometry governs the couplings of the supergravity theory.

To describe BPS states and the supersymmetry algebra, it is highly convenient to introduce the normalized period vector of Weyl weight zero,

$$\mathcal{V} = e^{\mathcal{K}/2}\,\Pi, \tag{2.3}$$

which satisfies the normalization condition $\langle \mathcal{V}, \bar{\mathcal{V}} \rangle = -i$.

A central quantity in the study of BPS states is the central charge $Z(\Gamma; z)$ appearing in the $\mathcal{N} = 2$ supersymmetry algebra. We use the notation $Z(\Gamma; z)$ as a shorthand for $Z(\Gamma; z, \bar{z})$, since this quantity is not holomorphic. For a state of charge Γ, the central charge is given by the symplectic pairing with the normalized period vector $\mathcal{V}$:

$$Z(\Gamma; z) = \langle \Gamma, \mathcal{V} \rangle = e^{\mathcal{K}/2}\left(P^\Lambda F_\Lambda - Q_\Lambda X^\Lambda\right). \tag{2.4}$$

The central charge dictates the BPS mass bound of the physical configuration. For a state of charge Γ, the mass M is bounded by the asymptotic value of the central charge evaluated at spatial infinity in units of the Planck mass:

$$M^2 \geq |Z(\Gamma; z_\infty)|^2 M_{\mathrm{Pl}}^2. \tag{2.5}$$

Finally, to formulate the equations of motion for black hole backgrounds, we introduce the Kähler covariant derivative $D_a \equiv \partial_a + \frac{1}{2}\partial_a \mathcal{K}$ acting on normalized quantities. Using the identities of special geometry, one verifies the orthogonality condition $\langle \mathcal{V}, D_a \mathcal{V} \rangle = 0$ as well as the metric identity $\langle D_a \mathcal{V}, \bar{D}_{\bar{b}} \bar{\mathcal{V}} \rangle = i g_{a\bar{b}}$. These relations underlie the BPS rewriting of the second-order supergravity equations of motion as first-order flow equations , thereby relating the radial evolution of the moduli fields directly to the central charge.

2.1.1 Single-Centered BPS Black Holes and Flow Equations

For static, spherically symmetric BPS states, the supergravity equations of motion admit exact solutions where the metric takes the Majumdar-Papapetrou form

$$ds^2 = -e^{2U} dt^2 + e^{-2U} d\vec{x}^2, \tag{2.6}$$

where the warp factor U depends only on the radial coordinate r. To preserve half of the supersymmetry in the background of a single charge center Γ, the second-order supergravity equations of motion reduce to a system of first-order differential equations. Introducing the inverse radial coordinate $\tau = 1/r$, the radial evolution of the warp factor U and the special Kähler moduli z^a is dictated by the so-called *attractor flow equations*:

$$\frac{dU}{d\tau} = -e^U |Z(\Gamma; z)|, \tag{2.7}$$

$$\frac{dz^a}{d\tau} = -2e^U g^{a\bar{b}} \partial_{\bar{b}} |Z(\Gamma; z)|. \tag{2.8}$$

These equations show that the radial evolution of the moduli z^a traces out gradient flow trajectories in the vector multiplet moduli space $\mathcal{M}$, with the central charge modulus $|Z|$ playing the role of an effective potential.

In the above convention, one finds that

$$\frac{d}{d\tau}|Z| = -4e^U g^{a\bar{b}} \partial_a |Z| \partial_{\bar{b}} |Z| \leq 0, \tag{2.9}$$

so that the central charge decreases monotonically as the flow proceeds from spatial infinity ($\tau = 0$) towards the core of the black hole ($\tau \to \infty$). At spatial infinity, the configuration saturates the BPS bound, yielding an asymptotic ADM mass $M_{\text{ADM}} = |Z(\Gamma; z_\infty)|$. As $\tau \to \infty$, the flow converges to a critical point in moduli space where $\partial_a |Z| = 0$, and the scalar fields take fixed "attractor" values $z_*(\Gamma)$ that depend only on the charge Γ, independently of their initial asymptotic values z_∞.

This charge-driven infrared fixed-point behavior is the content of the *attractor mechanism* for supersymmetric black holes. In the $\mathcal{N} = 2$ theory, the attractor point is characterized more precisely by the vanishing of the Kähler-covariant derivatives of the central charge,

$$D_a Z(\Gamma; z)\big|_{z=z_*(\Gamma)} = 0. \tag{2.10}$$

A useful feature of $\mathcal{N} = 2$ supergravity is that these differential flow equations can be integrated into algebraic generalized stabilization equations. For a general BPS configuration, the fields are determined by a symplectic vector of harmonic functions $H(\vec{x})$ evaluated on the flat $\mathbb{R}^3$ spatial base. The stabilization equations take the form

$$2e^{-U} \text{Im}(e^{-i\alpha} \mathcal{V}) = -H(\vec{x}), \tag{2.11}$$

where $\alpha = \arg Z(\Gamma; z)$ is the phase of the central charge. For a single-centered black hole located at the origin, the harmonic function is simply

$$H(\vec{x}) = \frac{\Gamma}{r} + h, \tag{2.12}$$

where the constant vector $h = -2\text{Im}(e^{-i\alpha_\infty} \mathcal{V}_\infty)$ is fixed by the asymptotic boundary conditions at spatial infinity to ensure asymptotic flatness ($e^{-2U(\infty)} = 1$).

The algebraic relations in (2.11) make it possible to express both the warp factor and the scalar fields in terms of a single homogeneous degree-two entropy function $\Sigma(H)$, with

$$e^{-2U(\vec{x})} = \Sigma(H(\vec{x}))$$

. Near the event horizon, located at $r \to 0$, the harmonic function is dominated by its pole,

$$H \sim \frac{\Gamma}{r},$$

so that

$$e^{-2U(r)} \sim \frac{\Sigma(\Gamma)}{r^2} = \frac{|Z_*(\Gamma)|^2}{r^2}.$$

The metric therefore approaches the Robinson–Bertotti form

$$ds^2_{\mathrm{NH}} = -\frac{r^2}{R_H^2}\, dt^2 + \frac{R_H^2}{r^2}\, dr^2 + R_H^2\, d\Omega_2^2, \tag{2.13}$$

which is locally $AdS_2 \times S^2$, with common radius

$$R_H^2 = \Sigma(\Gamma) = |Z_*(\Gamma)|^2. \tag{2.14}$$

It follows that the horizon area is

$$A_H = 4\pi R_H^2 = 4\pi\Sigma(\Gamma),$$

and hence the leading piece of the macroscopic Bekenstein–Hawking entropy is

$$S_{\mathrm{BH}} = \frac{A_H}{4} = \pi R_H^2 = \pi\Sigma(\Gamma) = \pi|Z_*(\Gamma)|^2 \tag{2.15}$$

in the conventions used here.

2.1.2 Moduli Dependence and Existence of BPS Solutions

The single-centered BPS flow is initiated by the choice of vacuum at spatial infinity, encoded by the asymptotic vector-multiplet moduli z_∞. For fixed charge Γ, varying z_∞ changes the initial value of the central charge and therefore the ADM mass, as well as the trajectory followed by the scalar fields along the radial evolution. The attractor flow equations thus determine, for each pair (Γ, z_∞), a distinguished path in moduli space from the asymptotic vacuum toward the infrared region. When this trajectory reaches a regular fixed point, the near-horizon values of the moduli are determined entirely by the charge. This charge-driven infrared universality is the basic form of the attractor mechanism.

The existence of a regular single-centered black hole is therefore a dynamical question in moduli space. For a given charge Γ, one must require that the corresponding attractor flow extend smoothly from spatial infinity to the horizon. A standard obstruction arises when the central charge vanishes at a regular point of the vector-multiplet moduli space before the flow reaches its attractor endpoint. In that case the radial evolution terminates at finite radius, and the putative single-centered solution does not develop a regular black-hole interior. The existence of a regular supersymmetric black hole is thus a property of the pair (Γ, z_∞), rather than of the charge vector alone.

This dependence on the asymptotic vacuum is one of the basic reasons that the BPS spectrum varies across moduli space. In particular, special codimension-one loci arise at which a charge Γ can align energetically with a decomposition into constituents $\Gamma_1 + \Gamma_2$. These loci are characterized by alignment of the phases of the constituent central charges and are known as walls of marginal

stability. Near such walls, the appropriate supersymmetric realization of a charge may involve a multicentered bound state whose stability depends on the asymptotic moduli. As the wall is approached, the bound state becomes arbitrarily weakly bound and may separate into independent constituents. The resulting moduli dependence of BPS bound states is the origin of wall-crossing, whose careful discussion will be given in Section 2.5.

2.2 Multicentered Black Holes and the Denef Formalism

When describing bound states of multiple extremal black holes, the assumption of spherical symmetry must be relaxed. If the constituent black holes carry mutually non-local charges (i.e., $\langle \Gamma_i, \Gamma_j \rangle \neq 0$), the corresponding electromagnetic field configurations source an intrinsic Poynting vector, endowing the spacetime with angular momentum. Consequently, the geometry is in general no longer static, but stationary. This section is based primarily on the Denef formalism for multicentered black hole solutions, following [35, 58, 72, 75].

The general stationary BPS solutions in $\mathcal{N} = 2$ supergravity describing such multicentered composites can be systematically constructed using the Denef–Bates formalism. The spacetime geometry is captured by a stationary, asymptotically flat metric ansatz generalizing the form of (2.6),

$$\mathrm{d}s^2 = -e^{2U(\vec{x})}(\mathrm{d}t + \omega)^2 + e^{-2U(\vec{x})}\mathrm{d}\vec{x}^2, \tag{2.16}$$

where the warp factor $U(\vec{x})$ and the rotation one-form $\omega = \omega_i \mathrm{d}x^i$ depend solely on the coordinates of the flat three-dimensional spatial base $\mathbb{R}^3$.

As for the case of single-centered black holes, a key feature of this formalism is that the stationary BPS equations reduce to a system determined by a symplectic vector of harmonic functions $H(\vec{x}) = (P^I(\vec{x}), Q_I(\vec{x}))$ valued in the electromagnetic charge lattice. For a composite of N distinct charge centers Γ_s located at spatial positions $\vec{x}_s$, the harmonic functions take the form

$$H(\vec{x}) = \sum_{s=1}^{N} \frac{\Gamma_s}{|\vec{x} - \vec{x}_s|} + h. \tag{2.17}$$

As before, the constant symplectic vector h is fixed by the asymptotic values of the scalar moduli at spatial infinity, $h = -2\,\mathrm{Im}(e^{-i\alpha_\infty}\mathcal{V}_\infty)$, where $\alpha_\infty = \arg Z(\Gamma, z_\infty)$ is the phase of the total central charge corresponding to the total charge $\Gamma = \sum_s \Gamma_s$.

The reconstruction of the full supergravity background, namely the metric, the scalar field profiles, and the gauge fields, from the harmonic functions $H(\vec{x})$ proceeds through algebraic generalized stabilization equations. Just as in the single-centered case, the field configurations at any point in spacetime are dictated by the local value of $H(\vec{x})$ via

$$2e^{-U(\vec{x})}\,\mathrm{Im}\left(e^{-i\alpha(\vec{x})}\mathcal{V}(\vec{x})\right) = -H(\vec{x}). \tag{2.18}$$

By solving (2.18), the normalized period vector $\mathcal{V}(\vec{x}) = \mathcal{V}(z(\vec{x}), \bar{z}(\vec{x}))$ and the local phase $\alpha(\vec{x})$ of the central charge are determined by $H(\vec{x})$.

Furthermore, as shown by Bates and Denef, the warp factor and the scalar moduli can in suitable cases be reconstructed explicitly using a single homogeneous degree-two function $\Sigma(H)$, already encountered for single-centered black holes. The warp factor is then given locally by

$$e^{-2U(\vec{x})} = \Sigma(H(\vec{x})). \tag{2.19}$$

Near a pole $\vec{x} = \vec{x}_s$ associated with a charge Γ_s supporting a regular single-centered solution, this reproduces the expected near-horizon behavior. More generally, the regularity of the full multicentered solution also requires the absence of additional pathologies, such as closed timelike curves.

The rotation one-form ω governing the stationary nature of the spacetime is reconstructed by solving the differential equation on the flat $\mathbb{R}^3$ base

$$*\mathrm{d}\omega = \langle \mathrm{d}H, H \rangle, \tag{2.20}$$

where $*$ is the Hodge star operator on flat $\mathbb{R}^3$. Since the right-hand side is built from the pairings of the harmonic functions, mutually non-local charges generically source a non-trivial ω, while mutually local configurations have $\omega = 0$.

Finally, the total electromagnetic field strength $\mathcal{F} = \mathrm{d}\mathcal{A}$ is obtained from the local gauge connection

$$\mathcal{A} = 2e^{U(\vec{x})} \mathrm{Re}\left(e^{-i\alpha(\vec{x})} \mathcal{V}(\vec{x}) \right) (dt + \omega) + \mathcal{A}_d, \tag{2.21}$$

where $\mathcal{A}_d$ is the spatial Dirac monopole vector potential satisfying $\mathrm{d}\mathcal{A}_d = *\mathrm{d}H$. Therefore, the task of constructing exact supersymmetric multicentered black hole solutions is reduced to specifying the harmonic functions (2.17) and integrating the rotation one-form (2.20), provided the corresponding entropy function $\Sigma(H)$ is known.

2.2.1 Integrability Equations

The requirement that ω be globally well defined, or equivalently that the metric be free of Dirac–Misner string singularities, imposes stringent restrictions on the allowed spatial positions $\vec{x}_s$ of the constituent black holes.

Applying the exterior derivative to both sides of (2.20) yields the integrability condition $0 = \langle \nabla^2 H, H \rangle$. Recalling that the harmonic function $H(\vec{x})$ possesses poles at the center positions $\vec{x}_s$ such that $\nabla^2 H = -4\pi \sum_s \Gamma_s \delta^{(3)}(\vec{x} - \vec{x}_s)$, one can evaluate this integrability condition at each pole. This results in a system of algebraic constraints tying the inter-center distances directly to the moduli at spatial infinity, namely the Denef equations:

$$\sum_{t \neq s} \frac{\langle \Gamma_s, \Gamma_t \rangle}{|\vec{x}_s - \vec{x}_t|} = 2 \,\mathrm{Im}\left(e^{-i\alpha_\infty} Z(\Gamma_s; z_\infty) \right) \quad \forall\, s. \tag{2.22}$$

These relations strongly constrain the phase space of multicentered BPS solutions. Unlike regular single-centered attractor black holes, whose near-horizon data are determined entirely by the total charge, multicentered bound states depend essentially on the asymptotic moduli through the Denef integrability equations. The simplest case is that of two centers, which gives:

$$|\vec{x}_1 - \vec{x}_2| = \frac{\langle \Gamma_1, \Gamma_2 \rangle}{2 \,\mathrm{Im}\left(e^{-i\alpha_\infty} Z_1(z_\infty) \right)} = \frac{1}{2} \langle \Gamma_1, \Gamma_2 \rangle \frac{|Z_1(z_\infty) + Z_2(z_\infty)|}{\mathrm{Im}\left(Z_1(z_\infty) \bar{Z}_2(z_\infty) \right)}, \tag{2.23}$$

where we have used the abbreviation $Z_i(z_\infty) \equiv Z(\Gamma_i; z_\infty)$.

Since the physical separation distance $|\vec{x}_1 - \vec{x}_2|$ must be strictly positive, the bound state can exist only in domains of the special Kähler moduli space $\mathcal{M}$ where the right-hand side of (2.23) is positive, i.e.,

$$\langle \Gamma_1, \Gamma_2 \rangle \ \mathrm{Im}\left(Z_1(z_\infty) \bar{Z}_2(z_\infty) \right) > 0. \tag{2.24}$$

If the asymptotic moduli are adiabatically varied so that this condition is violated, the corresponding bound-state solution ceases to exist.

The boundary separating the stable domain from the unstable domain is a codimension-one hypersurface in $\mathcal{M}$ known as a wall of marginal stability. Approaching this wall, the phases of the individual central charges align, meaning $\arg Z_1 \to \arg Z_2$. In this limit, the denominator $\mathrm{Im}(Z_1\bar{Z}_2)$ vanishes, and the equilibrium separation distance $|\vec{x}_1 - \vec{x}_2|$ diverges to infinity.

This provides a natural macroscopic picture of BPS state decay: as the background moduli are tuned toward marginal stability, the binding energy holding the composite together goes to zero, and the constituent black holes separate to infinite distance. Once the wall is crossed, the distance formula (2.23) would yield an unphysical negative separation, indicating that the corresponding supersymmetric bound-state solution no longer exists. This classical mechanism of discontinuous decay at walls of marginal stability provides the physical intuition underlying the wall-crossing formulae for BPS indices that we will discuss later in this chapter.

2.2.2 Angular Momentum

The presence of the rotation one-form ω in the multicentered metric ansatz signifies that bound states of mutually non-local BPS black holes are stationary rather than static. Physically, if the constituent black holes carry mutually non-local charges ($\langle\Gamma_1, \Gamma_2\rangle \neq 0$), their crossed electric and magnetic fields generate a non-vanishing local Poynting vector, which endows the spacetime with angular momentum.

By analyzing the asymptotic fall-off of the rotation one-form ω at spatial infinity ($\omega \sim O(1/r^2)$), the ADM angular momentum $\vec{J}$ of a general N-centered composite can be extracted. Using the supergravity equations on the flat $\mathbb{R}^3$ base, the total angular momentum vector can be written as:

$$\vec{J} = \frac{1}{2}\sum_{i<j}\langle\Gamma_i, \Gamma_j\rangle \frac{\vec{x}_i - \vec{x}_j}{|\vec{x}_i - \vec{x}_j|}. \tag{2.25}$$

This is a remarkable result: the angular momentum is fixed by the quantized Dirac–Zwanziger intersection products together with the relative orientation of the centers. It is independent of the magnitudes of the inter-center separations and of the precise asymptotic values of the special Kähler scalar fields.

This leads to a compelling physical interpretation of multicentered BPS solutions. They behave as composite electromagnetic and scalar bound states. In classical Maxwell electrodynamics, a static electron–monopole system famously carries a configurational angular momentum proportional to the product of its charges. The multicentered $\mathcal{N} = 2$ supergravity solutions represent the fully backreacted generalization of this phenomenon. In this supergravity context, the long-range gravitational attraction and the forces mediated by the exchange of massless scalar moduli precisely cancel the standard electromagnetic Coulomb repulsion, as required by the BPS no-force condition, leaving a stable macroscopic bound state supported by the topological interaction encoded in the symplectic pairing.

The existence of this intrinsic angular momentum implies that the quantum mechanics of these bound states possesses highly non-trivial features, providing the bridge between classical supergravity solutions and the microscopic BPS Hilbert space. Upon quantization of the relative position degrees of freedom, the symplectic pairing induces an effective magnetic flux on the relative moduli space, leading to a degeneracy of supersymmetric ground states which form the foundation of state counting in this setup.

For a simple two-centered system composed of charges Γ_1 and Γ_2, the classical electromagnetic angular momentum has magnitude $J_{\rm EM} = \frac{1}{2}|\langle\Gamma_1, \Gamma_2\rangle|$. As shown by Denef and Moore, a careful treatment of the supermultiplet structure of the probe particle mechanics reveals that the coupling of the spatial hypermultiplet fermions to the radial magnetic field shifts the effective spin of the ground state down by $1/2$. The resulting intrinsic angular momentum of the BPS ground state is therefore

$$J = \frac{1}{2}\left(|\langle\Gamma_1, \Gamma_2\rangle| - 1\right). \tag{2.26}$$

Quantizing this angular momentum gives rise to a ground-state degeneracy associated with the internal degrees of freedom of the bound state. Factoring out the center-of-mass degrees of freedom, the bound state contributes a multiplicity

$$2J + 1 = |\langle\Gamma_1, \Gamma_2\rangle| \tag{2.27}$$

to the BPS Hilbert space.

2.3 BPS States and Protected Indices

The supersymmetric black hole solutions discussed so far provide the classical gravitational description of charged BPS configurations in four-dimensional $\mathcal{N} = 2$ theories. Their quantum realization is furnished by BPS states in the Hilbert space, organized into shortened representations of the supersymmetry algebra and counted by protected indices. In Calabi–Yau compactifications, the basic indexed quantity is the second helicity supertrace, which captures the BPS spectrum in a fixed charge sector and varies with the moduli through the stability structure of the theory. This section introduces the representation-theoretic characterization of these states and the corresponding protected index that will be used throughout the rest of this chapter.

2.3.1 Short and Long Multiplets

The starting point is the four-dimensional $\mathcal{N} = 2$ supersymmetry algebra with a complex central extension. In a charge sector labeled by Γ, the central term is controlled by the corresponding central charge $Z(\Gamma; z_\infty)$, whose value depends both on the electromagnetic charge vector and on the asymptotic vector-multiplet moduli. The SUSY algebra takes the form

$$\{Q^A_\alpha, \bar{Q}_{\dot\beta B}\} = 2\,\sigma^\mu_{\alpha\dot\beta} P_\mu\,\delta^A{}_B, \qquad \{Q^A_\alpha, Q^B_\beta\} = \epsilon_{\alpha\beta}\epsilon^{AB}\,\overline{Z(\Gamma; z_\infty)}, \tag{2.28}$$

together with the complex-conjugate relation. The presence of the central term modifies the usual positivity argument and leads to the familiar BPS mass bound

$$M \geq |Z(\Gamma; z_\infty)|. \tag{2.29}$$

A BPS state is, by definition, a state in the fixed charge sector Γ that saturates this inequality. In four dimensions such a state preserves half of the supercharges and is therefore $1/2$-BPS. [75, 165]

This condition has an immediate consequence: For a generic massive state with $M > |Z|$, all supercharges act nontrivially and the state furnishes a long multiplet of the $\mathcal{N} = 2$ algebra. By contrast, when the bound is saturated, an appropriate linear combination of supercharges annihilates the state. The multiplet built from it therefore has fewer independent descendants and is

correspondingly shorter. It is this shortening that makes BPS states special: they are distinguished by the fact that they belong to a protected class of representations of the supersymmetry algebra.

In the present context, the moduli dependence of the central charge is crucial. For fixed electromagnetic charge $\Gamma = (P^\Lambda, Q_\Lambda)$, the central charge varies as the asymptotic vector-multiplet moduli vary, since it is determined by the special-geometric data reviewed earlier in the chapter. Thus the numerical value of the BPS bound, and in particular the phase of the quantity that enters it, is not fixed by the charge vector alone but also depends on the point z_∞ in moduli space.

It is also worth stressing that the notion of a BPS state here is broader than the single-centered black holes discussed in the previous sections. The charge sector Γ may contain elementary BPS particles, regular single-centered black holes, multicentered bound states, or combinations thereof, depending on the regime of moduli and on the amount of supersymmetry preserved by the relevant configuration. What is common to all such objects is that they contribute to the BPS Hilbert space only when they satisfy the same condition $M = |Z(\Gamma; z_\infty)|$.

2.3.2 Protected Indices and Moduli Dependence

Although BPS states are distinguished by their saturation of the BPS bound and by their membership in short multiplets, the raw number of such states in a given charge sector is not itself a protected quantity. The reason is that short multiplets need not remain isolated under continuous deformations. As the parameters of the theory are varied, several short multiplets can combine into a long multiplet, and once this happens the corresponding states can move away from the BPS bound without any contradiction. A naive degeneracy therefore depends too sensitively on details of the spectrum to serve as a robust counting function.

The standard remedy is to replace the naive degeneracy by an index which vanishes on long multiplets and is therefore insensitive to such recombinations. In the four-dimensional black-hole and Calabi–Yau context, the ordinary protected quantity is the second helicity supertrace,

$$\Omega(\Gamma; z_\infty) := -2\ \mathrm{Tr}_{\mathcal{H}(\Gamma;z_\infty)}(-1)^{2J_3} J_3^2. \tag{2.30}$$

Here $\mathcal{H}(\Gamma; z_\infty)$ denotes the BPS Hilbert space in the charge sector Γ at asymptotic moduli z_∞, and J_3 is a chosen generator of spatial rotations. The insertion of $(-1)^{2J_3} J_3^2$ is precisely what makes this trace sensitive to the short multiplets of interest while annihilating the generic long multiplets. [75] With the conventional normalization used in this subject, a single half-hypermultiplet contributes $+1$ to the index. [75]

This formula is the natural analog of the familiar idea that an index should count states with signs rather than count them absolutely. What matters is not the detailed multiplicity of every state, but the net contribution that survives the cancellations enforced by supersymmetry. In that sense, the protected index captures the part of the BPS spectrum that is stable under smooth deformations and is therefore physically meaningful beyond a particular weakly-coupled description.

In practice, it is often convenient to factor out the universal center-of-mass degrees of freedom carried by every one-particle BPS state. One then writes the BPS Hilbert space as

$$\mathcal{H}(\Gamma; z_\infty) = (0, 0; \tfrac{1}{2}) \otimes \mathcal{H}'(\Gamma; z_\infty), \tag{2.31}$$

where $(0, 0; \frac{1}{2})$ denotes the center-of-mass half-hypermultiplet and $\mathcal{H}'(\Gamma; z_\infty)$ is the reduced internal Hilbert space. After removing this universal factor, the protected index takes the simpler form

$$\Omega(\Gamma; z_\infty) = \mathrm{Tr}_{\mathcal{H}'(\Gamma;z_\infty)}(-1)^{2J_3'}. \tag{2.32}$$

This reduced trace isolates the intrinsic indexed degeneracy from the kinematical translational supermultiplet that accompanies any BPS particle in four dimensions. Therefore, the second helicity supertrace may be viewed either as a trace over the full BPS Hilbert space or, equivalently, as an ordinary signed trace over the internal Hilbert space after factoring out the universal half-hypermultiplet. [75]

The robustness of the index means that it is locally constant on moduli space. If one varies the asymptotic moduli z_∞ through a generic region in which no BPS state hits a stability threshold, then the value of $\Omega(\Gamma; z_\infty)$ cannot change. Individual states may move continuously, and the detailed realization of the BPS sector may vary, but long multiplets continue to contribute zero, while short multiplets that remain isolated continue to contribute the same net signed count. This is the precise sense in which the BPS index is protected. [165]

At the same time, this constancy is only local. Globally, the index is at best piecewise constant as a function of the asymptotic moduli. It can jump across codimension-one walls where a BPS bound state becomes marginally unstable. Physically, these are walls at which the phases of constituent central charges align. For a decomposition

$$\Gamma = \Gamma_1 + \Gamma_2, \tag{2.33}$$

one expects a wall of marginal stability when

$$\arg Z(\Gamma_1; z_\infty) = \arg Z(\Gamma_2; z_\infty). \tag{2.34}$$

At such a locus, a bound state of total charge Γ can sit at threshold against decay into constituents of charges Γ_1 and Γ_2, and the corresponding indexed count may discontinuously change as one crosses from one side of the wall to the other.

This is a good place to point out a subtlety: It is true that walls associated with phase alignment are the basic source of jumps in the BPS index, and it is precisely for this reason that wall-crossing occupies such a central role in the subject. However, it would be too loose to say that every codimension-one wall appearing in a supergravity description is automatically an ordinary wall of marginal stability with a corresponding jump of $\Omega(\Gamma; z_\infty)$. There are more subtle transformation walls for which the supergravity realization of a configuration changes without an accompanying discontinuity in the protected index. [21].

2.4 Refined and Rational Indices

The ordinary protected index $\Omega(\Gamma; z_\infty)$ introduced in the previous section is the basic deformation-invariant quantity used to count BPS states, but it is not always the most informative variable for later applications. Two natural refinements of this basic notion will play an important role in this thesis. First, one may ask whether some part of the spin content of the BPS spectrum can be retained, rather than collapsing it into a coarse signed count. Second, one may ask why wall-crossing and multicentered formulas are so naturally expressed in terms of rational rather than integer-valued invariants. This section is based primarily on [20, 75, 165].

2.4.1 Refined Indices: Spin-Sensitive BPS Counting

The ordinary BPS index is a protected and useful invariant, but it is also rather coarse: by taking an alternating trace, one discards most of the detailed angular-momentum information carried by the BPS states. In particular, different spin multiplets can contribute to the same net signed count,

so the integer index $\Omega(\Gamma; z_\infty)$ does not by itself resolve the spin content of the BPS spectrum. A natural refinement is therefore to introduce a fugacity y conjugate to the angular momentum and to define a spin-sensitive index by

$$\Omega_{\rm ref}(\Gamma; z_\infty; y) = \mathrm{Tr}'_{\mathcal{H}(\Gamma;z_\infty)}(-1)^{2J_3} y^{2J_3}, \tag{2.35}$$

where J_3 is the Cartan generator of spatial rotations, and the prime indicates the reduced trace on the BPS Hilbert space after removing the universal center-of-mass degrees of freedom. In this way, the extra variable y keeps track of the angular-momentum content of the states, and (2.35) refines the ordinary signed count into a spin-sensitive generating function.

At this stage, however, it remains to justify that the refinement (2.35) is itself protected. In four-dimensional $\mathcal{N} = 2$ supersymmetric quantum field theories, Gaiotto, Moore, and Neitzke identified the appropriate protected refinement, namely the *protected spin character* [98]. Because such theories possess an $SU(2)_R$ symmetry in addition to the spatial rotation group, one may define

$$\Omega_{\rm PSC}(\Gamma; z_\infty; y) = \mathrm{Tr}'_{\mathcal{H}(\Gamma;z_\infty)}(-1)^{2J_3} y^{2(I_3+J_3)}, \tag{2.36}$$

where I_3 denotes the Cartan generator of $SU(2)_R$. It is this combination $I_3 + J_3$, rather than J_3 alone, that yields the protected spin character in favorable four-dimensional $\mathcal{N} = 2$ settings.

A related statement is the *no-exotics* conjecture. Roughly speaking, after factoring out the universal Clifford vacuum, the reduced BPS Hilbert space is expected to transform trivially under $SU(2)_R$, so that the BPS states of interest are $SU(2)_R$ singlets. Equivalently, one expects that no non-trivial exotic $SU(2)_R$ quantum numbers occur in the protected BPS spectrum. When this conjecture holds, one has $I_3 = 0$ on the reduced BPS states, and the protected spin character (2.36) reduces precisely to the refined index (2.35):

$$\Omega_{\rm PSC}(\Gamma; z_\infty; y) = \Omega_{\rm ref}(\Gamma; z_\infty; y). \tag{2.37}$$

Thus, in the absence of exotics, the simpler spin-refined trace (2.35) is itself robust and protected.

In the following, we shall assume that the no-exotics property holds in the situations of interest, and accordingly identify the refined BPS index with the protected spin character. With this understanding, we shall simply write

$$\Omega(\Gamma; z_\infty; y) = \mathrm{Tr}'_{\mathcal{H}(\Gamma;z_\infty)}(-1)^{2J_3} y^{2J_3}, \tag{2.38}$$

keeping in mind that its protection is justified through the protected spin character together with the no-exotics assumption.

2.4.2 Rational Indices: Multi-Particle Structure

Rational BPS invariants arise naturally in the counting of multicentered configurations, especially when identical constituents are present. In that case, Bose–Fermi statistics may be reorganized into a Maxwell–Boltzmann form, and the corresponding wall-crossing and multi-particle formulas are most naturally written in terms of rational rather than integer invariants [146].

The unrefined rational BPS invariant is defined by

$$\bar{\Omega}(\Gamma; z_\infty) = \sum_{m|\Gamma} \frac{1}{m^2}\, \Omega(\Gamma/m; z_\infty), \tag{2.39}$$

where the sum runs over positive integers m such that Γ/m is again a charge vector in the lattice.

There is a direct refined analogue. One defines the refined rational index by

$$\bar{\Omega}(\Gamma; z_\infty; y) = \sum_{m|\Gamma} \frac{1}{m} \frac{y - y^{-1}}{y^m - y^{-m}} \Omega(\Gamma/m; z_\infty; y^m) \,. \tag{2.40}$$

The factor

$$\frac{1}{m} \frac{y - y^{-1}}{y^m - y^{-m}}$$

is the refined statistical weight appearing in the Maxwell–Boltzmann reorganization.

This redefinition is particularly useful for charge decompositions of the form

$$\Gamma = \sum_s \Gamma_s,$$

especially when some of the constituent charges Γ_s coincide.

The passage from integer to rational invariants is invertible. In the unrefined case, one recovers the integer index from the rational one by Möbius inversion:

$$\Omega(\Gamma; z_\infty) = \sum_{m|\Gamma} \frac{\mu(m)}{m^2} \bar{\Omega}(\Gamma/m; z_\infty), \tag{2.41}$$

where $\mu(m)$ is the arithmetic Möbius function defined as

$$\mu(m) = \begin{cases} 1, & m = 1, \\ (-1)^k, & m \text{ is a product of } k \text{ distinct primes}, \\ 0, & p^2 \mid m \text{ for some prime } p. \end{cases} \tag{2.42}$$

Likewise, the refined rational invariant can be inverted through

$$\Omega(\Gamma; z_\infty; y) = \sum_{m|\Gamma} \frac{\mu(m)}{m} \frac{y - y^{-1}}{y^m - y^{-m}} \bar{\Omega}(\Gamma/m; z_\infty; y^m) \,. \tag{2.43}$$

Thus rational invariants reorganize, but do not lose, the BPS data, and they provide the natural variables for non-primitive wall-crossing formulas.

2.5 Wall-Crossing and Chamber Structure

Sections 2.3 and 2.4 introduced the protected BPS index and its refinements. As emphasized, the important feature of these quantities is that they are locally constant on the vector-multiplet moduli space $\mathcal{M}$, but not globally constant: they may jump discontinuously across real codimension-one loci where a bound-state decomposition becomes marginally stable. The moduli dependence of the indexed BPS spectrum is therefore organized by a chamber structure on $\mathcal{M}$, separated by walls of marginal stability.

The purpose of the present section is to describe this chamber structure from the physical point of view. A more geometric realization of the same structure in terms of split attractor flows will be discussed in Section 2.6, while the scattering diagram formalism for wall-crossing will be revisited later in Section 3.3.

Consider a possible decay channel

$$\Gamma = \Gamma_1 + \Gamma_2.$$

A wall of marginal stability for this decomposition is characterized by the alignment of the phases of the corresponding central charges at the asymptotic moduli z_∞:

$$\mathrm{Im}\Big(Z(\Gamma_1; z_\infty)\,\overline{Z(\Gamma_2; z_\infty)}\Big) = 0, \qquad \mathrm{Re}\Big(Z(\Gamma_1; z_\infty)\,\overline{Z(\Gamma_2; z_\infty)}\Big) \tag{2.44}$$

Equivalently,

$$\arg Z(\Gamma_1; z_\infty) = \arg Z(\Gamma_2; z_\infty). \tag{2.45}$$

Such loci are real codimension-one subsets of $\mathcal{M}$ and divide moduli space into chambers. Within each chamber, the protected index is constant; it can jump only when one crosses one of these walls.

As reviewed in Section 2.2, for a two-centered configuration with constituent charges Γ_1 and Γ_2, the Denef integrability condition fixes the relative separation of the centers as

$$|\vec{x}_1 - \vec{x}_2| = \frac{\langle \Gamma_1, \Gamma_2 \rangle\, |Z(\Gamma_1 + \Gamma_2; z_\infty)|}{2\ \mathrm{Im}\Big(Z(\Gamma_1; z_\infty)\,\overline{Z(\Gamma_2; z_\infty)}\Big)}.$$

A physical bound state exists only on the side of the wall for which the right-hand side is positive. As the wall is approached from that side, the denominator tends to zero and the separation diverges, so the composite state becomes arbitrarily large. After crossing the wall, the putative separation would become negative, and the corresponding two-centered solution ceases to exist. In this way, the wall-crossing of the index is realized macroscopically as the decay of a composite BPS bound state.

More generally, for a decomposition

$$\Gamma = \sum_{s=1}^{n} \Gamma_s,$$

the existence of a multicentered solution depends on a set of integrability, positivity and regularity conditions. The resulting chamber structure is therefore richer than the two-centered case, but the basic mechanism is the same: the spectrum changes only when a previously stable decomposition becomes marginal, or when a new composite configuration becomes stable.

2.5.1 Primitive Wall-Crossing Formula

The jump of the BPS index across a wall of marginal stability can be understood physically from the behavior of multicentered bound states [75]. Consider the decay

$$\Gamma \to \Gamma_1 + \Gamma_2.$$

As stipulated in the arguments in the previous subsection, the states that become marginal are precisely those which, near the wall, decompose into two widely separated BPS clusters carrying charges Γ_1 and Γ_2.

In this regime the corresponding subspace of BPS states factorizes. Denoting by $\mathcal{H}'(\Gamma; z_\infty)$ the reduced Hilbert space of BPS states of total charge Γ, the near-wall sector associated with the split $\Gamma \to \Gamma_1 + \Gamma_2$ is expected to take the form

$$\mathcal{H}(\Gamma \to \Gamma_1 + \Gamma_2)\big|_{z_{\rm ms}} \;=\; \mathcal{H}_{\rm rel}(\Gamma_1, \Gamma_2) \otimes \mathcal{H}(\Gamma_1)\big|_{z_{\rm ms}} \otimes \mathcal{H}(\Gamma_2)\big|_{z_{\rm ms}},$$

where $z_{\rm ms}$ is a point on the wall. The first factor describes the relative supersymmetric quantum mechanics of the two centers, while the remaining factors encode the internal BPS degrees of freedom of the two constituent clusters.

The crucial input is then the quantization of the relative two-center dynamics. For a pair of primitive charges with Dirac–Schwinger–Zwanziger pairing

$$\Gamma_{12} := \langle \Gamma_1, \Gamma_2 \rangle,$$

the bosonic relative moduli space is a two-sphere endowed with magnetic flux Γ_{12}, and supersymmetric quantization produces an angular momentum multiplet of spin

$$J = \frac{|\Gamma_{12}| - 1}{2}.$$

Its contribution to the protected index is therefore

$$\mathrm{Tr}_{\mathcal{H}_{\rm rel}}(-1)^{2J_3} = (-1)^{\Gamma_{12}-1}|\Gamma_{12}|. \tag{2.46}$$

Multiplying this universal orbital factor by the indices of the two primitive constituents yields the primitive wall-crossing formula:

$$\Omega^+(\Gamma) - \Omega^-(\Gamma) = (-1)^{\langle \Gamma_1, \Gamma_2 \rangle - 1}\big|\langle \Gamma_1, \Gamma_2 \rangle\big|\, \Omega(\Gamma_1)\, \Omega(\Gamma_2). \tag{2.47}$$

where $\Omega^+(\Gamma)$ and $\Omega^-(\Gamma)$ are the indices in the chambers on the stable and unstable sides of the wall, respectively. Thus, the discontinuity is completely determined by two pieces of data: the intrinsic indices carried by the decay products, and the supersymmetric degeneracy of the relative two-center motion, which depends only on the symplectic pairing $\langle \Gamma_1, \Gamma_2 \rangle$.

2.6 The Split Attractor Flow Conjecture

The chamber structure on the vector-multiplet moduli space $\mathcal{M}$ admits a natural realization in terms of attractor flows in supergravity. Starting from asymptotic moduli $z_\infty \in \mathcal{M}$ and a total charge Γ, one considers the single-centered attractor flow reviewed in Section 2.1, which evolves toward the attractor point $z_*(\Gamma)$. For suitable values of the moduli, this flow may encounter walls at which a decomposition of the total charge into constituent charges becomes marginally possible. The flow then branches into separate trajectories associated with the constituent charges. Repeating this process produces a rooted tree in moduli space, whose vertices encode successive charge splittings and whose edges are ordinary attractor flows for the corresponding partial charges. In this way, a split attractor flow tree provides a geometric realization of the hierarchical decomposition of a BPS state into its constituents.

This picture suggests that the chamber-dependent index of a charge Γ at z_∞ should be reconstructed from chamber-independent data associated with the attractor endpoints of constituent charges, together with universal supergravity vertex factors attached to the intermediate splittings. The purpose of this section is to formulate this idea carefully, beginning with the basic split-flow mechanism. This section is primarily based on [16, 74]

2.6.1 Attractor Flows and Split Flows

We begin with the single-center attractor flow. In the stationary BPS ansatz, the flat spatial base is $\mathbb{R}^3$, and for spherically symmetric configurations it is natural to use the inverse radial variable

$$\tau = \frac{1}{r}, \tag{2.48}$$

so that $\tau = 0$ at spatial infinity and $\tau \to \infty$ at the attractor endpoint. Let

$$\alpha(\tau) = \arg Z(\Gamma, z(\tau)), \qquad \alpha_\infty = \arg Z(\Gamma, z_\infty). \tag{2.49}$$

Then the radial BPS flow can be written in symplectic form as

$$2e^{-U}\,\mathrm{Im}\big(e^{-\mathrm{i}\alpha}\mathcal{V}\big) = -\Gamma\,\tau + 2\,\mathrm{Im}\big(e^{-\mathrm{i}\alpha_\infty}\mathcal{V}\big)\Big|_{z=z_\infty}, \tag{2.50}$$

where U is the warp factor and $\mathcal{V}$ is the normalized non-holomorphic period vector. This equation expresses the fact that the flow is controlled by the central charge of the total charge Γ, and it is equivalent to the usual first-order attractor equations of four-dimensional $\mathcal{N} = 2$ supergravity (2.10).

Now assume the single center splits into two: $\Gamma = \Gamma_1 + \Gamma_2$. Contracting (2.50) with Γ_1 and using $Z(\Gamma; z) = \langle \Gamma, \mathcal{V}(z, \bar{z})\rangle$ gives

$$2e^{-U}\,\mathrm{Im}\big(e^{-\mathrm{i}\alpha} Z(\Gamma_1, z)\big) = -\langle \Gamma_1, \Gamma\rangle\,\tau + 2\,\mathrm{Im}\big(e^{-\mathrm{i}\alpha_\infty} Z(\Gamma_1, z_\infty)\big). \tag{2.51}$$

Since $\langle \Gamma_1, \Gamma\rangle = \langle \Gamma_1, \Gamma_2\rangle$, this may be rewritten in the equivalent form

$$2e^{-U}\,\mathrm{Im}\Big(Z(\Gamma_1, z)\,\overline{Z(\Gamma_2, z)}\Big) = -\langle \Gamma_1, \Gamma_2\rangle\,|Z(\Gamma, z)|\,\tau + 2\,\mathrm{Im}\Big(Z(\Gamma_1, z_\infty)\,\overline{Z(\Gamma_2, z_\infty)}\Big), \tag{2.52}$$

which governs the relative phase alignment of the two constituents along the flow of the total charge. In particular, the left-hand side vanishes precisely when the phases of $Z(\Gamma_1, z)$ and $Z(\Gamma_2, z)$ align, i.e. at the wall of marginal stability defined in (2.44).

A split flow is obtained when the attractor flow of the total charge Γ intersects such a wall at positive flow time. Setting the left-hand side of (2.52) equal to zero therefore determines the split point:

$$\tau_{\mathrm{ms}} = \frac{2\,\mathrm{Im}\Big(Z(\Gamma_1, z_\infty)\,\overline{Z(\Gamma_2, z_\infty)}\Big)}{\langle \Gamma_1, \Gamma_2\rangle\,|Z(\Gamma, z_\infty)|} = \frac{1}{r_{\mathrm{ms}}}. \tag{2.53}$$

A necessary condition for the split to be physically realized is therefore

$$\tau_{\mathrm{ms}} > 0, \qquad \text{equivalently} \qquad \langle \Gamma_1, \Gamma_2\rangle\,\mathrm{Im}\Big(Z(\Gamma_1, z_\infty)\,\overline{Z(\Gamma_2, z_\infty)}\Big) > 0, \tag{2.54}$$

which is precisely the supergravity stability condition for two centers (2.24) and the corresponding radius is the two-center equilibrium separation.

This agreement is the input behind the flow-tree picture: starting from z_∞, one follows the attractor trajectory of the total charge Γ. If the flow reaches a point on $\mathcal{W}(\Gamma_1, \Gamma_2)$ with $\tau_{\mathrm{ms}} > 0$, then the parent flow may split into two daughter flows carrying charges Γ_1 and Γ_2. Each daughter flow begins at the split point and continues toward the corresponding attractor point $z_*(\Gamma_1)$ or $z_*(\Gamma_2)$. If one of the daughter flows encounters a further wall of marginal stability, it can in turn split again, and so on. In this way one obtains an iterated split attractor flow.

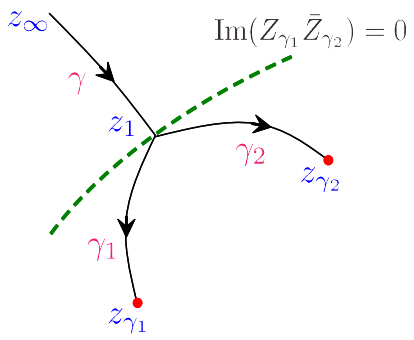


Figure 2.1: Elementary split attractor flow for a decomposition $\Gamma \to \Gamma_1 + \Gamma_2$. Taken from [16, Figure 1].

2.6.2 Attractor Flow Trees and Attractor Indices

The iterated splitting process described above leads to the notion of an attractor flow tree. Concretely, a rooted binary tree T consists of a root carrying the total charge Γ, a collection of internal vertices V_T, and a set of leaves carrying terminal charges Γ_i, $i = 1, \ldots, n$, such that

$$\Gamma = \sum_{i=1}^{n} \Gamma_i. \tag{2.55}$$

Each internal vertex $v \in V_T$ is decorated by a charge Γ_v and a non-trivial decomposition

$$\Gamma_v = \Gamma_{L(v)} + \Gamma_{R(v)}, \tag{2.56}$$

where $L(v)$ and $R(v)$ denote the left and right children of v. We write $p(v)$ for the parent of v. The root is attached to the asymptotic moduli z_∞, and each edge is a segment of a single-charge attractor flow in $\mathcal{M}$. We also write

$$\Gamma_v = \sum_{i=1}^{n} m_i^v \, \Gamma_i, \tag{2.57}$$

with coefficients m_i^v indicating which leaves descend from v.

It is useful to make the moduli on the tree explicit. For each internal vertex v we denote by $z_v \in \mathcal{M}$ the moduli at the split point associated with that vertex. The root begins at z_∞, and if v is the first split from the root then z_v lies on the attractor flow of the total charge Γ beginning at z_∞. More generally, if v lies below another internal vertex, then z_v lies on the attractor flow segment emanating from the split point of its parent. The tree is said to be stable if at every internal vertex v the charges $\Gamma_{L(v)}$ and $\Gamma_{R(v)}$ become aligned at z_v and satisfy the appropriate positivity condition. In other words,

$$\begin{aligned} \mathrm{Im}\Big(Z(\Gamma_{L(v)}, z_v)\,\overline{Z(\Gamma_{R(v)}, z_v)}\Big) &= 0, \\ \langle \Gamma_{L(v)}, \Gamma_{R(v)} \rangle \, \mathrm{Im}\Big(Z(\Gamma_{L(v)}, z_{p(v)})\,\overline{Z(\Gamma_{R(v)}, z_{p(v)})}\Big) &> 0. \end{aligned} \tag{2.58}$$

The leaves then terminate at the attractor points $z_*(\Gamma_i)$. Applying this procedure recursively and defining the stability parameters

$$c_v := \mathrm{Im}\Big(Z(\Gamma_v, z_\infty)\,\overline{Z(\Gamma, z_\infty)}\Big), \tag{2.59}$$

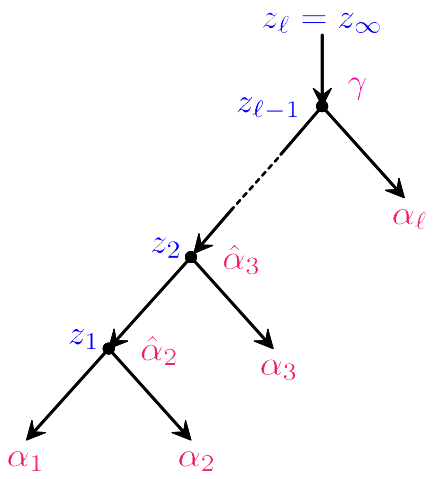


Figure 2.2: Discrete attractor flow data along a branch of a rooted tree. Taken from [16, Figure 5]

.

one is led to the discrete attractor flow equation

$$c_{v,i} = c_{p(v),i} - \frac{\langle \Gamma_v, \Gamma_i \rangle}{\langle \Gamma_v, \Gamma_{L(v)} \rangle} \sum_{j=1}^{n} m_j^{L(v)} \, c_{p(v),j}. \tag{2.60}$$

The flow-tree formalism separates the problem of counting BPS states into universal kinematics and model-dependent attractor data. The natural input attached to a leaf is the attractor index. We define

$$\Omega_\star(\Gamma, y) := \Omega(\Gamma; z_*(\Gamma), y), \tag{2.61}$$

namely the protected refined BPS index evaluated at the attractor stability condition of the charge Γ. If the attractor point lies on a non-generic locus, one should understand this as evaluation in the attractor chamber obtained by a generic infinitesimal deformation.

This quantity should be interpreted carefully. In particular, $\Omega_\star(\Gamma, y)$ is not, in general, identical to a single-centered Coulomb index defined in Section 2.7. In compact Calabi-Yau settings, multi-centered configurations may persist at or near the attractor point, especially in the presence of scaling sectors, and then the attractor index should be viewed as the basic index attached to the attractor stability condition rather than as an a priori purely single-centered object. For a more elaborate discussion of scaling solutions, see subsection 2.7.1.

Since the refined wall-crossing factors are most naturally expressed in terms of rational invariants, the attractor tree formulae are written at the level of the refined rational index. We continue to denote this by $\bar{\Omega}(\Gamma; z_\infty, y)$, in the notation established in Section 2.4. The unrefined rational invariant is recovered in the limit $y \to 1$, and the corresponding integral indices may then be reconstructed using the multicover relations recalled earlier.

The flow-tree formula takes the following form

$$\bar{\Omega}(\Gamma; z_\infty, y) = \sum_{n \geq 1} \sum_{\Gamma = \sum_{i=1}^n \Gamma_i} \frac{g_{\rm tr}(\{\Gamma_i\}, z_\infty, y)}{\big|\mathrm{Aut}\{\Gamma_i\}\big|} \prod_{i=1}^{n} \Omega_\star(\Gamma_i, y), \tag{2.62}$$

where the second sum runs over unordered decompositions of Γ into constituent charges $\{\Gamma_i\}$,

and $\big|\mathrm{Aut}\{\Gamma_i\}\big|$ is the symmetry factor of the multiset of charges. The coefficient

$$g_{\rm tr}(\{\Gamma_i\}, z_\infty, y) = \sum_{T\in\mathcal{T}_n(\{\Gamma_i\},z_\infty)} \Delta(T)\,\kappa(T,y) \tag{2.63}$$

is the tree index, obtained by summing over the set $\mathcal{T}_n(\{\Gamma_i\}, z_\infty)$ of stable rooted binary attractor flow trees with leaves labeled by $\{\Gamma_i\}$ and root moduli z_∞.

The factor $\Delta(T)$ encodes the supergravity stability conditions at the internal vertices (2.58). Writing V_T for the set of internal vertices of T, one has

$$\Delta(T) = \frac{1}{2^{n-1}} \prod_{v\in V_T} \left[\mathrm{sign}\Big(\mathrm{Im}\big(Z(\Gamma_{L(v)}, z_{p(v)})\,\overline{Z(\Gamma_{R(v)}, z_{p(v)})}\big)\Big) + \mathrm{sign}\big(\langle\Gamma_{L(v)}, \Gamma_{R(v)}\rangle\big)\right]. \tag{2.64}$$

This expression vanishes unless the corresponding split is compatible with the orientation of the wall-crossing.

The factor $\kappa(T, y)$ is the product of the two-center wall-crossing weights carried by the vertices,

$$\kappa(T,y) = (-1)^{n-1} \prod_{v\in V_T} \kappa\big(\langle\Gamma_{L(v)}, \Gamma_{R(v)}\rangle, y\big), \tag{2.65}$$

where the refined elementary factor is

$$\kappa(x,y) = (-1)^x\,\frac{y^x - y^{-x}}{y - y^{-1}}. \tag{2.66}$$

The unrefined specialization is obtained by taking $y \to 1$, which gives (2.46)

$$\kappa(x) = \lim_{y\to 1} \kappa(x,y) = (-1)^{x-1}|x|. \tag{2.67}$$

Thus the same rooted-tree structure controls both the refined and unrefined expansions.

The interpretation of (2.62) is worth stating explicitly. The chamber dependence of the rational index $\bar\Omega(\Gamma; z_\infty, y)$ is entirely carried by the set of stable trees and their vertex weights, that is, by the factor $g_{\rm tr}(\{\Gamma_i\}, z_\infty, y)$. By contrast, the factors $\Omega_\star(\Gamma_i, y)$ are evaluated at attractor stability conditions and are therefore taken as chamber-independent input data. In this sense, attractor indices provide the initial data from which the index at general asymptotic moduli is reconstructed.

For two centers, we reproduce the refined version of (2.47),

$$g_{\rm tr}(\{\Gamma_1,\Gamma_2\}, z_\infty, y) = -\frac{1}{2}\Big(\mathrm{sign}\, c_1 + \mathrm{sign}\langle\Gamma_1,\Gamma_2\rangle\Big)\,\kappa(\langle\Gamma_1,\Gamma_2\rangle, y), \tag{2.68}$$

$$\begin{aligned}\bar\Omega(\Gamma_1+\Gamma_2; z_\infty; y) = {}& \Omega_*(\Gamma_1+\Gamma_2, y)\\ &+ (-1)^{\Gamma_{12}-1}\frac{y^{\Gamma_{12}} - y^{-\Gamma_{12}}}{2(y-y^{-1})}\Big(\mathrm{sign}\, c_1 + \mathrm{sign}\,\Gamma_{12}\Big)\,\Omega_*(\Gamma_1, y)\,\Omega_*(\Gamma_2, y)\\ &+ \ldots \text{ (further splittings)},\end{aligned} \tag{2.69}$$

where $\Gamma_{12} = \langle\Gamma_1,\Gamma_2\rangle$.

The first non-trivial instance of this formalism is the three-center sector. Define

$$\Gamma_{ij} := \langle\Gamma_i,\Gamma_j\rangle, \qquad \Gamma_{i+j,k} := \langle\Gamma_i+\Gamma_j,\Gamma_k\rangle, \tag{2.70}$$

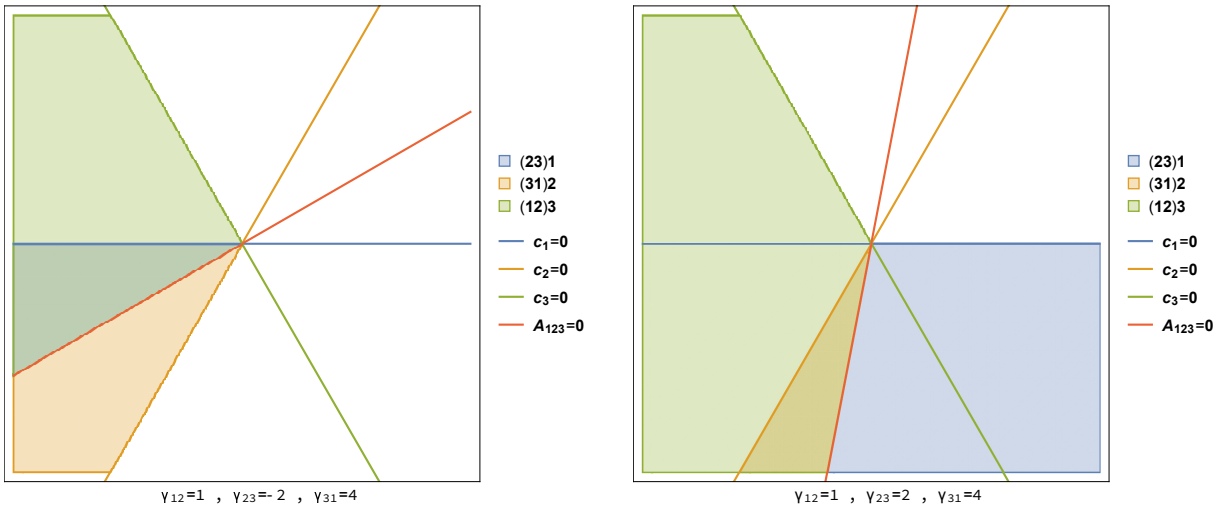


Figure 2.3: True walls and fake walls in the three-center stability plane. Taken from [16, Figure 4]

and introduce

$$c_i := \mathrm{Im}\Big(Z(\Gamma_i, z_\infty)\,\overline{Z(\Gamma, z_\infty)}\Big), \qquad i = 1, 2, 3. \tag{2.71}$$

Since $\Gamma = \Gamma_1 + \Gamma_2 + \Gamma_3$, these quantities satisfy $c_1 + c_2 + c_3 = 0$. It is also convenient to define

$$A_{123} := \Gamma_{23}\, c_1 + \Gamma_{31}\, c_2 + \Gamma_{12}\, c_3. \tag{2.72}$$

Finally, for any function $f(1, 2, 3)$ we define complete symmetrization by

$$\mathrm{Sym}\{f(1, 2, 3)\} := \frac{1}{3!} \sum_{\sigma \in S_3} f\big(\sigma(1), \sigma(2), \sigma(3)\big). \tag{2.73}$$

With this notation, the three-center tree index may be written as

$$\begin{aligned} g_{\mathrm{tr}}(\{\Gamma_1, \Gamma_2, \Gamma_3\}, z_\infty, y) = \frac{3}{4}\,\mathrm{Sym}\Big\{&\kappa(\Gamma_{12}, y)\,\kappa(\Gamma_{1+2,3}, y)\,\big[\mathrm{sign}(\Gamma_{1+2,3}) - \mathrm{sign}(c_3)\big] \\ &\times \big[\mathrm{sign}(\Gamma_{12}) + \mathrm{sign}(\Gamma_{1+2,3} A_{123})\big]\Big\}. \end{aligned} \tag{2.74}$$

The factor $\mathrm{sign}(\Gamma_{1+2,3}) - \mathrm{sign}(c_3)$ governs the existence of the first split, while the factor $\mathrm{sign}(\Gamma_{12}) + \mathrm{sign}(\Gamma_{1+2,3} A_{123})$ governs the second, nested split. The locus $A_{123} = 0$ is not itself a wall of marginal stability in $\mathcal{M}$; rather, it is an intermediate sign locus that appears in individual tree contributions. We sometimes refer to the locus $A_{123} = 0$ as a fake wall [20] since the structure of the trees change across this wall without an accompanied change of the index. The full symmetrized tree index is arranged so that any such unphysical discontinuities cancel in the complete expression.

To summarize: a stable rooted tree organizes a sequence of physically allowed splittings in moduli space. The tree index g_{tr} packages the corresponding stability factors and primitive wall-crossing weights. The attractor indices $\Omega_\star(\Gamma_i, y)$ furnish the terminal data at the leaves. The resulting sum (2.62) is the basic formula that underlies the split attractor flow conjecture.

Split attractor flow conjecture. Fix a total charge Γ and asymptotic moduli $z_\infty \in \mathcal{M}$. The split attractor flow conjecture asserts that the connected components of the moduli space of

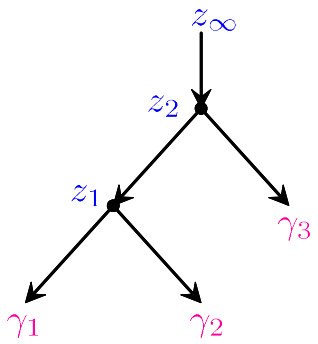


Figure 2.4: A three-leaf split attractor flow tree. Taken from [16, Figure 3].

multicentered BPS solutions of total charge Γ in the vacuum z_∞ are in one-to-one correspondence with stable rooted split attractor flow trees beginning at z_∞ and ending at attractor points of constituent charges Γ_i. Equivalently, the chamber-dependent BPS index is reconstructed by summing over stable flow trees, with attractor indices attached to the leaves and supergravity wall-crossing factors attached to the internal vertices.

It is important to distinguish the part of this picture that is under direct control from the stronger statement that remains conjectural. For two centers, the supergravity analysis is essentially explicit: one has the attractor flow equation (2.50), the phase-alignment identity (2.52), the two-center distance formula, and the positivity criterion (2.54). Together, these determine when a given binary split is physically admissible. The conjectural step is the promotion of this local two-center control to the global statement that, for general multicenter configurations, the admissible moduli space is partitioned into connected components labelled by stable split attractor flow trees.

The situation becomes sharper in non-compact and quiver-theoretic settings, where gravity decouples and the flow-tree formalism often admits a more direct mathematical realization. This regime, together with the local Calabi–Yau examples relevant for the present thesis, will be discussed in greater detail in the next chapter. A particularly important conjectural statement in that context is that, for suitable quiver realizations associated with local geometries, the attractor index should vanish unless the charge vector Γ corresponds to a simple representation, or lies in the kernel of the skew-symmetrized Euler form [37, 155]:

$$\Omega_*(\Gamma, y) = 0 \qquad \text{unless} \qquad \Gamma \text{ is simple} \quad \text{or} \quad \langle \Gamma, - \rangle = 0. \tag{2.75}$$

2.7 Coulomb Branch Formula

A complementary description of the BPS index is obtained from the Coulomb branch of the supersymmetric quantum mechanics governing multicentered black-hole configurations. This section is based primarily on [145, 148, 165].

For a fixed decomposition $\Gamma = \sum_{i=1}^{n} \Gamma_i$, the starting point is the moduli space of solutions to the Denef equilibrium equations, modulo overall translations,

$$M_n(\{\Gamma_{ij}\}; \{c_i\}) := \left\{ (\vec{r}_1, \ldots, \vec{r}_n) \in (\mathbb{R}^3)^n \;\middle|\; \sum_{j \neq i} \frac{\Gamma_{ij}}{|\vec{r}_i - \vec{r}_j|} = c_i, \quad i = 1, \ldots, n \right\} \Big/ \mathbb{R}^3, \tag{2.76}$$

where $\Gamma_{ij} = \langle \Gamma_i, \Gamma_j \rangle$ and

$$c_i = 2\ \mathrm{Im}\big(e^{-i\alpha_\infty} Z(\Gamma_i; z_\infty)\big)\,, \qquad \alpha_\infty = \arg Z(\Gamma; z_\infty), \qquad \sum_{i=1}^{n} c_i = 0. \tag{2.77}$$

For generic values of the parameters c_i, the space M_n is a $2n-2$-dimensional symplectic manifold. The ambient configuration space carries the closed two-form

$$\omega = \frac{1}{4}\sum_{i<j} \Gamma_{ij}\, \epsilon_{abc}\, \frac{dr^a_{ij} \wedge dr^b_{ij}\, r^c_{ij}}{|\vec{r}_{ij}|^3} = \frac{1}{2}\sum_{i<j} \Gamma_{ij}\ \sin\theta_{ij}\, d\theta_{ij} \wedge d\phi_{ij}, \tag{2.78}$$

whose restriction to M_n is non-degenerate and furnishes the required symplectic structure. The induced $SO(3)$ action is Hamiltonian, with moment map given by the total angular momentum (2.25)

$$\vec{J} = \frac{1}{2}\sum_{i<j} \Gamma_{ij}\, \frac{\vec{r}_{ij}}{|\vec{r}_{ij}|} = \frac{1}{2}\sum_{i=1}^{n} c_i\, \vec{r}_i. \tag{2.79}$$

Choosing a z-axis and writing J_3 for the corresponding component of $\vec{J}$, one first defines the classical refined contribution as the equivariant symplectic volume

$$g_{\text{classical}}(\{\Gamma_i\}; y) = \frac{(-1)^{\sum_{i<j}\Gamma_{ij}-n+1}}{(2\pi)^{n-1}(n-1)!}\int_{M_n} e^{2\nu J_3}\, \omega^{n-1}, \qquad \nu := \log y. \tag{2.80}$$

The quantum refined contribution is obtained by geometric quantization of M_n. Under the standard assumption that the relevant configurational index reduces to the equivariant index of the Dirac operator D, one defines

$$g_{\text{ref}}(\{\Gamma_i\}; y) = \mathrm{Tr}_{\mathrm{Ker}D^+}(-y)^{2J_3} - \mathrm{Tr}_{\mathrm{Ker}D^-}(-y)^{2J_3}. \tag{2.81}$$

Equivalently, for compact M_n,

$$g_{\text{ref}}(\{\Gamma_i\}; y) = \int_{M_n} \mathrm{Ch}(L, \nu)\, \hat{A}(M_n, \nu)\Big|_{2n-2}, \tag{2.82}$$

where

$$\mathrm{Ch}(L, \nu) = \exp\Big(2\nu J_3 + \frac{\omega}{2\pi}\Big)\,, \qquad \hat{A}(M_n, \nu) = \det\left(\frac{2\nu L + \frac{R}{2\pi}}{2\sinh\Big(\frac{1}{2}\big(2\nu L + \frac{R}{2\pi}\big)\Big)}\right). \tag{2.83}$$

Here L denotes the endomorphism induced by the J_3-action on the holomorphic tangent bundle, and R is its curvature two-form.

The index (2.82) can then be evaluated by the Atiyah–Bott–Lefschetz fixed-point formula,

$$g_{\text{ref}}(\{\Gamma_i\}; y) = \int_{M_n^{\text{fixed}}} \frac{\mathrm{Ch}(L, \nu)\, \hat{A}(M_n, \nu)}{\chi(NM_n^{\text{fixed}})}, \tag{2.84}$$

where $M_n^{\text{fixed}} \subset M_n$ is the fixed-point locus of the J_3-action and

$$\chi(NM_n^{\text{fixed}}) = \det\left(2\nu L + \frac{R}{2\pi}\right) \tag{2.85}$$

is the equivariant Euler class of the normal bundle to the fixed locus.

In the absence of scaling solutions, all fixed points are isolated and correspond precisely to collinear configurations. Writing z_i for the coordinate of the i-th center along the chosen axis, the fixed points satisfy

$$\sum_{\substack{j=1\\ j\neq i}}^{n} \frac{\Gamma_{ij}}{|z_i - z_j|} = c_i, \qquad \sum_{i=1}^{n} z_i = 0, \tag{2.86}$$

and may be described as critical points of the superpotential

$$\widehat{W}(\lambda, \{z_i\}) = -\sum_{i<j} \Gamma_{ij}\ \mathrm{sign}(z_j - z_i) \log|z_i - z_j| - \sum_{i=1}^{n} \left(c_i - \frac{\lambda}{n}\right) z_i. \tag{2.87}$$

For such isolated fixed points, the Atiyah–Bott formula reduces to the explicit localization formula

$$g_{\mathrm{ref}}(\{\Gamma_i\}; y) = \frac{(-1)^{\sum_{i<j}\Gamma_{ij}+n-1}}{(y - y^{-1})^{n-1}} \sum_{p} s(p)\, y^{\sum_{i<j}\Gamma_{ij}\ \mathrm{sign}(z_j - z_i)}, \tag{2.88}$$

where the sum runs over collinear solutions p, and

$$s(p) = \mathrm{sign}\,\det{}'\left(\frac{\partial^2 \widehat{W}}{\partial z_i\, \partial z_j}\right)_p \tag{2.89}$$

is the sign of the reduced Hessian, with the translational zero mode removed. The corresponding classical equivariant volume is

$$g_{\mathrm{classical}}(\{\Gamma_i\}; y) = \frac{(-1)^{\sum_{i<j}\Gamma_{ij}+n-1}}{(2\log y)^{n-1}} \sum_{p} s(p)\, y^{\sum_{i<j}\Gamma_{ij}\ \mathrm{sign}(z_j - z_i)}, \tag{2.90}$$

so that, in the non-scaling regime,

$$g_{\mathrm{ref}}(\{\Gamma_i\}; y) = \left(\frac{\nu}{\sinh \nu}\right)^{n-1} g_{\mathrm{classical}}(\{\Gamma_i\}; y). \tag{2.91}$$

The Coulomb branch formula is obtained by combining the configurational factor g_{ref} with the indices associated with the individual constituents. Changing the notation slightly to emphasize the Coulomb branch description, $g_C = g_{\mathrm{ref}}$, the rational refined index can be written as,

$$\bar{\Omega}(\Gamma; z_\infty, y) = \sum_{\Gamma=\sum_{i=1}^{n}\Gamma_i} \frac{g_C(\{\Gamma_i\}, z_\infty, y)}{|\mathrm{Aut}\{\Gamma_i\}|} \prod_{i=1}^{n} \left(\sum_{m_i|\Gamma_i} \frac{y - y^{-1}}{m_i(y^{m_i} - y^{-m_i})}\, \Omega_{\mathrm{tot}}(\Gamma_i/m_i; y^{m_i}) \right), \tag{2.92}$$

where $\mathrm{Aut}\{\Gamma_i\}$ is the automorphism group of the unordered multiset of constituents, and Ω_{tot} in the simplest cases is the single-centered Coulomb index Ω_S. In the presense of scaling solutions, however, Ω_{tot} is defined recursively as,

$$\Omega_{\mathrm{tot}}(\alpha; y) = \Omega_S(\alpha; y) + \sum_{\alpha=\sum_i m_i\beta_i} H_m(\{\beta_i\}, \{m_i\}, y) \prod_i \Omega_S(\beta_i; y^{m_i}). \tag{2.93}$$

The first term is the single-centered index. The remaining terms encode additional contributions associated with scaling sectors, organized by symmetric correction functions H_m for m constituents.

The role of the correction functions H_m is tied directly to the behavior of the classical phase space in the scaling regime. If no subset of the constituents can form a scaling configuration, then the reduced phase space is effectively compact and the Coulomb index (2.88) is already a Laurent polynomial in y. By contrast, when the charge data admit scaling solutions, subsets of centers can approach one another arbitrarily closely while keeping the total configuration BPS. In the simplest three-center case this happens, for example, when

$$\Gamma_{12} > 0, \qquad \Gamma_{23} > 0, \qquad \Gamma_{31} > 0, \tag{2.94}$$

together with the following triangle inequalities:

$$\Gamma_{12} < \Gamma_{23} + \Gamma_{31}, \qquad \Gamma_{23} < \Gamma_{31} + \Gamma_{12}, \qquad \Gamma_{31} < \Gamma_{12} + \Gamma_{23}. \tag{2.95}$$

In that regime, the naive fixed-point formula develops poles at $y = 1$. These poles are unphysical from the representation-theoretic point of view: the total refined index should be a Laurent polynomial, corresponding to a finite sum of $SU(2)$ characters, whereas the poles signal the non-compactness of the naive classical phase space description.

The minimal modification hypothesis provides the required correction. More precisely, it fixes the functions H_m by isolating the part of the naive Coulomb contribution responsible for the poles at $y = 1$: one extracts the polar part, namely the principal part of the Laurent expansion of the relevant rational function around $y = 1$, and then completes it to a symmetric Laurent polynomial in y which vanishes as $y \to \infty$. The resulting correction is added in such a way that the full Coulomb expansion becomes a proper Laurent polynomial, compatible with its interpretation as a finite $SU(2)$ character. In this way, the scaling contribution is isolated algebraically and the non-compact behavior of the naive classical phase space is removed from the final index.

2.7.1 Comparing Attractor and Single-Centered Indices

The comparison between the Coulomb and tree descriptions is sharpest when one asks which elementary index is reconstructed by these formulas. If no scaling solutions are present, then the Coulomb index and the tree index coincide:

$$g_C(\{\Gamma_i\}, z_\infty, y) = g_{\mathrm{tr}}(\{\Gamma_i\}, z_\infty, y). \tag{2.96}$$

This is the regime relevant for loopless quivers, or more generally for decompositions in which no subset of constituents can collapse into a scaling configuration. In that case, the attractor expansion involves no additional scaling sector, and one obtains

$$\Omega_*(\Gamma; y) = \Omega_S(\Gamma; y). \tag{2.97}$$

The situation changes substantially in the scaling regime. The first non-trivial example is the case of three constituents satisfying (2.94) and (2.95). Then the tree index g_{tr} remains a Laurent polynomial in y, while the Coulomb index g_C contains an additional polar contribution. More precisely, one finds

$$g_C - g_{\mathrm{tr}} = \frac{(-1)^{\Gamma_{12}+\Gamma_{23}+\Gamma_{31}}}{(y - y^{-1})^2} \left(y^{\Gamma_{23}+\Gamma_{31}-\Gamma_{12}} + y^{-\Gamma_{23}-\Gamma_{31}+\Gamma_{12}} \right), \tag{2.98}$$

which has a double pole at $y = 1$ produced by the naive Coulomb branch expression. The pole is absent from the tree index, which continues to behave as a genuine Laurent polynomial.

The discrepancy (2.98) is precisely the contribution that is absorbed into the minimal-modification term H_3. Introducing

$$\epsilon \equiv \Gamma_{12} + \Gamma_{23} + \Gamma_{31} \pmod 2, \tag{2.99}$$

with $\epsilon \in \{0, 1\}$ chosen to match the parity of the sum of pairings, one obtains the corrected relation

$$\Omega_*(\Gamma; y) = \Omega_S(\Gamma; y) + \kappa\left(\frac{\Gamma_{23} + \Gamma_{31} - \Gamma_{12} + \epsilon}{2}\right) \kappa\left(\frac{\Gamma_{23} + \Gamma_{31} - \Gamma_{12} - \epsilon}{2}\right) \prod_{i=1}^{3} \Omega_S(\Gamma_i; y). \tag{2.100}$$

The second term is the pure scaling contribution. It is absent in the loopless case, but it survives at the attractor point whenever the charges admit a genuine scaling solution.

2.8 Quiver Quantum Mechanics

Quiver quantum mechanics provides a complementary description of BPS bound states in terms of a one-dimensional $\mathcal{N} = 4$ supersymmetric gauge theory. For a given decomposition of the total charge into elementary constituents, the corresponding quiver encodes the charges in a finite combinatorial form: nodes represent constituent branes, arrows record their Dirac–Schwinger–Zwanziger pairings, and the asymptotic moduli enter through the associated Fayet–Iliopoulos parameters. The supersymmetric vacua of this quantum mechanics furnish a Higgs-branch realization of the BPS sector, and the cohomology of the resulting vacuum moduli space computes the protected index.

This description is closely related to the Coulomb-branch and flow-tree formalisms developed above, but it organizes the same bound-state problem in a more algebraic language. It is particularly useful because it distinguishes clearly between contributions associated with configurations of separated constituents and those carried by the intrinsic geometry of the Higgs branch itself. In the quiver setting, the former are encoded by cohomology inherited from the ambient D-term quotient, while the latter are captured by the additional middle cohomology of the complete intersection cut out by the F-term equations. This decomposition gives a precise Higgs-branch interpretation of the single-centered indices entering the Coulomb-branch formula. This section is primarily based on [73, 82, 147, 165].

2.8.1 Quivers from Charges and D-branes

Let

$$\Gamma = \sum_{i=1}^{K} N_i \, \Gamma_i \tag{2.101}$$

be a decomposition of the total charge into constituent charges Γ_i, with multiplicities $N_i \in \mathbb{Z}_{\geq 0}$. The index $i \in \{1, \ldots, K\}$ labels the nodes of the quiver, while the vector

$$\mathbf{N} = (N_1, \ldots, N_K) \tag{2.102}$$

is the corresponding dimension vector. The associated gauge group is

$$G = \prod_{i=1}^{K} U(N_i). \tag{2.103}$$

The arrows are determined by the antisymmetric Dirac–Schwinger–Zwanziger pairing

$$\Gamma_{ij} \equiv \langle \Gamma_i, \Gamma_j \rangle. \tag{2.104}$$

With the convention adopted here, $\Gamma_{ij} > 0$ gives Γ_{ij} arrows from node i to node j, while $\Gamma_{ij} < 0$ is represented by $|\Gamma_{ij}|$ arrows in the opposite direction. In this way, the quiver records the constituent charges together with their mutual electromagnetic pairings.

For each node i, the one-dimensional $\mathcal{N} = 4$ quiver quantum mechanics contains a vector multiplet valued in the adjoint of $U(N_i)$. Its bosonic components consist of a gauge field $A_{0,i}$, three real adjoint scalars X_i^a with $a = 1, 2, 3$, and an auxiliary field D_i, together with their fermionic partners. For each arrow $i \to j$, and for each copy

$$\alpha = 1, \ldots, |\Gamma_{ij}|, \tag{2.105}$$

one introduces a chiral multiplet

$$\phi_{ij,\alpha} \tag{2.106}$$

transforming in the bifundamental representation $(\mathbf{N}_i, \overline{\mathbf{N}}_j)$ of $U(N_i) \times U(N_j)$, together with its fermionic superpartner and auxiliary field. Thus the quiver determines both the gauge group and the matter content of the supersymmetric quantum mechanics.

The asymptotic moduli z_∞ enter through the Fayet–Iliopoulos parameters

$$c_i(z_\infty) = 2\ \mathrm{Im}\big(e^{-i\alpha_\infty} Z(\Gamma_i, z_\infty)\big)\,, \qquad \alpha_\infty = \arg Z(\Gamma, z_\infty), \tag{2.107}$$

which satisfy

$$\sum_{i=1}^{K} N_i\, c_i(z_\infty) = 0. \tag{2.108}$$

This relation reflects the decoupling of the overall diagonal $U(1)$, and matches the fact that the center-of-mass mode is removed in the Coulomb-branch description. The quantities $c_i(z_\infty)$ are precisely the quiver counterparts of the stability parameters appearing in the Denef equations.

The Lagrangian is that of a one-dimensional $\mathcal{N} = 4$ gauged sigma model built from these vector and chiral multiplets. Suppressing fermionic terms and numerical coefficients, its bosonic part takes the schematic form

$$L_{\mathrm{QQM}} = L_{\mathrm{vec}} + L_{\mathrm{chiral}} + L_D + L_{\mathrm{FI}} + L_W + \text{fermionic couplings}, \tag{2.109}$$

with

$$L_{\mathrm{vec}} \sim \sum_{i=1}^{K} \mathrm{Tr}\left[(D_t X_i^a)^2 + D_i^2 + \sum_{a<b} [X_i^a, X_i^b]^2 \right], \tag{2.110}$$

$$L_{\mathrm{chiral}} \sim \sum_{i,j,\alpha} \mathrm{Tr}\left[|D_t \phi_{ij,\alpha}|^2 + \sum_{a=1}^{3} \left| X_i^a\, \phi_{ij,\alpha} - \phi_{ij,\alpha}\, X_j^a \right|^2 + |F_{ij,\alpha}|^2 \right], \tag{2.111}$$

$$L_D + L_{\mathrm{FI}} \sim \sum_{i=1}^{K} \mathrm{Tr}\big[D_i\, \mu_i(\phi, \phi^\dagger) - c_i\, D_i \big]\,, \tag{2.112}$$

$$L_W \sim \sum_{i,j,\alpha} \left(F_{ij,\alpha}\, \frac{\partial W}{\partial \phi_{ij,\alpha}} + \mathrm{h.c.} \right). \tag{2.113}$$

Here D_t denotes the gauge-covariant time derivative, μ_i is the moment map for the $U(N_i)$-action on the chiral multiplets, and W is a gauge-invariant holomorphic superpotential constructed from traces of products of bifundamental fields along oriented closed loops in the quiver. The fermionic part contains the supersymmetric Yukawa couplings determined by gauge interactions and by the Hessian of W.

Supersymmetric vacua on the Higgs branch are obtained by setting the adjoint scalars X_i^a to zero and imposing the D-term and F-term equations. Writing T_i^a for generators of $U(N_i)$, the D-term equations take the form

$$\mu_i(\phi, \phi^\dagger) = c_i(z_\infty)\, \mathbf{1}_{N_i}, \tag{2.114}$$

or more explicitly,

$$\sum_{j:\,\Gamma_{ij}>0} \sum_{\alpha=1}^{\Gamma_{ij}} \phi_{ij,\alpha}\phi_{ij,\alpha}^\dagger - \sum_{k:\,\Gamma_{ki}>0} \sum_{\alpha=1}^{\Gamma_{ki}} \phi_{ki,\alpha}^\dagger \phi_{ki,\alpha} = c_i(z_\infty)\, \mathbf{1}_{N_i}, \tag{2.115}$$

while the F-term equations are

$$\frac{\partial W}{\partial \phi_{ij,\alpha}} = 0. \tag{2.116}$$

The Higgs-branch moduli space is therefore

$$\mathcal{M}_{\mathrm{H}}(\Gamma, z_\infty) = \left\{ \phi_{ij,\alpha} \;\middle|\; \mu_i(\phi, \phi^\dagger) = c_i(z_\infty)\, \mathbf{1}_{N_i}, \quad \frac{\partial W}{\partial \phi_{ij,\alpha}} = 0 \right\} \Big/ \prod_{i=1}^{K} U(N_i). \tag{2.117}$$

Equivalently, after complexifying the gauge group, one may regard $\mathcal{M}_{\mathrm{H}}$ as the moduli space of W-critical semistable representations of the quiver with stability parameters fixed by the FI terms.

It is often useful to separate the Kähler quotient defined by the D-terms from the final F-flat locus. Let

$$\mathcal{X} = \left\{ \mu_i(\phi, \phi^\dagger) = c_i(z_\infty)\, \mathbf{1}_{N_i} \right\} \Big/ \prod_{i=1}^{K} U(N_i) \tag{2.118}$$

denote the ambient Kähler quotient. Then the full Higgs branch is the critical locus of W inside $\mathcal{X}$,

$$\mathcal{M}_{\mathrm{H}} = \left\{ \frac{\partial W}{\partial \phi_{ij,\alpha}} = 0 \right\} \subset \mathcal{X}. \tag{2.119}$$

For acyclic quivers one may take $W = 0$, so that the Higgs branch is determined entirely by the D-term quotient. In many of the Abelian examples relevant for local Calabi–Yau geometries, $\mathcal{X}$ is a toric variety and $\mathcal{M}_{\mathrm{H}}$ is a complete intersection in $\mathcal{X}$.

Its complex dimension is

$$\dim_{\mathbb{C}} \mathcal{M}_{\mathrm{H}} = \sum_{\Gamma_{ij}>0} \Gamma_{ij} N_i N_j - \sum_{i=1}^{K} N_i^2 - f + 1, \tag{2.120}$$

where f denotes the number of independent F-term equations. The final $+1$ accounts for the decoupled overall diagonal $U(1)$. This dimension formula makes explicit how the Higgs branch is determined by the arrow multiplicities, the gauge quotient, and the superpotential constraints.

Physically, the quiver reformulates the same bound-state problem in the language of one-dimensional gauge theory. The parameters $c_i(z_\infty)$ that govern multicentered supergravity solutions appear here as Fayet–Iliopoulos terms, while the Higgs branch encodes the corresponding moduli space of bound states in quiver variables.

2.8.2 Quiver Moduli Spaces and the Higgs/Coulomb Dichotomy

The cohomology of the Higgs branch $\mathcal{M}_{\rm H}$ carries a natural Lefschetz $SU(2)$ action. If $h \in H^n(\mathcal{M}_{\rm H})$ is an n-form and ω_K is the Kähler form on $\mathcal{M}_{\rm H}$, the generators act as

$$J_+ \cdot h = \omega_K \wedge h, \qquad J_- \cdot h = \omega_K \lrcorner h, \qquad J_3 \cdot h = \frac{1}{2}(n-d)\, h, \tag{2.121}$$

where $d = \dim_{\mathbb{C}} \mathcal{M}_{\rm H}$ is the complex dimension. The important point is that the shifted cohomological degree $n - d$ plays the role of twice the third component of angular momentum.

The refined index on the Higgs branch is then given by the shifted Poincaré polynomial

$$Q(\mathcal{M}_{\rm H}; y) = \mathrm{Tr}'(-y)^{2J_3} = \sum_{p=0}^{2d} b_p(\mathcal{M}_{\rm H})\,(-y)^{p-d}, \tag{2.122}$$

where $b_p(\mathcal{M}_{\rm H})$ are the Betti numbers of $\mathcal{M}_{\rm H}$. This formula expresses the protected index directly in terms of the cohomology of the Higgs moduli space.

The cohomology of the moduli space of the Higgs branch $\mathcal{M}_{\rm H}$ separates naturally into a piece inherited from the ambient D-term quotient and a genuinely intrinsic piece. Let

$$i_{\mathcal{M}_{\rm H}} : \mathcal{M}_{\rm H} \hookrightarrow \mathcal{X} \tag{2.123}$$

denote the inclusion map. Then the cohomology splits as

$$H(\mathcal{M}_{\rm H}) = i^*_{\mathcal{M}_{\rm H}}(H(\mathcal{X})) \oplus \left[H^d(\mathcal{M}_{\rm H}) \Big/ i^*_{\mathcal{M}_{\rm H}}\Big(H^d(\mathcal{X})\Big)\right]. \tag{2.124}$$

The first summand is the pull-back of the ambient cohomology, while the second summand is a quotient of the middle cohomology. This is the mathematical form of the Higgs/Coulomb dichotomy.

Physically, the pull-back piece $i^*_{\mathcal{M}_{\rm H}}(H(\mathcal{X}))$ is identified with the multi-centered Coulomb sector. These are the states which admit a direct interpretation in terms of relative positions and orbital angular momentum of the constituent centers. By contrast, the quotient

$$H^d(\mathcal{M}_{\rm H}) \Big/ i^*_{\mathcal{M}_{\rm H}}\Big(H^d(\mathcal{X})\Big) \tag{2.125}$$

captures the pure-Higgs states. Since these states lie strictly in the middle cohomology, they satisfy

$$J_3 = 0, \tag{2.126}$$

and hence contribute to the refined index in a way which is independent of y. This is the underlying reason that the single-centered quantity $\Omega_S(\Gamma)$ is taken to be y-independent.

A simple cyclic example makes this structure explicit. Consider the Abelian three-node quiver with dimension vector $(1, 1, 1)$ and arrow multiplicities

$$\Gamma_{12} = a, \qquad \Gamma_{23} = b, \qquad \Gamma_{31} = c, \qquad a, b, c > 0. \tag{2.127}$$

Since the quiver contains an oriented loop, the superpotential is cubic,

$$W = \sum_{\alpha=1}^{a}\sum_{\beta=1}^{b}\sum_{\gamma=1}^{c} C_{\alpha\beta\gamma}\, \phi_{12,\alpha}\phi_{23,\beta}\phi_{31,\gamma}. \tag{2.128}$$

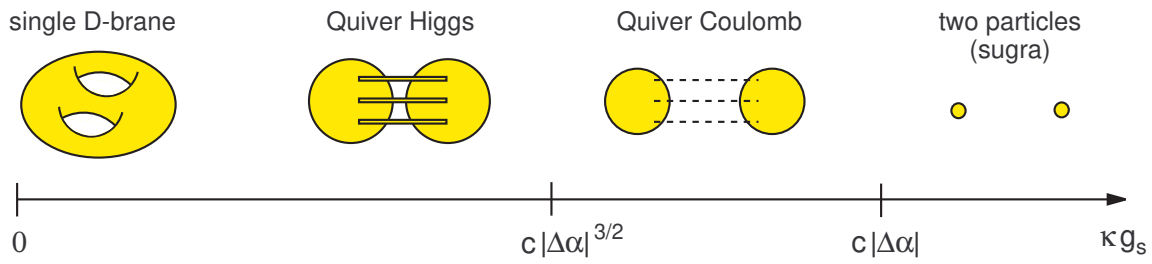


Figure 2.5: Schematic relation between Coulomb and Higgs descriptions of a quiver bound state. Taken from [73, Figure 6].

In a chamber where $\phi_{31,\gamma} = 0$, the D-term quotient is

$$\mathcal{X} = \mathbb{P}^{a-1} \times \mathbb{P}^{b-1}. \tag{2.129}$$

On this branch, the F-term equations $\partial W/\partial\phi_{12,\alpha} = 0$ and $\partial W/\partial\phi_{23,\beta} = 0$ are automatically satisfied, while

$$\frac{\partial W}{\partial \phi_{31,\gamma}} = 0, \qquad \gamma = 1, \dots, c, \tag{2.130}$$

imposes c independent bilinear constraints. For generic coefficients $C_{\alpha\beta\gamma}$, the Higgs branch is therefore a smooth complete intersection

$$\mathcal{M}_{\mathrm{H}} \subset \mathbb{P}^{a-1} \times \mathbb{P}^{b-1} \tag{2.131}$$

cut out by c sections of $\mathcal{O}(1,1)$, with complex dimension

$$d := \dim_{\mathbb{C}} \mathcal{M}_{\mathrm{H}} = (a-1) + (b-1) - c = a + b - c - 2. \tag{2.132}$$

Let $i : \mathcal{M}_{\mathrm{H}} \hookrightarrow \mathcal{X}$ denote the inclusion. Since $\mathcal{M}_{\mathrm{H}}$ is a smooth complete intersection in $\mathcal{X}$, the Lefschetz hyperplane theorem implies that the restriction map

$$i^* : H^k(\mathcal{X}) \to H^k(\mathcal{M}_{\mathrm{H}}) \tag{2.133}$$

is an isomorphism for $k < d$, and by Poincaré duality the same holds for $k > d$. Thus any cohomology of $\mathcal{M}_{\mathrm{H}}$ that is not inherited from $\mathcal{X}$ is confined to the middle degree d. In this example, the intrinsic part of the Higgs-branch cohomology is therefore

$$H^d_{\mathrm{prim}}(\mathcal{M}_{\mathrm{H}}) := H^d(\mathcal{M}_{\mathrm{H}}) \Big/ i^* H^d(\mathcal{X}). \tag{2.134}$$

Its net contribution is determined by the Euler characteristic. Using adjunction, one finds

$$\chi(\mathcal{M}_{\mathrm{H}}) = \int_{\mathcal{X}} \frac{(1+J_1)^a (1+J_2)^b}{(1+J_1+J_2)^c} \, (J_1+J_2)^c, \tag{2.135}$$

where J_1 and J_2 are the hyperplane classes of the two projective factors. Since the remaining Betti numbers are fixed by the ambient space, this determines the net middle-cohomology contribution, which in the quiver interpretation is identified with the single-centered invariant for the total charge $\Gamma_1 + \Gamma_2 + \Gamma_3$.

2.8.3 Kronecker Quivers

The most basic family of examples is provided by the m-arrow Kronecker quivers, which will be denoted by

$$K_m. \tag{2.136}$$

By definition, K_m has two nodes and m parallel arrows from the first node to the second. In the present notation this means

$$\mathbf{N} = (N_1, N_2), \qquad \Gamma_{12} = m > 0, \qquad \Gamma_{21} = -m. \tag{2.137}$$

The quiver K_m is acyclic, so there are no oriented loops and one may take

$$W = 0, \qquad f = 0. \tag{2.138}$$

For this reason K_m is especially simple: the Higgs branch is obtained from the D-term quotient alone, and the refined index can be computed exactly.

The simplest non-trivial case is the Abelian dimension vector

$$\mathbf{N} = (1, 1). \tag{2.139}$$

There are then m chiral fields

$$\phi_\alpha \equiv \phi_{12,\alpha}, \qquad \alpha = 1, \dots, m, \tag{2.140}$$

and the D-term equations reduce to

$$\sum_{\alpha=1}^{m} |\phi_\alpha|^2 = c_1, \qquad c_2 = -c_1. \tag{2.141}$$

For $c_1 > 0$, quotienting by the relative $U(1)$ gauge symmetry identifies configurations which differ by an overall complex phase. One therefore obtains

$$\mathcal{M}_{\mathrm{H}}(K_m, (1,1)) \cong \mathbb{P}^{m-1}. \tag{2.142}$$

The complex dimension is

$$d = m - 1, \tag{2.143}$$

in agreement with the general formula (2.120) for $N_1 = N_2 = 1$ and $f = 0$.

Since the cohomology of $\mathbb{P}^{m-1}$ is concentrated in even degree, with

$$b_{2k}\left(\mathbb{P}^{m-1}\right) = 1, \qquad k = 0, \dots, m-1, \tag{2.144}$$

and all odd Betti numbers equal to zero, the refined index is

$$\begin{aligned} Q(\mathbb{P}^{m-1}; y) &= \sum_{p=0}^{2m-2} b_p\left(\mathbb{P}^{m-1}\right) (-y)^{p-(m-1)} \\ &= (-y)^{-(m-1)} \left(1 + y^2 + \cdots + y^{2m-2}\right) \\ &= (-1)^{m-1} \frac{y^m - y^{-m}}{y - y^{-1}}, \quad \text{for } c_1 > 0. \end{aligned} \tag{2.145}$$

This is the exact Higgs-branch index for the Abelian representation of K_m.

This example is important because it reproduces exactly the corresponding two-particle Coulomb branch index. There are no scaling solutions for a two-center configuration, so no additional minimal-modification correction is required. In this sense the quiver K_m gives the cleanest instance of Higgs/Coulomb agreement: the Higgs branch is compact, explicitly computable, and directly matches the two-centered index discussed in Section 2.6.

It is useful to specialize further to the quiver K_2, both because it is the simplest non-trivial Kronecker quiver and because it already exhibits the familiar tower structure of stable representations. For the Abelian dimension vector $(1, 1)$ one finds

$$\mathcal{M}_{\mathrm{H}}(K_2, (1, 1)) \cong \mathbb{P}^1, \tag{2.146}$$

and hence

$$Q(\mathbb{P}^1; y) = -y - y^{-1}. \tag{2.147}$$

More generally, it is straightfoward to show that for K_2, the admissible dimension vectors relevant to the BPS spectrum are of the form

$$(k, k+1), \qquad (k+1, k), \qquad (1, 1), \qquad k \geq 0, \tag{2.148}$$

The two infinite families $(k, k+1), (k+1, k)$ are the analogues of hypermultiplet towers and carry unit index, $\Omega = 1$ while the dimension vector $(1, 1)$ gives the vectormultiplet-type state discussed above. In summary,

$$Q_{K_2,(k,k+1)}(y) = 1, \qquad Q_{K_2,(k+1,k)}(y) = 1, \qquad Q_{K_2,(1,1)}(y) = -y - y^{-1}. \tag{2.149}$$

2.9 Coherent Sheaves and Gieseker Stability

The preceding sections developed the general physical framework for BPS states in Calabi–Yau compactifications, in a language that does not depend on a particular Type IIA or Type IIB realization. Mirror symmetry relates these two descriptions and allows one to pass between A-brane and B-brane pictures according to the regime of interest. For the purposes of the present thesis, it is now convenient to specialize to the Type IIA description and to review the classical large-volume formulation of B-type branes in algebro-geometric terms.

In the large-volume regime, B-branes are modeled semiclassically by coherent sheaves, and supersymmetry is governed by stability conditions expressed in terms of numerical invariants associated with the sheaf. This classical framework already captures much of the geometry relevant for large-volume BPS configurations and provides the natural starting point for the enumerative and wall-crossing questions discussed later. The present section therefore reviews coherent sheaves, their basic numerical invariants, and the classical notions of slope and Gieseker stability, together with their relation to Hermitian–Yang–Mills geometry. The derived-category refinement and the corresponding notion of Bridgeland stability will be introduced in the next section. This section is primarily based on [28, 29].

2.9.1 Coherent Sheaves and Large-Volume B-branes

Let X be a smooth projective Calabi–Yau threefold equipped with a polarization H. In the large-volume B-model, a supersymmetric D-brane configuration is described by a holomorphic object on X. For a brane carrying a smooth gauge bundle on a holomorphic cycle, this object

is a holomorphic vector bundle; more generally, once degenerations and branes supported on lower-dimensional subvarieties are included, the appropriate language is that of coherent sheaves. A coherent sheaf on X is, by definition, a sheaf of $\mathcal{O}_X$-modules that is locally finitely generated and whose relations are also locally finitely generated. This class contains locally free sheaves, ideal sheaves, structure sheaves of subvarieties, and skyscraper sheaves, and hence provides a uniform framework for D6-, D4-, D2-, and D0-brane configurations in the large-volume limit.

From the physical point of view, the passage from vector bundles to coherent sheaves reflects the fact that B-branes are allowed to carry singularities, embedded lower-dimensional constituents, and degenerations along subvarieties. A locally free sheaf describes a brane with smooth bundle degrees of freedom on its support, while torsion sheaves describe branes whose support has smaller dimension. For instance, the structure sheaf $\mathcal{O}_C$ of a curve $C \subset X$ models a brane supported on C, and the skyscraper sheaf $\mathcal{O}_p$ at a point $p \in X$ models a pointlike brane. In this way the abelian category $\mathrm{Coh}(X)$ of coherent sheaves on X furnishes the classical large-volume category of B-branes.

Two elementary notions play an important role in the discussion of stability. A coherent sheaf $\mathcal{E}$ is called *torsion-free* if every nonzero local section has support of maximal dimension, or equivalently if no nonzero subsheaf of $\mathcal{E}$ is supported in codimension at least one. For sheaves of positive rank, torsion-freeness is the natural regularity condition entering slope stability. More generally, a coherent sheaf $\mathcal{E}$ is called *pure of dimension d* if every nonzero subsheaf of $\mathcal{E}$ has support of dimension exactly d. Purity is the appropriate condition for sheaves of lower-dimensional support, since it excludes embedded components of smaller dimension and ensures that stability is tested against subobjects of the same dimensional type.

The topological charge of a large-volume B-brane is encoded by the Chern character of the corresponding sheaf. For a coherent sheaf $\mathcal{E}$, one writes

$$\mathrm{ch}(\mathcal{E}) = \mathrm{ch}_0(\mathcal{E}) + \mathrm{ch}_1(\mathcal{E}) + \mathrm{ch}_2(\mathcal{E}) + \mathrm{ch}_3(\mathcal{E}). \tag{2.150}$$

One also defines the rank $\mathrm{rk}(\mathcal{E})$ as

$$\mathrm{rk}(\mathcal{E}) := \mathrm{ch}_0(\mathcal{E}).$$

When $\mathcal{E}$ is locally free, $\mathrm{rk}(\mathcal{E})$ agrees with the usual fiber rank. For a torsion sheaf, one has $\mathrm{rk}(\mathcal{E}) = 0$, and the first nonvanishing component of the Chern character records the dimension and homology class of the support. Thus the Chern character provides a single bookkeeping device for the Ramond–Ramond charge carried by the brane.

Given the polarization H, the degree of a torsion-free sheaf $\mathcal{E}$ is defined by intersecting its first Chern class with $H^{\dim X-1}$. Since X is a threefold, this gives

$$\deg_H(\mathcal{E}) := c_1(\mathcal{E}) \cdot H^2. \tag{2.151}$$

For a sheaf supported on a surface or a curve, one analogously evaluates the first relevant Chern class against the induced polarization on the support. On a fixed polarized variety, the pair $(\mathrm{rk}(\mathcal{E}), \deg_H(\mathcal{E}))$ gives the leading numerical information entering the large-volume notion of stability.

For every torsion-free coherent sheaf $\mathcal{E}$ of positive rank, one then defines its slope by

$$\mu_H(\mathcal{E}) := \frac{\deg_H(\mathcal{E})}{\mathrm{rk}(\mathcal{E})}. \tag{2.152}$$

The slope measures the degree per unit rank and governs the first approximation to supersymmetric stability at large volume. In particular, if

$$0 \to \mathcal{F} \to \mathcal{E} \to \mathcal{Q} \to 0$$

is a short exact sequence of torsion-free sheaves, then the relation

$$\mathrm{rk}(\mathcal{E}) = \mathrm{rk}(\mathcal{F}) + \mathrm{rk}(\mathcal{Q}), \qquad \deg_H(\mathcal{E}) = \deg_H(\mathcal{F}) + \deg_H(\mathcal{Q})$$

implies that $\mu_H(\mathcal{E})$ lies between $\mu_H(\mathcal{F})$ and $\mu_H(\mathcal{Q})$. This simple additivity property underlies the comparison of a sheaf with its subsheaves and quotient sheaves in the definition of slope stability.

For later applications, it is useful to keep in mind the geometric meaning of these objects on rigid surfaces inside local Calabi–Yau threefolds. When the relevant BPS sector is supported on a compact surface $S \subset X$, one often works with coherent sheaves on S itself and regards the corresponding brane on X as obtained by pushforward along the embedding $i : S \hookrightarrow X$. The numerical invariants of the sheaf on S, such as rank, first Chern class, and Euler characteristic, then furnish the discrete charge labels that organize the BPS spectrum in the large-volume chamber.

The classical large-volume picture of B-branes is therefore governed by the abelian category $\mathrm{Coh}(X)$, together with the numerical invariants extracted from Chern classes and the polarization.

2.9.2 Slope and Gieseker Stability

The first systematic moduli-theoretic notions of stability for sheaves emerged from Mumford's geometric invariant theory. In that setting, one seeks numerical conditions that single out objects admitting well-behaved moduli spaces, with bounded families and controlled automorphisms. For vector bundles on curves, the basic invariants are rank and degree, and the corresponding ratio defines slope stability. In higher dimensions, the Hilbert polynomial provides the natural invariant attached to the chosen polarization. Building on this perspective, Gieseker introduced a refinement of slope stability obtained by comparing reduced Hilbert polynomials, and used it to construct projective moduli spaces of semistable sheaves. These notions now occupy a central place in algebraic geometry and in the large-volume description of B-type branes.

Fix a polarization H on Y, and let $\mathcal{E}$ be a torsion-free coherent sheaf of positive rank. The slope introduced above provides the basic numerical criterion for comparing $\mathcal{E}$ with its subsheaves. If

$$0 \to \mathcal{F} \to \mathcal{E} \to \mathcal{Q} \to 0$$

is a short exact sequence of torsion-free sheaves, then rank and degree are additive, so $\mu_H(\mathcal{E})$ is a weighted average of $\mu_H(\mathcal{F})$ and $\mu_H(\mathcal{Q})$. This elementary observation is the starting point for the notion of slope stability.

A torsion-free coherent sheaf $\mathcal{E}$ is called *μ_H-stable* if every proper nonzero subsheaf

$$0 \neq \mathcal{F} \subsetneq \mathcal{E}$$

with $0 < \mathrm{rk}(\mathcal{F}) < \mathrm{rk}(\mathcal{E})$ satisfies

$$\mu_H(\mathcal{F}) < \mu_H(\mathcal{E}), \tag{2.153}$$

and it is called *μ_H-semistable* if

$$\mu_H(\mathcal{F}) \leq \mu_H(\mathcal{E}) \tag{2.154}$$

for all such subsheaves. Since saturation increases degree while preserving rank, it is enough to test these inequalities on saturated subsheaves. In this form, slope stability is the natural higher-dimensional analogue of the classical stability notion for bundles on curves.

Slope stability captures the leading asymptotic behavior of a sheaf with respect to the polarization. It also admits a canonical filtration theory. Every torsion-free sheaf $\mathcal{E}$ possesses a unique Harder–Narasimhan filtration

$$0 = \mathcal{E}_0 \subset \mathcal{E}_1 \subset \cdots \subset \mathcal{E}_\ell = \mathcal{E}, \tag{2.155}$$

whose successive quotients

$$\mathrm{gr}_i^{HN}(\mathcal{E}) := \mathcal{E}_i/\mathcal{E}_{i-1}$$

are μ_H-semistable and satisfy

$$\mu_H(\mathrm{gr}_1^{HN}(\mathcal{E})) > \mu_H(\mathrm{gr}_2^{HN}(\mathcal{E})) > \cdots > \mu_H(\mathrm{gr}_\ell^{HN}(\mathcal{E})).$$

This filtration organizes the maximal destabilizing pieces of $\mathcal{E}$ and gives a precise sense in which any torsion-free sheaf is assembled from semistable constituents of strictly decreasing slope.

For the construction of projective moduli spaces, one needs a stability notion that records more than the first two numerical coefficients. This leads to the Hilbert polynomial. For a coherent sheaf $\mathcal{E}$ on Y, define

$$P_{\mathcal{E}}(m) := \chi\big(Y, \mathcal{E}(m)\big), \qquad \mathcal{E}(m) := \mathcal{E} \otimes \mathcal{O}_Y(mH). \tag{2.156}$$

By the Hirzebruch–Riemann–Roch theorem, $P_{\mathcal{E}}(m)$ is a polynomial in m whose degree equals the dimension of the support of $\mathcal{E}$. If $\mathcal{E}$ is pure of dimension d, one may write

$$P_{\mathcal{E}}(m) = \frac{\alpha_d(\mathcal{E})}{d!}m^d + \frac{\alpha_{d-1}(\mathcal{E})}{(d-1)!}m^{d-1} + \cdots + \alpha_0(\mathcal{E}), \qquad \alpha_d(\mathcal{E}) > 0. \tag{2.157}$$

The coefficient $\alpha_d(\mathcal{E})$ measures the multiplicity of the support with respect to H, and the lower coefficients encode progressively finer intersection-theoretic information.

For torsion-free sheaves of positive rank on an n-dimensional smooth polarized variety, the first two coefficients recover rank and degree. In particular,

$$P_{\mathcal{E}}(m) = \frac{\mathrm{rk}(\mathcal{E})\, H^n}{n!}m^n + \frac{\deg_H(\mathcal{E})}{(n-1)!}m^{n-1} + O(m^{n-2}), \tag{2.158}$$

up to the standard Todd-class correction terms determined by Y. On a Calabi–Yau threefold, where $c_1(Y) = 0$, this expression simplifies further, and the slope appears directly in the ratio of the first two coefficients. Thus the Hilbert polynomial contains the slope as its leading stability datum and supplements it by lower-order information.

The appropriate normalized quantity is the *reduced Hilbert polynomial*

$$p_{\mathcal{E}}(m) = \frac{P_{\mathcal{E}}(m)}{\alpha_d(\mathcal{E})}, \tag{2.159}$$

defined for every pure sheaf $\mathcal{E}$ of dimension d. The use of purity is essential here. It ensures that every nonzero subsheaf has support of the same dimension and hence a Hilbert polynomial of the same degree, so that normalized comparison is meaningful. This point is especially important for

sheaves supported on divisors or curves, where rank vanishes and slope alone no longer provides the right invariant.

A pure coherent sheaf $\mathcal{E}$ is called *Gieseker stable* if for every proper nonzero subsheaf

$$0 \neq \mathcal{F} \subsetneq \mathcal{E}$$

one has

$$p_{\mathcal{F}}(m) < p_{\mathcal{E}}(m) \qquad \text{for all } m \gg 0, \tag{2.160}$$

and it is called *Gieseker semistable* if

$$p_{\mathcal{F}}(m) \leq p_{\mathcal{E}}(m) \qquad \text{for all } m \gg 0. \tag{2.161}$$

The symbol $m \gg 0$ means that the inequality holds for all sufficiently large integers m. Equivalently, one compares the coefficients of $p_{\mathcal{F}}$ and $p_{\mathcal{E}}$ lexicographically from the highest degree downward. The first coefficient after normalization is always $1/d!$, so the first nontrivial comparison occurs at the next coefficient; for torsion-free sheaves of positive rank, this first comparison reproduces slope. The subsequent coefficients refine the ordering whenever slopes coincide.

This refinement is particularly transparent in low dimension. On a smooth projective curve, the reduced Hilbert polynomial is determined entirely by rank and degree, so Gieseker stability and slope stability coincide. On surfaces and threefolds, the Hilbert polynomial contains additional coefficients, and Gieseker stability distinguishes sheaves having the same slope but different lower Chern-theoretic behavior. In this sense, Gieseker stability extends the classical slope condition to a fuller asymptotic comparison governed by the polarization.

The logical relation between the two notions is standard:

$$\mu_H\text{-stable} \Longrightarrow \text{Gieseker stable} \Longrightarrow \text{Gieseker semistable} \Longrightarrow \mu_H\text{-semistable}. \tag{2.162}$$

The first implication follows because a strict slope inequality already appears in the coefficient of m^{d-1} in the reduced Hilbert polynomial. The last implication follows because a violation of slope semistability would produce a subsheaf whose reduced Hilbert polynomial dominates at the first nontrivial coefficient. Hence Gieseker stability sits naturally between slope stability and slope semistability.

Gieseker's insight was that this stronger notion is precisely the one adapted to projective moduli. A bounded family of Gieseker semistable sheaves with fixed Hilbert polynomial admits a projective moduli space constructed by geometric invariant theory. Stable sheaves correspond to points with finite stabilizer, while semistable sheaves are organized by S-equivalence classes. Concretely, a Gieseker semistable sheaf $\mathcal{E}$ admits a Jordan–Hölder filtration

$$0 = \mathcal{E}_0 \subset \mathcal{E}_1 \subset \cdots \subset \mathcal{E}_r = \mathcal{E}, \tag{2.163}$$

whose successive quotients are Gieseker stable with the same reduced Hilbert polynomial as $\mathcal{E}$. The associated graded object

$$\mathrm{gr}^{JH}(\mathcal{E}) = \bigoplus_{i=1}^{r} \mathcal{E}_i/\mathcal{E}_{i-1}$$

is determined uniquely up to isomorphism, and two semistable sheaves define the same point of the moduli space precisely when their associated graded objects are isomorphic. This passage

from semistable sheaves to S-equivalence classes is one of the characteristic features of GIT moduli problems.

From the large-volume point of view, slope stability captures the first approximation to supersymmetric stability, while Gieseker stability records the full asymptotic ordering supplied by the Hilbert polynomial. The resulting hierarchy is both mathematically robust and geometrically natural: it applies to torsion-free sheaves of positive rank, extends to pure sheaves of lower-dimensional support, and supports the construction of moduli spaces that organize classical B-brane configurations in algebraic terms.

2.9.3 Hermitian–Yang–Mills Metrics and Classical Stability

The algebraic notions of slope stability and Gieseker stability admit a parallel differential-geometric formulation in terms of special unitary connections on holomorphic bundles over compact Kähler manifolds. This circle of ideas developed through work of Narasimhan and Seshadri on stable bundles over curves, was extended in higher dimension by Donaldson, and reached its general form in the theorem of Uhlenbeck and Yau. The guiding problem was to identify the correct algebraic condition on a holomorphic bundle that characterizes the existence of a canonical metric connection satisfying an Einstein-type equation. In the setting relevant for B-type branes at large volume, this relation supplies the bridge between holomorphic bundle geometry and supersymmetric gauge fields on the brane worldvolume.

Let (X, ω) be a compact Kähler manifold of complex dimension n, and let $\mathcal{E}$ be a holomorphic vector bundle on X. Choose a Hermitian metric h on $\mathcal{E}$, and let A be the associated Chern connection. Its curvature

$$F_A \in \Omega^{1,1}\big(X, \mathrm{End}(\mathcal{E})\big)$$

is automatically of type $(1, 1)$, since the Chern connection is compatible with both the Hermitian metric and the holomorphic structure. The Hermitian–Yang–Mills equation is the condition

$$\sqrt{-1}\,\Lambda_\omega F_A = \lambda\,\mathrm{Id}_{\mathcal{E}}, \tag{2.164}$$

where Λ_ω denotes contraction with the Kähler form and $\lambda \in \mathbb{R}$ is a topological constant determined by the rank of $\mathcal{E}$, its first Chern class, and the Kähler class $[\omega]$. If one defines the ω-degree by

$$\deg_\omega(\mathcal{E}) := \int_X c_1(\mathcal{E}) \wedge \frac{\omega^{n-1}}{(n-1)!}, \tag{2.165}$$

then the slope is

$$\mu_\omega(\mathcal{E}) := \frac{\deg_\omega(\mathcal{E})}{\mathrm{rk}(\mathcal{E})}, \tag{2.166}$$

and λ may be written as

$$\lambda = \frac{2\pi\,\mu_\omega(\mathcal{E})}{\mathrm{Vol}_\omega(X)}, \qquad \mathrm{Vol}_\omega(X) := \int_X \frac{\omega^n}{n!}, \tag{2.167}$$

up to the chosen normalization of curvature and degree.

Equation (2.164) is the higher-dimensional analogue of the constant-curvature condition familiar from bundles on curves. It singles out a unitary connection whose mean curvature is central, so that the trace-free part of $\sqrt{-1}\Lambda_\omega F_A$ vanishes. In local holomorphic coordinates, this condition may be written as

$$g^{j\bar{k}}\, F_{\alpha j\bar{k}}{}^{\beta} = -\sqrt{-1}\,\lambda\,\delta_\alpha^\beta, \tag{2.168}$$

where g is the Kähler metric associated with ω. The equation is elliptic modulo gauge, and its solutions are unique up to unitary automorphisms once the holomorphic bundle is fixed.

The relation with supersymmetry appears already at the classical level. A B-type brane wrapping a holomorphic cycle and carrying a gauge field preserves supersymmetry when the worldvolume connection is compatible with the complex structure and satisfies a primitivity condition. For a brane filling the ambient compact Kähler manifold, the leading large-volume form of this requirement is precisely the Hermitian–Yang–Mills equation. The holomorphicity of the bundle is encoded in the vanishing of $(0,2)$-component of the curvature, while the moment-map condition reduces to (2.164). In this way, a supersymmetric gauge configuration on the brane is described by a holomorphic bundle endowed with a Hermitian–Yang–Mills connection.

The mathematical problem of existence for such metrics was first understood in complex dimension one. For holomorphic vector bundles over a compact Riemann surface, the theorem of Narasimhan and Seshadri identifies stable bundles of degree zero with irreducible unitary representations of the fundamental group. This result gives a precise analytic classification of stable bundles on curves and already exhibits the link between an algebraic stability condition and a canonical unitary connection. In modern language, it is the one-dimensional prototype of the Kobayashi–Hitchin correspondence.

Donaldson carried this picture into higher dimension. In his work on projective algebraic surfaces, he studied anti-self-dual and Hermitian–Einstein connections and established the existence of Hermitian–Yang–Mills metrics on stable bundles over projective surfaces. His approach used gauge-theoretic methods, elliptic estimates, and a continuity argument adapted to the complex-geometric setting. One of the central motivations was to connect moduli of stable holomorphic bundles with moduli of gauge-theoretic instantons, thereby relating algebraic geometry and Yang–Mills theory on compact complex surfaces.

The general compact Kähler case was established by Uhlenbeck and Yau. Their theorem states that a holomorphic vector bundle on a compact Kähler manifold admits a Hermitian–Yang–Mills metric if and only if it is polystable, that is, a direct sum of stable bundles of the same slope:

$$\mathcal{E} \cong \bigoplus_{i=1}^{m} \mathcal{E}_i, \qquad \mu_\omega(\mathcal{E}_i) = \mu_\omega(\mathcal{E}), \qquad \mathcal{E}_i \ \mu_\omega\text{-stable}. \tag{2.169}$$

Equivalently, the existence of a Hermitian–Yang–Mills connection is characterized by μ_ω-polystability. This statement is often referred to as the Donaldson–Uhlenbeck–Yau theorem.

The appearance of polystability rather than stability is natural from the analytic point of view. If a bundle splits holomorphically as a direct sum of stable subbundles of common slope, then a block-diagonal Hermitian–Yang–Mills connection exists on the sum. Conversely, the presence of a Hermitian–Yang–Mills metric forces a holomorphic decomposition into stable summands whenever the connection is reducible. Stability therefore corresponds to the irreducible case, while polystability captures the full class of solutions to the Hermitian–Yang–Mills equation.

Although the theorem is usually stated for holomorphic vector bundles, moduli problems naturally lead to torsion-free and reflexive sheaves as well. In families of stable bundles, singular limits may occur, and these are most naturally described in the sheaf-theoretic language used in algebraic geometry. From this perspective, the Hermitian–Yang–Mills condition provides the differential-geometric counterpart of the classical slope-stability condition on smooth bundles, while the sheaf-theoretic framework accommodates the compactification of moduli spaces.

For large-volume B-branes, this correspondence gives a direct geometric interpretation of classical stability. A holomorphic vector bundle with fixed topological charges supports a

supersymmetric gauge connection precisely when it is μ-polystable with respect to the chosen Kähler class. In this way, slope stability is tied to the existence of Hermitian–Yang–Mills metrics, while Gieseker stability supplies the algebro-geometric refinement used in the construction of moduli spaces.

The Donaldson–Uhlenbeck–Yau theorem therefore identifies the classical notion of stability for holomorphic bundles with the existence of canonical solutions to the Yang–Mills equations compatible with the complex structure. This relation between algebraic stability and special metrics forms the differential-geometric foundation of the large-volume description of B-type branes.

2.10 Derived Categories and Bridgeland Stability Conditions

The large-volume description of B-branes in terms of coherent sheaves captures an important semiclassical regime, but it does not exhaust the full structure of the B-model. Bound states formed by tachyon condensation, brane–antibrane pairs, monodromy transformations, and the variation of stable objects across the Kähler moduli space are naturally expressed in a framework larger than the abelian category $\mathrm{Coh}(X)$. The appropriate setting is the bounded derived category of coherent sheaves,

$$D^b\,\mathrm{Coh}(X),$$

which packages sheaves, complexes of sheaves, and their extension data into a single triangulated category.

Derived categories arose in homological algebra through the work of Grothendieck and Verdier as a systematic way to retain the homological information of complexes while quotienting out quasi-isomorphisms. In the context of string theory, they entered the B-model through the identification of topological B-branes with objects of $D^b\,\mathrm{Coh}(X)$, and they provide the natural categorical language for open-string spectra and brane recombination. Bridgeland's notion of a stability condition then supplies the derived analogue of classical slope- and Gieseker-type stability, replacing the abelian category $\mathrm{Coh}(X)$ by a triangulated category equipped with a central charge and a notion of phase. The present section begins with the basic structure of $D^b\,\mathrm{Coh}(X)$ and its physical interpretation. This section is based primarily on [28, 48, 81].

2.10.1 Derived Categories and B-branes

Let X be a smooth projective Calabi–Yau threefold. A coherent sheaf $\mathcal{E} \in \mathrm{Coh}(X)$ may be viewed as a complex concentrated in degree zero,

$$\cdots \to 0 \to \mathcal{E} \to 0 \to \cdots .$$

Passing from sheaves to complexes allows one to describe extension data, bound states, and homological shifts in a uniform way. One therefore begins with the category $C^b\,\mathrm{Coh}(X)$ of bounded complexes of coherent sheaves,

$$\mathcal{E}^\bullet = \left(\cdots \longrightarrow \mathcal{E}^{i-1} \xrightarrow{d^{i-1}} \mathcal{E}^i \xrightarrow{d^i} \mathcal{E}^{i+1} \longrightarrow \cdots \right), \qquad d^{i+1} \circ d^i = 0, \tag{2.170}$$

where $\mathcal{E}^i = 0$ for $|i| \gg 0$. The i-th cohomology sheaf of $\mathcal{E}^\bullet$ is

$$H^i(\mathcal{E}^\bullet) := \frac{\ker(d^i : \mathcal{E}^i \to \mathcal{E}^{i+1})}{\mathrm{im}(d^{i-1} : \mathcal{E}^{i-1} \to \mathcal{E}^i)}. \tag{2.171}$$

A morphism of complexes $f : \mathcal{E}^\bullet \to \mathcal{F}^\bullet$ is called a *quasi-isomorphism* if it induces isomorphisms on all cohomology sheaves,

$$H^i(f) : H^i(\mathcal{E}^\bullet) \xrightarrow{\sim} H^i(\mathcal{F}^\bullet) \qquad \text{for all } i \in \mathbb{Z}. \tag{2.172}$$

The bounded derived category $D^b\,\mathrm{Coh}(X)$ is obtained from $C^b\,\mathrm{Coh}(X)$ by formally inverting quasi-isomorphisms. Equivalently, one may start from the homotopy category $K^b\,\mathrm{Coh}(X)$ and quotient by acyclic complexes. Thus

$$D^b\,\mathrm{Coh}(X) = K^b\,\mathrm{Coh}(X)\big[\text{quasi-isomorphisms}^{-1}\big]. \tag{2.173}$$

Two complexes that are quasi-isomorphic therefore define the same object of the derived category.

A simple example is provided by a short exact sequence of coherent sheaves

$$0 \longrightarrow \mathcal{A} \longrightarrow \mathcal{B} \longrightarrow \mathcal{C} \longrightarrow 0. \tag{2.174}$$

In the abelian category $\mathrm{Coh}(X)$, this sequence records an extension of $\mathcal{C}$ by $\mathcal{A}$. In the derived category it is encoded by the two-term complex

$$\big[\mathcal{A} \to \mathcal{B}\big]$$

together with a distinguished triangle

$$\mathcal{A} \longrightarrow \mathcal{B} \longrightarrow \mathcal{C} \longrightarrow \mathcal{A}[1]. \tag{2.175}$$

This passage from short exact sequences to triangles is one of the basic structural features of the derived category.

The category $D^b\,\mathrm{Coh}(X)$ is not abelian. Its natural structure is that of a *triangulated category*. Recall that a triangulated category $\mathcal{D}$ consists of an additive category equipped with an autoequivalence

$$[1] : \mathcal{D} \to \mathcal{D},$$

called the shift or translation functor, together with a distinguished class of exact triangles

$$A \longrightarrow B \longrightarrow C \longrightarrow A[1], \tag{2.176}$$

satisfying Verdier's axioms. In brief, these axioms state the following: every morphism $A \to B$ can be completed to a distinguished triangle; triangles are stable under isomorphism and under the shift functor; every distinguished triangle can be rotated; and morphisms between triangles can be completed in a compatible way, culminating in the octahedral axiom. The formal role of these axioms is to provide the triangulated analogue of exactness in homological algebra.

The shift functor acts on a complex by

$$(\mathcal{E}^\bullet[1])^i = \mathcal{E}^{i+1}, \qquad d^i_{\mathcal{E}[1]} = -d^{i+1}_{\mathcal{E}}. \tag{2.177}$$

Its inverse is denoted $[-1]$. In physics this shift has a direct interpretation: the object $\mathcal{E}[1]$ represents the anti-brane associated with $\mathcal{E}$, and more generally shifts change the grading of the open-string spectrum.

Given a morphism $f : \mathcal{A}^\bullet \to \mathcal{B}^\bullet$ of complexes, its mapping cone is the complex

$$\mathrm{Cone}(f)^i = \mathcal{B}^i \oplus \mathcal{A}^{i+1}, \qquad d^i_{\mathrm{Cone}(f)} = \begin{pmatrix} d^i_{\mathcal{B}} & f^{i+1} \\ 0 & -d^{i+1}_{\mathcal{A}} \end{pmatrix}. \tag{2.178}$$

The cone fits into a distinguished triangle

$$\mathcal{A}^\bullet \xrightarrow{f} \mathcal{B}^\bullet \longrightarrow \mathrm{Cone}(f) \longrightarrow \mathcal{A}^\bullet[1]. \tag{2.179}$$

This construction is the categorical form of brane recombination: a tachyon field represented by a morphism f between a brane and an anti-brane produces a bound state described by $\mathrm{Cone}(f)$.

The open-string spectrum between two B-branes is naturally expressed in terms of Ext-groups. If $\mathcal{E}, \mathcal{F} \in D^b\,\mathrm{Coh}(X)$, then

$$\mathrm{Ext}^k_X(\mathcal{E}, \mathcal{F}) \cong \mathrm{Hom}_{D^b\,\mathrm{Coh}(X)}(\mathcal{E}, \mathcal{F}[k]). \tag{2.180}$$

When $\mathcal{E}$ and $\mathcal{F}$ are honest coherent sheaves, this recovers the usual sheaf Ext-groups. If $\mathcal{E}$ is locally free, one also has

$$\mathrm{Ext}^k_X(\mathcal{E}, \mathcal{F}) \cong H^k\left(X, \mathcal{E}^\vee \otimes \mathcal{F}\right). \tag{2.181}$$

In the topological B-model, these groups furnish the graded space of open-string states stretching from $\mathcal{E}$ to $\mathcal{F}$. In particular, Ext^0 describes degree-zero string states, Ext^1 governs first-order deformations and extension classes, and higher Ext-groups capture higher obstruction and interaction data.

The charge of an object of $D^b\,\mathrm{Coh}(X)$ is encoded by its class in the Grothendieck group $K_0(X)$. For a bounded complex $\mathcal{E}^\bullet$, one defines

$$[\mathcal{E}^\bullet] = \sum_i (-1)^i [\mathcal{E}^i] \in K_0(X), \tag{2.182}$$

and hence

$$\mathrm{ch}(\mathcal{E}^\bullet) = \sum_i (-1)^i \,\mathrm{ch}(\mathcal{E}^i). \tag{2.183}$$

Thus the derived category preserves the additive charge familiar from coherent sheaves while enlarging the class of admissible objects.

It is also useful to record the natural embedding

$$\mathrm{Coh}(X) \hookrightarrow D^b\,\mathrm{Coh}(X),$$

which identifies a coherent sheaf with the corresponding degree-zero complex. In this sense, the abelian category $\mathrm{Coh}(X)$ appears as a distinguished full subcategory inside the derived category.

2.10.2 Bridgeland Stability Conditions

The passage from coherent sheaves to the derived category enlarges the class of admissible B-branes. A corresponding notion of stability must therefore be formulated directly on a triangulated category. The guiding physical input is the central charge. For a B-brane represented by an object $E \in D^b\,\mathrm{Coh}(X)$, the large-volume central charge is given by

$$Z_{B+\mathrm{i}J}(E) = -\int_X e^{-(B+\mathrm{i}J)}\,\mathrm{ch}(E)\,\sqrt{\mathrm{Td}(X)}, \tag{2.184}$$

where $B + \mathrm{i}J \in H^2(X, \mathbb{C})$ is the complexified Kähler class. The mass of a supersymmetric brane is proportional to $|Z_{B+\mathrm{i}J}(E)|$, and its phase is determined by the argument of $Z_{B+\mathrm{i}J}(E)$. This suggests that stability should be governed by a group homomorphism

$$Z : K_0(X) \to \mathbb{C}$$

together with a notion of semistable objects of fixed phase.

For an object E with $Z(E) \neq 0$, one writes

$$Z(E) = m(E)e^{\mathrm{i}\pi\phi(E)}, \qquad m(E) \in \mathbb{R}_{>0}, \qquad \phi(E) \in (0,1], \tag{2.185}$$

and calls $\phi(E)$ its phase. In the large-volume limit, expanding (2.184) in powers of J recovers the familiar asymptotic ordering by rank, first Chern class, and higher Chern data. On a Calabi–Yau threefold one finds

$$Z_{B+\mathrm{i}J}(E) = -\int_X \left(\mathrm{ch}_3^B(E) - \frac{J^2}{2}\mathrm{ch}_1^B(E)\right) + \mathrm{i}\int_X \left(J\mathrm{ch}_2^B(E) - \frac{J^3}{6}\mathrm{ch}_0^B(E)\right) + \cdots, \tag{2.186}$$

where $\mathrm{ch}^B(E) := e^{-B}\,\mathrm{ch}(E)$. The leading terms reproduce the classical large-volume hierarchy and motivate the derived notion of phase.

Bridgeland's definition packages this structure in an intrinsic form. Let $\mathcal{D}$ be a triangulated category. A *slicing* of $\mathcal{D}$ is a collection of full additive subcategories

$$\mathcal{P}(\phi) \subset \mathcal{D}, \qquad \phi \in \mathbb{R},$$

satisfying the following conditions:

1. $\mathcal{P}(\phi + 1) = \mathcal{P}(\phi)[1]$ for all $\phi \in \mathbb{R}$;
2. if $A_i \in \mathcal{P}(\phi_i)$ with $\phi_1 > \phi_2$, then
$$\mathrm{Hom}_{\mathcal{D}}(A_1, A_2) = 0;$$
3. every nonzero object $E \in \mathcal{P}(\phi)$ is assigned a phase ϕ, and will be called semistable of phase ϕ;
4. every nonzero object $E \in \mathcal{D}$ admits a finite filtration by distinguished triangles whose successive factors lie in $\mathcal{P}(\phi_j)$ with
$$\phi_1 > \phi_2 > \cdots > \phi_n.$$

The final condition is the Harder–Narasimhan property in the triangulated setting.

A *Bridgeland stability condition* on $\mathcal{D}$ is a pair

$$\sigma = (Z, \mathcal{P}), \tag{2.187}$$

where $Z : K(\mathcal{D}) \to \mathbb{C}$ is a group homomorphism, called the central charge, and $\mathcal{P}$ is a slicing such that for every nonzero object $E \in \mathcal{P}(\phi)$,

$$Z(E) \in \mathbb{R}_{>0}\, e^{\mathrm{i}\pi\phi}. \tag{2.188}$$

In practice one often restricts to *numerical* stability conditions, meaning that Z factors through the numerical Grothendieck group $K_{\mathrm{num}}(\mathcal{D})$, obtained by quotienting $K(\mathcal{D})$ by the kernel of the Euler pairing. Thus the phase of a semistable object is determined by the argument of its central charge. An object of $\mathcal{P}(\phi)$ is called *stable* if it is simple in the abelian category $\mathcal{P}(\phi)$,

and *semistable* otherwise. The stability condition is called *locally finite* if there exists $\varepsilon > 0$ such that each extension-closed subcategory

$$\mathcal{P}(\phi - \varepsilon, \phi + \varepsilon)$$

is of finite length.

An equivalent description may be given in terms of the heart of a bounded t-structure. Recall that a bounded t-structure on a triangulated category $\mathcal{D}$ determines a full subcategory

$$\mathcal{A} = \mathcal{D}^{\leq 0} \cap \mathcal{D}^{\geq 0},$$

called its *heart*. The heart $\mathcal{A}$ is an abelian category, so notions such as kernels, cokernels, subobjects, quotients, and short exact sequences are available inside $\mathcal{A}$. This provides the natural setting in which stability may again be formulated by comparing the phases of subobjects, in close analogy with the classical theory of coherent sheaves.

Accordingly, let $\mathcal{A} \subset \mathcal{D}$ be the heart of a bounded t-structure. A *stability function* on $\mathcal{A}$ is a group homomorphism

$$Z : K(\mathcal{A}) \to \mathbb{C} \tag{2.189}$$

such that for every nonzero object $E \in \mathcal{A}$,

$$Z(E) \in \mathbb{H} \cup \mathbb{R}_{<0}, \tag{2.190}$$

where $\mathbb{H}$ denotes the strict upper half-plane. One again defines the phase by

$$Z(E) = m(E)e^{i\pi\phi(E)}, \qquad m(E) > 0, \qquad \phi(E) \in (0, 1]. \tag{2.191}$$

An object $E \in \mathcal{A}$ is Z-semistable if every nonzero subobject $F \subset E$ satisfies

$$\phi(F) \leq \phi(E). \tag{2.192}$$

If every object of $\mathcal{A}$ admits a Harder–Narasimhan filtration with respect to this notion of semistability, then $(\mathcal{A}, Z)$ determines a Bridgeland stability condition.

The heart and the slicing determine one another. Given a stability condition $\sigma = (Z, \mathcal{P})$, one sets

$$\mathcal{A}_\sigma := \mathcal{P}((0, 1]), \tag{2.193}$$

which is the heart of a bounded t-structure on $\mathcal{D}$. Conversely, given a heart $\mathcal{A}$ together with a stability function Z satisfying the Harder–Narasimhan property, one reconstructs the slicing by declaring $\mathcal{P}(\phi)$ to be the full subcategory of Z-semistable objects of phase ϕ, together with their shifts. This equivalence is often the most practical way to construct examples: one chooses a heart by tilting an abelian category, then equips it with a central charge whose phase function defines semistability.

The Harder–Narasimhan property is central to the definition. For a heart $\mathcal{A}$ and stability function Z, it requires that every nonzero object $E \in \mathcal{A}$ admit a finite filtration

$$0 = E_0 \subset E_1 \subset \cdots \subset E_n = E \tag{2.194}$$

such that the quotients

$$F_j := E_j / E_{j-1}$$

are Z-semistable and satisfy

$$\phi(F_1) > \phi(F_2) > \cdots > \phi(F_n). \tag{2.195}$$

This is the derived analogue of the classical Harder–Narasimhan filtration for sheaves. It guarantees that every object can be decomposed into semistable factors ordered by phase, and it makes wall-crossing meaningful when the central charge varies.

A further technical requirement, now standard in the theory, is the *support property*. Fix a norm $\|\cdot\|$ on $K(\mathcal{D}) \otimes \mathbb{R}$. One asks that there exist a constant $C > 0$ such that every σ-semistable object E satisfies

$$\|[E]\| \leq C\,|Z(E)|. \tag{2.196}$$

Equivalently, there exists a quadratic form Q on $K(\mathcal{D}) \otimes \mathbb{R}$ which is negative definite on $\ker Z$, and such that

$$Q(E) \geq 0 \qquad \text{for every } \sigma\text{-semistable object } E. \tag{2.197}$$

This condition controls the classes of semistable objects with fixed phase and is part of the local structure theory of the stability manifold.

The physical origin of this formalism lies in Douglas' proposal of Π-stability. In the B-model, the exact worldsheet central charge of a brane determines a grade

$$\xi(E) = \frac{1}{\pi} \operatorname{Im} \log Z(E), \tag{2.198}$$

defined locally in moduli space. Stability is governed by the relative ordering of these grades, and decay occurs when phases align. This picture anticipates the mathematical structure of Bridgeland stability: the central charge determines phases, semistability is defined by phase inequalities, and walls of marginal stability are loci where the phases of potential constituents coincide. Bridgeland's definition may be viewed as a precise mathematical realization of this idea on a triangulated category. In regimes where the exact physical central charge is available and one has a suitable heart of branes, Π-stability fits naturally into the Bridgeland framework.

The collection of all stability conditions on a fixed triangulated category carries a natural geometry. Bridgeland showed that the space

$$\operatorname{Stab}(\mathcal{D})$$

of locally finite stability conditions satisfying the support property is a complex manifold, possibly with several connected components. The forgetful map

$$\pi : \operatorname{Stab}(\mathcal{D}) \to \operatorname{Hom}(K(\mathcal{D}), \mathbb{C}), \qquad (Z, \mathcal{P}) \mapsto Z, \tag{2.199}$$

is a local homeomorphism. Thus, locally, a stability condition is determined by its central charge. The walls of marginal stability form real codimension-one loci in $\operatorname{Stab}(\mathcal{D})$ where the phases of two classes align, and chambers are the connected components of the complement of these walls. Autoequivalences of $\mathcal{D}$ act naturally on $\operatorname{Stab}(\mathcal{D})$, reflecting monodromy and categorical symmetries of the B-model.

Bridgeland stability therefore extends the classical theory of stable sheaves from an abelian category to a triangulated category, while preserving the essential role of the central charge. The large-volume expression (2.184) provides the semiclassical model, the slicing and heart formalize semistability by phases, and the Harder–Narasimhan property furnishes canonical semistable decompositions. This framework supplies the derived notion of stability appropriate for B-branes on Calabi–Yau threefolds.

2.11 Generalized Donaldson–Thomas Invariants

Donaldson–Thomas theory originated as a holomorphic analogue of the Casson invariant [176]. Thomas showed that moduli spaces of stable sheaves on a Calabi–Yau threefold carry symmetric obstruction theories, so that one can form virtual counts of stable objects in fixed numerical classes. In rank one this framework already encompasses ideal sheaves of subschemes, and hence produces a curve-counting theory on Calabi–Yau threefolds. Behrend's reinterpretation of the virtual count as a weighted Euler characteristic made the local singularity structure of the moduli space intrinsic to the definition [38]. From the physical point of view, these invariants furnish protected indices for D-brane bound states in Type IIA compactifications.

The original Donaldson–Thomas invariant is formulated most directly when the chosen stability condition defines a moduli problem consisting entirely of stable objects. The presence of strictly semistable objects introduces decompositions, positive-dimensional stabilizers, and stack-theoretic contributions, so the stable theory no longer suffices. Joyce and Song addressed this by working in the Ringel–Hall algebra of stack functions and defining generalized Donaldson–Thomas invariants through the Hall-algebra logarithm of the semistable stack, weighted by the Behrend function [121]. The resulting invariants are rational numbers $\bar{\Omega}(\Gamma;\tau)$, from which the corresponding integral BPS invariants $\Omega(\Gamma;\tau)$ are recovered by the standard multicover inversion formula.

Kontsevich and Soibelman developed a parallel framework in which Donaldson–Thomas theory is lifted from numerical invariants to a motivic and, in particular, refined setting [128]. Their construction is formulated in terms of motivic Hall algebras, quantum tori, and wall-crossing structures, and it produces refined invariants that retain more information than the numerical Joyce–Song theory, notably the spin-sensitive content encoded by the refinement parameter. The numerical generalized Donaldson–Thomas invariants are recovered from this refined theory by specialization.

Several familiar enumerative theories arise as specializations of this general structure. Pure D0-brane charge is carried by skyscraper sheaves, whose basic counting problem is given by the Euler characteristic of their moduli spaces. The degree-zero Donaldson–Thomas theory, by contrast, belongs to the rank-one D6–D0 sector: it is defined by ideal sheaves of zero-dimensional subschemes, so that the relevant moduli spaces are the Hilbert schemes of points, and the corresponding partition function is governed by the MacMahon function. Pure curve counting is encoded by the genus-zero Gopakumar–Vafa invariants, which arise directly from the refined Donaldson–Thomas spectrum by extracting the scalar $SU(2)_L$ sector of the five-dimensional BPS Hilbert space. Rank-one torsion-free sheaves with trivial determinant describe the D6–D2–D0 sector and lead to the standard Donaldson–Thomas invariants of ideal sheaves. Stable pairs $(\mathcal{O}_X \to F)$, with F a pure one-dimensional sheaf, giving rise to the Pandharipande–Thomas (PT) invariants, provide a different chamber of the same D6–D2–D0 problem; the DT/PT correspondence relates the two generating series after removal of the degree-zero contribution. For fixed curve class, the stable-pair partition function admits the standard BPS expansion in terms of the Gopakumar–Vafa invariants $n_{g,\beta}$, and refined stable-pair theory packages the corresponding spin content of the BPS spectrum. For local surfaces $X = K_S$, compactly supported D4–D2–D0 states are described by sheaves pushed forward from S, and the associated generating series are organized by the Vafa–Witten theory of the surface.

2.11.1 Formal Definitions

Let X be a Calabi–Yau threefold and let τ be a stability condition on a heart $\mathcal{A} \subset D^b\operatorname{Coh}(X)$. For a numerical class $\Gamma \in K(\mathcal{A})$, write

$$\mathcal{M}_\Gamma^{\mathrm{st}}(\tau), \qquad \mathcal{M}_\Gamma^{\mathrm{ss}}(\tau)$$

for the moduli stack of τ-stable and τ-semistable objects of class Γ. The corresponding Donaldson–Thomas invariants are weighted counts of these moduli spaces or stacks, with the precise definition depending on whether the class admits strictly semistable representatives.

Suppose first that the class Γ admits no strictly τ-semistable objects, so that

$$\mathcal{M}_\Gamma^{\mathrm{st}}(\tau) = \mathcal{M}_\Gamma^{\mathrm{ss}}(\tau).$$

For a stable object E of class Γ, the infinitesimal deformation theory is governed by

$$\operatorname{Ext}^1(E,E), \qquad \operatorname{Ext}^2(E,E),$$

with tangent space $\operatorname{Ext}^1(E,E)$ and obstruction space $\operatorname{Ext}^2(E,E)$. On a Calabi–Yau threefold, Serre duality identifies

$$\operatorname{Ext}^2(E,E) \cong \operatorname{Ext}^1(E,E)^\vee,$$

and this self-duality is the origin of the *symmetric perfect obstruction theory* on the moduli space of stable objects. Concretely, a perfect obstruction theory on a scheme M is a two-term complex of vector bundles

$$\mathbb{E}^\bullet \longrightarrow \mathbb{L}_M$$

mapping to the cotangent complex and encoding the deformation–obstruction theory of the moduli problem. It is called *symmetric* if it is equipped with an isomorphism

$$\mathbb{E}^\bullet \cong (\mathbb{E}^\bullet)^\vee[1].$$

For moduli spaces of stable sheaves on a Calabi–Yau threefold this obstruction theory has virtual dimension zero, and therefore determines a zero-dimensional virtual fundamental class

$$[\mathcal{M}_\Gamma^{\mathrm{st}}(\tau)]^{\mathrm{vir}} \in A_0\big(\mathcal{M}_\Gamma^{\mathrm{st}}(\tau)\big).$$

The original Donaldson–Thomas invariant is the degree of this class,

$$DT_\Gamma(\tau) = \int_{[\mathcal{M}_\Gamma^{\mathrm{st}}(\tau)]^{\mathrm{vir}}} 1 = \deg\,[\mathcal{M}_\Gamma^{\mathrm{st}}(\tau)]^{\mathrm{vir}}. \tag{2.200}$$

Behrend gave an intrinsic reinterpretation of this virtual count in terms of a canonical constructible function. To every scheme or Deligne–Mumford stack M one associates a constructible function

$$\nu_M : M \to \mathbb{Z},$$

defined from the local Euler obstruction of the intrinsic normal cone. The Donaldson–Thomas invariant is then the weighted Euler characteristic

$$DT_\Gamma(\tau) = \chi\big(\mathcal{M}_\Gamma^{\mathrm{st}}(\tau), \nu_{\mathcal{M}}\big), \tag{2.201}$$

where

$$\chi(M, \nu_M) := \sum_{n\in\mathbb{Z}} n\, e\big(\nu_M^{-1}(n)\big), \tag{2.202}$$

and $e(M)$ denotes the ordinary topological Euler characteristic of M. If M is smooth, then $\nu_M = (-1)^{\dim M}$, so

$$\chi(M, \nu_M) = (-1)^{\dim M} e(M). \tag{2.203}$$

The stable theory does not suffice when $\mathcal{M}_\Gamma^{\mathrm{ss}}(\tau)$ contains strictly semistable objects. In that situation the coarse moduli space of semistable objects parametrizes S-equivalence classes rather than isomorphism classes. Two semistable objects are S-equivalent if their associated graded objects, obtained from Jordan–Hölder filtrations, are isomorphic. A direct count on the semistable moduli space therefore mixes indecomposable objects with direct sums of constituents of the same phase.

Joyce and Song address this by working on the moduli stack and organizing semistable objects in the Ringel–Hall algebra of stack functions. Let $\mathfrak{M}$ denote the Artin stack of objects of the heart $\mathcal{A}$. A stack function on $\mathfrak{M}$ is, roughly, a $\mathbb{Q}$-linear combination of isomorphism classes of morphisms

$$\rho : \mathfrak{R} \to \mathfrak{M}$$

from finite-type algebraic stacks, modulo the usual cut-and-paste relations. The Hall product $*$ is defined by the stack of short exact sequences in $\mathcal{A}$; it records the formation of extensions and turns the space of stack functions into an associative algebra. For a fixed class Γ, the characteristic stack function of the semistable locus is

$$\bar{\delta}_\Gamma^{\mathrm{ss}}(\tau) := \big[\mathcal{M}_\Gamma^{\mathrm{ss}}(\tau) \hookrightarrow \mathfrak{M}\big].$$

The Hall-algebra logarithm extracts the indecomposable contribution from the semistable stack. In particular, it is the stack function

$$\mathfrak{q}_\Gamma(\tau) = \sum_{\substack{n\geq 1,\ \Gamma_1+\cdots+\Gamma_n=\Gamma \\ \tau(\Gamma_i)=\tau(\Gamma)\ \forall i}} \frac{(-1)^{n-1}}{n}\, \bar{\delta}_{\Gamma_1}^{\mathrm{ss}}(\tau) * \cdots * \bar{\delta}_{\Gamma_n}^{\mathrm{ss}}(\tau). \tag{2.204}$$

This is the precise analogue of the logarithm of a generating function: products in the Hall algebra encode direct sums of semistable constituents of common phase, and the logarithm isolates the primitive stack-theoretic contribution of class Γ.

To pass from stack functions to numerical invariants, Joyce and Song construct a Lie algebra morphism

$$\tilde{\Psi} : \mathrm{SF}_{\mathrm{al}}^{\mathrm{ind}}(\mathfrak{M}) \to \tilde{L}(X),$$

from the Lie algebra of virtually indecomposable stack functions with algebra stabilizers to the Lie algebra $\tilde{L}(X)$ generated by basis elements $\tilde{\lambda}_\Gamma$. Its bracket is determined by the antisymmetrized Euler form,

$$[\tilde{\lambda}_{\Gamma_1}, \tilde{\lambda}_{\Gamma_2}] = (-1)^{\langle\Gamma_1,\Gamma_2\rangle}\langle\Gamma_1, \Gamma_2\rangle\, \tilde{\lambda}_{\Gamma_1+\Gamma_2}. \tag{2.205}$$

The generalized Donaldson–Thomas invariant is defined by

$$\tilde{\Psi}\big(\mathfrak{q}_\Gamma(\tau)\big) = -\bar{\Omega}(\Gamma;\tau)\, \tilde{\lambda}_\Gamma. \tag{2.206}$$

The coefficient $\bar{\Omega}(\Gamma;\tau) \in \mathbb{Q}$ is the generalized Donaldson–Thomas invariant of Joyce–Song. Its rationality reflects the stack-theoretic stabilizers and the subtraction of decomposable semistable

contributions. When the class Γ admits only stable objects, $\bar{\Omega}(\Gamma;\tau)$ reduces to the ordinary Donaldson–Thomas invariant.

The relation between the rational invariant $\bar{\Omega}(\Gamma;\tau)$ and the integer BPS invariant $\Omega(\Gamma;\tau)$ is given by the multicover formula and its Möbius inverse recalled earlier in (2.40) and (2.43). In particular, for primitive Γ the two invariants coincide.

2.11.2 Refined DT Invariants

Refined Donaldson–Thomas invariants are defined in four dimensions. In the Kontsevich–Soibelman framework, one first associates to a 3-Calabi–Yau category with stability condition a motivic Hall algebra and a homomorphism from this Hall algebra to a motivic quantum torus. The resulting motivic Donaldson–Thomas invariants are elements of this quantum torus, and the refined Donaldson–Thomas invariants are obtained by applying the weight-polynomial specialization from motives to Laurent polynomials in a refinement variable y. The numerical generalized Donaldson–Thomas invariants are recovered by the further specialization $y \to 1$.

For a charge class Γ, the refined invariant is therefore a Laurent polynomial

$$\Omega(\Gamma; y, \tau) \in \mathbb{Z}[y^{\pm 1}],$$

or, after rationalization, $\bar{\Omega}(\Gamma; y, \tau)$, whose unrefined limit reproduces the numerical Donaldson–Thomas invariant. At the level of the quantum torus, the refinement parameter enters through the noncommutative product

$$\hat{e}_{\Gamma_1}\hat{e}_{\Gamma_2} = (-y)^{\langle \Gamma_1,\Gamma_2\rangle}\,\hat{e}_{\Gamma_1+\Gamma_2}, \tag{2.207}$$

so that refined wall-crossing is governed by quantum dilogarithm identities rather than their classical limit.

For local Calabi–Yau threefolds, curve-class invariants admit an equivalent five-dimensional interpretation. M-theory on $X \times S^1$ is dual to Type IIA string theory on X, and BPS states in four dimensions arise by circle reduction of five-dimensional BPS objects. In particular, M2-branes wrapped on curves give D2–D0 states, M5-branes wrapped on divisors give D4–D2–D0 states, and Kaluza–Klein monopoles give D6-charge. Five-dimensional BPS particles are organized by the massive little group

$$\mathrm{Spin}(4) \cong SU(2)_L \times SU(2)_R,$$

while five-dimensional strings and black rings contribute after reduction to the same four-dimensional charge lattice. The spin refinement is therefore most naturally described in five dimensions, whereas the Donaldson–Thomas invariant itself remains a four-dimensional object.

For a curve class $\beta \in H_2(X,\mathbb{Z})$, let

$$\mathcal{H}_\beta^{\mathrm{BPS}} = \bigoplus_{j_L, j_R} N_\beta^{j_L, j_R}\,[j_L, j_R] \tag{2.208}$$

be the decomposition of the five-dimensional BPS Hilbert space into irreducible representations of $SU(2)_L \times SU(2)_R$. Writing

$$\chi_j(y) := \sum_{m=-j}^{j} y^{2m}, \tag{2.209}$$

one forms the two-variable spin character

$$\Omega_\beta(y_L, y_R) = \sum_{j_L, j_R} N_\beta^{j_L, j_R}\,\chi_{j_L}(y_L)\chi_{j_R}(y_R). \tag{2.210}$$

The single-variable refined series used in the Donaldson–Thomas and stable-pair literature is obtained from this master five-dimensional partition function by the diagonal specialization $y_L = y_R = y$, together with the standard indexed trace over the right-spin sector. Equivalently, one may work with the indexed $SU(2)_L$-character

$$\Omega_\beta(y) = \sum_{j_L, j_R} (-1)^{2j_R} (2j_R + 1)\, N_\beta^{j_L, j_R}\, \chi_{j_L}(y). \tag{2.211}$$

It is this single-variable object that enters the BPS expansion of refined DT/PT partition functions for curve classes.

The same indexed five-dimensional multiplicities determine the Gopakumar–Vafa invariants n_β^g. These are defined by expanding (2.211) in the basis

$$I_g(y) := \big(\chi_{1/2}(y) - 2\chi_0(y)\big)^g = \big(y^{1/2} - y^{-1/2}\big)^{2g}, \qquad g \geq 0, \tag{2.212}$$

namely

$$\sum_{j_L, j_R} (-1)^{2j_R} (2j_R + 1)\, N_\beta^{j_L, j_R}\, \chi_{j_L}(y) = \sum_{g \geq 0} n_\beta^g\, I_g(y). \tag{2.213}$$

This is the standard definition of the unrefined Gopakumar–Vafa invariants from the five-dimensional BPS spectrum.

The genus-zero invariant is extracted by the limit $y \to 1$. Since

$$I_0(y) = 1, \qquad I_g(y) \to 0 \quad (g \geq 1) \qquad \text{as } y \to 1,$$

one obtains

$$n_\beta^0 = \lim_{y \to 1} \sum_{j_L, j_R} (-1)^{2j_R} (2j_R + 1)\, N_\beta^{j_L, j_R}\, \chi_{j_L}(y). \tag{2.214}$$

Thus genus-zero Gopakumar–Vafa invariants are the $y \to 1$ limit of the indexed five-dimensional spin character. Higher-genus invariants measure the higher-order vanishing of the same character at $y = 1$.

For arbitrary charge classes Γ, refined Donaldson–Thomas invariants are defined by the Kontsevich–Soibelman motivic formalism and depend on the four-dimensional stability condition. For curve classes β on a local Calabi–Yau threefold, these refined invariants admit the five-dimensional interpretation above and are encoded by the same spin multiplicities $N_\beta^{j_L, j_R}$ that determine the Gopakumar–Vafa invariants.

2.11.3 PT Invariants and Special D-brane Sectors

Pandharipande and Thomas introduced stable pairs in order to isolate the curve contribution in rank-one Donaldson–Thomas theory from the free zero-dimensional contribution carried by points [163]. On a smooth projective Calabi–Yau threefold X, a *stable pair* is a morphism

$$s : \mathcal{O}_X \longrightarrow F \tag{2.215}$$

where F is a pure one-dimensional coherent sheaf, in the sense recalled in subsection 2.9.1, and the cokernel of s is zero-dimensional. If

$$[F] = \beta \in H_2(X, \mathbb{Z}), \qquad \chi(F) = n,$$

the moduli space of stable pairs is denoted by $P_n(X,\beta)$. For a Calabi–Yau threefold this moduli space carries a symmetric perfect obstruction theory of virtual dimension zero, and the corresponding PT invariant is

$$P_{n,\beta} = \int_{[P_n(X,\beta)]^{\mathrm{vir}}} 1 = \chi\big(P_n(X,\beta), \nu_{P_n(X,\beta)}\big). \tag{2.216}$$

The generating series in fixed curve class is

$$Z_{PT,\beta}(q) = \sum_{n\in\mathbb{Z}} P_{n,\beta}\, q^n. \tag{2.217}$$

A stable pair determines a canonical exact sequence

$$0 \longrightarrow I_C \longrightarrow \mathcal{O}_X \xrightarrow{s} F \longrightarrow Q \longrightarrow 0, \tag{2.218}$$

where $C \subset X$ is a Cohen–Macaulay curve and Q is a zero-dimensional sheaf supported on C. Here C is Cohen–Macaulay in the algebro-geometric sense that its structure sheaf $\mathcal{O}_C$ has depth equal to its dimension at every point; for a one-dimensional subscheme this excludes embedded and isolated zero-dimensional associated components. The sheaf F therefore records a curve together with zero-dimensional structure bound to it. By contrast, rank-one DT theory counts ideal sheaves

$$I_Z \subset \mathcal{O}_X \tag{2.219}$$

of one-dimensional subschemes $Z \subset X$, and the zero-dimensional contribution is allowed to move freely in the ambient threefold.

These moduli problems organize naturally by D-brane charge sector. Zero-dimensional sheaves represent pure D0-branes. Pure one-dimensional sheaves represent D2–D0 systems, with the curve class β giving the D2 charge and the Euler characteristic giving the accompanying D0 charge. Rank-one torsion-free sheaves, and in particular ideal sheaves I_Z, represent a single D6-brane bound to D2- and D0-charge. Stable pairs describe the same rank-one D6–D2–D0 sector in a different stability chamber. For local surface geometries $X = K_S$, compactly supported two-dimensional sheaves describe D4–D2–D0 systems; when such sheaves are written as i_*E for a sheaf E on the surface S, the corresponding invariants become invariants of moduli spaces of semistable sheaves on S.

The pure D0 sector is governed by the degree-zero Donaldson–Thomas invariants. For $\beta = 0$, rank-one DT theory reduces to the Hilbert scheme of points,

$$I_n(X,0) = \mathrm{Hilb}^n(X),$$

and

$$DT_{n,0} = \chi\big(\mathrm{Hilb}^n(X), \nu_{\mathrm{Hilb}^n(X)}\big). \tag{2.220}$$

Their generating series is universal:

$$Z_{DT,0}(q) := \sum_{n\geq 0} DT_{n,0}\, q^n = M(-q)^{\chi(X)}, \tag{2.221}$$

where

$$M(q) = \prod_{m\geq 1}(1-q^m)^{-m} \tag{2.222}$$

is the MacMahon function. The argument $-q$ reflects the Behrend-weighted sign in degree zero: the weighted Euler characteristic of $\mathrm{Hilb}^n(X)$ differs from the ordinary Euler characteristic by the factor $(-1)^n$.

For rank-one D6–D2–D0 states one fixes a curve class β and Euler characteristic n. The DT moduli space is the Hilbert scheme

$$I_n(X,\beta)$$

of ideal sheaves of one-dimensional subschemes $Z \subset X$ with

$$[Z] = \beta, \qquad \chi(\mathcal{O}_Z) = n.$$

The PT moduli space $P_n(X,\beta)$ describes the same charge sector in a different chamber. Their generating series are related by the DT/PT correspondence,

$$Z_{DT,\beta}(q) = M(-q)^{\chi(X)}\, Z_{PT,\beta}(q), \tag{2.223}$$

or equivalently

$$Z'_{DT,\beta}(q) := \frac{Z_{DT,\beta}(q)}{Z_{DT,0}(q)} = Z_{PT,\beta}(q). \tag{2.224}$$

This identity may be interpreted as wall-crossing between two stability conditions on the same rank-one D6–D2–D0 theory.

For fixed curve class, the PT partition function admits a product expansion in terms of the integral BPS multiplicities $n_{g,\beta}$:

$$Z_{PT}(q,Q) = \prod_{\beta>0}\prod_{j\geq 1}\left(1-(-q)^j Q^\beta\right)^{j\, n_{0,\beta}} \prod_{\beta>0}\prod_{g\geq 1}\prod_{k=0}^{2g-2}\left(1-(-q)^{g-1-k}Q^\beta\right)^{(-1)^{k+g}\binom{2g-2}{k} n_{g,\beta}}. \tag{2.225}$$

Thus PT theory packages the same integral BPS multiplicities that appear in the Gopakumar–Vafa expansion, while DT theory differs from it by the universal degree-zero factor $M(-q)^{\chi(X)}$. In primitive one-dimensional classes, the resulting integral BPS counts coincide with the genus-zero Gopakumar–Vafa invariants discussed above; more generally, the full PT partition function records the complete tower of Gopakumar–Vafa invariants $n_{g,\beta}$.

For local surface geometries $X = K_S$, compactly supported D4–D2–D0 states are described by sheaves on S pushed forward to X. The corresponding generalized Donaldson–Thomas invariants are therefore invariants of moduli spaces of semistable sheaves on S. In the gauge-theoretic chamber relevant to Vafa–Witten theory, the generating functions of these invariants are organized by the Vafa–Witten invariants of the surface. Generalized Donaldson–Thomas theory therefore contains, within one wall-crossing formalism, degree-zero DT theory for pure D0-branes, GV and PT theories for curve sectors, rank-one DT/PT theory for D6–D2–D0 states, and Vafa–Witten theory for compactly supported D4–D2–D0 systems.

3

BPS Spectrum in Local Calabi–Yau Models

This chapter specializes the general framework of the previous chapter to non-compact, or local, Calabi–Yau threefolds. These models provide a simplified but highly effective setting in which the structure of the BPS spectrum can be studied explicitly, while still retaining the essential wall-crossing, quiver, and enumerative features of the compact theory. Our main goal is to introduce the geometric and categorical tools that make the local problem tractable, and to prepare the ground for the explicit constructions in the later chapters.

The chapter is organized as follows. Section 3.1 explains the passage from compact Calabi–Yau compactifications to local models and the corresponding simplifications in the description of BPS states. Section 3.2 reviews exceptional collections and the quivers associated with local surfaces, which provide a concrete description of the categories of branes. Section 3.3 introduces scattering diagrams and their relation to the Kontsevich–Soibelman wall-crossing formalism. Finally, Section 3.4 reviews the local mirror-symmetry framework that will be used to compute central charges and analyze stability conditions in the examples studied later.

3.1 Non-compact toric Calabi-Yau models

The framework developed in the preceding sections—BPS indices, wall-crossing, attractor flow trees, quiver quantum mechanics—is naturally adapted to compact Calabi–Yau compactifications and their four-dimensional $\mathcal{N} = 2$ supergravity interpretation. The rest of this thesis works with non-compact local models, and the passage between the two settings requires understanding how the supergravity framework reduces, under a suitable degeneration, to a rigid supersymmetric theory supported on a neighborhood of a compact surface, in a way that preserves the charge lattices, stability structures, and BPS-counting problems that remain meaningful once gravity decouples. [14]

The relevant local models are non-compact Calabi–Yau threefolds of the form

$$X = \mathrm{Tot}(K_S),$$

where S is a rigid compact surface. The passage to this geometry has both a physical and a geometric aspect: the Planck scale diverges and surviving BPS states become D-brane bound states localized on compact cycles rather than asymptotically flat black-hole configurations, while simultaneously the vector-multiplet moduli space transitions from local to rigid special geometry. The following subsections make this transition explicit. Later sections will reformulate the same local setup in terms of coherent sheaves, exceptional collections, and stability conditions on S and on the associated local threefold.

3.1.1 Compact vs. Local Calabi–Yau Geometries

In compact Calabi–Yau compactifications of type II string theory, the low-energy effective theory is an $\mathcal{N} = 2$ theory coupled to gravity, whose vector-multiplet moduli space carries local

special Kähler geometry. BPS states appear as particles carrying electromagnetic charges in the four-dimensional supergravity theory; when these charges are large, or when multicentered configurations are considered, their indexed degeneracies are identified with those of asymptotically flat black-hole solutions. Wall-crossing refers to the discontinuous change of these degeneracies across walls of marginal stability in the compact moduli space.

The geometries relevant to the rest of the thesis arise in a different regime. Taking the bulk Calabi–Yau volume to infinity makes the four-dimensional Planck mass diverge and drives the Newton constant to zero,

$$G_{N,4} \sim \frac{g_s^2\,\ell_s^8}{\mathrm{Vol}(Y)} \to 0,$$

which decouples the gravitational sector entirely. The surviving BPS states are bound states of D-branes supported on compact cycles inside a non-compact Calabi–Yau threefold; in suitable field-theory limits they are reinterpreted as dyonic excitations on the Coulomb branch of the engineered rigid gauge theory.

The decoupling limit also changes the structure of the moduli space. For compact Calabi–Yau threefolds, the vector-multiplet moduli space is governed by local special geometry: holomorphic objects are sections of a gravitationally induced line bundle $\mathcal{L}$ over moduli space, and amplitudes and periods are twisted by this line bundle structure. In the non-compact limit $\mathcal{L}$ decouples, the moduli are described by rigid special coordinates, and the holomorphic three-form Ω_{hol} reduces, in the mirror description, to a meromorphic one-form λ on the mirror curve [1].

Two distinct limiting procedures appear in the discussion and should not be conflated. The first is the decoupling limit just described, which removes gravitational dynamics and isolates the local Calabi–Yau geometry. The second is a further field-theory scaling performed within a fixed local geometry in order to engineer a specific rigid gauge theory. In the $SU(2)$ geometric engineering construction of Katz, Klemm, and Vafa [124], one introduces Kähler parameters t_b and t_f for the base and fiber classes and takes

$$e^{-t_b} \sim \epsilon^4 \Lambda^4, \qquad t_f \sim \epsilon a, \qquad \epsilon \to 0. \tag{3.1}$$

Here Λ is the dynamical scale of the gauge theory and a the Coulomb-branch parameter. This extracts the field-theory regime from a geometry already decoupled from gravity, and should not be conflated with the degeneration

$$t_e \to \infty,$$

used in subsection 3.1.3 to pass from a compact elliptically fibered threefold to the local geometry itself.

3.1.2 Local Toric Models

The local models of primary interest are non-compact Calabi–Yau threefolds of the form

$$X = \mathrm{Tot}(K_S), \tag{3.2}$$

where S is a smooth projective surface and K_S its canonical bundle. The total space of the canonical bundle has trivial canonical class, so X is Calabi–Yau. Its compact geometry is carried entirely by the zero section $S \hookrightarrow X$, and compactly supported D-brane charges are accordingly described by sheaves supported on S. [60]

When S is toric, the geometry is encoded by a fan in an integral lattice: a collection of one-dimensional cones generated by primitive lattice vectors, together with their linear relations.

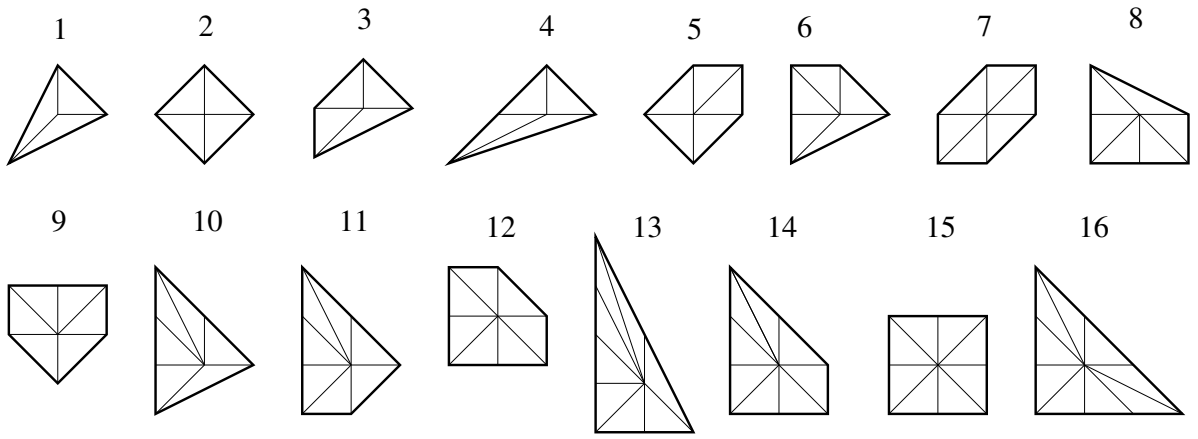


Figure 3.1: Reflexive Polyhedra Δ_B in two dimensions. $\hat{\Delta}_p = \Delta_{17-p}$ for $p = 1, \ldots, 6$. $\Delta_{7,8,9,10}$ are self-dual. Case 1 is the polyhedron representing $\mathbb{P}^2$; Cases 2, 3, and 4 are the Hirzebruch surfaces $\mathbb{F}_0 = \mathbb{P}^1 \times \mathbb{P}^1$, $\mathbb{F}_1$, $\mathbb{F}_2$, and the others are various blow-ups of these cases. Taken from [60, Figure 1].

In the gauged linear sigma model (GLSM) description, the same data are encoded by integer charge vectors, which determine the toric divisors, compact curve classes, Mori cone, and Kähler parameters. For local Calabi–Yau threefolds, the same input furnishes the toric diagram and the associated (p, q)-web, which will reappear in the discussion of local mirror symmetry in Section 3.4. [60]

The main example of Chapter 4 is the local Calabi–Yau threefold $X = \mathrm{Tot}(K_{\mathbb{F}_0})$, where $\mathbb{F}_0 \cong \mathbb{P}^1 \times \mathbb{P}^1$. The toric surface $\mathbb{F}_0$ is described by the complete fan in $N \cong \mathbb{Z}^2$ with one-dimensional cones generated by

$$v_1 = (1, 0), \qquad v_2 = (0, 1), \qquad v_3 = (-1, 0), \qquad v_4 = (0, -1). \tag{3.3}$$

The toric diagram is a square — Case 2 in Figure 3.1 — and its dual web diagram is the familiar rectangular four-valent web of local $\mathbb{F}_0$. [4]

The surface $\mathbb{F}_0$ has two independent compact curve classes, the classes of the two $\mathbb{P}^1$ factors, denoted

$$B, \qquad F.$$

Their intersection pairing is

$$B^2 = 0, \qquad F^2 = 0, \qquad B \cdot F = 1, \tag{3.4}$$

and the canonical class is

$$K_{\mathbb{F}_0} = -2B - 2F. \tag{3.5}$$

The Kähler form is

$$J = t_1\, \omega_B + t_2\, \omega_F, \tag{3.6}$$

where $\omega_B, \omega_F \in H^{1,1}(\mathbb{F}_0)$ are Poincaré dual to B and F, and t_1, t_2 are the corresponding Kähler parameters, equivalently the complexified volumes of the two rulings. By Poincaré duality, B and F will also denote the corresponding divisor classes in cohomology when no confusion can arise.

The GLSM description of the local threefold uses five homogeneous coordinates (x_1, x_2, x_3, x_4, p) with two $U(1)$ actions of charges

$$Q^{(1)} = (1, 1, 0, 0, -2), \qquad Q^{(2)} = (0, 0, 1, 1, -2). \tag{3.7}$$

The four coordinates x_i parametrize the toric surface $\mathbb{F}_0$, while p is the fiber coordinate of the canonical bundle. The Calabi–Yau condition is the vanishing of the charge sums,

$$\sum_i Q_i^{(a)} = 0,$$

and the two charge vectors generate the Mori cone of compact curve classes. The divisor relations

$$D_1 \sim D_2, \qquad D_3 \sim D_4$$

identify the toric divisors pairwise, with the two independent classes dual to B and F.

The toric data of S thus encode its compact curves, intersection pairing, and Kähler parameters which are all the input needed to set up the counting problem on the local threefold. The same data determine the mirror curve and its period structure, developed in Section 3.4.

3.1.3 Local Limit of Elliptically Fibered Compact CY3s

The compact-to-local transition is realized concretely by degenerating an elliptically fibered Calabi–Yau threefold. Following Alexandrov, Manschot, and Pioline [14], consider a smooth elliptically fibered Calabi–Yau threefold

$$\pi : Y \to S$$

with a single section over a compact, smooth almost Fano base S satisfying

$$b_1(S) = 0, \qquad b_2^+(S) = 1.$$

Under these conditions $\chi(\mathcal{O}_S) = 1$ and the divisor S is rigid inside Y. The allowed surfaces include Hirzebruch surfaces $\mathbb{F}_k$ with $0 \le k \le 2$ and del Pezzo surfaces B_k with $0 \le k \le 8$.

The Kähler moduli space of Y has dimension $h^{1,1}(Y) = b_2(S) + 1$. Let

$$(\omega_e, \omega_\alpha), \qquad \alpha = 1, \dots, h^{1,1}(S),$$

be generators of the Kähler cone, and let (D_e, D_α) denote the dual generators of the Mori cone. Writing

$$C_{\alpha\beta} = \int_S \omega_\alpha \wedge \omega_\beta, \qquad c_1(S) = c_1^\alpha\, \omega_\alpha, \tag{3.8}$$

the divisor intersections take the form

$$D_e^3 = C_{\alpha\beta} c_1^\alpha c_1^\beta, \quad D_e^2 \cap D_\alpha = C_{\alpha\beta} c_1^\beta, \quad D_e \cap D_\alpha \cap D_\beta = C_{\alpha\beta}, \quad D_\alpha \cap D_\beta \cap D_\gamma = 0, \tag{3.9}$$

encoding the intersection ring of Y in a basis adapted to the fiber and the base. The Euler characteristic and second Chern class are [14]

$$\chi(Y) = -60\, C_{\alpha\beta} c_1^\alpha c_1^\beta, \tag{3.10}$$

$$c_{2,e} = \int_S \big(11\, c_1(S)^2 + c_2(S)\big), \qquad c_{2,\alpha} = 12\, C_{\alpha\beta} c_1^\beta, \tag{3.11}$$

both expressed entirely in terms of the intersection form and Chern classes of S.

A distinguished divisor class is

$$[S] = D_e - c_1^\alpha D_\alpha, \tag{3.12}$$

which may be identified with the base surface viewed as the unique section of the fibration. It satisfies

$$[S]^3 = D_e^3, \qquad [S]^2 \cap D_\alpha = 0, \qquad [S] \cap D_\alpha \cap D_\beta = 0. \tag{3.13}$$

Rigidity of this divisor is verified directly: using the formula for the dimension of the deformation space of a divisor in a Calabi–Yau threefold, together with $\chi(\mathcal{O}_S) = 1$,

$$\frac{1}{3}S^3 + \frac{1}{6}c_2(TY)\cdot S - 2 = \frac{1}{6}\int_S \big(c_2(S) + c_1(S)^2\big) - 2 = 2\big(\chi(\mathcal{O}_S) - 1\big) = 0, \tag{3.14}$$

so the deformation space of S inside Y is trivial.

The local degeneration is obtained by splitting the complexified Kähler moduli as $t^a = (t_e, t^\alpha)$ and sending

$$t_e \to \infty. \tag{3.15}$$

Taking t_e large stretches the elliptic-fiber direction and localizes the geometry around the section S, producing the degeneration

$$Y \rightsquigarrow X = \mathrm{Tot}(K_S). \tag{3.16}$$

Once again, the limit (3.15) should not be confused with the field-theory scaling (3.1): the latter extracts a rigid gauge theory from a fixed local geometry, whereas the former produces the local geometry itself by degenerating the compact threefold.

The compact realization gives a precise correspondence between the D-brane charge vector in the compact model and the charge assignments in the local geometry. In the conventions of this thesis, the symplectic charge vector is

$$\Gamma = (P^\Lambda, Q_\Lambda),$$

with the index Λ decomposed as $\Lambda = (0, a)$, $a = (e, \alpha)$. Here 0 labels the D6/D0 component, e the elliptic-fiber direction, and α classes pulled back from the base. For a stack of N D4-branes wrapping S, the magnetic charge is

$$P^a = N P_0^a, \qquad P_0^a = (1, -c_1^\alpha), \tag{3.17}$$

fixed by the divisor class (3.12).

Let $i : S \hookrightarrow Y$ denote the inclusion of the section, and let F be the worldvolume sheaf with $c_1(F) \in H^2(S, \mathbb{Z})$. The electric charges are

$$Q_\alpha = -\int_S i^*(\omega_\alpha)\Big(c_1(F) + \tfrac{N}{2}c_1(S)\Big), \qquad Q_e = 0, \tag{3.18}$$

together with

$$Q_0 = \frac{1}{2N}\Big(c_1(F) + \tfrac{N}{2}c_1(S)\Big)^2 + \frac{N}{24}\chi(S) - N\,\Delta(F), \tag{3.19}$$

where $\Delta(F)$ is the Bogomolov discriminant [14].

The vanishing $Q_e = 0$ for a D4-brane wrapped on S is not accidental: it reflects the absence of electric charge in the elliptic-fiber direction after the local degeneration. Configurations with

$Q_e \neq 0$ necessarily wrap the fiber and are exponentially suppressed as $t_e \to \infty$, so the limit projects automatically onto the charge sector intrinsic to S.

The invariant D0-brane charge is defined by

$$\hat{Q}_0 = Q_0 - \frac{1}{2N} C^{\alpha\beta} Q_\alpha Q_\beta = -\int_S \Big[c_2(F) - \frac{N-1}{2N} c_1(F)^2 \Big] + \frac{N}{24}\chi(S), \tag{3.20}$$

where $C^{\alpha\beta}$ is the inverse intersection matrix. This is the local analogue of the invariant D0-charge appearing in generating functions for D4–D2–D0 states [14], and depends only on topological invariants of S and F.

For two reduced charge vectors $\check{\Gamma}_i = (N_i P_0^a, Q_{i,a})$, the Dirac pairing reduces to

$$\langle \Gamma_1, \Gamma_2 \rangle = c_1^\alpha \big(N_1 Q_{2,\alpha} - N_2 Q_{1,\alpha} \big) = K_S \cdot \big(N_1 c_1(F_2) - N_2 c_1(F_1) \big). \tag{3.21}$$

This is the pairing governing the local D4–D2 system and will enter wall-crossing and bound-state constructions throughout.

The local limit also affects the quadratic form induced by the magnetic charge:

$$\kappa_{ab} = \kappa_{abc} P^c = N \begin{pmatrix} 0 & 0 \\ 0 & C_{\alpha\beta} \end{pmatrix}. \tag{3.22}$$

The quadratic form is degenerate in the elliptic-fiber direction, reflecting the fact that $[S]$ is rigid but not ample. The standard decomposition of electric charges in the compact ample case therefore does not carry over; only the component intrinsic to the surface survives as a non-degenerate lattice, namely $\Lambda_S = H^2(S, \mathbb{Z})$ with intersection form $C_{\alpha\beta}$, as we have seen.

The remaining electric charges decompose as [14]

$$Q_\alpha = \mu_\alpha + N C_{\alpha\beta} \epsilon^\beta - \frac{N^2}{2} C_{\alpha\beta} c_1^\beta, \tag{3.23}$$

with $\epsilon^\alpha \in \Lambda_S = H^2(S, \mathbb{Z})$ and $\mu_\alpha \in \Lambda_S / (N\Lambda_S)$. For the surfaces considered in this thesis, Λ_S is unimodular, so (3.23) is the local analogue of the spectral-flow decomposition in the compact theory. The charges are thus classified by fluxes in $H^2(S, \mathbb{Z})$ together with residual classes modulo $N\Lambda_S$.

Once the charge system is localized on the rigid surface S, D-brane configurations are described by coherent sheaves and, more generally, by objects in the derived category on S and on the associated local threefold.

3.2 Exceptional collections and quivers on local surfaces

For local Calabi–Yau threefolds of the form $X = K_S$, with S a smooth rational surface, the derived category $D^b \operatorname{Coh}(S)$ often admits distinguished generating collections whose algebraic structure can be made completely explicit. The modern theory of exceptional collections grew out of Beilinson's description of $D^b \operatorname{Coh}(\mathbb{P}^n)$, and was subsequently developed through the work of Bondal, Kapranov, Gorodentsev, Rudakov, and others into a flexible framework involving mutations, dual collections, and helices. On rational surfaces this technology provides a concrete basis of branes adapted to the geometry of the surface and to the local Calabi–Yau obtained from its canonical bundle.

Its usefulness in the present context is twofold. First, exceptional collections furnish explicit fractional-brane bases and hence a direct route from geometric objects in $D^b\,\mathrm{Coh}(S)$ to quiver descriptions of the local BPS sector. Second, the resulting quiver data determine the antisymmetric pairing and the adjacency matrix that enter Coulomb-branch formulas and attractor-flow-tree computations of BPS indices. The aim of this section is therefore to recall the basic categorical structures associated with exceptional collections and to present them in a form adapted to local surfaces. This section is based on [28, 37, 46, 109].

3.2.1 Exceptional Objects, Mutations, and Helices

Let S be a smooth projective rational surface. For objects $\mathcal{E}, \mathcal{F} \in D^b\,\mathrm{Coh}(S)$, the basic bilinear form is the Euler pairing

$$\chi(\mathcal{E},\mathcal{F}) := \sum_{k\in\mathbb{Z}} (-1)^k \dim \mathrm{Ext}^k_S(\mathcal{E},\mathcal{F}). \tag{3.24}$$

By Hirzebruch–Riemann–Roch, this may be written as

$$\chi(\mathcal{E},\mathcal{F}) = \int_S \mathrm{ch}(\mathcal{E}^\vee)\ \mathrm{ch}(\mathcal{F})\ \mathrm{Td}(S). \tag{3.25}$$

When $\deg(\mathcal{E})$ is defined with respect to the anticanonical class by

$$\deg(\mathcal{E}) := -K_S \cdot c_1(\mathcal{E}),$$

the Euler form can be written as

$$\begin{aligned}\chi(\mathcal{E},\mathcal{F}) = \mathrm{rk}(\mathcal{E})\,\mathrm{rk}(\mathcal{F}) \ +\ \mathrm{rk}(\mathcal{E})\mathrm{ch}_2(\mathcal{F}) \ +\ \mathrm{rk}(\mathcal{F})\mathrm{ch}_2(\mathcal{E}) \\ -\ c_1(\mathcal{E})\cdot c_1(\mathcal{F}) \ +\ \frac{1}{2}\Big[\mathrm{rk}(\mathcal{E})\deg(\mathcal{F}) - \mathrm{rk}(\mathcal{F})\deg(\mathcal{E})\Big].\end{aligned} \tag{3.26}$$

Whereas the antisymmetrized pairing takes the form

$$\langle \mathcal{E},\mathcal{F}\rangle := \chi(\mathcal{E},\mathcal{F}) - \chi(\mathcal{F},\mathcal{E}) = \mathrm{rk}(\mathcal{E})\deg(\mathcal{F}) - \mathrm{rk}(\mathcal{F})\deg(\mathcal{E}). \tag{3.27}$$

This is the categorical counterpart of the physical symplectic pairing on charges and will later determine quiver adjacency matrices.

An object $\mathcal{E} \in D^b\,\mathrm{Coh}(S)$ is called *exceptional* if

$$\mathrm{Hom}(\mathcal{E},\mathcal{E}) = \mathbb{C}, \qquad \mathrm{Ext}^k_S(\mathcal{E},\mathcal{E}) = 0 \quad \text{for } k > 0. \tag{3.28}$$

In particular,

$$\chi(\mathcal{E},\mathcal{E}) = 1. \tag{3.29}$$

An ordered pair $(\mathcal{E},\mathcal{F})$ of exceptional objects is called an *exceptional pair* if

$$\mathrm{Ext}^k_S(\mathcal{F},\mathcal{E}) = 0 \qquad \text{for all } k \in \mathbb{Z}. \tag{3.30}$$

More generally, an ordered sequence

$$\mathbb{E} = (\mathcal{E}_1,\dots,\mathcal{E}_n)$$

is an *exceptional collection* if each $\mathcal{E}_i$ is exceptional and

$$\mathrm{Ext}^k_S(\mathcal{E}_i, \mathcal{E}_j) = 0 \qquad \text{for all } k \in \mathbb{Z} \text{ whenever } i > j. \tag{3.31}$$

Thus the collection is semiorthogonal in the prescribed order.

An exceptional collection is called *strong* if

$$\mathrm{Ext}^k_S(\mathcal{E}_i, \mathcal{E}_j) = 0 \qquad \text{for all } k > 0 \text{ and all } i, j, \tag{3.32}$$

so that only degree-zero morphisms remain. It is called *full* if the smallest thick triangulated subcategory containing the $\mathcal{E}_i$ coincides with $D^b\,\mathrm{Coh}(S)$,

$$\langle \mathcal{E}_1, \dots, \mathcal{E}_n \rangle = D^b\,\mathrm{Coh}(S). \tag{3.33}$$

For the rational surfaces relevant here, one often works with full strong exceptional collections of line bundles. These give explicit generators of the derived category and lead to tractable quiver descriptions.

Associated with a full exceptional collection are its dual collections. The *right dual* collection

$$\mathbb{E}^\vee = (\mathcal{E}_1^\vee, \dots, \mathcal{E}_n^\vee)$$

is characterized by the Euler-orthogonality relations

$$\chi(\mathcal{E}_i, \mathcal{E}_j^\vee) = \delta_{ij}, \tag{3.34}$$

while the *left dual* collection

$${}^\vee\mathbb{E} = ({}^\vee\mathcal{E}_1, \dots, {}^\vee\mathcal{E}_n)$$

is characterized by

$$\chi({}^\vee\mathcal{E}_i, \mathcal{E}_j) = \delta_{ij}. \tag{3.35}$$

For a full strong exceptional collection, the dual collections are naturally Ext-exceptional: the semiorthogonality is reversed and expressed in terms of vanishing Ext-groups rather than only Euler orthogonality. These dual objects provide the fractional-brane basis most naturally adapted to the quiver description of the local Calabi–Yau.

Starting from an exceptional pair $(\mathcal{F}, \mathcal{E})$, one obtains new exceptional objects by mutation. The *left mutation* of $\mathcal{E}$ through $\mathcal{F}$ is defined by the distinguished triangle

$$L_{\mathcal{F}}\mathcal{E} \longrightarrow \mathrm{Hom}^\bullet(\mathcal{F}, \mathcal{E}) \otimes \mathcal{F} \xrightarrow{\mathrm{ev}} \mathcal{E} \longrightarrow L_{\mathcal{F}}\mathcal{E}[1], \tag{3.36}$$

while the *right mutation* of $\mathcal{F}$ through $\mathcal{E}$ is defined by

$$\mathcal{F} \xrightarrow{\mathrm{coev}} \mathrm{Hom}^\bullet(\mathcal{F}, \mathcal{E})^\vee \otimes \mathcal{E} \longrightarrow R_{\mathcal{E}}\mathcal{F} \longrightarrow \mathcal{F}[1]. \tag{3.37}$$

Here

$$\mathrm{Hom}^\bullet(\mathcal{F}, \mathcal{E}) := \bigoplus_{k \in \mathbb{Z}} \mathrm{Ext}^k_S(\mathcal{F}, \mathcal{E})[-k]$$

denotes the total graded Hom-space. Mutations preserve exceptionality and generate the braid-group action on exceptional collections. In geometric terms, they produce new bases of $D^b\,\mathrm{Coh}(S)$ from old ones; in the brane picture, they correspond to changes of fractional-brane basis.

The left and right dual collections described above may be constructed explicitly by iterated mutations. The right dual is obtained by mutating each $\mathcal{E}_i$ successively through $\mathcal{E}_{i+1}, \dots, \mathcal{E}_n$, while the left dual is obtained by mutating each $\mathcal{E}_i$ successively through $\mathcal{E}_1, \dots, \mathcal{E}_{i-1}$.

When higher Ext-groups vanish except in a single degree, the mutation triangles reduce to short exact sequences of sheaves. For line-bundle collections on rational surfaces, this often leads to concrete recursive constructions of new exceptional bundles. It is in this form that mutations are especially useful in explicit local models, where one passes between different exceptional collections adapted to different quiver phases.

Exceptional collections on rational surfaces are naturally organized into *helices*. A geometric helix of period n is a bi-infinite sequence

$$\mathbb{H} = (\mathcal{E}_i)_{i \in \mathbb{Z}}$$

such that every consecutive thread

$$(\mathcal{E}_{i+1}, \dots, \mathcal{E}_{i+n})$$

is a full exceptional collection and

$$\mathcal{E}_{i+n} \cong \mathcal{E}_i \otimes \omega_S^{-1} \tag{3.38}$$

for all $i \in \mathbb{Z}$. Thus the helix is generated from any one thread by repeated mutation together with anticanonical twist. On del Pezzo and Hirzebruch surfaces this periodic structure is particularly effective, since it encodes the way exceptional collections recur under mutation and provides a natural organizing principle for the different quiver phases associated with the same local geometry.

3.2.2 From Exceptional Collections to Quivers on Local Surfaces

Let

$$\mathbb{E} = (\mathcal{E}_1, \dots, \mathcal{E}_r)$$

be a full strong exceptional collection on a smooth projective rational surface S. The direct sum

$$M := \bigoplus_{i=1}^{r} \mathcal{E}_i \tag{3.39}$$

is then a tilting object: one has

$$\mathrm{Ext}_S^k(M, M) = 0 \qquad \text{for all } k > 0, \tag{3.40}$$

and M generates $D^b \mathrm{Coh}(S)$ as a triangulated category. The associated endomorphism algebra

$$A := \mathrm{End}_S(M) \tag{3.41}$$

packages the morphism structure of the collection into a finite-dimensional algebra. Since the collection is strong, no higher Ext-groups occur among the $\mathcal{E}_i$, and the relevant algebraic structure is concentrated in degree zero.

A standard theorem of tilting theory, in the form due to Bondal and Kapranov, gives an equivalence of triangulated categories

$$\mathbf{R}\mathrm{Hom}_S(M, -) : D^b \mathrm{Coh}(S) \xrightarrow{\sim} D^b(\text{mod-}A), \tag{3.42}$$

with quasi-inverse $- \overset{\mathbf{L}}{\otimes}_A M$. Here mod-$A$ denotes the abelian category of finite-dimensional right A-modules. Thus the derived category of coherent sheaves on S may be described equivalently in terms of a finite-dimensional algebra determined by the exceptional collection. This is the categorical origin of the quiver description on local surfaces.

Any basic finite-dimensional algebra A is Morita equivalent to the path algebra of a quiver with relations,

$$A \cong \mathbb{C}Q/I, \tag{3.43}$$

where Q is a finite quiver and I is an admissible ideal of relations. In the present setting, the vertices of Q correspond to the objects $\mathcal{E}_i$, or more canonically to the primitive idempotents of A, and the arrows are determined by the spaces of irreducible morphisms between them. Because the collection is strong, one may work directly with the ordinary quiver algebra rather than a dg enhancement. The relations in I encode compositions among the basic morphisms and hence determine the path algebra that reproduces A.

For local Calabi–Yau threefolds of the form

$$X = K_S,$$

the compact B-brane sector is obtained by pushing sheaves on S forward along the zero-section embedding

$$i : S \hookrightarrow X. \tag{3.44}$$

Thus an object $\mathcal{F} \in D^b \operatorname{Coh}(S)$ gives an object $i_*\mathcal{F} \in D^b \operatorname{Coh}(X)$ supported on the compact surface $S \subset X$. In this way the surface theory furnishes the compactly supported part of the local Calabi–Yau category. The fractional branes relevant for quiver constructions are obtained from a dual exceptional collection on S, followed by pushforward to X, and in practice one often includes homological shifts so that the resulting basis is Ext-exceptional and the quiver arrows lie in degree one.

The key computational input is the relation between Ext-groups on the surface and Ext-groups on the local threefold. For $\mathcal{E}, \mathcal{F} \in D^b \operatorname{Coh}(S)$, one has

$$\operatorname{Ext}^k_X(i_*\mathcal{E}, i_*\mathcal{F}) \cong \operatorname{Ext}^k_S(\mathcal{E}, \mathcal{F}) \oplus \operatorname{Ext}^{k-1}_S(\mathcal{E}, \mathcal{F} \otimes K_S), \tag{3.45}$$

which, by Serre duality on the surface, may equally be written as

$$\operatorname{Ext}^k_X(i_*\mathcal{E}, i_*\mathcal{F}) \cong \operatorname{Ext}^k_S(\mathcal{E}, \mathcal{F}) \oplus \operatorname{Ext}^{3-k}_S(\mathcal{F}, \mathcal{E})^*. \tag{3.46}$$

This decomposition shows that the open-string spectrum on X is determined entirely by surface data together with its Serre-dual completion. It is precisely this feature that makes exceptional collections on S so effective in local quiver constructions.

Let

$$\mathbb{E}^\vee = (\mathcal{E}_1^\vee, \dots, \mathcal{E}_r^\vee)$$

be the right dual collection. The corresponding quiver nodes are represented by the pushed-forward objects

$$\mathcal{B}_i := i_*\mathcal{E}_i^\vee[n_i], \tag{3.47}$$

where the integers n_i are chosen so that the basis is Ext-exceptional in the desired chamber. The net number of arrows between two nodes is governed by the antisymmetrized Euler form,

$$\kappa_{ij} := \chi(\mathcal{E}_j^\vee, \mathcal{E}_i^\vee) - \chi(\mathcal{E}_i^\vee, \mathcal{E}_j^\vee) = \langle \mathcal{E}_i^\vee, \mathcal{E}_j^\vee \rangle. \tag{3.48}$$

Equivalently, in the physics convention one reads arrows from the degree-one Ext-groups

$$\mathrm{Ext}^1_X(\mathcal{B}_j, \mathcal{B}_i). \tag{3.49}$$

Thus the antisymmetric matrix κ_{ij} records the chiral arrow content of the quiver.

It is useful to distinguish two closely related layers of structure. The algebra $A = \mathrm{End}_S(M)$ determines a quiver with relations whose derived category is equivalent to $D^b\,\mathrm{Coh}(S)$. After passage to the local Calabi–Yau, the pushed-forward dual basis determines a quiver describing fractional branes and their open strings. The adjacency matrix is read off from the antisymmetrized Euler form, while the full superpotential requires the higher composition data encoded in the relations of the path algebra and, more intrinsically, in the A_∞-structure on the Ext-algebra.

In the toric local Calabi–Yau setting, this superpotential is often far from generic and is fixed by an additional combinatorial structure, namely a brane tiling or dimer model [155]. Concretely, for a wide class of toric Calabi–Yau threefolds, one starts from a bipartite graph G embedded in a two-torus. The dual graph is the quiver Q: its vertices correspond to faces of G, its arrows to edges shared by adjacent faces, and their orientation is determined by the bipartite coloring. The superpotential is then obtained as a signed sum of the oriented face cycles,

$$W = \sum_{F \in Q_2^+} w_F - \sum_{F \in Q_2^-} w_F, \tag{3.50}$$

where Q_2^+ and Q_2^- denote the faces associated with white and black vertices of the bipartite graph, respectively, and w_F is the cyclic word obtained by traversing the boundary of the face F. The corresponding relations are encoded by the Jacobian algebra

$$J(Q, W) = \mathbb{C}Q \,\big/\, (\partial W/\partial a : a \in Q_1)\,. \tag{3.51}$$

Thus, in quivers with oriented loops arising from local toric surfaces, the superpotential is canonically constrained by the brane-tiling geometry rather than chosen arbitrarily.

3.2.3 Some Toric Examples

The general discussion above becomes especially concrete for the toric surfaces that arise most often in local Calabi–Yau geometry. For these surfaces one can write down explicit full strong exceptional collections, compute their Euler matrices and dual collections, and thereby obtain concrete quiver descriptions of the compact B-brane sector on the local threefold $X = K_S$. We record here three basic examples: $\mathbb{P}^2$, $\mathbb{F}_0$, and $\mathbb{F}_1$.

$\mathbb{P}^2$. Let H denote the hyperplane class on $\mathbb{P}^2$. A standard full strong exceptional collection is the Beilinson collection

$$\mathbb{E}_{\mathbb{P}^2} = \big(\mathcal{O}_{\mathbb{P}^2},\, \mathcal{O}_{\mathbb{P}^2}(1),\, \mathcal{O}_{\mathbb{P}^2}(2)\big). \tag{3.52}$$

Its right dual is the Ext-exceptional collection

$$\mathbb{E}^\vee_{\mathbb{P}^2} = \big(\mathcal{O}_{\mathbb{P}^2},\, \Omega^1_{\mathbb{P}^2}(1)[1],\, \mathcal{O}_{\mathbb{P}^2}(-1)[2]\big), \tag{3.53}$$

where $\Omega^1_{\mathbb{P}^2}(1)$ is defined by the Euler sequence

$$0 \longrightarrow \Omega^1_{\mathbb{P}^2}(1) \longrightarrow \mathbb{C}^3 \otimes \mathcal{O}_{\mathbb{P}^2} \longrightarrow \mathcal{O}_{\mathbb{P}^2}(1) \longrightarrow 0. \tag{3.54}$$

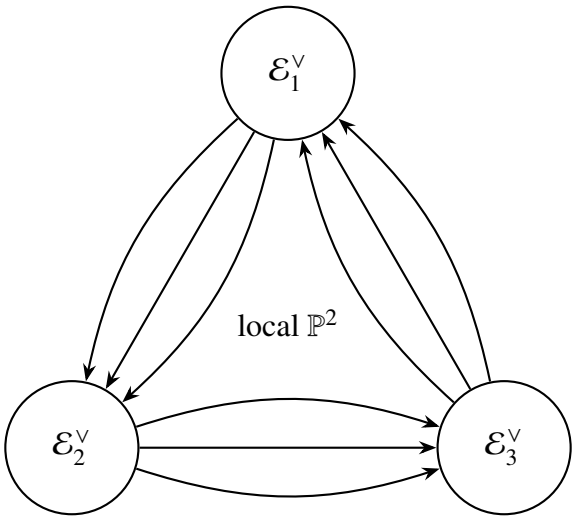


Figure 3.2: Three-node quiver for local $\mathbb{P}^2$, with fractional branes $\mathcal{E}_i^\vee$ at the nodes and three arrows along each edge corresponding to the relevant Ext-group generators.

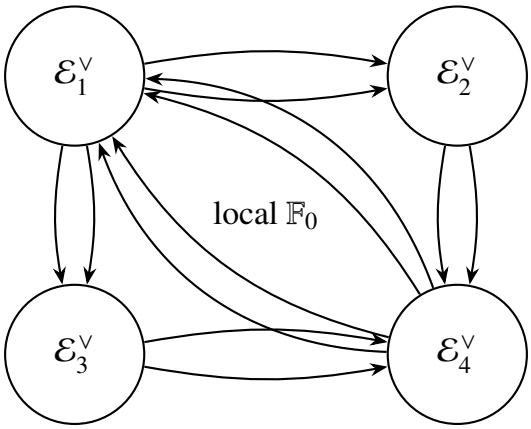


Figure 3.3: Phase-I quiver for local $\mathbb{F}_0$, associated with the fractional brane basis (3.57). The multiplicities of the arrows are determined by the antisymmetrized Euler form (3.61).

The corresponding antisymmetric Euler form is the cyclic 3×3 matrix

$$\kappa^{(\mathbb{P}^2)} = \begin{pmatrix} 0 & 3 & -3 \\ -3 & 0 & 3 \\ 3 & -3 & 0 \end{pmatrix}, \tag{3.55}$$

with three arrows between consecutive nodes, so that after pushforward to $K_{\mathbb{P}^2}$ one recovers the familiar three-node local $\mathbb{P}^2$ quiver (see Figure 3.2) with cubic superpotential.

$\mathbb{F}_0 \cong \mathbb{P}^1 \times \mathbb{P}^1$. Let $\pi_1, \pi_2 : \mathbb{P}^1 \times \mathbb{P}^1 \to \mathbb{P}^1$ be the two projections, and write

$$\mathcal{O}(p, q) := \pi_1^* \mathcal{O}_{\mathbb{P}^1}(p) \otimes \pi_2^* \mathcal{O}_{\mathbb{P}^1}(q). \tag{3.56}$$

A standard cyclic strong exceptional collection is

$$\mathbb{E}^{\mathrm{I}}_{\mathbb{F}_0} = \big(\mathcal{O}(0,0),\, \mathcal{O}(1,0),\, \mathcal{O}(0,1),\, \mathcal{O}(1,1)\big). \tag{3.57}$$

A mutation-equivalent strong exceptional collection, often referred to as a second quiver phase, is

$$\mathbb{E}^{\mathrm{II}}_{\mathbb{F}_0} = \big(\mathcal{O}(0,0),\, \mathcal{O}(1,0),\, \mathcal{O}(1,1),\, \mathcal{O}(2,1)\big). \tag{3.58}$$

At the level of quiver hearts, Arcara and Miles use the mutated collection

$$\mathbb{E}^{0}_{\mathbb{F}_0} = \big(\mathcal{O}_{\mathbb{F}_0},\, G,\, \mathcal{O}_{\mathbb{F}_0}(1,0),\, \mathcal{O}_{\mathbb{F}_0}(0,1)\big), \tag{3.59}$$

where G is a sheaf of rank 3, with

$$c_1(G) = c_1\big(\mathcal{O}_{\mathbb{F}_0}(1,1)\big), \qquad \mathrm{ch}_2(G) = -1.$$

Its right dual collection is

$$\mathbb{F}^{0}_{\mathbb{F}_0} = \big(\mathcal{O}_{\mathbb{F}_0}(-2,-1)[2],\, \mathcal{O}_{\mathbb{F}_0}(-1,-2)[2],\, \mathcal{O}_{\mathbb{F}_0}(-1,-1)[1],\, \mathcal{O}_{\mathbb{F}_0}\big), \tag{3.60}$$

and its extension closure is equivalent to a category of finite-dimensional quiver representations. These collections are related by mutations and provide equivalent descriptions of the same local geometry.

The phase I collection $\mathbb{E}^{\mathrm{I}}_{\mathbb{F}_0}$ generates the following antisymmetric Euler form

$$\kappa^{(\mathbb{F}_0)} = \begin{pmatrix} 0 & 2 & 2 & -4 \\ -2 & 0 & 0 & 2 \\ -2 & 0 & 0 & 2 \\ 4 & -2 & -2 & 0 \end{pmatrix}, \tag{3.61}$$

corresponding to the four-node quiver in Figure 3.3.

$\mathbb{F}_1$. It is convenient to describe $\mathbb{F}_1$ as the blow-up of $\mathbb{P}^2$ at one point:

$$\mathbb{F}_1 \cong \mathrm{Bl}_p\mathbb{P}^2.$$

Let H be the strict transform of the hyperplane class, let E be the exceptional divisor, and define

$$F := H - E. \tag{3.62}$$

Then

$$H^2 = 1, \qquad E^2 = -1, \qquad H\cdot E = 0, \qquad F^2 = 0, \qquad E\cdot F = 1. \tag{3.63}$$

In Hirzebruch notation, E is the negative section and F is the fiber class. A standard full strong exceptional collection is

$$\mathbb{E}_{\mathbb{F}_1} = \big(\mathcal{O}_{\mathbb{F}_1},\, \mathcal{O}_{\mathbb{F}_1}(F),\, \mathcal{O}_{\mathbb{F}_1}(E+F),\, \mathcal{O}_{\mathbb{F}_1}(E+2F)\big) = \big(\mathcal{O},\, \mathcal{O}(H-E),\, \mathcal{O}(H),\, \mathcal{O}(2H-E)\big). \tag{3.64}$$

Arcara and Miles further introduce two mutation-equivalent exceptional collections adapted to quiver hearts,

$$\mathbb{E}^{0}_{\mathbb{F}_1} = \big(\mathcal{O},\, G_1,\, \mathcal{O}(F),\, \mathcal{O}(E+F)\big), \tag{3.65}$$

and

$$\mathbb{E}^{00}_{\mathbb{F}_1} = \big(\mathcal{O},\, \mathcal{O}(E),\, G_2,\, \mathcal{O}(E+F)\big), \tag{3.66}$$

where G_1 and G_2 are rank-two sheaves with

$$c_1(G_1) = c_1(G_2) = E + F, \qquad \mathrm{ch}_2(G_1) = \mathrm{ch}_2(G_2) = -\frac{1}{2}.$$

Their right dual collections are

$$\mathbb{F}^0_{\mathbb{F}_1} = \big(\mathcal{O}_{\mathbb{F}_1}(-E-2F)[2],\, \mathcal{O}_{\mathbb{F}_1}(E)|_E[1],\, \mathcal{O}_{\mathbb{F}_1}(-E-F)[1],\, \mathcal{O}_{\mathbb{F}_1}\big), \tag{3.67}$$

and

$$\mathbb{F}^{00}_{\mathbb{F}_1} = \big(\mathcal{O}_{\mathbb{F}_1}(-E-2F)[2],\, \mathcal{O}_{\mathbb{F}_1}(-F)[1],\, \mathcal{O}_{\mathbb{F}_1}(E)|_E,\, \mathcal{O}_{\mathbb{F}_1}\big). \tag{3.68}$$

Here $\mathcal{O}_{\mathbb{F}_1}(E)|_E$ denotes the restriction of $\mathcal{O}_{\mathbb{F}_1}(E)$ to the exceptional curve E. These hearts are especially useful in the study of Bridgeland stability on $\mathbb{F}_1$, since they realize relevant chambers as quiver regions.

3.3 Scattering diagrams

In this section we study how generalized Donaldson–Thomas invariants vary with the stability condition. Their wall-crossing is encoded by a scattering diagram: a collection of walls in the space of central charges or stability conditions, each equipped with a formal automorphism recording the contribution of the corresponding BPS state. The fundamental requirement is consistency, meaning that the ordered product of these automorphisms is invariant under homotopy of paths avoiding the singular locus. This consistency condition is equivalent to the Kontsevich–Soibelman wall-crossing formula and furnishes the basic algebraic structure underlying the chamber decomposition of the BPS spectrum. This section is based on [21, 50].

3.3.1 Scattering Diagrams and Wall-Crossing Automorphisms

The abstract setting begins with a free abelian group N of finite rank and its dual lattice

$$M := \mathrm{Hom}_{\mathbb{Z}}(N, \mathbb{Z}), \qquad M_{\mathbb{R}} := M \otimes_{\mathbb{Z}} \mathbb{R}. \tag{3.69}$$

One also fixes a positive cone $N^+ \subset N$. In the examples relevant for wall-crossing, one may think of N as a lattice generated by BPS charges or, in quiver-theoretic language, by dimension vectors. We denote lattice elements by Γ.

Let

$$\mathfrak{g} = \bigoplus_{\Gamma \in N^+} \mathfrak{g}_\Gamma \tag{3.70}$$

be an N^+-graded Lie algebra. Its graded completion is

$$\hat{\mathfrak{g}} := \prod_{\Gamma \in N^+} \mathfrak{g}_\Gamma, \tag{3.71}$$

and the corresponding pro-unipotent group is

$$\hat{G} := \exp(\hat{\mathfrak{g}}), \tag{3.72}$$

where the exponential map is understood formally through the Baker–Campbell–Hausdorff series. The wall-crossing automorphisms attached to a scattering diagram take values in this group.

A wall is a codimension-one rational polyhedral cone

$$\mathfrak{d} \subset M_{\mathbb{R}} \tag{3.73}$$

contained in a hyperplane

$$\Gamma^{\perp} := \{\theta \in M_{\mathbb{R}} \mid \theta(\Gamma) = 0\} \tag{3.74}$$

for some primitive $\Gamma \in N^{+}$. To such a wall one assigns an element

$$\Phi_{\mathfrak{D}}(\mathfrak{d}) \in \hat{G} \tag{3.75}$$

lying in the subgroup

$$\exp\Big(\bigoplus_{k\geq 1} \mathfrak{g}_{k\Gamma}\Big) \subset \hat{G}. \tag{3.76}$$

A scattering diagram is then a pair

$$\mathfrak{D} = (\mathcal{S}, \Phi_{\mathfrak{D}}), \tag{3.77}$$

where $\mathcal{S}$ is a collection of such walls and $\Phi_{\mathfrak{D}}$ is the corresponding assignment of group elements. Its support is

$$\mathrm{supp}(\mathfrak{D}) := \bigcup_{\mathfrak{d}\in\mathcal{S}} \mathfrak{d}. \tag{3.78}$$

This is the algebraic object which encodes the chamber structure of the stability space.

The fundamental construction is the path-ordered product. Let $\gamma : [0,1] \to M_{\mathbb{R}}$ be a smooth path. It is called $\mathfrak{D}$-generic if its endpoints lie outside $\mathrm{supp}(\mathfrak{D})$, if it crosses walls transversely, and if it avoids intersections of walls of codimension greater than one. Suppose that γ crosses walls $\mathfrak{d}_1, \ldots, \mathfrak{d}_k$ at times

$$0 < t_1 < \cdots < t_k < 1, \tag{3.79}$$

and that $\mathfrak{d}_i \subset \Gamma_i^{\perp}$ with $\Gamma_i \in N^{+}$ primitive. One then defines

$$\epsilon_i := -\,\mathrm{sign}\left(\frac{\mathrm{d}}{\mathrm{d}t}\,\gamma(t)(\Gamma_i)\Big|_{t=t_i}\right), \tag{3.80}$$

and sets

$$\Phi_{\mathfrak{D}}(\gamma) = \Phi_{\mathfrak{D}}(\mathfrak{d}_k)^{\epsilon_k} \cdots \Phi_{\mathfrak{D}}(\mathfrak{d}_1)^{\epsilon_1}. \tag{3.81}$$

The convention is therefore that walls crossed later along the path appear further to the left in the product.

A scattering diagram $\mathfrak{D}$ is called *consistent* if for any two $\mathfrak{D}$-generic paths γ_1 and γ_2 with the same endpoints one has

$$\Phi_{\mathfrak{D}}(\gamma_1) = \Phi_{\mathfrak{D}}(\gamma_2). \tag{3.82}$$

Thus, for a consistent scattering diagram, the ordered product depends only on the endpoints and not on the chosen generic path. For a closed contractible loop this immediately implies that the corresponding ordered product is the identity. In the abstract algebraic setting this is the defining consistency condition; in the physical setting discussed below it becomes a statement about the invariance of framed BPS generating functions under transport around non-singular contractible loops in moduli space.

It is instructive to record the simplest explicit example. For the A_2 quiver one finds three relevant rays corresponding to Γ_1, Γ_2, and $\Gamma_1 + \Gamma_2$. Consistency implies the pentagon identity

$$\Phi_{\Gamma_2} \circ \Phi_{\Gamma_1} = \Phi_{\Gamma_1} \circ \Phi_{\Gamma_1+\Gamma_2} \circ \Phi_{\Gamma_2}. \tag{3.83}$$

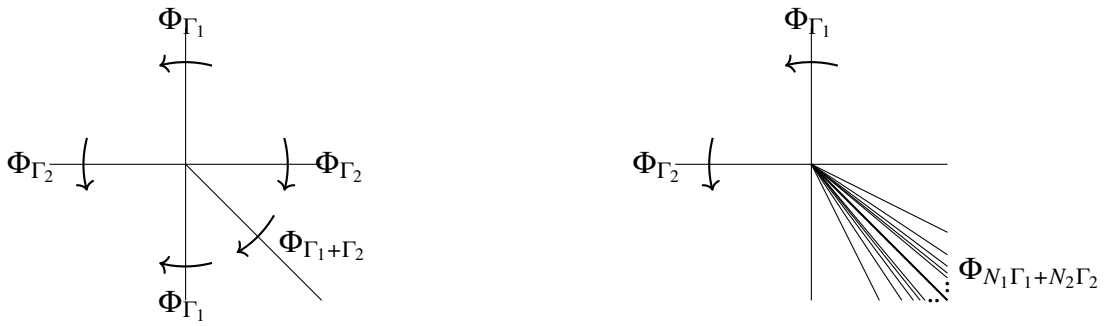


Figure 3.4: Examples of two-dimensional scattering diagrams. Left: the A_2 quiver, with walls corresponding to the three indecomposable representations. Right: the Kronecker quiver, with walls corresponding to the dimension vectors of indecomposable representations. Adapted from [50, Figures 1 and 2].

This identity expresses the fact that the direct crossing of the two initial walls must agree with the alternative path in which a new wall for $\Gamma_1 + \Gamma_2$ is inserted. It is the simplest instance of the general principle that consistency forces the appearance of additional walls.

A second example, already substantially richer, is provided by the Kronecker quiver. In that case one obtains infinitely many rays, and the corresponding consistency relation takes the form

$$\Phi_{\Gamma_2} \circ \Phi_{\Gamma_1} = \Phi_{\Gamma_1} \circ \Phi_{2\Gamma_1+\Gamma_2} \circ \Phi_{3\Gamma_1+2\Gamma_2} \circ \cdots \circ \Phi^{-2}_{\Gamma_1+\Gamma_2} \circ \cdots \circ \Phi_{2\Gamma_1+3\Gamma_2} \circ \Phi_{\Gamma_1+2\Gamma_2} \circ \Phi_{\Gamma_2}. \tag{3.84}$$

This identity shows that consistency can require infinitely many additional walls and can lead to accumulation phenomena even in rank two.

3.3.2 Physical Derivation of the KS Product Formula

The following physical derivation is based on the idea of a *BPS galaxy*, namely a system consisting of a very massive BPS core black hole together with lighter BPS objects orbiting around it, introduced in [21]. In the halo picture, a halo particle of charge Γ_s bound to a core of charge Γ_c has equilibrium radius

$$R = \frac{\langle \Gamma_s, \Gamma_c \rangle}{2\ \mathrm{Im}\big(e^{-\mathrm{i}\alpha_\infty} Z(\Gamma_s, z_\infty)\big)}. \tag{3.85}$$

As usual, z_∞ denotes the asymptotic vector-multiplet moduli, and α_∞ is the phase of the total central charge as measured at infinity. The denominator vanishes when

$$\arg\big[e^{-\mathrm{i}\alpha_\infty} Z(\Gamma_s, z_\infty)\big] = 0, \tag{3.86}$$

at which point the equilibrium radius diverges and the halo becomes marginally unbound. This defines the BPS wall

$$W_{\Gamma_s} = \Big\{ z_\infty \in \mathcal{M} \,\Big|\, \arg\big[e^{-\mathrm{i}\alpha_\infty} Z(\Gamma_s, z_\infty)\big] = 0 \Big\}. \tag{3.87}$$

For a single primitive halo charge one may already see the structure of the wall-crossing operator directly from the halo Fock space. If the halo consists of particles of primitive charge Γ_s, the corresponding Fock-space generating function is

$$G^{\mathrm{Fock}}_{\Gamma_c}(X) = \big(1 - (-1)^{\langle \Gamma_s, \Gamma_c \rangle} X^{\Gamma_s}\big)^{\Omega(\Gamma_s)\,|\langle \Gamma_s, \Gamma_c \rangle|}\, X^{\Gamma_c}, \tag{3.88}$$

which is the framed version of the usual semi-primitive halo formula. In the full problem, however, the effective interior charge seen by a given halo depends on the total charge enclosed by it.

To isolate a genuinely framed problem, one considers a family of cores whose charge scales as

$$\Gamma_c = \Lambda^2\Gamma_0 + \Lambda\Gamma_0' + \Gamma_{c,0}, \qquad \Lambda \to \infty, \tag{3.89}$$

with

$$\langle \Gamma_0, \Gamma_0' \rangle \neq 0, \qquad \langle \Gamma_{c,0}, \Gamma_0 \rangle = 0 = \langle \Gamma_{c,0}, \Gamma_0' \rangle, \tag{3.90}$$

and with Γ_0 chosen so that it supports a single-centered BPS black hole. The associated orbit lattice is

$$L_{\rm orb} := \left\{ \Gamma \in \Gamma \,\middle|\, \langle \Gamma, \Gamma_0 \rangle = 0 = \langle \Gamma, \Gamma_0' \rangle \right\}. \tag{3.91}$$

Only charges in $L_{\rm orb}$ remain as finite orbital excitations in the large-core limit. The anisotropic hierarchy Λ^2, Λ is essential: it removes precisely those tunneling channels which would otherwise lead to mixing with different core sectors.

The reason the large-core limit produces a closed framed system is that nonperturbative mixing becomes entropically suppressed. More precisely, if one compares two galaxy configurations whose core charges differ by a charge δ, the tunneling process between them is weighted by the entropy difference

$$\Delta S = S_{\rm BH}(\Lambda^2\Gamma_0 + \Lambda\Gamma_0' + \Gamma_{c,0}) - S_{\rm BH}(\Lambda^2\Gamma_0 + \Lambda\Gamma_0' + \Gamma_{c,0} - \delta). \tag{3.92}$$

For $\delta \in L_{\rm orb}$ one finds, roughly

$$\Delta S = 2\pi\Lambda^2 \, {\rm Re}\big(Z_{\Gamma_0}\overline{Z_\delta}\big)\big|_{t_*(\Gamma_0)} + O(1) = \pm 2\pi\Lambda^2 \, |Z_{\Gamma_0}| \, m_\delta\big|_{t_*(\Gamma_0)} + O(1), \tag{3.93}$$

so that the tunneling amplitude is exponentially suppressed as $\Lambda \to \infty$. The only exception occurs if a charged particle in $L_{\rm orb}$ becomes massless at the attractor point $t_*(\Gamma_0)$. In the absence of such massless charges, galaxies with different core charge do not mix, and the framed BPS problem becomes a closed quantum system. This physical closure of the Hilbert space is the key ingredient in the derivation of the KS product formula.

Once the core has been decoupled in this sense, one can define framed BPS indices by factoring out the internal states of the core. For orbital charge $\Gamma_{\rm orb} \in L_{\rm orb}$ let $\Omega_C(\Gamma_{\rm orb}; z_\infty)$ denote the corresponding framed galaxy index. The natural generating function is then

$$G_C(X; z_\infty) = \sum_{\Gamma_{\rm orb} \in L_{\rm orb}} \Omega_C(\Gamma_{\rm orb}; z_\infty) \, X^{\Gamma_{c,0}+\Gamma_{\rm orb}}. \tag{3.94}$$

At the attractor point of the core there are no multicentered bound states involving the core, so the generating function reduces to the single monomial

$$G_C(X)\big|_{t_*(\Gamma_c)} = X^{\Gamma_{c,0}}. \tag{3.95}$$

This plays the role of an initial condition: the entire framed spectrum away from the attractor point is reconstructed by composing wall-crossing operators along a path in moduli space.

The halo wall crossing is encoded by a derivation. For any charge Γ define

$$D_\Gamma(X^\mu) := \langle \Gamma, \mu \rangle \, X^\mu. \tag{3.96}$$

Following Andriyash et al., one introduces the refined variables

$$\tau_\Gamma := (-1)^{D_\Gamma} X^\Gamma. \tag{3.97}$$

These satisfy

$$\tau_{\Gamma_1}\tau_{\Gamma_2} = (-1)^{\langle\Gamma_1,\Gamma_2\rangle}\,\tau_{\Gamma_1+\Gamma_2}, \tag{3.98}$$

which is the natural quadratic refinement of the mod-two symplectic pairing.

The primitive wall-crossing operator attached to a halo charge Γ_s is

$$T_{\Gamma_s} := \left(1 - (-1)^{D_{\Gamma_s}} X^{\Gamma_s}\right)^{D_{\Gamma_s}}. \tag{3.99}$$

Equivalently, its action on a monomial is

$$T_{\Gamma_s}(X^\mu) = \left(1 - (-1)^{\langle\Gamma_s,\mu\rangle} X^{\Gamma_s}\right)^{\langle\Gamma_s,\mu\rangle} X^\mu. \tag{3.100}$$

If the wall W_{Γ_s} is crossed in the direction of increasing $\arg\left[e^{-\mathrm{i}\alpha_\infty} Z(\Gamma_s, z_\infty)\right]$ then the framed generating function transforms as

$$G_C(X) \longmapsto U_{\Gamma_s}(z_\infty)\, G_C(X), \tag{3.101}$$

where the full ray operator is

$$U_\Gamma(z_\infty) := \prod_{k\in\mathbb{Z}_{>0}} T_{k\Gamma}^{\Omega(k\Gamma;z_\infty)}. \tag{3.102}$$

The product over positive integers appears because the walls $W_{k\Gamma}$ coincide for all $k > 0$.

The content of the Wall-crossing formulae is obtained by transporting the generating function around a non-singular contractible loop $\mathcal{P} \subset \mathcal{M}$. Suppose that $\mathcal{P}$ crosses walls of marginal stability at points z_i with associated charges Γ_i. Since the loop is contractible, the total composition of wall-crossing operators must act trivially on the framed generating function:

$$\prod_i U_{\Gamma_i}(z_i) \cdot G_C(X) = G_C(X). \tag{3.103}$$

Here the product is ordered according to the sequence of wall crossings, and walls crossed later along the path are written to the left. Since the collection of generating functions obtained by varying the core data is sufficiently rich, one concludes that the operator identity itself must hold:

$$\prod_i U_{\Gamma_i}(z_i) = 1. \tag{3.104}$$

This is the central product formula arising from the galaxy picture. It is the physical counterpart of the consistency condition (3.82) for scattering diagrams.

To recover the usual KS wall-crossing formula from (3.104), one zooms in on a generic codimension-two intersection

$$W_{\Gamma_1} \cap W_{\Gamma_2}, \qquad \langle\Gamma_1,\Gamma_2\rangle \neq 0, \tag{3.105}$$

and considers the charges

$$\Gamma_{r_1,r_2} := r_1\Gamma_1 + r_2\Gamma_2. \tag{3.106}$$

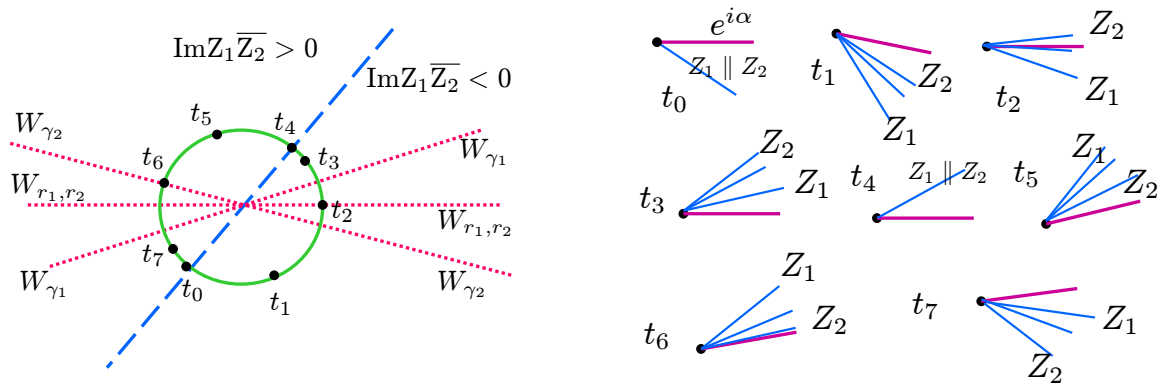


Figure 3.5: Contractible loop and reordering of central-charge rays in the derivation of the KS product formula. Taken from [21, Figures 1 and 2].

For a sufficiently small loop around the intersection, the walls are precisely those associated with such combinations. If one orders the walls by increasing ratio r_1/r_2, then the physical loop argument gives, as before,

$$\prod_{r_1/r_2 \nearrow}^{\leftarrow} T_{r_1,r_2}^{-\Omega^+_{r_1,r_2}} \prod_{r_1/r_2 \nearrow}^{\leftarrow} T_{r_1,r_2}^{\Omega^-_{r_1,r_2}} = 1, \tag{3.107}$$

where

$$T_{r_1,r_2} := T_{\Gamma_{r_1,r_2}}, \qquad \Omega^{\pm}_{r_1,r_2} := \Omega^{\pm}(\Gamma_{r_1,r_2}), \tag{3.108}$$

and where increasing values of r_1/r_2 are written to the left. Using the relation between this slope ordering and the ordering of the phases of the corresponding central charges, one may rewrite the same identity in the more familiar form

$$\prod_{\arg Z \nearrow}^{\curvearrowright} T_{r_1,r_2}^{\Omega^+_{r_1,r_2}} = \prod_{\arg Z \nearrow}^{\curvearrowleft} T_{r_1,r_2}^{\Omega^-_{r_1,r_2}}. \tag{3.109}$$

3.3.3 From Scattering-Diagram Consistency to the KS Formula

The original Kontsevich–Soibelman formalism is naturally phrased in a motivic or quantum torus

$$\hat{X}^{\Gamma_1}\hat{X}^{\Gamma_2} = \mathbb{L}^{\frac{1}{2}\langle\Gamma_1,\Gamma_2\rangle}\hat{X}^{\Gamma_1+\Gamma_2}. \tag{3.110}$$

In the "semi-classical" limit, $q^{1/2} \to -1$, one obtains a commutative algebra of formal generators, still denoted here by X^{Γ}, with twisted multiplication law

$$X^{\Gamma_1}X^{\Gamma_2} = (-1)^{\langle\Gamma_1,\Gamma_2\rangle}\, X^{\Gamma_1+\Gamma_2}, \tag{3.111}$$

and Poisson bracket

$$\{X^{\Gamma_1}, X^{\Gamma_2}\} = (-1)^{\langle\Gamma_1,\Gamma_2\rangle}\,\langle\Gamma_1,\Gamma_2\rangle\, X^{\Gamma_1+\Gamma_2}. \tag{3.112}$$

This Poisson torus is the classical limit relevant for numerical DT invariants and for the wall-crossing identities, as aluded to in Section 2.11.

The KS wall-crossing formula is most naturally expressed in terms of sector elements. Let $V \subset \mathbb{C}$ be a strict sector in the central-charge plane. The associated KS element is

$$A_V = \prod_{\Gamma \in C(V,Z)}^{\curvearrowright} \exp\left(-\Omega(\Gamma) \sum_{n=1}^{\infty} \frac{X^{n\Gamma}}{n^2}\right), \tag{3.113}$$

where the product is taken in clockwise order of the rays $\mathbb{R}_{>0} Z(\Gamma)$. If $V = V_1 \sqcup V_2$ is a decomposition into strict sectors in clockwise order, then these elements satisfy the factorization property

$$A_V = A_{V_1} A_{V_2}. \tag{3.114}$$

This factorization property is the abstract form of wall crossing. It says that the same total sector element admits different ordered factorizations when the stability condition is varied and the ordering of rays changes.

At this point the dictionary between the three languages can be stated explicitly. In the scattering-diagram formalism one has walls

$$\mathfrak{d} \subset M_{\mathbb{R}} \qquad \text{with automorphisms} \qquad \Phi_{\mathfrak{D}}(\mathfrak{d}) \in \hat{G}. \tag{3.115}$$

In the physical galaxy picture one has BPS walls

$$W_\Gamma \subset \mathcal{M} \qquad \text{with operators} \qquad U_\Gamma = \prod_{k \geq 1} T_{k\Gamma}^{\Omega(k\Gamma)}. \tag{3.116}$$

In the KS formalism one has rays

$$\mathbb{R}_{>0} Z(\Gamma) \subset \mathbb{C} \qquad \text{with sector factors} \qquad \exp\left(-\Omega(\Gamma) \sum_{n \geq 1} \frac{X^{n\Gamma}}{n^2}\right). \tag{3.117}$$

The content of the preceding discussion is that these are not three unrelated constructions. Rather, $\Phi_{\mathfrak{D}}(\mathfrak{d})$ is the abstract algebraic version of the physical ray operator U_Γ, and the sector element A_V is the ordered product of the same ray operators over all charges whose central charges lie in the sector V.

The equivalence between scattering-diagram consistency and the KS formula is now straightforward to state. Consistency means that the ordered product of wall automorphisms depends only on the endpoints of a generic path. For a contractible loop, this means that the product is the identity. In the galaxy language, the same statement is (3.104), obtained from the requirement that the framed generating function be single-valued after transport around a contractible loop. In the Poisson-torus language, this identity becomes the equality of the two ordered products in (3.109), or equivalently the equality of two factorizations of the same sector element A_V.

It is worth noting again that the A_2 and Kronecker quiver cases displayed earlier are concrete manifestations of this equivalence. In the A_2 case, the single additional wall for $\Gamma_1 + \Gamma_2$ is precisely what is required for path independence, and the resulting pentagon identity is the simplest KS re-factorization. In the Kronecker case, the infinite tower of walls realizes a more elaborate re-factorization pattern, again dictated entirely by consistency.

3.4 Local mirror symmetry and Pi-Stability

For the toric local Calabi–Yau threefolds studied in this thesis, mirror symmetry produces an explicit B-model description in terms of algebraic families of curves, period integrals, and Picard–Fuchs systems whose analytic continuation encodes the global structure of the complex structure moduli space. Throughout, K_S denotes the total space of the canonical bundle over a toric surface S; the examples of primary interest are $K_{\mathbb{P}^2}$, $K_{\mathbb{F}_0}$, and $K_{\mathbb{F}_1}$. The complexified Kähler parameters of the A-model are written as

$$t^a = B^a + \mathrm{i}J^a \,, \tag{3.118}$$

with $a = 1, \ldots, k$. On the B-model side, the algebraic complex structure moduli are z^a, with logarithmic derivatives

$$\Theta_a := z^a \partial_{z^a} \,. \tag{3.119}$$

Near the large complex structure limit, the flat coordinates extracted from periods are T^a, and one sets $Q^a := e^{2\pi \mathrm{i} T^a}$. The mirror map $z^a = z^a(Q)$ then identifies the two descriptions. [60, 111, 112]

3.4.1 From GLSM to the local mirror geometry

The local mirror geometry is obtained by dualizing the two-dimensional $(2,2)$ GLSM that defines K_S. The model has a $U(1)^k$ gauge group with $N = k + 3$ chiral multiplets Φ_i of integer charges Q_i^a, subject to the D-term constraints

$$\sum_{i=1}^{N} Q_i^a |\phi_i|^2 = r^a \,, \qquad a = 1, \ldots, k \,, \tag{3.120}$$

and the Calabi–Yau condition

$$\sum_{i=1}^{N} Q_i^a = 0 \qquad \text{for each } a \,. \tag{3.121}$$

In the Hori–Vafa construction [111], the phases of the charged multiplets are dualized to twisted chiral superfields Y_i, yielding the exact twisted superpotential

$$\widetilde{W} = \sum_{a=1}^{k} \Sigma_a \left(\sum_{i=1}^{N} Q_i^a Y_i - t^a \right) + \mu \sum_{i=1}^{N} e^{-Y_i} \,, \tag{3.122}$$

where $t^a = r^a + \mathrm{i}\theta^a$ are the complexified FI parameters. Integrating out Σ_a imposes the constraints $\sum_i Q_i^a Y_i = t^a$, which in the variables $x_i := e^{-Y_i}$ become

$$\prod_{i=1}^{N} x_i^{Q_i^a} = e^{-t^a} \,, \qquad a = 1, \ldots, k \,. \tag{3.123}$$

Solving these relations reduces the geometry to a conic bundle over $(\mathbb{C}^*)^2$,

$$w_+ w_- = H(x, y; z^a) \,, \tag{3.124}$$

whose zero section is the affine mirror curve $H(x, y; z^a) = 0$. The algebraic complex structure parameters are

$$z^a = (-1)^{Q_0^a} \prod_{i=1}^{k+3} x_i^{Q_i^a} \,. \tag{3.125}$$

The period integrals of the holomorphic three-form reduce, in the local model, to integrals of the meromorphic one-form

$$\lambda = \log(y)\, \frac{\mathrm{d}x}{x} \tag{3.126}$$

over one-cycles $\gamma \in H_1(H = 0, \mathbb{Z})$:

$$\Pi_\gamma(z) = \oint_\gamma \lambda \,. \tag{3.127}$$

The mirror curve and its differential thus encode the full special geometry of the local B-model. [60, 111, 113]

3.4.2 GKZ systems, periods, and the mirror map

The periods (3.127) are annihilated by GKZ operators built directly from the charge matrix:

$$\mathcal{D}_a = \prod_{Q_i^a > 0} \partial_{x_i}^{Q_i^a} - \prod_{Q_i^a < 0} \partial_{x_i}^{-Q_i^a} \,, \qquad a = 1, \dots, k \,. \tag{3.128}$$

Passing to the moduli z^a via the chain rule

$$\theta_i := x_i \partial_{x_i} = \sum_{a=1}^{k} Q_i^a \Theta_a \tag{3.129}$$

converts the GKZ system into a Picard–Fuchs system in the Θ_a.

Near the large complex structure point $z^a = 0$, the periods admit a Frobenius expansion. The deformed fundamental solution is

$$w_0(z, \rho) = \sum_{n_a \geq 0} \frac{\prod_{a=1}^{k} \left((-1)^{Q_0^a} z^a \right)^{n_a + \rho_a}}{\prod_{i=1}^{k+3} \Gamma\!\left(1 + \sum_{a=1}^{k} Q_i^a (n_a + \rho_a)\right)} \,, \tag{3.130}$$

where ρ_a are auxiliary deformation parameters. The flat coordinates are

$$T^a = \frac{1}{2\pi \mathrm{i}} \frac{\partial}{\partial \rho_a} w_0(z, \rho) \bigg|_{\rho = 0} \,, \tag{3.131}$$

the higher logarithmic solutions are

$$X^{(a_1 \cdots a_n)} = \frac{1}{(2\pi \mathrm{i})^n} \frac{\partial^n w_0(z, \rho)}{\partial \rho_{a_1} \cdots \partial \rho_{a_n}} \bigg|_{\rho = 0} \,, \tag{3.132}$$

and the mirror map is obtained by exponentiation and formal inversion,

$$Q^a = e^{2\pi \mathrm{i} T^a} \,, \qquad z^a = z^a(Q) \,. \tag{3.133}$$

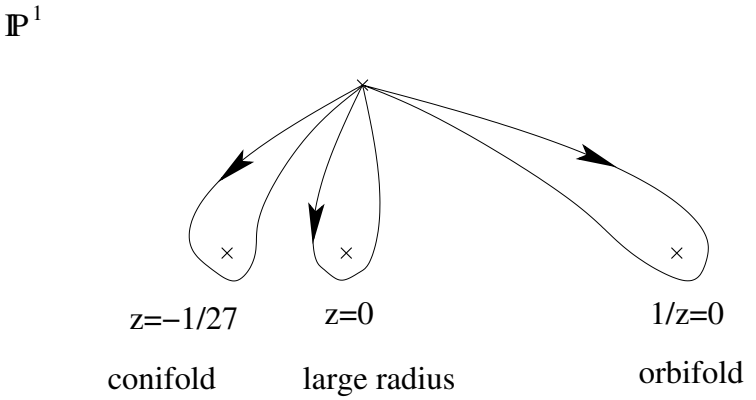


Figure 3.6: One-dimensional moduli space of local $K_{\mathbb{P}^2}$, showing the large-radius point $z = 0$, the conifold point $z = -1/27$, and the orbifold point $1/z = 0$, together with generators of the corresponding monodromies. Taken from [105, Figure 1].

Local $K_{\mathbb{P}^2}$. The charge vector is $Q = (-3, 1, 1, 1)$, giving the one-parameter Picard–Fuchs operator

$$\mathcal{D} = \Theta^3 + 3z(3\Theta - 2)(3\Theta - 1)\Theta\,. \tag{3.134}$$

The discriminant is

$$\Delta = 1 + 27z\,, \tag{3.135}$$

so the moduli space has three distinguished loci: the large-radius point $z = 0$, the conifold point $z = -1/27$, and the orbifold point at $1/z = 0$. The large-radius mirror map begins as

$$z(Q) = Q - 6Q^2 + 9Q^3 + \cdots\,. \tag{3.136}$$

A period basis adapted to special geometry is

$$\hat{\Pi} = \begin{pmatrix} T_D \\ T \\ 1 \end{pmatrix} = \begin{pmatrix} -9\,\partial_T F_0 \\ T \\ 1 \end{pmatrix}, \tag{3.137}$$

in which the monodromies around the three singular loci generate $\Gamma_0(3)$. [60, 112]

Local $K_{\mathbb{F}_0}$. For $K_{\mathbb{F}_0} \cong \mathcal{O}(-2,-2) \to \mathbb{P}^1 \times \mathbb{P}^1$, the charge vectors are

$$Q_i^1 = (-2, 1, 0, 1, 0)\,, \qquad Q_i^2 = (-2, 0, 1, 0, 1)\,, \tag{3.138}$$

yielding the two-parameter Picard–Fuchs operators

$$\mathcal{D}_1 = \Theta_1^2 - 2z^1(\Theta_1 + \Theta_2)(1 + 2\Theta_1 + 2\Theta_2)\,, \tag{3.139}$$

$$\mathcal{D}_2 = \Theta_2^2 - 2z^2(\Theta_1 + \Theta_2)(1 + 2\Theta_1 + 2\Theta_2)\,, \tag{3.140}$$

with discriminant

$$\Delta = 1 - 8(z^1 + z^2) + 16(z^1 - z^2)^2\,. \tag{3.141}$$

For later use, a convenient conifold chart is

$$z_c^1 = 1 - \frac{z^1}{z^2}\,, \qquad z_c^2 = 1 - 8z^2 - 8z^1\,, \tag{3.142}$$

with z_c^2 normal to the discriminant and z_c^1 tangential to it. [105, 115]

Figure 3.7: Placeholder: resolved moduli space of local $K_{\mathbb{F}_0}$, showing the large-radius divisors L_1, L_2, the conifold divisors E, C, and the additional components F_1, F_2. [105]

Local $K_{\mathbb{F}_1}$. For $K_{\mathbb{F}_1} \cong \mathcal{O}(-2,-3) \to \mathbb{F}_1$, one may take

$$Q_i^1 = (-2,1,0,1,0)\,, \qquad Q_i^2 = (-1,0,1,-1,1)\,, \tag{3.143}$$

giving

$$\mathcal{D}_1 = \Theta_1(\Theta_1 - \Theta_2) - z^1(2\Theta_1 + \Theta_2)(1 + 2\Theta_1 + 2\Theta_2)\,, \tag{3.144}$$

$$\mathcal{D}_2 = \Theta_2^2 - z^2(\Theta_2 - \Theta_1)(2\Theta_1 + \Theta_2)\,, \tag{3.145}$$

with discriminant

$$\Delta = (1 - 4z^1)^2 - z^2(1 - 36z^1 + 27z^1z^2)\,. \tag{3.146}$$

The Frobenius analysis near $z^1 = z^2 = 0$ proceeds as in the general case and produces the flat coordinates and mirror map. The analytic continuation of the periods away from large radius is particularly important for the physical ω-stability slice studied in Chapter 5. [105, 115]

3.4.3 Analytic continuation and moduli space singularities

The global structure of the complex structure moduli space $\mathcal{M}$ is governed by the discriminant locus $\Delta(z) = 0$, which detects degenerations of the mirror curve. For $K_{\mathbb{P}^2}$ the singular set consists of the three points identified from (3.135); for $K_{\mathbb{F}_0}$ and $K_{\mathbb{F}_1}$ the discriminant defines a divisor in the two-dimensional moduli space with correspondingly richer structure. [60, 105, 112]

Analytic continuation between patches of $\mathcal{M}$ is carried out efficiently via Mellin–Barnes integral representations. In the one-parameter case one writes

$$w_0(x) = \frac{1}{2\pi\mathrm{i}} \int_C \mathrm{d}s\, \frac{\Gamma(-s)\Gamma(4s+1)(-1)^s}{\Gamma(s+1)^3}\, x^s\,, \tag{3.147}$$

where the contour C separates poles corresponding to different expansion regions. Closing in one direction recovers the Frobenius expansion near the large-radius point; closing in the other direction yields the expansion adapted to the orbifold region. The technique extends to the multi-parameter examples. [56, 112]

At the level of period vectors, continuation between singular loci produces connection matrices:

$$\Pi^{(\infty)} = N\,\Pi^{(0)}\,, \tag{3.148}$$

and monodromy matrices M_0, M_∞, M_{conifold} around the respective singular points. In the local $K_{\mathbb{P}^2}$ example these generate $\Gamma_0(3)$; in the multi-parameter cases one obtains monodromy representations associated to loops around the components of the discriminant divisor. [60, 112]

To interpret the monodromy action integrally, one works with a basis compatible with the A-model brane lattice via the monodromy-invariant pairing of Hosono [112, 113]:

$$I:\ K_{\text{hol}}(X) \otimes H_3(X^\vee, \mathbb{Z}) \to \mathbb{Q}\,. \tag{3.149}$$

In this integral basis, monodromy acts by Fourier–Mukai transformations. The translation between the analytic basis adapted to prepotential computations and this integral basis depends on the

Figure 3.8: Placeholder: local geometry of the conifold coordinates $z_c^1 = 0$ and $z_c^2 = 0$ for local $K_{\mathbb{F}_0}$, showing their intersection with the discriminant locus $\Delta = 0$. [105]

chosen symplectic pairing and must be matched to the sign conventions used for electromagnetic charges elsewhere in the thesis.

Near a conifold branch, the flat coordinate t_c normal to the discriminant vanishes linearly:

$$t_c \sim 0 \qquad \text{as } \Delta \to 0\,. \tag{3.150}$$

The higher-genus free energies satisfy the conifold gap condition

$$F_g^c = \frac{B_{2g}}{2g(2g-2)\,t_c^{2g-2}} + O(t_c^0)\,, \qquad g \geq 2\,, \tag{3.151}$$

with B_{2g} the Bernoulli numbers. The absence of intermediate negative powers of t_c is the essential content: it supplies the polar boundary condition for the direct-integration approach to the holomorphic anomaly equations. [105, 115]

Loci at which the Picard–Fuchs system appears singular while the physical monodromy is nevertheless trivial,

$$M_{\text{app}} = \mathbf{1}\,, \tag{3.152}$$

are apparent singularities of the differential presentation rather than genuine singular points of the moduli space.

3.4.4 Coulomb branch and the u-plane

The same moduli space admits a reformulation as the base of an elliptic fibration. For the rank-one systems obtained from the local toric models above, the Coulomb branch is a complex curve with coordinate u, and the low-energy effective theory is governed by a holomorphic prepotential $\mathcal{F}(a)$ with dual period and gauge coupling

$$a_D = \frac{\partial \mathcal{F}}{\partial a}\,, \qquad \tau = \frac{\partial^2 \mathcal{F}}{\partial a^2} = \frac{\partial a_D}{\partial a}\,. \tag{3.153}$$

The special Kähler metric is

$$ds^2 = \mathrm{Im}(\tau)\,|da|^2 = -\frac{\mathrm{i}}{2}\big(da_D\, d\bar{a} - da\, d\bar{a}_D\big)\,, \qquad \mathrm{Im}(\tau) > 0\,. \tag{3.154}$$

For this section, we write the electromagnetic charge of a rank-one BPS state as $\Gamma = (P, Q)$, the Dirac pairing as $\langle \Gamma_1, \Gamma_2 \rangle = P_1 Q_2 - Q_1 P_2$, and the central charge as

$$Z(\Gamma, u) = P\, a_D(u) + Q\, a(u) + \sum_i q_i^F \mu_i + n_{KK}\,, \tag{3.155}$$

with the BPS bound $M \geq |Z(\Gamma, u)|$. [65, 171]

The period vector

$$\Pi(u) = \begin{pmatrix} a_D(u) \\ a(u) \end{pmatrix} \tag{3.156}$$

is a section of a rank-two holomorphic affine bundle over the Coulomb branch with structure group $\mathbb{C}^2 \rtimes SL(2,\mathbb{Z})$. Its multi-valuedness is encoded by monodromy: analytic continuation around a singular point u_* acts as

$$\Pi \longmapsto M_* \, \Pi + b_* \,, \qquad M_* \in SL(2,\mathbb{Z}) \,. \tag{3.157}$$

The physical periods are obtained by integrating the Seiberg–Witten differential λ_{SW} over a symplectic basis $\gamma_1, \gamma_2 \in H_1(E_u, \mathbb{Z})$:

$$a_D(u) = \oint_{\gamma_1} \lambda_{SW} \,, \qquad a(u) = \oint_{\gamma_2} \lambda_{SW} \,, \tag{3.158}$$

and the exact gauge coupling is the period ratio

$$\tau(u) = \frac{da_D/du}{da/du} = \frac{\int_{\gamma_1} \omega_u}{\int_{\gamma_2} \omega_u} \,, \qquad \mathrm{Im}(\tau) > 0 \,. \tag{3.159}$$

The compactified Coulomb branch is a rational elliptic surface, with the elliptic fibration

$$E \longrightarrow \mathcal{S} \xrightarrow{\pi} \mathbb{P}^1_u \,, \tag{3.160}$$

written in minimal Weierstrass form as

$$y^2 = 4x^3 - g_2(u) x - g_3(u) \,, \tag{3.161}$$

with discriminant and absolute invariant

$$\Delta(u) = g_2(u)^3 - 27 g_3(u)^2 \,, \qquad J(u) = \frac{g_2(u)^3}{\Delta(u)} \,, \qquad j(\tau) = 1728 \, J(u) \,. \tag{3.162}$$

There is also a useful universal Picard–Fuchs equation in the invariant J:

$$\frac{d^2\Omega}{dJ^2} + \frac{1}{J}\frac{d\Omega}{dJ} + \frac{31J - 4}{144 J^2 (1-J)^2} \, \Omega = 0 \,, \tag{3.163}$$

with physical periods related by

$$\omega_a(u) = \frac{\sqrt{g_2(u)}}{\sqrt{g_3(u)}} \, \Omega(J(u)) \,. \tag{3.164}$$

3.4.5 Kodaira classification and rational elliptic surface constraints

At a singular point u_*, the degeneration type is determined by the vanishing orders $\mathrm{ord}_{u_*}(g_2)$, $\mathrm{ord}_{u_*}(g_3)$, $\mathrm{ord}_{u_*}(\Delta)$, and Kodaira's theorem associates a unique fiber type to each combination. The relevant entries for rank-one Seiberg–Witten geometry are collected in Table 3.1.

At an I_1 singularity, a single hypermultiplet of charge $\Gamma = (P, Q)$ becomes massless with local monodromy

$$M_\Gamma = \begin{pmatrix} 1 + PQ & Q^2 \\ -P^2 & 1 - PQ \end{pmatrix} . \tag{3.165}$$

Table 3.1: Kodaira singular fibers for rank-one Seiberg–Witten geometries. Monodromy entries are representatives of conjugacy classes in $SL(2,\mathbb{Z})$.

Fiber	$\mathrm{ord}(g_2)$	$\mathrm{ord}(g_3)$	$\mathrm{ord}(\Delta) = e(F_v)$	M_*	physics
I_k	0	0	k	T^k	k mutually local light states
II	≥ 1	1	2	ST	strongly-coupled cusp
III	1	≥ 2	3	S	strongly-coupled cusp
IV	≥ 2	2	4	$(ST)^{-1}$	strongly-coupled cusp
I_k^*	2	3	$k+6$	$-T^k$	asymptotic weak-coupling fiber
IV^*	≥ 3	4	8	$-(ST)^{-1}$	enhanced flavor symmetry
III^*	3	≥ 5	9	$-S$	enhanced flavor symmetry
II^*	≥ 4	5	10	$-ST$	enhanced flavor symmetry

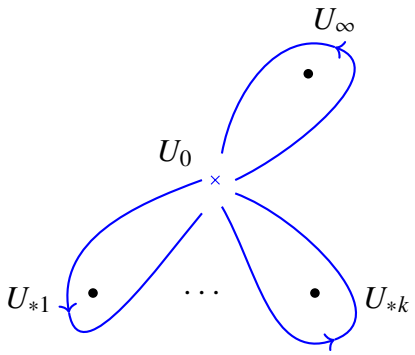


Figure 3.9: Paths γ_v generating the fundamental group of the U-plane. The path around infinity is equal to minus the sum of all the other paths, $\gamma_\infty = -(\gamma_1 + \cdots + \gamma_k)$. Taken from [65, Figure 1].

More generally, an I_k fiber has monodromy conjugate to T^k and corresponds to k mutually local light states in a suitable duality frame. With branch cuts oriented so that monodromy acts from the left on the column vector $\Pi = (a_D, a)^T$, the global constraint around the compactified u-plane is

$$M_\infty \prod_{\ell=1}^{k} M_{*\ell} = I\,. \tag{3.166}$$

Since the compactified total space is a rational elliptic surface, the set of singular fibers is constrained globally by

$$\sum_v e(F_v) = 12\,, \qquad \sum_v \mathrm{rank}(F_v) \leq 8\,, \tag{3.167}$$

where $e(F_v) = \mathrm{ord}_{u_{*,v}}(\Delta)$ and $\mathrm{rank}(F_v)$ is the rank of the ADE algebra associated to the reducible part of the fiber, equivalently $m_v - 1$ if the resolved fiber has m_v irreducible components. The fiber at infinity F_∞ encodes the asymptotic weak-coupling regime and determines the rank of the non-abelian flavor algebra via

$$\mathrm{rank}(\mathfrak{g}_F) = 8 - \mathrm{rank}(F_\infty)\,, \tag{3.168}$$

while the free part of the Mordell–Weil group satisfies

$$\mathrm{rk}(\Phi) = 8 - \mathrm{rank}(T)\,, \tag{3.169}$$

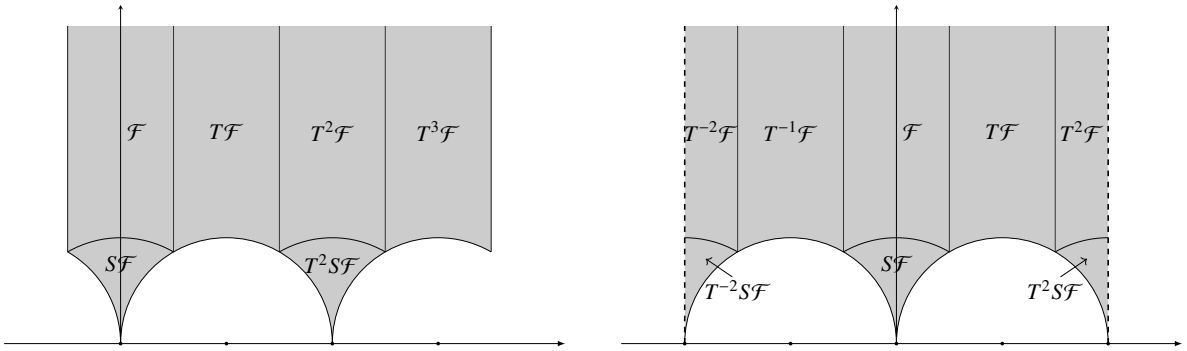


Figure 3.10: Fundamental domains for $\Gamma^0(4)$ governing the modular parametrization of the pure $SU(2)$ Coulomb branch. The left panel shows a standard choice of fundamental domain, with width-one cusps at $\tau = 0$ and $\tau = 2$ and the width-four cusp at $\tau = i\infty$. The right panel shows an equivalent presentation in which the cusp at $\tau = \pm 2$ is split, with the branch cut of the periods indicated by the dashed line. Adapted from [65, Figure 4].

with T the root lattice of the reducible fiber components. For the standard 4d $SU(2)$ families one has $F_\infty = I^*_{4-N_f}$, so that the pure theory corresponds to $F_\infty = I^*_4$ with two finite I_1 fibers. For circle-compactified 5d rank-one theories the large-volume monodromy takes the form

$$M_\infty = T^{9-n} = \begin{pmatrix} 1 & 9-n \\ 0 & 1 \end{pmatrix}. \tag{3.170}$$

3.4.6 Modular parametrization of the u-plane

In favorable cases the Coulomb branch admits an identification

$$\Gamma\backslash\mathfrak{H} \;\cong\; \mathbb{P}^1_u \setminus \{\text{singular points}\}\,, \tag{3.171}$$

where $\Gamma \subset PSL(2,\mathbb{Z})$ is a finite-index subgroup. When the quotient has genus zero, the coordinate $u(\tau)$ is a Hauptmodul for Γ, and the geometry of the Coulomb branch is equivalent to that of a modular curve.

This identification is formalized by Shioda's elliptic modular surface. If $\tilde{u} \in \mathcal{U}$ is a lift of $u \in \Delta_\Gamma$ to the universal cover, and $\omega : \mathcal{U} \to \mathfrak{H}$ is the period-ratio map, then

$$J_\Gamma(\pi(\tilde{u})) = j(\omega(\tilde{u}))\,. \tag{3.172}$$

Here $J_\Gamma(u)$ is a function on the physical base curve while $j(\tau)$ is the standard modular function on the upper half-plane; the lifted coordinate $\tilde{u}$ is needed because the period ratio is defined on the universal cover. [65, 172]

Cusps of $\Gamma\backslash\mathfrak{H}$ correspond to multiplicative singular fibers. A width-n cusp at $\tau = Q/P \in \mathbb{Q}$ gives a local monodromy conjugate to T^n and corresponds to n light BPS states of charge

$$\pm(P, -Q)\,, \tag{3.173}$$

with monodromy

$$M_{\text{cusp}} = \sigma\, T^n\, \sigma^{-1}\,, \tag{3.174}$$

where $\sigma \in PSL(2,\mathbb{Z})$ sends $i\infty$ to Q/P. The modular picture thus reproduces the exact monodromy of the Seiberg–Witten geometry and identifies the light BPS charges from cusp locations. [65, 139]

The basic example is the pure $SU(2)$ theory, with monodromy group $\Gamma_0(4)$ and Hauptmodul

$$u(\tau) = 1 + \frac{1}{8}\left(\frac{\eta(\tau/4)}{\eta(\tau)}\right)^8 = \frac{\vartheta_2(\tau)^4 + \vartheta_3(\tau)^4}{2\,\vartheta_2(\tau)^2\vartheta_3(\tau)^2}\,. \tag{3.175}$$

The quotient $\Gamma_0(4)\backslash\mathfrak{H}$ has two width-one cusps at $\tau = 0$ and $\tau = 2$, describing the monopole and dyon loci with charges $\pm(1,0)$ and $\pm(1,-2)$, and a width-four cusp at $\tau = i\infty$ mapping to the I_4^* fiber at $u = \infty$. [65, 139, 171]

4

BPS Dendroscopy on Local $\mathbb{P}^1 \times \mathbb{P}^1$

This chapter is based entirely on the paper *BPS Dendroscopy on Local* $\mathbb{P}^1 \times \mathbb{P}^1$ [132], written in collaboration with Bruno Le Floch and Boris Pioline, and is reproduced here with only minor editorial changes. The main object of study is the BPS spectrum of D-brane bound states on the non-compact toric Calabi–Yau threefold local $\mathbb{P}^1 \times \mathbb{P}^1$. The chapter constructs the corresponding scattering diagram in several complementary regimes: near the orbifold point using the quiver description, on the large-volume slice, and along the physical slice of Π-stability conditions. It then uses these descriptions to analyze attractor indices and wall-crossing, and to formulate a proof of the Split Attractor Flow Tree Conjecture in this example for a restricted range of the central-charge phase.

4.1 Introduction

The BPS spectrum in type II string theory compactified on a Calabi-Yau (CY) threefold X has been a favorite playground for physicists and mathematicians alike. One reason is that the indices $\Omega_\sigma(\gamma)$ counting stable BPS states with fixed electromagnetic charge γ have a rigorous definition, as the generalized Donaldson-Thomas invariants associated to the derived category of coherent sheaves $\mathcal{C} = D^b \operatorname{Coh} X$. They depend on a choice of Bridgeland stability condition[1] $\sigma = (Z, \mathcal{A}) \in \operatorname{Stab} \mathcal{C}$, which formalizes and generalizes the physical notion of stability [49]. For compact CY threefolds, direct computations of DT invariants are generally out of reach, and explicit results typically rely on wall-crossing from an empty chamber in $\operatorname{Stab} \mathcal{C}$ where $\Omega_\sigma(\gamma)$ vanishes (see e.g. [13, 92–94, 178] for recent progress using this strategy). Instead, for non-compact toric CY threefolds, the category $\mathcal{C}$ is isomorphic to the derived category of representations of a quiver with potential $D^b \operatorname{Rep}(Q, W)$, and one may hope to describe the complete BPS spectrum at any point $\sigma \in \operatorname{Stab} \mathcal{C}$, or at least be able to compute the BPS index $\Omega_\sigma(\gamma)$ at any such point. This in turn determines the BPS spectrum of the five-dimensional superconformal field theory on $\mathbb{R}^{3,1} \times S^1$ arising in the reduction of M-theory on X, after compactifying further on a circle down to 3+1 dimensions.

In [47], we carried out this program for $X = K_{\mathbb{P}^2}$, the total space of the canonical bundle over the projective plane, also known as local $\mathbb{P}^2$; let us briefly recall the salient results. In this case, since $b_2(\mathbb{P}^2) = 1$ the space of stability conditions has complex dimension 3, but the BPS spectrum is invariant under the action[2] of $GL(2, \mathbb{R})^+$, effectively leaving a complex one-dimensional space of inequivalent stability conditions. We found that the BPS spectrum can be efficiently encoded into the scattering diagram $\mathcal{D}_\psi \subset \operatorname{Stab} \mathcal{C}$, defined as the union of the loci

[1] Here Z is the usual central charge determining the mass of BPS states, and $\mathcal{A}$ is the 'heart', an Abelian subcategory of $\mathcal{C}$ locally determined by Z and and determining the allowed decays.

[2] More precisely, the space of stability conditions carries an action of the universal cover $\widetilde{GL(2, \mathbb{R})^+}$, but to avoid cluttering we omit the tilde.

(also called rays) $\mathcal{R}_\psi(\gamma)$ where there exist semi-stable objects of central charge of fixed phase $Z(\gamma) \in \mathrm{i}e^{\mathrm{i}\psi}\mathbb{R}^+$, decorated at every point with a certain automorphism of the quantum torus algebra encoding the refined BPS index $\Omega_\sigma(\gamma, y)$. This concept, introduced in the context of quivers in [50], is the natural framework for the attractor flow tree representation of BPS bound states [16, 25, 74, 75], at least in the context of non-compact CY threefolds where the phase ψ is constant along the flow [47].

Specifically, in *loc. cit.* we constructed the scattering diagram $\mathcal{D}_\psi$ along the large volume slice Λ, generalizing the analysis of [45] to arbitrary phase ψ, and along the physical slice Π singled out by mirror symmetry. This slice is isomorphic to the universal cover of the Kähler moduli space $\mathbb{H}/\Gamma_1(3)$, which is equal to the Poincaré upper half-plane $\mathbb{H}$ itself, and it admits an action of the modular group $\Gamma_1(3)$ by autoequivalences [36, 48]. In particular, the central charge has a contour integral representation in terms of a certain weight 3 Eisenstein series of $\Gamma_1(3)$, which allows for a straightforward analytic extension to the full Poincaré upper half-plane. The large volume slice Λ is also parametrized by $\mathbb{H}$, and is in fact related to Π under $GL(2,\mathbb{R})^+$ above a certain curve which passes through the conifold points $\tau \in \mathbb{Z}$ but stays away from the orbifold points $\tau \in \tau_o + \mathbb{Z}$ with $\tau_o = -\frac{1}{2} + \frac{\mathrm{i}}{2\sqrt{3}}$. Along the slice Λ, the only initial rays are those emanating from the conifold points $\tau = m \in \mathbb{Z}$, associated to the fluxed D4 and anti-D4 branes $\mathcal{O}_{\mathbb{P}^2}(m)$ and $\mathcal{O}_{\mathbb{P}^2}(m)[1]$, and the full BPS spectrum at large volume arises by iterated scattering of these rays. The scattering diagram along the slice Π is much more complicated, since there are initial rays for all $\Gamma_1(3)$ images of $\mathcal{O}_{\mathbb{P}^2}$, emanating from every $\tau = \frac{p}{q} \in \mathbb{Q}$ with $(p,q) = 1, q \neq 0 \mod 3$. This includes in particular all homological shifts $\mathcal{O}_{\mathbb{P}^2}(m)[k]$ at $\tau = m$. However, as long as $|\psi|$ is less than a certain critical phase ψ_c, the only initial rays which can reach $\tau = \mathrm{i}\infty$ are the same as those in Λ. The scattering diagram of the orbifold quiver (Q, W) is embedded in a neighbourhood of the orbifold point τ_o and its $\Gamma_1(3)$ images, which shrinks as $|\psi| \to \frac{\pi}{2}$. When $|\psi| = \frac{\pi}{2}$, the scattering diagram simplifies drastically as rays coincide with level sets of a certain slope function $s(\tau)$, which only intersect at τ_o and its images.

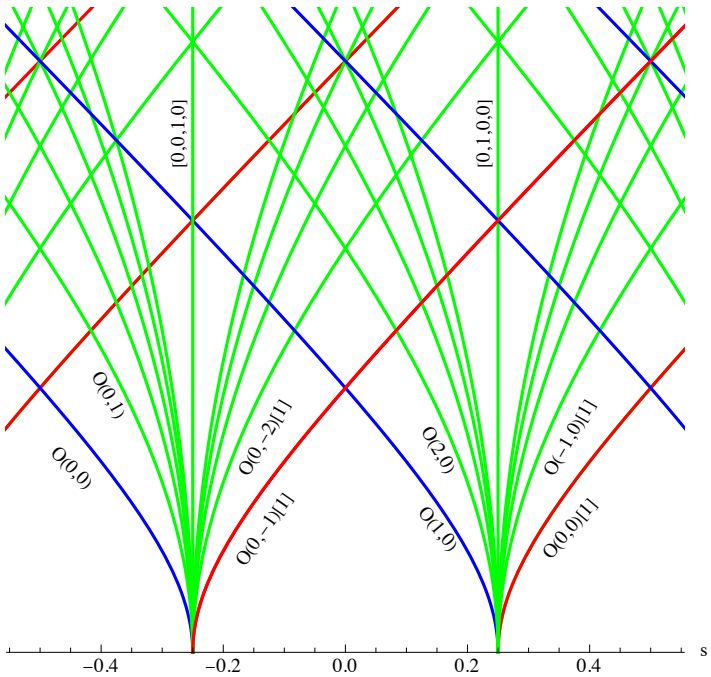


Figure 4.1: Initial rays for the large volume scattering diagram of local $\mathbb{F}_0$ in the (s,t) plane at $m = 1/2$.

Our aim in this chapter is to extend this study to the next simplest toric CY threefold, namely $X = K_{\mathbb{F}_0}$, the canonical bundle over the Hirzebruch surface $\mathbb{F}_0 = \mathbb{P}^1 \times \mathbb{P}^1$, also known as local $\mathbb{F}_0$. Unlike the local $\mathbb{P}^2$ case, M-theory compactified on $\mathbb{F}_0$ yields a weakly coupled five-dimensional gauge theory at low energies, with gauge group $SU(2)$ and vanishing discrete theta angle. Because $b_2(\mathbb{F}_0) = 2$, the space of stability conditions has complex dimension 4, reduced to 2 after modding out by the action of $GL(2,\mathbb{R})^+$. Fixing only the $\mathbb{C}^\times \subset GL(2,\mathbb{R})^+$ action, we can write the central charge for an object of Chern character $\gamma(E) = [r, d_1, d_2, \mathrm{ch}_2]$ as

$$Z(\gamma) = -2rT_D + d_1T_1 + d_2T_2 - \mathrm{ch}_2 \tag{4.1}$$

where $(T_1, T_2) \in \mathbb{H} \times \mathbb{H}$ can be viewed as the complexified Kähler parameters measuring the area and B-field along the two $\mathbb{P}^1$ factors. The large volume slice $\Lambda \subset \mathrm{Stab}\,\mathcal{C}$ is obtained by setting $T_D = \frac{1}{2}T_1T_2$, and choosing a particular heart $\mathcal{A}_{T_1,T_2}$ obtained from the Abelian category of coherent sheaves on $\mathbb{F}_0$ by tilting (see §4.2.3 for details). Since we shall mostly focus on the canonical polarization $\mathrm{Im}\,T_1 = \mathrm{Im}\,T_2$, we set $T_1 = T, T_2 = T + m$ and assume that m is real, unless stated otherwise. For fixed real m, the rays $\mathcal{R}_\psi(\gamma)$ in the half-plane $(s \in \mathbb{R}, t \in \mathbb{R}^+)$ with $T = s - \frac{m}{2} + \mathrm{i}t$ are portions of hyperbolae centered on the real axis $t = 0$, while walls of marginal stability $\mathcal{W}(\gamma, \gamma')$ are half-circles centered on the same axis, as in [47]. However, unlike local $\mathbb{P}^2$ where there are only a pair of rays emanating from each integer point along the boundary $t = 0$, we find that the scattering diagram $\mathcal{D}^\Lambda_{\psi,m}$ admits an infinite set of initial rays emanating from each of the points $s \in \mathbb{Z} + \frac{m}{2}$ and $s = \mathbb{Z} + \frac{m}{2} - \mathrm{Fr}(m)$ on the boundary, where the following objects become massless (see Fig. 4.1 for $m = 1/2$):

$$\begin{array}{lll} s = k + \frac{m}{2}: & \mathcal{O}(k+1+\lfloor m\rfloor + n, k), & \mathcal{O}(k+\lfloor m\rfloor - n, k)[1], \quad GV_{-y-1/y}(1,0,k) \\ s = k - \frac{m}{2}: & \mathcal{O}(k, k-\lfloor m\rfloor + n), & \mathcal{O}(k, k-\lfloor m\rfloor - n - 1)[1], \quad GV_{-y-1/y}(0,1,k) \end{array} \tag{4.2}$$

for all $n \geq 0$. Here $\mathrm{Fr}(m) := m - \lfloor m\rfloor \in [0,1)$ denotes the fractional part of m, $\mathcal{O}(k_1,k_2)$ is the line bundle with first Chern class (k_1,k_2) on $\mathbb{P}^1 \times \mathbb{P}^1$, corresponding to a pure D4-brane with (k_1,k_2) units of flux, while $GV_\Omega(d_1,d_2,k)$ denotes a D2-D0 brane with Chern vector $[0,d_1,d_2,k]$ and BPS index Ω. Fortunately, upon extending the scattering diagram slightly below the $t = 0$ axis[3], one finds that each of these infinite sets of rays originate from the scattering of just two rays with Dirac product $\langle\gamma_1,\gamma_2\rangle = \pm 2$, each of them carrying $\Omega(\gamma_i) = 1$, corresponding to the objects with $n = 0$ in (4.2). [4] With the knowledge of these initial rays, one can determine the BPS spectrum at any point (s,t) along the slice Λ by enumerating all possible scattering sequences in the past 'light-cone', as in [47]. As m varies, the location of the initial rays also varies and some sequences may (dis)appear, leading to further wall-crossing phenomena beyond those occurring at fixed m. For m integer (the values relevant for duality with Chern-Simons on the lens space $L(1,2)$ [3]), the sets of initial rays coalesce in pairs and the structure of the initial rays becomes more complicated, see Fig. 4.27.

In order to rule out initial rays entering the large volume slice Λ through the intervals in between the points $s = k \pm \frac{m}{2}$ on the boundary, we follow the same strategy as in [45] and use

[3] More precisely, below the parabola $y = -\frac{1}{2}x(x+\mu)$ in affine coordinates introduced in (4.91), defined such that rays become straight lines in the (x,y) plane.

[4] In particular, we observe that i) the initial rays $\mathcal{O}(k,k), \mathcal{O}(k+1,k), \mathcal{O}(k+1,k+1), \mathcal{O}(k+2,k+1)$ in an interval of length 2 (corresponding to tensoring with the canonical class $K_{\mathbb{F}_0} = \mathcal{O}(2,2)$) form the foundation of a geometric helix [52], and ii) the large volume scattering diagram coincides with the scattering diagram controlling the Gromov-Witten invariants of the log Calabi-Yau surface $(\mathbb{F}_0, D)$, where D is a smooth very ample anticanonical divisor, obtained by unfolding the spanning polytope of the toric fan of $\mathbb{F}_0$ [102].

the isomorphism $D^b\,\mathrm{Coh}(X) \sim D^b\,\mathrm{Rep}(Q,W)$ with the derived category of representations of the 'orbifold' quiver (see Fig. 4.2) associated to the Ext-exceptional collection generated by the objects

$$E_1 = \mathcal{O}(0,0), \quad E_2 = \mathcal{O}(-1,0)[1], \quad E_3 = \mathcal{O}(1,-1)[1], \quad E_4 = \mathcal{O}(0,-1)[2] \tag{4.3}$$

Physically, the quiver with potential (Q,W) describes the fractional branes on the $\mathbb{Z}_2$ orbifold of the resolved conifold, which arises in a particular degeneration of local $\mathbb{F}_0$. In fact, the region of validity[5] of the orbifold quiver itself does not overlap with the large volume slice Λ, but suitable mutations of (Q,W), including the phase I quiver shown in Fig. 4.22, do. By the same reasoning as in [47, §5.2], one can show that the orbifold quiver satisfies the Attractor Conjecture [37, 155], namely that the only non-vanishing attractor invariants are those associated to the simple dimension vectors $\gamma_i = \mathrm{ch}\,E_i$ and to D0-branes[6]

$$\Omega_\star(\gamma_i) = 1, \quad \Omega_\star(k\delta) = -y^3 - 2y - 1/y \tag{4.4}$$

with $\Omega_\star(\gamma) = 0$ otherwise. Using these initial rays, it is easy to construct the scattering diagram $\mathcal{D}_m^o$ for the orbifold quiver (see Fig. 4.3), as well as for the related type I quiver (see Fig. 4.23). We note that the BPS spectrum of local $\mathbb{F}_0$ in special chambers of the quiver region has been studied previously in [70, 71, 136] and proven rigorously in [51, 184].

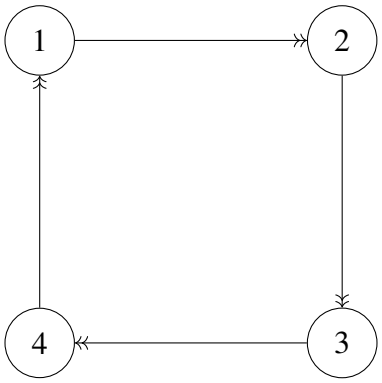


Figure 4.2: Quiver associated to the Ext-exceptional collection (4.3), sometimes known as phase II or orbifold quiver. This is accompanied by the quartic superpotential W in (4.65).

In order to study the BPS spectrum along the Π-stability slice, it is convenient to trade the coordinate T for the modulus τ of the genus one mirror curve. From the point of view of the five-dimensional $SU(2)$ gauge theory compactified on a circle, τ parametrizes the Coulomb branch while m keeps track of the 5D gauge coupling, in units of the circle radius. The study of the mirror curve in Appendix 4.6 shows that the Coulomb branch is a double cover of $\mathbb{H}/\Gamma_0(4)$, ramified over a point τ_B determined in terms of m by the condition[7]

$$J_4(\tau_B) = -8\cos\pi m, \quad J_4(\tau) := 8 + \left(\frac{\eta(\tau)}{\eta(4\tau)}\right)^8 \tag{4.5}$$

[5] Namely, the region in $\mathrm{Stab}\,C$ where the objects E_i are stable simultaneously and have central charges in a common half-plane, such that the heart σ is related by a tilt to the quiver heart.

[6] Since the dimension vector $\delta = (1,1,1,1)$ for D0-branes (or skyscraper sheaves) is in the kernel of the Dirac pairing, the associated rays decouple from the scattering diagram and the value of $\Omega_\star(k\delta)$ does not affect other indices. We thank P. Descombes for confirming that the proof of the Attractor Conjecture in [47, §5.2] carries over to this model.

[7] An equivalent modular parametrization was proposed in [125], see (4.137) for the dictionary.

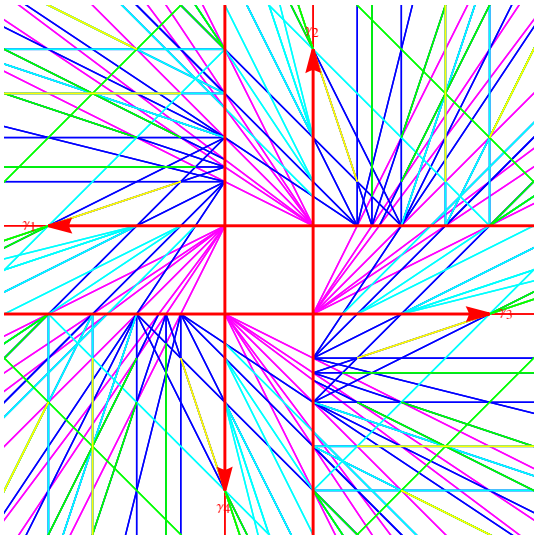


Figure 4.3: Scattering diagram of the orbifold quiver for $m = 1/2$, keeping rays with height $\sum_i N_i \leq 8$.

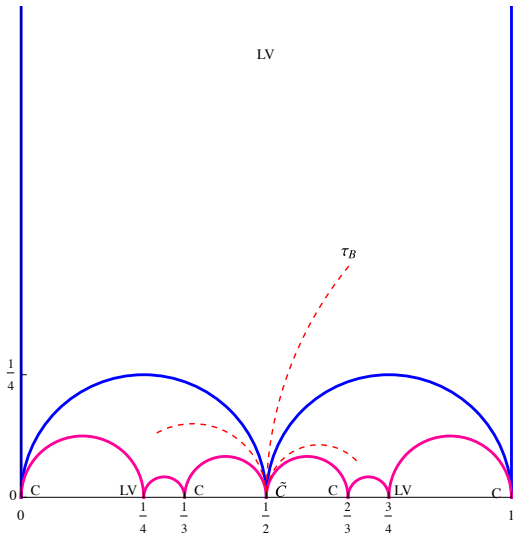


Figure 4.4: Fundamental domain $\mathcal{F}$ (in blue) for the action of $\Gamma_0(4)$ on the upper half-plane, and its images under $\tau \mapsto \frac{\tau-1}{4\tau-3}$ and $\tau \mapsto \frac{3\tau-1}{4\tau-1}$. The cusps at $\tau = (i\infty, 0, \frac{1}{2})$ correspond to the large volume limit $z = 0$, conifold point $z = \frac{1}{4(1+\sqrt{\lambda})^2}$ and dual conifold point $z = \frac{1}{4(1-\sqrt{\lambda})^2}$, while the branch point τ_B corresponds to $z = \infty$. The dotted lines show the cuts joining τ_B and its images to $\tau = \frac{1}{2}$ along geodesic circles.

where $J_4(\tau)$ is the Hauptmodul mapping $(\mathrm{i}\infty, 0, \frac{1}{2})$ to $(\infty, 8, -8)$ (we choose τ_B such that it lies in the fundamental domain $\mathcal{F}$ shown in Fig. 4.4). The point $\tau = \tau_B$ corresponds to the limit where $K_{\mathbb{F}_0}$ degenerates into a $\mathbb{Z}_2$ orbifold of the resolved conifold. For m real, both τ_B and its $\Gamma_0(4)$ image $\tilde{\tau}_B = \frac{\tau_B - 1}{4\tau_B - 3} = 1 - \overline{\tau_B}$ lie on the half-circles at the boundary of the fundamental domain. At the special points $m \in \mathbb{Z}$ (or $\lambda := e^{2\pi i m} = 1$, which much of the literature on local $\mathbb{F}_0$ focuses on), the ramification point τ_B coalesces with the conifold point $\tau = \frac{1}{2}$.

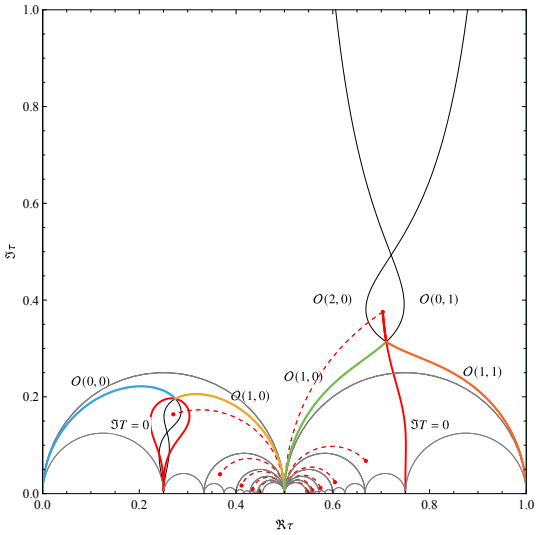


Figure 4.5: (Putative) boundary of the space of geometric stability conditions, for $m = 0.4 + 0.3\mathrm{i}$. The red solid line is the locus $\mathrm{Im}\, T = 0$. Along the blue, yellow, green and orange lines, the central charge associated to $\mathcal{O}(0,0), \mathcal{O}(1,0), \mathcal{O}(0,1)$ (or rather its image $\mathcal{O}(1,0)$ through the cut) and $\mathcal{O}(1,1)$ become real and negative, destabilizing skyscraper sheaves. The green and orange lines intersect at a point τ_b where $\mathrm{Im}\, T = \mathrm{Im}\, T_D = 0$, and similarly the blue and yellow lines intersect at $\tilde{\tau}_b$ where where $\mathrm{Im}\, T = \mathrm{Im}\, T_D = 0$. Along the segment of the locus $\mathrm{Im}\, T = 0$ joining τ_b to τ_B, skyscraper sheaves are instead destabilized by D2-branes. The fundamental domain $\widehat{\mathcal{F}}$ is defined as the region above the blue, yellow, green, orange lines with the red segment from τ_b to τ_B excised.

The space of Π_m-stability conditions $(Z, \mathcal{A})$ is defined as the universal cover of Kähler moduli space at fixed m, equipped with a central charge function $Z : \mathbb{Z}^4 \to \mathbb{C}$ determined by periods of a certain one-form with logarithmic singularities on the mirror, and a compatible heart $\mathcal{A}$ which coincides with the large volume heart $\mathcal{A}_{T,T+m}$ for $\mathrm{Im}\,\tau$ large enough. For $m \in \mathbb{Z}$, the universal cover of Kähler moduli space is simply the Poincaré upper half-plane $\mathbb{H}$, and the central charge is given by a contour integral of a weight 3 modular form under[8] $\Gamma_0(4)$, similar to [47],

$$\begin{pmatrix} T \\ T_D \end{pmatrix}(\tau) = \begin{pmatrix} T(\tau_0) \\ T_D(\tau_0) \end{pmatrix} + \int_{\tau_0}^{\tau} \begin{pmatrix} 1 \\ u \end{pmatrix} C(u, m)\mathrm{d}u \tag{4.6}$$

with $m = 0$ and

$$C(\tau, 0) = \frac{\eta(\tau)^4 \eta(2\tau)^6}{\eta(4\tau)^4} = 1 - 4\sum_{n \geq 1} \frac{n^2 \chi_4(n) q^n}{1 - q^n} \tag{4.7}$$

where $\chi_4(n)$ is the Dirichlet character modulo 4, equal to ± 1 for $n = \pm 1 \mod 4$ and 0 otherwise. In the fundamental domain and its translates $\mathcal{F} + \mathbb{Z}$, the heart $\mathcal{A}_\tau$ is constructed by the usual

[8] More precisely, $C(\tau, 0)$ is modular under $\Gamma_1(4)$, as $\Gamma_0(4)$ admits no modular forms of odd weight. Note that the quotient $\mathbb{Z}_2 = \Gamma_1(4)/\Gamma_0(4)$ acts trivially on τ.

tilting construction, and extended to $\mathbb{H}$ by the action of auto-equivalences. For $m \notin \mathbb{Z}$, the fundamental domain of $\Gamma_0(4)$ can still be unfolded to $\mathbb{H}$, but at the cost of introducing $\mathbb{Z}_2$ branch cuts between the $\Gamma_0(4)$ images of τ_B and the corresponding $\Gamma_0(4)$ images of $\tau = \frac{1}{2}$. Since the monodromies around different ramification points do not commute, the physical slice Π_m is now an infinite cover of $\mathbb{H}$, with sheets labeled by a rank 4 lattice[9] $\mathbb{Z}^4$, ramified at all $\Gamma_0(4)$ images of τ_B. The central charge along Π_m is still given by contour integral of the form (4.6), but now

$$C(\tau, m) := \frac{\eta(\tau)^4 \eta(2\tau)^6}{\eta(4\tau)^4} \sqrt{\frac{J_4(\tau) + 8}{J_4(\tau) + 8\cos \pi m}} \tag{4.8}$$

has square root singularities at τ_B and images thereof. The integral now depends on the choice of path avoiding the $\mathbb{Z}_2$-ramification points. We refer to the sheet reached by analytic continuation along a path from τ_0 near $i\infty$ to τ which does not cross any of the branch cuts[10] as the principal sheet. In §4.2.4 we explain how to construct the heart $\mathcal{A}_\tau$ by tilting in a fundamental domain $\widehat{\mathcal{F}}$ which differs slightly from $\mathcal{F}$ when m is complex (see Fig. 4.5), and then extend it to the full slice of Π-stability conditions by auto-equivalences. [11]

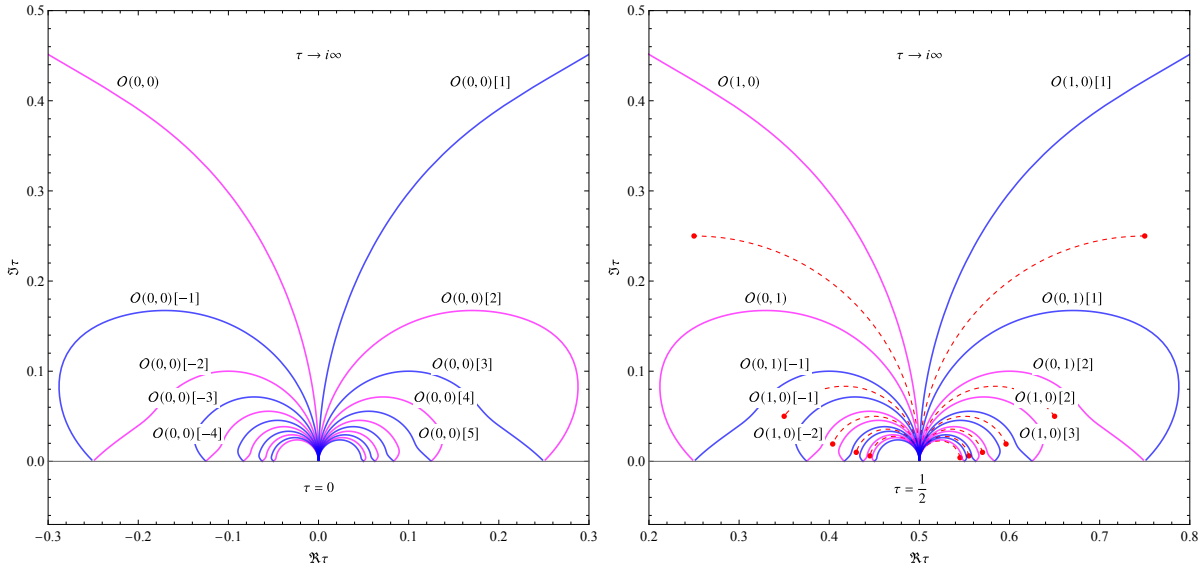


Figure 4.6: Initial rays emitted from $\tau = 0$ (left) and $\tau = \frac{1}{2}$ (right), for $m = 1/2$ and $\psi = 0$. Rays with positive and negative rank r are shown in magenta and blue, respectively.

The scattering diagram $\mathcal{D}^{\Pi}_{\psi,m}$ along Π, for fixed values of the mass parameter m and phase ψ, is then uniquely determined by requiring that it reduces to the large volume scattering diagram $\mathcal{D}^{\Lambda}_{\psi,m}$ as $\tau \to i\infty$, to the orbifold scattering diagram $\mathcal{D}^{o}_{m}$ as $\tau \to \tau_B$, and by requiring invariance

[9] More precisely, the monodromy group Γ preserving a generic m is an extension $1 \to \mathbb{Z}^4 \to \Gamma \to \Gamma_0(4) \to 1$.

[10] In order to evaluate the periods T, T_D, we find it convenient to choose branch cuts along hyperbolic geodesics from τ_B to $\tau = \frac{1}{2}$ and $\Gamma_0(4)$ images thereof, which differ slightly from the locus where the argument of the square root in (4.8) crosses the negative real axis. In view of the discussion of geometric stability conditions in §4.2.4, another natural choice of branch cut would be the locus $\mathrm{Im}\, T = 0$ in $\mathcal{F}$ and $\Gamma_0(4)$ images thereof, but it is less convenient for numerics.

[11] For the mathematically minded reader, we find evidence that the space of geometric stability conditions (modulo tensoring with line bundles) provides a fundamental domain in a connected component of the space of Bridgeland stability conditions modulo the action of auto-equivalences, similar to the local $\mathbb{P}^2$ case [36].

under the monodromy group Γ. In particular, it includes an infinite set of rays emanating from every conifold point $\tau = \frac{p}{q}$ with $(p, q) = 1, q \neq 0 \mod 4$. The structure of the initial rays near $\tau = 0$ and $\tau = \frac{1}{2}$ on the particular sheet reached by analytic continuation from $\tau = \mathrm{i}\infty$ is shown in Fig. 4.6.

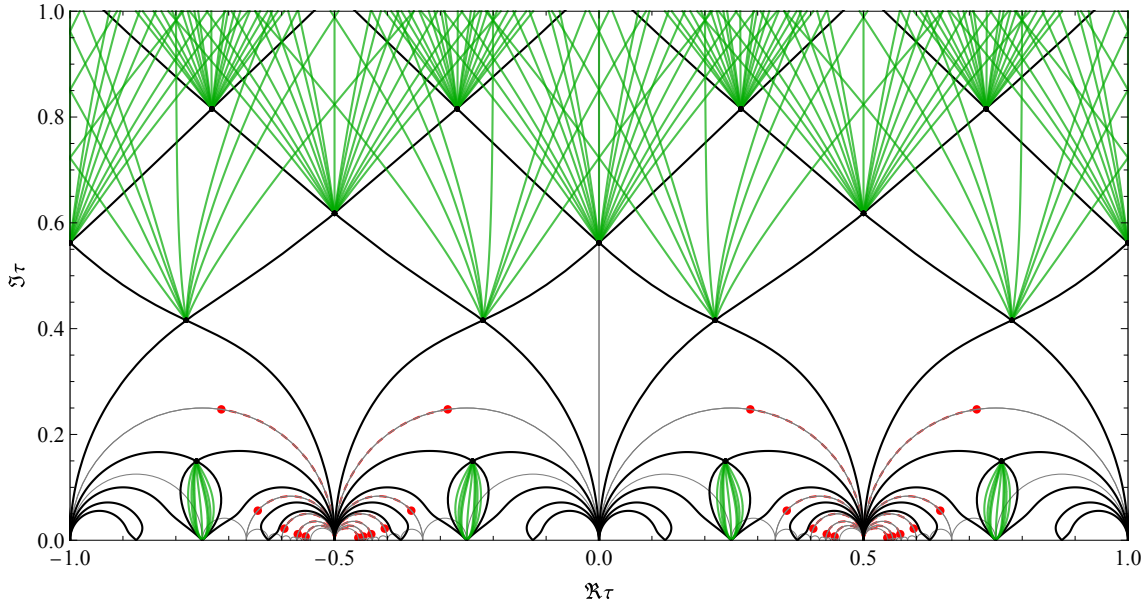


Figure 4.7: Scattering diagram $\mathcal{D}^{\Pi}_{m,\psi}$ along the Π-stability slice for $m = 0.4$, $\psi = 0$. For clarity, only primary scatterings are shown.

For small phase $|\psi|$, the structure of $\mathcal{D}^{\Pi}_{\psi,m}$ along the fundamental domain $\mathcal{F}$ and its translates turns out to be similar to that along the extended large volume slice, with initial rays $\mathcal{O}(k,k), \mathcal{O}(k,k)[1]$ emitted at $\tau = k$ and $\mathcal{O}(k+1,k), \mathcal{O}(k+1,k)[1]$ emitted at $\tau = k + \frac{1}{2}$ (see Fig. 4.7). These rays do not cross the cuts and asymptote to $\tau = \mathrm{i}\infty$ as in the large volume slice. As ψ increases, some of these initial rays curl back and end up at $\Gamma_0(4)$ images of the large volume point, potentially after crossing cuts, while suitable homological shifts of the original rays manage to escape to $\mathrm{i}\infty$ (see Figs. 4.8-4.10). In particular, for ψ bigger than both[12]

$$\psi_{\mathrm{cr}} = \arctan\left(\frac{\mathrm{Im}\,\mathcal{V}(m)}{\mathrm{Re}\,\mathcal{V}(m)}\right), \quad \tilde{\psi}_{\mathrm{cr}} = \arctan\left(\frac{\mathrm{Im}[\tilde{\mathcal{V}}(m) + \mathrm{i}(1-m)]}{\mathrm{Re}[\tilde{\mathcal{V}}(m) + \mathrm{i}(1-m)]}\right), \tag{4.9}$$

where $\mathcal{V}(m)$ and $\tilde{\mathcal{V}}(m)$ are the 'quantum volumes' defined in (4.212) and (4.235), the rays $\mathcal{R}(\gamma_i)$ associated to the simple objects in the Ext-exceptional collection (4.3) (tensored by $\mathcal{O}(1,1)$) circle around the ramification point τ_B, intersecting exactly as predicted by the orbifold scattering diagram, before exiting to the large volume points $\tau = \mathrm{i}\infty$ or $\tau = 1/4$. It is worth noting that the rays γ_i and γ_{i+2} live on different sheets, although they project to the same ray on the τ-plane (see Fig. 4.11). For $\psi = \frac{\pi}{2}$ and real m, the scattering diagram simplifies drastically since geometric rays coincide with contours of $s = \mathrm{Im}\,T_D/\mathrm{Im}\,T$, and intersect only at τ_B and its $\Gamma_0(4)$ images, see Fig. 4.12. As in [47], this explains why the quiver index agrees with the Gieseker index for normalized torsion-free sheaves in canonical polarization, as observed in [37].[13] When m takes

[12] Here we assume $\psi > 0$, the critical values for $\psi < 0$ can be found in (4.116). For $m = 1/2$, the two critical values coincide, $\psi_{\mathrm{cr}} = \tilde{\psi}_{\mathrm{cr}} \simeq 0.68641$.

[13] For m complex, this simple argument no longer works since the polarization $\eta = 1 + \frac{\mathrm{Im}\,m}{\mathrm{Im}\,T}$ is now τ-dependent, and objects with the same slope $s = \frac{d_1 + \eta d_2}{2r}$ may have non-trivial Dirac product.

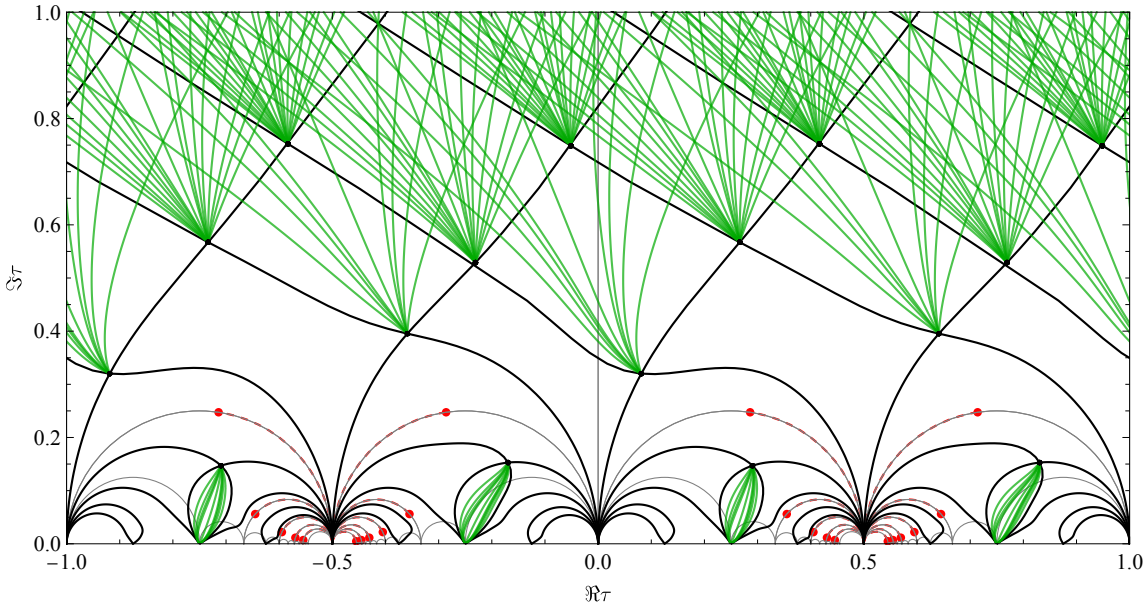


Figure 4.8: Scattering diagram $\mathcal{D}^{\Pi}_{m,\psi}$ for $m = 0.4$, $\psi = 0.4$ below the first critical value $\psi_{cr} \simeq 0.545$.

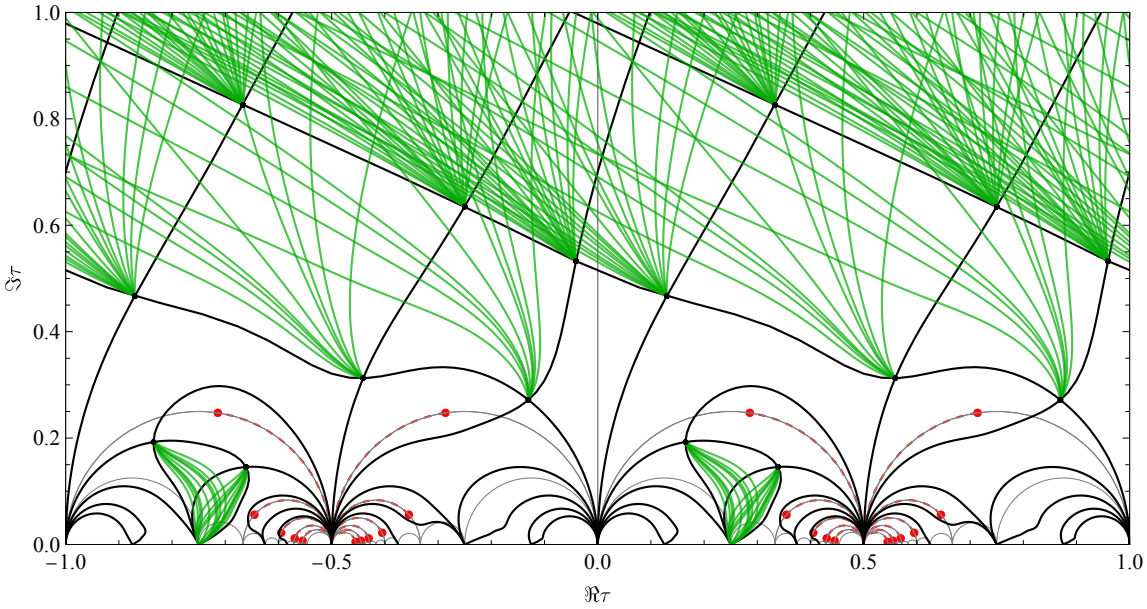


Figure 4.9: Scattering diagram $\mathcal{D}^{\Pi}_{m,\psi}$ for $m = 0.4$, $\psi = 0.68$ between the first two critical values $\psi_{cr} \simeq 0.545$ and $\tilde{\psi}_{cr} \simeq 0.832$.

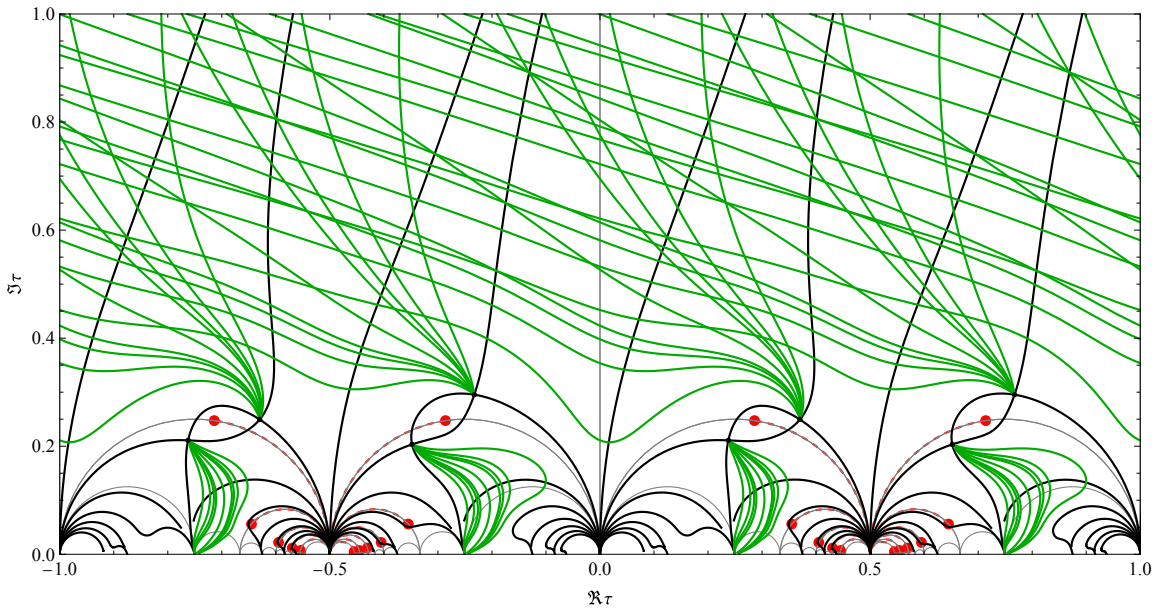


Figure 4.10: Scattering diagram $\mathcal{D}^{\Pi}_{m,\psi}$ for $m = 0.4$, $\psi = 0.98$ above $\tilde{\psi}_{cr} \simeq 0.832$.

integer values, the structure of the diagram on the one hand simplifies due to the absence of branch cuts, but on the other hand is complicated by coalescence of various intersection points, due to initial rays related by fiber/base duality, see Fig. 4.29.

In general, we conjecture that the scattering diagram in $\mathcal{F} + \mathbb{Z}$ (translates of the fundamental domain) arises from the scattering of rays associated to orbifold quivers with lone rays emanating from $\tau \in \mathbb{Z}$ and $\tau \in \mathbb{Z} + \frac{1}{2}$. In other words, attractor flow trees (see §4.5.3) can always be decomposed into a finite set of 'shrubs' (i.e. trees rooted at elements in the exceptional collection (4.3) or one of its translates or images under fiber/base duality, and supported in the corresponding quiver region) and a finite set of 'lone branches' emanating from $\tau \in \mathbb{Z}$ and $\tau \in \mathbb{Z} + \frac{1}{2}$. We sketch a possible strategy for proving this claim, and hence the validity of the Split Attractor Flow Conjecture, at least in some range $\psi \in \mathcal{I}_{\rm cvx}$ around $\psi = 0$ where we can use convexity arguments to rule out rays entering quiver regions.

We conclude this introduction and summary by listing a few open questions for future research. First, we have mostly focused on the scattering diagram at fixed mass parameter m, which at large $\mathrm{Im}\, T$ determines the counting of Gieseker semi-stable sheaves on $\mathbb{F}_0$ with canonical polarization $H \propto c_1(S)$. It would be of interest to understand the scattering diagram at $m = M_1 + M_2 T$ with fixed (M_1, M_2), as it should determine the counting of η-Gieseker semi-stable sheaves with generic polarization. Second, it would be interesting to extend our study to higher del Pezzo surfaces, at least along the large volume slice, and see whether the coincidence between the large volume scattering diagram and the unfolding of the spanning polytope of the log CY surface, noted in footnote 4, continues to hold. Third, it would be useful to clarify the relation between attractor flow trees and exponential spectral networks, introduced in [84] and applied to the case of local $\mathbb{F}_0$ in [34]. Finally, it would be of great interest to determine the spectrum of framed BPS states in these geometries. Indeed, as the phase ψ of the framing defect is varied, framed BPS indices jump precisely along the rays of the scattering diagram $\mathcal{D}_{\psi,m}$ [21, 98], and one expects that the generating series of framed BPS indices should interpolate between the generating series of molten crystals near the orbifold point [155, 156, 162] and the topological string amplitude

in the large volume limit, generalizing the picture of [119] to the case of CY threefolds with compact divisors.

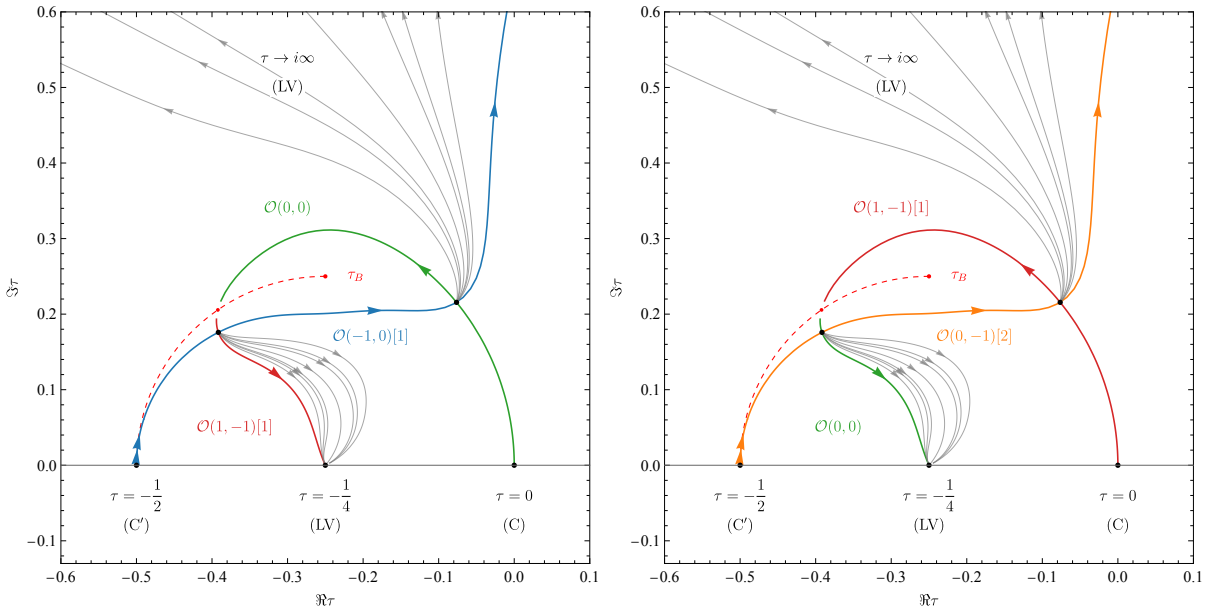


Figure 4.11: Embedding of the orbifold scattering diagram into the Π-stability scattering diagram around $\tau_B - 1 = \frac{i-1}{4}$, for $m = 1/2$ and $\psi = 0.72$. The initial rays $\mathcal{R}(\gamma_i)$ for the exceptional collection (4.117) are shown in green, blue, red and orange. The scatterings of $\{\gamma_1, \gamma_2\}$ and $\{\gamma_2, \gamma_3\}$ take place on one sheet, and those of $\{\gamma_3, \gamma_4\}$ and $\{\gamma_4, \gamma_1\}$ on another sheet, glued along the branch cut (shown in red dashed line).

The rest of this chapter is organized as follows. In §4.2 we recall relevant properties of bundles and coherent sheaves on $\mathbb{F}_0$, collect some known results for the Gieseker index of rank 0 sheaves, and their relation to Gopakumar-Vafa invariants, and outline the construction of Bridgeland stability conditions along the slice of Π-stability conditions. In §4.3, we introduce two useful exceptional collections and their respective quivers, related by mutation, and construct a two-dimensional slice in their respective scattering diagrams. In §4.4, we construct the scattering diagram in the large volume slice with fixed parameter m, identifying the initial rays, and use it to reproduce some known Gieseker indices for coherent sheaves with low rank. In §4.5, we combine the orbifold and large volume scattering diagrams with invariance under $\Gamma_0(4)$, and construct the scattering diagram in the slice of Π stability conditions, for fixed real mass parameter m, and discuss phase transitions as the phase ψ is varied. We sketch the proof of the SAFC, and illustrate the complexity of the scattering diagram by identifing the scattering sequences contributing to the index of the structure sheaves $\mathcal{O}_S := \mathcal{O}(0,0)$ and $\mathcal{O}_C$ for varying values of ψ. In Appendix §4.6 we establish the contour integral representation (4.6) for the central charge, and use it to obtain expansions near cusp and ramification points in the fundamental domain. A Mathematica package `F0Scattering.m` and accompanying worksheets allowing to reproduce our computations, in particular evaluating the central charge on the principal sheet over any point in the Poincaré upper half-plane, is provided in a publicly available repository. [14]

[14] `https://github.com/bpioline/F0Scattering`

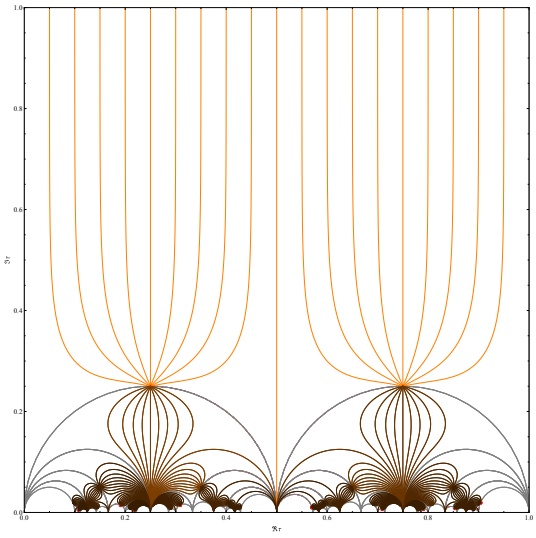


Figure 4.12: Contour lines of $s = \frac{\operatorname{Im} T_D}{\operatorname{Im} T}$ for $m = 1/2$.

4.2 Generalities

4.2.1 Coherent sheaves on $K_{\mathbb{F}_0}$

The Hirzebruch surface $S = \mathbb{F}_0$ is biholomorphic to $\mathbb{P}^1 \times \mathbb{P}^1$. We denote by (C, F) the classes in $H_2(S, \mathbb{Z})$ corresponding to the two $\mathbb{P}^1$ factors, such that $C^2 = F^2 = 0$ and $C.F = 1$. The effective cone and nef cone are both spanned by C and F. Every ample divisor is an integer multiple of $H = C + \eta F$ for some rational $\eta > 0$, which we also call the polarization. For any coherent sheaf E on S, we denote the Chern character by $\gamma(E) = [r(E), d_1(E), d_2(E), \mathrm{ch}_2(E)] \in \mathbb{Z}^4$, with $d_1(E) = C.c_1(E)$, $d_2(E) = F.c_1(E)$, and $\mathrm{ch}_2(E) := \int_S \mathrm{ch}(E)$. When the rank $r(E)$ is non-zero, we define the slope and Bogomolov discriminant by

$$\mu_\eta(\gamma) = \frac{d_1 + \eta d_2}{2r}, \quad \Delta(\gamma) = \frac{d_1 d_2}{r^2} - \frac{\mathrm{ch}_2}{r} \tag{4.10}$$

and set $\mu_\eta(\gamma) = +\infty$ if $r = 0$. Since the canonical class is $K_S = -c_1(S) = -2C - 2F$, the canonical slope is obtained by setting $\eta = 1$. The Euler form is given by the Grothendieck-Riemann-Roch theorem,

$$\begin{aligned} \chi(E, E') &= \dim \mathrm{Hom}(E, E') - \dim \mathrm{Ext}^1(E, E') + \dim \mathrm{Ext}^2(E, E') \\ &= rr' + r(d_1' + d_2') - r'(d_1 + d_2) + r\mathrm{ch}_2' + r'\mathrm{ch}_2 - (d_1 d_2' + d_1' d_2) \end{aligned} \tag{4.11}$$

We define the antisymmetrized Euler form (or Dirac product) as

$$\langle \gamma, \gamma' \rangle = 2r(d_1' + d_2') - 2r'(d_1 + d_2) \tag{4.12}$$

When the moduli space $\mathcal{M}_\eta(\gamma)$ of Gieseker-semistable sheaves[15] with Chern character $\gamma = [r, d_1, d_2, \mathrm{ch}_2]$ is non empty, then it is an irreducible projective variety of complex dimension

$$d_{\mathbb{C}}(\gamma) = 1 - \chi(E, E) = 2(d_1 d_2 - r\mathrm{ch}_2) - r^2 + 1 \tag{4.13}$$

[15] Recall that a torsion-free coherent sheaf E is Gieseker-semistable if $\mu_\eta(F) \leq \mu_\eta(E)$ for every subsheaf $F \subset E$, and if $\frac{\mathrm{ch}_2(F)}{r(F)} + \frac{c_1(S).c_1(F)}{2r(F)} \leq \frac{\mathrm{ch}_2(E)}{r(E)} + \frac{c_1(S).c_1(E)}{2r(E)}$ whenever $\mu_\eta(F) = \mu_\eta(E)$, see e.g. [142, §2].

which is smooth whenever γ is primitive, i.e. $\gcd(r, d_1, d_2, \mathrm{ch}_2) = 1$. For $r > 0$, the classical Bogomolov identity implies that $\mathcal{M}_\eta(\gamma)$ is empty unless $\Delta(\gamma) \geq 0$. A sharp lower bound analogous to the Drézet-Le Potier condition in the projective plane case [83] was established in [67] using exceptional bundles, which we summarize below.

Exceptional bundles are defined by the conditions $\mathrm{Hom}(E, E) = \mathbb{C}$ and $\mathrm{Ext}^{i>0}(E, E) = 0$. Since $d_{\mathbb{C}}(\gamma) = 0$, their discriminant is $\Delta(E) = \frac{1}{2}(1 - \frac{1}{r^2(E)})$ by (4.13) hence $r(E)$ is necessarily odd [67, Lemma 6.7]. The discriminant vanishes in the rank 1 case $E = \mathcal{O}(d_1, d_2)$, and is otherwise at least $\frac{4}{9}$. The first few exceptional bundles with rank ≤ 19 have (up to fiber/base duality and tensoring with line bundles) Chern characters $[2k+1, 1, k, -k]$, along with sporadic cases $[11, 4, 4, -4]$, $[17, 5, 5, -7]$ and $[19, 4, 7, -8]$ (see [67, Table 1]). All exceptional bundles are stable for the canonical polarization $\eta = 1$, but they get destabilized when $|\eta - 1|$ is large enough, except in the rank 1 case. The list $\mathcal{E}_\eta$ of Gieseker-stable exceptional bundles then determines a lower bound $\Delta(E) \geq \delta_{\mathrm{DLP}}(\eta, a, b)$ on the discriminant of non-exceptional Gieseker-stable torsion-free sheaves with slope $(a, b) = (d_1, d_2)/r$, given by [67, Proposition 6.15][16]

$$\delta_{\mathrm{DLP}}(\eta, a, b) := \sup_{F \in \mathcal{E}_\eta, |2\mu_\eta(F) - a - \eta b| \leq \eta + 1} \left[P_\epsilon\left(a - \tfrac{d_1(F)}{r(F)}, b - \tfrac{d_2(F)}{r(F)}\right) - \Delta(F) \right] \tag{4.14}$$

where $P_\epsilon(a, b) = (\epsilon a + 1)(\epsilon b + 1)$ and $\epsilon(F) = \mathrm{sign}[2\mu_\eta(F) - a - \eta b]$. Note that $\delta_{\mathrm{DLP}}(\eta, a, b)$ is invariant under $(a, b) \to (a+1, b), (a, b+1), (-a, -b), (b, a)$ and is at least $1/2$ by [67, Corollary 8.15]. Conversely, $\mathcal{M}_\eta(\gamma)$ is non-empty if γ is the Chern character of an exceptional stable bundle (or an integer multiple thereof) or if $\Delta(\gamma) \geq \delta_{\mathrm{DLP}}(\eta, d_1/r, d_2/r)$ [67, Corollary 7.6]. The function $\delta_{\mathrm{DLP}}(M, a, b)$ for the canonical polarization $\eta = 1$ is plotted in Fig. 4.13.[17]

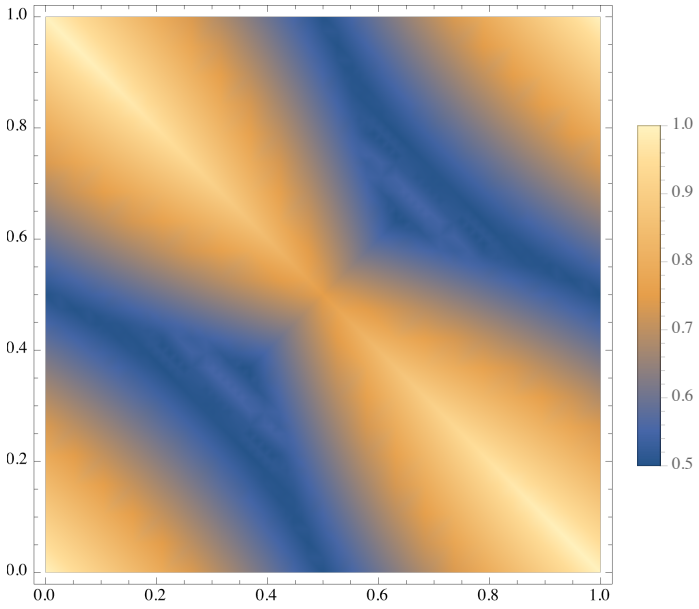


Figure 4.13: Lower bound $\delta_{\mathrm{DLP}}(\eta, a, b)$ on the discriminant of non-exceptional H-stable sheaves for $\eta = 1$, obtained by retaining exceptional sheaves with rank up to 19. Figure adapted from [67, Fig. 5].

For γ primitive, we define the refined Gieseker index $\Omega_\eta(\gamma)$ as the Poincaré-Laurent

[16] The parameter m in [67] corresponds to η in our notations.

[17] We are grateful to Jack Huizenga for sharing the code used for producing this picture.

polynomial for the moduli space $\mathcal{M}_\eta(\gamma)$,

$$\Omega_\eta(\gamma, y) = \sum_{p=0}^{2d_{\mathbb{C}}(\gamma)} b_p(\mathcal{M}_\eta(\gamma))\,(-y)^{p-d_{\mathbb{C}}(\gamma)} \tag{4.15}$$

For $r \neq 0$ and arbitrary polarization $\eta > 0$, the Gieseker indices were determined in [142], using wall-crossing from the degenerate polarization $\eta = 0$, where the indices are computable using the Hall algebra of $\mathbb{P}^1$ [153]. For $r = 1$, the indices are independent of η, and determined by the modular generating series

$$\begin{aligned}\sum_{n\geq 0} \Omega_\eta([1,0,0,-n])\,q^n =& \frac{\mathrm{i} q^{1/6}(y-1/y)}{\eta(q)\,\theta_1(q,y^2)} = 1 + (y^2+2+1/y^2)q + (y^4+3y^2+6+\dots)q^2 \\ &+ (y^6+3y^4+9y^2+14+\dots)q^3 + O(q^4)\end{aligned} \tag{4.16}$$

where $\eta(q) = q^{1/24}\prod_{n\geq 1}(1-q^n)$, $\theta_1(q,y) = \mathrm{i}\sum_{r\in\mathbb{Z}+\frac{1}{2}}(-1)^{r-1/2}q^{r^2/2}y^r$ are the usual Dedekind and Jacobi theta series, and the dots are determined by invariance under Poincaré duality, $y \to 1/y$. Explicit results for rank $r \leq 4$ can be found in [37, 142, 144].

For rank 0, the Gieseker invariants $\Omega_\eta(0, d_1, d_2, \mathrm{ch}_2)$ are independent of ch_2 [149], presumably also of the polarization η, and are related to the refined BPS invariants $N^{j_L,j_R}_{d_1,d_2}$ by

$$\Omega_\eta(0,d_1,d_2,\cdot,y) = \sum_{j_L,j_R\in\frac{1}{2}\mathbb{Z}_{\geq 0}} (-1)^{2j_L+2j_R}\chi_{j_L}(y)\chi_{j_R}(y)\,N^{j_L,j_R}_{d_1,d_2} \tag{4.17}$$

where $\chi_j(y) = (y^{2j+1}-y^{-2j-1})/(y-1/y)$. In particular, for $y = 1$ they reduce to the genus 0 GV invariant $GV^{(0)}_{d_1,d_2}$. The GV invariants for local $\mathbb{F}_0$ were first computed at genus 0 in [60], and higher genus in [3]. The refined BPS invariants $N^{j_L,j_R}_{d_1,d_2}$ were obtained in [118, p34], [116, Table 4], and are summarized in the following table of multiplets (j_L, j_R) for low degrees (d_1, d_2):

$d_1\backslash d_2$	0	1	2	3
0	0	$(0,\frac{1}{2})$	0	0
1	$(0,\frac{1}{2})$	$(0,\frac{3}{2})$	$(0,\frac{5}{2})$	$(0,\frac{7}{2})$
2	0	$(0,\frac{5}{2})$	$(0,\frac{7}{2}\oplus\frac{5}{2})\oplus(\frac{1}{2},4)$	$(1,\frac{11}{2})\oplus(\frac{1}{2},5\oplus 4)$ $\oplus(0,\frac{9}{2}^{\oplus 2}\oplus\frac{7}{2}\oplus\frac{5}{2})$
3	0	$(0,\frac{7}{2})$	$(1,\frac{11}{2})\oplus(\frac{1}{2},5\oplus 4)$ $\oplus(0,\frac{9}{2}^{\oplus 2}\oplus\frac{7}{2}\oplus\frac{5}{2})$	$(2,\frac{15}{2})\oplus(\frac{3}{2},7\oplus 6)$ $\oplus(1,\frac{13}{2}^{\oplus 3}\oplus\frac{11}{2}^{\oplus 2}\oplus\frac{9}{2})$ $\oplus(\frac{1}{2},7\oplus 6^{\oplus 3}\oplus 5^{\oplus 3}\oplus 4^{\oplus 2}\oplus 3)$ $\oplus(0,\frac{11}{2}^{\oplus 4}\oplus\frac{9}{2}^{\oplus 3}\oplus\frac{7}{3}^{\oplus 4}\oplus\frac{5}{2}\oplus\frac{3}{2})$

(4.18)

leading to the refined D2-D0 indices

$$\begin{aligned}
\Omega_\eta(0,1,d,\cdot) &= -(y^{2d+2} - y^{-2d-2})/(y-1/y) \overset{y\to 1}{\to} -(2d-2) \\
\Omega_\eta(0,2,2,\cdot) &= -y^9 - 3y^7 - 4y^5 - 4y^3 - 4y - \ldots \overset{y\to 1}{\to} -32 \\
\Omega_\eta(0,2,3,\cdot) &= -y^{13} - 3y^{11} - 8y^9 - 10y^7 - 11y^5 - 11y^3 - 11y + \ldots \overset{y\to 1}{\to} -110 \\
\Omega_\eta(0,3,3,\cdot) &= -y^{19} - 3y^{17} - 10y^{15} - 22y^{13} \\
&\quad - 41y^{11} - 53y^9 - 60y^7 - 62y^5 - 63y^3 - 63y + \ldots \overset{y\to 1}{\to} -756
\end{aligned} \tag{4.19}$$

The leading power of y matches the expected dimension $d_{\mathbb{C}}(\gamma) = 2d_1d_2 + 1$. Moreover, $\Omega_\eta(0, d_1, d_2, \mathrm{ch}_2)$ vanishes if $d_1d_2 < 0$, i.e. if the curve class lies outside the Mori cone.

4.2.2 Derived category of coherent sheaves on $K_{\mathbb{F}_0}$

The (compactly supported, bounded) derived category $\mathcal{C} = D^b_c\mathrm{Coh}K_{\mathbb{F}_0}$ is the category of finite length complexes $\mathcal{E} = \cdots \to E_k \to E_{k+1} \ldots$ (up to quasi-isomorphisms) where the component E_k in cohomological degree k is a coherent sheaf on $K_{\mathbb{F}_0}$ supported set-theoretically on $\mathbb{F}_0$. The category $\mathcal{C}$ is graded by the lattice $\Gamma := \mathbb{Z}^4$ corresponding to the Chern character $\gamma(\mathcal{E}) := [r(\mathcal{E}), d_1(\mathcal{E}), d_2(\mathcal{E}), \mathrm{ch}_2(\mathcal{E})] := \sum_k (-1)^k \gamma(E_k)$. The Euler form on $\mathcal{C}$ coincides with the antisymmetrized Euler form $\langle -, - \rangle$ in (4.12).

The category $\mathcal{C}$ admits several natural auto-equivalences:

- Homological shift $\mathcal{E} \mapsto \mathcal{E}[1]$, mapping $\gamma(\mathcal{E}) \mapsto -\gamma(\mathcal{E})$
- Tensoring by the line bundle $\mathcal{O}(k_1, k_2)$, also known as spectral flow, mapping

$$[r, d_1, d_2, \mathrm{ch}_2] \mapsto [r, d_1 + rk_1, d_2 + rk_2, \mathrm{ch}_2 + d_2k_1 + d_1k_2 + rk_1k_2] \tag{4.20}$$

- 'Fiber-base duality' exchanging the two $\mathbb{P}^1$ factors, and acting on the charge vector as

$$FB: \quad [r, d_1, d_2, \mathrm{ch}_2] \mapsto [r, d_2, d_1, \mathrm{ch}_2] \tag{4.21}$$

- Seidel-Thomas twist ST_S by any spherical object S, acting as[18]

$$\mathrm{ch}\, E \mapsto \mathrm{ch}\, E - \langle \mathrm{ch}\, S, \mathrm{ch}\, E \rangle \,\mathrm{ch}\, S \tag{4.22}$$

In particular, the composition $FB \circ ST_{\mathcal{O}(0,0)} \circ (\mathcal{O}(0,1) \otimes -)$ gives an order 4 automorphism, acting as

$$\mathbb{Z}_4: \quad [r, d_1, d_2, \mathrm{ch}_2] \mapsto [-2d_1 - 2d_2 - r, d_2 + r, d_1, d_1 + \mathrm{ch}_2] \tag{4.23}$$

In addition, under derived duality $\mathcal{E} \mapsto \mathcal{E}^\vee$, the charge vector $\gamma(\mathcal{E})$ transforms as

$$[r, d_1, d_2, \mathrm{ch}_2] \mapsto [-r, d_1, d_2, -\mathrm{ch}_2] \tag{4.24}$$

[18] Although the Chern vector ch S is invariant under (4.22), the object S itself is not invariant, rather it is mapped to its homological shift $S[2]$.

4.2.3 Bridgeland stability conditions

Donaldson-Thomas invariants $\Omega_\sigma(\gamma)$ depend on a charge vector $\gamma \in \Gamma = K(C)$ and a choice of Bridgeland stability condition $\sigma = (Z, \mathcal{A})$ on the derived category $C = D^b_c \mathrm{Coh} X$. The latter consists of a group homomorphism $Z : \Gamma \to \mathbb{C}$, called the central charge, and an Abelian subcategory $\mathcal{A} \subset C$, often called the heart, satisfying certain axioms [49] (see e.g. [138] for an introduction of stability conditions, or the lightning review in [47, §2.4]). Key among those is the fact that for any nonzero element $E \in \mathcal{A}$, the central charge is either in the strict upper half-plane, $\mathrm{Im}\, Z(E) > 0$, or on the negative real semi-axis, $Z(E) < 0$. The space of such stability conditions $\mathrm{Stab}\, C$ forms a complex manifold of dimension equal to the rank of the lattice Γ. It admits a left-action by auto-equivalences of C, and a right action by (the universal cover of) $GL(2,\mathbb{R})^+$, acting on the central charge Z viewed as a vector in $\mathbb{R}^2$. Given a stability condition σ and a charge vector $\gamma \in \Gamma$, one defines the moduli space (or rather, moduli stack) $\mathcal{M}_\sigma(\gamma)$ of σ-semi-stable objects $E \in \mathcal{A}$ with class $\gamma(E) = \gamma$ (i.e. objects $E \in \mathcal{A}$ such that $\arg Z(F) \leq \arg Z(E)$ for any subobject $F \subset E$). The refined (or motivic) DT invariant $\Omega_\sigma(\gamma, y)$ is an invariant of $\mathcal{M}_\sigma(\gamma)$, which reduces to the (shifted) Poincaré polynomial

$$\Omega_\sigma(\gamma, y) = \sum_{p=0}^{2d_{\mathbb{C}}(\gamma)} \dim H^p(\mathcal{M}_\sigma(\gamma), \mathbb{Q})\, (-y)^{p-d_{\mathbb{C}}(\gamma)} \tag{4.25}$$

whenever $\mathcal{M}_\sigma(\gamma)$ is a smooth projective variety of complex dimension $d_{\mathbb{C}}(\gamma)$ [121, 127]. The invariant $\Omega_\sigma(\gamma, y)$ is a Laurent polynomial with integer coefficients whenever σ is generic (which means that the only subobjects which can saturate the condition $\arg Z(F) \leq \arg Z(E)$ are those such that $\gamma(F)$ divides $\gamma(E)$). The invariant $\Omega_\sigma(\gamma, y)$ is the mathematical counterpart of the BPS index in physics, which counts stable BPS states in type II string theory on $\mathbb{R}^{3,1} \times X$, with a fugacity y conjugate to angular momentum J_3 in $\mathbb{R}^3$. Being integer valued, it is a locally constant function of σ, but may jump across walls of marginal stability $\mathcal{W}(\gamma, \gamma')$, where the phase of a semistable object E of charge γ becomes aligned with the phase of a subject $F \subset E$ of charge γ'. It is convenient to introduce the *rational* invariant $\bar{\Omega}_\sigma(\gamma, y)$

$$\bar{\Omega}_\sigma(\gamma, y) = \sum_{k|\gamma} \frac{y - y^{-1}}{k(y^k - y^{-k})} \Omega_\sigma(\gamma/k, y^k)\,, \tag{4.26}$$

which has simpler transformation properties under wall-crossing [121, 127, 146]. The Gieseker indices $\Omega_\eta(\gamma, y)$ defined in (4.15), counting H-semi-stable coherent sheaves on a surface S for the polarization $H = C + \eta F$, coincide with the DT invariants $\Omega_\sigma(\gamma, y)$ for the local CY threefold $X = K_S$ with Kähler class H in a suitable large volume limit.

In the present case $X = K_{\mathbb{F}_0}$, the space of Bridgeland stability conditions $\mathrm{Stab}\, C$ has complex dimension 4. Upon fixing the $\mathbb{C}^\times \subset GL(2,\mathbb{R})^+$ action, we get a three-dimensional slice with central charge

$$Z(\gamma) = -2rT_D + d_1 T_1 + d_2 T_2 - \mathrm{ch}_2 \tag{4.27}$$

parametrized by T_1, T_2 and T_D in some suitable domain $U \subset \mathbb{C}^3$. The parameters T_1 and T_2 can be viewed as the complexified Kähler parameters of the two factors in $S = \mathbb{P}^1 \times \mathbb{P}^1$, while T_D measures the size of S. In terms of the rank one 5D gauge theory engineered by M-theory compactified on K_S, $T_1 + T_2$ parametrizes the Coulomb branch while $T_1 - T_2$ corresponds to the 5D gauge coupling (or mass deformation of the superconformal point). Thus, it is natural to define

$$T_1 = T, \quad T_2 = T + m \tag{4.28}$$

and introduce the 'period vector' (so called because it is determined by periods of the mirror curve along the Π-stability slice) $\Pi = (1, m, T, T_D)$ such that

$$Z(\gamma) = \gamma \Sigma \Pi^t \,, \quad \Sigma = \begin{pmatrix} 0 & 0 & 0 & -2 \\ 0 & 0 & 1 & 0 \\ 0 & 1 & 1 & 0 \\ -1 & 0 & 0 & 0 \end{pmatrix} \tag{4.29}$$

In order for the central charge $Z(\gamma)$ to stay invariant under an autoequivalence acting as $\gamma \mapsto \gamma g$ on the Chern vector, the period vector should transform as $\Pi^t \mapsto M \Pi^t$ with $M = \Sigma^{-1} g^{-1} \Sigma$. For the autoequivalences listed in the previous subsection, the matrices M are given by

$$M_{k_1,k_2} = \begin{pmatrix} 1 & 0 & 0 & 0 \\ k_1 - k_2 & 1 & 0 & 0 \\ k_2 & 0 & 1 & 0 \\ \frac{k_1 k_2}{2} & \frac{k_2}{2} & \frac{k_1+k_2}{2} & 1 \end{pmatrix}, \quad M_{FB} = \begin{pmatrix} 1 & 0 & 0 & 0 \\ 0 & -1 & 0 & 0 \\ 0 & 1 & 1 & 0 \\ 0 & 0 & 0 & 1 \end{pmatrix} \tag{4.30}$$

$$M_C = \begin{pmatrix} 1 & 0 & 0 & 0 \\ 0 & 1 & 0 & 0 \\ 0 & 0 & 1 & -4 \\ 0 & 0 & 0 & 1 \end{pmatrix}, \quad M_{\tilde{C}} = \begin{pmatrix} 1 & 0 & 0 & 0 \\ 0 & 1 & 0 & 0 \\ 0 & 0 & 3 & -4 \\ 0 & 0 & 1 & -1 \end{pmatrix}, \quad M_{\mathbb{Z}_4} = \begin{pmatrix} 1 & 0 & 0 & 0 \\ 1 & -1 & 0 & 0 \\ 0 & -1 & -1 & -4 \\ 0 & \frac{1}{2} & \frac{1}{2} & 1 \end{pmatrix} \tag{4.31}$$

where M_C and $M_{\tilde{C}}$ implement the Seidel-Thomas twist with respect to $\mathcal{O}(0,0)$ and $\mathcal{O}(1,0)$, respectively. For later reference, we note that the only invariant period vector under $M_{\mathbb{Z}_4}$ is $(1, m, T, T_D) = (1, \frac{1}{2}, -\frac{1}{2}, \frac{1}{8})$, while invariance under the order 2 autoequivalence

$$M_B := (M_{\mathbb{Z}_4})^2 = M_C \cdot M_{\tilde{C}} \cdot M_{1,1} = \begin{pmatrix} 1 & 0 & 0 & 0 \\ 0 & 1 & 0 & 0 \\ -1 & 0 & -1 & 0 \\ \frac{1}{2} & -\frac{1}{2} & 0 & -1 \end{pmatrix} \tag{4.32}$$

only requires $(T, T_D) = (-\frac{1}{2}, \frac{1-m}{4})$, irrespective of the value of m. The matrices which preserve a generic m are all of the form

$$M = \begin{pmatrix} 1 & 0 & 0 & 0 \\ 0 & 1 & 0 & 0 \\ n_1 & n_2 & 1 & 0 \\ \frac{\ell_1}{2} & \frac{\ell_2}{2} & 0 & 1 \end{pmatrix} \cdot \begin{pmatrix} 1 & 0 & 0 & 0 \\ 0 & 1 & 0 & 0 \\ 0 & 0 & d & c \\ 0 & 0 & b & a \end{pmatrix} \tag{4.33}$$

where a, b, c, d, n_i, ℓ_i integers, $ad - bc = 1, c = 0 \mod 4$. In particular, the monodromy group Γ for fixed m is an extension of $\Gamma_0(4)$ by a rank 4 lattice, as anticipated in footnote 9. When m is integer or half-integer, Γ gets extended by the generator $M_{k_1,k_2} M_{FB}$ with $2m = k_1 - k_2$.

There is a simple two-dimensional slice inside U which is preserved under tensoring with $\mathcal{O}(k_1, k_2)$, namely the locus $T_D = \frac{1}{2} T(T + m)$. This is recognized as (minus half) the central charge of a D4-brane wrapped on $\mathbb{F}_0$ in the large volume limit. We thus define the large volume central charge by

$$Z^{\mathrm{LV}}_{T,m}(\gamma) = -rT(T + m) + d_1 T + d_2(T + m) - \mathrm{ch}_2 \tag{4.34}$$

In addition to being invariant under tensoring with $O(k_1, k_2)$, the central charge (4.34) is also invariant under fiber-base duality,

$$Z^{\rm LV}_{T,m}(r, d_1, d_2, {\rm ch}_2) = Z^{\rm LV}_{T+m,-m}(r, d_2, d_1, {\rm ch}_2) \tag{4.35}$$

and transforms into (minus) its complex conjugate under derived duality,

$$Z^{\rm LV}_{-\overline{T},-\overline{m}}(-r, d_1, d_2, -{\rm ch}_2) = -\overline{Z^{\rm LV}_{T,m}(r, d_1, d_2, {\rm ch}_2)} \tag{4.36}$$

We note that this slice does not contain any invariant point under $M_{\mathbb{Z}_4}$ or M_B.

Another way to reduce the dimension of the space of Bridgeland stability conditions is to consider orbits under the action of the (universal cover of the) group $GL(2,\mathbb{R})^+$, acting by positive-determinant linear transformations of $({\rm Re}\, Z, {\rm Im}\, Z)$, and corresponding tilting of the heart. Using this action, one may transform the general central charge (4.27) into $Z^{\rm LV}_{T_1^{\rm LV}, T_2^{\rm LV} - T_1^{\rm LV}}$ provided

$$\frac{2\,{\rm Im}(T_D\overline{T_1})}{{\rm Im}\, T_2} = |T_1^{\rm LV}|^2\,, \quad \frac{{\rm Im}(T_D + \frac{1}{2}\overline{T_1}T_2)}{{\rm Im}\, T_2} = {\rm Re}\, T_1^{\rm LV} \tag{4.37}$$

for some $T_1^{\rm LV}$ with ${\rm Im}\, T_1^{\rm LV} > 0$, and the same equation with indices 1 and 2 exchanged. This is possible provided

$${\rm Im}\, T_1 > 0, \quad {\rm Im}\, T_2 > 0, \quad 2\,{\rm Im}(T_D\overline{T_1})\ {\rm Im}\, T_2 - \Big({\rm Im}(T_D + \tfrac{1}{2}\overline{T_1}T_2)\Big)^2 > 0 \tag{4.38}$$

Note that this is invariant under the exchange of T_1 and T_2, thanks to the identity

$${\rm Im}\, T_1\ {\rm Im}(T_D\overline{T_2}) - {\rm Im}\, T_2\ {\rm Im}(T_D\overline{T_1}) = {\rm Im}\, T_D\ {\rm Im}(T_1\overline{T_2}) \tag{4.39}$$

It will be useful to define the $GL(2,\mathbb{R})^+$-invariant coordinates

$$s := \frac{{\rm Im}\, T_D}{{\rm Im}\, T}, \quad w := \frac{{\rm Im}(T_D\overline{T})}{{\rm Im}\, T}, \quad M_1 := -\frac{{\rm Im}(m\overline{T})}{{\rm Im}\, T}, \quad M_2 := \frac{{\rm Im}\, m}{{\rm Im}\, T} \tag{4.40}$$

such that $T_D = -w + sT, m = M_1 + M_2 T$, or alternatively

$$\eta := M_2 + 1, \quad s_1 := \frac{s - \frac{M_1}{2}}{\eta}, \quad w_1 := \frac{w}{\eta} - \frac{1}{2}s_1^2 \tag{4.41}$$

In terms of these coordinates, one has

$$2\,{\rm Im}(T_D\overline{T_1})\ {\rm Im}\, T_2 - \Big({\rm Im}(T_D + \tfrac{1}{2}\overline{T_1}T_2)\Big)^2 = 2\eta^2({\rm Im}\, T)^2 w_1 \tag{4.42}$$

so the inequalities (4.38) can be written as

$${\rm Im}\, T > 0, \quad \eta > 0, \quad w_1 > 0 \tag{4.43}$$

Under spectral flow (4.20), ${\rm Im}\, T$ and η stay invariant while

$$(s, w, M_1) \mapsto \Big(s + \tfrac{k_1+\eta k_2}{2}, w + k_2(s - \tfrac{M_1}{2}) + \tfrac{\eta k_2^2}{2}, M_1 + k_1 - \eta k_2\Big) \tag{4.44}$$

leaving the inequalities (4.43) invariant.

Now, let us discuss the construction of a heart $\mathcal{A}$ for the general central charge (4.27), such that $(Z, \mathcal{A})$ provides an actual Bridgeland stability condition. As recalled in the beginning of this section, a necessary condition on the heart $\mathcal{A}$ is that, for all non-zero objects $E \in \mathcal{A}$, $\mathrm{Im}\, Z(E) \geq 0$ and $\mathrm{Re}\, Z(E) < 0$ whenever $\mathrm{Im}\, Z(E) = 0$. Assuming that $r(E) \neq 0$, the imaginary part of the central charge is expressed in terms of the slope defined in (4.10) via

$$\mathrm{Im}\, Z(\gamma) = (-2rs + d_1 + \eta d_2)\, \mathrm{Im}\, T = -2r\, \big(s - \mu_\eta(\gamma)\big)\, \mathrm{Im}\, T \tag{4.45}$$

Moreover, when $\mathrm{Im}\, Z(\gamma)$ vanishes, the real part evaluates to

$$\begin{aligned} \mathrm{Re}\, Z(\gamma) &= 2rw + d_2 M_1 - \mathrm{ch}_2 \\ &= r\left[2w - \frac{1}{\eta}(s - \tfrac{M_1}{2})^2 + \Delta + \frac{(d_1 - \eta d_2 - M_1 r)^2}{4\eta r^2}\right] \end{aligned} \tag{4.46}$$

Although this is guaranteed by construction, one may check using (4.44) that (4.46) is invariant under spectral flow, as long as the condition $s = \mu_\eta(\gamma)$ is imposed. If $r = 0$, then $\mathrm{Im}\, Z(\gamma) = (d_1 + d_2\eta)\, \mathrm{Im}\, T$, which is always positive as long as $\mathrm{Im}\, T > 0, \eta > 0$ and $d_1, d_2 \geq 0$.

Let us now define

$$\delta(s, \eta, M_1) := \inf_E \left[\Delta(E) + \frac{(d_1(E) - \eta d_2(E) - M_1 r(E))^2}{4\eta r^2(E)}\right] \tag{4.47}$$

where the infimum runs over all slope-semistable sheaves $E \in \mathcal{E}_\eta$ of positive rank and slope $\mu_\eta(E) = s$. The function (4.47) is related to (4.14) through[19]

$$\delta(s, \eta, M_1) = \inf_{a+\eta b = 2s} \left[\hat{\delta}_{\mathrm{DLP}}(\eta, a, b) + \frac{1}{4\eta}(a - \eta b - M_1)^2\right] \tag{4.48}$$

where $\hat{\delta}_{\mathrm{DLP}}(\eta, a, b) = \min(\delta_{\mathrm{DLP}}(\eta, a, b), \Delta(F))$ where $F \in \mathcal{E}_\eta$ runs over all Gieseker-stable exceptional bundles with slope (a, b), see Fig. 4.14 for an illustrative case $M_1 = 1/4, \eta = 1$. Note that the term in bracket is a piecewise linear function (in general discontinuous for $\eta \neq 1$) of (a, b) along the line $a + \eta b = 2s$, thanks to a cancellation between the quadratic terms in (4.48) and (4.14). Moreover, $\delta(s, \eta, M_1) \geq \frac{4}{9}$ except at points where there exists integer values (a, b) such that $a + \eta b = 2s$ and $|a - \eta b - M_1| < (4/3)\eta^{1/2}$.

Then, inside the domain (which contains the large volume region (4.43))

$$U_{\mathrm{geo}} = \left\{\mathrm{Im}\, T > 0, \quad \eta > 0, \quad w_1 > -\frac{\delta(s, \eta, M_1)}{2\eta}\right\} \subset U \tag{4.49}$$

we can define the heart $\mathcal{A}$ by the standard tilt construction, i.e. generated by length-two complexes $\mathcal{E} \to \mathcal{F}$ where $\mathcal{E}$ (in degree -1) is a slope-semistable torsion-free sheaf of slope $\mu_\eta(\mathcal{E}) \leq s$ and $\mathcal{F}$ (in degree 0) is a slope-semistable torsion-free sheaf of slope $\mu_\eta(\mathcal{F}) > s$ or a torsion sheaf. This produces a stability condition such that skyscraper sheaves are stable, also known as a *geometric* stability condition. Along the loci $\mathrm{Im}\, T = 0$ or $\eta = 0$, the central charge of D2-branes wrapping C or F becomes aligned with the central charge of D0-branes, corresponding to a boundary of the space of geometric stability conditions. The loci where the last inequality in (4.49) becomes saturated correspond to boundaries where skyscraper sheaves are destabilized by torsion-free sheaves.

[19] Observe that if $\delta_{\mathrm{DLP}}(\eta, a, b)$ was constant, the infimum would be obtained for $(a, b) = (s + \frac{M_1}{2}, \frac{1}{\eta}(s - \frac{M_1}{2}))$.

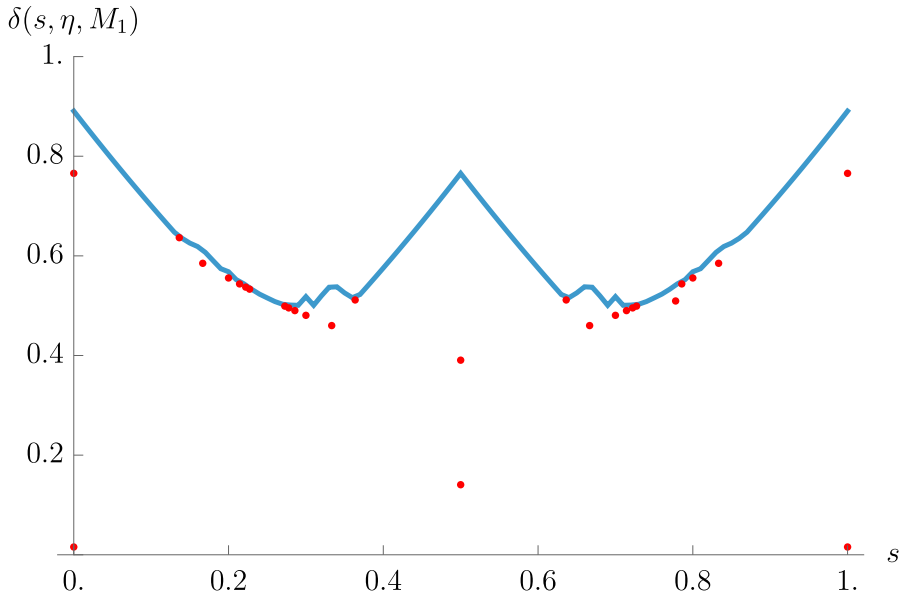


Figure 4.14: Approximate shape of $\delta(s,\eta,M_1)$ for $\eta = 1, M_1 = 1/4$. The red dots indicate the corresponding lowest values arising from exceptional stable bundles.

4.2.4 Stability conditions on the Π-stability slice

As explained in Appendix 4.6, mirror symmetry singles out a particular complex two-dimensional slice in $\operatorname{Stab} C$ where the coefficients T, T_D are expressed in terms of the modular parameter $\tau \in \mathbb{H}$ of the mirror curve and the mass parameter m via the contour integral representation (4.6). The general strategy to construct the corresponding heart is to check that the conditions (4.49) are satisfied in a fundamental domain of $\Gamma_0(4)$, use the tilt construction in that domain, and extend it to the full ($\mathbb{Z}^4$ cover over the) Poincaré upper half-plane using autoequivalences of C. The details however differ depending whether m is integer, real or complex valued.

$m \in \mathbb{Z}$

Upon tensoring with $\mathcal{O}(0,m)$ we can assume that $m = 0$. In this case, the modular form (4.8) is an ordinary weight 3 Eisenstein series for $\Gamma_1(4)$, with no square root singularities. The universal cover of the Kähler moduli space (with integer m) is therefore the Poincaré upper half plane, and it suffices to construct stability conditions for τ in the fundamental domain $\mathcal{F}$ bounded by the vertical lines $\tau \in \mathrm{i}\mathbb{R}, \tau \in 1 + \mathrm{i}\mathbb{R}$ and the half-circles $C := C(\frac{3}{4}, \frac{1}{4}), \tilde{C} := C(\frac{1}{4}, \frac{1}{4})$, and extend them elsewhere by acting with the autoequivalences $ST_{\mathcal{O}(0,0)}$ and $\mathcal{O}(1,1) \otimes -$, which generate the group $\Gamma_0(4)$.

As for the inequality $\operatorname{Im} T > 0$, the q-series expansion (4.194) with $m = 0$ shows that it holds at the boundaries $\tau \in \mathrm{i}\mathbb{R}^+, \tau \in 1 + \mathrm{i}\mathbb{R}^+$, and numerical analysis shows that it also holds along the half-circles C and $\tilde{C}$, although it becomes saturated at the dual conifold point $\tau = \frac{1}{2}$. Since T is holomorphic inside $\mathcal{F}$, the inequality holds everywhere in $\mathcal{F}$ (and its translates $\mathcal{F}(k)$ for $k \in \mathbb{Z}$).

Using the reality conditions (4.198), we see that $s = \operatorname{Re} \tau$ along the vertical lines $\operatorname{Re} \tau \in \mathbb{Z}$ and $\operatorname{Re} \tau \in \mathbb{Z} + \frac{1}{2}$. Moreover, similar to [47, (A.57)], we can use the fact that M_C restricts to $\tau \mapsto -\bar{\tau}$ along $\tilde{C}$, to conclude that $\operatorname{Im} T_D = 0$ along C, hence $s = 0$. Similarly, since $M_{\tilde{C}}$ restricts to $\tau \mapsto 1 - \bar{\tau}$ along C, one finds $\operatorname{Im} T_D = \operatorname{Im} T$ hence $s = 1$. In the vicinity of the dual conifold point, s varies from 0 on $\tilde{C}$ to $\frac{1}{2}$ on the vertical axis $\frac{1}{2} + \mathrm{i}\mathbb{R}^+$ to 1 on C (see Fig. 4.15). Using

(4.170) and the equality $w = s\,\mathrm{Re}\,T - \mathrm{Re}\,T_D$, it follows that $w = \frac{s}{2} - \frac{1}{4}$ grows linearly with s around the cusp $\tau = \frac{1}{2}$. Tensoring with $\mathcal{O}(k,k)$, we find that the union of the fundamental domains $\mathcal{F}(k)$ maps to the region in the (s,w) plane above the piecewise linear curve joining the points $(k, \frac{1}{2}k^2 - \frac{1}{4})$ with $k \in \mathbb{Z}$, see Fig. 4.16.

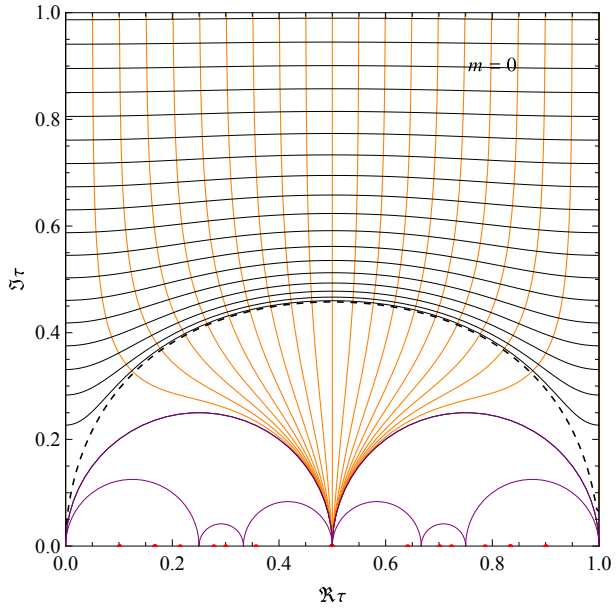


Figure 4.15: For $m = 0$ (hence $\lambda = 1$), the contours with fixed $s = \frac{\mathrm{Im}\,T_D}{\mathrm{Im}\,T}$ in the strip $\tau_1 \in (0,1)$, shown in orange, all converge to $\tau = \frac{1}{2}$. The contours with fixed (and real) $t = \sqrt{2w - s^2}$ approach $\tau = 0$ and $\tau = 1$ when $t \to 0$ (shown in dashed line), but stay away from $\tau = \frac{1}{2}$. In the region above the dashed line, Π stability is related to large volume stability by $GL(2,\mathbb{R})^+$.

In order to apply the tilting construction explained below (4.40), we need to check that the condition (4.49) (with $\eta = 1, M_1 = 0$)

$$w - \frac{1}{2}s^2 > -\frac{1}{2}\delta(s,1,0) \tag{4.50}$$

is also satisfied. The lower bound is the blue jagged curve shown in Figure 4.16 along the red dots corresponding to exceptional bundles. Since the left-hand side of (4.50) is greater than $-\frac{1}{4}$, attained at the points $(k, \frac{1}{2}k^2 - \frac{1}{4})$, while $\delta(s,1,0) \geq \frac{1}{2}$ except when s is the slope of exceptional bundles of rank 1 or 3; in both cases, inspection of Fig. (4.16) shows that the bound still holds. Thus, every point in the interior of the fundamental domain and its translates is endowed with a geometric stability condition, while the skyscraper sheaves become destabilized by $\mathcal{O}(k,k)$ and $\mathcal{O}(k+1,k+1)$ along the half-circles $\tilde{C}(k)$ and $C(k)$, respectively.

$m \in \mathbb{R}\backslash\mathbb{Z}$

When m is real but not integer, we can tensor with $\mathcal{O}(0,\lfloor m \rfloor)$ and assume $0 < m < 1$. The modular form (4.8) now has square root singularities on the boundary of the fundamental domain at $\tau_B \in C$ and[20] $\tilde{\tau}_B := \frac{\tau_B - 1}{4\tau_B - 3} \in \tilde{C}$. As indicated before, we choose branch cuts along semi-circles from τ_B to $\tau = \frac{1}{2}$, and similarly from $\tilde{\tau}_B$ to $\tau = \frac{1}{2}$. Using the reality conditions (4.198) implies

[20] For m real, $\frac{\tau_B - 1}{4\tau_B - 3}$ actually coincides with $1 - \bar{\tau}_B$.

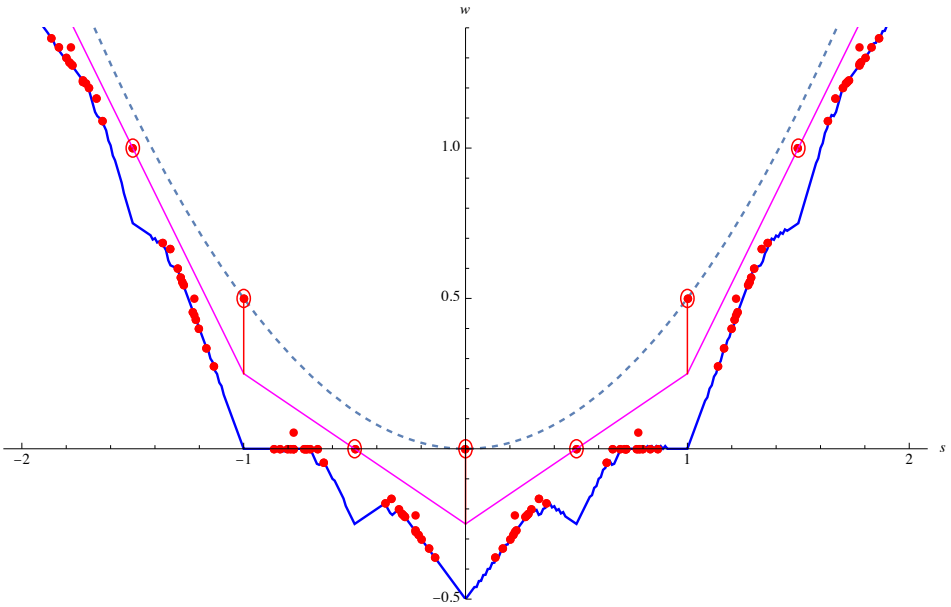


Figure 4.16: Image of the fundamental domain $\mathcal{F}$ and its translates into the (s, w) plane for $m = 0$. The dashed line is the parabola $w = \frac{1}{2}s^2$, the red vertical segments are the images of the half-circles on the boundary of the fundamental domain and its translates and the segments in magenta correspond to the values of (s, w) around the dual conifolds $\tau \in \frac{1}{2} + \mathbb{Z}$. The blue curve denotes the (continuous part of the) lower bound $\frac{1}{2}s^2 - \frac{1}{2}\delta(s, 1, 0)$ of w in the geometric domain (4.49), and the red dots are the discontinuous values occurring at slopes of exceptional stable bundles. The circled ones are those which are massless at the conifold points $\tau = k$ and $\tau = k + \frac{1}{2}$.

that $s = \operatorname{Re}\tau$ along the vertical lines $\operatorname{Re}\tau \in \mathbb{Z}$ and $\operatorname{Re}\tau \in \mathbb{Z} + \frac{1}{2}$. Moreover, one may check that $\operatorname{Im} T > 0$ on the fundamental domain $\mathcal{F}(k)$ for any $k \in \mathbb{Z}$ (except at the branch points on $\tilde{C}(k)$ and $C(k)$). When $m = 0$, τ_B collides with the dual conifold singularity at $\tau = \frac{1}{2}$ and the branch cuts disappear.

Due to the branch points on C and $\tilde{C}$, it now turns out that s is discontinuous along the boundary of the fundamental domain, namely $s = 0$ along the half-circle $\tilde{C}$ from $\tau = 0$ up to $\tilde{\tau}_B$, $s = \frac{1}{2}$ on the two arcs in between $\tilde{\tau}_B$ and τ_B and $s = 1$ along C from τ_B to 1. Along these arcs, the central charge associated to $\mathcal{O}(0,0), \mathcal{O}(1,0)$ and $\mathcal{O}(1,1)$ becomes real and negative, respectively. Moreover, along infinitesimal half-circles around $\tilde{\tau}_B$ and τ_B, s increases continuously from 0 to $\frac{1}{2}$ and from $\frac{1}{2}$ to 1, respectively (see Fig. 4.17 for the example of $m = \frac{1}{2}$). Using (4.213), (4.234) and the equality $w = s \operatorname{Re} T - \operatorname{Re} T_D$, one finds that (s, w) lies on the segment $w = \left(\frac{1}{2} - m\right) s + \frac{m-1}{4}$ with $s \in (0, \frac{1}{2})$ on an infinitesimal half-circle around $\tilde{\tau}_B$, and on the segment $w = \frac{1}{2}s - \frac{m+1}{4}$ with $s \in (\frac{1}{2}, 1)$ on an infinitesimal half-circle around τ_B, with the two segments intersecting at $(s, w) = (\frac{1}{2}, -\frac{m}{4})$. On the other hand, the boundary circle arcs map to vertical segments at $s \in \mathbb{Z}/2$, ending at the images of the conifold points $\tau = k$ and dual conifold points $\tau = k + \frac{1}{2}$ (see (4.217), (4.237))

$$(s, w) = \left(k, \tfrac{1}{2}k(k-m)\right) \quad \text{or} \quad (s, w) = \left(k + \tfrac{1}{2}, \tfrac{1}{2}k(k+1-m)\right) \tag{4.51}$$

Hence, the union of the fundamental domains $\mathcal{F}(k)$ is mapped to the region above the piecewise

linear curve (shown in magenta in Fig. 4.17) joining the points

$$\left(k, \tfrac{k(k-m)}{2} + \tfrac{m-1}{4}\right) \to \left(k + \tfrac{1}{2}, \tfrac{k(k+1-m)}{2} - \tfrac{m}{4}\right) \to \left(k+1, \tfrac{(k+1)(k+1-m)}{2} + \tfrac{m-1}{4}\right) \to \dots \tag{4.52}$$

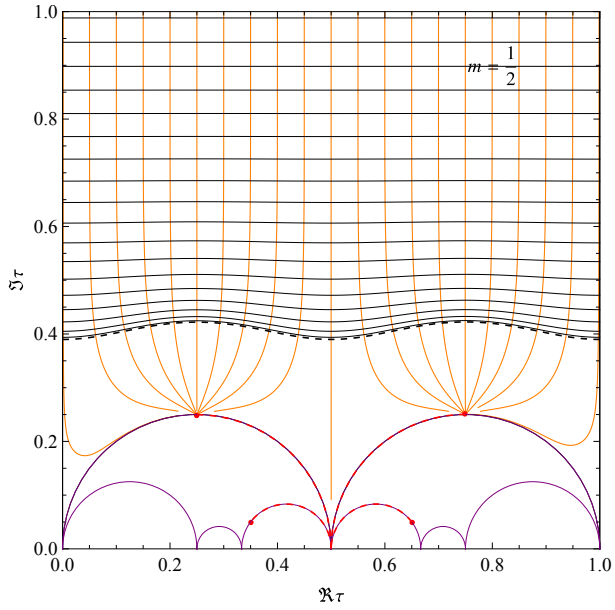


Figure 4.17: For $m = \frac{1}{2}$, the contours with fixed $s = \frac{\mathrm{Im}\, T_D}{\mathrm{Im}\, T}$ in the strip $\tau_1 \in (0,1)$, shown in orange, converge either to $\tau = \frac{1+\mathrm{i}}{4}$ or $\tau = \frac{3+\mathrm{i}}{4}$. The contours with fixed (and real) $t = \sqrt{2w - (s - \frac{1}{4})^2}$ stay well above the conifold and branch points In the region above the dashed line $t = 0$, Π stability is related to large volume stability by $GL(2,\mathbb{R})^+$.

In order to apply the tilting construction explained below (4.40), we need to check that the condition (4.49) (with $\eta = 1$)

$$w - \frac{1}{2}(s - \tfrac{m}{2})^2 > -\frac{1}{2}\delta(s, 1, m) \tag{4.53}$$

is also satisfied. The lower bound is the blue jagged curve shown in Fig. 4.18, along with the red dots corresponding to exceptional bundles. The left-hand side of (4.53) is greater than $-\frac{1+\max(m,1-m)^2}{8}$, attained at the corners of the piecewise linear curve (4.52), while $\delta(s,1,m) \geq \frac{1}{2}$ except when s coincides with the slope of rank 1 or rank 3 exceptional bundles, where inspection of Fig. 4.18 shows that the bound (4.53) is still satisfied. Thus, every point in the interior of the fundamental domain and its translates is endowed with a geometric stability condition, while the skyscraper sheaves become destabilized by $\mathcal{O}(k,k), \mathcal{O}(k+1,k)$ or $\mathcal{O}(k+1,k+1)$ along the half-circles $\tilde{C}(k)$ and $C(k)$.

m complex

When $\mathrm{Im}\, m \neq 0$, there are several complications:

i) The $GL(2,\mathbb{R})^+$-invariant parameters M_1, η entering in the construction of the heart become non-trivial functions of τ (assuming, as we always do, that the parameter $m = M_1 + (\eta - 1)T$

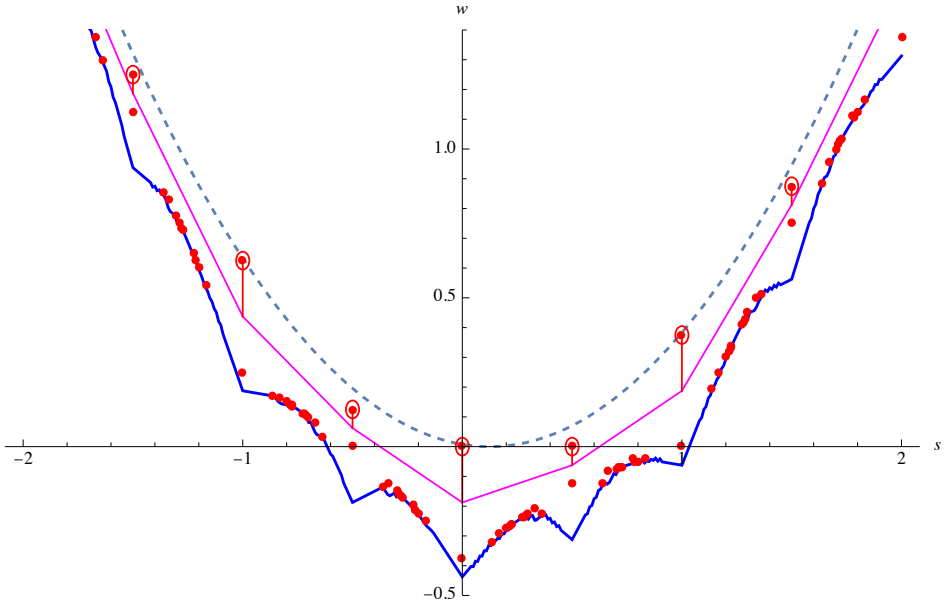


Figure 4.18: Image of the fundamental domain $\mathcal{F}$ and its translates into the (s, w) plane, shown for $m = 1/4$. The dashed line is the parabola $w = \frac{1}{2}(s - \frac{m}{2})^2$, the red vertical segments are the images of the half-circles on the boundary of the fundamental domain and its translates and the segments in magenta correspond to the values of (s, w) on an infinitesimal circle around the branch points. The blue curve denotes the (continuous part of the) lower bound $\frac{1}{2}(s - \frac{m}{2})^2 - \frac{1}{2}\delta(s, 1, m)$ on w in the geometric domain (4.49), and the red dots are the discontinuous values occurring at slopes of exceptional stable bundles. The circled ones are those which are massless at the conifold points $\tau = k$ and $\tau = k + \frac{1}{2}$, lying along the shifted parabolas $w - \frac{1}{2}(s - \frac{m}{2})^2 = -\frac{m^2}{8}$ and $-\frac{(1-m)^2}{8}$, respectively.

is held fixed). This is already easily seen using the expansions (4.194) for large $\mathrm{Im}\,\tau$, where (denoting $\tau = \tau_1 + \mathrm{i}\tau_2, m = m_1 + \mathrm{i}m_2$

$$M_1 \simeq \frac{m_1\tau_2 - m_2\tau_1}{\tau_2 - \frac{m_2}{2}}, \quad \eta \simeq \frac{\tau_2 + \frac{m_2}{2}}{\tau_2 - \frac{m_2}{2}}, \quad s \simeq \frac{\tau_1\tau_2 - \frac{m_1m_2}{4}}{\tau_2 - \frac{m_2}{2}} \tag{4.54}$$

up to worldsheet instanton corrections. As a result, we cannot map the fundamental domain in the (s_1, w_1) plane without also keeping track of (η, M_1).

ii) The branch point τ_B moves inside the fundamental domain $\mathcal{F}$, and the inequality $\mathrm{Im}\,T > 0$ fails along a curve extending from[21] τ_B to $\tau = \frac{3}{4}$. For the purpose of the current discussion, it is thus natural to choose this curve $\mathrm{Im}\,T = 0$ as the branch cut. Moreover, the locus where $\mathrm{Im}\,Z(\mathcal{O}(1,0)) = 0$ intersects the cut at a point τ_b where $\mathrm{Im}\,T_D$ also vanishes, and likewise the locus $\mathrm{Im}\,Z(\mathcal{O}(1,1)) = 0$ reaches the same point τ_b on the other side of the cut (see Fig. 4.5);

iii) Simultaneously, the branch point $\tilde{\tau}_B$ and the loci where $Z(\mathcal{O}(0,0))$ and $Z(\mathcal{O}(1,0))$ are real and negative leave the fundamental domain $\mathcal{F}$, and move into its image $\tilde{\mathcal{F}}$ under M_S. They intersect the locus $\mathrm{Im}\,T = 0$ at a point $\tilde{\tau}_b$, but this locus lies below the arcs $\mathrm{Im}\,Z(\mathcal{O}(0,0)) = 0$ and $\mathrm{Im}\,Z(\mathcal{O}(1,0)) = 0$.

The last two bullet points show that the space of geometric boundary conditions cannot extend beyond the loci $s = 0$, $s = \frac{1}{2}$ and $s = \frac{1+\eta}{2}$, along which skyscraper sheaves are destabilized by $\mathcal{O}(0,0)$, $\mathcal{O}(1,0)$ and $\mathcal{O}(1,1)$, respectively, nor across the segment from τ_b to τ_B along the locus $\mathrm{Im}\,T = 0$, along which skyscraper sheaves are destabilized by D2-branes. Let $\widehat{\mathcal{F}}$ be the domain bounded by these loci in the strip $0 \le \mathrm{Re}(\tau_1) < 1$. Since $\mathcal{O}(1,1)$ and $\mathcal{O}(1,0)$ are mapped to $\mathcal{O}(0,0)$ and $\mathcal{O}(0,1)$ under M_S, $\widehat{\mathcal{F}}$ is still a fundamental domain under $\Gamma_0(4)$, and it suffices to check that it satisfies the inequalities in (4.49). We shall not attempt to prove it, but rather give some numerical evidence that it does.

In Fig. 4.20, we show the value of w_1 along the boundary of the fundamental domain $\widehat{\mathcal{F}}$, including the two sides of the locus $\mathrm{Im}\,T = 0$. This requires applying the monodromy $M_B(0)$ around τ_B, acting as

$$\begin{aligned} (T, T_D) &\mapsto (1 - T, \tfrac{1+m}{2} - T_D) \\ (s, w, \eta, M_1) &\mapsto \left(s + \tfrac{1}{2}(1-\eta), -w + s - \tfrac{\eta + M_1}{2}, 2 - \eta, M_1 + \eta - 1\right) \end{aligned} \tag{4.55}$$

We first observe that the inequality $w_1 > 0$, which characterizes the large volume region, fails when $\mathrm{Im}\,\tau$ becomes small enough along the vertical boundaries at $\tau_1 = 0$ and $\tau_1 = 1$, consistent with Fig. 4.19. Second, we observe that $w_1 > -\frac{2}{9\eta}$ everywhere except on the two sides of the segment $\mathrm{Im}\,T = 0$ on the boundary (as well as tiny segments along $\mathrm{Im}\,Z(\mathcal{O}(1,0)) = 0$ and $\mathrm{Im}\,Z(\mathcal{O}(1,1)) = 0$ in the vicinity of τ_b). Since $\delta(s, \eta, M_1) \ge \frac{4}{9}$ away from integer and half-integer slopes, this indicates that the inequality $w_1 > -\delta(s, \eta, M_1)/(2\eta)$ is satisfied everywhere in $\widehat{\mathcal{F}}$, except perhaps inside a tiny sliver along the segment $\mathrm{Im}\,T = 0$. We speculate that, using more refined information about $\delta(s, \eta, M_1)$, the inequalities (4.49) could be shown to hold everywhere in the interior of the fundamental domain $\widehat{\mathcal{F}}$, so that geometric stability conditions can be obtained

[21] To see this, one can use the expansion (4.245) around τ_B to find that $\mathrm{Im}\,T = 0$ along the infinitesimal segment $\tau = \tau_B - \frac{\mathrm{i}\eta^8(2\tau_B)}{\sin^2(\pi m/2)\eta^8(\tau_B)\eta^8(4\tau_B)}\epsilon + O(\epsilon^2)$ for small $\epsilon > 0$, which points towards the real axis.

using the tilting construction. If so, the intersection between the slice of Π-stability conditions and the space of geometric stability conditions would again coincide with the domain $\widehat{\mathcal{F}}$ and its translates. Stability conditions on the full $\mathbb{Z}^4$ cover of the Poincaré half-plane can then be obtained from those in $\mathcal{F}$ by applying the autoequivalences $ST_{\mathcal{O}(0,0)}, \mathcal{O}(1,1)\otimes -$ and $M_B(0)$.

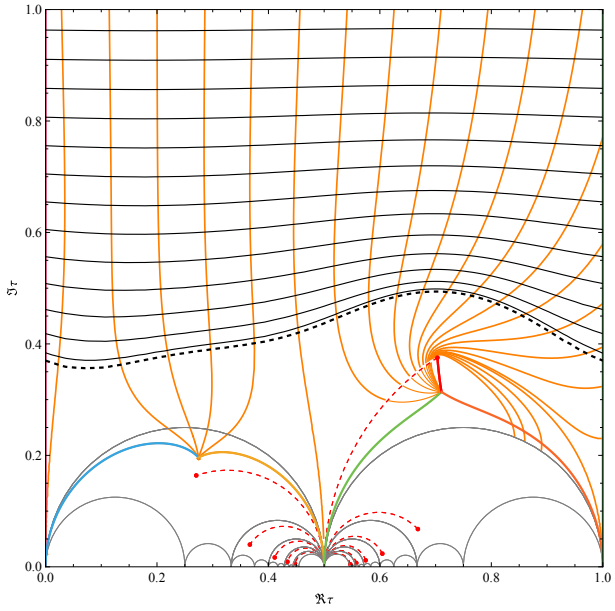


Figure 4.19: Contours with fixed s (orange) or fixed $t = \sqrt{2w_1}$ (black) in the τ half-plane, for $m = 0.4+0.3\mathrm{i}$. In the region above the dashed line, corresponding to $t = 0$, Π stability is related to large volume stability by $GL(2,\mathbb{R})^+$. The blue, yellow, green, dark orange and red lines delimit (putatively) the domain of geometric stability conditions, as in Fig. 4.5.

4.3 Quiver scattering diagram

The derived category of (compactly supported) coherent sheaves on $K_{\mathbb{F}_0}$ is equivalent to the derived category of representations of quivers attached to cyclic strong exceptional collections [31, 43]. In this section we discuss the scattering diagram associated to the orbifold exceptional collection (4.3), also known as phase II quiver, and to one of its mutations, sometimes known as phase I quiver, reproducing some of the results obtained in [37, §4.1].

4.3.1 Basics of quiver scattering diagrams

For completeness, we include a brief review of scattering diagrams for quivers with relations, heavily based on §3.1 in our earlier work [47], with minor changes of notation.

Let (Q,W) be a quiver with potential. A representation R of (Q,W) is a set of finite dimensional vector spaces M_i for every node $i \in Q_0$, and linear maps $f_a\colon M_i \to M_j$ for every arrow $(a\colon i\to j)\in Q_1$ such that for any arrow $a\in Q_1$, the element $\partial W/\partial a$ in the path algebra of Q evaluates to zero on R. The set of representations R forms an Abelian category $\mathcal{A}$ graded by the lattice $\mathbb{Z}^{Q_0}$ spanned by the dimension vector $\vec{N} = \dim R = (\dim M_i)_{i\in Q_0}$. Given a choice of *King stability parameters* $\zeta\in\mathbb{R}^{Q_0}$, a representation R is called ζ-semi-stable if and only if $(\zeta,\vec{N}) = 0$ and $(\zeta,\vec{N}')\le 0$ for any subrepresentation $R'\subset R$ of dimension vector $\vec{N}'$. This coincides with

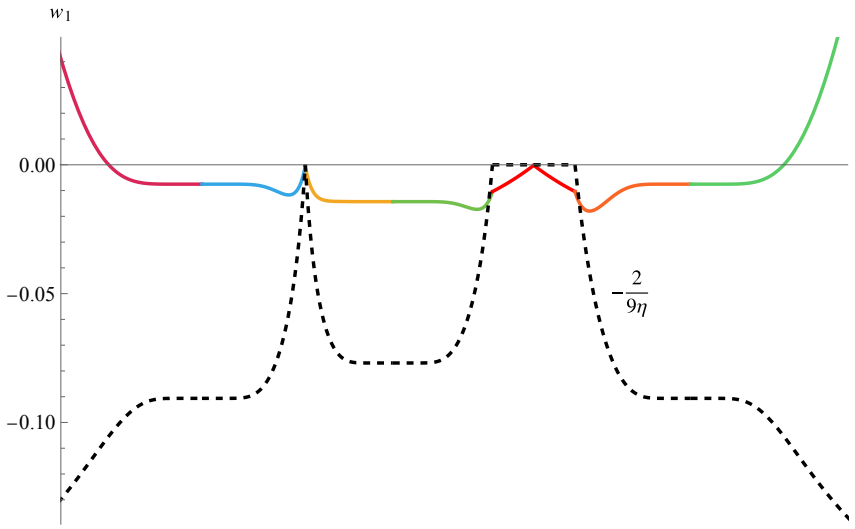


Figure 4.20: Values of w_1 (defined in (4.41)) along the various components of the boundary of the space of geometric stability conditions, including either side of the locus $\mathrm{Im}\, T = 0$, compared to the sufficient lower bound $-2/(9\eta)$ (dashed line) following from $\delta(s, \eta, M_1) > \frac{4}{9}$. The value of m and the color coding for the boundary components is the same as in Figs. 4.5 and 4.19.

the usual notion of σ-semistability for a stability condition $\sigma = (Z, \mathcal{A})$ with central charge $Z(\vec{N}) = \sum_{i\in Q_0}(-\zeta_i + \mathrm{i}\rho_i)N_i$ for any choice of $\rho_i > 0$, provided one restricts to objects with $Z(E) \in \mathrm{i}\mathbb{R}^+$. We denote by $\mathcal{M}_\zeta(\vec{N})$ the moduli space of ζ-semi-stable representations of dimension vector $\vec{N}$, by $\Omega_\zeta(\vec{N})$ its refined Donaldson-Thomas invariant (4.25) and by $\bar{\Omega}_\zeta(\vec{N})$ its rational counterpart (4.26). These invariants vanish unless $\vec{N}$ belongs to the positive quadrant $\Gamma_+ = \mathbb{N}^{Q_0}$, in particular if all the ζ_i's have the same sign.

The set of DT invariants is conveniently encoded in a stability scattering diagram $\mathcal{D}_Q$ in the space $\mathbb{R}^{Q_0}$ spanned by King stability parameters, defined as follows [50]. We first introduce the hyperplane orthogonal to $\vec{N}$, called *geometric ray*,

$$\mathcal{R}_Q^{\mathrm{geo}}(\vec{N}) = \{\zeta : (\zeta, \vec{N}) = 0\} \tag{4.56}$$

and define the *active ray* $\mathcal{R}_Q(\vec{N})$ as the subset of $\mathcal{R}_Q^{\mathrm{geo}}(\vec{N})$

$$\mathcal{R}_Q(\vec{N}) = \{\zeta : (\zeta, \vec{N}) = 0, \quad \bar{\Omega}_\zeta(\vec{N}) \neq 0\} \tag{4.57}$$

Furthermore, to each point $\zeta \in \mathcal{R}_Q(\vec{N})$ we associate an automorphism $\mathcal{U}_\zeta(\vec{N})$ of the quantum torus algebra (or a suitable pronilpotent completion thereof) generated by formal variables $\mathcal{X}_{\vec{N}}$ for any $\vec{N} \in \Gamma_+$, subject to the relations

$$\mathcal{X}_{\vec{N}}\, \mathcal{X}_{\vec{N}'} = (-y)^{\langle \vec{N}, \vec{N}' \rangle} \mathcal{X}_{\vec{N}+\vec{N}'} \tag{4.58}$$

where

$$\langle \vec{N}, \vec{N}' \rangle = \sum_{a:(i\to j)\in Q_1} (n_i' n_j - n_i n_j') \tag{4.59}$$

is the antisymmetrization of the Euler form $\chi_Q(\vec{N}, \vec{N}') = \sum_{i\in Q_0} n_i n_i' - \sum_{a:(i\to j)\in Q_1} n_i n_j'$. The

automorphism $\mathcal{U}_\zeta(\vec{N})$ then encodes the rational DT invariant $\bar{\Omega}_\zeta(\vec{N})$ via

$$\mathcal{U}_\zeta(\vec{N}) = \exp\left(\frac{\bar{\Omega}_\zeta(\vec{N})\mathcal{X}_{\vec{N}}}{y^{-1}-y}\right) \tag{4.60}$$

The scattering diagram $\mathcal{D}_Q$ is defined as the union of the active rays $\{\mathcal{R}_Q(\vec{N}) : \vec{N} \in \Gamma_+\}$ for all $\vec{N}$ equipped with the automorphism $\mathcal{U}_\zeta(\vec{N})$ at each point. Since $\bar{\Omega}_\zeta(\vec{N})$ is invariant under rescaling $\zeta \to \lambda\zeta$ with $\lambda \in \mathbb{R}_{>0}$, and since it can only jump on a finite set of hyperplanes $\mathcal{R}^{\rm geo}_Q(\vec{N}')$ corresponding to the destabilization by a subobject of dimension vector $\vec{N}' < \vec{N}$, $\mathcal{D}_Q$ decomposes into a complex of convex rational polyhedral cones in $\mathbb{R}^{Q_0}$.

The wall-crossing formula ensures that $\mathcal{D}_Q$ is consistent in the following sense [50]: for any generic closed path $\mathcal{P}\colon t \in [1,0] \to \mathbb{R}^{Q_0}$ (where generic means that the intersection of $\mathcal{P}$ with a ray $\mathcal{R}(\vec{N}_i)$ at $t = t_i$ is transverse and does not meet any cone of codimension larger than one), the ordered product of automorphisms associated to each intersection is trivial,

$$\prod_i \mathcal{U}_{\zeta(t_i)}(\vec{N}_i)^{\epsilon_i} = 1\,, \quad \epsilon_i = \mathrm{sign}\left(\frac{\mathrm{d}\zeta}{\mathrm{d}t}, \vec{N}_i\right) \tag{4.61}$$

This consistency property ensures that all rays can be deduced from the knowledge of the initial rays, defined as those rays $\mathcal{R}_\star(\vec{N})$ which contain the self-stability condition $\zeta_\star(\vec{N}) := \langle -, \vec{N}\rangle$ (such that $(\zeta_\star(\vec{N}), \vec{N}') = \langle \vec{N}', \vec{N}\rangle$ for all $\vec{N}'$). We define the *attractor invariant* $\Omega_\star(\vec{N})$ as the index on the initial ray $\mathcal{R}_\star(\vec{N})$. The attractor tree formula of [16] or its variant in [154] provide an algorithm to compute $\Omega_\zeta(\vec{N})$ on the attractor invariants, which is essentially equivalent to summing over all possible scattering sequences of the initial rays [25, 47].

For acyclic quivers (hence trivial potential), the only initial rays are those associated to the standard basis vectors $\vec{N}_i$, carrying $\Omega_\star(\vec{N}_i) = 1$, and the construction of the scattering diagram is straightforward. For a general quiver with potential (Q, W), determining the initial rays is a difficult problem. For quivers associated to non-compact Calabi-Yau threefolds, the case of interest in this work, it was conjectured in [37, 76, 155] that $\Omega_\star(\vec{N}) = 0$ unless $\vec{N}$ is a standard basis vector, or $\vec{N}$ belongs to the kernel of the antisymmetrized Euler form. See [47, §3] for examples of scattering diagrams for Kronecker quivers, and for a definition of the scattering diagram $\mathcal{D}_\psi$ in the full space of Bridgeland stability conditions.

4.3.2 Orbifold quiver

We first consider the cyclic strong exceptional collection

$$C = (\mathcal{O}(0,0), \mathcal{O}(1,0), \mathcal{O}(1,1)\,, \mathcal{O}(2,1)) \tag{4.62}$$

dual[22] to the Ext-exceptional collection

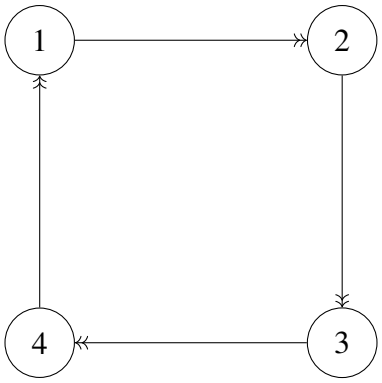
$$C^\vee = (\mathcal{O}(0,0), \mathcal{O}(-1,0)[1], \mathcal{O}(1,-1)[1]\,, \mathcal{O}(0,-1)[2]) \tag{4.63}$$

The Chern vectors of the objects E^i in C and dual objects E_i in $C^\vee$ are

$$\begin{array}{rclcrcl} \gamma^1 &=& [1,0,0,0] & & \gamma_1 &=& [1,0,0,0] \\ \gamma^2 &=& [1,1,0,0] & & \gamma_2 &=& [-1,1,0,0] \\ \gamma^3 &=& [1,1,1,1] & & \gamma_3 &=& [-1,-1,1,1] \\ \gamma^4 &=& [1,2,1,2] & & \gamma_4 &=& [1,0,-1,0] \end{array} \tag{4.64}$$

[22] In the sense that $\chi(E^i, E_j) = \delta^i_j$ for all i, j, see e.g. [37, §2.3, 2.4] for some background on exceptional collections. The collection (4.62) appears in [164] and arises by mutation from the more familiar collection (4.81) discussed in the next subsection.

The corresponding quiver (sometimes called phase II quiver) is



with quartic superpotential [88],[89, (2.2)]

$$W = \sum_{(\alpha\beta)\in S_2} \sum_{(\gamma\delta)\in S_2} \mathrm{sign}(\alpha\beta)\ \mathrm{sign}(\gamma\delta)\, \Phi_{12}^{\alpha}\, \Phi_{23}^{\gamma}\, \Phi_{34}^{\beta}\, \Phi_{41}^{\delta}\ . \tag{4.65}$$

A general Chern character $\gamma = [r, d_1, d_2, \mathrm{ch}_2]$ decomposes as $\gamma = \sum_i n_i \gamma_i$ with

$$\begin{aligned} n_1 &= d_1 + d_2 + \mathrm{ch}_2 + r \\ n_2 &= d_1 + \mathrm{ch}_2 \\ n_3 &= \mathrm{ch}_2 \\ n_4 &= -d_2 + \mathrm{ch}_2 \end{aligned} \tag{4.66}$$

It is straightforward to check that the $\mathbb{Z}_4$ cyclic symmetry $\gamma_i \to \gamma_{i+1}$ acts on the Chern vector as in (4.23).

As in [37], we set $N_i = -n_i$ such that N_i are all positive for large negative ch_2. With these identifications, the expected dimension of the moduli space of Gieseker stable sheaves coincides with the expected dimension of the moduli space of stable quiver representations in the chamber $\zeta_1 \geq 0, \zeta_4 \leq 0$ where the arrows Φ_{41}^{α} can be set to zero. In order to match King stability with Gieseker stability for the canonical polarization $H = C + F$, one needs to take

$$\zeta_1 = -\rho(d_1 + d_2) - \mathrm{ch}_2, \quad \zeta_2 = \rho(r + d_1 + d_2) + \mathrm{ch}_2, \quad \zeta_3 = \rho(d_1 + d_2) + r + \mathrm{ch}_2, \quad \zeta_4 = -\zeta_2 \tag{4.67}$$

with ρ large and positive [37, (4.27)] (after fixing a sign mistake in loc. cit.). We refer to the chamber (4.67) as the canonical chamber[23]. With these identifications, the quiver index $\Omega_c(\vec{N})$ in the canonical chamber is expected to agree with the Gieseker index $\Omega_1(\gamma)$ whenever $-r \leq d_1 + d_2 \leq 0$. More generally, in order to reproduce Gieseker indices $\Omega_\eta(\gamma)$ for polarization $H = C + \eta F$, the stability parameters should be chosen as [37, (4.32)]

$$\begin{aligned} \zeta_1 &= -\mu_1 d_2 - \mu_2 d_1 - \mathrm{ch}_2 = \mu_1(N_3 - N_4) + \mu_2(N_2 - N_3) + N_3 \\ \zeta_2 &= \mu_1 d_2 + \mu_2(r + d_1) + \mathrm{ch}_2 = \mu_1(N_4 - N_3) + \mu_2(2N_3 - N_1 - N_4) - N_3 \\ \zeta_3 &= \mu_1(r + d_2) + \mu_2(d_1 - r) + r + \mathrm{ch}_2 = \mu_1(N_2 - N_1) + \mu_2(N_1 + N_4 - 2N_2) + N_2 - N_1 - N_4 \\ \zeta_4 &= -\mu_1(r + d_2) - \mu_2 d_1 - \mathrm{ch}_2 = \mu_1(N_1 - N_2) + \mu_2(N_2 - N_3) + N_3 \end{aligned} \tag{4.68}$$

[23]The canonical chamber is also called anti-attractor chamber, since the stability parameter (4.67) is opposite to the attractor parameter $\zeta_i = -\kappa_{ij} N_j$, with κ_{ij} the number of arrows $i \to j$ minus the number of arrows $j \to i$.

with $\mu_1, \mu_2 \gg 1$ such that $\eta = \mu_1/\mu_2$. These identifications ensure that

$$\sum_i N_i\zeta_i = 0\,, \quad \sum_i N'_i\zeta_i = r(\mu_1 d'_2 + \mu_2 d'_1) - r'(\mu_1 d_2 + \mu_2 d_1) + r\,\mathrm{ch}'_2 - r'\mathrm{ch}_2 \tag{4.69}$$

The conditions $\zeta_1 \geq 0, \zeta_4 \leq 0$ for the validity of the quiver description now translate into $-\eta r \leq d_1 + \eta d_2 \leq 0$.

Since the kernel of the antisymmetrized Euler form is spanned by the dimension vectors $(1,0,1,0)$ and $(0,1,0,1)$, it is natural to consider two-dimensional slices of the scattering diagram with fixed values of $\zeta_1 + \zeta_3$ and $\zeta_2 + \zeta_4$. Motivated by the values of the parameters ζ_i at the ramification point τ_B along the Π-stability slice, we choose

$$\zeta_1 + \zeta_3 = \mu - 1, \quad \zeta_2 + \zeta_4 = -\mu \tag{4.70}$$

with μ a fixed real number. We can parametrize this slice by $(u, v) \in \mathbb{R}^2$ such that

$$\zeta_1 = v + \tfrac{\mu-1}{2}, \quad \zeta_2 = u - \tfrac{\mu}{2}, \quad \zeta_3 = -v + \tfrac{\mu-1}{2}, \quad \zeta_4 = -u - \tfrac{\mu}{2} \tag{4.71}$$

The geometric rays $\mathcal{R}_\gamma$ are then straight lines

$$(N_2 - N_4)u + (N_1 - N_3)v + \tfrac{\mu}{2}(N_1 - N_2 + N_3 - N_4) - \tfrac{N_1+N_3}{2} = 0 \tag{4.72}$$

oriented along the vector $v_\gamma = (N_3 - N_1, N_2 - N_4)$. Observe that the inner product $v_\gamma \wedge v'_\gamma$ is equal to the Dirac product $\langle\gamma, \gamma'\rangle$, up to a factor $-1/2$. Moreover, the angular momentum is constant along the rays, and positive for $0 < \mu < 1$,

$$(u, v) \wedge v_\gamma = \tfrac{N_1+N_3}{2} - \tfrac{\mu}{2}(N_1 - N_2 + N_3 - N_4) \tag{4.73}$$

so rays tend to rotate counterclockwise around the origin $u = v = 0$.

By the same reasoning as in [47, §5.2] one can show that the only initial rays are those associated to γ_i, with unit BPS index $\Omega_\star(\gamma_i) = 1$, and to the D0-branes (or skyscaper sheaves) $k\delta$ with $\delta = (1,1,1,1)$. The indices $\Omega_c(\vec{N})$ in the canonical chamber for a selection of Chern vectors in the window $-r \leq d_1 + d_2 \leq 0$ are then given by the following scattering sequences (or

trees, for brevity):

$[r, d_1, d_2, \mathrm{ch}_2]$	$\vec{N}$	Trees	$\Omega_c(\vec{N})$
$[1,0,0,-1]$	$(0,1,1,1)$	$\{\gamma_2, \{\gamma_3, \gamma_4\}\}$	$y^2 + 2 + 1/y^2$
$[1,0,0,-2]$	$(1,2,2,2)$	$\{\{\{\gamma_1, 2\gamma_4\}, 2\gamma_3\}, 2\gamma_2\}$ $\{\{\{\{\gamma_1, \gamma_2\}, 2\gamma_4\}, 2\gamma_3\}, \gamma_2\}$ $\{\{\{\{\gamma_1, \gamma_4\}, 2\gamma_3\}, \gamma_4\}, 2\gamma_2\}$	$y^4 + 3y^2 + 6 + 3/y^2 + 1/y^4$
$[2,0,0,-2]$	$(0,2,2,2)$	$\{2\gamma_2, \{2\gamma_3, 2\gamma_4\}\}$	$-y^5 - 2y^3 - 3y - \ldots$
$[2,-1,0,-1]$	$(0,2,1,1)$	$\{2\gamma_2, \{\gamma_3, \gamma_4\}\}$	$-y - 1/y$
$[2,-1,0,-2]$	$(1,3,2,2)$	$\{\gamma_1, \{3\gamma_2, \{2\gamma_3, 2\gamma_4\}\}\}$ $\{\{\{\{\gamma_1, \gamma_2\}, 2\gamma_4\}, 2\gamma_3\}, 2\gamma_2\}$	$-y^5 - 3y^3 - 7y - \ldots$
$[2,0,-1,-1]$	$(0,1,1,0)$	$\{\gamma_2, \gamma_3\}$	$-y - 1/y$
$[2,0,-1,-2]$	$(1,2,2,1)$	$\{\gamma_1, \{2\gamma_2, \{2\gamma_3, \gamma_4\}\}\}$ $\{\gamma_1, \{\{2\gamma_2, \{\gamma_3, \gamma_4\}\}, \gamma_3\}\}$ $\{\{\{\gamma_1, \gamma_4\}, 2\gamma_3\}, 2\gamma_2\}$	$-y^5 - 3y^3 - 7y - \ldots$
$[2,-1,-1,-1]$	$(1,2,1,0)$	$\{\gamma_1, \{\gamma_2, \gamma_3\}\}$	$-y^3 - y - 1/y - 1/y^3$
$[3,0,0,-3]$	$(0,3,3,3)$	$\{3\gamma_2, \{3\gamma_3, 3\gamma_4\}\}$	$y^{10} + 2y^8 + 5y^6 + 8y^4 + 9y^2 + 10 + \ldots$
$[3,0,-1,-2]$	$(0,2,2,1)$	$\{2\gamma_2, \{2\gamma_3, \gamma_4\}\}$ $\{\{2\gamma_2, \{\gamma_3, \gamma_4\}\}, \gamma_3\}$	$y^4 + 2y^2 + 4 + \ldots$
$[3,-1,-1,-1]$	$(0,2,1,0)$	$\{2\gamma_2, \gamma_3\}$	1
$[3,-1,-2,-2]$	$(2,3,2,0)$	$\{2\gamma_1, \{3\gamma_2, 2\gamma_3\}\}$ $\{\{2\gamma_1, \{\gamma_2, \gamma_3\}\}, \{2\gamma_2, \gamma_3\}\}$	$y^8 + 2y^6 + 4y^4 + 4y^4 + 5 + \ldots$

This reproduces the table in [37, §4.1.1]. Note that whenever $-r \le d_1 + d_2 \le 0$, the ray exits in the first quadrant $u > 0, v > 0$, and the index $\Omega_c(\vec{N})$ in the canonical chamber coincides with the Gieseker index for canonical polarization.

We further note that the BPS spectrum of this quiver has been studied in [62, 70, 71, 136]. In particular, in [71], elaborating on [62, Appendix D], the authors show that the spectrum simplifies drastically in the 'collimation chamber' defined by[24]

$$Z(\gamma_3) = Z(\gamma_1) + \delta, \quad Z(\gamma_4) = Z(\gamma_2) - \delta, \quad \arg Z(\gamma_1) > \arg Z(\gamma_2), \quad Z(\gamma_1 + \gamma_2) < 0 \tag{4.74}$$

with $-\frac{1}{2} < \delta < \frac{1}{2}$. Namely, in this chamber the spectrum is the union of bound states of $\{\gamma_1, \gamma_2\}$, described by the Kronecker quiver K_2, and bound states of $\{\gamma_3, \gamma_4\}$, described by the same quiver. More generally, the same conclusion holds when

$$Z(\gamma_3) = \rho Z(\gamma_1) + \delta, \quad Z(\gamma_4) = \rho Z(\gamma_2) - \delta, \quad \arg Z(\gamma_1) > \arg Z(\gamma_2), \quad Z(\gamma_1 + \gamma_2) < 0 \tag{4.75}$$

where $\rho > 0$ and $-\frac{\rho}{1+\rho} < \delta < \frac{\rho}{1+\rho}$. When $\arg Z(\gamma_1) > \arg Z(\gamma_2)$, we similarly expect bound states of $\{\gamma_4, \gamma_1\}$ and $\{\gamma_2, \gamma_3\}$ only. Central charges of the form (4.75) arise for

$$T = -\frac{1}{1+\rho}, \quad T_D = \frac{(1 + \delta - \mu)}{2(1+\rho)} \tag{4.76}$$

This intersects the Π-stability slice at the orbifold point where $\delta = 0, \rho = 1$. In terms of the King stability parameters

$$\zeta_i = \frac{\mathrm{Re}(e^{-i\psi} Z(\gamma_i))}{\cos\psi} \tag{4.77}$$

[24] We rescale the central charges in [71] by a factor of $-R/(2\pi)$, such that the D0-brane central charge is -1. Furthermore, we identify $\tau = 1/\sqrt{\lambda} = e^{-i\pi m}, \kappa = U/\sqrt{\lambda}$.

(with the phase ψ chosen such that all central charges lie in the half-plane $\mathrm{Im}(e^{-\mathrm{i}\psi} Z(\gamma_i)) \geq 0$), the chamber (4.75) lies along the locus

$$\zeta_3 = \rho\zeta_1 + \delta, \quad \zeta_4 = \rho\zeta_2 - \delta \tag{4.78}$$

Further enforcing the conditions (4.70), we get

$$u = \frac{\mu}{2} + \frac{\delta - \mu}{1+\rho}, \quad v = \frac{1-\mu}{2} + \frac{\mu - 1 - \delta}{1+\rho} \tag{4.79}$$

Solving for (ρ, δ) in terms of (u, v), we see that the region where $\rho > 0, -\frac{\rho}{1+\rho} < \delta < \frac{\rho}{1+\rho}$ is bounded by the two hyperbolae

$$(u+v)^2 \pm \mu(u+v) \mp u - \frac{1}{4} < 0 \tag{4.80}$$

One may check that this region contains only rays coming from the primary scattering of $\{\gamma_1, \gamma_4\}$ and $\{\gamma_2, \gamma_3\}$, as predicted in [62] (see Fig. 4.21).

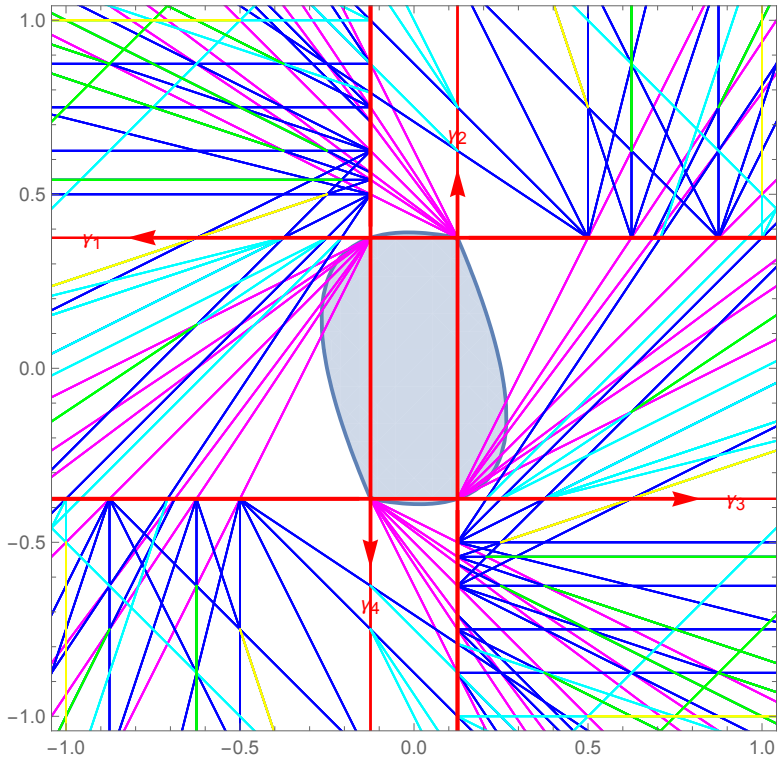


Figure 4.21: Scattering diagram $\mathcal{D}^o_\mu$ for the orbifold quiver at $\mu = 1/4$. The shaded area corresponds to the generalized 'collimation chamber' (4.75).

4.3.3 Phase I quiver

We now consider the cyclic strong exceptional collection [52, Example 2.8]

$$C = (\mathcal{O}(0,0), \mathcal{O}(1,0), \mathcal{O}(0,1), \mathcal{O}(1,1)) \tag{4.81}$$

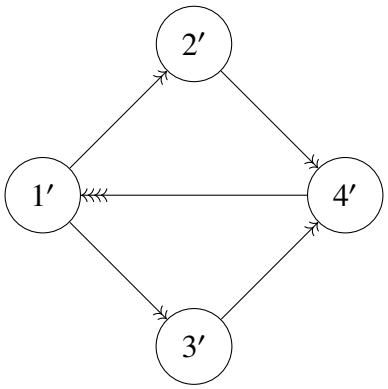


Figure 4.22: Quiver associated to the Ext-exceptional collection (4.82), sometimes known as phase I quiver. This is accompanied by the cubic superpotential W in (4.84).

dual to the Ext-exceptional collection

$$C^\vee = (\mathcal{O}(0,0), \mathcal{O}(-1,0)[1], \mathcal{O}(0,-1)[1], \mathcal{O}(-1,-1)[2]) \tag{4.82}$$

This is obtained from the orbifold collection (4.63) by applying a mutation with respect to node 4, and then exchanging the nodes 3 and 4. Note that $C^\vee$ is no longer invariant under the order 4 autoequivalence $M_{\mathbb{Z}_4}$, but it is invariant under fiber-base duality. The Chern vectors of the objects E^i and dual objects E_i are

$$\begin{array}{llll} \gamma'^1 &= [1,0,0,0] & \gamma'_1 &= [1,0,0,0] = \gamma_1 \\ \gamma'^2 &= [1,1,0,0] & \gamma'_2 &= [-1,1,0,0] = \gamma_2 \\ \gamma'^3 &= [1,0,1,0] & \gamma'_3 &= [-1,0,1,0] = -\gamma_4 \\ \gamma'^4 &= [1,1,1,1] & \gamma'_4 &= [1,-1,-1,1] = \gamma_3 + 2\gamma_4 \end{array} \tag{4.83}$$

The corresponding quiver, shown in Fig. 4.22, is accompanied by the cubic superpotential [88]

$$\begin{aligned} W \;=\; & \Phi^1_{12}\Phi^1_{24}\Phi^4_{41} - \Phi^1_{12}\Phi^2_{24}\Phi^3_{41} - \Phi^2_{12}\Phi^1_{24}\Phi^2_{41} + \Phi^2_{12}\Phi^2_{24}\Phi^1_{41} \\ & -\Phi^1_{13}\Phi^1_{34}\Phi^4_{41} + \Phi^1_{13}\Phi^2_{34}\Phi^2_{41} + \Phi^2_{13}\Phi^1_{34}\Phi^3_{41} - \Phi^2_{13}\Phi^2_{34}\Phi^1_{41} \end{aligned} \tag{4.84}$$

A general Chern character $\gamma = [r, d_1, d_2, \mathrm{ch}_2]$ decomposes as $\gamma = \sum_i n'_i \gamma_i$ with

$$\begin{array}{lll} n'_1 &=& d_1 + d_2 + \mathrm{ch}_2 + r \\ n'_2 &=& d_1 + \mathrm{ch}_2 \\ n'_3 &=& d_2 + \mathrm{ch}_2 \\ n'_4 &=& \mathrm{ch}_2 \end{array} \tag{4.85}$$

As in [37], we set $N'_i = -n'_i$ such that N'_i are all positive for large negative ch_2. The dimension vector $\vec{N}'$ with respect to $C'^\vee$ is related to the dimension vector $\vec{N}$ with respect to $C^\vee$ by $(N'_1, N'_2, N'_3, N'_4) = (N_1, N_2, 2N_3 - N_4, N_3)$.

With these identifications, the expected dimension of the moduli space of Gieseker stable sheaves again coincides with the expected dimension of the moduli space of stable quiver representations in the chamber $\zeta'_1 \geq 0, \zeta'_4 \leq 0$ where the arrows Φ^α_{41} can be set to zero. This

coincides with the canonical (or anti-attractor) chamber whenever $-2r \le d_1 + d_2 \le 0$. In order to match King stability with Gieseker stability, one needs to take

$$\zeta'_1 = -\rho(d_1+d_2) - \mathrm{ch}_2, \quad \zeta'_2 = \zeta'_3 = \rho(r+d_1+d_2) + \mathrm{ch}_2, \quad \zeta'_4 = -\rho(d_1+d_2+2r) + r - \mathrm{ch}_2, \tag{4.86}$$

with ρ large and positive [37, (4.11)] (after fixing a sign mistake in loc. cit.). The stability parameters for Gieseker stability with respect to $H = C + \eta F$ can be obtained from (4.68) by equating $(\zeta'_1, \zeta'_2, \zeta'_3, \zeta'_4) = (\zeta_1, \zeta_2, -\zeta_4, \zeta_3 + 2\zeta_4)$.

Since the objects E_1 and E_2 are identical in the two collections $\mathcal{C}^\vee$ and $\mathcal{C}'^\vee$, it is natural to choose the same two-dimensional slice as in (4.70),

$$\zeta'_1 = v + \frac{\mu-1}{2}, \quad \zeta'_2 = u - \frac{\mu}{2}, \quad \zeta'_3 = u + \frac{\mu}{2}, \quad \zeta'_4 = -2u - v - \frac{\mu+1}{2} \tag{4.87}$$

such that the rays $\mathcal{R}(\gamma'_1)$ and $\mathcal{R}(\gamma'_2)$ agree with the corresponding rays in the scattering diagram of the orbifold quiver (4.70). The geometric rays $\mathcal{R}_\gamma$ are now straight lines

$$(N'_2 + N'_3 - 2N'_4)u + (N'_1 - N'_4)v + \frac{\mu}{2}(N'_1 - N'_2 + N'_3 - N'_4) + \frac{N'_1 + N'_4}{2} = 0 \tag{4.88}$$

oriented along $v_\gamma = (N'_4 - N'_1, N'_2 + N'_3 - 2N'_4)$.

As shown in [152], the scattering diagram for the mutated collection $\mathcal{C}'^\vee$ coincides with the scattering diagram for the original collection $\mathcal{C}^\vee$ on the half-space $\zeta_4 < 0$. It follows that the Attractor Conjecture must also hold for the phase I quiver, namely the only initial rays are those associated to γ'_i, with BPS index $\Omega_\star(\gamma'_i) = 1$, and to the D0-branes $k\delta$ with $\delta = (1,1,1,1)$. From these initial rays, we can compute the canonical indices for the same Chern vectors as in the previous subsection, and check that the same result arises, in general from different scattering sequences:

$[r, d_1, d_2, \mathrm{ch}_2]$	$\vec{N}'$	Trees	$\Omega_c(\vec{N}')$
$[1,0,0,-1]$	$(0,1,1,1)$	$\{\{\gamma'_3,\gamma'_4\},\gamma'_2\}$	$y^2 + 2 + 1/y^2$
$[1,0,0,-2]$	$(1,2,2,2)$	$\{2\gamma'_2,\{2\gamma'_3,\{2\gamma'_4\,\gamma'_1\}\}\}$ $\{\gamma'_2,\{2\gamma'_3,\{2\gamma'_4,\{\gamma'_1,\gamma'_2\}\}\}\}$ $\{2\gamma'_2,\{\gamma'_3,\{2\gamma'_4,\{\gamma'_1,\gamma'_3\}\}\}\}$	$y^4 + 3y^2 + 6 + \dots$
$[2,0,0,-2]$	$(0,2,2,2)$	$\{\{2\gamma'_3,2\gamma'_4\},2\gamma'_2\}$	$-y^5 - 2y^3 - 3y - \dots$
$[2,-1,0,-1]$	$(0,2,1,1)$	$\{\{\gamma'_3,\gamma'_4\},2\gamma'_2\}$	$-y - 1/y$
$[2,-1,0,-2]$	$(1,3,2,2)$	$\{\gamma'_1,\{3\gamma'_2,\{2\gamma'_3,2\gamma'_4\}\}\}$ $\{2\gamma'_2,\{2\gamma'_3,\{2\gamma'_4,\{\gamma'_1,\gamma'_2\}\}\}\}$	$-y^5 - 3y^3 - 7y - \dots$
$[2,0,-1,-1]$	$(0,1,2,1)$	$\{\{2\gamma'_3,\gamma'_4\},\gamma'_2\}$	$-y - 1/y$
$[2,-1,-1,-1]$	$(1,2,2,1)$	$\{\gamma'_1,\{2\gamma'_2,\{2\gamma'_3,\gamma'_4\}\}\}$	$-y^3 - y - 1/y - 1/y^3$
$[3,0,0,-3]$	$(0,3,3,3)$	$\{\{3\gamma'_3,3\gamma'_4\},3\gamma'_2\}$	$y^{10} + 2y^8 + 5y^6 + 8y^4 + 9y^2 + 10 + \dots$
$[3,-1,0,-2]$	$(0,3,2,2)$	$\{3\gamma'_2,\{2\gamma'_3,2\gamma'_4\}\}$	$y^4 + 2y^2 + 4 + \dots$
$[3,-1,-1,-1]$	$(0,2,2,1)$	$\{\gamma'_2,\{2\gamma'_3,\gamma'_4\}\}$	1

In all cases, the index $\Omega_c(\vec{N}')$ in the canonical chamber coincides with the Gieseker index.

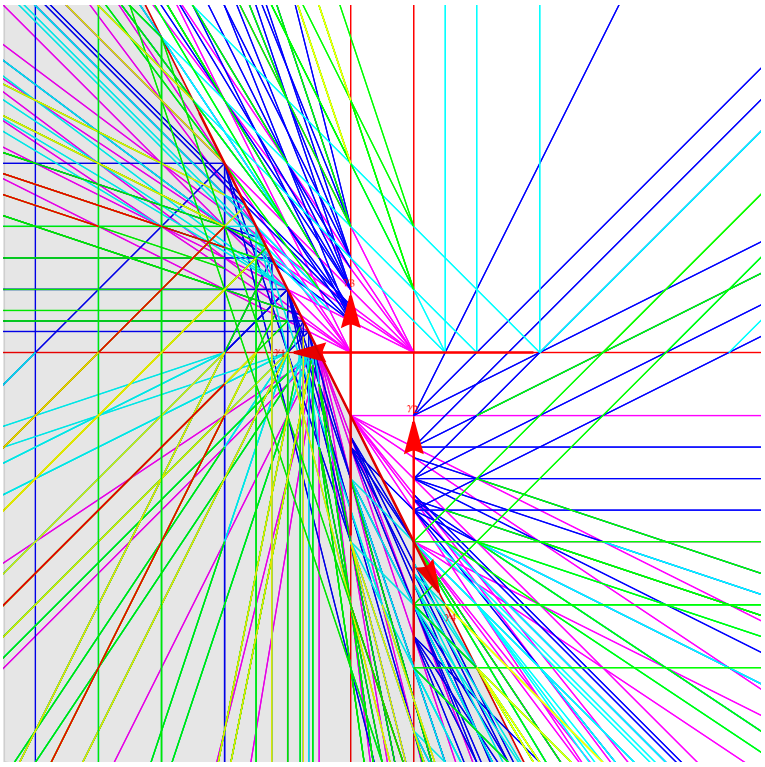


Figure 4.23: Scattering diagram $\mathcal{D}^I_\mu$ for the phase I quiver at $\mu = 1/2$, keeping rays with height $\sum_i N'_i \leq 8$, with $\max(n_1, n_2) \leq 4$ at each intersection. Up to truncation effects, it coincides with the scattering diagram for the orbifold quiver in Fig. 4.3 when $\zeta_4 < 0$, i.e. outside the shaded region.

4.4 Large volume scattering diagram

In this section, we construct the scattering diagram for the large volume stability condition with central charge (4.34), which we repeat for convenience,

$$Z^{\mathrm{LV}}_{T,m}(\gamma) = -rT(T+m) + d_1 T + d_2(T+m) - \mathrm{ch}_2 \tag{4.89}$$

Due to the identity (similar to [47, (4.26)])

$$\mathrm{Re}\left(e^{-\mathrm{i}\psi} Z^{\mathrm{LV}}_{T,m}(\gamma)\right) = \cos\psi \ \mathrm{Re}\left(Z^{\mathrm{LV}}_{T_\psi, m_\psi}(\gamma)\right), \quad \begin{cases} T_\psi := & \mathrm{Re}\, T + \mathrm{Im}\, T \tan\psi + \frac{\mathrm{i}\,\mathrm{Im}\, T}{\cos\psi} \\ m_\psi := & \mathrm{Re}\, m + \mathrm{Im}\, m \tan\psi + \frac{\mathrm{i}\,\mathrm{Im}\, m}{\cos\psi} \end{cases} \tag{4.90}$$

there is no loss of generality in restricting attention to the scattering diagram for $\psi = 0$, since the rays $\mathcal{R}_\psi(\gamma)$ in the T-plane coincide with the rays $\mathcal{R}_0(\gamma)$ in the T_ψ-plane after redefining $m \mapsto m_\psi$ (a trivial operation if m is real). The identity (4.90) can be traced back to the fact both sides lead to the same values of the affine coordinates

$$x = \frac{\mathrm{Re}\left(e^{-\mathrm{i}\psi} T\right)}{\cos\psi}, \quad y = -\frac{\mathrm{Re}\left(e^{-\mathrm{i}\psi} T_D\right)}{\cos\psi}, \quad \mu = \frac{\mathrm{Re}\left(e^{-\mathrm{i}\psi} m\right)}{\cos\psi} \tag{4.91}$$

such that the rays $\mathcal{R}_\psi(\gamma)$ become straight segments in the (x, y) plane,

$$2ry + (d_1 + d_2)x + d_2\mu - \mathrm{ch}_2 = 0 \tag{4.92}$$

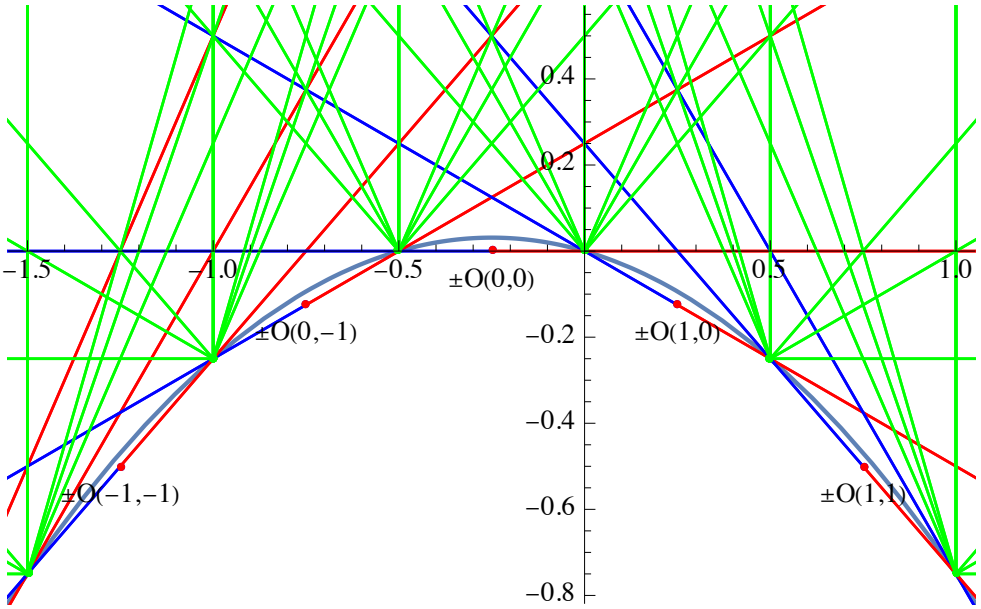


Figure 4.24: Scattering diagram in the (x, y) plane at $m = \frac{1}{2}$, including only primary scattering of initial rays.

The region $\mathrm{Im}\, T > 0$ in the T-plane maps to region above the parabola $y > -\frac{1}{2}x(x+\mu)$, in the regime $\mathrm{Im}\, m > 0$ that we consider (for $\mathrm{Im}\, m < 0$ the large-volume region is $\mathrm{Im}(T+m) > 0$, which has the same (x, y) image), see Fig. 4.24.

For $\psi = 0$, the real part of T coincides with the coordinate x, and m_1 with μ, so we set $T = x + \mathrm{i}t, m = \mu + \mathrm{i}m_2$. The coordinate $s = \frac{\mathrm{Im}\, T_D}{\mathrm{Im}\, T}$ determining the heart is $s = x + \frac{\mu}{2} + \frac{m_2 x}{t}$, so coincides with $x + \frac{m}{2}$ when m is real. The rays $\mathcal{R}_0(\gamma)$ satisfy

$$\mathrm{Re}\, Z(\gamma) = r(t^2 - x^2) + (d_1 + d_2 - \mu r)x + \mu d_2 - \mathrm{ch}_2 + m_2 r t = 0 \tag{4.93}$$

For $r = 0$, the ray is a vertical line at $x = \frac{\mathrm{ch}_2 - \mu d_2}{d_1 + d_2}$. For $r \neq 0$, it is a branch of hyperbola centered at $(x, t) = (\frac{d_1+d_2-\mu r}{2r}, -\frac{m_2}{2})$, intersecting the real axis $t = 0$ at $x = \frac{d_1+d_2-\mu r \pm \sqrt{\Delta_\mu}}{2r}$ with

$$\Delta_\mu = 4(d_1 d_2 - r\mathrm{ch}_2) + (d_2 - d_1 + \mu r)^2 \tag{4.94}$$

Note that the first term is proportional to the Bogomolov discriminant (4.10), and that the same combination appeared in (4.47) for $\eta = 1, M_1 = \mu$. For $\Delta_\mu > r^2 m_2^2$, the hyperbola consists of two branches intersecting the axis $t = 0$ at two distinct points, while for $\Delta_\mu < r^2 m_2^2$, it consists of a single branch intersecting the real axis twice.

Walls of marginal stability where $\mathrm{Im}\, Z(\gamma)\overline{Z(\gamma')} = 0$ are in general cubic curves in the (x, t) plane, which reduce to half-circles centered on the real axis when $m_2 = 0$ (see Fig. 4.28 for an example of walls of marginal stability for $m_2 > 0$). For fixed charge γ, we expect a finite number of nested walls [22, 23, 137], outside which the index $\Omega_{T,m}(\gamma)$ should reduce to a variant of the Gieseker index $\Omega_\eta(\gamma)$ with $\eta = 1$, where the semi-stability condition for sheaves with equal slope is in general different from the standard Gieseker prescription in footnote 15. Indeed, for large t the ratio

$$\frac{\mathrm{Im}\, Z(\gamma)}{\mathrm{Re}\, Z(\gamma)} = \frac{\frac{d_1+d_2}{r} - m_1 - 2x}{t} + \frac{m_2(m_1 + x - \frac{d_1}{r})}{t^2} + O(1/t^3) \tag{4.95}$$

is dominated by the slope $\mu_1(\gamma) = \frac{d_1+d_2}{2r}$, up to a charge independent constant; when the slopes are equal and $m_2 \neq 0$, the subleading term requires comparing the ratios $\frac{d_1}{r}$ (or equivalently $\frac{d_2}{r}$), while ch_2 enters only at sub-subleading order. When $m_2 = 0$, the subleading term vanishes and the sub-subleading term requires comparing $\frac{\mathrm{ch}_2 - m_1 d_2}{r}$, which reduces to the Gieseker prescription for $m_1 = 0$ only (see [78] for an early discussion of such discrepancies). We expect that these subtleties do not affect the index, at least for sufficiently generic charges.

Focusing now on $\gamma = \pm \mathrm{ch}\, \mathcal{O}(d_1, d_2)$, the Bogomolov discriminant vanishes so the rays intersect the real axis at $x = d_1 - \mu$ and $x = d_2$. More precisely, the ray $\mathcal{R}_0(\mathcal{O}(d_1, d_2))$ starts at $(\min(d_1 - \mu, d_2), 0)$ and bends to the left, while the ray $\mathcal{R}_0(\mathcal{O}(d_1, d_2))[1]$ starts at $(\max(d_1 - \mu, d_2), 0)$ and bends to the right. In the (x, y) plane, the rays $\mathcal{R}_\psi(\mathcal{O}(d_1, d_2))$ and $\mathcal{R}_\psi(\mathcal{O}(d_1, d_2)[1]$ start at $x = d_1 - \mu$ or $x = d_2$ along the parabola $y = -\frac{1}{2}x(x + \mu)$, where the respective large volume central charges vanish. Note that the ray $\mathcal{R}_0(\mathcal{O}(d_1, d_2))$ intersects $\mathcal{R}_0(\mathcal{O}(d_1', d_2'))[1]$ if and only if $d_1 \geq d_1'$ and $d_2 \geq d_2'$.

Similar to [47, §6.2], we regulate the scattering diagram using the cost function

$$\varphi_x(\gamma) = d_1 + d_2 - r(2x + \mu) = \frac{\mathrm{Im}\, Z^{\mathrm{LV}}(\gamma)}{\mathrm{Im}\, T} + m_2(rx - d_2) \tag{4.96}$$

which increases along any ray and is additive at each vertex. Since the qualitative structure of the large volume scattering diagram $\mathcal{D}^{\Lambda}_{m_1 + \mathrm{i}m_2, \psi}$ turns out to be insensitive to m_2, we henceforth set $m_2 = 0, m = \mu$ and $\psi = 0$.

4.4.1 $m \notin \mathbb{Z}$

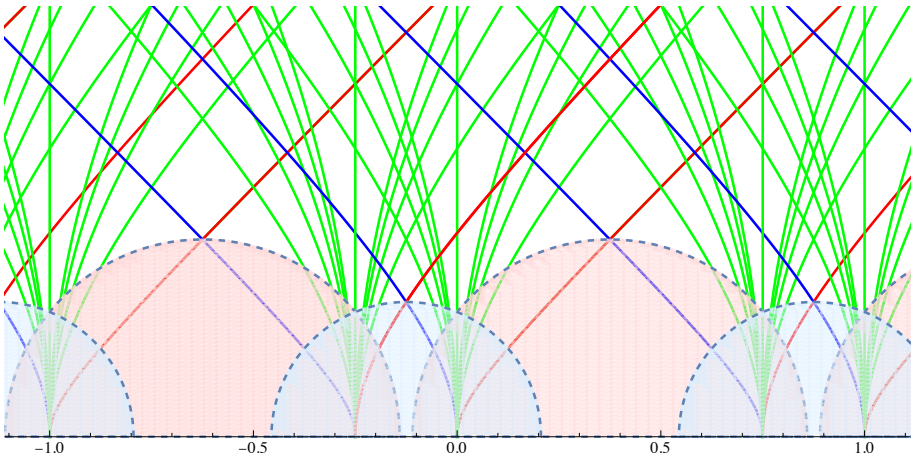


Figure 4.25: Initial rays for the large volume scattering diagram in the (x, t) plane at $m = 1/4$. The shaded blue and red regions correspond to the validity of the Ext-exceptional collection (4.82) tensored with $\mathcal{O}(k, k)$ and $\mathcal{O}(k, k-1)$, respectively.

In view of the spectral flow invariance (4.30), we can assume $0 < m < 1$. One may check that the region of validity (in the sense of footnote 5 on page 90) of the phase I quiver attached to the exceptional collection (4.81) includes the interval $(-1, m-1)$ on the real axis, while the interval $(m-1, 0)$ is covered by the same exceptional collection (4.81) tensored with $\mathcal{O}(1, 0)$ (see Fig. 4.25). By applying a sequence of mutations, one finds that there is an infinite number of rays emerging from $x = -m$ associated to $\mathcal{O}(0, k)$ with $k > 0$ and $\mathcal{O}(0, -k)[1]$ with $k \geq 0$. Similarly,

there is an infinite number of rays emerging from $x = 0$, associated to $\mathcal{O}(k, 0)$ with $k > 0$ and $\mathcal{O}(-k, 0)[1]$ with $k \geq 0$. The two set of rays emerging from $x = -m$ and $x = 0$ are related by the combination of fiber/base duality $(x, m) \mapsto (x + m, -m)$ and derived duality $(x, m) \mapsto (-x, -m)$. For $m = 1/2$, the diagram is symmetric with respect to the axis $x = -1/2$, see Fig. 4.1.

In fact, the infinite set of initial rays emerging from $x = -m$ can be can be understood as arising from the scattering of the two extremal rays $\mathcal{O}(0, -1)[1]$ and $\mathcal{O}(0, 0)$ with charge $\gamma_1 = [-1, 0, 1, 0]$ and $\gamma_2 = [1, 0, 0, 0]$, described by the Kronecker quiver K_2 (also known as affine A_1 quiver). Indeed, it is well known that the only populated dimension vectors for K_2 are of the form $(k, k + 1)$, $(k + 1, k)$ and (k, k), corresponding to outgoing rays

$$k\gamma_1 + (k + 1)\gamma_2 = \mathrm{ch}\,\mathcal{O}(0, k), \quad (k + 1)\gamma_1 + k\gamma_2 = \mathrm{ch}\,\mathcal{O}(0, -k - 1)[1] \tag{4.97}$$

with unit index, as well as $k\gamma_1 + k\gamma_2 = [0, 0, k, 0]$ with index $\Omega_\star(k\gamma_1 + k\gamma_2) = -y - 1/y$. For $k = 1$, the latter is recognized as the vertical ray $GV(0, 1, 0)$ associated the D2-D0 bound states with index $-y - 1/y$ (see the first line in (4.19), with $d = 0$). Similarly, the rays emerging from $x = 0$ arise from the scattering of the two extremal rays $\mathcal{O}(1, 0)$ and $\mathcal{O}(0, 0)[1]$, with unit DT invariant, and also include the vertical ray $GV(1, 0, 0)$ with index $-y - 1/y$.

Thus the full large volume scattering diagram $\mathcal{D}^{\Lambda}_{m,0}$ can be obtained from the initial rays $\mathcal{O}(k, k)$, $\mathcal{O}(k, k - 1)[1]$ starting from $x = k - m$ with $k \in \mathbb{Z}$, slightly displaced into the lower half-plane, and $\mathcal{O}(k + 1, k)$, $\mathcal{O}(k, k)[1]$ starting from $x = k$, slightly displaced into the lower half-plane. More precisely, in the affine coordinates (x, y), we can take the starting point for $\mathcal{O}(k, k)$ and $\mathcal{O}(k, k)[1]$ to be any point along the ray below the parabola $y = -\frac{1}{2}x(x + m)$, and similarly for $\mathcal{O}(k + 1, k)$ and $\mathcal{O}(k + 1, k)[1]$. A natural choice[25] is the midpoint along the chord (see the red dots in Fig. 4.24):

$$\begin{array}{rcl} (x, y) = (k - \frac{m}{2}, -\frac{k^2}{2}) & : & \mathcal{O}(k, k) \text{ and } \mathcal{O}(k, k)[1] \\ (x, y) = (k + \frac{1-m}{2}, -\frac{k(k+1)}{2} + \frac{m-1}{4}) & : & \mathcal{O}(k + 1, k) \text{ and } \mathcal{O}(k + 1, k)[1] \end{array} \tag{4.98}$$

Note that the initial points for $\pm\mathcal{O}(k, k)$ lie along the parabola $y = -\frac{1}{2}x(x + m) - \frac{m^2}{8}$ while the initial points for $\pm\mathcal{O}(k + 1, k)$ lie along the parabola $y = -\frac{1}{2}x(x + m) - \frac{(1-m)^2}{8}$.

More generally, when m lies outside the interval $(0, 1)$, decomposing $m = \lfloor m \rfloor + \mathrm{Fr}(m)$ and tensoring by $\mathcal{O}(\lfloor m \rfloor, 0)$, we get the initial rays

$$\begin{array}{rcl} (x, y) = \Big(k - \frac{\mathrm{Fr}(m)}{2}, -\frac{k^2}{2} - \frac{k}{2}\lfloor m \rfloor + \frac{1}{4}\lfloor m \rfloor \,\mathrm{Fr}(m)\Big) & : & \pm\mathcal{O}(k + \lfloor m \rfloor, k) \\ (x, y) = \Big(k + \frac{1-\mathrm{Fr}(m)}{2}, -\frac{k^2}{2} - \frac{k}{2}(1 + \lfloor m \rfloor) - \frac{1}{4}(1 - \mathrm{Fr}(m))(1 + \lfloor m \rfloor)\Big) & : & \pm\mathcal{O}(k + 1 + \lfloor m \rfloor, k) \end{array} \tag{4.99}$$

Their intersection on the parabola produces the initial rays at the boundary of the upper half-plane,

$$\begin{array}{rcccc} x = k: & \mathcal{O}(k + 1 + \lfloor m \rfloor + n, k), & \mathcal{O}(k + \lfloor m \rfloor - n, k)[1], & GV(1, 0, k) \\ x = k - \mathrm{Fr}(m): & \mathcal{O}(k + \lfloor m \rfloor, k + n), & \mathcal{O}(k + \lfloor m \rfloor, k - n - 1)[1], & GV(0, 1, k + \lfloor m \rfloor) \end{array} \tag{4.100}$$

for all $n \geq 0$. Setting $s = x + \frac{m}{2}$ and shifting $k \mapsto k - \lfloor m \rfloor$ in the second line, we recover the initial rays announced in (4.2).

[25] This corresponds to the image in the (x, y) plane of the points along the Π-stability slice where $\mathcal{O}(k, k)$ and $\mathcal{O}(k + 1, k)$ are massless, for m real and $\psi = 0$. Along the large volume slice, $\mathcal{O}(k, k)$ and $\mathcal{O}(k, k - 1)[1]$ are instead massless at $x = k$ on the parabola $y = -\frac{1}{2}x(x + m)$, while $\mathcal{O}(k, k)[1]$ and $\mathcal{O}(k + 1, k)$ are massless at $x = k - m$ along the same parabola.

It is now straightforward to determine the scattering sequences contributing to the Gieseker index for low enough Chern invariants, using as a cut-off the cost function (4.96). As the ray crosses the parabola, or equivalently at $t = 0$, one has

$$\varphi_{\text{in}}(\pm\mathcal{O}(k, k + \lfloor m \rfloor)) = \text{Fr}(m), \quad \varphi_{\text{in}}(\pm\mathcal{O}(k + 1 + \lfloor m \rfloor, k)) = 1 - \text{Fr}(m) \tag{4.101}$$

Moreover, $\varphi_x(\gamma)$ vanishes along these rays (whose discriminant vanishes, namely $\text{ch}_2 = d_1 d_2/r$) at

$$(x, y) = \left(\frac{d_1 + d_2}{2r} - m, -\frac{d_1^2 + d_2^2}{4r^2} + \frac{m(d_1 - d_2)}{4r} \right) \tag{4.102}$$

such that $y + \frac{1}{2}x(x + m) = -\frac{1}{8}(m + \frac{d_2 - d_1}{r})^2$. The same arguments as in [47, §4.2] guarantee that only a finite number of trees contribute to the index, hence the SAFC holds in the large volume slice.

$[r, d_1, d_2, \text{ch}_2]$	Trees	Range	$\Omega(\gamma)$
$[0, 1, 0, 0]$	$\{\mathcal{O}(0,0)[1], \mathcal{O}(1,0)\}$	$\mathbb{R}$	$K_2(1,1) = -y - 1/y$
$[0, 1, 1, 0]$	$\{\mathcal{O}(0,-1)[1], \mathcal{O}(1,0)\}$	$[0, 2]$	$K_4(1,1) = -y^3 - y - \ldots$
$[0, 1, 2, 0]$	$\{\mathcal{O}(0,-2)[1], \mathcal{O}(1,0)\}$	$[0, 3]$	$K_6(1,1) = -y^5 - y^3 - y - \ldots$
$[0, 2, 2, 0]$	$\{\mathcal{O}(-1,-1)[1], \mathcal{O}(1,1)\}$ $\{\mathcal{O}(0,-1)[1]^{\oplus 2}, \mathcal{O}(1,0)^{\oplus 2}\}$ $\{\mathcal{O}(0,-2)[1], \mathcal{O}(2,0)\}$	$[-2, 2]$ $[0, 2]$ $[0, 4]$	$K_4(2,2) + 2K_8(1,1)$ $= -y^9 - 3y^7 - 4y^5 - 4y^3 - 4y + \ldots$
$[0, 2, 3, 0]$	$\{\{\mathcal{O}(-1,-1)[1], GV(0,1,0)\}, \mathcal{O}(1,1)\}$ $\{\mathcal{O}(0,-3)[1], \mathcal{O}(2,0)\}$ $\{\{\mathcal{O}(0,-1)[1], \mathcal{O}(1,0)^{\oplus 2}\}, \mathcal{O}(0,-2)[1]\}$	$[-\frac{5}{3}, \frac{5}{2}]$ $[0, 5]$ $[0, \frac{10}{3}]$	$(K_2(1,1)^2 + K_4(1,2) + 1)\, K_{10}(1,1)$ $= -y^{13} - 3y^{11} - 8y^9 - 10y^7$ $-11y^5 - 11y^3 - 11y + \ldots$
$[1, 0, 0, -1]$	$\{\mathcal{O}(0,-1), GV(0,1,-1)\}$	$\mathbb{R}^+$	$K_2(1,1)^2 = y^2 + 2 + \ldots$
$[1, 0, 0, -2]$	$\{\mathcal{O}(0,-1), GV(0,1,-2)\}$ $\{\mathcal{O}(-1,0), GV(1,0,-2)\}$ $\{\mathcal{O}(-2,-2)[1], \mathcal{O}(-1,-1)^{\oplus 2}\}$	$[-1, \infty]$ $[-\infty, 1]$ $[-1, 1]$	$2K_2(1,1)^2 + K_4(1,2)$ $= y^4 + 3y^2 + 6 + \ldots$
$[1, 0, 0, -3]$	$\{\mathcal{O}(0,-1), GV(0,1,-3)\}$ $\{\mathcal{O}(-1,0), GV(1,0,-3)\}$ $\{\mathcal{O}(-1,-1), \{\mathcal{O}(-1,-2), \mathcal{O}(-2,-3)[1]\}\}$ $\{GV(0,1,-2), \{GV(1,0,-2), \mathcal{O}(-1,-1)\}\}$	$[-2, \infty]$ $[-\infty, 2]$ $[-2, 2]$ $[-\frac{1}{2}, \infty]$	$2K_2(1,1)^2 + K_4(1,1)^2 + K_2(1,1)^4$ $= y^6 + 3y^4 + 9y^2 + 14 + \ldots$
$[2, 0, 0, -2]$	$\{\mathcal{O}(0,-1)^{\oplus 2}, GV(0,2,-2)\}$	$\mathbb{R}^+$	$-y^5 - 2y^3 - 3y - \ldots$
$[2, -1, 0, -1]$	$\{\mathcal{O}(0,-1), \mathcal{O}(-1,1)\}$	$\mathbb{R}^+$	$K_2(1,1) = -y - 1/y$
$[2, 0, -1, -1]$	$\{2\mathcal{O}(0,-1), GV(0,1,-1)\}$	$\mathbb{R}^+$	$K_2(2,1) = -y - 1/y$
$[2, -1, -1, -1]$	$\{\mathcal{O}(-1,-1)^{\oplus 3}, \mathcal{O}(-2,-2)[1]\}$	$[-1, 1]$	$K_4(3,1) = -y^3 - y - \ldots$
$[3, 1, 1, -1]$	$\{\mathcal{O}(0,0)^{\oplus 4}, \mathcal{O}(-1,-1)[1]\}$	$[-1, 1]$	$K_4(4,1) = 1$
$[3, 2, 2, 0]$	$\{\mathcal{O}(1,0)^{\oplus 2}, \mathcal{O}(0,2)\}$	$\mathbb{R}^+$	$K_2(2,1) = 1$
$[5, 1, 2, -2]$	$\{\mathcal{O}(0,0)^{\oplus 6}, \mathcal{O}(-1,-2)[1]\}$	$[-1, 2]$	$K_6(6,1) = 1$
$[5, 3, 4, 0]$	$\{\mathcal{O}(1,0)^{\oplus 3}, \mathcal{O}(0,2)^{\oplus 2}\}$	$\mathbb{R}^+$	$K_2(3,2) = 1$

Table 4.1: Trees contributing to the index $\Omega_{s,t}(\gamma)$ at $t \to \infty$, for m in the range specified in the third column. As m reaches the ends of the interval, the last wall of marginal stability shrinks to zero radius.

In Table 4.1, we display the trees contributing to the index at large t, for m in an interval containing $m = \frac{1}{2}$. For m outside this range, the index is still the same at large t, but BPS states arise from a different set of constituents. For example,

- For $\gamma = [0, 1, 0, 0]$, the ray $GV(1, 0, 0)$ exists for all m, but it arises as a bound state from different constituents: e.g $\{\mathcal{O}(1, 0), \mathcal{O}(0, 0)[1]\}$ when $0 < m < 1$, or more generally

$$\{\mathcal{O}(\lfloor m \rfloor + 1, 0), \mathcal{O}(\lfloor m \rfloor, 0)[1]\} \tag{4.103}$$

  when $m \notin \mathbb{Z}$.

- For $\gamma = [0, 1, 1, 0]$ and $\lfloor m \rfloor$ even, the contributing tree is

$$\{\mathcal{O}(1 + \tfrac{1}{2}\lfloor m \rfloor, -\tfrac{1}{2}\lfloor m \rfloor), \mathcal{O}(\tfrac{1}{2}\lfloor m \rfloor, -1 - \tfrac{1}{2}\lfloor m \rfloor)[1]\} \tag{4.104}$$

  For odd $\lfloor m \rfloor$, the contributing tree is instead

$$\{\mathcal{O}(\tfrac{1}{2} + \tfrac{1}{2}\lfloor m \rfloor, \tfrac{1}{2} - \tfrac{1}{2}\lfloor m \rfloor), \mathcal{O}(-\tfrac{1}{2} + \tfrac{1}{2}\lfloor m \rfloor, -\tfrac{1}{2} - \tfrac{1}{2}\lfloor m \rfloor)[1]\} \tag{4.105}$$

  Writing $m = 2d + p + \mathrm{Fr}(m)$ with $p \in \{0, 1\}$, this can be rewritten in both cases as

$$\{\mathcal{O}(d + 1, -d), \mathcal{O}(d, -1 - d)[1]\} \tag{4.106}$$

  When m varies in an interval $]2n, 2n + 2[$, the tree stays the same, but the circle of marginal stability shrinks as m approaches the end of the interval. For m even integer, the state arises as an initial ray.

- For $\gamma = [0, 1, 2, 0]$ and $m = 3d + p + \mathrm{Fr}(m)$ with $d = \lfloor \frac{m}{3} \rfloor$, the contributing tree is

$$\{\mathcal{O}(d + 1, -2d), \mathcal{O}(d, -2 - 2d)[1]\} \tag{4.107}$$

  This is independent of $p \in \{0, 1, 2\}$, but jumps as d changes.

- For $\gamma = [1, 0, 0 - 1]$, we find the following trees, setting $d = \lfloor m \rfloor$ with $m > 0$,

$$\begin{cases} 0 < m < 1 : & \{\mathcal{O}(0, -1), \{\mathcal{O}(-1, -1), \mathcal{O}(-1, -2)[1]\}\} \\ 1 < m < 2 : & \{\mathcal{O}(0, -1), \{\mathcal{O}(-1, -2), \mathcal{O}(-1, -3)[1]\}\} \\ m > 2 : & \{\{\mathcal{O}(0, -d)^{\oplus d}, \mathcal{O}(0, -d - 1)[1]^{\oplus d+1}\}, \{\mathcal{O}(0, -d - 1), \mathcal{O}(-1, -d - 2)\}\} \end{cases} \tag{4.108}$$

  whose first node is the same $\{\mathcal{O}(0, -1), GV(0, 1, -1)\}$ for any $m > 0$. For $m < 0$, we have the same trees upon setting $d = \lfloor -m \rfloor$ and applying fiber/base duality.

4.4.2 $m \in \mathbb{Z}$

When m is an integer, the initial rays at $x \in \mathbb{Z}$ and $x \in \mathbb{Z} - \mathrm{Fr}(m)$ coalesce and the structure of the scattering diagram becomes more complicated. In particular, assuming $m = 0$ without loss of generality, we see that four initial rays $\mathcal{O}(0, 0), \mathcal{O}(0, 0)[1], \mathcal{O}(1, 0), \mathcal{O}(0, -1)[1]$ intersect at the origin $(x, y) = 0$. In order to determine the outcoming rays, we start from the phase I collection and apply mutations μ_1 and $\mu_2\mu_3$ alternatively (see Fig. 4.26). Under these mutations, the charge γ'_4 attached to node 4 and the number of arrows $1 \leftrightarrow 2, 1 \leftrightarrow 3$ remain unchanged (with the

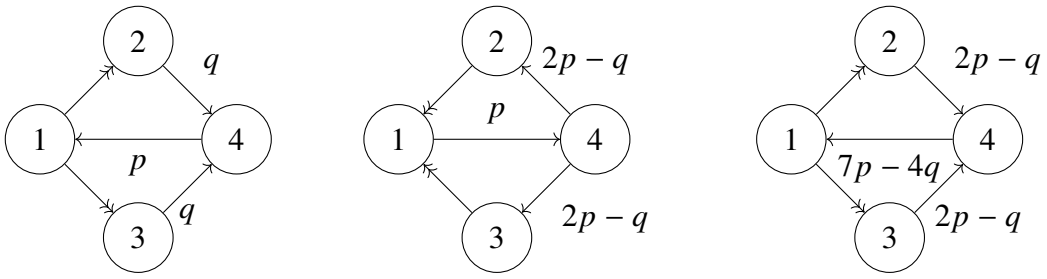


Figure 4.26: Images of the phase I quiver under mutations μ_1 and $\mu_2\mu_3$.

direction of the arrow being inverted at each step), but the charge vectors $\gamma'_{1,2,3}$ attached to nodes 1,2,3 and the numbers p of arrows $4 \leftrightarrow 1$ and q of arrows $2 \leftrightarrow 4, 3 \leftrightarrow 4$, change according to

$$\begin{pmatrix} q \\ p \end{pmatrix} \mapsto \begin{pmatrix} -1 & 2 \\ -4 & 7 \end{pmatrix} \begin{pmatrix} q \\ p \end{pmatrix}, \quad \begin{pmatrix} \gamma'_1 \\ \gamma'_2 \\ \gamma'_3 \end{pmatrix} \mapsto \begin{pmatrix} 7 & 2 & 2 \\ -2 & -1 & 0 \\ -2 & 0 & -1 \end{pmatrix} \begin{pmatrix} \gamma'_1 \\ \gamma'_2 \\ \gamma'_3 \end{pmatrix} \tag{4.109}$$

Starting with the phase I collection (4.82) with $(p, q) = (4, 2)$ at $k = 0$ and denoting by $(\alpha_{2k+1}, -\alpha_{2k})$ the charge vectors $(\gamma'_1, -\gamma'_3)$ after the k-th iteration, we find an infinite series of simple rays emitted at $(x, y) = (0, 0)$, with charges

$$\alpha_1 = \mathcal{O}(0,0),\ \alpha_2 = \mathcal{O}(0,1),\ \alpha_3 = [3,2,2,0],\ \alpha_4 = [5,4,3,0],\ \alpha_5 = [17,12,12,0], \ldots \tag{4.110}$$

along with their images under fiber/base duality. Explicitly,

$$r_k = \frac{(1+\sqrt{2})^k + (1+\sqrt{2})^{-k}}{2^{1+\mathrm{Fr}(k/2)}}, \qquad (d_{1k}, d_{2k}) = \frac{(1+\sqrt{2})^k - (1+\sqrt{2})^{-k}}{2^{3/2+\mathrm{Fr}(k/2)}} \pm (-1)^{(k+1)/2}\, \mathrm{Fr}(k/2). \tag{4.111}$$

such that $(d_1, d_2)/r_k$ tens to $1/\sqrt{2}$. Similarly, there is a discrete set of rays $\tilde{\alpha}_k$ with negative rank emitted at $(x, y) = (0, 0)$, related to α_k by derived duality. Beyond these discrete sets of rays, the diagram becomes dense and we shall not attempt to characterize it further, see Fig. 4.27.

4.5 Scattering diagram in the Π-stability slice

In this section, we combine our understanding of the large volume and quiver scattering diagrams with the action of $\Gamma_0(4)$ (or rather, the monodromy group Γ) to elucidate the structure of the scattering diagram along the Π-stability slice. In view of the complications introduced by the branch cuts, we do not aim for mathematical rigour, but rather propose a compelling physical picture supported by numerous numerical checks. In §4.5.3 we outline the proof that this picture is correct, together with the proof of the Split Attractor Flow Conjecture, which go hand in hand. Throughout, we assume $0 < \mathrm{Re}\, m < 1$ and $\mathrm{Im}\, m \geq 0$.

4.5.1 Uncovering the scattering diagram

By the same arguments as in [47], we know that initial rays can only be emitted from conifold points along the boundary. By invariance under $\Gamma_0(4)$, this includes all rational points $\tau = \frac{p}{q}$ with (p, q) coprime and $q \neq 0 \mod 4$, while rational points with $4|q$ correspond to images of

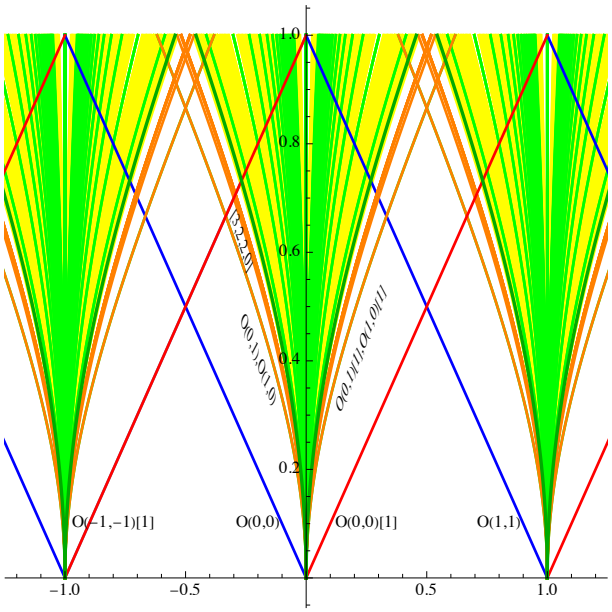


Figure 4.27: Initial rays in the (x,t) plane for $m = 0$. The orange rays are obtained from the phase I collection by iterating the mutations μ_1 and $\mu_2\mu_3$. The dense yellow rays arise from the scattering of $\mathcal{R}(O(1,0))$ and $\mathcal{R}(O(0,-1)[1])$ with $|\langle\gamma_1,\gamma_2\rangle| = 4$.

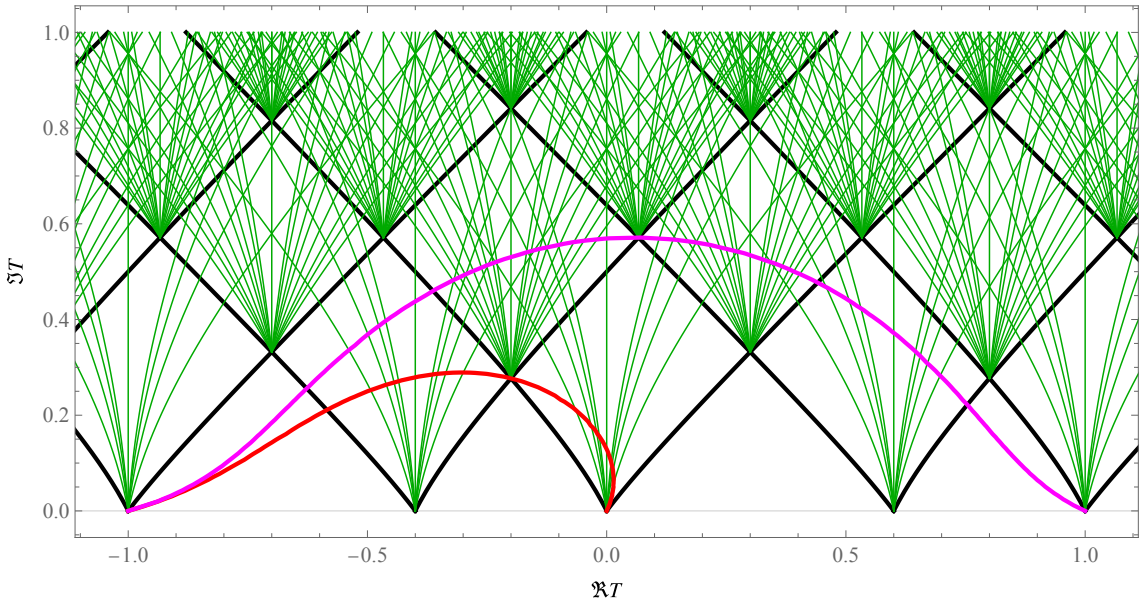


Figure 4.28: Initial rays for the large volume scattering diagram $\mathcal{D}^{\Lambda}_{m,0}$ for fixed $m = 0.4 + 0.3\mathrm{i}$, and their primary scatterings. The red and magenta lines denote the walls of marginal stability for the binary trees $\{O(1,0), O(0,-1)[1]\}$ and $\{O(1,1), O(0,-1)[1]\}$.

the large volume point $\tau = \mathrm{i}\infty$. However, due to the existence of $\mathbb{Z}_2$ ramification points at all $\Gamma_0(4)$ images of τ_B, each fraction $\frac{p}{q}$ actually corresponds to a tower of conifold points indexed by $\mathbb{Z}^4$. On the principal sheet, obtained by analytic continuation from $\tau = \mathrm{i}\infty$ without crossing any cut, the initial rays at $\tau = 0$ correspond to all homological shifts $\mathcal{O}(0,0)[n]$ of the structure sheaf, while the initial rays at $\tau = \frac{1}{2}$ correspond to $\mathcal{O}(1,0)[n]$ or $\mathcal{O}(0,1)[n]$, depending on the angular sector (see Fig. 4.6). Initial rays on the principal sheet near other conifold points $\tau = \frac{p}{q}$ can be obtained by applying the autoequivalences $ST_{\mathcal{O}(0,0)}$ and $\mathcal{O}(1,1) \otimes -$ generating $\Gamma_0(4)$.

For $|\psi|$ small enough (and $\mathrm{Re}\, m$ far enough from the endpoints of the interval $0 < \mathrm{Re}\, m < 1$, depending on ψ), numerical analysis indicates that the only initial rays which can reach the large volume point $\tau = \mathrm{i}\infty$ are the rays $\mathcal{O}(k,k)$ and $\mathcal{O}(k,k)[1]$ starting from $\tau = k$ on the principal sheet, and the rays $\mathcal{O}(k+1,k)$ and $\mathcal{O}(k+1,k)[1]$ starting from $\tau = k + \frac{1}{2}$ on the principal sheet. As discussed in §4.4, those are the same rays which generate the infinite collections of initial rays emanating from $x \in \mathbb{Z}$ and $x \in \mathbb{Z} - m$ in the large volume scattering diagram for m real. In fact, using the affine coordinates (x, y) and parameter μ introduced in (4.91), the part of the Π-stability scattering diagram which is connected to $\tau = \mathrm{i}\infty$ is identical to the large volume scattering diagram $\mathcal{D}_\mu^\Lambda$, except that the origin of the initial rays is shifted to

$$\begin{aligned} \tau = k &: \left(k + \mathcal{V}_\psi, -\frac{1}{2}k(k+\mu) - k\mathcal{V}_\psi\right) \\ \tau = k + \tfrac{1}{2} &: \left(k + \tilde{\mathcal{V}}_\psi, -\frac{1}{2}k(k+\mu) - (k+\tfrac{1}{2})\tilde{\mathcal{V}}_\psi\right) \end{aligned} \tag{4.112}$$

where

$$\mathcal{V}_\psi := \frac{\mathrm{Re}[\mathrm{i}e^{-\mathrm{i}\psi}\mathcal{V}(m)]}{\cos\psi}, \quad \tilde{\mathcal{V}}_\psi := \frac{\mathrm{Re}[\mathrm{i}e^{-\mathrm{i}\psi}\tilde{\mathcal{V}}(m)]}{\cos\psi} \tag{4.113}$$

For m real and $\psi = 0$, one has $(\mathcal{V}_0, \tilde{\mathcal{V}}_0) = (-\frac{m}{2}, \frac{1-m}{2})$ so the initial points coincide with (4.98), namely the midpoint along the chord between $k - \mu < x < k$ and $k < x < k + 1 - \mu$ below the parabola. For later reference, we also note that the 'jagged parabola' joining the successive points (4.112) is convex only if the following two conditions are obeyed

$$\mathcal{V}_\psi(2\mathcal{V}_\psi + \mu + 1) \le \tilde{\mathcal{V}}_\psi(2\mathcal{V}_\psi + \mu), \quad \tilde{\mathcal{V}}_\psi(2\tilde{\mathcal{V}}_\psi + \mu - 2) \le \mathcal{V}_\psi(2\tilde{\mathcal{V}}_\psi + \mu - 1) \tag{4.114}$$

Indeed, the first inequality saturates when the points associated to $\tau \in \{k, k+\frac{1}{2}, k+1\}$ become aligned, while the second saturates when the points $\tau \in \{k-\frac{1}{2}, k, k+\frac{1}{2}\}$ become aligned. Furthermore, the two equations are exchanged under $(\mathcal{V}_\psi, \tilde{\mathcal{V}}_\psi, \mu) \mapsto (-\tilde{\mathcal{V}}_\psi, -\mathcal{V}_\psi, 1-\mu)$. We denote by $\mathcal{I}_{\mathrm{cvx}}$ the range of ψ such that the convexity conditions (4.114) are satisfied. This range is obviously contained in the range where the initial rays (4.112) are ordered horizontally, namely $\mathcal{V}_\psi < \tilde{\mathcal{V}}_\psi < \mathcal{V}_\psi + 1$, and one may check (numerically) that it always contains $\psi = 0$.

As long as the initial points stay on the aforementioned chords, i.e. when

$$-\mu < \mathcal{V}_\psi < 0 \quad \text{and} \quad 0 < \tilde{\mathcal{V}}_\psi < 1 - \mu \tag{4.115}$$

the topology of the scattering diagram stays unaffected, and is identical to the large volume diagram (see Figs. 4.7 and 4.8). This description clearly breaks down for $m = 0$ or $m = 1$, where one of the ranges in (4.115) becomes empty. Focusing for definiteness on the case $m = 0$, we have $(\mathcal{V}_\psi, \tilde{\mathcal{V}}_\psi) = (\frac{4G}{\pi^2}\tan\psi, \frac{1}{2})$ where G is Catalan's constant. For arbitrarily small $\psi > 0$, we

find that the initial rays $\mathcal{O}(0,1), \mathcal{O}(1,0)$ starting from $\tau = \frac{1}{2}$ approach $\tau = 0$ before curling back to another large volume point $\tau = \frac{1}{4}$, while the initial rays $\mathcal{O}(0,-1)[1], \mathcal{O}(-1,0)[1]$ starting from $\tau = -\frac{1}{2}$ approach $\tau = 0$ and narrowly escape to $\tau = \mathrm{i}\infty$, crossing the ray $\mathcal{O}(0,0)$ emanating from $\tau = 0$ on their way (see Fig. 4.29). The scattering of $\mathcal{O}(0,-1)[1]^{\oplus n_1}$, $\mathcal{O}(0,0)^{\oplus n_2}$ and $\mathcal{O}(-1,0)[1]^{\oplus n_3}$ is described by a 3-node quiver with $\kappa_{12} = \kappa_{32} = 2$, leading to an infinite number of outgoing rays, all of them with $\mathrm{ch}_2 = 0$, which reproduce the dense set of rays in the large volume scattering diagram Fig. 4.27.

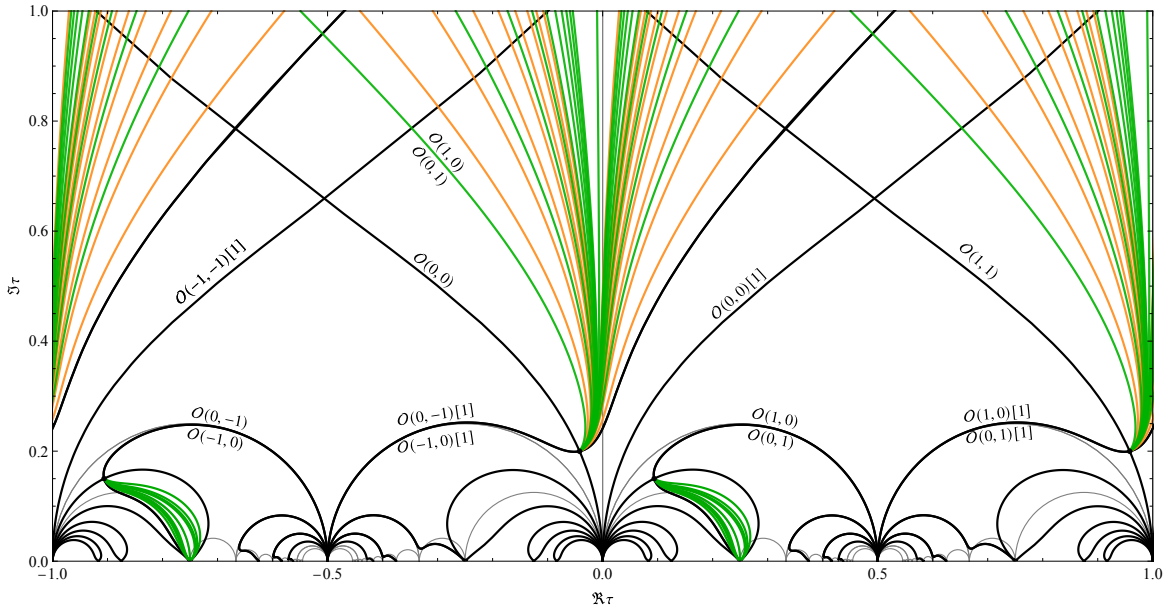


Figure 4.29: Scattering diagram $\mathcal{D}^{\Pi}_{m,\psi}$ for $m = 0, \psi = 0.01$, keeping only primary scatterings. Note that rays related by fiber-based duality are indistinguishable, with further degeneracies when $r = 0$. As $\psi \to 0$, the intersection point between $\mathcal{O}(0,-1)[1], \mathcal{O}(-1,0)[1]$ and $\mathcal{O}(0,0)$ coalesces with $\tau = 0$, similar to Fig. 4.27.

Returning to the case where $\mathrm{Re}\, m$ is not integer, we find that as $|\psi|$ increases beyond certain critical values, such that either of the inequalities (4.115) get violated, the initial points cross the primary intersection points at $x = k$ or $k - \mu$, and the topology of the scattering diagram changes: this occurs at phases $\psi^-_{\mathrm{cr}} < 0 < \psi^+_{\mathrm{cr}}$ where $\mathcal{V}_\psi = -\mu$ and $\mathcal{V}_\psi = 0$ respectively, and phases $\tilde{\psi}^-_{\mathrm{cr}} < 0 < \tilde{\psi}^+_{\mathrm{cr}}$ where $\tilde{\mathcal{V}}_\psi = 0$ and $\tilde{\mathcal{V}}_\psi = 1 - \mu$, respectively. Explicitly,

$$\begin{aligned} \psi^-_{\mathrm{cr}} &= \arctan\left(\frac{\mathrm{Im}[\mathcal{V}(m) - \mathrm{i}m]}{\mathrm{Re}[\mathcal{V}(m) - \mathrm{i}m]}\right), & \tilde{\psi}^-_{\mathrm{cr}} &= \arctan\left(\frac{\mathrm{Im}\,\tilde{\mathcal{V}}(m)}{\mathrm{Re}\,\tilde{\mathcal{V}}(m)}\right), \\ \psi^+_{\mathrm{cr}} &= \arctan\left(\frac{\mathrm{Im}\,\mathcal{V}(m)}{\mathrm{Re}\,\mathcal{V}(m)}\right), & \tilde{\psi}^+_{\mathrm{cr}} &= \arctan\left(\frac{\mathrm{Im}[\tilde{\mathcal{V}}(m) + \mathrm{i}(1-m)]}{\mathrm{Re}[\tilde{\mathcal{V}}(m) + \mathrm{i}(1-m)]}\right) \end{aligned} \tag{4.116}$$

For concreteness we consider positive ψ, and assume $\psi^+_{\mathrm{cr}} < \tilde{\psi}^+_{\mathrm{cr}}$, which holds for $m \in (0, 1/2)$, and more generally for small positive $\mathrm{Re}\, m$. For $\psi > \psi^+_{\mathrm{cr}}$, the initial rays $\mathcal{O}(k+1,k)$ starting from $\tau = k + \frac{1}{2}$ no longer reach $\tau = \mathrm{i}\infty$ but instead curl back and escape to another large volume point $\tau = k + \frac{1}{4}$, while the rays $\mathcal{O}(k,k+1)[1]$ (which previously were curling back to $\tau = k + \frac{3}{4}$) now escape to $\tau = \mathrm{i}\infty$ (see Fig. 4.9). For $\psi > \tilde{\psi}^+_{\mathrm{cr}}$, a similar transition occurs where $\mathcal{O}(k,k)$ crosses the cut and falls back on $\tau = k - \frac{1}{4}$ (on a different sheet) and $\mathcal{O}(k+1,k-1)[1]$ instead

comes from $\tau = k$ on a different sheet, emerges into the principal sheet by crossing a cut, and escapes to i∞. At that point, the rays $\mathcal{O}(0,0)$ and $\mathcal{O}(-1,0)[1]$ (along with their images under the monodromy $M_B(-1)$) surround the ramification point at $\tau_B - 1$ (see Fig. 4.10). Those are precisely the rays associated to the objects in the orbifold collection (4.63), which we recall for convenience,

$$\gamma_1 : \mathcal{O}(0,0), \quad \gamma_2 : \mathcal{O}(-1,0)[1], \quad \gamma_3 : \mathcal{O}(1,-1)[1], \quad \gamma_4 : \mathcal{O}(0,-1)[2] \tag{4.117}$$

Note that their central charges at $\tau = \tau_B - 1$ are equal in pairs, namely $\{\frac{m-1}{2}, -\frac{m}{2}, \frac{m-1}{2}, -\frac{m}{2}\}$, and become all equal to $-1/4$ when $m = 1/2$. A portion of the orbifold scattering diagram embeds inside the exact scattering diagram by equating ζ_i with (4.77), or in terms of the affine coordinates (4.71),

$$u = x - 2y + \tfrac{\mu}{2}, \quad v = 2y + \tfrac{1-\mu}{2} \tag{4.118}$$

The monodromy $M_B(-1)$ maps $(T, T_D) \mapsto (-1 - T, \frac{1-m}{2} - T_D)$ hence $(u, v) \mapsto (-u, -v)$, so the branch point maps to the origin in the (u, v) plane. Unlike in the orbifold scattering diagram of §4.3.2, the rays $\mathcal{R}(\gamma_1)$ and $\mathcal{R}(\gamma_2)$ no longer come from infinity, but start at $\tau = 0$ and $\tau = -\frac{1}{2}$ (approached on the principal sheet), which map to

$$\gamma_1 : (u, v) = \left(\tfrac{\mu}{2} + \mathcal{V}_\psi, \tfrac{1-\mu}{2}\right), \qquad \gamma_2 : (u, v) = \left(\tfrac{\mu}{2}, \tfrac{1-\mu}{2} - \tilde{\mathcal{V}}_\psi\right) \tag{4.119}$$

while the starting points for γ_3, γ_4 are the images under $(u, v) \mapsto (-u, -v)$. For $\psi = 0$ and m real, the rays start at the midpoints on the rectangle bounded by the lines $u = \pm\frac{\mu}{2}, v = \pm\frac{1-\mu}{2}$, so do not intersect. The rays $\{\gamma_1, \gamma_2\}$ (and similarly $\{\gamma_3, \gamma_4\}$) start intersecting when $\mathcal{V}_\psi \geq 0$, while the rays $\{\gamma_2, \gamma_3\}$ (and similarly $\{\gamma_4, \gamma_1\}$) start intersecting when $\tilde{\mathcal{V}}_\psi \geq 1 - \mu$.

Similarly, the rays $\mathcal{O}(1,0)$ and $\mathcal{O}(1,-1)[1]$ (along with their two images under the monodromy $\widetilde{M}_B(0)$) surrounding the ramification point at $\tau = \tilde{\tau}_B = \frac{\tau_B - 1}{4\tau_B - 3}$ are recognized as those associated to the Ext-exceptional collection

$$\gamma_1' : \mathcal{O}(1,0), \quad \gamma_2' : \mathcal{O}(1,-1)[1], \quad \gamma_3' : \mathcal{O}(0,1)[1], \quad \gamma_4' : \mathcal{O}(0,0)[2] \tag{4.120}$$

related to (4.117) by applying fiber/base duality and then tensoring with $\mathcal{O}(1,0)$. Affine coordinates (u, v) defined by $\zeta_1' = v - \frac{\mu}{2}, \zeta_2' = u + \frac{\mu-1}{2}$ (related to (4.71) by $\mu \mapsto 1 - \mu$) are related to (x, y) by

$$u = -2y + \tfrac{\mu-1}{2}, \quad v = x + 2y + \tfrac{\mu}{2}. \tag{4.121}$$

The rays now originate from $\tau = \frac{1}{2}$ (on the principal sheet) and $\tau = 0$ (across the branch cut from $\tau = \tilde{\tau}_B$ to $\tau = \frac{1}{2}$), which map to

$$\gamma_1' : (u, v) = \left(\tfrac{\mu-1}{2} + \tilde{\mathcal{V}}_\psi, \tfrac{\mu}{2}\right), \qquad \gamma_2' : (u, v) = \left(\tfrac{1-\mu}{2}, -\tfrac{\mu}{2} - \mathcal{V}_\psi\right) \tag{4.122}$$

For $\psi = 0$ and m real, the rays start at the midpoints on the rectangle, so do not intersect. The rays $\{\gamma_1', \gamma_2'\}$ start intersecting for $\tilde{\mathcal{V}}_\psi \geq 1 - \mu$, while $\{\gamma_2', \gamma_3'\}$ start intersecting for $\mathcal{V}_\psi \geq 0$.[26]

We shall describe momentarily the scattering diagram for generic ψ beyond those critical phases. Let us first discuss the extreme value $\psi = \frac{\pi}{2}$ (the same happens *mutatis mutandis* for $\psi = -\frac{\pi}{2}$). It follows from (4.45) that the rays $\operatorname{Im} Z(\gamma) = 0$ coincide with the loci $s = \frac{d_1 + \eta d_2}{2r}$. For

[26] As one can see in Figure 4.9, in the regime where $\mathcal{V}_\psi > 0$ and $\tilde{\mathcal{V}}_\psi < 1 - \mu$, the rays of bound states of γ_2' and γ_3' do not reach the $\tau =$ i∞ large volume region.

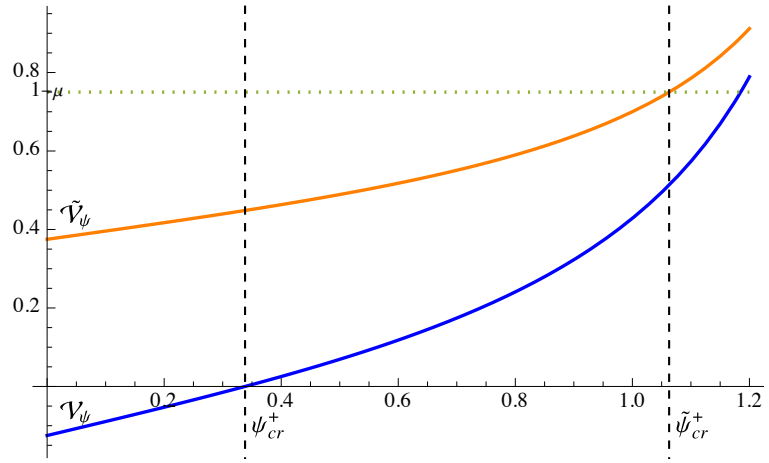


Figure 4.30: $\mathcal{V}_\psi$ and $\tilde{\mathcal{V}}_\psi$ as a function of ψ, for $m = 1/4$. The values $\psi^+_{\rm cr}$ and $\tilde{\psi}^+_{\rm cr}$ correspond to the transitions where $\mathcal{V}_\psi = 0$ and $\tilde{\mathcal{V}}_\psi = 1 - \mu$, respectively. For $m = 1/2$, $\tilde{\mathcal{V}}_\psi = \mathcal{V}_\psi + \frac{1}{2}$ and the two critical values coincide.

m real, $\eta = 1$ and these are level sets of $s = \frac{\operatorname{Im} T_D}{\operatorname{Im} T}$. Hence they can only intersect at the branch point where s becomes ill-defined, hence there can be no wall-crossing between the branch point and $\tau = \mathrm{i}\infty$. For $\operatorname{Im} m > 0$ however, η becomes a function of τ, which asymptotes to 1 as $\tau_2 \to \mathrm{i}\infty$, see (4.54). Rays can intersect whenever $\frac{d_1+\eta d_2}{2r} = \frac{d_1'+\eta d_2'}{2r'}$ and $\langle \gamma, \gamma' \rangle \neq 0$, i.e. $\frac{d_1}{r} \neq \frac{d_1'}{r'}$ and $\frac{d_2}{r} \neq \frac{d_2'}{r'}$. Since $\langle \gamma, \gamma' \rangle = 2(1-\eta)(r d_2' - r' d_2)$ must be a non-zero even integer, this can only happen when η is a rational number such that $|(1-\eta)(r d_2' - r' d_2)| \geq 1$, hence for large charges if η is close to one.

4.5.2 Building the scattering diagram on the Π-stability slice

The orbifold diagram associated to the collection (4.117) (resp. (4.120)) is valid in the region (dubbed 'orbifold region') around $\tau_B - 1$ (resp. $\tilde{\tau}_B$) where all central charges $Z(\gamma_i)$ (resp. $Z(\gamma_i')$) remain in the same half-plane. In stark contrast to the local $\mathbb{P}^2$ case of [47], these orbifold regions (depicted in Fig. 4.31) and their $\tau \to \tau + 1$ translates, together with the region where the central charge is $\widetilde{\mathrm{GL}}^+(2,\mathbb{R})$-equivalent to the large-volume central charge, do not cover the whole fundamental domain $\mathcal{F}$ for $\Gamma_0(4)$: the neighborhood of $\tau = \frac{1}{2}$ is not covered. Another issue is that the large volume description, while correctly counting BPS states through the large-volume scattering diagram, does not correctly describe the exact scattering diagram in the Π-stability slice, since the $\widetilde{\mathrm{GL}}^+(2,\mathbb{R})$ transformation affects the phase of the central charge, hence affects the rays.

To describe the exact scattering diagram we first define subregions Δ_ψ (resp. $\tilde{\Delta}_\psi$) of the orbifold regions near $\tau_B - 1$ (resp. $\tilde{\tau}_B$), defined in the local affine coordinates (u, v) adapted to the given exceptional collection as being the convex hull of the four initial points (4.119) (resp. (4.122)) of the rays, in other words, parallelograms in affine coordinates (u, v) or (x, y). Each of their sides maps in the τ-plane to a curve joining the conifold and dual conifold points $\tau = 0, -\frac{1}{2}$ (resp. $\tau = 0, \frac{1}{2}$) and opposite sides of the parallelogram map to the same curve since the monodromy around the branch point rotates the exceptional collection by two steps. See

Figure 4.31.[27] We also define[28] W_ψ as the connected component containing the large-volume point $\tau = \mathrm{i}\infty$ in the complement of Δ_ψ, $\tilde{\Delta}_\psi$ and their $\Gamma_0(4)$ images. The image of its boundary ∂W_ψ in the (x, y) plane is the 'jagged parabola' introduced above (4.114). The Π-stability slice is partitioned in this way into Δ_ψ, W_ψ and their images under $\Gamma_0(4)$. (In fact, $\tilde{\Delta}_\psi$ is one of the $\Gamma_0(4)$ images of Δ_ψ.)

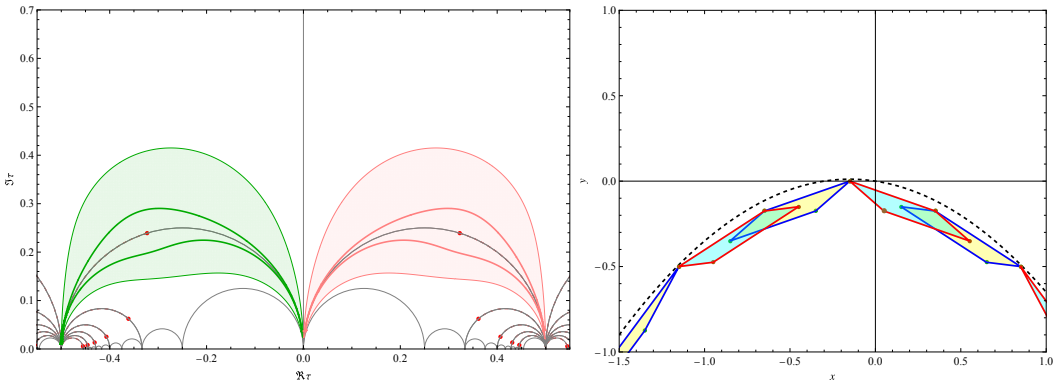


Figure 4.31: Left: Domain of validity of the quiver descriptions based on the collections (4.117), (4.120), for $m = 0.3$. The solid green and red lines are the boundaries of Δ_ψ and $\tilde{\Delta}_\psi$ and correspond to straight lines in the (x, y) plane. Right: the same regions in the (x, y) plane, together with some of their translates; the overlaps correspond to different stability conditions that map to the same values of x, y coordinates. The region above all of these translates is W_ψ.

The following picture emerges for the scattering diagram $\mathcal{D}^{\Pi}_{\psi,m}$ along Π, for fixed m and ψ.

- For $|\psi| < \min(\psi^+_{\rm cr}, \tilde{\psi}^+_{\rm cr})$, the region Δ_ψ and its $\Gamma_0(4)$ images do not contain any active[29] ray so that the scattering diagram is a disjoint union of $\Gamma_0(4)$ images of the W_ψ region, in which the scattering diagram coincides with the large-volume scattering diagram in affine coordinates (x, y, μ) given in (4.91). The initial rays participating in that connected component are $\mathcal{O}(k, k)$ and $\mathcal{O}(k, k)[1]$ emerging at each integer (conifold) point $\tau = k$, and $\mathcal{O}(k + 1, k)$ and $\mathcal{O}(k + 1, k)[1]$ emerging at half-integer (dual conifold) points $\tau = k + \frac{1}{2}$.
- If $\psi^+_{\rm cr} < \tilde{\psi}^+_{\rm cr}$ then for $\psi^+_{\rm cr} < \psi < \tilde{\psi}^+_{\rm cr}$ the collision of the initial rays $\mathcal{O}(k - 1, k)[1]$ and $\mathcal{O}(k, k)$ (emerging from $\tau = k - \frac{1}{2}$ and $\tau = k$, respectively) produces an infinite set of bound state rays that exit from Δ_ψ into W_ψ. These bound states are described by the Kronecker quiver K_2, and they admit a large volume description[30] as $\mathcal{O}(k - n - 1, k)[1]$ and $\mathcal{O}(k + n, k)$, and D2–D0 brane bound states with charge $[0, n, 0, nk]$, for $n \geq 1$. The scattering diagram within W_ψ can then be built starting from these infinitely many rays together with $\mathcal{O}(k, k - 1)[1]$ emerging from $\tau = k - \frac{1}{2}$ and $\mathcal{O}(k, k)[1]$ emerging from

[27] We checked numerically for a broad range of m with $\mathrm{Im}\, m \geq 0$ and $0 < \mathrm{Re}\, m < 1$ that Δ_ψ and $\tilde{\Delta}_\psi$ are in the region of validity of the respective quiver descriptions.

[28] In [47] the large-volume components were called $\diamond_\psi$ instead of W_ψ, but this could cause confusion since now the orbifold points are surrounded by four-sided regions.

[29] A ray is active if there exists a semi-stable object with that charge vector, namely if the corresponding index is nonzero.

[30] As ψ varies across $\psi^+_{\rm cr}$, this same collection of states goes from being described as bound states of $\mathcal{O}(k, k)[1]$ and $\mathcal{O}(k + 1, k)$ for $\psi < \psi^+_{\rm cr}$ to the present description as bound states of $\mathcal{O}(k - 1, k)[1]$ and $\mathcal{O}(k, k)$. The dictionary involves shifting the label n, which means for instance that $\mathcal{O}(k + 1, k)$ goes from being an initial ray for small ψ to a composite one for $\psi > \psi^+_{\rm cr}$, while conversely $\mathcal{O}(k - 1, k)[1]$ goes from composite to initial.

$\tau = k$. Altogether, the initial rays participating in the connected component of $\tau = \mathrm{i}\infty$ are $\mathcal{O}(k,k)$ and $\mathcal{O}(k,k)[1]$ emerging from $\tau = k$, and $\mathcal{O}(k,k+1)[1]$ and $\mathcal{O}(k+1,k)[1]$ emerging from $\tau = k + \frac{1}{2}$.

- If $\tilde{\psi}^+_{\rm cr} < \psi^+_{\rm cr}$ then for $\tilde{\psi}^+_{\rm cr} < \psi < \psi^+_{\rm cr}$ the situation is similar. The initial rays $\mathcal{O}(k,k)$ exit (translates of) Δ_ψ towards different images of the large volume region W_ψ. A new set of initial rays participate in the diagram in the region $\tau \to \mathrm{i}\infty$ of interest to us: $\mathcal{O}(k+1,k-1)[1]$ emerges from $\tau = k$ on a different sheet, enters through the cut from $k + \tau_B$ to $k + \frac{1}{2}$, collides with $\mathcal{O}(k+1,k)$ emerging from $\tau = k + \frac{1}{2}$, thus producing bound states with large-volume description as $\mathcal{O}(k+1,k+n)$, $\mathcal{O}(k+1,k-n-1)[1]$, and D2-D0 bound state with charge $[0,0,n,n(k+1)]$, for $n \geq 1$. The initial rays participating in the connected component of $\tau = \mathrm{i}\infty$ are $\mathcal{O}(k,k)[1]$ and $\mathcal{O}(k+1,k-1)[1]$ emerging from $\tau = k$ on two different sheets, and $\mathcal{O}(k+1,k)$ and $\mathcal{O}(k+1,k)[1]$ emerging from $\tau = k + \frac{1}{2}$.

- For $\psi > \max(\psi^+_{\rm cr}, \tilde{\psi}^+_{\rm cr})$ the scattering diagram is fully connected. Within the region $k + \Delta_\psi$ (resp. $k + \tilde{\Delta}_\psi$), rays of the exceptional collection (4.117) (resp. (4.120)) tensored with $\mathcal{O}(k,k)$ interact according to the quiver scattering diagram. Their bound state rays exit towards different $\Gamma_0(4)$ images of W_ψ. Those that enter W_ψ combine with the rays $\mathcal{O}(k,k)[1]$ and $\mathcal{O}(k+1,k)[1]$ emerging from $\tau = k, k + \frac{1}{2}$ directly into the region W_ψ to produce the scattering diagram in that region. Overall, the initial rays that participate to the scattering diagram in the large-volume region W_ψ are $\mathcal{O}(k,k)$, $\mathcal{O}(k,k)[1]$, $\mathcal{O}(k,k)[2]$, $\mathcal{O}(k+1,k)$, $\mathcal{O}(k+1,k)[1]$, $\mathcal{O}(k,k+1)[1]$ from the principal sheet, $\mathcal{O}(k+2,k)[1]$ and $\mathcal{O}(k+1,k)[2]$ from behind a cut joining $k + \tau_B$ to $k + \frac{1}{2}$, and finally $\mathcal{O}(k+1,k-1)[1]$ and $\mathcal{O}(k,k+1)[1]$ from behind a cut joining $k + \tilde{\tau}_B$ to $k + \frac{1}{2}$. Note that two different rays labeled $\mathcal{O}(k,k+1)[1]$ and emerging from different points with the same coordinate $\tau = k + \frac{1}{2}$ are involved, and likewise the two different rays[31] $\mathcal{O}(k+1,k-1)[1]$ emerge from $\tau = k$ on different sheets.

For negative ψ the situation is similar with different exceptional collections. We only describe the case $\psi < \min(\psi^-_{\rm cr}, \tilde{\psi}^-_{\rm cr})$, as the intermediate phases $\min(\psi^-_{\rm cr}, \tilde{\psi}^-_{\rm cr}) < \psi < \max(\psi^-_{\rm cr}, \tilde{\psi}^-_{\rm cr})$ are simpler in that many of the rays mentioned below simply enter W_ψ directly. The rays $\mathcal{O}(k,k-1)[1]$ and $\mathcal{O}(k,k)[-1]$ on the principal sheet, together with rays $\mathcal{O}(k-1,k)$ and $\mathcal{O}(k+1,k-1)$ from across the cut joining $\tau_B - 1$ to $\tau = \frac{1}{2}$ interact to generate an orbifold scattering diagram in $k + \Delta_\psi$. The rays $\mathcal{O}(k,k+1)$ and $\mathcal{O}(k,k)[1]$ on the principal sheet, together with rays $\mathcal{O}(k+1,k)[-1]$ and $\mathcal{O}(k+1,k-1)$ from across the cut joining $\tilde{\tau}_B$ to $\tau = \frac{1}{2}$ interact to generate an orbifold scattering diagram in $k + \tilde{\Delta}_\psi$. These two collections of four rays correspond to the exceptional collections (4.117) and (4.120) tensored with $\mathcal{O}(k,k)$ and shifted by $[-1]$. They generate infinitely many rays exiting from $k + \Delta_\psi$ and $k + \tilde{\Delta}_\psi$ into W_ψ. Together with the rays $\mathcal{O}(k,k)$ and $\mathcal{O}(k+1,k)$ that emerge directly into W_ψ, they generate the scattering diagram in that region.

4.5.3 Split Attractor Flow Conjecture

An important claim underlying the above picture is that the only active rays that enter into Δ_ψ (and likewise its $\Gamma_0(4)$ images) are the four initial rays participating in the exceptional collection,

[31] One of them is listed here as $\mathcal{O}(k+2,k)[1]$, which simply amounts to shifing k.

namely that collisions within W_ψ do not produce any rays that can re-enter Δ_ψ and that could then participate in other large volume regions. This ensures that portions of the scattering diagram in different $\Gamma_0(4)$ images of W_ψ are completely independent. The proof of this claim relies on the Split Attractor Flow Conjecture (SAFC), which itself relies on a closely related claim that attractor flow trees (see below) can only enter Δ_ψ and not exit it. We discuss these related issues here and outline a proof of the SAFC, at least in the range $\psi \in \mathcal{I}_{\rm cvx}$ defined below (4.114), such that the initial points bound a convex region in the (x, y) plane. We reiterate that we do not aim for mathematical rigour, hence will content ourselves with sketching the proof, letting the interested reader fill in the gaps.[32]

The SAFC posits a mostly-combinatorical formula for the index $\Omega_\sigma(\gamma)$ for a given charge vector γ and Π-stability condition σ as a sum over 'attractor flow trees' [16, 74, 75]. Edges of these trees are paths in the space of Π-stability conditions defined by gradient flow of the central charge $|Z(\gamma_i)|$ for some charge vectors γ_i labeling the edge. Nodes must obey charge conservation $\gamma_p = \gamma_1 + \cdots + \gamma_k$ when a parent edge with label γ_p splits into children edges with labels $\gamma_1, \ldots, \gamma_k$, and the central charges $Z(\gamma_i)$ involved at a given node must all have the same phase. Finally, the first (root) edge of the tree starts at the stability condition σ and is labeled by γ. The contribution of a given tree is given by the product of indexes of the constituents (charge vectors of the leaves), multiplied by some combinatorial factors that account for multiplicities at each node of the tree.

An important observation in the noncompact setting [47] is that the central charge $Z(\gamma)$ is a holomorphic function of τ and m (i.e. the normalizing factor $e^{-K/2}$ is absent). The gradient flow with respect to its modulus $|Z(\gamma)|$ thus preserves its phase. Since at each node the central charges $Z(\gamma_i)$ also have the same phase, all central charges involved in an attractor flow tree have the same phase as the central charge $Z_\tau(\gamma)$ at the initial point of the flow. Moreover, the metric determining the gradient flow is degenerate in such a way that the attractor flow in the (τ, m) space leaves m invariant. Thus, attractor flow trees lie in the scattering diagram $\mathcal{D}^\Pi_{\psi,m}$, for fixed m and ψ.

We are now ready to outline the proof of the SAFC for the scattering diagram $\mathcal{D}^\Pi_{\psi,m}$. First, we should clear out a potential source of confusion, namely that the attractor flow is oriented towards smaller values of $|Z(\gamma)|$, while when discussing scattering diagrams it is much more natural to think of rays as oriented in the opposite direction: exiting points where the object is massless, and pointing towards growing central charges. We will mostly use the 'scattering diagram direction', but it is sometimes necessary to mention the 'attractor flow direction'. We say that an oriented ray segment in W_ψ (oriented in the scattering diagram direction) is *outgoing* if the half-line in (x, y) coordinates obtained by continuing the ray in that direction does not intersect ∂W_ψ, but the full line does. Note that this definition excludes any ray that belongs to an (x, y) line that does not intersect the 'jagged parabola' ∂W_ψ at all. Note also that, at least when ψ belongs to the range $\mathcal{I}_{\rm cvx}$ introduced below (4.114), an outgoing ray cannot exit W_ψ, due to the complement $\mathbb{R}^2 \setminus W_\psi$ in the (x, y) plane being convex. It is possible that this property continues to be satisfied by active rays when the inequalities (4.114) are no longer satisfied, but we shall not attempt to prove this.

The first part of the proof is to understand how attractor flow trees decompose into W_ψ, Δ_ψ,

[32] A non-trivial gap, as in the local $\mathbb{P}^2$ case, is to justify rigorously our claims about bijectivity properties of the map from the τ plane to the (x, y) plane. Other minor gaps should be easy to fill by following the analogous proofs in [47].

$\tilde{\Delta}_\psi$ regions.

- In an attractor flow tree, by an induction going up from the leaves towards the root, we find that all ray segments that lie in W_ψ are outgoing. Indeed, rays that enter W_ψ are necessarily outgoing, and then if several outgoing rays combine at a given node, then their bound state, whose ray lies in the convex hull of the children rays, must also be outgoing.

- Thus, edges of attractor flow trees can only cross the boundary of W_ψ one way: in the flow direction they can exit W_ψ into one of the regions $k + \Delta_\psi$ or $k + \tilde{\Delta}_\psi$, but they can then never leave those regions.

- In particular, any attractor flow tree with root in W_ψ can be decomposed into 'shrubs' in the regions $k + \Delta_\psi$ or $k + \tilde{\Delta}_\psi$ produced by the exceptional collections (4.117) and (4.120) and translates thereof, and a 'trunk' in the region W_ψ that combines these shrubs together with additional lone branches $\mathcal{O}(k,k)[1]$ and $\mathcal{O}(k+1,k)[1]$ (for $\psi > 0$) or $\mathcal{O}(k,k)$ and $\mathcal{O}(k+1,k)$ (for $\psi < 0$).[33]

The main part of the proof is to make sense of the sum over attractor flow trees by proving that there are finitely many of them, as follows.

- In the (x,y) plane the trunk of any attractor flow tree with root at a given point $(x,y) \in W_\psi$ must lie within the convex hull of ∂W_ψ and (x,y). Trees can thus only involve shrubs from finitely many exceptional collections.

- Then one exhibits a cost function

$$\varphi_\tau(\gamma) = \begin{cases} d_1 + d_2 + r\lfloor \mathcal{V}_\psi - x \rfloor + r\lfloor \tilde{\mathcal{V}}_\psi - x \rfloor & \text{in } W_\psi, \\ c_\psi(N_1 + N_2 + N_3 + N_4) & \text{in } \Delta_\psi, \\ c_\psi(\tilde{N}_1 + \tilde{N}_2 + \tilde{N}_3 + \tilde{N}_4) & \text{in } \tilde{\Delta}_\psi, \end{cases} \tag{4.123}$$

  where the vectors (N_1, N_2, N_3, N_4) and $(\tilde{N}_1, \tilde{N}_2, \tilde{N}_3, \tilde{N}_4)$ are dimension vectors of γ with respect to the exceptional collections (4.117) and (4.120), and $c_\psi > 0$ is a sufficiently small constant.

- One checks that $\varphi_\tau(\gamma) \geq 1$ for the rays $\mathcal{O}(k,k)[1]$ and $\mathcal{O}(k+1,k)[1]$ near $\tau = k$ and $\tau = k + \frac{1}{2}$ respectively, and for other initial rays one has $\varphi_\tau(\gamma) \geq c_\psi > 0$ since dimension vectors are non-negative (and non-zero).

- The cost function decreases monotonically along each branch of an attractor flow tree in the flow direction: in the large volume region, the variation of x is appropriately correlated to the sign of r, and one only needs to check the transition from W_ψ to Δ_ψ or $\tilde{\Delta}_\psi$.

Note that this leads to explicit bounds hence an explicit algorithm for listing the trees for a given Chern vector.

As explained in [47, §3.4–3.5], once it has been shown that there are finitely many trees, a suitable choice of combinatorial factors (found in [16, 25, 154]) ensures that the index calculated

[33] While this step looks like a restatement of the structure of the scattering diagram proposed in the previous section, it concerns here all attractor flow trees, even if their branches are actually not active rays. This phenomenon is ubiquitous and occurs due to cancellation between trees: for instance the SAFC applied to quivers produces trees for all non-negative dimension vectors even when the index happens to vanish.

by the Split Attractor Flow formula obeys the wall-crossing formula of [127], or in other words that it defines a consistent scattering diagram.

It remains to prove that the scattering diagram has the correct initial data and is uniquely characterized by consistency. Large parts of the proof should mimic [47, Appendix C].

- The idea to compute $\Omega_\tau(\gamma)$ is to apply the KS wall-crossing formula starting from τ and tracking all relevant indices at every wall of marginal stability.
- Concretely, one considers a notion of split attractor flow, which is a close cousin of attractor flow trees. A split attractor flow starting from τ, with charge vector γ is obtained by the same gradient flow as for attractor flow trees, and the same type of splitting of a parent charge $\gamma_p = \gamma_1 + \cdots + \gamma_k$ into children charges, but now every edge has to be active (in the sense of footnote 29), and the flow is not a priori required to reach initial rays in a finite number of steps.
- The Kähler moduli space being compact except for large volume and conifold points, one finds that any such split attractor flow must in fact have finitely many branches, and must eventually reach the only non-compact points which are (dual) conifold points or the large volume point. The large volume point is excluded by considering the asymptotics of the central charge. Near the (dual) conifold points, suitable quiver descriptions force the split attractor flow to be given by initial rays that we have identified.
- Altogether, repeatedly applying the wall-crossing formula to compute $\Omega_\tau(\gamma)$ in terms of simpler indices is a finite process. It expresses the index in terms of split attractor flows, which are among attractor flow trees (with the added constraint that all rays be active). The SAFC follows, after some bookkeeping to ensure that trees with some non-active rays do indeed cancel.

4.5.4 Exploring the forest in the Π-stability slice

Given the complexity of the structure of initial rays, the above discussion of the SAFC only gives a somewhat impractical algorithm for determining the trees contributing to the index for an arbitrary Chern vector. As ψ varies, the trees will in general jump, even if the index is constant.

To illustrate this phenomenon, we consider the simple cases of the Chern characters for the structure sheaves $\mathcal{O}_S$ and $\mathcal{O}_C$, namely the pure D4-brane $\gamma = [1,0,0,0]$ and pure D2-brane $\gamma = [0,1,0,0]$. In this case, we find evidence that for fixed ψ, only one 'shrub' contributes, even though the exceptional collection on which it is rooted varies as a function of ψ. The tree gets more complicated as $|\psi| \to \frac{\pi}{2}$, albeit in a controlled fashion, as we now explain.

For these Chern characters, the dimension vectors with respect to the collection (4.117) tensored with $\mathcal{O}(-k,-k)$ (which we denote by $C(-k)$) are given by

$$\mathcal{O}_S : ((k+1)^2, k^2+k, k^2, k^2-k)\,, \quad \mathcal{O}_C : (k+1, k+1, k, k) \tag{4.124}$$

while the dimension vectors with respect to the collection (4.120) tensored with $\mathcal{O}(-k,-k)$ (which we denote by $C'(-k)$) are given by

$$\mathcal{O}_S : (k^2+k, k^2, k^2-k, (k-1)^2)\,, \quad \mathcal{O}_C : (k+1, k, k, k-1) \tag{4.125}$$

In general under shifting $k \mapsto k+1$, both dimension vectors transform as

$$(N_1, N_2, N_3, N_4) \mapsto (4N_1 - 2N_2 - 3N_3 + 2N_4, N_4 + 2N_1 - 2N_3, N_1, N_2) \tag{4.126}$$

In fact, the dimension vector along (4.120) is mapped to the dimension vector along (4.117) via

$$(N_1, N_2, N_3, N_4) \mapsto (2N_1 - 2N_3 + N_4, N_1, N_2, N_3) \tag{4.127}$$

and the transformation (4.126) follows by acting with (4.127) twice. The transformation (4.127) suggests that under shifting $C(-k)$ to $C'(-k+1)$, and then further to $C(-k+1)$, the trees transform by a cyclic permutation σ of the charges $\gamma_i \mapsto \gamma_{i+1}$, and adding an extra leg carrying $\langle \gamma, \gamma_2 \rangle$ units of charge γ_1,

$$T \mapsto \{\langle \gamma, \gamma_2 \rangle \gamma_1, \sigma \cdot T\} \tag{4.128}$$

Of course, this only makes sense if $\langle \gamma, \gamma_2 \rangle > 0$, and the full quiver scattering diagram could in principle contain additional trees. However, for the two cases mentioned above, we find that this prescription correctly produces a tree contributing the same index (namely 1 for $\mathcal{O}_S$, and $-y - 1/y$ for $\mathcal{O}_C$) for increasing values of ψ, see Figures 4.32 and 4.33, so it is presumably the only contributing tree.

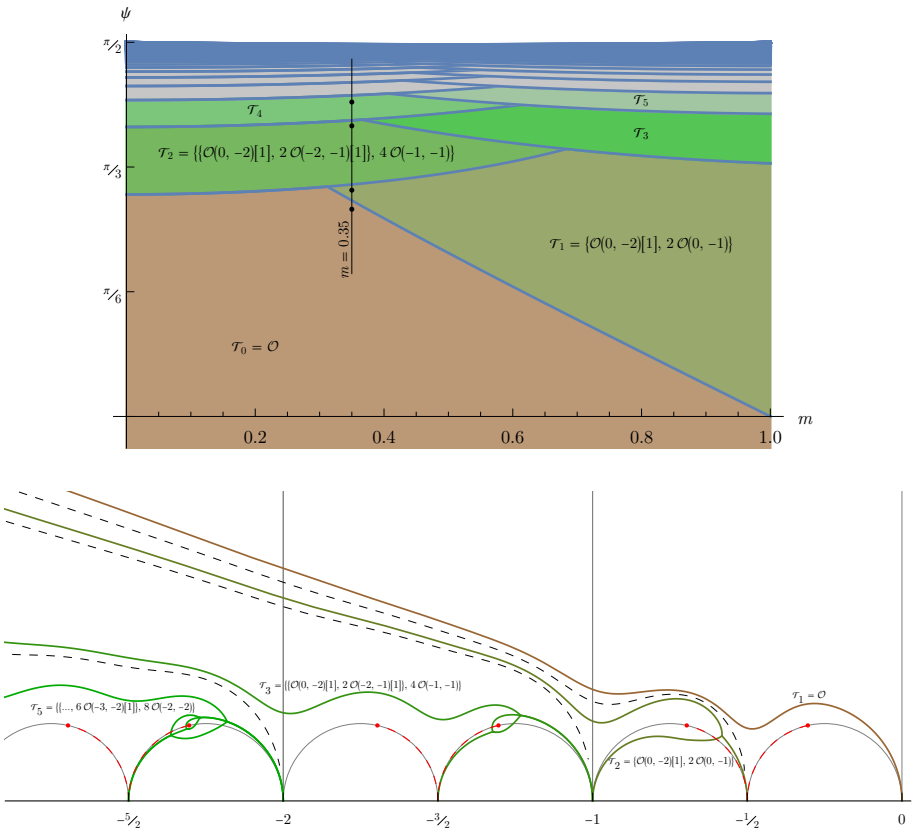


Figure 4.32: Top: Trees contributing to the structure sheaf index $\Omega([1,0,0,0])$ as function of m (real) and ψ. Bottom: Trees in τ-plane for $m = 0.35$, varying ψ. Note that the tree $\mathcal{T}_4$ does not arise for this value.

4.6 Appendix: Central charge as Eichler Integrals

In this Appendix, we determine the central charge at a general point along the slice of Π-stability conditions, extending earlier studies of mirror symmetry for local $\mathbb{F}_0$ [1, 2, 105, 114–116, 124] (or its close cousin $\mathbb{F}_2$ [55]). In particular, we express the coefficients T, T_D as Eichler integrals

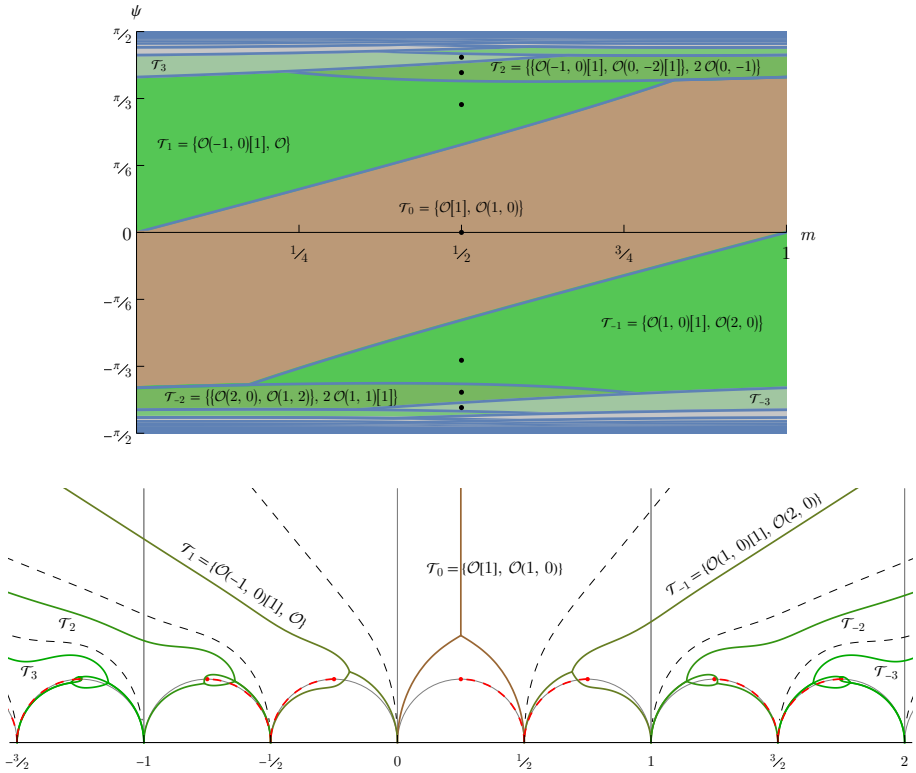


Figure 4.33: Top: Trees contributing to the D2 index $\Omega([0,1,0,0])$ as function of m (real) and ψ. Bottom: Trees in τ-plane for $m = 0.5$, varying ψ.

of a certain weight 3 modular form under $\Gamma_1(4)$, and determine the asymptotic expansions near the large volume, conifold, dual conifold and branch points.

4.6.1 Mirror curve

Local mirror symmetry [60] relates type IIA strings on $K_{\mathbb{F}_0}$ to type IIB strings on a conic bundle over the genus one curve with equation

$$y_1 + \frac{z_1}{y_1} + y_2 + \frac{z_2}{y_2} + 1 = 0 \tag{4.129}$$

where y_1, y_2 are coordinates in $\mathbb{C}^\times \times \mathbb{C}^\times$ and z_1, z_2 are complex structure parameters. Setting

$$\lambda = \frac{z_1}{z_2}\,, \quad U = -\frac{1}{\sqrt{z_2}}\,, \quad y_1 = t\sqrt{z_1}\,, \quad y_2 = w\sqrt{z_2} \tag{4.130}$$

we arrive at the form of the mirror curve used in [65]:

$$\sqrt{\lambda}\left(\frac{1}{t} + t\right) + \frac{1}{w} + w - U = 0\,, \tag{4.131}$$

Fiber-base duality acts by exchanging z_1 and z_2, or equivalently

$$\lambda \mapsto \frac{1}{\lambda}\,, \quad U \mapsto \frac{U}{\sqrt{\lambda}} \tag{4.132}$$

It will be convenient to define

$$\lambda = e^{2\pi i m} \tag{4.133}$$

and choose $0 \leq \mathrm{Re}(m) \leq \frac{1}{2}$, which is always possible by fiber-base duality. Upon defining $U = \frac{1}{Q_b}, \lambda = \frac{Q_f^2}{Q_b^2}$, or equivalently $(Q_f, Q_b) = (-\sqrt{z_1}, -\sqrt{z_2})$, and rescaling t and w, one arrives at the representation in [34]

$$Q_b \left(w + \frac{1}{w}\right) + Q_f \left(t + \frac{1}{t}\right) - 1 = 0 \tag{4.134}$$

The curve (4.129) can be recast into the Weierstrass form

$$y^2 = x^3 + fx + g\,, \tag{4.135}$$

with coefficients given by

$$\begin{aligned} f =& -\frac{1}{48}\left(1 - 8z_1 + 16z_1^2 - 8z_2 - 16z_1z_2 + 16z_2^2\right)\,, \\ g =& \frac{1}{864}\left(1 - 4z_1 - 4z_2\right)\left(1 - 8z_1 + 16z_1^2 - 8z_2 - 40z_1z_2 + 16z_2^2\right)\,, \end{aligned} \tag{4.136}$$

Equivalently, one may write (4.135) as a quartic [125]

$$Y^2 = (X^2 + UX + 1)^2 - 4X^2\mathcal{R}^4\,, \quad \mathcal{R} = \sqrt{\lambda}, \quad U = -\frac{1}{\sqrt{z_2}} \tag{4.137}$$

The curve (4.135) becomes singular when the discriminant Δ vanishes, with

$$\Delta = 4f^3 + 27g^2 = -\frac{1}{16}z_1^2z_2^2\left(1 - 8(z_1 + z_2) + 16(z_1 - z_2)^2\right)\,. \tag{4.138}$$

The discriminant locus $\Delta = 0$ decomposes into 3 components, the two large volume limits $z_1 = 0$, $z_2 = 0$ and the conifold locus $C = \{1 - 8(z_1 + z_2) + 16(z_1 - z_2)^2 = 0\}$ (or equivalently $U = \pm 2(\mathcal{R}^2 \pm 1)$). The symmetric slice $\{z_1 = z_2 = z\}$ (corresponding to $\lambda = 1$) intersects the discriminant locus at $z = 0$ and $z = 1/16$. A generic slice $\{z_1 = \lambda z_2\}$ with $\lambda \neq 1$ intersects Δ in 3 points, for example $z = 0, z = \pm i/8$ when $\lambda = -1$.

The Klein invariant of the elliptic curve (4.135) evaluates to

$$J(z_1, z_2) = 1728\frac{4f^3}{27g^2 + 4f^3} = \frac{\left[(1 - 4z_1 - 4z_2)^2 - 48z_1z_2\right]^3}{z_1^2z_2^2\left(1 - 8(z_1 + z_2) + 16(z_1 - z_2)^2\right)}\,. \tag{4.139}$$

For fixed $\lambda = z_1/z_2$, the Klein invariant produces a 6:1 cover from the punctured sphere parametrized by $z := z_2$ to $\mathbb{H}/PSL(2,\mathbb{Z})$. In order to trivialize this cover, we reduce the modular group $SL(2,\mathbb{Z})$ to the subgroup $\Gamma_0(4)$, generated by integer matrices $\left(\begin{smallmatrix} a & b \\ c & d \end{smallmatrix}\right)$ with $ad - bc = 1$ and $c = 0 \mod 4$. [34]. The congruence subgroup $\Gamma_0(4)$ is an index 6 subgroup of $SL(2,\mathbb{Z})$, with cusps at $\tau = i\infty$ (and images thereof, $\tau = \frac{p}{q}$ with $q = 0 \mod 4$), $\tau = 0$ (and images thereof, $\tau = \frac{p}{q}$ with $q = 1$ or $q = 3 \mod 4$) and $\tau = \frac{1}{2}$ (and images thereof, $\tau = \frac{p}{q}$ with $q = 2 \mod 4$). It

[34] Note that the authors of [32, 65] consider instead $\Gamma^0(4)$, related by $\tau \mapsto \tau/4$. Moreover, $\Gamma_0(4)$ differs from $\Gamma_1(4)$ by the additional generator $\mathrm{diag}(-1,-1)$, which acts trivially on τ.

will be convenient to choose the following fundamental domain of $\Gamma_0(4)$ in the Poincaré upper half-plane $\mathbb{H}$ (see Fig. 4.4)

$$\mathcal{F} = \left\{\tau \in \mathbb{H}, 0 \leq \mathrm{Re}\,\tau < 1,\ |\tau - \tfrac{1}{4}| > \tfrac{1}{4}, \quad |\tau - \tfrac{3}{4}| \geq \tfrac{1}{4}\right\} \tag{4.140}$$

In particular, the lower boundary of $\mathcal{F}$ consists of two half circles of radius 1/4, which we denote by $C = C(\frac{3}{4}, \frac{1}{4})$ and $C' = C(\frac{1}{4}, \frac{1}{4})$. The quotient $\mathbb{H}/\Gamma_0(4)$ is in 1:1 correspondence with the punctured sphere $\mathbb{P}^1\backslash\{\infty, \pm 8\}$ via the Hautpmodul

$$J_4(\tau) = 8 + \left(\frac{\eta(\tau)}{\eta(4\tau)}\right)^8 = \frac{1}{q} + 20q - 62q^3 + 216q^5 - 641q^7 + \dots \tag{4.141}$$

which maps

$$J_4(\mathrm{i}\infty) = \infty, \quad J_4(0) = 8\,, \quad J_4(\tfrac{1}{2}) = -8, \quad J_4(\tfrac{\mathrm{i}+1}{4}) = J_4(\tfrac{\mathrm{i}+3}{4}) = 0 \tag{4.142}$$

Using the relation between J_4 and the Klein invariant $J(\tau) = \frac{E_4^3}{\eta^{24}(\tau)}$

$$J(\tau) = \frac{(J_4^2(\tau) + 240J_4(\tau) + 2112)^3}{(J_4(\tau) - 8)^4(J_4(\tau) + 8)} \tag{4.143}$$

and setting $u = \frac{U^2}{4} - \lambda - 1$, we find that

$$\frac{u}{2\sqrt{\lambda}} = \frac{J_4(\tau) + 24}{J_4(\tau) - 8} \tag{4.144}$$

This can be further simplified by introducing the Fricke transform

$$\begin{aligned} J_4'(\tau) =& J_4\left(-\frac{1}{4\tau}\right) = 8 + 256\left(\frac{\eta(4\tau)}{\eta(\tau)}\right)^8 = 8 + \frac{256}{J_4(\tau) - 8} \\ =& 8 + 256q + 2048q^2 + 11264q^3 + \dots \end{aligned} \tag{4.145}$$

Indeed, (4.144) now becomes $\frac{u}{\sqrt{\lambda}} = \frac{1}{4}J_4'(\tau)$ or equivalently

$$z = \frac{1}{\sqrt{\lambda}J_4'(\tau) + 4(\lambda + 1)} \tag{4.146}$$

In order to map the large volume limit $z \to 0$ to $\mathrm{i}\infty$, we shall henceforth trade τ for its Fricke transform $\tau' = -1/(4\tau)$ (i.e. perform the isogeny $\tau \mapsto 4\tau$ followed by the inversion) and write

$$z = \frac{1}{\sqrt{\lambda}J_4(\tau) + 4(\lambda + 1)} \tag{4.147}$$

This relation gives a 1:1 map from $\mathbb{H}/\Gamma_0(4)$ to the punctured line parametrized by z,

$$\mathbb{P}^1\backslash\{0, \frac{1}{4(1 + \sqrt{\lambda})^2}, \frac{1}{4(1 - \sqrt{\lambda})^2}, \infty\} \tag{4.148}$$

corresponding to the images of $\tau = \mathrm{i}\infty, 0, \frac{1}{2}, \tau_B$, respectively, where τ_B is the point in the fundamental domain $\mathcal{F}$ defined by

$$J_4(\tau_B) = -4(\lambda^{1/2} + \lambda^{-1/2}) = -8\cos\pi m \tag{4.149}$$

Circling around the point τ_B, z is single valued but $U = -1/\sqrt{z}$ changes sign. Thus, for generic values of λ, the U-line is a double cover of $\mathbb{H}/\Gamma_0(4)$. We choose the branch cut starting from τ_B and ending at $\tau = \frac{1}{2}$ along a hyperbolic geodesic (equivalently, we require that its image under the Atkin-Lehner involution $\tau'' = \frac{\tau}{1-2\tau}$ mapping $(\mathrm{i}\infty, 0, \frac{1}{2})$ to $(-\frac{1}{2}, 0, \mathrm{i}\infty)$ lies along a vertical line with fixed $\mathrm{Re}\,\tau''$), and extend this choice to the full Poincaré upper half-plane by $\Gamma_0(4)$ invariance. We observe the following simplifications at special values of λ:

- For $|\lambda| = 1$ (or m real), the branch point τ_B lies along the half circle $C := C(\frac{3}{4}, \frac{1}{4})$ while its image under $\tau \mapsto \frac{\tau-1}{4\tau-3}$ lies along the half circle $\tilde{C} := C(\frac{1}{4}, \frac{1}{4})$, see Fig. 4.4.

- For $\mathrm{Re}(m) = 0$, τ_B lies along the vertical axis $\mathrm{Re}\,\tau_B = 1/2$. For $\mathrm{Re}(m) = \frac{1}{2} + \mathrm{i}0^+$ (respectively $\mathrm{Re}(m) = \frac{1}{2} - \mathrm{i}0^+$), the branch point τ_B lies on the vertical axis $\mathrm{Re}(\tau) = \frac{1}{4}$ (respectively $\mathrm{Re}(\tau) = \frac{3}{4}$)

- For $\lambda \to 1$ (or rather $m \to 0$), the branch point τ_B collides with the cusp at $\tau = \frac{1}{2}$, so the branch cut disappears. The coordinate U then becomes single-valued on the doubled fundamental domain $\mathcal{F} \cup (\mathcal{F} + 1)$, which can be viewed as a fundamental domain of $\Gamma_0(8)$ after rescaling $\tau \mapsto \tau/2$ [65].

- For $\lambda \to -1$ (or rather $m \to 1/2$) we have $J_4(\tau_B) \to 0$ so τ_B coincides with the $\mathbb{Z}_4$-orbifold point $\frac{\mathrm{i}+3}{4}$, and its image with $\frac{\mathrm{i}+1}{4}$. The auto-equivalence $M_{0,1} \cdot M_{FB}$ from (4.30) gives an extra symmetry $\tau \mapsto \tau + \frac{1}{2}$, which extends $\Gamma_0(4)$ to $\Gamma_0(2)$, now acting on 2τ. Indeed, for $\lambda = -1$ the Coulomb branch parameter $U = -1/\sqrt{z}$ can be written in terms of the Hauptmodul for $\Gamma_0(2)$

  $$J_2(\tau) = \left(\frac{\eta(\tau)}{\eta(2\tau)}\right)^{24} + 24 = \frac{1}{q} + 276q - 2048q^2 + 11202q^3 + \ldots \tag{4.150}$$

  as

  $$U^4 = -(J_2(2\tau) + 40) \tag{4.151}$$

  where we used $J_2(2\tau) = J_4^2(\tau) - 40$. Thus, the U-line becomes a $4:1$ cover of $\mathbb{H}/\Gamma_0(2)$ [65].

- For $\lambda \to +\infty$ (or $m \to -\mathrm{i}\infty$), corresponding to the 4D limit (see §4.6.6), the branch point τ_B moves off to infinity

4.6.2 Picard-Fuchs equations and mirror map

The dependence of the coefficients T_D, T_1, T_2 on the Kähler parameters z_1, z_2 is dictated by mirror symmetry. The Picard-Fuchs (PF) system annihilating the periods is generated by the two operators [124]

$$\begin{aligned} \mathcal{D}_1 &= \theta_1^2 - 2z_1(\theta_1 + \theta_2)(2\theta_1 + 2\theta_2 + 1)\,, \\ \mathcal{D}_2 &= \theta_2^2 - 2z_2(\theta_1 + \theta_2)(2\theta_1 + 2\theta_2 + 1)\,. \end{aligned} \tag{4.152}$$

Setting $z = z_2, \lambda = \frac{z_1}{z_2}$, the first operator is rewritten as

$$\mathcal{D}_1 = (\lambda\partial_\lambda)^2 - 2\lambda z(2\theta+1)\theta \tag{4.153}$$

where $\theta = z\partial_z$, while the second operator can be traded for a third order differential operator in z [116]

$$\mathcal{D} = \left[\theta^2 - 2(1+\lambda)z(2\theta+1)^2 + 4(1-\lambda)^2 z^2(2\theta+1)(2\theta+3)\right]\theta\,, \tag{4.154}$$

where λ plays the role of an external parameter. This operator has 4 singularities at

$$z = 0, \quad z = \frac{1}{4(1+\sqrt{\lambda})^2}, \quad z = \frac{1}{4(1-\sqrt{\lambda})^2}, \quad z = \infty \tag{4.155}$$

corresponding to the large volume point $\tau = \mathrm{i}\infty$, conifold point $\tau = 0$, 'dual conifold' point $\tau = \frac{1}{2}$ and branch point τ_B, respectively. The constants

$$\varpi_0 = 1\,, \quad \varpi_1 = \log\lambda = 2\pi\mathrm{i}m \tag{4.156}$$

are manifestly annihilated by $\mathcal{D}$ and $\mathcal{D}_1$, while non-constant solutions of $\mathcal{D}_1 = 0$ have a logarithmic or doubly logarithmic singularities at $z = 0$,

$$\begin{aligned}
\varpi_2 &= \log z + 2\sum_{k+\ell>0}\frac{(2k+2\ell-1)!}{(k!)^2(\ell!)^2}z^{k+\ell}\lambda^\ell \\
&= \log z + 2z(1+\lambda) + (3+12\lambda+3\lambda^2)z^2 + \frac{20}{3}(1+9\lambda+9\lambda^2+\lambda^3)z^3 + \dots\,, \\
\varpi_3 &= -\log^2 z + (2\log z + \log\lambda)\,\varpi_2 - 2\sum_{k+\ell>0}\frac{(2k+2\ell)!}{(k!)^2(\ell!)^2(k+\ell)}\left(H_k + H_\ell - 2H_{2k+2\ell} + \frac{1}{k+\ell}\right)z^{k+\ell}\lambda^\ell \\
&= -\log^2 z + \varpi_2\,[\log(\lambda) + 2\log(z)] + 4z(1+\lambda) + (13+40\lambda+13\lambda^2)z^2 + \dots\,.
\end{aligned} \tag{4.157}$$

where $H_k = 1 + \frac{1}{2} + \cdots + \frac{1}{k}$ are the harmonic numbers. Note that ϖ_2 is invariant under fiber-base duality, $(z,\lambda) \mapsto (z\lambda, 1/\lambda)$, whereas ϖ_3 transforms by a shift proportional to ϖ_1. On the other hand, the period ϖ_1 is independent of the complex structure of the mirror curve, odd under fiber-base duality, and is the residue of the meromorphic differential.

Guided by the large volume limit of the D4-brane central charge T_D, we define the period T and dual period T_D (or $(2a, \frac{1}{2}a_D)$ in the notations of [65]) via

$$T = \frac{1}{2\pi i}\varpi_2\,, \quad T_D = \frac{1}{2}\frac{1}{(2\pi i)^2}\varpi_3 + \frac{1}{12}\,, \tag{4.158}$$

Setting $Q = e^{2\pi\mathrm{i}T}$, we can obtain the mirror map order by order in Q,

$$\begin{aligned}
z(Q) =& Q - 2(1+\lambda)Q^2 + 3(1+\lambda^2)Q^3 \\
&- 4(1+\lambda+\lambda^2+\lambda^3)Q^4 + 5(1-5\lambda^2+\lambda^4)Q^5 + \mathcal{O}(Q^6)\,,
\end{aligned} \tag{4.159}$$

The prepotential F_0 is obtained by integrating the relation $T_D = \partial_T F_0$,

$$F_0 = \frac{1}{6}T^3 + \frac{1}{4}mT^2 + \frac{T}{12} + \frac{1}{(2\pi\mathrm{i})^3}\left[2(1+\lambda)Q + \frac{1}{4}(1+16\lambda+\lambda^2)Q^2 + \mathcal{O}(Q^3)\right]. \tag{4.160}$$

In the large volume limit, we get the expected large volume expression of the D4-brane central charge, including the Todd-class correction $\chi(\mathbb{F}_0)/48 = 1/12$,

$$T_D = \frac{1}{2}T(T+m) + \frac{1}{12} + \mathcal{O}(Q) \tag{4.161}$$

The modular parameter of the mirror curve is given by the second derivative of the prepotential,

$$\tau = \partial_T T_D = \partial_T^2 F_0 \tag{4.162}$$

such that

$$q = e^{2\pi i\tau} = Q\sqrt{\lambda}\left[1 + 2(1+\lambda)Q + (3 + 20\lambda + 3\lambda^2)Q^2 + \mathcal{O}(Q^3)\right], \tag{4.163}$$

After inverting the series, we can express Q a in terms of τ,

$$\sqrt{\lambda}Q = q - 2\left(\lambda^{-\frac{1}{2}} + \lambda^{\frac{1}{2}}\right)q^2 + \left(5\lambda^{-1} - 4 + 5\lambda\right)q^3 + \mathcal{O}(q^4) \tag{4.164}$$

and therefore z in terms of τ

$$z = \frac{q}{\sqrt{\lambda}} - 4\frac{1+\lambda}{\lambda}q^2 + \frac{4(4+3\lambda+4\lambda^2)}{\lambda^{3/2}}q^3 - \frac{32(2+\lambda+\lambda^2+2\lambda^3)}{\lambda^2}q^4 + \dots \tag{4.165}$$

which agrees with the q-expansion of (4.147).

4.6.3 Explicit solutions at $\lambda = \pm 1$

When $\lambda = 1$ (more precisely $m = 0$), one of the singularities (4.155) moves off to infinity and the PF equation (4.154) admits explicit solutions in terms of Meijer G functions,

$$\begin{aligned}
\varpi_2(z) &= -\frac{1}{\pi}G^{2,2}_{3,3}\left(\begin{matrix}\frac{1}{2} & \frac{1}{2} & 1\\ 0 & 0 & 0\end{matrix}\,\middle|\, -16z\right) - \mathrm{i}\pi\,,\\
\varpi_3(z) &= -\frac{2}{\pi}G^{3,2}_{3,3}\left(\begin{matrix}\frac{1}{2} & \frac{1}{2} & 1\\ 0 & 0 & 0\end{matrix}\,\middle|\, 16z\right) - \frac{4\pi^2}{3}
\end{aligned} \tag{4.166}$$

such that

$$\tau = \frac{z\partial_z T_D}{z\partial_z T} = \frac{\mathrm{i}}{2}\frac{{}_2F_1(\frac{1}{2},\frac{1}{2};1;1-16z)}{{}_2F_1(\frac{1}{2},\frac{1}{2};1;16z)}, \quad z = \frac{1}{J_4(\tau)+8} \tag{4.167}$$

One easily checks that the expansion near $z = 0$ (assuming $\mathrm{Im}\, z < 0$) reproduces (4.157), while the value at the conifold point $z = 1/16$, corresponding to $\tau = 0$ or $U = \pm 4$ yields

$$\varpi_2 = -\frac{8G}{\pi}, \quad \varpi_3 = \frac{2\pi^2}{3} \tag{4.168}$$

where $G = \mathrm{Im}\,\mathrm{Li}_2(\mathrm{i}) \simeq 0.915966$ is Catalan's constant, hence

$$m = 0: \qquad T(0) = \mathrm{i}\frac{4G}{\pi^2}, \quad T_D(0) = 0 \tag{4.169}$$

The expansion near $z = \infty$ (or $U \to \infty$) is more subtle, due to the branch cut in the Meijer G-function. For $\mathrm{Im}\, z < 0$, the Meijer G-function goes to zero and $\tau \to -\frac{1}{2}$, yielding $(T, T_D) =$

$(-\frac{1}{2}, \frac{1}{4})$. For $\mathrm{Im}\, z > 0$, τ instead goes to $+\frac{1}{2}$ and we obtain the image of the previous result under spectral flow,

$$m = 0: \qquad T(\tfrac{1}{2}) = \tfrac{1}{2}, \quad T_D(\tfrac{1}{2}) = \tfrac{1}{4} \tag{4.170}$$

We shall recompute these values below (4.200) using L-series. By using analytic properties of the Meijer-G functions, we find the monodromies of the reduced period vector $(1, T, T_D)^t$ around $z = 0$, $z = 1/16$ and $z = \infty$,

$$M_{LV} = \begin{pmatrix} 1 & 0 & 0 \\ 1 & 1 & 0 \\ \frac{1}{2} & 1 & 1 \end{pmatrix}, \quad M_C = \begin{pmatrix} 1 & 0 & 0 \\ 0 & 1 & -4 \\ 0 & 0 & 1 \end{pmatrix}, \quad M_o = \begin{pmatrix} 1 & 0 & 0 \\ 1 & 1 & -4 \\ \frac{1}{2} & 1 & -3 \end{pmatrix} \tag{4.171}$$

This reduces to the matrices in [65, (5.22-23)] upon ignoring the mixing with the constant solution and translating notations. The corresponding actions on the τ parameter are the $\Gamma_0(4)$ transformations

$$\tau \mapsto \tau + 1, \quad \tau \mapsto -\frac{\tau}{4\tau - 1}, \quad \tau \mapsto \frac{3\tau - 1}{4\tau - 1} \tag{4.172}$$

For $\lambda = -1$, the PF equation (4.154) becomes invariant under $z \to -z$, with singularities at $z \in \{0, \pm\frac{\mathrm{i}}{8}, \infty\}$, and also admits explicit solutions in terms of Meijer G functions. Matching the behavior (4.157) near $z = 0^+$, we find [65, (5.69)],

$$\begin{aligned} \varpi_2(z) &= -\frac{1}{2\pi\sqrt{2}}\, G^{2,2}_{3,3}\left(\begin{matrix} \frac{1}{4} & \frac{3}{4} & 1 \\ 0 & 0 & 0 \end{matrix} \,|\, 64z^2 \right), \\ \varpi_3(z) &= -\frac{1}{2\pi\sqrt{2}}\, G^{3,2}_{3,3}\left(\begin{matrix} \frac{1}{4} & \frac{3}{4} & 1 \\ 0 & 0 & 0 \end{matrix} \,|\, -64z^2 \right) - \frac{\pi^2}{3} \end{aligned} \tag{4.173}$$

such that

$$\tau = \frac{\mathrm{i}}{2\sqrt{2}} \frac{{}_2F_1(\frac{1}{4}, \frac{3}{4}; 1; 1 + 64z^2)}{{}_2F_1(\frac{1}{4}, \frac{3}{4}; 1; -64z^2)}, \quad z = \frac{\mathrm{i}}{J_4(\tau)} \tag{4.174}$$

In the limit $z \to \infty$, corresponding to $\tau \to \tau_B$, the Meijer G functions go to 0, so that

$$m = -\frac{1}{2}: \quad T(\tau_B) = 0, \quad T_D(\tau_B) = \frac{1}{8} \tag{4.175}$$

with $\tau_B = \frac{\mathrm{i}+3}{4}$. If instead we match the expansion near $z = 0^-$, we find

$$\begin{aligned} \varpi_2(z) &= -\frac{1}{2\pi\sqrt{2}}\, G^{2,2}_{3,3}\left(\begin{matrix} \frac{1}{4} & \frac{3}{4} & 1 \\ 0 & 0 & 0 \end{matrix} \,|\, 64z^2 \right) + \mathrm{i}\pi \\ \varpi_3(z) &= -\frac{1}{2\pi\sqrt{2}}\, G^{3,2}_{3,3}\left(\begin{matrix} \frac{1}{4} & \frac{3}{4} & 1 \\ 0 & 0 & 0 \end{matrix} \,|\, -64z^2 \right) + 2\pi\mathrm{i}\varpi_2(z) - \frac{\pi^2}{3} \end{aligned} \tag{4.176}$$

leading to

$$m = \frac{1}{2}: \quad T(\tau_B) = \frac{1}{2}, \quad T_D(\tau_B) = \frac{3}{8} \tag{4.177}$$

At the conifold points $z = \pm\mathrm{i}/8$, the period T_D vanishes, while T is given (in agreement with the results for the E_7 model in [151, (3.57)]) by

$$T = \mp\frac{1}{4} + \frac{3}{64\pi\mathrm{i}}\, {}_3F_4(1, 1, \tfrac{5}{4}, \tfrac{7}{4}; 2, 2, 2; 1) - \frac{\log 8}{2\pi\mathrm{i}} \simeq \pm\frac{1}{4} + \mathrm{i} \times 0.305131 \tag{4.178}$$

where the upper (lower) sign corresponds to (4.173) and (4.176), respectively. These correspond to the values at $\tau = \frac{1}{2}$ and $\tau = 0$, respectively.

4.6.4 Eichler integral representation

We shall now establish an Eichler integral representation for the periods, similar to the one obtained in [47][35] for local $\mathbb{P}^2$. For this, we need to compute $C(\tau, m) := \partial_\tau T = 1/\partial_T \tau = 1/C_{TTT}$, the inverse of the Yukawa coupling. Defining $e(\tau, m) = z\partial_z \varpi_2$ and using

$$q\partial_q J_4 = -16\frac{\theta_3^4(2\tau)\theta_4^4(2\tau)}{\theta_2^4(2\tau)} \tag{4.179}$$

we easily compute the ratio

$$\frac{C}{e} = \frac{q}{z}\frac{\partial z}{\partial q} = 16\frac{\theta_3^4(2\tau)\theta_4^4(2\tau)}{\theta_2^4(2\tau)}(J_4 + 4\lambda^{1/2} + 4\lambda^{-1/2})^{-1} \tag{4.180}$$

The l.h.s. of (4.180) should be identified as C/e, where $C = 1/C_{zzz}$ is the inverse Yukawa coupling. On the other hand, the ratio C/e^3 is equal to the discriminant,

$$\frac{C}{e^3} = \frac{1}{(2\pi \mathrm{i} z\partial_z T)^3 C_{TTT}} = \frac{1}{(2\pi \mathrm{i} z)^3 C_{zzz}} = 1 - 8z(1+\lambda) + 16z^2(\lambda-1)^2 \tag{4.181}$$

It follows that e and C are given separately by

$$\begin{aligned} e(\tau, m) &= \frac{4\theta_3^2(2\tau)\,\theta_4^2(2\tau)\,z^{1/2}\lambda^{1/4}}{\theta_2^2(2\tau)\sqrt{1-8z(1+\lambda)+16z^2(\lambda-1)^2}} = \frac{4\theta_3^2(2\tau)\theta_4^2(2\tau)}{\theta_2^2(2\tau)}\sqrt{\frac{J_4 + 4\lambda^{1/2} + 4\lambda^{-1/2}}{J_4^2 - 64}} \\ C(\tau, m) &= \frac{64\theta_3^6(2\tau)\theta_4^6(2\tau)\,z^{3/2}\lambda^{3/4}}{\theta_2^6(2\tau)\sqrt{1-8z(1+\lambda)+16z^2(\lambda-1)^2}} = \frac{64\theta_3^6(2\tau)\theta_4^6(2\tau)}{\theta_2^6(2\tau)\sqrt{(J_4^2-64)(J_4 + 4\lambda^{1/2} + 4\lambda^{-1/2})}} \end{aligned} \tag{4.182}$$

For $\lambda = 1$, the branch cuts disappear and e, C become simple ratios of Dedekind eta functions, in turn equal to Eisenstein series of weight 1 and 3 under $\Gamma_1(4)$, respectively,

$$\begin{aligned} e(\tau, 0) &= \frac{\eta(2\tau)^{10}}{\eta(\tau)^4\eta(4\tau)^4} = 1 + 4\sum_{n\geq 1}\frac{\chi_4(n)q^n}{1-q^n} = 1 + 4q + 4q^2 + 4q^4 + 8q^5 + O(q^6)\,, \\ C(\tau, 0) &= \frac{\eta(\tau)^4\eta(2\tau)^6}{\eta(4\tau)^4} = 1 - 4\sum_{n\geq 1}\frac{n^2\chi_4(n)q^n}{1-q^n} = 1 - 4q - 4q^2 + 32q^3 - 4q^4 - 104q^5 + O(q^6) \end{aligned} \tag{4.183}$$

Using these expressions, we can simplify the expression of e and C for arbitrary λ,

$$\begin{aligned} e(\tau, m) &= \frac{\eta(2\tau)^{10}}{\eta(\tau)^4\eta(4\tau)^4}\sqrt{\frac{J_4 + 4\lambda^{1/2} + 4\lambda^{-1/2}}{J_4 + 8}} \\ &= 1 + 2q(\lambda^{\frac{1}{2}} + \lambda^{-\frac{1}{2}}) - 2q^2(\lambda - 4 + \lambda^{-1}) + 4q^3(\lambda^{\frac{3}{2}} - \lambda^{\frac{1}{2}} - \lambda^{-\frac{1}{2}} + \lambda^{-\frac{3}{2}}) + \dots\,, \\ C(\tau, m) &= \frac{\eta(\tau)^4\eta(2\tau)^6}{\eta(4\tau)^4}\sqrt{\frac{J_4 + 8}{J_4 + 4\lambda^{1/2} + 4\lambda^{-1/2}}} \\ &= 1 - 2q(\lambda^{\frac{1}{2}} + \lambda^{-\frac{1}{2}}) + q^2(6\lambda - 16 + 6\lambda^{-1}) + q^3(-20\lambda^{\frac{3}{2}} + 36\lambda^{\frac{1}{2}} + 36\lambda^{-\frac{1}{2}} - 20\lambda^{-\frac{3}{2}}) + \dots \end{aligned} \tag{4.184}$$

[35] With hindsight, such a representation could have been extracted from [1], Sections 6 and 7.

We determine the sign of the square root in the same way as described below (4.149), namely we choose a branch cut extending from $\tau = \tau_B$ to $\tau = \frac{1}{2}$ along a geodesic circle. Moreover, the product eC is independent of λ, and is modular of weight 4 under $\Gamma_0(2)$ after rescaling $\tau \to \tau/2$,

$$e(\tau, m)C(\tau, m) = \frac{\eta(2\tau)^{16}}{\eta(4\tau)^8} \tag{4.185}$$

For $\lambda = -1$, using the identities

$$\theta_2(\tau) = \frac{2\eta^2(2\tau)}{\eta(\tau)}\,, \quad \theta_3(\tau) = \frac{\eta^5(\tau)}{\eta^2(\tau/2)\eta^2(2\tau)}\,, \quad \theta_4(\tau) = \frac{\eta^2(\tau/2)}{\eta(\tau)}\,, \quad \frac{\theta_3\theta_4}{\theta_2} = \frac{\eta^5(\tau)}{2\eta^4(2\tau)} \tag{4.186}$$

we find the simpler expressions

$$e(\tau, \tfrac{1}{2}) = \frac{1}{\sqrt{2}}\sqrt{\theta_3^4(2\tau) + \theta_4^4(2\tau)}\,, \quad C(\tau, \tfrac{1}{2}) = \frac{\sqrt{2}\,\theta_4^8(4\tau)}{\sqrt{\theta_3^4(2\tau) + \theta_4^4(2\tau)}} \tag{4.187}$$

From the fact that $\partial_\tau(T, T_D) = C(1, \tau)$, we conclude that

$$\begin{pmatrix} T \\ T_D \end{pmatrix}(\tau) = \begin{pmatrix} T(\tau_0) \\ T_D(\tau_0) \end{pmatrix} + \int_{\tau_0}^{\tau} \begin{pmatrix} 1 \\ u \end{pmatrix} C(u)\mathrm{d}u \tag{4.188}$$

for any point τ_0 where (T, T_D) takes a finite value. It is natural to choose $\tau_0 = \tau_B$, the branch point where the factor $J_4 + 4\lambda^{1/2} + 4\lambda^{-1/2}$ in the expression (4.182) for C vanishes. Although we have not been able to derive this directly, we have computed numerically the periods at $\tau = \tau_B$ by integrating (4.188) to large values of $\mathrm{Im}\,\tau$, and found overwhelming confirmation for the following formulae for $\mathrm{Im}\,m > 0$, $0 < \mathrm{Re}\,m < 1$, and $\mathrm{Im}\,\tau \geq \mathrm{Im}\,\tau_B$

$$\begin{pmatrix} T \\ T_D \end{pmatrix} = \begin{pmatrix} \frac{1}{2} \\ \frac{1+m}{4} \end{pmatrix} + \int_{\tau_B}^{\tau} \begin{pmatrix} 1 \\ u \end{pmatrix} C(u)\mathrm{d}u \tag{4.189}$$

where the contour runs from τ_B to τ without crossing the cut. For $\mathrm{Im}\,m < 0$ and $0 < \mathrm{Re}\,m < 1$ and $\mathrm{Im}\,\tau \geq \mathrm{Im}\,\tau_B$, one finds instead

$$\begin{pmatrix} T \\ T_D \end{pmatrix} = \begin{pmatrix} \frac{1}{2} - m \\ \frac{1-m}{4} \end{pmatrix} + \int_{\tau_B}^{\tau} \begin{pmatrix} 1 \\ u \end{pmatrix} C(u)\mathrm{d}u \tag{4.190}$$

with the same choice of contour. These formulae can then be used to analytically continue T, T_D into the Poincaré upper half-plane, although the result will of course depends on the path, due to the square root branch cuts in C. We note that the two values for opposite signs of $\mathrm{Im}\,m$ are related by fiber-base duality (4.21).

Moreover, the values at τ_B are invariant under the order 2 monodromies $M_B(0)$ and $\widetilde{M}_B(0)$ respectively, where

$$\begin{aligned} M_B(k) &= \begin{pmatrix} 1 & 0 & 0 & 0 \\ 0 & 1 & 0 & 0 \\ 2k+1 & 0 & -1 & 0 \\ k^2+k+\frac{1}{2} & k+\frac{1}{2} & 0 & -1 \end{pmatrix}, \quad M_{B,k}^2 = 1 \\ \widetilde{M}_B(k) &= \begin{pmatrix} 1 & 0 & 0 & 0 \\ 0 & 1 & 0 & 0 \\ 2k+1 & -2 & -1 & 0 \\ k^2+k+\frac{1}{2} & -\frac{1}{2}-k & 0 & -1 \end{pmatrix}, \quad \widetilde{M}_{B,k}^2 = 1 \end{aligned} \tag{4.191}$$

It is worth noting that $M_B(k)$ and $\widetilde{M}_B(k)$ are themselves the square of order 4 matrices,

$$\begin{aligned} M_{\mathbb{Z}_4}(k) &= \begin{pmatrix} 1 & 0 & 0 & 0 \\ 1 & -1 & 0 & 0 \\ -2k(k+1) & 2k+1 & 4k+3 & -4 \\ -2k(k+1)^2 & \frac{1}{2}(2k+1)^2 & 4k^2+6k+\frac{5}{2} & -4k-3 \end{pmatrix} \\ \widetilde{M}_{\mathbb{Z}_4}(k) &= \begin{pmatrix} 1 & 0 & 0 & 0 \\ 1 & -1 & 0 & 0 \\ -2k^2 & 2k+1 & 4k+1 & -4 \\ -k^2(2k+1) & 2k^2+k+\frac{1}{2} & 4k^2+2k+\frac{1}{2} & -4k-1 \end{pmatrix} \end{aligned} \tag{4.192}$$

which preserve the values $(\tau, m) = (\frac{3+k+\mathrm{i}}{4}, \frac{1}{2})$ and $(\frac{1+k+\mathrm{i}}{4}, \frac{1}{2})$, respectively. For $k = -1$ the matrices $M_{\mathbb{Z}_4}(-1)$ and $M_B(-1)$ coincide with $M_{\mathbb{Z}_4}$ and M_B in (4.31) and (4.32).

4.6.5 Expansions around singular points

We shall now obtain the expansion of the periods near $\tau = \mathrm{i}\infty$, $\tau = 0$, $\tau = \frac{1}{2}$ and $\tau = \tau_B$. The expansion near all other singular points in the Poincaré upper half-plane are then determined by the action of $\Gamma_0(4)$.

Large volume expansion

At large $\mathrm{Im}\,\tau$ the argument of the square root behaves as $1 + q(1 - \cos\pi m) + O(q)$ as $\tau \to \mathrm{i}\infty$ so the path does not cross the cut. Upon Fourier expanding

$$C = \sum_{n\geq 0} c_n(m)\, q^n\,, \quad \lambda = e^{2\pi \mathrm{i} m} \tag{4.193}$$

and integrating term by term, we easily obtain expansions near $\tau \to \mathrm{i}\infty$,

$$\begin{aligned} T_1 &= T = \tau - \frac{1}{2}m + \frac{1}{2\pi\mathrm{i}} f_1(\tau, m) \\ T_2 &= T + m = \tau + \frac{1}{2}m + \frac{1}{2\pi\mathrm{i}} f_1(\tau, m) \\ T_D &= \frac{1}{2}\tau^2 - \frac{1}{8}m^2 + \frac{1}{12} + \frac{\tau}{2\pi\mathrm{i}} f_1(\tau, m) + \frac{1}{(2\pi\mathrm{i})^2} f_2(\tau, m) \end{aligned} \tag{4.194}$$

with

$$f_1(\tau, m) = \sum_{n\geq 1} \frac{c_n(m)}{n} q^n, \quad f_2(\tau, m) = -\sum_{n\geq 1} \frac{c_n(m)}{n^2} q^n \tag{4.195}$$

The radius of convergence is fixed by the distance to the nearest singularity, so the series f_1 and f_2 converge uniformly when $\mathrm{Im}\,\tau > \mathrm{Im}\,\tau_B$. Their value at τ_B is determined by consistency with the Eichler integral representation (4.189), e.g. for $\mathrm{Im}\, m > 0$

$$\begin{aligned} \tau_B + \frac{f_1(\tau_B, m)}{2\pi\mathrm{i}} &= \frac{m+1}{2} \\ \frac{1}{2}\tau_B^2 + \frac{\tau_B}{2\pi\mathrm{i}} f_1(\tau_B, m) + \frac{f_2(\tau_B, m)}{(2\pi\mathrm{i})^2} &= \frac{m^2}{8} + \frac{m}{4} + \frac{1}{6} \end{aligned} \tag{4.196}$$

Since $f_i(\tau - \frac{1}{2}, m \pm 1) = f_i(\tau, m)$, we find that the periods (T, T_D) transform according to (4.30) under tensoring with $\mathcal{O}(1,1)$, $\mathcal{O}(-1,0)$, $\mathcal{O}(0,-1)$ and $\mathcal{O}(-1,1)$, respectively,

$$\begin{aligned}
T(\tau+1,m) &= T(\tau,m)+1, & T_D(\tau+1,m) &= T_D(\tau,m)+T(\tau,m)+\tfrac{m+1}{2}\\
T(\tau-\tfrac{1}{2},m-1) &= T(\tau,m), & T_D(\tau-\tfrac{1}{2},m-1) &= T_D(\tau,m)-\frac{1}{2}T(\tau,m)\\
T(\tau-\tfrac{1}{2},m+1) &= T(\tau,m)-1, & T_D(\tau-\tfrac{1}{2},m+1) &= T_D(\tau,m)-\frac{1}{2}(T(\tau,m)+m)\\
T(\tau,m-2) &= T(\tau,m)+1, & T_D(\tau,m-2) &= T_D(\tau,m)+\tfrac{m-1}{2}
\end{aligned} \tag{4.197}$$

Note however that these formulae no longer hold when $\operatorname{Im}\tau < \operatorname{Im}\tau_B$, due to the presence of branch cuts. Moreover, from (4.194) and the fact that $c_n(m) = \overline{c_n(\bar{m})} = c_n(-m)$ we see that T, T_D satisfy the reality conditions

$$T(-\bar{\tau},-\bar{m}) = -\overline{T(\tau,m)}\,, \quad T_D(-\bar{\tau},-\bar{m}) = \overline{T_D(\tau,m)} \tag{4.198}$$

As a result, the central charge along the Π-stability slice has the same transformation property as the large volume central charge (4.36),

$$Z_{-\overline{\tau},-\overline{m}}(-r,d_1,d_2,-\mathrm{ch}_2) = -\overline{Z_{\tau,m}(r,d_1,d_2,\mathrm{ch}_2)} \tag{4.199}$$

As in [47], we can use these expansions and zeta function regularization to compute the values of the periods at the conifold points when $m = 0$. For this purpose, we compute the L-series associated to f_1 and f_2,

$$\begin{aligned}
L_{f_1}(s) &\coloneqq \sum_{n\geq 1}\frac{c_n(0)}{n^{1+s}} = -4\zeta(s+1)\,L(\chi_4,s-1)\\
L_{f_2}(s) &\coloneqq -\sum_{n\geq 1}\frac{c_n(0)}{n^{2+s}} = 4\zeta(s+2)\,L(\chi_4,s)
\end{aligned} \tag{4.200}$$

where $L(\chi_4,s) \coloneqq \sum_{m\geq 1}\chi_4(m)m^{-s} = 4^{-s}\left(\zeta(s,\frac{1}{4}) - \zeta(s,\frac{3}{4})\right)$ is the Dirichlet L-series. Therefore

$$\begin{aligned}
f_1(0,0) &= -4\lim_{s\to 0}\zeta(s+1)\,L(\chi_4,s-1) = -\frac{8G}{\pi}\\
f_2(0,0) &= 4\lim_{s\to 0}\zeta(s+2)\,L(\chi_4,s) = \frac{\pi^2}{3}
\end{aligned} \tag{4.201}$$

where we used $L(\chi_4,0) = 1/2$. Similarly, the periods at $\tau = \frac{1}{2}$ can be computed by noting that the insertion of a sign $(-1)^n$ replaces $\zeta(s)$ by $\zeta_2(s) \coloneqq \sum_{k\geq 1}(-1)^k/k^s = (2^{1-s}-1)\zeta(s)$, leading to

$$\begin{aligned}
f_1(\tfrac{1}{2},0) &= -4\lim_{s\to 0}\zeta_2(s+1)\,L(\chi_4,s-1) = 0\\
f_2(\tfrac{1}{2},0) &= 4\lim_{s\to 0}\zeta_2(s+2)\,L(\chi_4,s) = -\frac{\pi^2}{6}
\end{aligned} \tag{4.202}$$

Inserting these results in (4.194), we reproduce the values (4.169) and (4.170). Unfortunately, we do not know how to reproduce the values (4.178) at $m = \frac{1}{2}$ from the L-series associated to (4.187).

Expansion near $\tau = 0$

We can now obtain the expansion $\tau = 0$ by performing a Fricke transform $\tau \mapsto -1/(4\tau)$, $u \mapsto -1/(4u)$ in the Eichler integral representation (4.189). This involution maps the fundamental domain $\mathcal{F}$ to its shift $\mathcal{F}(-1)$. Since $J_4(-1/(4\tau)) = 8 + \frac{256}{J_4(\tau)-8}$, we get (assuming $\mathrm{Im}\, m > 0$)

$$\begin{pmatrix} T \\ T_D \end{pmatrix}\left(-\frac{1}{4\tau}\right) = \begin{pmatrix} \frac{1}{2} \\ \frac{1+m}{4} \end{pmatrix} + 8\mathrm{i}\int_{-1/(4\tau_B)}^{\tau} \begin{pmatrix} 4u \\ -1 \end{pmatrix} C'(u)\mathrm{d}u \tag{4.203}$$

with

$$\begin{aligned} C'(\tau) &= \frac{C(-1/(4\tau))}{128\mathrm{i}\tau^3} \\ &= \frac{\eta(4\tau)^4\eta(2\tau)^6}{\eta(\tau)^4}\sqrt{\frac{4(J_4+8)}{2J_4+48+(J_4-8)(\lambda^{1/2}+\lambda^{-1/2})}} \\ &= \frac{2q}{\lambda^{1/4}+\lambda^{-1/4}} + 8\frac{3\sqrt{\lambda}-2+3/\sqrt{\lambda}}{(\lambda^{1/4}+\lambda^{-1/4})^3}q^2 + 16\frac{9\lambda-44\sqrt{\lambda}+86-44/\sqrt{\lambda}+9/\lambda}{(\lambda^{1/4}+\lambda^{-1/4})^5}q^3 \end{aligned} \tag{4.204}$$

It follows that

$$T(-1/(4\tau)) = -\frac{8\mathrm{i}}{\pi^2}f_2'(\tau,m) + \mathrm{cte}\,, \quad T_D(-1/(4\tau)) = -\frac{4}{\pi}f_1'(\tau,m) + \mathrm{cte} \tag{4.205}$$

where c_n' are the Fourier coefficients of $C'(\tau,m)$,

$$f_1'(\tau,m) = \sum_{n\geq 1}\frac{c_n'}{n}q^n, \quad f_2'(\tau,m) = 2\pi\mathrm{i}\tau f_1'(\tau,m) - \sum_{n\geq 1}\frac{c_n'}{n^2}q^n \tag{4.206}$$

In particular, under $\tau \to \tau+1$, the period vector $\Pi^t = (1,m,T,T_D)^t$ transforms into $M_C\Pi^t$, where M_C was defined in (4.31). This is the expected action of the Seidel-Thomas twist (4.22) with respect to the spherical object $\mathcal{O}(0,0)$, which is massless at $\tau = 0$, the fixed point of the action $\tau \mapsto \frac{\tau}{1-4\tau}$ of M on τ.

To determine the additive constants in (4.205), we solve the PF equation (4.154) around $z = \frac{1}{4(1+\sqrt{\lambda})^2}$. It is convenient to use the variable $z' = \frac{1}{\sqrt{\lambda}J_4'+4(\lambda+1)}$ obtained by Fricke involution, which vanishes at that point,

$$z = \frac{1}{4(1+\sqrt{\lambda})^2} - \frac{16\lambda z'}{(1+\sqrt{\lambda})^4 - 4z'(1-\lambda)^2(1+6\sqrt{\lambda}+\lambda)} \tag{4.207}$$

The regular and logarithmic solutions are given by

$$\begin{aligned} \varpi_2' =& \frac{\lambda^{3/4}z'}{\sqrt{\lambda}+1} + \frac{\lambda^{3/4}\left(2\sqrt{\lambda}\left(2\sqrt{\lambda}+7\right)(\lambda+1)+4\right)z'^2}{(\sqrt{\lambda}+1)^3} + \dots \\ \varpi_3' =& \varpi_2'\log(z'\sqrt{\lambda}) + \frac{\mathrm{i}}{8}\left(\mathrm{Li}_2(\mathrm{i}\lambda^{1/4}) - \mathrm{Li}_2(-\mathrm{i}\lambda^{1/4})\right) + \frac{\lambda^{3/4}z'}{\sqrt{\lambda}+1} \\ &+ \frac{\lambda^{3/4}\left(8\lambda^2+25\lambda^{3/2}+10\lambda+25\sqrt{\lambda}+8\right)z'^2}{(\sqrt{\lambda}+1)^3} + \dots \end{aligned} \tag{4.208}$$

where the y-dependent normalization and constant terms are fixed by (4.153). Rewriting this in terms of q', we find

$$\frac{\partial_{z'}\varpi'_3}{\partial_{z'}\varpi'_2} = 2 + \log q' \tag{4.209}$$

and recognize

$$\varpi'_2 = \frac{1}{2}f'_1, \quad \varpi'_3 = f'_1 + \frac{1}{2}f'_2 + \frac{\mathrm{i}}{8}\left(\mathrm{Li}_2(\mathrm{i}\lambda^{1/4}) - \mathrm{Li}_2(-\mathrm{i}\lambda^{1/4})\right) \tag{4.210}$$

Hence, we conclude that, possibly up to linear terms in m,

$$\begin{aligned} T(-1/(4\tau)) =& \frac{16\mathrm{i}}{\pi^2}(2\varpi'_2 - \varpi'_3) = -\frac{8\mathrm{i}}{\pi^2}f'_2(\tau) + \mathrm{i}\mathcal{V}(m) \\ T_D(-1/(4\tau)) =& -\frac{8}{\pi}\varpi'_2 = -\frac{4}{\pi}f'_1(\tau) \end{aligned} \tag{4.211}$$

where

$$\mathcal{V}(m) = \frac{2\mathrm{i}}{\pi^2}\left(\mathrm{Li}_2(-\mathrm{i}e^{\mathrm{i}\pi m/2}) - \mathrm{Li}_2(\mathrm{i}e^{\mathrm{i}\pi m/2})\right) \tag{4.212}$$

In particular, as $\tau \to \mathrm{i}\infty$ we get

$$T(0,m) = \mathrm{i}\mathcal{V}(m), \quad T_D(0,m) = 0 \tag{4.213}$$

so that (4.189) may be written as

$$\begin{pmatrix} T \\ T_D \end{pmatrix}\left(-\frac{1}{4\tau}\right) = \begin{pmatrix} \mathrm{i}\mathcal{V}(m) \\ 0 \end{pmatrix} + 8\mathrm{i}\int_{\mathrm{i}\infty}^{\tau}\begin{pmatrix} 4u \\ -1 \end{pmatrix} C'(u)\mathrm{d}u \tag{4.214}$$

We have checked the absence of additional linear terms in m by numerical integration. Remarkably, the value of $T(0)$ for $m = 0$ and $m = 1/2$ reproduces (4.169) and (4.178), respectively. Note that $\mathcal{V}(m)$ is anti-periodic under $m \mapsto m + 2$, in fact using the expansion near $\tau = 0$ we find

$$T(\tau, m-2) = -T(\tau,m), \quad T_D(\tau,m-2) = -T_D(\tau,m), \tag{4.215}$$

in contrast to the periodicity at large volume (4.197). For m real, using Joncquière's identity we get

$$\mathrm{Im}\,\mathcal{V}(m) = 2B_2\left(\mathrm{Fr}(\tfrac{m-1}{4})\right) - 2B_2\left(\mathrm{Fr}(\tfrac{m+1}{4})\right) \tag{4.216}$$

where $\mathrm{Fr}(x) = x - \lfloor x \rfloor$ and $B_2(x) = x^2 - x + \frac{1}{6}$ is the second Bernoulli polynomial. For $m \in [-1,1]$, this evaluates to $\mathrm{Im}\,\mathcal{V}(m) = \frac{m}{2}$, while for $m \in [1,3]$, $\mathrm{Im}\,\mathcal{V}(m) = 1 - \frac{m}{2}$. The real part oscillates between $\pm 4G/(\pi^2)$. By using the second equation (4.197) , we get, for $k \in \mathbb{Z}$ and $0 < \mathrm{Re}(m) < 1$,

$$T(k,m) \;=\; k + \mathrm{i}\mathcal{V}(m), \quad T_D(k,m) = \frac{k(k+m)}{2} + k\mathrm{i}\mathcal{V}(m) \tag{4.217}$$

such that $\mathcal{O}(k,k)$ is massless at $\tau = k$.

Expansion near $\tau = \frac{1}{2}$

Let us now define

$$J_4''(\tau) = J_4\left(\frac{\tau}{2\tau+1}\right), \quad C_1''(\tau) = -\frac{1}{4(2\tau+1)^3} C_1\left(\frac{\tau}{2\tau+1}\right) \tag{4.218}$$

In particular, setting $\tau' = -1/4\tau, \tau'' = \frac{\tau}{1-2\tau}$ we have

$$J_4(\tau) = J_4'(\tau') = J_4''(\tau''), \quad \tau' = -\frac{1}{4\tau''} - \frac{1}{2} \tag{4.219}$$

Note that when τ lies in the standard fundamental domain in the interval $(0,1)$, τ'' belongs to the standard fundamental domain in the interval $(-1,0)$. The large volume point is now at $\tau'' = -\frac{1}{2}$, while the conifold and shifted conifold points are now at $\tau'' = 0$ and $\tau'' = \mathrm{i}\infty$. Using a sequence of S and T transformations we find

$$\begin{aligned}
\eta\left(\frac{\tau}{2\tau+1}\right) &= -(-1)^{5/6}\sqrt{2\tau+1}\,\eta(\tau) \\
\eta\left(\frac{2\tau}{2\tau+1}\right) &= -(-1)^{11/12}\sqrt{2\tau+1}\,\eta(2\tau) \\
\eta\left(\frac{4\tau}{2\tau+1}\right) &= \frac{1}{\sqrt{2}}\sqrt{2\tau+1}\,\eta(\tau-\tfrac{1}{2})
\end{aligned} \tag{4.220}$$

We further note the relation

$$\eta(\tau - \tfrac{1}{2}) = e^{-\frac{\mathrm{i}\pi}{24}} \frac{\eta^3(2\tau)}{\eta(\tau)\eta(4\tau)} \tag{4.221}$$

Using these relations, we get

$$J_4''(\tau) = -8 + \frac{256}{J_4(\tau)+8} = 8 - \frac{16\eta^{16}(\tau)\eta^8(4\tau)}{\eta^{24}(2\tau)} = -8 + 256q - 2048q^2 + \dots \tag{4.222}$$

and

$$C_1''(\tau) = (-1)^{1/3}\frac{\eta^6(2\tau)\eta^4(\tau)}{\eta^4(\tau-\frac{1}{2})} = \frac{\eta^8(\tau)\eta^4(4\tau)}{\eta^6(2\tau)} = \sqrt{q} - 8q^{3/2} + 26q^{5/2} - 48q^{7/2} + \dots \tag{4.223}$$

More generally, for $\lambda \neq 1$,

$$\begin{aligned}
C''(\tau,m) =& \frac{\eta^8(\tau)\eta^4(4\tau)}{\eta^6(2\tau)} \frac{8}{\sqrt{48 - 2J_4 + (J_4+8)(\lambda^{1/2}+\lambda^{-\frac{1}{2}})}} \\
=& \frac{8q}{\lambda^{1/4}-\lambda^{-1/4}} - \frac{32(3\lambda^{1/2}+2+3\lambda^{-1/2})q^2}{(\lambda^{1/4}-\lambda^{-1/4})^3} + \dots
\end{aligned} \tag{4.224}$$

Note that the leading power jumps from $q^{1/2}$ at $\lambda = 1$ to q at $\lambda \neq 1$. For $\lambda = -1$, we have $\lambda^{1/4} - \lambda^{-1/4} = \mathrm{i}\sqrt{2}$ hence

$$C''(\tau, \pm\tfrac{1}{2}) \to -4\mathrm{i}\sqrt{2}\left(q + 4q^2 + 136q^3 + 2576q^4 + \dots\right) \tag{4.225}$$

Moreover, note the relation between the Fourier coefficients of C' and C'',

$$c_n'(m-1) = \frac{\mathrm{i}}{4}(-1)^{n+1} c_n''(m) \tag{4.226}$$

Similarly as above, we solve the PF equation (4.154) around $z = \frac{1}{4(1-\sqrt{\lambda})^2}$, by using the variable $z'' = \frac{1}{\sqrt{\lambda}J_4'' + 4(\lambda+1)}$ obtained by Fricke involution, which vanishes at that point,

$$z = \frac{1}{4(1-\sqrt{\lambda})^2} - \frac{16\lambda z''}{(1-\sqrt{\lambda})^4 - 4z''(1-\lambda)^2(1-6\sqrt{\lambda}+\lambda)} \tag{4.227}$$

The regular and logarithmic solutions are given by

$$\begin{aligned}
\varpi_2'' =& \frac{\lambda^{3/4} z''}{1-\sqrt{\lambda}} + \frac{\lambda^{3/4}\left(4 - 14\sqrt{\lambda} + 4\lambda - 14\lambda^{3/2} + 4\lambda^2\right) z''^2}{(1-\sqrt{\lambda})^3} + \dots \\
\varpi_3'' =& \varpi_2'' \log(z''\sqrt{\lambda}) + \frac{1}{8}\left(\mathrm{Li}_2(\lambda^{1/4}) - \mathrm{Li}_2(-\lambda^{1/4})\right) + \frac{\lambda^{3/4} z''}{1-\sqrt{\lambda}} \\
&+ \frac{\lambda^{3/4}\left(8\lambda^2 - 25\lambda^{3/2} + 10\lambda - 25\sqrt{\lambda} + 8\right) z''^2}{(1-\sqrt{\lambda})^3} + \dots
\end{aligned} \tag{4.228}$$

This agrees with the continuation of (4.208) under $\sqrt{\lambda} \to -\sqrt{\lambda}$. Moreover,

$$\frac{\partial_{z''}\varpi_3''}{\partial_{z''}\varpi_2''} = 2 + \log q'' \,, \quad q''\partial_{q''}\varpi_2'' = -\frac{1}{8}C'' \tag{4.229}$$

Setting

$$f_1''(\tau, m) = \sum_{n\geq 1} \frac{c_n''(m)}{n} q^n, \quad f_2''(\tau, m) = 2\pi \mathrm{i}\tau f_1''(\tau, m) - \sum_{n\geq 1} \frac{c_n''(m)}{n^2} q^n \tag{4.230}$$

we recognize

$$\varpi_2'' = -\frac{1}{8} f_1'', \quad \varpi_3'' = -\frac{1}{8}(2f_1'' + f_2'') + \frac{1}{8}\left(\mathrm{Li}_2(\lambda^{1/4}) - \mathrm{Li}_2(-\lambda^{1/4})\right) \tag{4.231}$$

In particular, under $\tau \to \tau + 1$, the period vector $\Pi^t = (1, m, T, T_D)^t$ transforms into $M_{\tilde{C}}\Pi^t$ where $M_{\tilde{C}}$ is the Seidel-Thomas twist (4.22) with respect to the spherical object $O(1,0)$. The latter is indeed massless at $\tau = \frac{1}{2}$, the fixed point under the action $\tau \mapsto \frac{\tau-1}{4\tau-3}$ of $M_{\tilde{C}}$ on the upper half-plane.

By demanding consistency with the Eichler integral representation

$$\begin{pmatrix} T \\ T_D \end{pmatrix}\left(\tfrac{\tau}{2\tau+1}, m\right) = \begin{pmatrix} a'' \\ b'' \end{pmatrix} + 4\int_{\mathrm{i}\infty}^{\tau} \begin{pmatrix} 2u+1 \\ u \end{pmatrix} C''(u, m)\mathrm{d}u \tag{4.232}$$

we conclude that

$$\begin{aligned}
T\left(\tfrac{\tau}{2\tau+1}, m\right) =& \frac{16}{\pi^2}(\varpi_3'' - 2\varpi_2'') + \frac{16\mathrm{i}}{\pi}\varpi_2'' = -\frac{2}{\pi^2} f_2'' - \frac{2\mathrm{i}}{\pi} f_1'' + \mathrm{i}\tilde{\mathcal{V}}(m) \\
T_D\left(\tfrac{\tau}{2\tau+1}, m\right) =& \frac{8}{\pi^2}(\varpi_3'' - 2\varpi_2'') = -\frac{1}{\pi^2} f_2'' + \frac{\mathrm{i}}{2}\tilde{\mathcal{V}}(m)
\end{aligned} \tag{4.233}$$

up to an additive constant and additive multiple of $\log\lambda$. In particular, as $\tau \to \mathrm{i}\infty$,

$$T(\tfrac{1}{2}, m) = 2T_D(\tfrac{1}{2}, m) = \mathrm{i}\tilde{\mathcal{V}}(m) \tag{4.234}$$

with

$$\tilde{\mathcal{V}}(m) := \frac{2\mathrm{i}}{\pi^2}\left(\mathrm{Li}_2(-\lambda^{1/4}) - \mathrm{Li}_2(\lambda^{1/4})\right) = \mathcal{V}(m-1) \tag{4.235}$$

This determines the constants a'', b'' in (4.232), possibly up to linear terms in m,

$$\begin{pmatrix} T \\ T_D \end{pmatrix}\left(\tfrac{\tau}{2\tau+1}, m\right) = \begin{pmatrix} \mathrm{i}\tilde{\mathcal{V}}(m) \\ \frac{1}{2}\mathrm{i}\tilde{\mathcal{V}}(m) \end{pmatrix} + 4\int_{\mathrm{i}\infty}^{\tau} \begin{pmatrix} 2u+1 \\ u \end{pmatrix} C''(u,m)\mathrm{d}u \tag{4.236}$$

We have checked by numerical integration that there are no additional linear terms. By spectral flow, we find the periods at the conifold points $\tau = k + \frac{1}{2}$,

$$T(k+\tfrac{1}{2}, m) = k + \mathrm{i}\tilde{\mathcal{V}}(m), \quad T_D(k+\tfrac{1}{2}, m) = \frac{k(k+m)}{2} + (k+\tfrac{1}{2})\mathrm{i}\tilde{\mathcal{V}}(m) \tag{4.237}$$

such that $\mathcal{O}(k+1,k)$ is massless at $\tau = k + \frac{1}{2}$.

Expansion near $\tau = \tau_B$

For completeness, we finally solve the Picard-Fuchs equations near the branch point $z = \infty$. Choosing the Ansatz $\varpi = \sum_{n\geq 0} a_n(\lambda) z^{-n-\frac{1}{2}}$ and expanding in $1/z$, one finds that the equation $\mathcal{D}\varpi = 0$ determines all coefficients in terms of $a_0(\lambda)$ and $a_1(\lambda)$ via

$$-8n(2n^2-n-1)(1-\lambda)^2 a_n(\lambda) + 4(n-1)^2(2n-1)(1+\lambda)a_{n-1}(\lambda) - \frac{1}{8}(2n-3)^3 a_{n-2}(\lambda) = 0 \tag{4.238}$$

in particular

$$\begin{aligned} a_2(\lambda) &= -\frac{a_0(\lambda) - 96(\lambda+1)a_1(\lambda)}{640(\lambda-1)^2} \\ a_3(\lambda) &= \frac{3\left(23\lambda^2+82\lambda+23\right)a_1(\lambda) - (\lambda+1)a_0(\lambda)}{2688(\lambda-1)^4}, \\ a_4(\lambda) &= \frac{384\left(11\lambda^3+85\lambda^2+85\lambda+11\right)a_1(\lambda) - \left(71\lambda^2+242\lambda+71\right)a_0(\lambda)}{884736(\lambda-1)^6} \end{aligned} \tag{4.239}$$

Moreover, the equation $\mathcal{D}_1\varpi = 0$ implies that a_1 is determined from a_0, which must satisfy the second order differential equation

$$a_1(\lambda) = \frac{1}{6}(a_0' + \lambda a_0''), \quad 4\lambda(1-\lambda)a_0'' - 4(2y-1)a_0' - a_0 = 0 \tag{4.240}$$

where the prime denotes the derivative with respect to λ. The solutions are linear combinations of elliptic functions $K(\lambda)$ and $K(1-\lambda)$. The regular solution at $\lambda = 1$ is obtained by choosing $a_0(\lambda) = \frac{2}{\pi}K(1-\lambda)$,

$$\begin{aligned} \varpi_2^B =& \frac{2K(1-\lambda)}{\pi\sqrt{z}} + \frac{(1+\lambda)K(1-\lambda) - 2E(1-\lambda)}{12\pi(\lambda-1)^2 z^{3/2}} + \dots \\ =& \frac{1}{\sqrt{z}}\left(1 + \frac{1}{4}(1-\lambda) + \frac{9}{64}(1-\lambda)^2 + \dots\right) \\ &+ \frac{1}{192 z^{3/2}}\left(1 + \frac{3}{4}(1-\lambda) + \frac{75}{128}(1-\lambda)^2 + \dots\right) + \dots \end{aligned} \tag{4.241}$$

The logarithmic solution is obtained by choosing $a_0(\lambda) = \frac{4\log 4}{\pi}K(1-\lambda) - 2K(\lambda))$,

$$\begin{aligned}\varpi_3^B &= \left(\frac{4\log 4}{\pi}K(1-\lambda) - 2K(\lambda)\right) z^{-1/2} + \\ &\quad + \frac{\pi(1-\lambda)K(\lambda) - 2\pi E(\lambda) + 2\log 4\,((1+\lambda)K(1-\lambda) - 2E(1-\lambda))}{12\pi(1-\lambda)^2} z^{-3/2} + \dots \\ &= \varpi_2^B \log(1-\lambda) + \frac{1}{\sqrt{z}}\left(\frac{1}{2}(1-\lambda) + \frac{21}{64}(1-\lambda)^2 + \dots\right) \\ &\quad + \frac{1}{z^{3/2}}\left(-\frac{1}{6(1-\lambda)^2} + \frac{1}{24(1-\lambda)} + \frac{5}{384} + \frac{5}{512}(1-\lambda) + \frac{255}{32768}(1-\lambda)^2 + \dots\right) + \dots\end{aligned} \tag{4.242}$$

One may check that the expansions around $z = \infty$ and $\lambda = 1$ satisfy the recursion in [2, §6.3], and agree with [105, (5.24)] at low orders.

Notice that both ϖ_2^B and ϖ_3^B vanish at $z = \infty$. The periods at the branch point are therefore linear combinations of 1 and $\varpi_1^B = -\log\lambda$. In order to fix the relevant combination, we can evaluate the Eichler integral (4.189) in the vicinity of the branch point using (4.179) and (4.186),

$$z = \frac{1}{\sqrt{\lambda}(J_4(\tau) - J_4(\tau_B))} \sim -\frac{1}{2\pi\mathrm{i}\sqrt{\lambda}}\frac{\eta^{16}(4\tau_B)}{\eta^{20}(2\tau_B)(\tau-\tau_B)} \tag{4.243}$$

$$C(\tau, m) \sim \frac{\eta^4(\tau_B)\eta^6(2\tau_B)}{\eta^4(4\tau_B)}\sqrt{\frac{8 - 4\lambda^{1/2} - 4\lambda^{-1/2}}{(\tau-\tau_B)\partial_\tau J_4(\tau_B)}} = \pm\frac{2\eta^4(\tau_B)\eta^4(4\tau_B)(\lambda^{1/4} - \lambda^{-1/4})}{\eta^4(2\tau_B)\sqrt{(2\pi\mathrm{i})(\tau-\tau_B)}} \tag{4.244}$$

hence

$$\begin{aligned}\int_{\tau_B}^{\tau}\begin{pmatrix}1\\u\end{pmatrix} C(u,m)\mathrm{d}u &\sim \pm\begin{pmatrix}1\\\tau_B\end{pmatrix}\frac{4(\lambda^{1/4} - \lambda^{-1/4})\eta^4(\tau_B)\eta^4(4\tau_B)\sqrt{(\tau-\tau_B)}}{\eta^4(2\tau_B)\sqrt{2\pi\mathrm{i}}} \\ &\sim \pm\begin{pmatrix}1\\\tau_B\end{pmatrix}\frac{2\eta^{12}(4\tau_B)\eta^4(\tau_B)}{\eta^{14}(2\tau_B)}\frac{1-\lambda^{-1/2}}{\pi\sqrt{z}}\end{aligned} \tag{4.245}$$

Moreover, we can use the fact that for $k = \frac{\theta_2^4(4\tau)}{\theta_3^4(4\tau)}$,

$$K(k) = \frac{\pi}{2}\theta_3^2(4\tau), \qquad E(k) = \frac{\theta_3^4(4\tau) + \theta_4(4\tau)^4}{3\theta_3^4(4\tau)}K(k) + \frac{\pi^2 E_2(4\tau)}{12K(k)}\,, \quad 4\tau = \frac{\mathrm{i}K(1-k)}{K(k)} \tag{4.246}$$

The identification $k = \lambda$ is justified by the observation that the branch point where $J_4(\tau_B) + 4(\lambda^{1/2} + \lambda^{-1/2}) = 0$ satisfies

$$\left(\frac{\theta_2(2\tau_B)}{\theta_3(2\tau_B)}\right)^4 = \frac{4\sqrt{\lambda}}{(1+\sqrt{\lambda})^2} \;\Rightarrow \left(\frac{\theta_2(4\tau_B)}{\theta_3(4\tau_B)}\right)^4 = \lambda \tag{4.247}$$

where the second equality follows from the doubling identities

$$\theta_2(4\tau) = \frac{1}{\sqrt{2}}\sqrt{\theta_3^2(2\tau) - \theta_4^2(2\tau)}\,, \quad \theta_3(4\tau) = \frac{1}{\sqrt{2}}\sqrt{\theta_3^2(2\tau) + \theta_4^2(2\tau)} \tag{4.248}$$

and holds whenever τ_B is in the fundamental domain of $\Gamma_0(4)$ (if not the r.h.s seems to evaluate to $1/\lambda$ rather than λ).

To evaluate the precise linear combination, we evaluate the coefficient of $1/\sqrt{z}$ at $\lambda = -1$. Using the Meijer-G representation (4.166) above, we expect

$$\varpi_2 = -\frac{\Gamma(\frac{1}{4})^2}{2\sqrt{2}\pi^{3/2}} z^{-1/2} + \dots, \quad \varpi_3 = -\frac{\pi^2}{3} + 2K(2)\, z^{-1/2} + \dots \tag{4.249}$$

where we used (or observed)

$$\begin{aligned} \Gamma(\tfrac{5}{4}) =& \frac{1}{4}\Gamma(\tfrac{1}{4}), \quad \Gamma(\tfrac{3}{4}) = \frac{\pi\sqrt{2}}{\Gamma(\frac{1}{4})} \\ K(2) =& \frac{1-\mathrm{i}}{8}\sqrt{\frac{2}{\pi}}\Gamma(\tfrac{1}{4})^2\,, \quad E(2) = \frac{1+\mathrm{i}}{2}\sqrt{\frac{2}{\pi}}\Gamma(\tfrac{3}{4})^2 \\ K(-1) =& \frac{1+\mathrm{i}}{2}K(2), \quad E(-1) = \frac{8\pi^2 + \Gamma\left(\frac{1}{4}\right)^4}{4\sqrt{2\pi}\Gamma\left(\frac{1}{4}\right)^2} \end{aligned} \tag{4.250}$$

On the other hand, the eta functions in (4.245) evaluate to

$$\eta(\tfrac{1+\mathrm{i}}{4}) = \frac{e^{-\mathrm{i}\pi/24}\Gamma(\frac{1}{4})}{2^{5/8}\pi^{3/4}}\,, \quad \eta(\tfrac{1+\mathrm{i}}{2}) = \frac{e^{\mathrm{i}\pi/24}\Gamma(\frac{1}{4})}{2^{3/4}\pi^{3/4}}\,, \quad \eta(1+\mathrm{i}) = \frac{e^{\mathrm{i}\pi/12}\Gamma(\frac{1}{4})}{2\pi^{3/4}}\,, \tag{4.251}$$

Using these relations for $\lambda = -1$ we find

$$\varpi_2 = -\left(1 + \frac{4\mathrm{i}\log 2}{\pi}\right)\varpi_2^B + \frac{\mathrm{i}}{\pi}\varpi_3^B, \quad \varpi_3 = -\frac{\pi^2}{3} + (8\log 2 - \mathrm{i}\pi)\varpi_2^B - 2\varpi_3^B \tag{4.252}$$

Using (4.158), we find, for $\lambda = -1$,

$$T = \frac{1}{(2\pi\mathrm{i})^2}\left((8\log 2 - 2\pi\mathrm{i})\varpi_2^B - 2\varpi_3^B\right), \quad T_D = \frac{3}{8} + \frac{1}{(2\pi\mathrm{i})^2}\left(\left(4\log 2 + \frac{\mathrm{i}\pi}{2}\right)\varpi_2^B - \varpi_3^B\right) \tag{4.253}$$

These relations are found to persist for any m with any For $0 < \mathrm{Re}\, m < 1, \mathrm{Im}\, m > 0$, with a judicious choice of constant term, invariant under $M_B(0)$,

$$\begin{aligned} T =& \tfrac{1}{2} + \frac{1}{(2\pi\mathrm{i})^2}\left(8\log 2\,\varpi_2^B - 2\varpi_3^B\right), \\ T_D =& \tfrac{1+m}{4} + \frac{1}{(2\pi\mathrm{i})^2}\left(\left(4\log 2 + \frac{\mathrm{i}\pi}{2}\right)\varpi_2^B - \varpi_3^B\right) \end{aligned} \tag{4.254}$$

For $0 < \mathrm{Re}\, m < 1, \mathrm{Im}\, m < 0$, we find instead

$$\begin{aligned} T =& \tfrac{1}{2} - m + \frac{1}{(2\pi\mathrm{i})^2}\left((8\log 2 - 2\pi\mathrm{i})\,\varpi_2^B - 2\varpi_3^B\right) \\ T_D =& \tfrac{1-m}{4} + \frac{1}{(2\pi\mathrm{i})^2}\left(\left(4\log 2 - \tfrac{\mathrm{i}\pi}{2}\right)\varpi_2^B - \varpi_3^B\right) \end{aligned} \tag{4.255}$$

where the constant term is invariant under $\widetilde{M}_B(0)$. These relations are consistent with the value of $\tau_B = \frac{\mathrm{d}T_D}{\mathrm{d}T}$, except for a shift by $\frac{1}{2}$ and $\Gamma_0(4)$ action,

$$\begin{aligned} &\mathrm{Im}\, m > 0: \quad \tau_B = \tfrac{\mathrm{d}T_D}{\mathrm{d}T}|_{\tau=\tau_B} = \tfrac{1}{2} + \tfrac{\mathrm{i}K(1-\lambda)}{4K(\lambda)} \\ &\mathrm{Im}\, m < 0: \quad \tau_B = \tfrac{2K(\lambda)-\mathrm{i}\,K(1-\lambda)}{4K(\lambda)-4\mathrm{i}\,K(1-\lambda)} \quad \Leftrightarrow \quad \tfrac{3\tau_B-1}{4\tau_B-1} = \tfrac{1}{2} + \tfrac{\mathrm{i}K(1-\lambda)}{4K(\lambda)} \end{aligned} \tag{4.256}$$

Note that τ_B evaluates to $\frac{3+\mathrm{i}}{4}$ or $\frac{1+\mathrm{i}}{4}$ as $\lambda \to -1$ with $\mathrm{Im}\, m > 0$ or $\mathrm{Im}\, m < 0$, respectively.

Convergence domains and numerical evaluation

The convergence domain of the expansions near $\tau = \mathrm{i}\infty, 0, 1/2$ are determined by the nearest branch point, namely τ_B in the τ plane, $-1/(4\tau_B)$ or $-1/(4\tau_B-4)$ in the τ' plane and $\tau_B/(2\tau_B-1)$ in the τ'' plane (see Fig. 4.34). Together with the expansion around $\tau = 1$ obtained by translation, they cover the whole fundamental domain. However, all three expansions break down both as τ approaches the branch point, and as τ approaches $1 - \overline{\tau_B}$, which also lies at the boundary of the convergence disks. Instead of completing the set of expansions using the large z expansion (4.254)–(4.255), we find it more efficient to solve numerically the Picard–Fuchs equation order by order in powers of $\tau'' - \tau''_B$, for a fixed value of m. The convergence radius of the resulting series expansion is determined by the $\Gamma_1(4)$ image of τ''_B nearest to τ''_B.

We find numerical evidence that the large volume expansion agrees with the expansions around $0, \frac{1}{2}, 1$ in their common domain of convergence. In contrast, the expansions around $\tau = 0$ and $\tau = \frac{1}{2}$ agree for $\mathrm{Im}\, m > 0$, but satisfy

$$\begin{aligned} T'(\tau, m) &= -T''(\tau, m) + 1 - 2m, \\ T'_D(\tau, m) &= -T''_D(\tau, m) + \frac{1-m}{2} \end{aligned} \tag{4.257}$$

when $\mathrm{Im}\, m < 0$. This corresponds to the action of the monodromy matrix $\widetilde{M}_{B,0}$ in (4.191), and and is consistent with the value of $(T, T_D) = (\frac{1}{2} - m, \frac{1-m}{4})$ at the branch point, see (4.190). Similarly, the expansions around $\tau = 1$ and $\tau = \frac{1}{2}$ agree for $\mathrm{Im}\, m < 0$, but satisfy

$$\begin{aligned} T'(\tau - 1, m) + 1 &= -T''(\tau, m) + 1 \\ T'_D(\tau - 1, m) + T'(\tau - 1, m) + \frac{1+m}{2} &= -T''_D(\tau, m) + \frac{1+m}{2} \end{aligned} \tag{4.258}$$

when $\mathrm{Im}\, m > 0$. This corresponds to the action of the monodromy matrix $M_{B,0}$ in (4.191), and is consistent with the value of $(T, T_D) = (\frac{1}{2}, \frac{1+m}{4})$ at the branch point (4.189).

As a result, we arrive at the following prescription for computing $T(\tau, m), T_D(\tau, m)$ for any τ in the Poincaré upper half-plane on the principal sheet (defined below (4.188)). First, we bring τ in the fundamental domain $\mathcal{F}$ by a suitable sequence of $\Gamma_0(4)$ transformations $\tau \mapsto \tau + 1$ and $\tau \mapsto \frac{\tau-1}{4\tau-3}$ (as well as their inverses), keeping track of its action on the period vector Π^t via the following lifts to Γ:

$$\begin{aligned} \tau \mapsto \tau + 1: \quad & M_{LV} = \begin{pmatrix} 1 & 0 & 0 & 0 \\ 0 & 1 & 0 & 0 \\ 1 & 0 & 1 & 0 \\ \frac{1}{2} & \frac{1}{2} & 1 & 1 \end{pmatrix} \\ \tau \mapsto \frac{\tau-1}{4\tau-3}: \quad & M_S = \begin{pmatrix} 1 & 0 & 0 & 0 \\ 0 & 1 & 0 & 0 \\ 1 & -2 & -3 & 4 \\ \frac{1}{2} & -\frac{1}{2} & -1 & 1 \end{pmatrix} = M_C^{-1} M_{LV}^{-1} \end{aligned} \tag{4.259}$$

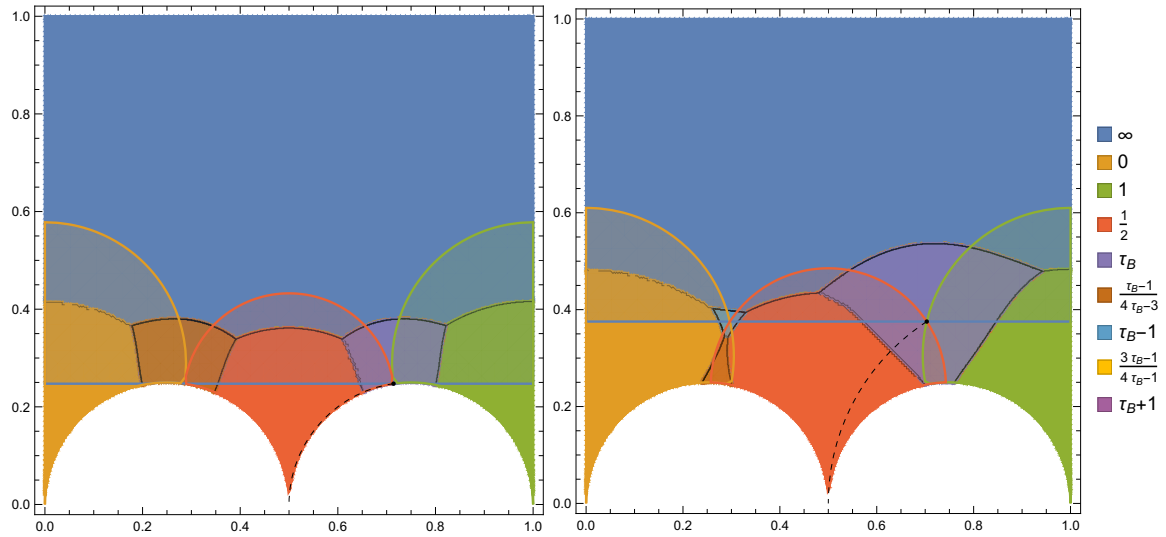


Figure 4.34: Convergence regions of the expansions around $\tau = i\infty, 0, 1, \frac{1}{2}$ (halfplane and disks intersected with the fundamental domain, shaded in blue, orange, green, red, respectively), and domains where each of these expansions are used, as well as expansion around images of the branch point τ_B (black dot, connected to $\tau = \frac{1}{2}$ by the cut). Different values of m require different subsets of the expansions. Left: $m = 0.4$, involving the first six expansions. Right: $m = 0.4 + 0.3i$, involving the first seven expansions (the last two would become relevant for other values of m).

Second, when τ belongs to $\mathcal{F}$, for all 9 expansions that are needed to cover the whole fundamental domain depending on the value of m (namely the expansions around $\tau = \infty, 0, 1/2, 1, \tau_B$, $\frac{\tau_B-1}{4\tau_B-3}, \tau_B - 1, \frac{3\tau_B-1}{4\tau_B-1}, \tau_B + 1$), we compute the expansion parameters (such as q or $\tau'' - \tau''_B$), divided by the radius of convergence of the respective series. The expansion for which this ratio is the smallest provides the best-converging series, which we use to perform the computation (see Fig. 4.34), taking into account the branch cut. An important optimization is to compute the series expansion coefficients only once for each value of m. This algorithm is implemented as `EichlerZ[{r_,d1_,d2_,ch2_},tau_,m_]` in the Mathematica package `F0Scattering.m` (see footnote 14).

4.6.6 4D limit

While the scattering diagrams studied in this chapter determine the BPS spectrum in pure 5D super-Yang-Mills theory with $SU(2)$ gauge group (and vanishing theta angle) compactified on a circle, it is natural to ask if they reproduce the usual BPS spectrum of 4D super Yang-Mills theory [171] in the limit where the circle shrinks to zero size. Here we take some steps in this direction, making contact with earlier results in the literature.

Starting from the representation (4.134), the authors of [34] show that the 4D limit is obtained by setting

$$Q_b = -\Lambda^2 R^2, \quad Q_f = \frac{1}{2} + R^2 u_{\rm SW} + \dots \tag{4.260}$$

and taking $R \to 0$ keeping $\Lambda, u_{\rm SW}$ fixed. In this limit, we have

$$\lambda \sim \frac{1}{\Lambda^4 R^4} \to \infty\,, \quad u \sim -\frac{u_{\rm SW}}{R^2\Lambda^4} \to \infty \tag{4.261}$$

Since the ratio $u/\sqrt{\lambda}$ goes to a constant, the modular parameter τ is fixed, with $J_4'(\tau) = -8u_{\rm SW}/\Lambda^2$.

Up to a subleading term in u, this agrees with the geometric engineering limit introduced in [124] (see [116, (6.19)]),

$$z_1 = \frac{1}{4}\exp\left(-4\epsilon^2 u_{\rm SW}\right)\ , \quad z_2 = \epsilon^4\Lambda^4, \quad \epsilon \to 0 \tag{4.262}$$

keeping $u_{\rm SW}, \Lambda$ fixed.

We can also make contact with the periods of the SW curve as follows. In [18, §4.2.4], the authors provide a representation of the periods $Z_{\rm SW}(\gamma_1)$, $Z_{\rm SW}(\gamma_2)$ associated to the states that become massless at $u = 1$ and $u = -1$ as quasi-modular forms

$$\begin{aligned} Z_{\rm SW}(\gamma_1) =& \frac{A^2 - 2B^2 + E}{16A} = q - 6q^2 + 24q^3 + \dots, \\ Z_{\rm SW}(\gamma_2) =& \frac{\pi\tau(A^2 - 2B^2 + E) - 2\mathrm{i}}{16\pi A} \end{aligned} \tag{4.263}$$

where

$$A = \theta_3^2(2\tau) = \frac{\eta(2\tau)^{10}}{\eta(\tau)^4\eta(4\tau)^4}, \quad B = \theta_4^2(2\tau) = \frac{\eta(\tau)^4}{\eta(2\tau)^2}, \quad C = \theta_2^2(2\tau) = \frac{4\eta(4\tau)^4}{\eta(2\tau)^2} \tag{4.264}$$

$$E = \partial_\tau \log B^2C^2 = \frac{1}{3}E_2 + \frac{2}{3}B^2 + \frac{1}{3}C^2\ , \quad A^2 = B^2 + C^2 \tag{4.265}$$

The u variable is

$$u = -1 + \frac{2B^2}{A^2} = \frac{24 - J_4}{8 + J_4} \tag{4.266}$$

such that $u = 1, -1, \infty$ correspond to the cusps $\tau = 0, \tau = \mathrm{i}\infty, \tau = \frac{1}{2}$. Fricke transform $\tau \mapsto -1/(4\tau)$ exchanges B and C, $Z_{\rm SW}(\gamma_1)$ with $Z_{\rm SW}(\gamma_2)$ and sends $u \to -u$.

The formulae (4.263) are obtained by integrating the equations

$$\partial_\tau \begin{pmatrix} Z_{\rm SW}(\gamma_1) \\ Z_{\rm SW}(\gamma_2) \end{pmatrix} = C_{\rm SW}(\tau) \begin{pmatrix} -1 \\ \tau \end{pmatrix} \tag{4.267}$$

with

$$C_{\rm SW}(\tau) = \frac{1}{16}\left(AB^2 - \frac{B^4}{A}\right) = \frac{\eta(\tau)^{12}\eta(4\tau)^{12}}{\eta(2\tau)^{18}} \tag{4.268}$$

Using

$$J_4 + 8 = 16\frac{A^2}{C^2} = 16\frac{\eta(2\tau)^{24}}{\eta(\tau)^8\eta(4\tau)^{16}} \tag{4.269}$$

we see agreement with the limit $\lambda \to \infty$ of C'' in (4.224), up to rescaling by a factor of $\lambda^{1/4}$,

$$C''(\tau, m) \sim \frac{\eta^8(\tau)\eta^4(4\tau)}{\eta^6(2\tau)}\frac{8}{\lambda^{1/4}\sqrt{J_4 + 8}} \tag{4.270}$$

Of course, one can perform a Fricke-type transform $\tau \mapsto \tau/(2\tau + 1)$ in the formulae from [18], such that $u = 1, -1, \infty$ get mapped to $\tau = 0, 1/2, \mathrm{i}\infty$. Under this transformation, B is invariant but A and C get exchanged, and $J_4 \mapsto \frac{256}{J_4+8} - 8$. As a result, the new identifications are

$$u = \frac{1}{8}J_4(\tau)\ , \quad C_{SW}(\tau) = \frac{\eta(2\tau)^{18}}{\eta(4\tau)^{12}} = \frac{1}{q^{1/2}} - 18q^{3/2} + 147q^{7/2} + \dots \tag{4.271}$$

which is recognized as the $\lambda \to \infty$ limit of $C(\tau)$, up to a factor of $2\lambda^{1/4}$,

$$C(\tau, m) \sim \frac{\eta(\tau)^4 \eta(2\tau)^6}{\eta(4\tau)^4} \frac{\sqrt{J_4 + 8}}{2\lambda^{1/4}} = \frac{\eta(2\tau)^{18}}{2\lambda^{1/4}\eta(4\tau)^{12}} \tag{4.272}$$

In fact, we can rewrite the periods appropriate to the weak coupling regime (see e.g. [134])

$$a = \frac{u^{1/2}}{\sqrt{2}}\, {}_2F_1\left(-\frac{1}{4}, \frac{1}{4}, 1; 1/u^2\right), \quad a_D = \frac{\mathrm{i}}{4}(u^2 - 1)\, {}_2F_1\left(\frac{3}{4}, \frac{3}{4}, 2; 1 - u^2\right), \tag{4.273}$$

in terms of Eichler-type integrals of $C_{SW} = \sum_{n\geq 0} c_n q^{2n-\frac{1}{2}}$:

$$a = -\frac{1}{4\sqrt{2}} f_1, \quad a_D = \frac{1}{4\pi\mathrm{i}} \left(f_2 - f_1 \log q\right) \tag{4.274}$$

with

$$\begin{aligned} f_1 &= \sum_{n\geq 0} \frac{c_n}{2n - \frac{1}{2}} q^{2n-\frac{1}{2}} = -\frac{2}{q^{1/2}} - 12q^{3/2} + 42q^{7/2} + \cdots = 2\frac{E_2 - C^2 + 5A^2}{3C} \\ f_2 &= \sum_{n\geq 0} \frac{c_n}{(2n - \frac{1}{2})^2} q^{2n-\frac{1}{2}} = \frac{4}{q^{1/2}} - 8q^{3/2} + 12q^{7/2} + \cdots = \frac{16}{C} \end{aligned} \tag{4.275}$$

We expect (but cannot show yet) that in the limit $\lambda \to +\infty$, or $m \to -\mathrm{i}\infty$, the scattering diagram $\mathcal{D}^{\Pi}_{m,\psi}$ should simplify drastically, leaving only the primary scatterings of the initial rays $O(k, k)$ and $O(k + 1, k)$ in every strip $\mathrm{Re}\,\tau \in (k, k + 1)$, reproducing the spectrum of monopoles and dyons in the weakly coupled 4D limit $\tau \to \mathrm{i}\infty$. Independently of this, it would be interesting to unfold the u-plane analysis of attractor flow trees for 4D $SU(2)$ super Yang-Mills theory in [18] into the modular upper half-plane, which would avoid the need for branch cuts. It is also interesting to ask if a similar representation in terms of quasi-modular forms exists for the Eichler integrals (4.195) away from the 4D limit $\lambda = \infty$.

5

BPS Dendroscopy on Local $\mathbb{F}_1$

This chapter is based entirely on ongoing joint work with Boris Pioline, currently under preparation, and is included here in essentially the same form, with only minor editorial changes. The aim is to extend the framework of BPS dendroscopy from local $\mathbb{P}^2$ and local $\mathbb{P}^1 \times \mathbb{P}^1$ to the Hirzebruch surface local $\mathbb{F}_1$. The chapter studies the BPS spectrum of compactly supported D-brane bound states on this geometry, constructs the corresponding scattering diagrams in the large-volume and physical Π-stability regimes, and analyzes how the presence of the exceptional curve modifies the structure of initial rays and wall-crossing. It also develops the local mirror-symmetry description of the relevant central charges, including special loci in parameter space such as the Argyres–Douglas point, which leads to a modular description in terms of a non-congruence subgroup.

5.1 Introduction

Mapping out the spectrum of BPS states in type II string theories compactified on a Calabi-Yau threefold is an important problem in mathematical physics, with applications to supersymmetric black holes, supersymmetric gauge theories, algebraic geometry, representation theory and more. In previous works [47, 132], we studied this problem for two of the simplest non-trivial toric Calabi-Yau threefolds, the total spaces of the canonical bundle $X = K_S$ over the complex projective space $S = \mathbb{P}^2$ and the product of two lines $S = \mathbb{F}_0 = \mathbb{P}^1 \times \mathbb{P}^1$. Upon compactifying type IIA strings on K_S, these two geometries engineer rank 1 5D superconformal field theories on $\mathbb{R}_{3,1} \times S_1$, decoupled from gravity. The goal of this work is to carry out a similar study for the Hirzebruch surface $S = \mathbb{F}_1$, a non-trivial $\mathbb{P}^1$ bundle over $\mathbb{P}^1$ which arises by blowing up $\mathbb{P}^2$ at one point, and provides the UV completion of $5D$ $\mathcal{N} = 1$ super-Yang-Mills theory with gauge group $SU(2)$ and half-unit theta angle.

Unlike the (arguably trivial) case of the resolved conifold and other small resolutions of toric singularities, where the finite mass BPS spectrum consists only of mutually local D2-D0 brane bound states, the existence of a compact divisor S leads to a rich chamber structure for the Donalson-Thomas (DT) invariants $\Omega_\sigma(\gamma)$ counting semi-stable objects in the derived category $\mathcal{C} = D^b \operatorname{Coh}_c X$ of compactly supported sheaves for given stability condition $\sigma \in \operatorname{Stab} X$ (Physically, $\Omega_\sigma(\gamma)$ reduces to the BPS index counting D4-D2-D0 bound states for given Kähler moduli on X along the slice of Pi-stability conditions). The stability scattering diagram, introduced first in the context of moduli spaces of quiver representations in [50], provides a powerful way to determine the DT invariants at any point $\sigma \in \operatorname{Stab} X$, from the knowledge of the initial rays emitted at the boundary of $\operatorname{Stab} X$ where certain spherical objects become massless. As anticipated in [129] and demonstrated in [25], this is the natural mathematical framework for the attractor flow tree formula [16, 74, 75, 155] allowing to express BPS indices at any point in moduli space, in terms of the indices $\Omega_\star(\gamma)$ counting BPS in their attractor chamber, also known as self-stability condition.

In previous work [47, 132], we constructed the scattering diagram for $S = \mathbb{P}^2$ and $S = \mathbb{F}_0$ both along the large volume slice (corresponding to divisorial stability conditions, generalizing the analysis of [45]), and along the physical slice of Π-stability conditions (determined by local mirror symmetry). In particular, the scattering diagram along the physical slice was manifestly invariant under the full group of autoequivalences (suitable extensions of the congruence subgroups $\Gamma_0(3)$ and $\Gamma_0(4)$, respectively, corresponding to the monodromy group of the family of elliptic curves). The case $S = \mathbb{F}_1$, associated by local mirror symmetry to the family of elliptic curves in $\mathbb{C}_x^\times \times \mathbb{C}_y^\times$ [60, 105, 116]

$$x + y + \frac{\ell}{xy} + \frac{\ell}{x} = \frac{1}{\mathrm{u}}\,, \tag{5.1}$$

where ℓ and u parametrized the gauge coupling and Coulomb branch parameter in the 5D gauge theory on $\mathbb{R}^{3,1} \times S_1$, is significantly more complicated for several reasons, which we believe warrant the present study:

i) Due to the existence of effective curves with negative self-intersection (namely the base B of the $\mathbb{P}^1$ fibration, with $B^2 = -1$), line bundles are in general not everywhere stable in the large volume slice [23]. As result, the initial rays are not just pure D4 and anti-D4-branes (invertible sheaves $\mathcal{O}(d_F, d_B)$ and their homological shift $\mathcal{O}(d_F, d_B)[1]$, in mathematical terms) but also include spherical D2-branes wrapped on B. Nonetheless, upon extending the scattering diagram 'below the parabola' in affine coordinates, the initial rays turn out to be pure D4-anti-D4 brane pairs associated to a *geometric helix of invertible sheaves*. A similar phenomenon was observed for $S = \mathbb{F}_0$ in [132], and is expected to hold true for any del Pezzo surface with canonical polarization.

ii) For generic values of of the gauge coupling (or'mass parameter) ℓ, the family (5.1) has the same ramification structure over the u-plane as for local $\mathbb{F}_0$, namely type $I_8 + 4I_1$ in Kodaira's notation, where the I_8 fiber corresponds to $\mathrm{u} = 0$ and the I_1 fibers to the four roots of the reduced discriminant

$$\Delta_4(\mathrm{u}, \ell) = 1 + \mathrm{u} - 8\ell\mathrm{u}^2 - 36\ell\mathrm{u}^3 + \ell\,(16\ell - 27)\,\mathrm{u}^4\,. \tag{5.2}$$

In contrast to local $\mathbb{F}_0$, the Klein invariant $J(\mathrm{u}, \ell)$ is in general not a Hauptmodul for any subgroup of $PSL(2, \mathbb{Z})$, which prevents us from unfolding the scattering diagram from the u plane to the Poincaré upper half-plane. Moreover, the fact that the discriminant is a general quartic polynomial in u (as opposed to a quadratic polynomial in u^2) makes it challenging to compute the periods at the four I_1 fibers, where we expect massless states to arise. Fortunately, we find that by passing to an 8:1 cover of the ℓ-plane, the roots can be expressed as rational functions in a new complex parameter[1] $b \in \mathbb{P}^1$,

$$\ell = -\frac{b\left(b^2 + b + 1\right)^3}{(b+1)^8}, \quad \mathrm{u} = -\frac{(b+1)^4}{\left(b^2 + b + 1\right)\left(b^2 + 4b + 1\right)} \quad \Rightarrow\ \Delta_4(\mathrm{u}, \ell) = 0. \tag{5.3}$$

This change of variable naturally arises when computing the regulator period of nodal curves in the family (5.1) using the method of [80], allowing to express the periods at the conifold point (sometimes called quantum volume) as linear combinations of Bloch-Wigner dilogarithms in b and its powers, along with standard logarithms.

[1] Simpler rational expressions exist in terms of $\beta = b + 1/b$, see (5.129), given a 4:1 cover of the ℓ-plane, but periods need not be invariant under $b \to 1/b$.

iii) For the special value $\ell = -27/256$, two I_1 fibers collide to form a type II degeneration, known in physics as Argyres-Douglas (AD) point of type H_0 (in contrast, local $\mathbb{F}_0$ admits a degeneration $I_1 + I_1 \to I_2$, whose physics is simply unHiggsing). As a consequence, the monodromy group does reduces to (an extension) of a *non-congruence subgroup* $\Gamma \subset PSL(2,\mathbb{Z})$, a genus zero subgroup of index 10 with 3 cusps (corresponding to the I_8 and two I_1 fibers) and one elliptic point of order 3 (corresponding to the AD point) first identified in [139]. The Coulomb branch parameter u then becomes a Hauptmodul for Γ, allowing to parametrize the universal cover of the Coulomb branch by a modulus τ in the Poincaré upper half-plane. As in the case of local $\mathbb{P}^2$ and local $\mathbb{F}_0$ at the special point $\lambda = 1$, this allows to construct full Γ-invariant scattering diagram avoiding the need for branch cuts.

iv) For the other special value $\ell = 0$, one I_1 fiber collides with the I_8 fiber at $\mathrm{u} = 0$ to produce an I_9 fiber, resulting in the same ramification structure as for local $\mathbb{P}_2$. Indeed, geometrically ℓ controls the size of the exceptional divisor when viewing $\mathbb{F}_1$ as the one-point blow-up of $\mathbb{P}^2$. Since this degeneration changes the large volume structure, we refrain from studying it here.

The rest of this chapter is organized as follows. Section 5.2 reviews the basic geometry of local $\mathbb{F}_1$, the relevant charges and moduli spaces of Gieseker-semistable sheaves, the associated Gopakumar–Vafa data, and the structure of Bridgeland stability conditions. Section 5.3 then discusses the quiver descriptions arising from exceptional collections and their mutations. In Section 5.4 we construct and analyze the scattering diagram on the large-volume slice. Section 5.5 turns to the physical Π-stability slice, developing the local mirror-symmetry description of the central charges, their large-volume and conifold expansions, the limit to local $\mathbb{P}^2$, and the corresponding monodromies. Finally, Sections 5.6 and 5.7 are devoted to two further interesting aspects of the model: the appearance of a distinguished non-congruence subgroup and an explicit description of the conifold periods in terms of dilogarithmic functions.

5.2 Generalities

5.2.1 Coherent sheaves on $K_{\mathbb{F}_1}$

The Hirzebruch surface $S = \mathbb{F}_1$ is a $\mathbb{P}^1$ bundle over $\mathbb{P}^1$, given by the projectivization of the $\mathcal{O} + \mathcal{O}(-1)$ bundle over $\mathbb{P}^1$. We denote by F and B the fiber and base $\mathbb{P}^1$, respectively. They satisfy $F^2 = 0, B^2 = -1, B.F = 1$. Alternatively, one may view $\mathbb{F}_1$ as the blow-up of $\mathbb{P}^2$ at one point. The second homology is then spanned by the hyperplane class $H = F + B$ and the exceptional divisor C, with $H^2 = 1, C^2 = -1, H.C = 0$. Although the exceptional divisor class C coincides with the base divisor class B, we use different letters to distinguish the bases (F, B) and (H, C). The Mori cone is spanned by (F, B), while the nef cone is spanned by (H, F). The anticanonical class is $c_1(S) = 3F + 2B = 3H - C$. For any coherent sheaf E on S, we decompose the first Chern class as $c_1(E) = d_F(E)\, F + d_B(E)\, B$ and denote the Chern character by $\gamma(E) = [r(E), d_F(E), d_B(E), \mathrm{ch}_2]$. Alternatively, we can decompose $c_1(E) = d_H(E)\, H + d_C(E)\, C$, with

$$(d_H, d_C) = (d_B, d_B - d_F) \quad \Leftrightarrow \quad (d_F, d_B) = (d_H, d_H + d_C) \tag{5.4}$$

We denote by $\mathcal{O}(m_F, m_B)$ the unique line bundle on S with first Chern class $m_F\, F + m_B\, B$; its Chern vector is $[1, m_F, m_B, m_F m_B - \frac{1}{2}m_B^2]$. Under tensoring $E \mapsto E \otimes \mathcal{O}(m_F, m_B)$, an operation we call spectral flow, the Chern vector transforms as

$$[r, d_F, d_B, \mathrm{ch}_2] \mapsto [r, d_F + r m_F, d_B + r m_B, \mathrm{ch}_2 + (d_F - d_B)m_B + d_B m_F + r(m_B m_F - \tfrac{1}{2}m_B^2)] \tag{5.5}$$

For two coherent sheaves E, E' of Chern characters $[r, d_B, d_F, \mathrm{ch}_2]$ and $[r', d'_B, d'_F, \mathrm{ch}'_2]$, the Euler form is given by the Grothendieck-Riemann-Roch theorem,

$$\begin{aligned}\chi(E, E') :=& \dim \mathrm{Hom}(E, E') - \dim \mathrm{Ext}^1(E, E') + \dim \mathrm{Ext}^2(E, E') \\ =& r r' + \frac{1}{2} r(2d'_F + d'_B) - \frac{1}{2} r'(2d_F + d_B) + r\mathrm{ch}'_2 + r'\mathrm{ch}_2 - (d_F d'_B - d_B d'_F) + d_B d'_B\end{aligned} \tag{5.6}$$

We define the antisymmetrized Euler form, or Dirac product, as

$$\langle \gamma, \gamma' \rangle := \chi(E, E') - \chi(E', E) = r(2d'_F + d'_B) - r'(2d_F + d_B) \tag{5.7}$$

The Euler form and Dirac product are invariant under spectral flow. For $r \neq 0$, so is the Bogomolov discriminant, defined by

$$\Delta(\gamma) = \frac{2d_F d_B - d_B^2}{2r^2} - \frac{\mathrm{ch}_2}{r} \tag{5.8}$$

5.2.2 Moduli space of Gieseker-semistable sheaves

Up to scaling, we can parametrize ample divisors D by a real number M, such that $D \propto H_M := 3F + (M+2)B = 3H + (M-1)C$. For $M = 0$, H_0 coincides with the anticanonical class $c_1(S)$. We define the slope by

$$\mu_M(\gamma) = \frac{3d_H + d_C}{r} - M\frac{d_C}{r}\,, \tag{5.9}$$

for $r \neq 0$, and $\mu_M(\gamma) = +\infty$ for $r = 0$ and denote by $\mathcal{M}_M(\gamma)$ the moduli space of Gieseker-semistable sheaves with Chern character γ. When $\mathcal{M}_M$ is non empty, it has complex dimension

$$d_{\mathbb{C}}(\gamma) = 1 - \chi(E, E) = 2d_B d_F - d_B^2 - 2r\mathrm{ch}_2 - r^2 + 1 \tag{5.10}$$

We denote by $\Omega_M(\gamma)$ the Donaldson-Thomas invariant associated to the moduli space (or moduli stack, if γ is not primitive of M not generic) $\mathcal{M}_M(\gamma)$. For $r > 0$, the non-emptiness of $\mathcal{M}_M(\gamma)$ requires that the Bogomolov discriminant s positive, $\Delta(\gamma) \geq 0$. Sufficient conditions for $\mathcal{M}_M(\gamma)$ being non-empty are discussed in [67, 135, 188]. As in the classic case of the projective plane [83], these conditions are determined from the list of stable exceptional bundles E, with $\dim \mathrm{Hom}(E, E) = 1, \dim \mathrm{Ext}^{1,2}(E, E) = 0$. The list of the first few exceptional bundles, and their stability range, can be found in [67, Table 2],

$$[1,0,0,0]_0, [2,1,1,-\tfrac{1}{2}]_{\frac{3}{8}}, [4,2,1,-\tfrac{3}{2}]_{\frac{15}{32}}, [5,2,2,-2]_{\frac{12}{25}}, [6,3,5,-\tfrac{5}{2}]_{\frac{35}{72}}, [8,4,1,-\tfrac{7}{2}]_{\frac{63}{128}}, \dots \tag{5.11}$$

where we wrote the discriminant $\Delta = \frac{1}{2}(1 - \frac{1}{r^2})$ in subscript. All exceptional bundles are stable for the canonical polarization $M = 0$, but (except for the first of them) get destabilized outside some finite range $[M_-, M_+]$. The list $\mathcal{E}_M$ of stable exceptional bundles determines a lower bound

$\Delta(E) \geq \delta_{\rm DLP}(M,a,b)$ on the discriminant of non-exceptional H-stable torsion-free sheaves with slope $(a,b) = (d_B, d_F)/r$, given by [67][2]

$$\delta_{\rm DLP}(M,a,b) := \sup_{F\in\mathcal{E}_M, |\mu_M(F)-(a+2b)-M(b-a)|\leq 2\frac{M+8}{M+2}} \left[P_\epsilon\left(a-\tfrac{d_B(F)}{r(F)}, b-\tfrac{d_F(F)}{r(F)}\right) - \Delta(F)\right] \tag{5.12}$$

where $P_\epsilon(a,b) = (\epsilon a+1)(\epsilon b+1-\frac{1}{2}\epsilon a)$ and $\epsilon(F) = \text{sign}[\mu_M(F)-(a+2b)-M(b-a)| \leq 2\frac{M+8}{M+2}]$. Note that $\delta_{\rm DLP}(M,a,b)$ is invariant under $(a,b)\to(a+1,b),(a,b+1),(-a,-b)$ and greater than $1/2$. Conversely, $\mathcal{M}_H(\gamma)$ is non-empty if γ is the Chern character of an exceptional stable bundle or $\Delta(\gamma) > \delta_{\rm DLP}(M, d_B/r, d_F/r)$. The function $\delta_{\rm DLP}(M,a,b)$ for the canonical polarization $M=0$ is plotted in Figure 5.1.

5.2.3 Gopakumar-Vafa invariants

For rank 0, Gieseker indices $[0, d_F, d_B, \text{ch}_2]$ are conjecturally independent of M and of ch_2, and reduce to the genus 0 GV invariants $\text{GV}^{(0)}_{d_F,d_B}$. For $S=\mathbb{F}_1$, the latter were computed in [60, Table 10]:

$d_F\backslash d_B$	0	1	2	3	4
0	0	1	0	0	0
1	−2	3	0	0	0
2	0	5	−6	0	0
3	0	7	−32	27	0
4	0	9	−110	286	−192

(5.13)

They vanish unless $d_F\geq 0, d_B\geq 0$ and $d_B\leq d_F$, except for the entry $(d_F,d_B)=(0,1)$, which lies outside the cone of moveable curves. The fact that they vanish for $d_B > 2d_F$ is a consequence of the formula for the expected dimension of the moduli space, $\dim_{\mathbb{C}}\mathcal{M}_M(\gamma) = 2d_Bd_F - d_B^2 + 1$. The vanishing in the range $d_F < d_B < 2d_F$ is instead a consequence of the existence of second geometric phase related by a flop $(T_B,T_F)\mapsto(-T_B,T_F+T_B)$. After flop, the GV invariants become $\text{GV}'^{(0)}_{d'_F,d'_B} = \text{GV}'^{(0)}_{d_F,d_F-d_B}$ for $d_F\geq d_B$ and zero otherwise, except for $\text{GV}'^{(0)}_{0,1} = \text{GV}^{(0)}_{0,1}$:

$d'_F\backslash d'_B$	0	1	2	3	4
0	0	1	0	0	0
1	3	−2	0	0	0
2	−6	5	0	0	0
3	27	−32	7	0	0
4	−192	286	−110	9	0
5	1695	−3038	1651	−288	11

(5.14)

In particular, the diagonal invariants $\text{GV}^{(0)}_{d,d}$, or the equivalently the invariants $\text{GV}'^{(0)}_{d,0}$ in the first column of the previous table, are recognized as the GV invariants of local $\mathbb{P}_2$.

The refined BPS invariants $\text{GV}^{(j_L,j_R)}_{d_B,d_F}$, counting multiplicities of representations of the 5D little group $SU(2)_L\times SU(2)_R$, were found in [118, p34], see also [116, Table 5]. The refined D2-D0 invariants follow from the refined BPS invariants by evaluating the character of the

[2]The parameter m in [67] corresponds to $\frac{1-M}{2+M}$ in our notations.

$SU(2)_L \times SU(2)_R$ representation on the diagonal locus $y_L = y_R$,

$$\begin{aligned}
\Omega([0,0,1,\mathrm{ch}_2]) &= 1 \\
\Omega([0,1,0,\mathrm{ch}_2]) &= -y - 1/y \\
\Omega([0,1,1,\mathrm{ch}_2]) &= y^2 + 1 + 1/y^2 \\
\Omega([0,2,1,\mathrm{ch}_2]) &= y^4 + y^2 + 1 + 1/y^2 + 1/y^4 \\
\Omega([0,2,2,\mathrm{ch}_2]) &= -y^5 - y^3 - y - 1/y - 1/y^3 - 1/y^5 \\
\Omega([0,3,2,\mathrm{ch}_2]) &= -y^9 - 3y^7 - 4y^5 - 4y^3 - 4y - \dots \\
\Omega([0,3,3,\mathrm{ch}_2]) &= y^{10} + 2y^8 + 3y^6 + 3y^4 + 3y^2 + 3 + \dots \\
\Omega([0,4,2,\mathrm{ch}_2]) &= -y^{13} - 3y^{11} - 8y^9 - 10y^7 - 11y^5 - 11y^3 - 11 + \dots
\end{aligned} \tag{5.15}$$

The first and second line are straightforward consequences of the fact that the base curve B is isolated, while the fiber comes in a $\mathbb{P}^1$ family.

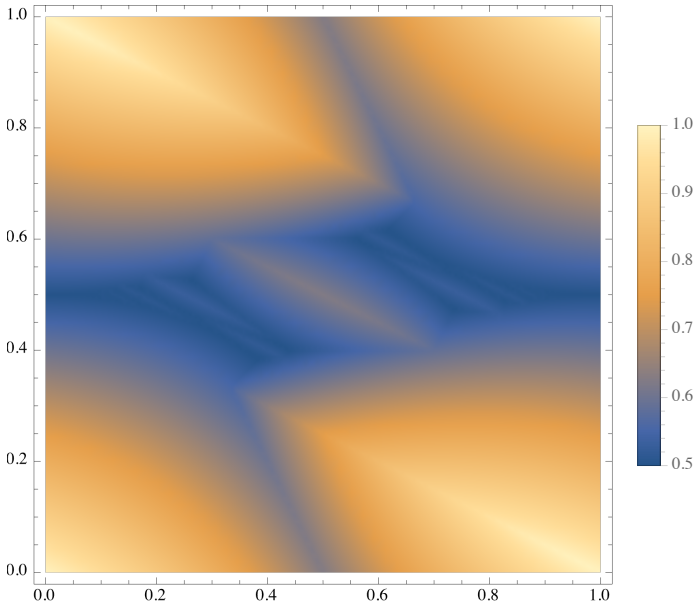


Figure 5.1: Lower bound $\delta_{\mathrm{DLP}}(M,a,b)$ on the discriminant of non-exceptional H_M-stable sheaves for $M = 0$, obtained by retaining exceptional sheaves with rank up to 19. Figure adapted from [67, Fig. 6].

5.2.4 Bridgeland stability conditions

Let C be the derived category of compactly supported coherent sheaves on $K_{\mathbb{F}_1}$. For a bounded complex of sheaves $\mathcal{E} = \cdots \to E_k \to E_{k+1} \dots$, we define the Chern vector as the alternating sum $\gamma(\mathcal{E}) = \sum_k (-1)^k \gamma(E_k)$. The image of the Grothendieck group $K(C)$ under the Chern map is a rank 4 lattice Λ, corresponding physically to the lattice of D4-,D2- and D0-brane charges. The Donaldson-Thomas invariant $\Omega_\sigma(\gamma)$, counting BPS states of fixed charges γ, depends on a choice of stability condition $\sigma = (Z, \mathcal{A})$, consisting of a linear map $Z : \Lambda \to \mathbb{C}$ (the central charge), and an abelian subcategory $\mathcal{A} \subset C$ (the heart) satisfying certain axioms. As shown in [49], the space of stability conditions $\mathrm{Stab}\, C$ is a complex manifold of complex dimension $\mathrm{rk}\,\Lambda = 4$. It admits commuting actions by auto-equivalences $\mathrm{Aut}\, C$ (from the left) and by the universal cover of $GL(2,\mathbb{R})^+$ (from the right). Up to a $\mathbb{C}^\times \subset GL(2,\mathbb{R})^+$ actin, one can assume

that D0-branes (or skyscraper sheaves) have central charge -1, such that the central charge takes the form

$$Z(\gamma) = -rT_D + d_F T_F + d_B T_B - \mathrm{ch}_2 \tag{5.16}$$

The parameters T_B and T_F are complexified Kähler parameters measuring the size of the base and the fiber, such that the complexified Kähler form is $J_{\mathbb{C}} = T_B F + T_F(B+F)$. The Kahler cone condition is $\mathrm{Im}\, T_B, \mathrm{Im}\, T_F > 0$. The parameter T_D corresponds to the central charge of a D4-brane wrapped on S. Under tensoring by $\mathcal{O}(m_F, m_B)$, such that the Chern vector transform as in (5.5), the central charge remains invariant provided

$$(T_F, T_B, T_D) \mapsto (T_F + m_B, T_B + m_F - m_B, T_D + m_F T_F + m_B T_B + m_B m_F - \frac{1}{2} m_B^2) \tag{5.17}$$

Furthermore, it is invariant Under derived duality provided T_F, T_B, T_D are suitably conjugated,

$$Z_{-\overline{T_F}, -\overline{T_B}, \overline{T_D}}(-r, d_F, d_B, -\mathrm{ch}_2) = -\overline{Z_{T_F, T_B, T_D}(r, d_F, d_B, \mathrm{ch}_2)} \tag{5.18}$$

On the physical slice, T_D is determined by T_F and T_B by local mirror symmetry. In the large volume limit, the physical central charge reduces to $Z_{\mathrm{LV}}(\gamma) = -\int_S e^{-J_{\mathbb{C}}} \mathrm{ch}(E)\mathrm{Tod}(S)$, up to exponentially small corrections, leading to a quadratic function of T_F and T_B, (consistent with [37, (4.34)] upon setting $m_1 = T_F, m_2 = T_B$)

$$T_D = \frac{1}{2} T_F^2 + T_B T_F + \frac{1}{6} \tag{5.19}$$

The canonical polarization, such that $\mathrm{Im}\, J_{\mathbb{C}} \propto c_1(S)$, corresponds to $\mathrm{Im}\, T_F = 2\,\mathrm{Im}\, T_B$. In fact, on the physical slice the combination $T_F - 2T_B$ turns out to be directly expressible in terms of the coefficients of the mirror curve (i.e. it has a trivial mirror map), so it is natural to define

$$T_F = 2T + m, \quad T_B = T - m \tag{5.20}$$

such that, in the large volume limit $T \to \mathrm{i}\infty$ the central charge (5.19) becomes

$$Z(\gamma) = -r\left(T(4T+m) - \tfrac{m^2}{2} + \tfrac{1}{6}\right) + d_F(2T+m) + d_B(T-m) - \mathrm{ch}_2 \tag{5.21}$$

In this parametrization, the complexified Kähler form is $J_{\mathbb{C}} = T(3F+2B) + mB$, and its imaginary part is proportional to H_M with $M = \mathrm{Im}\, m / \mathrm{Im}\, T$. Invariance under spectral flow is maintained provided

$$(T, m) \mapsto \left(T + \frac{1}{3} m_F, m + m_B - \frac{2}{3} m_F\right) \tag{5.22}$$

In particular, tensoring with the anticanonical class $\mathcal{O}(3F+2B)$ leaves m invariant but shifts $T \mapsto T+1$. Note that the flop acts by

$$(T, m) \mapsto \left(\frac{2T+m}{3}, \frac{5T-2m}{3}\right) \tag{5.23}$$

leaving the locus $T = m$ invariant.

As in the case of $\mathbb{F}_0$, the construction of stability conditions depends on

$$\delta(s, m) := \inf_E \left[\Delta(E) + \tfrac{1}{4}\left(\tfrac{d_H(E) + 3d_C(E)}{2r(E)} + m\right)^2\right] \tag{5.24}$$

where the infimum runs over slope-stable bundles E with slope $s = \frac{3d_H(E)+d_C(E)}{4r(E)}$, or equivalently $s = \frac{d_B+2d_F}{4r}$. The function $\delta(\mu, m)$ is related to $\delta_{\mathrm{DLP}}(0, a, b)$,

$$\delta(s, m) = \inf_{\frac{a}{4}+\frac{b}{2}=s} \left[\delta_{\mathrm{DLP}}(0, a, b) + \frac{1}{4} \left(\frac{3a-2b}{2} + m \right)^2 \right] \tag{5.25}$$

see Figure 5.2.

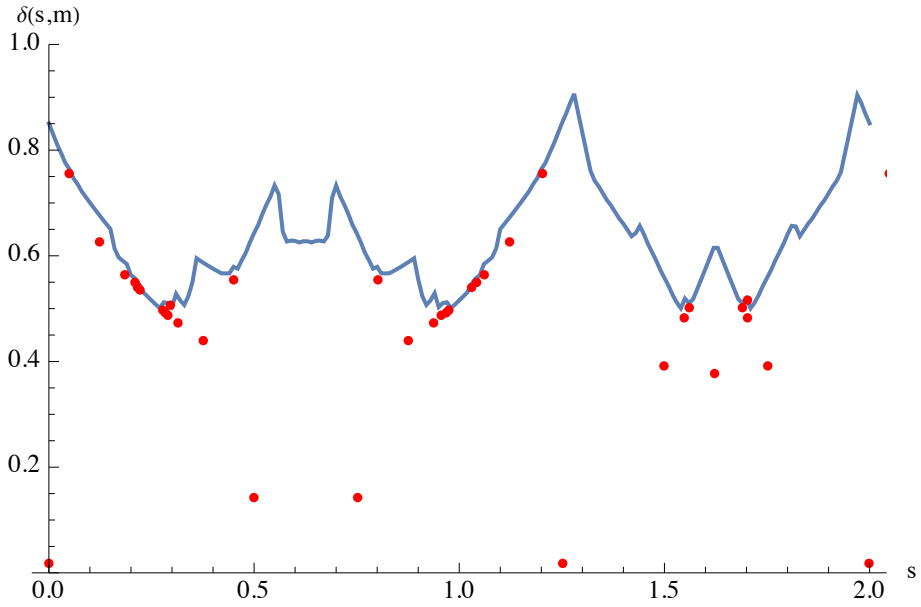


Figure 5.2: Approximate shape of $\delta(s, m)$ for $m = 1/4$. The red dots indicate the corresponding lowest values arising from exceptional stable bundles.

5.3 Quiver descriptions

In this section, we introduce three exceptional collections on $S = \mathbb{F}_1$, which give rise to three equivalent quiver descriptions of the category $\mathcal{C} = D^b \operatorname{Coh}(S)$. As shown in [23, 24], these collections play a distinguished role in studying the stability of line bundles and proving that the moduli space of semi-stable objects are projective. In the next Section, we will show that these quiver descriptions are sufficient to determine all incoming rays in the large volume scattering diagram.

We start by recalling some definitions and basic facts. For a given projective surface S, an exceptional collection is an ordered list $\mathcal{E} = (E^1, \ldots, E^n)$ of coherent sheaves such that

$$\operatorname{Hom}(E^i, E^i) \simeq \mathbb{C}, \quad \operatorname{Ext}^k(E^i, E^j) = 0 \quad \forall k \geq 0, 1 \leq j \leq i \leq r \tag{5.26}$$

In particular, the objects E_i are exceptional sheaves. $\mathcal{E}$ is a *strongly* exceptional collection if for all i, j, $\operatorname{Ext}^k(E^i, E^j) = 0$ whenever $k > 0$. The matrix $S^{ij} = \chi(E^i, E^j)$ is then upper triangular with ones along the diagonal and non-negative entries. It is a *full* exceptional collection if the objects span the K-theory lattice; for a simply connected surface, this implies $r = \chi(S) = b_2(S) + 2$. In order to generate the category $\mathcal{C}$, we need the following stronger condition, sometimes called *cyclicity*: let $\mathcal{H} = \{E^i\}_{i\in\mathbb{Z}}$ be the bi-infinite sequence of coherent sheaves defined by the condition

$E^{i+r} = E^i \otimes K_S^{-1}$. We require that $\mathcal{H}$ forms a *geometric helix*, i.e. that each finite sequence $(E_i, E_{i+1}, \ldots, E_{i+r})$ of length r (called foundation of the helix) is a full exceptional collection and that

$$\forall i < j, \quad \mathrm{Ext}^k(E^i, E^j) = 0 \quad \text{unless} \quad k = 0 \tag{5.27}$$

We then define the dual collection $\mathcal{E}^\vee = (E_1, \ldots, E_r)$ of objects in $D^b\,\mathrm{Coh}(S)$ by

$$E_i = L_{E^1} L_{E^2} \ldots L_{E^{i-1}} E^i \tag{5.28}$$

where $L_E F$ denotes the left mutation of F with respect to E. In particular, it follows that $\chi(E^i, E_j) = \delta^i_j$, and $S_{ij} := \chi(E_j, E_i)$ (equal to the inverse of S^{ij}) is an upper triangular matrix with ones along the diagonal (but other entries may be negative). The dual collection $\mathcal{E}^\vee$ is exceptional but in general not strongly so. Nonetheless, it generates the derived category C, in the sense that the latter is isomorphic to the category of representation $D^b(Q, R)$ of a quiver with potential, where the vertices $i \in Q_0$ correspond to the dual objects E_i, the arrows $(i \to j) \in Q_1$ to the negative entries $S_{ij} < 0$, and the relations R_a to the positive off-diagonal entries. Equivalently, it is isomorphic to the category of representation $D^b(Q', W)$ of a quiver with potential, where the quiver Q' includes additional arrows $a : (j \to i)$ for any off-diagonal positive entry $S_{ij} > 0$, and a (super)potential $W = \sum_a \phi_a R_a$ linear in the additional arrows.

5.3.1 Bridgeland-Stern-Perling collection

The simplest exceptional collections come from geometric helices of invertible sheaves (i.e. rank 1 sheaves with vanishing discriminant). In the case of $S = \mathbb{F}_1$, there is a unique geometric helix, up to translation of the index i and tensoring by $\mathcal{O}(m_F F + m_B B)$ [52, Example 8.6(a), 109]

$$\ldots, \mathcal{O}(-F-B), \mathcal{O}, \mathcal{O}(F), \mathcal{O}(F+B), \mathcal{O}(2F+B), \mathcal{O}(3F+2B), \mathcal{O}(4F+2B), \ldots \tag{5.29}$$

first constructed in [169, p. 100], as quoted in [108, §4.1]. Choosing the foundation

$$C = (\mathcal{O}, \mathcal{O}(F), \mathcal{O}(F+B), \mathcal{O}(2F+B)) = (\mathcal{O}, \mathcal{O}(H-C), \mathcal{O}(H), \mathcal{O}(2H-C)) \tag{5.30}$$

we arrive at the dual Ext-exceptional collection $C^\vee = (E_1, E_2, E_3, E_4)$ with

$$E_1 = \mathcal{O}, \quad E_2 = \mathcal{O}(-F)[1], \quad E_3 = \mathcal{O}(-B)[1], \quad E_4 = \mathcal{O}(-B-F)[2] \tag{5.31}$$

The Chern characters $\gamma^i = \mathrm{ch}\, E^i$, $\gamma_i = \mathrm{ch}\, E_i$ of the corresponding objects are given, in components $[r, d_F, d_B, \mathrm{ch}_2]$ by

$$\begin{array}{lllll} \gamma^1 &=& [1,0,0,0] & \gamma_1 &=& [1,0,0,0] \\ \gamma^2 &=& [1,1,0,0] & \gamma_2 &=& [-1,1,0,0] \\ \gamma^3 &=& \left[1,1,1,\tfrac{1}{2}\right] & \gamma_3 &=& \left[-1,0,1,\tfrac{1}{2}\right] \\ \gamma^4 &=& \left[1,2,1,\tfrac{3}{2}\right] & \gamma_4 &=& \left[1,-1,-1,\tfrac{1}{2}\right] \end{array} \tag{5.32}$$

The resulting quiver is shown in Figure 5.3 (left), accompanied by the superpotentiel [30, 89][3]

$$W = -\Phi_{23}\Phi^1_{34}\Phi^2_{41}\Phi^2_{12} + \Phi_{23}\Phi^2_{34}\Phi^2_{41}\Phi^1_{12} + \Phi_{24}\Phi^1_{41}\Phi^2_{12} - \Phi_{24}\Phi^3_{41}\Phi^1_{12} + \Phi^1_{34}\Phi^3_{41}\Phi_{13} - \Phi^2_{34}\Phi^1_{41}\Phi_{13} \tag{5.33}$$

[3] Note that the same quiver arises for the strong exceptional collection $C_0 = (\mathcal{O}, \mathcal{O}(B), \mathcal{O}(B+F), \mathcal{O}(2B+2F)) = (\mathcal{O}, \mathcal{O}(C), \mathcal{O}(H), \mathcal{O}(2H))$, mentioned in [107, (5.6)] and used in [37, §4.2]. C_0 arises as a foundation of the helix (5.29) tensored by $\mathcal{O}(-F)$. While the quivers are identical, the dimension vectors for fixed Chern character will be different.

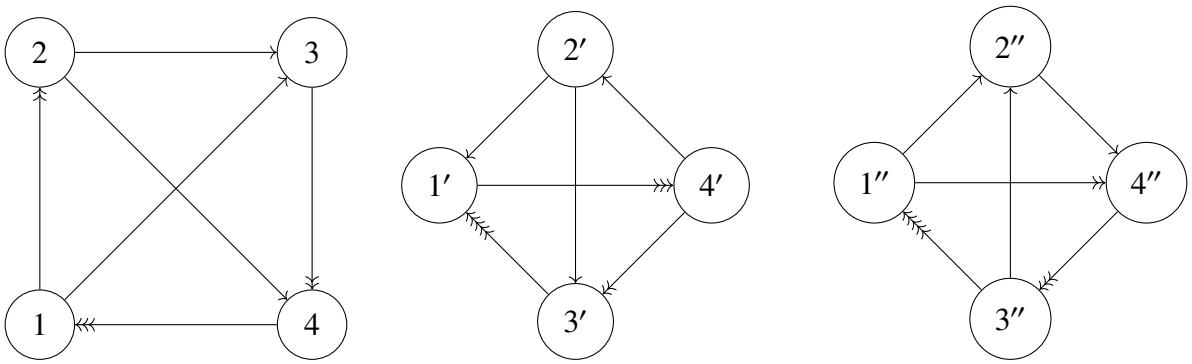


Figure 5.3: Quivers corresponding to the exceptional collections C, C', C''. Observe that the usual quiver for $S = \mathbb{P}^2$ arises by merging the nodes 2 and 3 in the first quiver (a procedure called Higgsing). This is possible because there is only one arrow from 2 to 3,

A general Chern character $\gamma = [r, d_F, d_B, \mathrm{ch}_2]$ decomposes as $\gamma = \sum_i n_i \gamma_i$ with

$$\begin{aligned} n_1 &= d_F + \frac{1}{2} d_B + \mathrm{ch}_2 + r\,, \quad n_2 = d_F - \frac{1}{2} d_B + \mathrm{ch}_2 \\ n_3 &= \frac{1}{2} d_B + \mathrm{ch}_2\,, \quad n_4 = -\frac{1}{2} d_B + \mathrm{ch}_2 \end{aligned} \tag{5.34}$$

In order that the dimension vector be positive for large negative ch_2, we set $N_i = -n_i$. In the chamber $\zeta_1 \leq 0, \zeta_2 \geq 0$, such that the arrows Φ_{12}, Φ_{13} are set to zero, the dimension of the moduli space of stable quiver representations of dimension vector $\vec{N}$ agrees with the expected dimension of the moduli space of stable sheaves with Chern character γ.

Since the kernel of the antisymmetrized Euler form is spanned by the dimension vectors $(1, -1, 2, 0)$ and $(0, 2, -1, 1)$ (which sum up to the D0-brane charge $(1, 1, 1, 1)$), it is natural to restrict the scattering diagram to the two-dimensional slice

$$\zeta_1 - \zeta_2 + 2\zeta_3 = -\frac{1}{2} = 2\zeta_2 - \zeta_3 + \zeta_4 \tag{5.35}$$

We parametrize it as

$$\zeta_1 = v - 2u, \quad \zeta_2 = v - \frac{1}{2}, \quad \zeta_3 = u - \frac{1}{2}, \quad \zeta_4 = u - 2v, \tag{5.36}$$

The geometric rays are then lines

$$(N_3 + N_4 - 2N_1)u + (N_1 + N_2 - 2N_4)v - \frac{1}{2}(N_2 + N_3) = 0 \tag{5.37}$$

oriented along $v_\gamma = (2N_4 - N_1 - N_2, N_3 + N_4 - 2N_1)$. We conjecture that the only initial rays are those associated to γ_i, with BPS index $\Omega_\star(\gamma_i) = 1$, and to the D0-branes $k\delta$ with $\delta = (1, 1, 1, 1)$, with unspecified BPS index $\Omega_\star(k\delta)$.

We find the following trees:

$[r, d_F, d_B, \mathrm{ch}_2]$	$\vec{N}$	Trees	$\Omega_c(\vec{N})$
$[1,0,0,-1]$	$(0,1,1,1)$	$\{\gamma_2,\{\gamma_3,\gamma_4\}\}$ $\{\{\gamma_2,\gamma_4\},\gamma_3\}$	y^2+2+1/y^2
$[1,0,0,-2]$	$(1,2,2,2)$	$\{\{\{\gamma_1,\{\{\gamma_2,\gamma_4\},\gamma_3\},\gamma_2\}\},\gamma_4\},\gamma_3\}$ $\{\{\{\{\gamma_1,\gamma_2\},2\gamma_4\},2\gamma_3\},\gamma_2\}$ $\{(\{\{\{\gamma_1,\gamma_4\},\gamma_3\},\{\{\gamma_2,\gamma_4\},\gamma_3\}\}),\gamma_2\}$	$y^4+3y^2+6+3/y^2+1/y^4$
$[2,0,0,-2]$	$(0,2,2,2)$	$\{2\gamma_2,\{2\gamma_3,2\gamma_4\}\}$ $\{\{\{\{\gamma_2,\gamma_4\},\gamma_3\},\gamma_2\},\{\gamma_3,\gamma_4\}\}$	$-y^5-2y^3-3y-\ldots$
$\left[2,-1,-1,-\frac{3}{2}\right]$	$(1,2,2,1)$	$\{\{2\gamma_2,\{2\gamma_3,\gamma_4\}\},\gamma_1\}$ $\{\{\{2\gamma_2,\{\gamma_3,\gamma_4\}\},\gamma_1\},\gamma_3\}$	$y^4+3y^2+5+\ldots$
$\left[3,-1,-1,-\frac{3}{2}\right]$	$(0,2,2,1)$	$\{2\gamma_2,\{2\gamma_3,\gamma_4\}\}$	y^2+1+1/y^2
$[3,0,0,-3]$	$(0,3,3,3)$	$\{3\gamma_2,\{3\gamma_3,3\gamma_4\}\}$ $\{2\gamma_2,\{\{\{\gamma_2,\gamma_4\},\gamma_3\},\{2\gamma_3,2\gamma_4\}\}\}$	$y^{10}+2y^8+5y^6+8y^4+10y^2+11$
$[3,-2,-2,-1]$	$(1,2,2,0)$	$\{\{2\gamma_2,2\gamma_3\},\gamma_1\}$	y^2+1+1/y^2
$\left[4,-1,-1,-\frac{5}{2}\right]$	$(0,3,3,2)$	$\{3\gamma_2,\{3\gamma_3,2\gamma_4\}\}$ $\{\{2\gamma_2,\{\gamma_3,\gamma_4\}\},\{\gamma_2,\{2\gamma_3,\gamma_4\}\}\}$	$y^6+2y^4+5y^2+6+\ldots$

5.3.2 Arcara-Miles and other mutated collections

In [24, §5.1], the authors introduce two strong exceptional collections, which no longer consist of invertible sheaves. The first one C' is obtained by mutating (5.30) with respect to node 4 (with + sign). This leads to the objects

$$E'^1 = \mathcal{O}, \quad E'^2 = \mathcal{O}(F), \quad E'^3 = \mathcal{O}(F+B), \quad E'^4 = V_2 \tag{5.38}$$

where V_2 is the rank 2 exceptional vector bundle of Chern class $B+F$, with dual objects

$$E'_1 = \mathcal{O}, \quad E'_2 = \mathcal{O}(B)|_B[1], \quad E'_3 = \mathcal{O}(-2F-B)[2], \quad E'_4 = \mathcal{O}(-F-B)[1] \tag{5.39}$$

Their respective Chern vectors are given by

$$\begin{array}{lcl} \gamma'^1 = [1,0,0,0] & & \gamma'_1 = [1,0,0,0] \\ \gamma'^2 = [1,1,0,0] & & \gamma'_2 = \left[0,0,-1,\frac{1}{2}\right] \\ \gamma'^3 = \left[1,1,1,\frac{1}{2}\right] & , & \gamma'_3 = \left[1,-2,-1,\frac{3}{2}\right] \\ \gamma'^4 = \left[2,1,1,-\frac{1}{2}\right] & & \gamma'_4 = \left[-1,1,1,-\frac{1}{2}\right] \end{array} \tag{5.40}$$

and the quiver is shown in Fig. 5.3 (center).

The second strong exceptional collection C'' is obtained from (5.40) by mutating with respect to node 2 (with + sign), leading to the objects

$$E''^1 = \mathcal{O}, \quad E''^2 = \mathcal{O}(B), \quad E''^3 = \mathcal{O}(F+B), \quad E''^4 = V_2 \tag{5.41}$$

with dual objects

$$E''_1 = \mathcal{O}, \quad E''_2 = \mathcal{O}(B)|_B, \quad E''_3 = \mathcal{O}(-2F-B)[2], \quad E''_4 = \mathcal{O}(-F)[1] \tag{5.42}$$

Equivalently, C'' can be obtained from the collection C_0 mentioned in footnote 3 by mutating with respect to node 4 (with + sign). The Chern vectors of the respective objects are

$$\begin{array}{rclcrcl} \gamma''^1 &=& [1,0,0,0] & & \gamma''_1 &=& [1,0,0,0] \\ \gamma''^2 &=& \left[1,0,1,-\frac{1}{2}\right] & & \gamma''_2 &=& \left[0,0,1,-\frac{1}{2}\right] \\ \gamma''^3 &=& \left[1,1,1,\frac{1}{2}\right] & , & \gamma''_3 &=& \left[1,-2,-1,\frac{3}{2}\right] \\ \gamma''^4 &=& \left[2,1,1,-\frac{1}{2}\right] & & \gamma''_4 &=& [-1,1,0,0] \end{array} \tag{5.43}$$

and the quiver is shown in Fig. 5.3 (right). Note that the D0-brane dimension vector is $(1,1,1,2)$ for both C and C'.

5.4 Large volume Scattering diagram

In this section, we study the scattering diagram along the large volume slice, obtained by dropping the constant $1/6$ for the central charge (5.21):

$$Z^{\mathrm{LV}}(\gamma) = -r\left(T(4T+m) - \frac{m^2}{2}\right) + d_F(2T+m) + d_B(T-m) - \mathrm{ch}_2 \tag{5.44}$$

For simplicity, we assume that m is a fixed real parameter, and aim to construct the scattering diagram in the (s,t) half-plane, where $T = s + \mathrm{i}t$. By spectral flow invariance, we may restrict m to a width 1 interval, for example $-1/3 < m < 2/3$. Moreover, the diagram is periodic under $s \mapsto s+1$, with a suitable relabelling of the charges. As in previous studies, there is no loss in assuming that the phase $\psi = 0$, since other phases (distinct from $\pm\pi/2$) can be reached by transforming

$$(s,t) \mapsto \left(s - t\tan\psi, \frac{t}{\cos\psi}\right) \tag{5.45}$$

Note that this only holds for real m, and on the large volume slice. For $\psi = 0$, geometric rays for $r \neq 0$ are branches of hyperbolae centered at $s = \frac{d_F+2d_B-mr}{8r}$ on the real axis, or for $r = 0$, vertical rays at $s = \frac{\mathrm{ch}_2+m(d_F-d_B)}{d_F+2d_B}$. In particular, for pure D4-branes with flux, the geometric ray $\mathcal{R}(\mathcal{O}(d_F,d_B))$ starts at $s = \min(\frac{1}{4}(2d_F - d_B + m), \frac{1}{2}(d_B - m))$ on the real axis and bends to the left, while $\mathcal{R}(\mathcal{O}(d_F,d_B)[1])$ starts at $s = \max(\frac{1}{4}(2d_F - d_B + m), \frac{1}{2}(d_B - m))$ and bends to the right. Importantly, in contrast to the local $\mathbb{P}^2$ and local $\mathbb{F}_0$ cases studied in [47, 132], the structure sheaf and its shifts are *not* in general stable for any (s,t), so the actual ray may not intersect the real axis.

We shall also be interested in the diagram in affine (x,y) coordinates defined (in analogy to [45]) by

$$x = \frac{\mathrm{Re}(e^{-\mathrm{i}\psi}T}{\cos\psi} = s, \quad y = -\frac{\mathrm{Re}(e^{-\mathrm{i}\psi}T_D}{\cos\psi}, \quad \mu = \frac{\mathrm{Re}(e^{-\mathrm{i}\psi}m)}{\cos\psi} = m \tag{5.46}$$

where the upper half-plane $t > 0$ maps to the region above the parabola

$$P = \{(x,y), y = -4x^2 - \mu x + \frac{1}{2}\mu^2\} \tag{5.47}$$

In these coordinates, all rays are straight segments

$$ry + x(d_B + 2d_F) - \mathrm{ch}_2 + \mu(d_F - d_B) = 0 \tag{5.48}$$

where $\mu = m$ when m is real, the case of interest here. In order to regulate the scattering diagram (both in (s,t) and (x,y) plane), we use the cost function

$$\varphi_s(\gamma) = \frac{\mathrm{Im}\, Z^{\mathrm{LV}}(\gamma)}{\mathrm{Im}\, T} = d_B + 2d_F - r(8s+m) \tag{5.49}$$

which coincides with $\mathrm{Im}\, Z^{\mathrm{LV}}/\mathrm{Im}\, T$, and increases along the rays (with the orientation pointing away from the real axis).

In order to determine the structure of the initial rays along the boundary at $t = 0$, we can use the Ext-exceptional collections C, C', C'' introduced in Eqs. (5.32), (5.40), (5.43) of the previous Section to rule out incoming rays from all but a finite set of points (in a finite width integral). In particular, assuming that $3m$ is not an integer, we find that for any fixed integer $m_F \in \mathbb{Z}$, there is a unique integer m_B such that the domain of validity of the collection $C \otimes \mathcal{O}(m_F, m_B)$ includes an open integral on the axis $t = 0$:

$$C: \qquad m_B = \left\lceil \frac{2m_F - 1}{3} + m \right\rceil \tag{5.50}$$

$$C': \qquad m_B = \left\lceil \frac{2m_F - 3}{3} + m \right\rceil, \tag{5.51}$$

$$C'': \qquad m_B = \left\lceil \frac{2m_F - 1}{3} + m \right\rceil. \tag{5.52}$$

In this way, we find that the full real axis is covered by the quiver descriptions listed in Table 5.1 (see Figures 5.4, 5.5, 5.6 for their domain of validity extending into the upper half-plane $t > 0$). We conclude that the only rays entering through the real axis are those listed on the last column of Table 5.1. In particular, in sharp contrast to the local $\mathbb{P}^2$ and local $\mathbb{F}_0$ case, the pure D4-branes and anti-D4-branes (in other words, the structure sheaf $\mathcal{O}(d_F, d_B)$ and its homological shift $\mathcal{O}(d_F, d_B)[1]$) are in general *not* stable throughout the upper half plane $t > 0$, while the D2-D0 branes with charge $[0,1,0,n]$ and $\pm[0,0,1,n+\frac{1}{2}]$ for some $n \in \mathbb{Z}$/ *are* stable throughout the upper half plane. Indeed, as shown in [23], most of pure D4 and anti D4-branes decay precisely by emitting a D2-D0 brane with charge $[0,0,1,n+\frac{1}{2}]$. This is consistent with their index being 1 at large t, since the latter D2-D0 brane, associated with the curve B with negative self-intersection, also has unit DT invariant $\mathrm{GV}^{(0)}_{(0,1)} = 1$. This can be seen from the trees contributing the corresponding indices, displayed in Table 5.2.

In order to understand the origin of the infinite family of rays entering at $t = 0$, we can use the affine coordinates (x,y) and extend the scattering diagram below the parabola P. In this way we find

i) the infinite bunches of rays emerging at $s \in -\frac{m}{2} + \mathbb{Z}$ originate from the scattering of a pair $\mathcal{O}(d_F, d_B), \mathcal{O}(d_F - 1, d_B)[1]$ of pure (anti) D4-branes with Dirac product ± 2.

ii) The corresponding bound states $k\mathcal{O}(d_F, d_B) + (k+1)\mathcal{O}(d_F - 1, d_B)[1]$ and $(k+1)\mathcal{O}(d_F, d_B) + k\mathcal{O}(d_F - 1, d_B)[1]$ account for the rays $\mathcal{O}(d_F + k, d_B)$ and $\mathcal{O}(d_F - k - 1, d_B)[1]$, while the D4-anti D4 bound state $\mathcal{O}(d_F, d_B) + \mathcal{O}(d_F - 1, d_B)[1]$ accounts for the D2-D0 bound state $\mathrm{GV}(1, 0, d_B)$ with index $\mathrm{GV}^{(0)}_{(1,0)} = -y - 1/y$

iii) In contrast, the spherical D2-D0 branes $\mathrm{GV}(0, 1, n + \frac{1}{2})$ entering at $s = n \in \mathbb{Z}$ arise from the scattering of two rays with Dirac product ± 1 intersectinhg below the parabola P.

As a result, all rays emerging at $t = 0$ arise from the scattering of D4-branes and anti D4-branes associated to the helix (5.29), or its tensor product with $\mathcal{O}(F + B)$ ($0 < m < \frac{1}{3}$) or with $\mathcal{O}(-F)$ ($\frac{1}{3} < m < \frac{2}{3}$):

$$\left|\begin{array}{c|l} -\frac{1}{3} < m < 0 & \dots, \mathcal{O}(-1,-1), \mathcal{O}(0,0), \mathcal{O}(1,0), \mathcal{O}(1,1), \mathcal{O}(2,1), \mathcal{O}(3,2), \dots \\ 0 < m < \frac{1}{3} & \dots, \mathcal{O}(-1,0), \mathcal{O}(0,0), \mathcal{O}(1,1), \mathcal{O}(2,1), \mathcal{O}(2,2), \mathcal{O}(3,2), \dots \\ \frac{1}{3} < m < \frac{2}{3} & \dots, \mathcal{O}(-2,-1), \mathcal{O}(0,0), \mathcal{O}(0,1), \mathcal{O}(1,1), \mathcal{O}(2,2), \mathcal{O}(3,2), \dots \end{array}\right| \tag{5.53}$$

Dirac products of consecutive elements of the helix are $\kappa = 1, 2, 3, 2, \dots$. Collisions with $\kappa = 1, 2, 3$ occur below, at and above the parabola P, respectively, reproducing the above list of rays entering at $t = 0$ (see Figure 5.7). The initial point at which a pair $\pm\mathcal{O}(d_B, d_F)$ in the helix is emitted is irrelevant, provided it lies along the segment joining two consecutive intersections. For $|m|$ small enough, it can be chosen to be the point where the cost function (5.49) vanishes. In Section 5.5 we shall determine the exact location for the physical slice, corresponding to the values of (x, y) where the corresponding BPS state becomes massless.

m	$s_- < s < s_+$	Quiver	Incoming rays at s_+
$-\frac{1}{3} < m < 0$	$\frac{m-1}{4} < s < \frac{m}{4}$	C	$\mathcal{O}(0,0)$
	$\frac{m}{4} < s < -\frac{m}{2}$	$C'' \otimes \mathcal{O}(1,0)$	$\mathcal{O}(k+1,0), \mathcal{O}(-k,0)[1], \mathrm{GV}(1,0,0)$
	$-\frac{m}{2} < s < \frac{m+1}{4}$	$C \otimes \mathcal{O}(1,1)$	$\mathcal{O}(1,1)$
	$\frac{m+1}{4} < s < m + \frac{1}{2}$	$C'' \otimes \mathcal{O}(2,1)$	$\mathrm{GV}(0,1,\frac{1}{2})$
	$m + \frac{1}{2} < s < \frac{m+2}{4}$	$C' \otimes \mathcal{O}(2,1)$	$\mathcal{O}(1,0)[1]$
	$\frac{m+2}{4} < s < \frac{1-m}{2}$	$C \otimes \mathcal{O}(2,1)$	$\mathcal{O}(k+2,1), \mathcal{O}(1-k,1)[1], \mathrm{GV}(1,0,1)$
	$\frac{1-m}{2} < s < \frac{m+3}{4}$	$C' \otimes \mathcal{O}(3,2)$	$\mathcal{O}(2,1)[1]$
$0 < m < \frac{1}{3}$	$-\frac{m}{2} < s < \frac{m}{4}$	$C' \otimes O(1,1)$	$\mathcal{O}(0,0)[1]$
	$\frac{m}{4} < s < \frac{m+1}{4}$	$C \otimes O(1,1)$	$\mathcal{O}(1,1)$
	$\frac{m+1}{4} < s < \frac{1-m}{2}$	$C'' \otimes O(2,1)$	$\mathcal{O}(k+2,1), \mathcal{O}(1-k,1)[1], \mathrm{GV}(1,0,1)$
	$\frac{1-m}{2} < s < \frac{m+2}{4}$	$C \otimes O(2,2)$	$\mathcal{O}(2,2)$
	$\frac{m+2}{4} < s < m + \frac{1}{2}$	$C'' \otimes O(3,2)$	$\mathrm{GV}(0,1,\frac{1}{2})$
	$m + \frac{1}{2} < s < \frac{m+3}{4}$	$C' \otimes O(3,2)$	$\mathcal{O}(2,1)[1]$
	$\frac{m+3}{4} < s < 1 - \frac{m}{2}$	$C \otimes O(3,2)$	$\mathcal{O}(k+3,2), \mathcal{O}(2-k,2)[1], \mathrm{GV}(1,0,2)$
$\frac{1}{3} < m < \frac{2}{3}$	$-\frac{m}{2} < s < \frac{m-1}{4}$	$C \otimes \mathcal{O}(0,1)$	$\mathcal{O}(0,1)$
	$\frac{m-1}{4} < s < m - \frac{1}{2}$	$C'' \otimes \mathcal{O}(1,1)$	$\mathrm{GV}(0,1,-\frac{1}{2})$
	$m - \frac{1}{2} < s < \frac{m}{4}$	$C' \otimes \mathcal{O}(1,1)$	$\mathcal{O}(0,0)[1]$
	$\frac{m}{4} < s < \frac{1-m}{2}$	$C \otimes \mathcal{O}(1,1)$	$\mathcal{O}(1+k,1), \mathcal{O}(-k,1)[1], \mathrm{GV}(1,0,1)$
	$\frac{1-m}{2} < s < \frac{m+1}{4}$	$C' \otimes \mathcal{O}(2,2)$	$\mathcal{O}(1,1)[1]$
	$\frac{m+1}{4} < s < \frac{m+2}{4}$	$C \otimes \mathcal{O}(2,2)$	$\mathcal{O}(2,2)$
	$\frac{m+2}{4} < s < 1 - \frac{m}{2}$	$C'' \otimes \mathcal{O}(3,2)$	$\mathcal{O}(k+3,2), \mathcal{O}(2-k,2)[1], \mathrm{GV}(1,0,2)$

Table 5.1: Quiver descriptions at $t = 0$, obtained by tensoring one of the Ext-collections C (5.32), C' (5.40) and C'' (5.43) with a suitable line bundle $\mathcal{O}(m_F, m_B)$. When both a D4-brane $\mathcal{O}(d_F, d_B)$ and an anti D4-brane $\mathcal{O}(d'_F, d'_B)[1]$ with $|\langle\gamma, \gamma'\rangle| = 2$ enter the boundary at the same point, they produce an infinite set of rays, indexed by $k \in \mathbb{N}$. Quiver descriptions outside the range $s_{\min} < s < s_{\min} + 1$ covered in the table can be obtained by tensoring with $\mathcal{O}(3k, 2k)$.

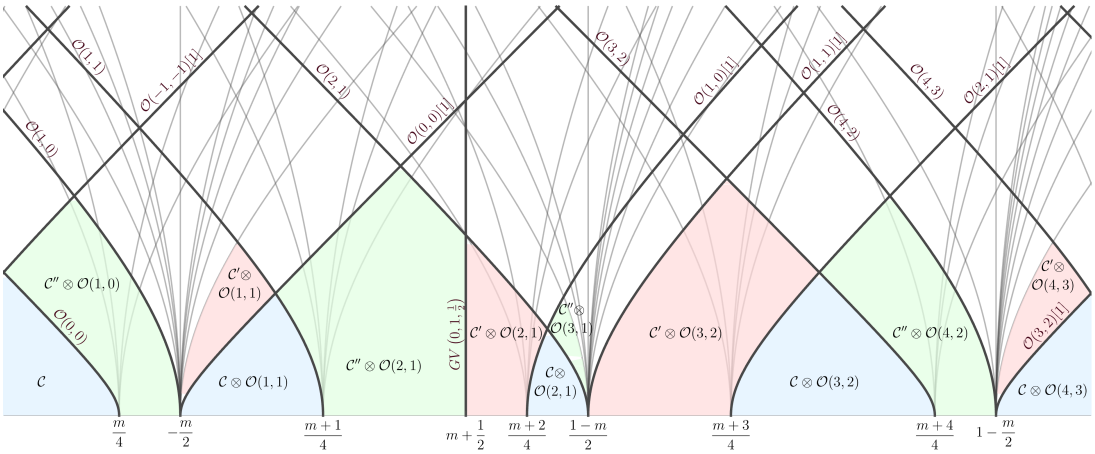


Figure 5.4: Domains of validy of the quiver descriptions covering the real axis, assuming that $-\frac{1}{3} < m < 0$ (plotted here for $m = -\frac{1}{10}$). Quivers obtain by tensoring the Ext-exceptional collections C (5.32), C' (5.40) and C'' (5.43) with a suitable line bundle $O(m_F, m_B)$ are plotted in blue, red and green, respectively. Grey lines correspond to the geometric rays for $O(d_F, d_B)$ and $O(d_F, d_B)[1]$. Those which lie inside quiver domains must necessarily decay before reaching this domain. Initial rays coming from below the parabola are plotted in thick black lines.

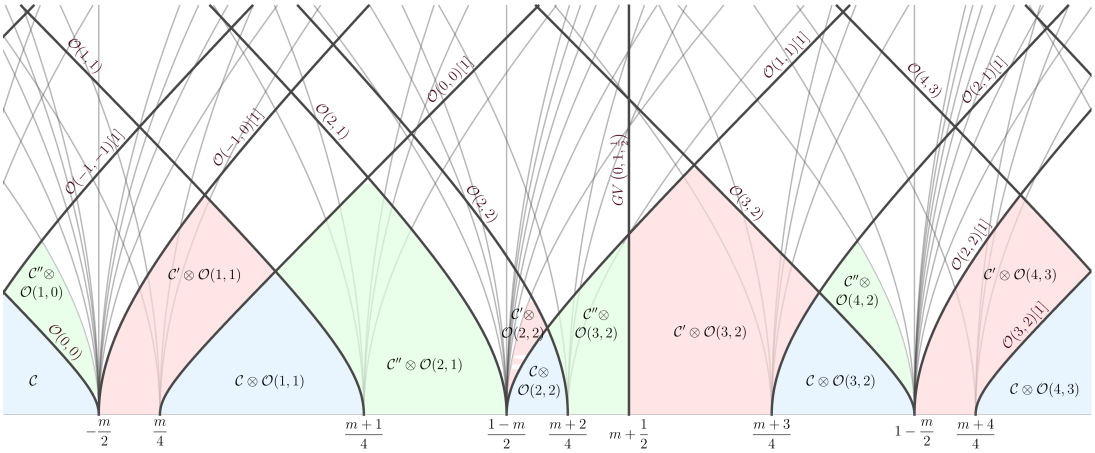


Figure 5.5: Similar as Figure 5.4, now assuming $0 < m < \frac{1}{3}$ (plotted for $m = \frac{1}{10}$).

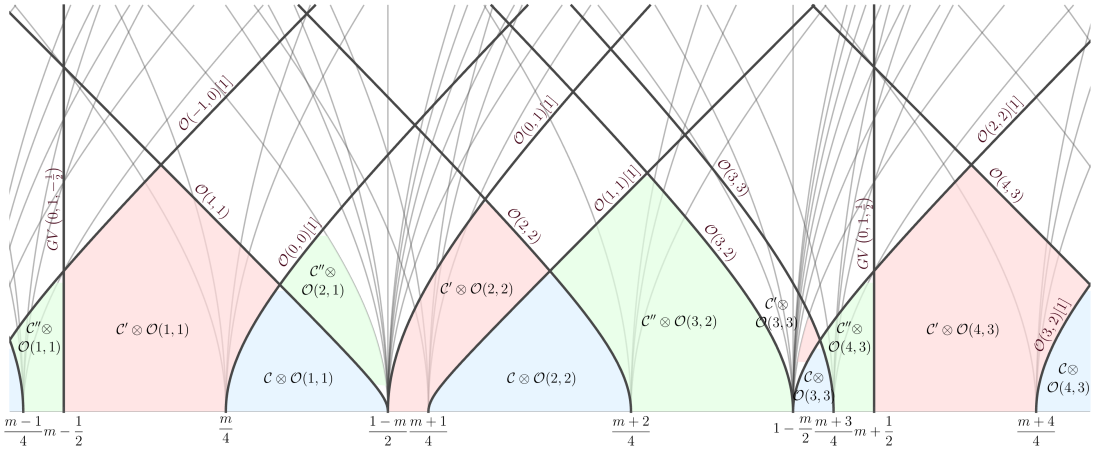


Figure 5.6: Similar as Figure 5.4, now assuming $\frac{1}{3} < m < \frac{2}{3}$ (plotted for $m = \frac{2}{5}$).

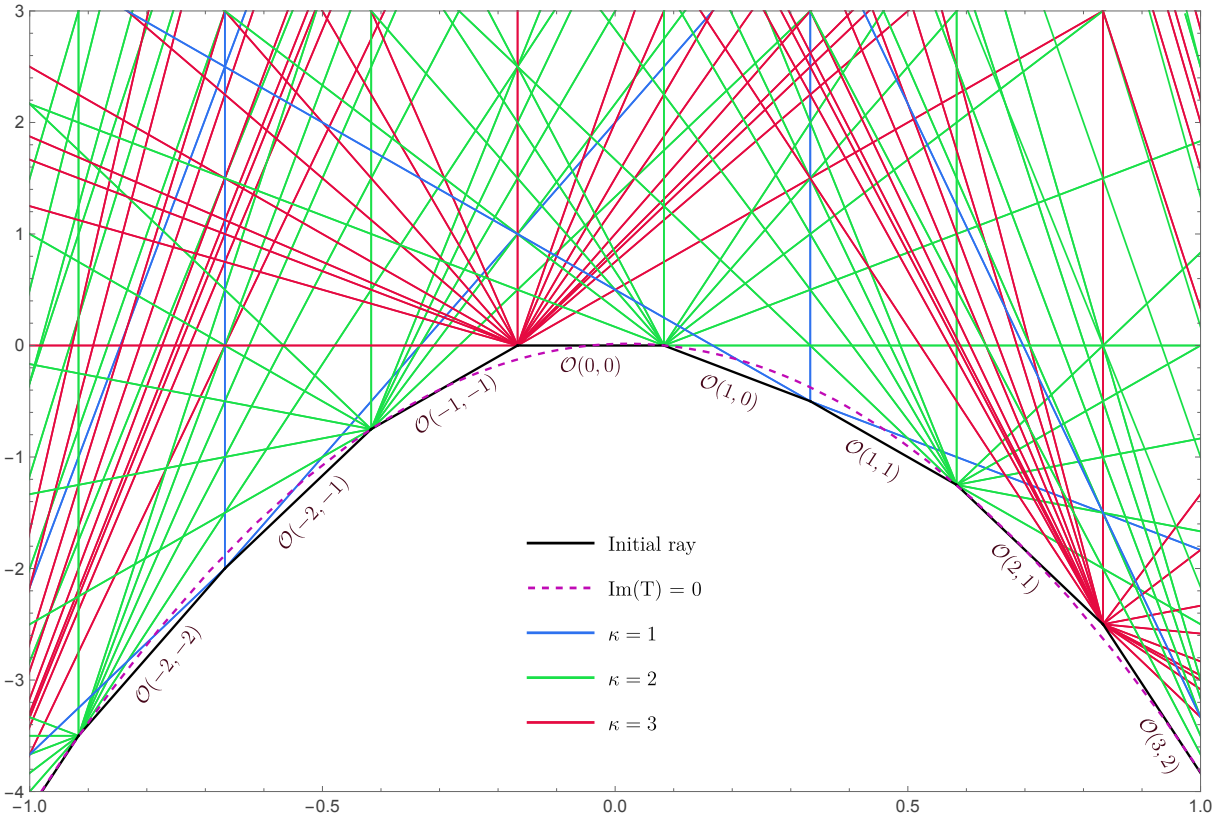


Figure 5.7: Initial and secondary rays in affine coordinates (x, y) for $-\frac{1}{3} < m < 0$ (here drawn for $m = -\frac{1}{6}$). Secondary rays originating from collisions with Dirac product $\kappa = 1, 2, 3$ are shown in blue, green, red, respectively. Collisions with $\kappa = 1, 2, 3$ occur below, at and above the parabola, respectively.

Charge (FB)	**Charge (HC)**	**Contributing tree(s)**	**Index $\Omega_H(y)$** (nonneg. part)
$[0,0,1,\frac{1}{2}]$	$[0,0,1,\frac{1}{2}]$	$\{\mathcal{O}(1,0)[1],\ \mathcal{O}(1,1)\}$	1
$[0,1,0,0]$	$[0,1,-1,0]$	$\{\mathcal{O}(0,0)[1],\ \mathcal{O}(1,0)\}$	$-y$
$[0,1,1,\frac{1}{2}]$	$[0,1,0,\frac{1}{2}]$	$\{\mathcal{O}(0,0)[1],\ \mathcal{O}(1,1)\}$	y^2+1
$[0,2,1,\frac{1}{2}]$	$[0,2,-1,\frac{1}{2}]$	$\{\mathcal{O}(1,1),\ \{2\,\mathcal{O}(0,0)[1],\ \mathcal{O}(1,0)\}\}$	y^4+y^2+1
$[0,2,2,0]$	$[0,2,0,0]$	$\{\mathcal{O}(1,1),\ \mathcal{O}(-1,-1)[1]\}$	$-y^5-y^3-y$
$[0,3,2,0]$	$[0,3,-1,0]$	$\{\mathcal{O}(-1,-1)[1],\ \{\mathcal{O}(1,1),\ \{\mathcal{O}(0,0)[1],\ \mathcal{O}(1,0)\}\}\}$	$-y^9-3y^7-4y^5-4y^3-4y$
$[0,3,3,\frac{1}{2}]$	$[0,3,0,\frac{1}{2}]$	$\{\mathcal{O}(-1,-1)[1],\ \{\mathcal{O}(0,0)[1],\ 2\,\mathcal{O}(1,1)\}\}$	$y^{10}+2y^8+3y^6+3y^4+3y^2+3$
$[0,4,2,0]$	$[0,4,-2,0]$	① $\{\mathcal{O}(-2,-1)[1],\ \mathcal{O}(2,1)\}$ ② $\{\mathcal{O}(-1,-1)[1],\ \{\mathcal{O}(1,1),\ \{2\,\mathcal{O}(0,0)[1],\ 2\,\mathcal{O}(1,0)\}\}\}$	$-y^{13}-3y^{11}-8y^9-10y^7-11y^5-11y^3-11y$
$[1,2,2,2]$	$[1,2,0,2]$	$\{\mathcal{O}(2,1),\ \{\mathcal{O}(1,0)[1],\ \mathcal{O}(1,1)\}\}$	1
$[1,0,1,-\frac{1}{2}]$	$[1,0,1,-\frac{1}{2}]$	$\{\mathcal{O}(0,0),\ \{\mathcal{O}(-2,-2)[1],\ \mathcal{O}(-2,-1)\}\}$	1
$[1,1,2,0]$	$[1,1,1,0]$	$\{\mathcal{O}(1,1),\ \{\mathcal{O}(-2,-2)[1],\ \mathcal{O}(-2,-1)\}\}$	1
$[1,2,3,\frac{3}{2}]$	$[1,2,1,\frac{3}{2}]$	$\{\{\mathcal{O}(-2,-2)[1],\ \mathcal{O}(-2,-1)\},$ $\{\mathcal{O}(2,1),\ \{\mathcal{O}(1,0)[1],\ \mathcal{O}(1,1)\}\}\}$	1
$-[1,0,-1,-\frac{1}{2}]$	$-[1,0,-1,-\frac{1}{2}]$	$\{\mathcal{O}(0,0)[1],\ \{\mathcal{O}(1,0)[1],\ \mathcal{O}(1,1)\}\}$	1
$-[1,2,1,\frac{3}{2}]$	$-[1,2,1,\frac{3}{2}]$	$\{\mathcal{O}(2,1)[1]\}$	1
$[1,0,0,-1]$	$[1,0,0,-1]$	① $\{\mathcal{O}(-2,-2)[1],\ 2\,\mathcal{O}(-1,-1)\}$ ② $\{\{\mathcal{O}(-2,-2)[1],\ \mathcal{O}(-2,-1)\},$ $\{\mathcal{O}(-2,-1)[1],\ 2\,\mathcal{O}(-1,-1)\}\}$	y^2+2
$[1,0,0,-2]$	$[1,0,0,-2]$	① $\{\mathcal{O}(-1,-1),\ \{\mathcal{O}(-3,-2)[1],\ \mathcal{O}(-2,-1)\}\}$ ② $\{\{\mathcal{O}(-5,-4)[1],\ \mathcal{O}(-5,-3)\},$ $\{\mathcal{O}(-2,-1)[1],\ 2\,\mathcal{O}(-1,-1)\}\}$ ③ $\{\{\mathcal{O}(-3,-2)[1],\ \mathcal{O}(-2,-2)\},$ $\{\mathcal{O}(-1,-1),\ \{\mathcal{O}(-2,-2)[1],\ \mathcal{O}(-2,-1)\}\}\}$	y^4+3y^2+6
$[2,1,1,-\frac{1}{2}]$	$[2,1,0,-\frac{1}{2}]$	$\{3\,\mathcal{O}(0,0),\ \mathcal{O}(-1,-1)[1]\}$	1
$[2,1,0,-1]$	$[2,1,-1,-1]$	$\{2\,\mathcal{O}(0,0),\ \{\mathcal{O}(-2,-1)[1],\ \mathcal{O}(-1,-1)\}\}$	$-y$

Table 5.2: Charges, contributing trees for $m=-\frac{1}{10}$, and the nonnegative-power part of the refined index $\Omega_H(y)$ (the full Laurent polynomial is symmetric under $y\leftrightarrow y^{-1}$). The rank 0 entries are consistent with the refined D2-D0 indices in (5.15).

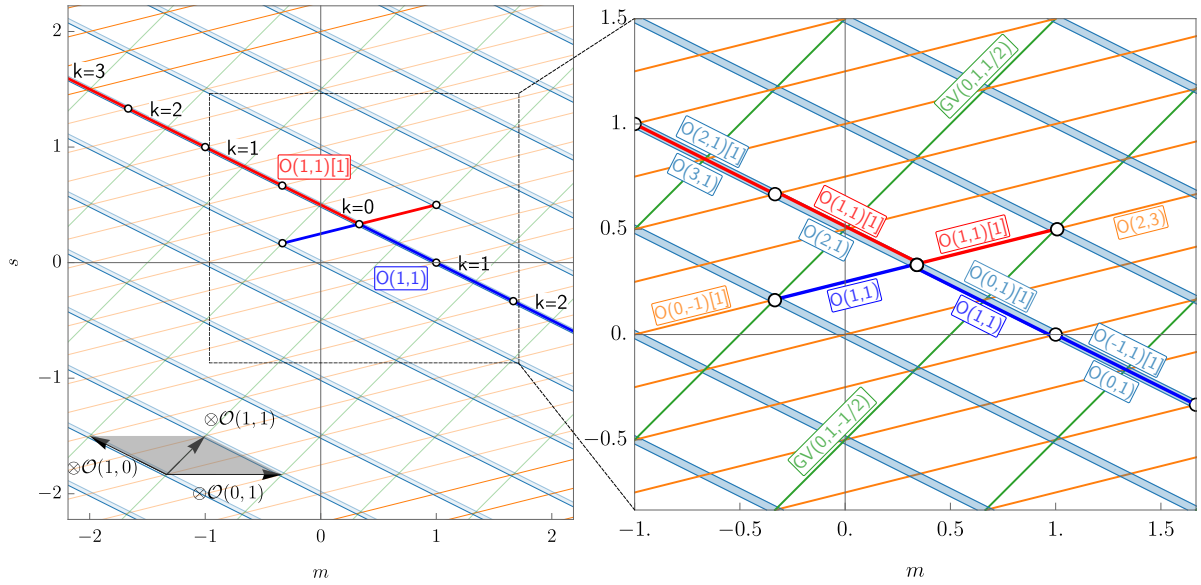


Figure 5.8: Initial rays in the (m, s) plane at the boundary $t = 0$ of the large volume slice. The structure sheaf tensored with $\mathcal{O}(1,1)$ is stable only for $m > -\frac{1}{3}$ (thick blue line), while the correspond anti-brane is stable only for $m < 1$ (in red). In the range $-\frac{1}{3} < m < 1$, both objects are initial rays of the scattering diagram below the parabola; outside this range, they are level-k bound states of the Kronecker quiver K_2 associated to the same initial rays, shown in light blue in plot on the left and labelled in the magnified plot on the right. The remaining initial rays are shown in orange and green.

5.5 Π-stability slice

5.5.1 Mirror curve

The canonical bundle over $\mathbb{F}_1$ is described by the following toric data,

$$\left.\begin{array}{ccc|cc} 0 & 0 & 1 & -2 & -1 \\ 1 & 0 & 1 & 1 & 0 \\ -1 & -1 & 1 & 0 & 1 \\ -1 & 0 & 1 & 1 & -1 \\ 0 & 1 & 1 & 0 & 1 \end{array}\right. \tag{5.54}$$

The mirror curve in $\mathbb{C}^\times \times \mathbb{C}^\times$ then takes the form

$$H(e^x, e^p; z_1, z_2) = 1 + e^x + e^p + z_1\, e^{-x} + z_1 z_2\, e^{-x-p}\,. \tag{5.55}$$

After choosing coordinates $y_1 = e^x,\ y_2 = e^p$ and rescaling the equation we arrive at

$$H(y_{1,2}; z_{1,2}) = y_1^2 y_2 + y_1 y_2^2 + y_1 y_2 + z_1 \cdot y_2 + z_1 z_2 \cdot y_1^2\,. \tag{5.56}$$

This can be mapped to into the Weierstrass form

$$Y^2 = 4X^3 - g_2 X - g_3\,, \tag{5.57}$$

with coefficients given by

$$\begin{aligned} g_2 =& 108(1 - 8z_1 + 16z_1^2 + 24z_1 z_2)\,, \\ g_3 =& -216(1 - 12z_1 + 48z_1^2 - 64z_1^3 + 36z_1 z_2 - 144z_1^2 z_2 + 216z_1^2 z_2^2)\,, \end{aligned} \tag{5.58}$$

and the discriminant takes the form

$$\Delta = g_2^3 - 27g_3^2 = 2^{12} \cdot 3^{12} \cdot z_1^3 z_2^2 \left[(1-4z_1)^2 - z_2(1-36z_1+27z_1z_2)\right] \tag{5.59}$$

such that the Klein invariant[4] takes the form [105, (6.4)]

$$J(z_1,z_2) = 1728\frac{g_2^3}{\Delta} = \frac{\left[(1-4z_1)^2+24z_1z_2\right]^3}{z_1^3z_2^2\left[(1-4z_1)^2 - z_2(1-36z_1+27z_1z_2)\right]} \tag{5.60}$$

The conifold locus $C = \{(1-4z_1)^2 - z_2(1-36z_1+27z_1z_2) = 0\}$ intersects $z_1 = 0$ at $z_2 = 1$ normally, and is tangent to $z_2 = 0$ at $z_1 = 1/4$. It will be useful to define

$$z_1 = \lambda u^2, \quad z_2 = -\frac{u}{\lambda} \quad \leftrightarrow \quad u = -(z_1z_2)^{1/3}, \quad \lambda = \frac{z_1^{1/3}}{z_2^{2/3}} \tag{5.61}$$

and alternative coordinates,

$$\mathrm{u} = u/\lambda = -z_2, \quad \ell = \lambda^3 = \frac{z_1}{z_2^2} \tag{5.62}$$

such that (5.60) becomes

$$J(\mathrm{u},\ell) = \frac{\left(1-8\ell\mathrm{u}^2-24\mathrm{u}^3+16\ell^2 r u^4\right)^3}{\ell^3\mathrm{u}^8\left(1+\mathrm{u}-8\ell\mathrm{u}^2-36\ell\mathrm{u}^3+\ell\left(16\ell-27\right)\mathrm{u}^4\right)} \tag{5.63}$$

$$= \frac{Q_4^3}{\ell^3\mathrm{u}^8\Delta_4} = 1728 + \frac{Q_6^2}{\ell^3\mathrm{u}^8\Delta_4} \tag{5.64}$$

where

$$\begin{aligned}
\Delta_4 =& 1+\mathrm{u}-8\ell\mathrm{u}^2-36\ell\mathrm{u}^3+\ell\left(16\ell-27\right)\mathrm{u}^4\\
Q_4 =& 1-8\ell\mathrm{u}^2-24\mathrm{u}^3+16\ell^2\mathrm{u}^4\\
Q_6 =& 1-12\mathrm{u}^2\ell-36\mathrm{u}^3\ell+48\mathrm{u}^4\ell^2+144\mathrm{u}^5\ell^2+\mathrm{u}^6\ell^2(216-64\ell)
\end{aligned} \tag{5.65}$$

For generic λ, the discriminant $\Delta = \ell^3\mathrm{u}^8\Delta_4$ has 4 distinct roots at finite u and an order 8 root at $\mathrm{u} = 0$, so the elliptic fibration is of Kodaira type $I_8, 4I_1$ in the notations of [65]. The equation $J(\mathrm{u},\ell) = j$ is polynomial of degree 12 in u, with discriminant proportional to

$$(27+256\ell)^3 j^8 (j-1728)^6\left[(27+256\ell)(243+256\ell)^3 - 2^{24}\ell^3 j\right] \tag{5.66}$$

Generically, u is a 12:1 covering[5] of the j-line with ramification profile $1^4, 8$ at $j = \infty$, 3^4 at the $\mathbb{Z}_3$ orbifold point $j = 0$ (i.e. 4 pairs of multiplicity 3 roots, corresponding to the zeros of Q_4), 2^6 at the $\mathbb{Z}_2$ orbifold point $j = 1728$ (i.e. 6 pairs of multiplicity 2 roots, corresponding to the zeros of Q_6), and $1^{10}2$ at $j = j_B$ with

$$j_B = \frac{(27+256\ell)(243+256\ell)^3}{2^{24}\ell^3} \tag{5.67}$$

[4] defined such that $J(\tau) = q^{-1} + 744 + 196884q + \ldots$ such that $J(\mathrm{i}) = 1728, J(e^{2\pi\mathrm{i}/3}) = 0$.

[5] Note that the ramification structure of the u-line over the j-line satisfies the Riemann-Hurwitz formula $\chi(S') = N\chi(S) - \sum_{P\in S'}(e_P - 1)$ for the Euler characteristic of an $N:1$ cover $S' \to S$, where e_P is the ramification index at point P. Here, $\chi(S) = \chi(S') = 2 = 24 - (7+1)\times(2-1) - 4\times(3-1) - 1\times(8-1)$.

The corresponding double root is at $\mathrm{u} = -\frac{8}{9}$, around which

$$J(\mathrm{u},\ell) = j_B - \frac{3^8(256\ell+243)^2\left(65536\ell^2-124416\ell-19683\right)}{2^{28}\ell^3(256\ell+27)}\left(\mathrm{u}+\tfrac{8}{9}\right)^2 + O\left(\mathrm{u}+\tfrac{8}{9}\right)^3 \quad (5.68)$$

As we shall see later, the point $\mathrm{u} = -\frac{8}{9}$ is an apparent singularity of the Picard-Fuchs equation, where the solutions are actually regular.

In contrast, for $\ell = -\frac{27}{256}$, the degree of the equation $J(\mathrm{u},\ell) = j$ drops to 10, with Δ_4, Q_4 and Q_6 all acquiring a common factor $9\mathrm{u}+8$ (of multiplicity 2 in the case of Δ_4):

$$\begin{aligned}
\Delta_4 =& \frac{1}{4096}(9\mathrm{u}+8)^2\left(153\mathrm{u}^2-80\mathrm{u}+64\right)\\
Q_4 =& \frac{1}{4096}(9\mathrm{u}+8)\left(81\mathrm{u}^3+1080\mathrm{u}^2-576\mathrm{u}+512\right)\\
Q_6 =& \frac{1}{262144}(9\mathrm{u}+8)\left(72171\mathrm{u}^5-17496\mathrm{u}^4+31104\mathrm{u}^3+82944\mathrm{u}^2-36864\mathrm{u}+32768\right)
\end{aligned} \quad (5.69)$$

In particular, the elliptic fibration is now of type $I_8, 2I_1, II$, with the fiber II corresponds to the Argyres-Douglas theory H_0, with an elliptic point of order 3 [65, §5.2]. The u-line is now a 10:1 covering[6] of the j-line with ramification profile $1^2, 8$ at $j = \infty$, $1, 3^3$ at $j = 0$ and 2^5 at $j = 1728$. We can now invoke [33, Theorem 1][7] to conclude that u is a Hauptmodul for a subgroup Γ of index 10 in $PSL(2,\mathbb{Z})$. This subgroup was identified in [139, Table 7] as the non-congruence subgroup $\Gamma(10;0,3,0,1;8)$ of index 10 in $PSL(2,\mathbb{Z})$, with genus 0, 3 cusps of width (8,1,1) and one $\mathbb{Z}_3$ orbifold point (using the notation of [173] for subgroups of $PSL(2,\mathbb{Z})$; note that the parameter λ in [65] corresponds to $\lambda^{3/2}$ in our conventions). By unfolding the standard fundamental domain $\mathcal{F}$ of $PSL(2,\mathbb{Z})$ into the fundamental domain $\mathcal{F}_\Gamma$ of Γ, we can associate a unique value $\mathrm{u}(\tau)$ among the ten solutions u_i with the same values of $J(\mathrm{u},\ell) = J(\tau)$, related to the standard Hauptmodul of Γ (see Appendix) by

$$\underline{\mathrm{u}}(\tau) = \frac{8w}{J_\Gamma(\tau)+w} \quad (5.70)$$

where $w := -(-1/3^9)^{1/8} \simeq -0.268444 - 0.111193\mathrm{i}$. The universal cover of the Kähler moduli space at $\ell = -27/256$ is therefore the Poincaré upper half-plane.

Away from the locus $\ell = \underline{\ell} := -\frac{27}{256}$, we can still attempt to parametrize the u-line by τ, by equating the Klein Hauptmodul at $\mathrm{u}(\tau,\ell)$ with its value at $\underline{\mathrm{u}}(\tau)$,

$$J(\tau) = \frac{Q_4^3}{\ell^3\mathrm{u}^8\Delta_4} = \frac{\underline{Q}_4^3}{\underline{\ell}^3\underline{\mathrm{u}}^8\underline{\Delta}_4} \quad (5.71)$$

[6] Similar to footnote 5, it is easy to check that the ramification structure satisfies the Riemann-Hurwitz formula, $2 = 2\times 10 - 5\times(2-1) - 3\times(3-1) - 1\times(8-1)$. Equivalently, the genus of the congruence subgroup Γ is given by $g = 1 + \frac{\mu}{12} - \frac{|\mathcal{E}_2|}{4} - \frac{|\mathcal{E}_3|}{3} - \frac{|C|}{2} = 1 + \frac{10}{12} - \frac{1}{3} - \frac{3}{2}$, where $|\mathcal{E}_2|$ is the number of elliptic points of order 2, $|\mathcal{E}_3|$ is the number of elliptic points of order 3, and $|C|$ the number of cusps.

[7] Namely: *A necessary and sufficient condition that $f(\tau)$ is a modular function on a subgroup of finite index in $PSL(2,\mathbb{Z})$ is that $f(\tau)$ should be an algebraic function of the Klein invariant J, and that its only branch points should be branch points of order dividing 2 at which $J = 1728$, branch points of order dividing 3 at which $J = 0$, and branch points at which J is infinite.*

In order to solve this equation, we can introduce an unknown non-vanishing function $f(\underline{u}, \ell)$ and solve instead

$$Q_4 = f\underline{Q}_4, \quad Q_6 = f^{3/2}\underline{Q}_6, \quad \mathrm{u}^8\ell^3\Delta_4 = f^3\underline{u}^8\underline{\ell}^3\underline{\Delta}_4 \tag{5.72}$$

where the last equation is a consequence of the first two. For $|\ell - \underline{\ell}|$ sufficiently small, ten of the roots of (5.71), which we denote by u_i ($i = 1, \ldots, 10$) are small perturbations of $\underline{u}_i$, which can be determined as a Taylor series in $\ell - \underline{\ell}$,

$$\begin{aligned}
\mathrm{u} =& \underline{u}\left(1 - \frac{4}{9}(\underline{u} - 8)\left(\ell - \underline{\ell}\right) + \frac{16\left(27\underline{u}^3 - 300\underline{u}^2 + 2624\underline{u} + 2816\right)}{243(9\underline{u} + 8)}\left(\ell - \underline{\ell}\right)^2 + \ldots\right) \\
f =& 1 - \frac{16\underline{u}^2}{9\underline{u} + 8}\left(\ell - \underline{\ell}\right) + \frac{32\underline{u}^2\left(45\underline{u}^2 - 56\underline{u} - 128\right)}{9(9\underline{u} + 8)^2}\left(\ell - \underline{\ell}\right)^2 + \ldots \\
=& 1 - \frac{16\mathrm{u}^2}{9\mathrm{u} + 8}\left(\ell - \underline{\ell}\right) + \frac{32\mathrm{u}^2\left(27\mathrm{u}^2 + 56\mathrm{u} + 128\right)}{9(9\mathrm{u} + 8)^2}\left(\ell - \underline{\ell}\right)^2 + \ldots
\end{aligned} \tag{5.73}$$

Note that this expansion blows up at $9\mathrm{u} + 8 = 0$, reflecting the existence of a branch point at $\tau = \tau_B$ (and all its images under Γ), where τ_B is one of the 10 pre-images of $j = j_B$). The two additional roots, which we denote by $\mathrm{u}_\pm$, instead emerge from the ramification point, $\mathrm{u}_\pm = -\frac{8}{9} + O(\ell - \underline{\ell})$. The expansion can be determined by matching the sum and product over all roots, which are easily determined from the coefficients in the degree 12 polynomial $Q_{12} = Q_4^3 - j\ell^3\mathrm{u}^8\Delta_4$,

$$\sum_{i=1}^{10}\underline{u}_i = \frac{16(5j - 621)}{9(17j + 27)}, \quad \prod_{i=1}^{10}\underline{u}_i = \frac{2^{30}}{3^{11}(17j + 27)} \tag{5.74}$$

$$\sum_{i=\pm,1}^{10}\mathrm{u}_i = \frac{36(j - 512\ell)}{j(16\ell - 27) - 4096\ell^2}, \quad \prod_{i=\pm,1}^{10}\mathrm{u}_i = \frac{1}{j(27 - 16\ell)\ell^4 + 4096\ell^6} \tag{5.75}$$

Using this and the expansion (5.73) for each u_i, we find

$$\begin{aligned}
\mathrm{u}_+ + \mathrm{u}_- &= -\frac{16}{9} - \frac{2048}{729}\left(\ell - \underline{\ell}\right) - \frac{1736704\left(\ell - \underline{\ell}\right)^2}{59049} - \frac{1024458752\left(\ell - \underline{\ell}\right)^3}{4782969} + \ldots \\
\mathrm{u}_+\mathrm{u}_- &= \frac{64}{81} + \frac{16384}{6561}\left(\ell - \underline{\ell}\right) + \frac{4980736\left(\ell - \underline{\ell}\right)^2}{177147} + \frac{1098907648\left(\ell - \underline{\ell}\right)^3}{4782969} + \ldots
\end{aligned} \tag{5.76}$$

In particularm the dependence on j drops, and the discriminant $(\mathrm{u}_+ - \mathrm{u}_-)^2$ vanishes up to order $O\left(\ell - \underline{\ell}\right)^3$. As a result, we find

$$\mathrm{u}_\pm = -\frac{8}{9} - \frac{1024}{729}\left(\ell - \underline{\ell}\right) \pm \frac{4096\sqrt{5}\left(\ell - \underline{\ell}\right)^{3/2}}{6561} - \frac{868352\left(\ell - \underline{\ell}\right)^2}{59049} + O\left(\ell - \underline{\ell}\right)^{5/2} \tag{5.77}$$

Finally, for $\lambda = 0$, one of the I_1 fibers collide with the I_8 fiber at $\mathrm{u} = 0$, leading to a configuration of type $I_9, 3I_1$. This corresponds to the blow-down limit where the exceptional curve C shrinks to a point (see below). The Coulomb branch is now a modular curve for the congruence subgroup $\Gamma_0(9)$, which has index 12 in $SL(2,\mathbb{Z})$ and 4 cusps of width (9,1,1,1). Keeping $z = z_1z_2 = -u^3$ fixed and taking the limit $z_1 \to 0$, the discriminant and J-invariant reduce to

$$\Delta \to -z^3(1 + 27z), \quad J \to -\frac{(1 + 24z)^3}{z^3(1 + 27z)} \tag{5.78}$$

Equating

$$J(\tau) = \frac{(J_3+15)(J_3+231)^3}{(J_3-12)^3}, \quad J_3 = \frac{(J_9-3)^3}{J_9^2+3J_9+9} + 12 \tag{5.79}$$

we can express u in terms of J_9 order by order in λ,

$$1/u = \frac{3(J_9+6)}{J_9-3}\left(1 + \frac{(J_9+6)\lambda}{3(J_9-3)} - \frac{\left(J_9^3+72J_9^2+270J_9+702\right)\lambda^2}{9(J_9-3)^2(J_9+6)} + \dots\right) \tag{5.80}$$

In terms of the Fricke transform $\hat{J}_9 = \frac{27}{J_9-3} + 3$,

$$1/u = \hat{J}_9\left(1 + \frac{\hat{J}_9\lambda}{9} + \frac{\left(18-\hat{J}_9^3\right)\lambda^2}{27\hat{J}_9} + \frac{7\left(5\hat{J}_9^3-108\right)\lambda^3}{2187} - \frac{11\hat{J}_9\left(13\hat{J}_9^3-297\right)\lambda^4}{19683} + \dots\right) \tag{5.81}$$

We note two further special cases:

- For $\ell^3 = \frac{27}{16}$, one of the roots of Δ_4 moves off to u = ∞, but this does not affect the structure of the singular fibers.
- In the limit $\lambda \to \infty$, the 4 roots of Δ_4 split into two pairs

$$1/u_\pm = -2\sqrt{\lambda}\left(1 \pm \frac{\mathrm{i}}{\lambda^{3/4}} + \frac{1}{8\lambda^{3/2}} \mp \frac{\mathrm{i}}{32\lambda^{9/4}} + \dots\right), \tag{5.82}$$

$$1/u'_\pm = 2\sqrt{\lambda}\left(1 \pm \frac{1}{\lambda^{3/4}} - \frac{1}{8\lambda^{3/2}} \pm \frac{1}{32\lambda^{9/4}} + \dots\right) \tag{5.83}$$

Setting $1/u = -2\sqrt{\lambda}\left(1 + \frac{\mathrm{i}u_{\mathrm{SW}}}{2\lambda^{3/4}} + O(\lambda^{-3/2})\right)$ or $1/u = 2\sqrt{\lambda}\left(1 + \frac{u_{\mathrm{SW}}}{2\lambda^{3/4}} + O(\lambda^{-3/2})\right)$ and taking the limit $\lambda \to \infty$ with u_{SW} fixed[8], we recover in either case the usual Klein invariant for $SU(2)$ Seiberg-Witten theory in 4 dimensions,

$$J = \frac{256(u_{\mathrm{SW}}^2-3)^3}{u_{\mathrm{SW}}^2-4} + O(\lambda^{-3/4}) \tag{5.84}$$

To match the notations in [65], we define (note a missing term $+144U\lambda_{CM}$ in the formula for $g_3(U)$ in (5.85), loc.cit.)

$$U = \frac{1}{\sqrt{z_1}}, \quad \lambda_{CM} = -\frac{z_2}{\sqrt{z_1}} = -\lambda^{-3/2} \tag{5.85}$$

such that the mirror curve [65, (2.94)] becomes

$$\sqrt{\lambda_{CM}}\left(\frac{1}{t} + tw\right) + w + \frac{1}{w} - U = 0 \tag{5.86}$$

The mirror curve of local $\mathbb{P}^2$

$$\frac{1}{t} + \frac{1}{w} + tw - 3U = 0 \tag{5.87}$$

is recovered upon redefining $(t, w, U) \to (\lambda_{CM}^{1/6}t, w/\lambda_{CM}^{1/3}, 3U\lambda_{CM}^{1/3})$ and taking the limit $\lambda_{CM} \to \infty$ keeping z fixed. Equivalently, one can set $z_2 = z/z_1$ and take the limit $z_1 \to 0$.

[8] This is equivalent to the prescription $z_1 \to \frac{1}{4}\exp(-2\sqrt{2}\epsilon^2\tilde{u})$, $z_2 \sim \epsilon^4\Lambda^4$ from [116, p. 6.33].

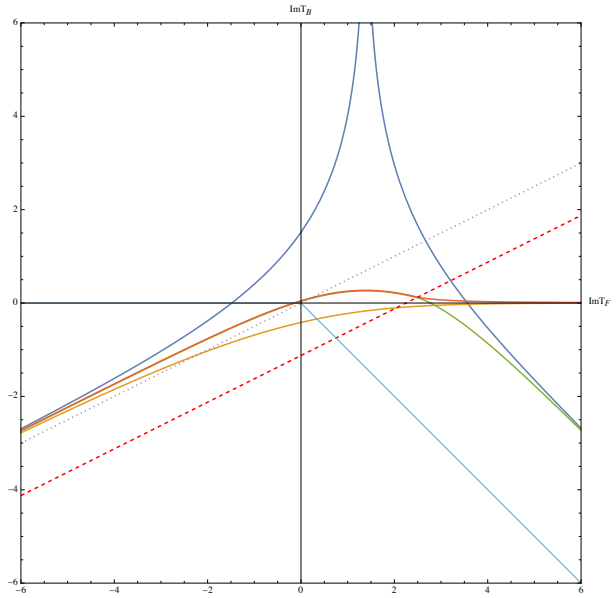


Figure 5.9: Real slice of the discriminant locus for local $\mathbb{F}_1$. The slices $|\lambda| = cte$ correspond to lines of fixed $\mathrm{Im}(T_F - 2T_B)$. The Kähler cone of $\mathbb{F}_1$ corresponds to the first quadrant $\mathrm{Im}\, T_F > 0, \mathrm{Im}\, T_B > 0$. The Kähler cone of the flopped geometry corresponds to $\mathrm{Im}\, T_B < 0, \mathrm{Im}(T_F + T_B) > 0$ i.e. $\mathrm{Im}\, T_C > 0, \mathrm{Im}\, T_H > 0$. The dashed and dotted lines correspond to loci with fixed λ equal to $(-27/256)^{1/3}$ and 1, respectively.

5.5.2 Large volume expansion

The Picard-Fuchs system is given by [105] (after fixing a typo in loc. cit.)

$$\begin{aligned}\mathcal{D}_1 =&\theta_1(\theta_1 - \theta_2) - z_1(2\theta_1 + \theta_2)(1 + 2\theta_1 + \theta_2)\\ \mathcal{D}_2 =&\theta_2^2 - z_2(\theta_2 - \theta_1)(2\theta_1 + \theta_2)\end{aligned} \tag{5.88}$$

In terms of the coordinates $(\tilde{u} = -1/u, \lambda)$ defined in (5.61),

$$\begin{aligned}3\mathcal{D}_1 =& -3u^4\lambda\partial_u^2 - 6u^3\lambda\partial_u + u\partial_u\lambda\partial_\lambda + \lambda\partial_\lambda f + \lambda^2\partial_{\lambda^2}\\ 9\mathcal{D}_2 =&4\lambda^2\partial_\lambda^2 + 4\lambda\partial_\lambda + u\partial_u - (4\lambda + 9u)u\partial_u\partial_\lambda + u^2\partial_u^2\end{aligned} \tag{5.89}$$

Combining the two equations one arrives at the third order differential operator

$$\begin{aligned}\mathcal{D}_3 =&(8\lambda + 9u)\left(\lambda + \left(16\lambda^3 - 27\right)u^4 - 36\lambda u^3 - 8\lambda^2u^2 + u\right)\theta_u^3\\ &- u\left(\lambda + \left(729 - 432\lambda^3\right)u^4 + 8\lambda\left(189 - 64\lambda^3\right)u^3 + 936\lambda^2u^2 + 128\lambda^3u\right)\theta_u^2\\ &+ 2u^2\left(-32\lambda^3 + 9\left(16\lambda^3 - 27\right)u^3 + 6\lambda\left(32\lambda^3 - 81\right)u^2 - 282\lambda^2u\right)\theta_u\\ \lambda\mathcal{D}_3 =&(9\mathrm{u} + 8)\left(16\mathrm{u}^4\ell^2 - (9\mathrm{u}(3\mathrm{u} + 4) + 8)\mathrm{u}^2\ell + \mathrm{u} + 1\right)\theta_\mathrm{u}^3\\ &+ \mathrm{u}\left(16(27\mathrm{u} + 32)\mathrm{u}^3\ell^2 - \left(729\mathrm{u}^3 + 1512\mathrm{u}^2 + 936\mathrm{u} + 128\right)\mathrm{u}\ell - 1\right)\theta_\mathrm{u}^2\\ &+ 2\mathrm{u}^2\ell\left(9\mathrm{u}^3(16\ell - 27) + 6\mathrm{u}^2(32\ell - 81) - 282\mathrm{u} - 32\right)\theta_\mathrm{u}\end{aligned} \tag{5.90}$$

with $\theta_u = u\partial_u$, $\theta_\mathrm{u} = \mathrm{u}\partial_\mathrm{u}$, along with

$$\mathcal{D}_4 = (8\lambda + 9u)\partial_u\partial_\lambda f - \left(24\lambda u^2 + 1\right)\partial_u f - u\left(12\lambda u^2 + 1\right)\partial_u^2 f \tag{5.91}$$

One may check that (5.90) agrees with [116, (6.28)] upon renaming $(\tilde{u}, m)$ into $(-1/u, \lambda)$ and reordering the derivatives.

Importantly, the coefficient of θ_{u}^3 is proportional to $(9\mathrm{u}+8)\Delta_4$, hence vanishes on the finite discriminant locus as well as for $\mathrm{u} = -8/9$. For $\ell \neq \underline{\ell}$, the latter coincides with the ramification point (5.68) and corresponds to an apparent singularity with trivial monodromy. Indeed a local analysis shows that the characteristic exponents at that point are $0, 1, 3$, compared to $0, 1, 2$ at an ordinary regular point. For $\ell = \underline{\ell}$, it coincides instead with the $\mathbb{Z}_3$ orbifold point of Γ and corresponds to an irregular point with characteristic exponents $(0, \frac{5}{6}, \frac{7}{6})$.

The operators $\mathcal{D}_3$ and $\mathcal{D}_4$ annihilate constants as well as $\log\lambda = \frac{1}{3}\log(z_1/z_2^2)$, so $\varpi_0 = 1$ and $\varpi_1 = \log z_1 - 2\log z_2 = 3\log\lambda$. The other logarithmic and double logarithmic solutions have expansions at small u given by

$$\begin{aligned}
\varpi_2 &= \log u + u^2\lambda + 2u^3 + \frac{3}{2}\lambda^2 u^4 + 12\lambda u^5 + \dots \\
\varpi_3 &= (\log u)^2 - \varpi_2(2\log u + \frac{1}{4}\log\lambda) + \frac{1}{8}(\log\lambda)^2 - \frac{u}{4\lambda} + \frac{1-16\lambda^3}{16\lambda^2}u^2 - \frac{90\lambda^3+1}{36\lambda^3}u^3 \\
&\quad + \frac{-208\lambda^6 - 24\lambda^3 + 1}{64\lambda^4}u^4 + \frac{6450\lambda^6 - 50\lambda^3 + 3}{300\lambda^5}u^5 + \dots
\end{aligned} \tag{5.92}$$

We can in fact obtain an all-order solution as follows. First, observe that the operator (5.90) factorizes as $\mathcal{D}_3 = \mathcal{D}\theta_u$ where $\mathcal{D}$ is a second order differential operator. This operator must annihilate the periods ω_1, ω_2 of the elliptic curve. The fundamental period ω_1 is easily found from the GLSM charges,

$$\omega_1 = \sum_{k,\ell\geq 0} \frac{(k+2\ell)!}{(k!)^2\ell!(\ell-k)!} u^{k+2\ell}\lambda^{\ell-k} = \sum_{k,\ell\geq 0} \frac{(3k+2\ell)!}{(k!)^2\ell!(k+\ell)!} u^{3k+2\ell}\lambda^{\ell} \tag{5.93}$$

where in the second expression we shifted $\ell \mapsto \ell + k$, observing that terms with $k > \ell$ do not contribute in the sum in the first line. Using the Frobenius method (i.e. shifting $k \to k + x$, or $\ell \to \ell + y$, and taking the coefficient in the linear term in x or y), we find two logarithmic solutions

$$\begin{aligned}
\omega_2 =& (\log u - \log\lambda)\omega_1 + 2\sum_{-2\ell<k\leq\ell} \frac{(k+2\ell)!\,(H_{2\ell+k} + H_{\ell-k} - 2H_k)}{(k!)^2(k)!(\ell-k)!} u^{k+2\ell}\lambda^{\ell-k} \\
&+ \sum_{0\leq\ell<k} (-1)^{k+\ell}\frac{\Gamma(k-\ell)(k+2\ell)!}{\ell!\,(k!)^2} u^{k+2\ell}\lambda^{\ell-k} \\
\omega_2' =& (2\log u + \log\lambda)\omega_1 + 2\sum_{-2\ell<k\leq\ell} \frac{(k+2\ell)!\,(2H_{2\ell+k} - H_{\ell-k} - H_\ell)}{(k!)^2(k)!(\ell-k)!} u^{k+2\ell}\lambda^{\ell-k} \\
&- \sum_{0\leq\ell<k} (-1)^{k+\ell}\frac{\Gamma(k-\ell)(k+2\ell)!}{\ell!\,(k!)^2} u^{k+2\ell}\lambda^{\ell-k}
\end{aligned} \tag{5.94}$$

where $H_n = \sum_{k=1}^n (1/k)$ are the harmonic numbers. In fact, only the linear combination $2\omega_2 + 3\omega_2'$ is annihilated by $\mathcal{D}$, while ω_2 and ω_2' satisfy it with a source term proportional to $9\lambda/u^4 + 96\lambda^3/u^3$. In particular, we find that the modular parameter is given by

$$\tau = \frac{2\omega_2 + 3\omega_2'}{2\pi\mathrm{i}\omega_1} = \frac{1}{2\pi\mathrm{i}}\left[8\log u + \log\lambda + \frac{u}{\lambda} + \frac{\left(32\lambda^3 - 1\right)u^2}{2\lambda^2} + \frac{\left(132\lambda^3 + 1\right)u^3}{3\lambda^3} + \dots\right] \tag{5.95}$$

The CY periods satisfy $u\partial_u\varpi_2 = \omega_1, u\partial_u\varpi_3 = -\frac{1}{4}(2\omega_2 + 3\omega_2')$. Hence they are obtained by integrating once with respect to u,

$$\begin{aligned}
\varpi_2 &= \log u + \sum_{3k+2\ell>0} \frac{(3k+2\ell-1)!}{(k!)^2(\ell!)(k+\ell)!} u^{3k+2\ell}\lambda^\ell \\
\varpi_3 &= \log^2 u - (2\log u + \frac{1}{4}\log\lambda)\varpi_2 + \frac{1}{8}\log^2\lambda \\
&\quad - 2\sum_{-2\ell<k\le\ell} \frac{(k+2\ell-1)!\,(2H_{2\ell+k} - H_{\ell-k} - H_\ell)}{(k!)^2(k)!(\ell-k)!} u^{k+2\ell}\lambda^{\ell-k} \\
&\quad + \sum_{0\le\ell<k} (-1)^{k+\ell} \frac{\Gamma(k-\ell)(k+2\ell-1)!}{\ell!\,(k!)^2} u^{k+2\ell}\lambda^{\ell-k} - 2\sum_{k+2\ell>0} \frac{(k+2\ell-1)!}{(k+2\ell)(k!)^2\ell!(\ell-k)!} u^{k+2\ell}\lambda^{\ell-k}
\end{aligned} \tag{5.96}$$

As an aside, a simple way to express the periods in terms of the u–ℓ coordinates is as follows:

$$m = \frac{1}{3}X^{(1)}, \qquad t = X^{(2)} + \frac{1}{3}X^{(1)}, \qquad t_D = 4X^{(3)} + \frac{1}{6}X^{(0)}, \tag{5.97}$$

where

$$X^{(0)} = 1, \qquad X^{(1)} = \frac{1}{2\pi\mathrm{i}}\log\ell, \qquad X^{(2)} = \frac{1}{2\pi\mathrm{i}}\big(\log\mathrm{u} + \sigma_1(\mathrm{u},\ell)\big), \tag{5.98}$$

$$\begin{aligned}
X^{(3)} = \frac{1}{(2\pi\mathrm{i})^2}\Big[&(\log\mathrm{u})^2 + \frac{3}{4}\log\ell\log\mathrm{u} + \frac{1}{8}(\log\ell)^2 + \Big(2\log\mathrm{u} + \frac{3}{4}\log\ell\Big)\sigma_1(\mathrm{u},\ell) \\
&+ \sigma_2(\mathrm{u},\ell)\Big],
\end{aligned} \tag{5.99}$$

are the solutions of the Picard-Fuchs equations in standard Frobenius basis and σ_i are the following series

$$\begin{aligned}
\sigma_1 &= \sum_{n=2}^{\infty}(n-1)!\Big(\sum_{r=\lceil n/3\rceil}^{\lfloor n/2\rfloor} \frac{\ell^r}{r!(n-2r)!^2(3r-n)!}\Big)\mathrm{u}^n \\
&= \ell\,\mathrm{u}^2 + 2\ell\,\mathrm{u}^3 + \frac{3}{2}\ell^2\mathrm{u}^4 + 12\ell^2\mathrm{u}^5 + O(\mathrm{u}^6),
\end{aligned} \tag{5.100}$$

$$\begin{aligned}
\sigma_2 = &-\sum_{n=1}^{\infty}\frac{(n-1)!}{4}\Bigg[\sum_{r=0}^{\lfloor (n-1)/3\rfloor}\frac{(-1)^{n-r}(n-3r-1)!}{r!\,(n-2r)!^2}\,\ell^r \\
&\qquad + \sum_{r=\lceil n/3\rceil}^{\lfloor n/2\rfloor}\frac{\ell^r}{r!\,(n-2r)!^2\,(3r-n)!}\,(4H_{n-2r} + 3H_r + H_{3r-n} - 8H_{n-1})\Bigg]\mathrm{u}^n \\
= &\frac{\mathrm{u}}{4} + \left(\ell - \frac{1}{16}\right)\mathrm{u}^2 + \left(\frac{1}{36} + \frac{5\ell}{2}\right)\mathrm{u}^3 + \frac{-1+24\ell+208\ell^2}{64}\,\mathrm{u}^4 + O(\mathrm{u}^5).
\end{aligned} \tag{5.101}$$

It follows that for $\tau = \frac{\partial_{\mathrm{u}} T_D}{\partial_{\mathrm{u}} T}$,

$$\begin{aligned}\log q = 2\pi\mathrm{i}\,\tau &= \big(8\log \mathrm{u} + 3\log \ell\big) + \frac{4\mathrm{u}\sigma_2' + 8\sigma_1}{1+\mathrm{u}\sigma_1'} \\ &= \big(8\log \mathrm{u} + 3\log \ell\big) + \mathrm{u} + \frac{1}{2}(-1+32\ell)\mathrm{u}^2 + \frac{1}{3}(1+132\ell)\mathrm{u}^3 \\ &\quad + \frac{1}{4}(-1+4\ell+128\ell^2)\mathrm{u}^4 + \frac{1}{5}(1-5\ell+1680\ell^2)\mathrm{u}^5 + O(\mathrm{u}^6).\end{aligned} \tag{5.102}$$

At any rate, in the large volume limit $u \to 0$, we get

$$\begin{aligned}\varpi_2 &\to \log u = \frac{1}{3}\log z_1 + \frac{1}{3}\log z_2 \\ \varpi_3 &\to -(\log u)^2 - \frac{1}{4}\log u \log\lambda + \frac{1}{8}(\log\lambda)^2 = -\frac{1}{8}(\log z_1)^2 - \frac{1}{4}\log z_1\ \log z_2\end{aligned} \tag{5.103}$$

In order to match the desired large volume limit, we define

$$2\pi\mathrm{i}T_1 = 2\varpi_2 + \log\lambda, \quad 2\pi\mathrm{i}T_2 = \varpi_2 - \log\lambda, \quad T_D = -4\frac{\varpi_3}{(2\pi\mathrm{i})^2} + \frac{1}{6} \tag{5.104}$$

Setting $T = \frac{1}{3}(T_1+T_2) = \varpi_2/(2\pi\mathrm{i})$, $Q = e^{2\pi\mathrm{i}T}$ and inverting the series, we get

$$-u = Q - \lambda Q^3 + 2Q^4 + \lambda^2 Q^5 - (\lambda^3+1)Q^7 + 4\lambda^2 Q^8 + \dots \tag{5.105}$$

and therefore

$$\varpi_3 = -(\log Q)^2 - \frac{1}{4}\log Q\log\lambda + \frac{1}{8}(\log\lambda)^2 + \frac{Q}{4\lambda} + \frac{1-16\lambda^3}{16\lambda^2}Q^2 + \frac{81\lambda^3+1}{36\lambda^3}Q^3 + \frac{1-16\lambda^6}{64\lambda^4}Q^4 + \dots \tag{5.106}$$

Integrating T_D/Q with respect to Q to get the free energy and substituting $Q = (Q_1Q_2)^{1/3}$, $\lambda = (Q_1/Q_2^2)^{1/3}$, we recover the known GV invariants,

$$\begin{aligned}F =& -\frac{1}{6}\left(-3\log(\lambda)\log^2(Q) + 3\log^2(\lambda)\log(Q) + \frac{1}{6}\log Q - 8\log^3(Q)\right) \\ & - \frac{Q}{\lambda} - \frac{\left(1-16\lambda^3\right)Q^2}{8\lambda^2} - \frac{\left(81\lambda^3+1\right)Q^3}{27\lambda^3} - \frac{\left(1-16\lambda^6\right)Q^4}{64\lambda^4} - \frac{\left(625\lambda^6+1\right)Q^5}{125\lambda^5} \\ & - \frac{\left(-16\lambda^9-1215\lambda^6+1\right)Q^6}{216\lambda^6} - \frac{\left(2401\lambda^9+1\right)Q^7}{343\lambda^7} + \frac{\left(16\lambda^{12}+16384\lambda^9-1\right)Q^8}{512\lambda^8} + \dots \\ =& \frac{1}{162}(T_1+T_2)(8T_1^2+25T_1T_2-10T_2^2) - (\mathrm{Li}_3(Q_2) - 2\,\mathrm{Li}_3(Q_1) + 3\,\mathrm{Li}_3(Q_1Q_2) \\ & +5\,\mathrm{Li}_3(Q_1^2Q_2) - 6\,\mathrm{Li}_3(Q_1^2Q_2^2) + 7\,\mathrm{Li}_3(Q_1^3Q_2) - 32\,\mathrm{Li}_3(Q_1^3Q_2^2) + 27\,\mathrm{Li}_3(Q_1^3Q_2^3) + \dots\Big)\end{aligned} \tag{5.107}$$

Note in particular that the diagonal invariants $n^{(0)}_{d,d} = 3, -6, 27, \dots$ reproduce the genus 0 GV invariants of local $\mathbb{P}^2$. After the flop transition, using $\mathrm{Li}_3(e^{-2\pi\mathrm{i}x}) = \mathrm{Li}_3(e^{2\pi\mathrm{i}x}) + \frac{(2\pi\mathrm{i})}{6}(x^3 - \frac{3x^2}{2} + \frac{x}{2})$ we find that the polynomial term in F becomes

$$F' = \frac{16T_1'^3 - 18T_1'^2T_2' - 54T_1'T_2'^2 - 54T_2'^3 + 18T_1' + 81T_2'^2 - 27T_2'}{324} + O(Q') \tag{5.108}$$

We can now express the periods in terms of the modulus τ by expanding the J-invariant in (5.60) at small u, and inverting the q-expansion:

$$2\pi \mathrm{i}\tau = 8\log u + \log\lambda + \frac{u}{\lambda} + \frac{32\lambda^3-1}{2\lambda^2}u^2 + \frac{132\lambda^3+1}{3\lambda^3}u^3 + \frac{128\lambda^6+4\lambda^3-1}{4\lambda^4}u^4 + \dots \quad (5.109)$$

$$q_8 := e^{2\pi\mathrm{i}\tau/8} = \lambda^{1/8}u + \frac{u^2}{8\lambda^{7/8}} - + \frac{\left(256\lambda^3-7\right)u^3}{128\lambda^{15/8}} + \frac{\left(5888\lambda^3+35\right)u^4}{1024\lambda^{23/8}} + \dots \quad (5.110)$$

leading to

$$u^{-1} = \frac{\lambda^{1/8}}{q_8} + \frac{1}{8\lambda} + \frac{256\lambda^3-9}{128\lambda^{17/8}}q_8 + \frac{5\left(256\lambda^3+3\right)}{256\lambda^{13/4}}q_8^2 + \frac{\left(256\lambda^3+11\right)\left(256\lambda^3+171\right)}{32768\lambda^{35/8}}q_8^3 + \dots \quad (5.111)$$

Plugging into the large volume expansions (5.96), (5.104), we find

$$\begin{aligned} 2\pi\mathrm{i}T &= \log\left(\frac{q_8}{\lambda^{1/8}}\right) - \frac{q_8}{8\lambda^{9/8}} + \frac{5-64\lambda^3}{64\lambda^{9/4}}q_8^2 - \frac{9216\lambda^3+209}{3072\lambda^{27/8}}q_8^3 + \dots \\ (2\pi\mathrm{i})^2 T_D &= \frac{-27\log^2\lambda + 192\log^2 q_8}{48} + \frac{(2\pi\mathrm{i})^2}{6} - \frac{\log q_8 - 1}{\lambda^{9/8}}q_8 - \frac{\left(64\lambda^3-5\right)(2\log q_8 - 1)}{16\lambda^{9/4}}q_8^2 \\ &\quad - \frac{\left(9216\lambda^3+209\right)(3\log q_8 - 1)}{1152\lambda^{27/8}}q_8^3 + \frac{\left(768\lambda^6+672\lambda^3+35\right)(4\log q_8 - 1)}{256\lambda^{9/2}}q_8^4 + \dots \end{aligned} \quad (5.112)$$

In order to express this as an Eichler type integral, we recall that the algebraic Yukawa couplings are [105, (6.9)] (Note the likely sign error in front of coefficient 60)

$$\begin{aligned} C_{111} &= \frac{-1-4z_1^2+z_2-z_1(7-6z_2)}{3\Delta' z_1^3}, \quad C_{112} = \frac{-1+8z_1^2+z_2+z_1(2-3z_2)}{3\Delta' z_1^2 z_2}, \\ C_{122} &= \frac{z_2(1-12z_1)-(1-4z_1)^2}{3\Delta' z_1 z_2^2}, \quad C_{222} = \frac{2(1-4z_1)^2+z_2(1+60z_1)}{3\Delta' z_2^3} \end{aligned} \quad (5.113)$$

Changing coordinates, one finds

$$C_{uuu} = C_{111}(\partial_u z_1)^3 + 3C_{112}(\partial_u z_1)^2\partial_u z_2 + 3C_{122}\partial_u z_1(\partial_u z_2)^2 + C_{222}(\partial_u z_2)^3 = -\frac{9u+8\lambda}{u^3\Delta'} \quad (5.114)$$

The holomorphic Yukawa coupling, normalized to agree with $\partial_T^3 F$ (up to powers of $2\pi\mathrm{i}$), is then

$$C_{TTT} = C_{uuu}/(\partial_u \varpi_2)^3 \quad (5.115)$$

Defining

$$\begin{aligned} C :=& \frac{8}{C_{TTT}} := \sum_{n\geq 0} c_n(\lambda) q_8^n \\ =& 1 - \frac{q_8}{8\lambda^{9/8}} + \frac{\left(5-64\lambda^3\right)q_8^2}{32\lambda^{9/4}} - \frac{209+9216\lambda^3}{1024\lambda^{27/8}}q_8^3 + \frac{\left(768\lambda^6+672\lambda^3+35\right)q_8^4}{128\lambda^{9/2}} + \dots \end{aligned} \quad (5.116)$$

we get

$$2\pi \mathrm{i} T = \log q_8 - \frac{1}{8}\log\lambda + \sum_{n\geq 1}\frac{c_n(\lambda)}{n} q_8^n \tag{5.117}$$

$$(2\pi\mathrm{i})^2 T_D = 4(\log q_8)^2 - \frac{9}{16}(\log\lambda)^2 + \frac{(2\pi\mathrm{i})^2}{6} + 8\log q_8 \sum_{n\geq 1}\frac{c_n(\lambda)}{n} q_8^n - 8\sum_{n\geq 1}\frac{c_n(\lambda)}{n^2} q_8^n \tag{5.118}$$

such that $\partial T_D/\partial T = \frac{8\log q_8}{2\pi\mathrm{i}} = \tau$. Equivalently,

$$\boxed{\begin{pmatrix} T \\ T_D \end{pmatrix} = \mathrm{cte} + \int^{\tau} \begin{pmatrix} 1 \\ \rho \end{pmatrix} C(\rho)\mathrm{d}\rho} \tag{5.119}$$

To obtain an explicit expression for C, we introduce $\omega_1 = u\partial_u \varpi_2$ and note that

$$\frac{C}{\omega_1} = u^{-1}\partial_\tau u, \quad \frac{C}{(\omega_1)^3} = \frac{1}{u^3 C_{uuu}} = -\frac{\Delta'}{9u+8\lambda} \tag{5.120}$$

which allows to compute C and ω_1 separately, up to sign:

$$C^2 = -\left(u^{-1}\partial_\tau u\right)\frac{9u+8\lambda}{\Delta'}, \quad \omega_1^2 = -\left(u^{-1}\partial_\tau u\right)^3 \frac{9u+8\lambda}{\Delta'} \tag{5.121}$$

For $\lambda = \underline{\lambda}$, we find that C^2 is a holomorphic modular form of weight 6 under the non-congruence subgroup Γ, with a simple zero at the $\mathbb{Z}_3$ orbifold point double zeros at the conifold points

$$C^2 = \frac{(q_8\partial_{q_8} J_\Gamma)^3}{(J_\Gamma + 10w)(J_\Gamma^2 - 8wJ_\Gamma + 144w^2)}, \tag{5.122}$$

while $(\omega_1)^2$ is a meromorphic modular form of weight 2, with a simple pole at the orbifold point and a double zero at $u = \infty$,

$$\omega_1^2 = \frac{(J_\Gamma + w)^2\, q_8\partial_{q_8} J_\Gamma}{(J_\Gamma + 10w)(J_\Gamma^2 - 8wJ_\Gamma + 144w^2)} \tag{5.123}$$

The ratio C/ω_1^3 is modular invariant, vanishes at the orbifold and conifold points but has a triple pole at $u = \infty$,

$$\frac{C}{\omega_1^3} = -\frac{(J_\Gamma + 10w)(J_\Gamma^2 - 8wJ_\Gamma + 144w^2)}{(J_\Gamma + w)^3} = -\frac{1}{54}(8u + 8\underline{\lambda})(153u^2 - 80u\underline{\lambda} + 64\underline{\lambda}^2) \tag{5.124}$$

For general values of λ, we can compute C by deriving the Klein Hauptmodul (5.71) with respect to u and and $\underline{\mathrm{u}}$,

$$\partial_{\mathrm{u}} J = -\frac{(9\mathrm{u}+8)Q_4^2 Q_6}{\mathrm{u}^9\ell^3\Delta_4^2}, \quad \partial_{\underline{\mathrm{u}}} J = -\frac{(9\underline{\mathrm{u}}+8)\underline{Q}_4^2\underline{Q}_6}{\underline{\mathrm{u}}^9\underline{\ell}^3\underline{\Delta}_4^2}, \tag{5.125}$$

giving access to the derivative

$$\frac{\partial \mathrm{u}}{\partial \underline{\mathrm{u}}} = \frac{(9\underline{\mathrm{u}}+8)\underline{\mathrm{u}}^7\underline{\ell}^3}{(9\mathrm{u}+8)\mathrm{u}^7\ell^3} f^{5/2} \tag{5.126}$$

hence to the ratio

$$\left(\frac{C}{\underline{C}}\right)^2 = \frac{(9\underline{\mathrm{u}}+8)^2\underline{\mathrm{u}}^{16}\underline{\ell}^6}{(9\mathrm{u}+8)^2\mathrm{u}^{16}\ell^6} f^{9/2} \tag{5.127}$$

Note that f can only vanish when Q_4 and Q_6 admit a common root, which only occurs when their resultant vanishes, i.e. when $\ell = \underline{\ell}$ (but then $f = 1$) or $\ell = 0$ (but then $Q_4 = Q_6 = 1$, unless one rescales u).

5.5.3 Expansion near conifold points

Here, we analyze the behavior of the periods T and T_D near points u_c where $\Delta(\mathrm{u}, \ell) = 0$. As mentioned in the introduction, it is advantageous to parametrize ℓ in terms of a new complex variable b, such tthat both ℓ and u_c are rational functions in b:

$$\ell = -\frac{b\left(b^2+b+1\right)^3}{(b+1)^8}, \quad \mathrm{u}_c = -\frac{(b+1)^4}{\left(b^2+b+1\right)\left(b^2+4b+1\right)} \tag{5.128}$$

For given ℓ, there are in general 8 solutions for b, which appear in pairs $(b, 1/b)$. The b-plane is therefore an 8:1 cover of the ℓ-plane, ramified at $\ell \in \{-27/256, 0, \infty\}$, In fact, it is possible to choose a simpler parametrization in terms of $\beta = b + 1/b$,

$$\ell = -\frac{(\beta+1)^3}{(\beta+2)^4}, \quad \mathrm{u}_c = -\frac{(\beta+2)^2}{(\beta+1)(\beta+5)} \tag{5.129}$$

where there are now in general 4 values of β for a given ℓ, which correspond to the four roots of the polynomial Δ_4. However, it will turn out that the periods are not invariant under $b \to 1/b$, so we prefer to use the variable b throughout.

Because the characteristic exponents at $\mathrm{u} = \mathrm{u}_c$ of the third-order Picard-Fuchs equation $\mathcal{D}_3\varpi = 0$ are $(0, 1, 1)$, the solutions to the s $\mathcal{D}_1\varpi = \mathcal{D}_2\varpi = 0$ behave either as $O(\delta)$, where $\delta = \mathrm{u} - \mathrm{u}_c$, or as $O(\delta \log \delta)$. In the first case, plugging in the ansatz

$$\varpi_2^c = A_1(b)\delta + A_2(b)\delta^2 + A_3(b)\delta^3 + \ldots \tag{5.130}$$

the Picard-Fuchs equation $\mathcal{D}_1\varpi = 0$ implies that $A_1(b)$ satisfies the differential equation

$$\left(b^6+5b^5+5b^4-5b^2-5b-1\right)\partial_b A_1 + \left(5b^4+4b^3+18b^2+4b+5\right)A_1(b) = 0 \tag{5.131}$$

which is solved by (up to an overall multiplicative constant),

$$A_1(b) = \frac{\left(b^2+b+1\right)\left(b^2+4b+1\right)^2}{(1-b)(b+1)^5} \tag{5.132}$$

To leading order in δ, this also solves the Picard-Fuchs equation $\mathcal{D}_2\varpi = 0$. At next-to-leading order, we find that $\mathcal{D}_1\varpi = 0$ implies that A_2 satisfies a non-homogenous differential equation similar to (5.131), with a right-hand side determined by A_2. The equation $\mathcal{D}_2\varpi = 0$ uniquely determines the homogenous solution, leading to

$$\begin{aligned} A_2(b) &= \frac{\left(b^2+b+1\right)^2\left(b^2+4b+1\right)^3}{2(b-1)^7(b+1)^{11}} p_8(b) \\ p_8(b) &= b^8 - 18b^7 - 32b^6 - 74b^5 - 114b^4 - 74b^3 - 32b^2 - 18b + 1 \end{aligned} \tag{5.133}$$

This procedure may be continued at higher order, for example

$$A_3(b) = -\frac{\left(b^2+b+1\right)^3\left(b^2+4b+1\right)^4}{3(b-1)^{13}(b+1)^{17}}p_{16}(b) \tag{5.134}$$

$$\begin{aligned} p_{16}(b) = {} & b^{16} - 6b^{15} + 508b^{14} + 2930b^{13} + 11572b^{12} + 31310b^{11} + 60840b^{10} \\ & + 90470b^9 + 103710b^8 + 90470b^7 + 60840b^6 + 31310b^5 + 11572b^4 \\ & + 2930b^3 + 508b^2 - 6b + 1 \end{aligned} \tag{5.135}$$

In the second case, plugging in the Ansatz

$$\varpi_3^c = \varpi_1^c \log\delta + G_0(b) + G_1(b)\delta + G_2(b)\delta^2 + \dots \tag{5.136}$$

we find we find that $G_0(b)$ satisfies an inhomogenous second order differential equation,

$$b^2\left(b^4+b^3-b-1\right)\partial_b^2 G_0 + b\left(b^4-4b^3-8b^2-6b-1\right)\partial_b G_0 = (b-1)^4 \tag{5.137}$$

The homogeneous solutions are linear combinations of 1 and $\log(-\frac{b\left(b^2+b+1\right)^3}{(b+1)^8})$, which are just the usual constant periods 1 and m. A particular inhomogeneous solution, valid in the half-plane $\mathrm{Re}(b) > 0$, is given by

$$G_0(b) = -\left[\mathrm{Li}_2(b^3) - 4\,\mathrm{Li}_2(b^2) + 5\,\mathrm{Li}_2(b)\right] - \frac{1}{2}(\log b)^2 - 3\log b\,\log(b^2+b+1) + 8\log b\,\log(b+1) \tag{5.138}$$

For $\mathrm{Re}(b) < 0$, this expression is no longer a solution for the standard choice of branch cuts for the logarithm and dilogarithm, nor is it a continuous function of b, but this may be repaired by adding a term proportional to $\log b$ with piecewise constant coefficient, along with a piecewise constant,

$$\begin{aligned} \tilde{G}_0(b) = {} & G_0(b) - 6\pi\mathrm{i}\,\Theta(-b_1-\frac{1}{2})\,\mathrm{sign}(b_2)\left(1-\Theta(b_2-\sqrt{3}b_1)\,\Theta(-b_2-\sqrt{3}b_1)\,\Theta(b_2)\right)\log b \\ & - 2\pi^2\Theta(-b_1)\left[2\Theta(|b|-1)\Theta(b_2-\sqrt{3}b_1)\,\Theta(-b_2-\sqrt{3}b_1) + \mathrm{sign}(1-|b|)\right] + \frac{\pi^2}{3} \end{aligned} \tag{5.139}$$

where $b = b_1 + \mathrm{i}b_2$ and $\Theta(x)$ is the Heaviside function, equal to 1 for $x > 0$ and 0 otherwise. With this definition, $\tilde{G}_0(b)$ is continuous for all $b \in \mathbb{C}\backslash(-\infty, 0) \cup \{\pm e^{\mathrm{i}\pi/6}\}$, and satisfies the differential equation (5.137). In Appendix 5.7, we shall rederive this expression in a completely different way, by computing the regulator period of the family of nodal curves.

At the next order, we find that both Picard-Fuchs equations produce the same inhomogeneous first order ODE for $G_1(b)$, where the homogenous part is the same as for $A_1(b)$ (5.131),

$$\begin{aligned} & \left(b^6+5b^5+5b^4-5b^2-5b-1\right)G_1'(b) + \left(5b^4+4b^3+18b^2+4b+5\right)G_1(b) = f_1(b) \\ & f_1(b) = \frac{3\left(b^2+b+1\right)\left(b^2+4b+1\right)^2\left(b^6+8b^5+15b^4+24b^3+15b^2+8b+1\right)}{(b-1)b(b+1)^5} \end{aligned} \tag{5.140}$$

The inhomogenous solution is given by

$$G_1(b) = -\frac{\left(b^2+b+1\right)\left(b^2+4b+1\right)^2}{(b-1)(b+1)^5}\log\left(\frac{b^3\left(b^2+b+1\right)\left(b^2+4b+1\right)^2}{\left(1-b^2\right)^6}\right) \tag{5.141}$$

Let us now express the periods in terms of the modular parameter τ, which lies at a cusp $\tau_c \in \mathbb{R}$ as $\mathrm{u} \to \mathrm{u})_c$. For this it is convenient to introduce a new modular parameter τ', related to τ by an element of $PGL(2,\mathbb{Z})$ such that the limit $\tau = \tau_c$ becomes $\tau' = \mathrm{i}\infty$. To relate δ and τ', it suffices to equate the Laurent expansion of the Klein Hauptmodul $J(\mathrm{u}_c+\delta,\ell)$ as $\delta \to 0$ with the q'-expansion of $J(\tau)$. In this way, we find

$$\delta = -\frac{\left(b^2-1\right)^6}{b^3\left(b^2+b+1\right)\left(b^2+4b+1\right)^2}q' + \frac{2\left(b^2-1\right)^6\left(4b^8+37b^7+106b^6+199b^5+244b^4+199b^3+106b^2+37b+4\right)}{b^6\left(b^2+b+1\right)\left(b^2+4b+1\right)^3}q'^2+\ldots \tag{5.142}$$

To obtain the expansion near a zero u_c of Δ_4, corresponding to $\tau = \tau_c$, let us introduce a local coordinate τ', related to τ by an element of $PGL(2,\mathbb{Z})$ which maps $\tau = \tau_c$ to $\tau' = \mathrm{i}\infty$. We can then expand the Klein J-invariant near u_c, and equate it with the expansion of $J(\tau')$ near $\mathrm{i}\infty$. In practice, we introduce the ratio

$$\begin{aligned} P(\mathrm{u}) := \frac{\Delta_4(\mathrm{u})}{\mathrm{u}-\mathrm{u}_c} =& \ell^3\left(4\mathrm{u}_c^3\ell(16\ell-27)-108\mathrm{u}_c^2\ell-16\mathrm{u}_c\ell+1\right) \\ &+2\ell^4(\mathrm{u}-\mathrm{u}_c)\left(\mathrm{u}_c^2(48\ell-81)-54\mathrm{u}_c-4\right)+4\ell^4(\mathrm{u}-\mathrm{u}_c)^2(\mathrm{u}_c(16\ell-27)-9) \\ &+\ell^4(16\ell-27)(\mathrm{u}-\mathrm{u}_c)^3 \end{aligned} \tag{5.143}$$

which is a cubic polynomial whenever $\Delta_4(\mathrm{u}_c)=0$, and Laurent expand $J(u) = \frac{(Q_4(\mathrm{u}))^3}{\mathrm{u}^8(\mathrm{u}-\mathrm{u}_c)P(\mathrm{u})}$ near u_c. In this way we arrive at

$$\mathrm{u} = \mathrm{u}_c + \frac{\left(16\mathrm{u}_c^4\ell^2-24\mathrm{u}_c^3\ell-8\mathrm{u}_c^2\ell+1\right)^3}{\mathrm{u}_c^8\ell^3\left(4\mathrm{u}_c^3\ell(16\ell-27)-108\mathrm{u}_c^2\ell-16\mathrm{u}_c\ell+1\right)}q' + O\left(q'^2\right) \tag{5.144}$$

where higher order corrections are readily computed. For $\ell = \underline{\ell}$, the conifold points are given by the roots of a quadratic polynomial, and the expansion can be computed more directly,

$$\mathrm{u} = \frac{8}{153}\left(5\pm 8\mathrm{i}\sqrt{2}\right) - \frac{2048\mathrm{i}\left(\pm 11369\sqrt{2}-6976\mathrm{i}\right)}{5688387}q' + \frac{16384\left(1680185024\pm 3039785485\mathrm{i}\sqrt{2}\right)}{1903396862457}q'^2+\ldots \tag{5.145}$$

5.5.4 Limit to local $\mathbb{P}^2$

As $\lambda \to 0$ keeping u fixed, the Klein Hauptmodul reduces to

$$J \to \frac{(1-24u^3)^3}{u^9(1-27u^3)} = 1728 + \frac{(1-36u^3+216u^6)^2}{u^9(1-27u^3)} \tag{5.146}$$

This agrees with [47, A.7] upon identifying $z' = -u^3$ hence $z = u^3 - \frac{1}{27}$. The algebraic Yukawa coupling (5.114) also reduces to the algebraic Yukawa coupling of local $\mathbb{P}^2$,

$$C_{uuu}(\mathrm{d}u)^3 \to -\frac{(\mathrm{d}z)^3}{3z^3(1+27z)} \tag{5.147}$$

The A-periods similarly reduce to those of local $\mathbb{P}^2$, up to an overall factor,

$$\begin{aligned} -\omega_1 &\to 1 - 6z + 90z^2 - 1680z^3 + \dots \\ 3\varpi_2 &\to \log z - 6z + 45z^2 - 560z^3 + \dots \end{aligned} \tag{5.148}$$

5.5.5 Monodromies

The spectral flow (5.5) acts on the period vector $\Pi = (1, m, T, T_D)^t$ by

$$\Pi \mapsto \begin{pmatrix} 1 & 0 & 0 & 0 \\ m_B - \frac{2m_F}{3} & 1 & 0 & 0 \\ \frac{m_F}{3} & 0 & 1 & 0 \\ m_B m_F - \frac{m_B^2}{2} & m_F - m_B & m_B + 2m_F & 1 \end{pmatrix} \Pi = \begin{pmatrix} 1 & 0 & 0 & 0 \\ 0 & 1 & 0 & 0 \\ k & 0 & 1 & 0 \\ 4k^2 & k & 8k & 1 \end{pmatrix} \Pi \tag{5.149}$$

where in the second equality, we specialized to $(m_F, m_B) = k(3, 2)$, which leaves m invariant and sends $T \mapsto T + 8k$. Moreover, the *inverse* of the monodromy matrix associated to a Seidel-Thomas twist with respect to $\mathcal{O}(m_F, m_B)$ acts by

$$M_{(m_F,m_B)} := \begin{pmatrix} 1 & 0 & 0 & 0 \\ 0 & 1 & 0 & 0 \\ \frac{1}{2}m_B(m_B - 2m_F) & m_F - m_B & m_B + 2m_F + 1 & -1 \\ \frac{1}{2}m_B\left(m_B^2 - 4m_F^2\right) & -m_B^2 - m_B m_F + 2m_F^2 & (m_B + 2m_F)^2 & -m_B - 2m_F + 1 \end{pmatrix} \tag{5.150}$$

such that $\mathcal{O}(m_F, m_B)$ becomes massless at

$$\tau = 2m_F + m_B, \quad T_D = (2m_F + m_B)T + m(m_F - m_B) + \frac{1}{2}m_B^2 - m_B m_F \tag{5.151}$$

Using the sagemath package `ore_algebra.analytic.monodromy` [150], we find the following monodromies:

- For $\lambda = 1$, around the roots $u_1, \dots, u_4$ of Δ', ordered as $\{0.2632, -3.0257, -0.2551 + 0.2216i, -0.2551 - 0.2216i\}$

$$\begin{aligned} M_1 &= \begin{pmatrix} 1 & 0 & 0 & 0 \\ 0 & 1 & 0 & 0 \\ 0 & 0 & 1 & 1 \\ 0 & 0 & 0 & 1 \end{pmatrix}, \quad M_2 = \begin{pmatrix} 1 & 0 & 0 & 0 \\ 0 & 1 & 0 & 0 \\ 0 & -1 & -1 & 1 \\ 0 & -2 & -4 & 3 \end{pmatrix}, \\ M_3 &= \begin{pmatrix} 1 & 0 & 0 & 0 \\ 0 & 1 & 0 & 0 \\ \frac{1}{2} & 0 & -2 & 1 \\ \frac{3}{2} & 0 & -9 & 4 \end{pmatrix}, \quad M_4 = \begin{pmatrix} 1 & 0 & 0 & 0 \\ 0 & 1 & 0 & 0 \\ \frac{1}{2} & 0 & 4 & 1 \\ -\frac{3}{2} & 0 & -9 & -2 \end{pmatrix} \end{aligned} \tag{5.152}$$

  Note in particular that

$$M_3 \cdot M_2 \cdot M_1 \cdot M_4 = M_{LV} := \begin{pmatrix} 1 & 0 & 0 & 0 \\ 0 & 1 & 0 & 0 \\ 1 & 0 & 1 & 0 \\ 4 & 1 & 8 & 1 \end{pmatrix} \tag{5.153}$$

  Using (5.150), the corresponding massless objects are $\mathcal{O}(0,0), \mathcal{O}(1,0), \mathcal{O}(1,1)$ and $\mathcal{O}(-1,-1)$, respectively, which become massless at $\tau = 0, -2, 3, -3$.

- For $27 + 256\lambda^3 = 0$, specifically $\lambda = \underline{\lambda} := -\frac{3}{4\cdot 2^{2/3}}$ we find instead 4 monodromy matrices, M_{LV} along with

$$M_1' = \begin{pmatrix} 1 & 0 & 0 & 0 \\ 0 & 1 & 0 & 0 \\ -\frac{1}{2} & 1 & 0 & 1 \\ -\frac{1}{2} & 1 & -1 & 1 \end{pmatrix}, \quad M_2' = \begin{pmatrix} 1 & 0 & 0 & 0 \\ 0 & 1 & 0 & 0 \\ 0 & 1 & 3 & 1 \\ 0 & -2 & -4 & -1 \end{pmatrix}, \quad M_3' = \begin{pmatrix} 1 & 0 & 0 & 0 \\ 0 & 1 & 0 & 0 \\ \frac{1}{2} & 0 & -2 & 1 \\ \frac{3}{2} & 0 & -9 & 4 \end{pmatrix} \tag{5.154}$$

around the points

$$u_1' = -\frac{8\underline{\lambda}}{9} \simeq 0.420, \quad u_2' = \frac{8\underline{\lambda}}{153}(5 - 8\mathrm{i}\sqrt{2}) \simeq -0.123 - 0.279\mathrm{i}, \quad u_3' = \frac{8\underline{\lambda}}{153}(5 + 8\mathrm{i}\sqrt{2}), \tag{5.155}$$

such that

$$M_3' M_1' M_2' M_{LV} = 1\,, \quad (M_1')^6 = 1, \quad (M_1')^3 = \begin{pmatrix} 1 & 0 & 0 & 0 \\ 0 & 1 & 0 & 0 \\ -1 & 2 & -1 & 0 \\ 0 & 0 & 0 & -1 \end{pmatrix} \tag{5.156}$$

The point u_1' is an Argyres-Douglas type point, where both $\mathcal{O}(0,0)$ and $\mathcal{O}(0,1)$ are massless, since of $T = m - \frac{1}{2}, T_D = 0$ at that point. In fact, the inverse of M_1' is the product of two ST twists, $(M_1')^{-1} = M_{(0,0)} \cdot M_{(0,1)}$. On the other hand, u_2' and u_3' are conifold points where $\mathcal{O}(-1,0)$ and $\mathcal{O}(1,1)$ are massless, respectively.

- For $\lambda = -1/4$, $m = \frac{\log(1/4)}{2\pi\mathrm{i}} + \frac{1}{2}$, we find

$$\begin{aligned} M_1'' &= \begin{pmatrix} 1 & 0 & 0 & 0 \\ 0 & 1 & 0 & 0 \\ 0 & 0 & 1 & 0 \\ -\frac{1}{2} & 1 & -1 & 1 \end{pmatrix}, \quad M_2'' = \begin{pmatrix} 1 & 0 & 0 & 0 \\ 0 & 1 & 0 & 0 \\ 0 & 1 & 3 & 1 \\ 0 & -2 & -4 & -1 \end{pmatrix}, \\ M_3'' &= \begin{pmatrix} 1 & 0 & 0 & 0 \\ 0 & 1 & 0 & 0 \\ \frac{1}{2} & 0 & -2 & 1 \\ \frac{3}{2} & 0 & -9 & 4 \end{pmatrix}, \quad M_4'' = \begin{pmatrix} 1 & 0 & 0 & 0 \\ 0 & 1 & 0 & 0 \\ 0 & 0 & 1 & 1 \\ 0 & 0 & 0 & 1 \end{pmatrix} \end{aligned} \tag{5.157}$$

correspond to SD twists with respect to $[0,0,1,-\frac{1}{2}], \mathcal{O}(-1,0), \mathcal{O}(1,1), \mathcal{O}(0,0)$, which are massless at $\tau = \mathrm{i}\infty, 3, 1, -1$, respectively. Note that $M_1' = M_4'' M_1'', M_2' = M_2'', M_3' = M_3'' = M_3, M_1 = M_4''$.

- For $\lambda = -(-1)^{1/3}/4 \simeq \frac{1}{8} + .216\mathrm{i}$, the four monodromies are associated to $\mathcal{O}(0,0), \mathcal{O}(1,1), \mathcal{O}(-1,-1)$ and $GV(0,1,-\frac{1}{2})$. The product of the last two gives the monodromy of the AD point.

- For $\lambda = -(-1)^{2/3}/4 \simeq \frac{1}{8} - .216\mathrm{i}$, the four monodromies are associated to $\mathcal{O}(0,0)$, $\mathcal{O}(-1,-1), \mathcal{O}(1,1)$ and $GV(0,1,\frac{1}{2})$. The product of the last two gives the monodromy of the AD point.

Finally, at the orbifold point $u = -8\lambda/9$ for λ real, we seem to find

$$\operatorname{Re} T_D = -2 \operatorname{Re} T, \quad \operatorname{Im} T = -\frac{1}{2} \operatorname{Im} m, \quad \operatorname{Re} \tau = -\frac{1}{4} \tag{5.158}$$

while $\operatorname{Im} T_D$ and $\operatorname{Re} T$ seem to be random values.

Redoing the analysis in (u, ℓ) coordinates, we find

- For $\ell = 1$, around the roots $\mathrm{u}_1, \ldots, \mathrm{u}_4$ for Δ_4, ordered as $\{-0.255099+0.221553\mathrm{i}, -0.255099-0.221553\mathrm{i}, -3.02572, 0.263185\}$

$$\begin{pmatrix} 1 & 0 & 0 & 0 \\ 0 & 1 & 0 & 0 \\ \frac{1}{2} & 0 & -2 & 1 \\ \frac{3}{2} & 0 & -9 & 4 \end{pmatrix}, \begin{pmatrix} 1 & 0 & 0 & 0 \\ 0 & 1 & 0 & 0 \\ \frac{1}{2} & 0 & 4 & 1 \\ -\frac{3}{2} & 0 & -9 & -2 \end{pmatrix}, \begin{pmatrix} 1 & 0 & 0 & 0 \\ 0 & 1 & 0 & 0 \\ 0 & 0 & 1 & 0 \\ \frac{1}{2} & 1 & -1 & 1 \end{pmatrix}, \begin{pmatrix} 1 & 0 & 0 & 0 \\ 0 & 1 & 0 & 0 \\ 0 & 0 & 1 & 1 \\ 0 & 0 & 0 & 1 \end{pmatrix} \tag{5.159}$$

  corresponding to spherical twist with respect to $\mathcal{O}(1,1), \mathcal{O}(-1,-1), GV[0,1,1/2], \mathcal{O}(0,0)$, respectively.

- For $\ell = 2$, around the roots $\mathrm{u}_1, \ldots, \mathrm{u}_4$ for Δ_4, ordered as $\{0.2, 7.41375, -0.206875 + 0.156987\mathrm{i}, -0.206875 - 0.156987\mathrm{i}\}$

$$\begin{pmatrix} 1 & 0 & 0 & 0 \\ 0 & 1 & 0 & 0 \\ 0 & 0 & 1 & 1 \\ 0 & 0 & 0 & 1 \end{pmatrix}, \begin{pmatrix} 1 & 0 & 0 & 0 \\ 0 & 1 & 0 & 0 \\ 0 & -1 & -1 & 1 \\ 0 & -2 & -4 & 3 \end{pmatrix}, \begin{pmatrix} 1 & 0 & 0 & 0 \\ 0 & 1 & 0 & 0 \\ \frac{1}{2} & 0 & -2 & 1 \\ \frac{3}{2} & 0 & -9 & 4 \end{pmatrix}, \begin{pmatrix} 1 & 0 & 0 & 0 \\ 0 & 1 & 0 & 0 \\ \frac{1}{2} & 0 & 4 & 1 \\ -\frac{3}{2} & 0 & -9 & -2 \end{pmatrix} \tag{5.160}$$

  corresponding to spherical twist with respect to $\mathcal{O}(0,0), \mathcal{O}(1,0), \mathcal{O}(1,1), \mathcal{O}(-1,-1)$, respectively.

- For $\ell = -1$, around the roots $\mathrm{u}_1, \ldots, \mathrm{u}_4$ for Δ_4, ordered as $\{-0.512108+0.1945\mathrm{i}, -0.512108-0.1945\mathrm{i}, 0.0935038 + 0.262211\mathrm{i}, 0.0935038 - 0.262211\mathrm{i}\}$,

$$\begin{pmatrix} 1 & 0 & 0 & 0 \\ 0 & 1 & 0 & 0 \\ \frac{3}{2} & -1 & -4 & 1 \\ \frac{15}{2} & -5 & -25 & 6 \end{pmatrix}, \begin{pmatrix} 1 & 0 & 0 & 0 \\ 0 & 1 & 0 & 0 \\ 0 & 1 & 3 & 1 \\ 0 & -2 & -4 & -1 \end{pmatrix}, \begin{pmatrix} 1 & 0 & 0 & 0 \\ 0 & 1 & 0 & 0 \\ \frac{1}{2} & 0 & -2 & 1 \\ \frac{3}{2} & 0 & -9 & 4 \end{pmatrix}, \begin{pmatrix} 1 & 0 & 0 & 0 \\ 0 & 1 & 0 & 0 \\ 0 & 0 & 1 & 1 \\ 0 & 0 & 0 & 1 \end{pmatrix} \tag{5.161}$$

  corresponding to spherical twist with respect to $\mathcal{O}(2,1), \mathcal{O}(-1,0), \mathcal{O}(1,1), \mathcal{O}(0,0)$, respectively.

- For $\ell = -27/256$, more precisely $m = -1/6 + 0.119331\mathrm{i}$ around the 3 roots $\mathrm{u}_1, \ldots, \mathrm{u}_3$ of Δ_4 ordered as

$$\mathrm{u}_1 = -\frac{8}{9}, \quad \mathrm{u}_2 = \frac{8}{153}(5+8\mathrm{i}\sqrt{2}) \simeq 0.261+0.592\mathrm{i}, \quad \mathrm{u}_3 = \frac{8}{153}(5-8\mathrm{i}\sqrt{2}) \simeq 0.261-0.592\mathrm{i}, \tag{5.162}$$

$$\begin{pmatrix} 1 & 0 & 0 & 0 \\ 0 & 1 & 0 & 0 \\ \frac{1}{2} & 0 & -2 & 1 \\ \frac{3}{2} & 1 & -7 & 3 \end{pmatrix}, \begin{pmatrix} 1 & 0 & 0 & 0 \\ 0 & 1 & 0 & 0 \\ 0 & 0 & 1 & 1 \\ 0 & 0 & 0 & 1 \end{pmatrix}, \begin{pmatrix} 1 & 0 & 0 & 0 \\ 0 & 1 & 0 & 0 \\ \frac{1}{2} & 0 & 4 & 1 \\ -\frac{3}{2} & 0 & -9 & -2 \end{pmatrix} \tag{5.163}$$

The last two correspond to spherical twists with respect to $\mathcal{O}(0,0)$ and $\mathcal{O}(-1,-1)$, while the first one, associated to the Argyres-Douglas point, is a monodromy of order 6, equal to the inverse of $M_{\mathcal{O}(1,1)} \cdot M_{\mathrm{GV}(0,1,1/2)}$. The values of (τ, T, T_D) at this point are $(\frac{5}{2} + \mathrm{i}\frac{\sqrt{3}}{2}, m + \frac{1}{2}, 3m + 1)$, invariant under monodromy as they should.

5.6 The Non-congruence subgroup $\Gamma(10; 0, 3, 0, 1; 8)$

The monodromy group for $\lambda = \underline{\lambda} := -\frac{3}{4\cdot 2^{2/3}}$ is an extension of a subgroup of $PSL(2,\mathbb{Z})$ generated by the lower-right blocks of the monodromy matrices (5.154),

$$g_1 = \begin{pmatrix} 1 & -1 \\ 1 & 0 \end{pmatrix}, \quad g_2 = \begin{pmatrix} -1 & -4 \\ 1 & 3 \end{pmatrix}, \quad g_3 = \begin{pmatrix} -1 & -1 \\ 4 & 3 \end{pmatrix}, \tag{5.164}$$

such that

$$g_1^3 = \begin{pmatrix} -1 & 0 \\ 0 & -1 \end{pmatrix}, \quad g_1 \cdot g_3 \cdot g_2 = \begin{pmatrix} 1 & 8 \\ 0 & 1 \end{pmatrix}, \quad g_1 \cdot g_3 \cdot g_1^{-1} = \begin{pmatrix} 4 & -9 \\ 1 & -2 \end{pmatrix} \tag{5.165}$$

As anticipated in [139] on the basis of the classification of rational elliptic surfaces, this is a non-congruence subgroup of $PSL(2,\mathbb{Z})$ of index 10, genus zero, with 3 cusps of widths $(8, 1, 1)$, no elliptic point of order 2, and one elliptic point of order 3 (corresponding to the Argyres-Douglas point). Non-congruence subgroups of index ≤ 11 were classified in [173], and a conjugate of Γ, denoted by $\Gamma' = \Gamma(10; 0, 3, 0, 1; 8)$, appears as the last in the index 10 subgroups in Table 2. As noted in [173, Example 34], Γ' has width one cusps at $\tau = 2$ and 5 modulo 8, whereas Γ has width one cusps at $\tau = 3$ and $\tau = 6$ modulo 8, so $\Gamma = T\Gamma' T^{-1}$.

In general, subgroups of $PSL(2,\mathbb{Z})$ are classified by the permutations σ_S, σ_R through which the order two and three generators $S = \left(\begin{smallmatrix} 0 & -1 \\ 1 & 0 \end{smallmatrix}\right)$, $R = \left(\begin{smallmatrix} 0 & -1 \\ 1 & 1 \end{smallmatrix}\right)$ act on the cosets $PSL(2,\mathbb{Z})/\Gamma$. Relabelling those cosets such that the generator $T = \left(\begin{smallmatrix} 1 & 1 \\ 0 & 1 \end{smallmatrix}\right)$ acts by cyclic permutations of the first 8 of them, $\sigma_T = (1,2,3,4,5,6,7,8)(9)(10)$, we have

$$\sigma_S = (1,8)(2,4)(5,7)(3,9)(6,10), \quad \sigma_R = (8,2,5)(4,3,9)(7,6,10) \tag{5.166}$$

Using Sagemath package `sage.modular.arithgroup.arithgroup_perm`[9], we readily check that Γ is generated by the matrices in (5.164), and obtain an explicit list of cosets:

$$\{c_i\}_{i=1\ldots 10} = \{1, T^7, T^6, T^5, T^4, T^3, T^2, T, \begin{pmatrix} 6 & -1 \\ 1 & 0 \end{pmatrix}, \begin{pmatrix} 3 & -1 \\ 1 & 0 \end{pmatrix}\} \tag{5.167}$$

A fundamental domain of Γ can thus be obtained as the union of the images of the standard 'keyhole' fundamental domain of $PSL(2,\mathbb{Z})$ under the cosets c_i (see Figure 5.10).

Note that the generators g_i in (5.164) leave the points $\tau = -2, -\frac{1}{2}, e^{i\pi/3}$ invariant, respectively. Under these generators, we find the orbit of the three cusps and the elliptic point in the range $0 \leq \tau_1 < 8$,

$$\{i\infty, 0, 1, 2, 4, 5, 7, \tfrac{1,7,9,13}{2}, \tfrac{4,5,7,8,10,11,13,14,16,17,19,20}{3}, \ldots\}, \tag{5.168}$$

$$\{3, \tfrac{15}{2}, \tfrac{2}{3}, \ldots\}, \quad \{6, \tfrac{3}{2}, \tfrac{1}{3}, \ldots\}, \quad \{e^{i\pi/3}, \tfrac{9}{2} + \tfrac{i}{2\sqrt{3}}, \tfrac{175+i\sqrt{3}}{26}, \ldots\} \tag{5.169}$$

The dots indicate images with larger denominators, or, in the case of the elliptic point, smaller imaginary parts. In particular, the fixed points $\tau = -2$, $\tau = -1/2$ under g_1, g_2 are in the orbit of $\tau = 6$ and $\tau = 3$, respectively, and these two orbits are exchanged under $\tau \mapsto 1 - \bar{\tau}$.

[9] Define `G = ArithmeticSubgroup_Permutation(S2="(1,8)(2,4)(5,7)(3,9)(6,10)", S3="(8,2,5) (4,3,9) (7,6,10)")` and type `G.generators(), G.cosets()`

Modular forms for the non-congruence subgroup Γ' were computed in [40, 41][10]. The generators provided by Sage,

$$g_1' = \begin{pmatrix} 1 & 1 \\ -1 & 0 \end{pmatrix}, \quad g_2' = \begin{pmatrix} 3 & -1 \\ 4 & -1 \end{pmatrix}, \quad g_3' = \begin{pmatrix} 3 & -4 \\ 1 & -1 \end{pmatrix} \tag{5.170}$$

satisfy

$$(g_1')^3 = \begin{pmatrix} -1 & 0 \\ 0 & -1 \end{pmatrix}, \quad g_3' g_2' g_1'^{-1} = \begin{pmatrix} 1 & 8 \\ 0 & 1 \end{pmatrix}, \tag{5.171}$$

and are related to those in (5.164) by

$$g_1' = T^{-1} g_1^{-1} T, \quad g_2' = T^{-1} g_1 g_2 g_1^{-1} T, \quad g_3' = T^{-1} g_1 g_3 g_1^{-1} T. \tag{5.172}$$

confirming that Γ' is therefore conjugate to Γ under T. In particular, Γ' has cusps of width 1 at $\tau = 2, 5$, and width 8 at $\tau = \mathrm{i}\infty$. The Hauptmodul $J_{\Gamma'}$ was determined in [40] via the Belyi map relating it to the Klein J-invariant,

$$\begin{aligned} J(\tau) =& \frac{(10w + J_{\Gamma'})\left(208w^3 + 120w^2 J_{\Gamma'} - 6wJ_{\Gamma'}^2 + J_{\Gamma'}^3\right)^3}{J_{\Gamma'}^2 - 8wJ_{\Gamma'} + 144w^2} \\ =& 1728 + \frac{\left(70624w^5 - 760w^4 J_{\Gamma'} + 928w^3 J_{\Gamma'}^2 + 136w^2 J_{\Gamma'}^3 - 4wJ_{\Gamma'}^4 + J_{\Gamma'}^5\right)^2}{J_{\Gamma'}^2 - 8wJ_{\Gamma'} + 144w^2} \end{aligned} \tag{5.173}$$

where $w := -(-1/3^9)^{1/8} \simeq -0.268444 - 0.111193\mathrm{i}$. Inserting the q-expansion $J(\tau) = 1/q_8^8 + 744 + \ldots$, where $q_8 := e^{2\pi \mathrm{i}\tau/8}$, one obtains the q_8-series expansion

$$\begin{aligned} J_{\Gamma'} =& \frac{1}{q_8} - 18q_8w^2 - 240q_8^2w^3 + 288q_8^3w^4 - 2304q_8^4w^5 - 10176q_8^5w^6 + 31680q_8^6w^7 \\ & - 111987q_8^7w^8 + 243712q_8^8w^9 + 712170q_8^9w^{10} + 19958112q_8^{10}w^{11} - 28207584q_8^{11}w^{12} + \ldots \end{aligned} \tag{5.174}$$

Note that after rescaling $q_8 \to q_8/w$, the Fourier coefficients are integer up to an overall factor of w.

As explained in [41, §5.3], a basis of holomorphic modular forms of (even) weight k for a subgroup Γ with Hauptmodul J can be constructed from powers of the τ-derivative $q\partial_q J$, multiplied by a suitable rational function in J. Indeed, $q\partial_q J$ transforms as a modular form of weight 2 and vanishes at finite cusps and at elliptic points. Denoting by C, $\mathcal{E}_2$ and $\mathcal{E}_3$ the set of finite cusps, elliptic points of order 2 and elliptic points of order 3, the following ratio is then a holomorphic modular form:

$$\phi_{2k,i} = \frac{(q\partial_q J)^{k/2}\, J^{d-k/2-i}}{\prod_{e\in\mathcal{E}_2}(J-j_e)^{\lfloor k/4\rfloor} \prod_{e\in\mathcal{E}_3}(J-j_e)^{\lfloor k/3\rfloor} \prod_{c\in C}(J-j_c)^{k/2}} \tag{5.175}$$

with $d = |\mathcal{E}_2|\lfloor k/4\rfloor + |\mathcal{E}_3|\lfloor k/3\rfloor + (|C|-1)\frac{k}{2}$ is the degree of the denominator and i runs over the range $0 \le i \le d - k/2$. For the group Γ' with one order 3 elliptic point and two cusps, this reduces to

$$\phi_{2k,i} = \frac{(q_8\partial_{q_8} J_{\Gamma'})^{k/2}\, J_{\Gamma'}^{\lfloor k/3\rfloor + k/2 - i}}{(J_{\Gamma'} + 10w)^{\lfloor k/3\rfloor}(J_{\Gamma'}^2 - 8wJ_{\Gamma'} + 144w^2)^{k/2}} \tag{5.176}$$

[10] The unique LMFDB identifier is `10T30-8.1.1_3.3.3.1_2.2.2.2.2-a`, where `10T30` stands for the finite group $PGL(2,\mathbb{F}_9) = A_6 \rtimes C_2$ spanned by σ_S and σ_R of order 720 inside the permutation group $\mathcal{S}_{10}$.

for $0 \le i \le \lfloor k/3 \rfloor + k/2$, leading to a two-dimensional space of modular forms of weight 2, respectively 4-dimensional space of weight 4, 6-dimensional space of weight 6, etc. A basis of cusp forms can similarly be obtained by requiring a factor $(\prod_{c\in C}(J - j_c))/J$ in the numerator,

$$\psi_{2k,i} = \frac{(q_8\partial_{q_8} J_{\Gamma'})^{k/2}\, J_{\Gamma'}^{\lfloor k/3\rfloor + k/2 - i - 2}}{(J_{\Gamma'} + 10w)^{\lfloor k/3\rfloor}(J_{\Gamma'}^2 - 8wJ_{\Gamma'} + 144w^2)^{\frac{k}{2}-1}} \tag{5.177}$$

for $0 \le i \le \lfloor k/3 \rfloor + k/2 - 3$. The first cusp form $\psi_{4,0}$ thus occurs in weight 4.

For $\lambda = \underline{\lambda}$, we find that the q_8-expansion of $1/u$ in (5.111) matches the q'_8 expansion (5.174) of the Hauptmodul of Γ', upon replacing $q_8 \mapsto e^{-i\pi/4} q'_8$ (taking into account that Γ and Γ' are conjugate under T), up to an additive constant and multiplicative factor,

$$1/u = \frac{J_{\Gamma'} + w}{8\underline{\lambda} w} \tag{5.178}$$

Indeed, under this identification, (5.173) reduces to

$$\begin{aligned} J(\tau) =& -\frac{(8\underline{\lambda} + 9u)\left(81u^3 + 1080\underline{\lambda}u^2 - 576\underline{\lambda}^2 u - 54\right)^3}{3^9 u^8\left(153u^2 - 80\underline{\lambda}u + 64\underline{\lambda}^2\right)} \\ =& 1728 - \frac{\left(72171u^5 - 17496\underline{\lambda}u^4 + 31104\underline{\lambda}^2u^3 - 8748u^2 - 36864\underline{\lambda}^4 u + 32768\underline{\lambda}^5\right)^2}{3^9 u^8\left(153u^2 - 80\underline{\lambda}u + 64\underline{\lambda}^2\right)} \end{aligned} \tag{5.179}$$

which matches the Klein Hauptmodul (5.63) at $\lambda = \underline{\lambda}$, using the fact that

$$\begin{aligned} 1 - 8\underline{\lambda}u^2 - 24u^3 + 16\underline{\lambda}^2u^4 &= -\frac{(9u + 8\underline{\lambda})}{432\underline{\lambda}}\left(81u^3 + 1080u^2\underline{\lambda} - 576u\underline{\lambda}^2 - 54\right) \\ \underline{\lambda} + u - 8\underline{\lambda}^2u^2 - 36\underline{\lambda}u^3 + \left(16\underline{\lambda}^3 - 27\right)u^4 &= -\frac{(9u + 8\underline{\lambda})^2}{432}\left(153u^2 - 80u\underline{\lambda} + 64\underline{\lambda}^2\right) \end{aligned} \tag{5.180}$$

Moreover, the square of the inverse Yukawa $C^2 = (1/C_{TTT})^2$ can be identified as a weight 6 holomorphic modular form, see (5.122), while the square of the A-period $(\omega_1)^2$ is identified as a weight 2 meromorphic modular form with a simple pole at the orbifold point, see (5.123).

Away from the locus $\lambda = \underline{\lambda}$, it seems that one should express u in terms of the Hauptmodul $\underline{u} = \frac{8\underline{\lambda}w}{J_{\Gamma'}+w}$ by equating the numerators and denominators, up to a scale factor f,

$$\begin{aligned} 1 - 8\lambda u^2 - 24u^3 + 16\lambda^2u^4 &= -f\frac{(9\underline{u} + 8\underline{\lambda})}{432\underline{\lambda}}\left(81\underline{u}^3 + 1080\underline{u}^2\underline{\lambda} - 576\underline{u}\underline{\lambda}^2 - 54\right) \\ u^8\left(\lambda + u - 8\lambda^2u^2 - 36\lambda u^3 + \left(16\lambda^3 - 27\right)u^4\right) &= -f^3\underline{u}^8\frac{(9\underline{u} + 8\underline{\lambda})^2}{432}\left(153\underline{u}^2 - 80\underline{u}\underline{\lambda} + 64\underline{\lambda}^2\right) \end{aligned} \tag{5.181}$$

Solving order by order in powers of $\lambda - \underline{\lambda}$, we find

$$\begin{aligned} u =& \underline{u} - \frac{\left(\underline{u}\left(32\underline{\lambda}^2\underline{u}\left(891\underline{u}^6 - 126\underline{u}^3 + 4\right) + 72\underline{\lambda}\underline{u}^2\left(15\underline{u}^3 - 2\right) + 3\left(243\underline{u}^6 - 90\underline{u}^3 + 4\right)\right)\right)}{6\left(192\underline{\lambda}^2\left(12\underline{u}^3 - 1\right)\underline{u}^2 + 4\underline{\lambda}\left(891\underline{u}^6 - 144\underline{u}^3 + 4\right) - 81\underline{u}^4\right)}(\lambda - \underline{\lambda}) \\ &+ O\left((\lambda - \underline{\lambda})^2\right) \\ f =& 1 - \frac{12\left(16\underline{\lambda}^2\left(891\underline{u}^6 - 144\underline{u}^3 + 4\right)\underline{u}^2 - 324\underline{\lambda}\underline{u}^6 - 972\underline{u}^7 + 81\underline{u}^4\right)}{\left(8\underline{\lambda} + 9\underline{u}\right)\left(192\underline{\lambda}^2\left(12\underline{u}^3 - 1\right)\underline{u}^2 + 4\underline{\lambda}\left(891\underline{u}^6 - 144\underline{u}^3 + 4\right) - 81\underline{u}^4\right)}(\lambda - \underline{\lambda}) \\ &+ O\left((\lambda - \underline{\lambda})^2\right) \\ =& 1 - \frac{12\left(16\underline{\lambda}^2\left(891u^6 - 144u^3 + 4\right)u^2 - 324\underline{\lambda}u^6 - 972u^7 + 81u^4\right)}{\left(8\underline{\lambda} + 9u\right)\left(192\underline{\lambda}^2\left(12u^3 - 1\right)u^2 + 4\underline{\lambda}\left(891u^6 - 144u^3 + 4\right) - 81u^4\right)}(\lambda - \underline{\lambda}) + O\left((\lambda - \underline{\lambda})^2\right) \end{aligned} \tag{5.182}$$

The value of J_Γ where $j = j_B$ is given by

$$J_\Gamma/w = -10 - \frac{2^{52}}{3^{17}}(\ell - \underline{\ell}) - \frac{2^{57}\cdot 103\cdot 199\cdot 401\cdot 857\cdot 871621}{3^{38}}(\ell - \underline{\ell})^2 + \ldots \tag{5.183}$$

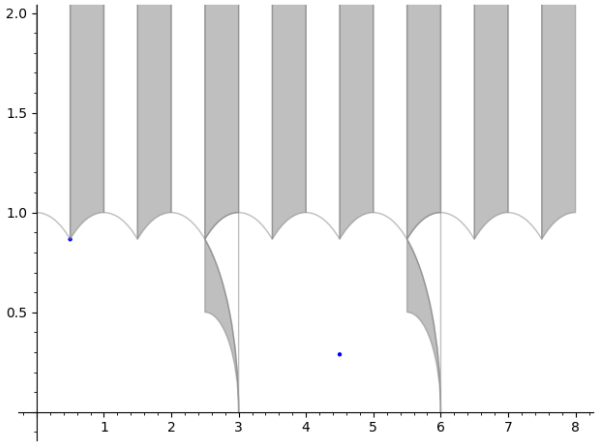


Figure 5.10: A fundamental domain for the non-congruence subgroup Γ. The blue dots correspond to elliptic points of order 3.

5.7 Conifold periods from dilogarithms

In [80], a formalism was developped for computing the regulator period of singular elliptic curves in toric ambient spaces. In the simplest case of a type I_1 nodal degeneration, the key step is to obtain a rational parametrization of the nodal curve of the form

$$X = A\prod_j (1 - \alpha_j/z)^{d_j}, \quad Y = B\prod_k (1 - z/\beta_k)^{e_k} \tag{5.184}$$

such that the node connects the points $z = 0$ and $z = \infty$. The regulator period is then given by [80, (4.12)] (after overall rescaling

$$\begin{aligned} 4\pi^2 \mathcal{Q} = & \sum_{j,k} d_j e_k \left[\mathrm{Li}_2(\frac{\alpha_j}{\beta_k}) + (\log \alpha_j - \log \beta_k) \log(1 - \frac{\alpha_j}{\beta_k}) \right] \\ & - \log Y(0)(\log X(0) - \log X(\infty)) + \log Y(0) \sum_j d_j \log \alpha_j \\ & - \log X(\infty) \sum_k e_k \log \beta_k . \end{aligned} \tag{5.185}$$

Note that $\sum_j d_j = \sum_k e_k = 0$ in order for X, Y to take finite values at $z = 0, \infty$.

Here we apply this formalism to compute the values of T and T_D at conifold points, where the mirror curve admits a nodal degeneration.[11] We start with the mirror curve in toric coordinates

$$x + y + \frac{\ell}{xy} + \frac{\ell}{x} = \frac{1}{\mathrm{u}} \tag{5.186}$$

In order to put the curve in Weierstrass form (5.57), we perform the birational change of coordinates

$$x = \frac{\frac{Y}{12\mathrm{u}} + 18\ell \mathrm{u}^2}{X + 12\ell \mathrm{u}^2 - 3}, \qquad y = -\frac{36\ell \mathrm{u}^2}{X + 12\ell \mathrm{u}^2 - 3}. \tag{5.187}$$

Now, when $\Delta_4(\mathrm{u}) = 0$, the Weierstrass form (5.57) degenerates into

$$Y^2 = 4(X - X_0)^2 (X - X_1), \quad X_0 = -\frac{3g_3}{2g_2}, \quad X_1 = -2X_0 \tag{5.188}$$

The nodal curve then admits the rational parametrization

$$X = t^2 - 2X_0, \qquad Y = t\left(2t^2 - 3X_0\right). \tag{5.189}$$

where $t \in \mathbb{C}$, such that the original toric coordinates are given by

$$\begin{aligned} x &= \frac{3(t^2 - 2X_0) + t(t^2 - 3X_0) - 9 + 36\ell \mathrm{u}^2 (1 + 3\mathrm{u})}{6\mathrm{u}\left(t^2 - 2X_0 - 3 + 12\ell \mathrm{u}^2\right)}, \\ y &= \frac{36\ell \mathrm{u}^2}{2X_0 + 3 - 12\ell \mathrm{u}^2 - t^2}. \end{aligned} \tag{5.190}$$

Introducing the parameter $t_1 = \sqrt{2X_0 + 3 - 12\ell \mathrm{u}^2}$, such that the denominator of y becomes $t^2 - t_1^2$, one verifies that on the discriminant locus, the numerator of x factorizes as

$$3(t^2 - 2X_0) + t(t^2 - 3X_0) - 9 + 36\ell \mathrm{u}^2 (1 + 3\mathrm{u}) = (t - t_1)^2 (t + 2t_1 + 3), \tag{5.191}$$

Moreover, in terms of t_1 we have

$$\ell = \frac{27(t_1 + 1)^3 (t_1 + 3)}{16 t_1^4}, \quad \mathrm{u} = \frac{2t_1^2}{9(t_1 + 1)}, \quad X_0 = t_1(t_1 + 2) \tag{5.192}$$

[11] We are grateful to Marcos Marino for sharing a note outlining the key steps in this computation.

Going back to the original toric coordinates, we obtain the rational parametrization

$$x = \frac{(t-t_1)(t+2t_1+3)}{6\mathrm{u}(t+t_1)}, \qquad y = -\frac{36\mathrm{u}^2}{t^2-t_1^2}. \tag{5.193}$$

such that the nodes lie at $t = \pm\sqrt{3X_0}$. In order to map them to 0 and ∞, it suffices to perform the $SL(2,\mathbb{C})$ transformation

$$z = \frac{t-\sqrt{3X_0}}{t+\sqrt{3X_0}}. \tag{5.194}$$

In terms of z, the parametrization (5.193) takes the form

$$x = A\,\frac{(z-1/b^2)(z-b)}{(z-1/b)(z-1)}, \qquad y = B\,\frac{(z-1)^2}{(z-b)(z-1/b)}, \tag{5.195}$$

where

$$b = \frac{t_1-\sqrt{3X_0}}{t_1+\sqrt{3X_0}}, \quad A = -\frac{b\left(b^2+b+1\right)}{(b+1)^4}, \quad B = -\frac{b^2+b+1}{(b+1)^2} \tag{5.196}$$

We note that on the discriminant locus, u, ℓ and t_1 can all be expressed as rational functions of b,

$$\ell = -\frac{b\left(b^2+b+1\right)^3}{(b+1)^8}, \quad \mathrm{u} = -\frac{(b+1)^4}{\left(b^2+b+1\right)\left(b^2+4b+1\right)}, \quad t_1 = -\frac{3(b+1)^2}{b^2+4b+1} \tag{5.197}$$

For fixed ℓ, there are generically 8 values of b, related in pairs under the involution $b \to 1/b$. At the special value $\ell = -27/256$, the root $b = 1$ occurs with multiplicity 4, corresponding to $\mathrm{u} = -8/9$, along with two additional pairs of roots corresponding to $\mathrm{u} = \frac{8}{153}(5 \pm 8\mathrm{i}\sqrt{2})$. At $\ell = 0$, the roots $e^{2\pi\mathrm{i}/3}, e^{4\pi\mathrm{i}/3}$ each occur with multiplicity 3, while $b = 0$ occurs with multiplicity 1. At $\ell = \infty$, the root $b = -1$ occurs with multiplicity 8. This ramification structure is of course consistent with Riemann-Hurwitz formula (see footnote 5).

ℓ	b	u	$Q(b)$	T	T_D	massless
1	$-0.7251497610 - 0.6885911879\mathrm{i}$	0.263	$-0.1841935331\mathrm{i}$	Q	0	$\mathcal{O}(0,0)$
	-4.402515245	-3.026	-0.2309698649	$\frac{1}{2}$	$\frac{3}{2} - Q$	$\mathrm{GV}(0,1,\frac{1}{2})$
	$-1.016583417 - 1.122079973\mathrm{i}$	$-0.255 - 0.222\mathrm{i}$	$0.3753225891 - 0.1550612280\mathrm{i}$	Q	$-3Q - \frac{1}{2}$	$\mathcal{O}(-1,-1)$
	$-1.016583417 + 1.122079973\mathrm{i}$	$-0.255 + 0.222\mathrm{i}$	$0.3753225891 + 0.1550612280\mathrm{i}$	$-Q$	$-3Q - \frac{1}{2}$	$\mathcal{O}(1,1)$
2	-0.2810370499	7.413	$0.2068883162 + 0.0551589000\mathrm{i}$	$-Q - 2m$	$-2Q - 3m$	$\mathcal{O}(1,0)$
	$-0.7500000000 + 0.6614378278\mathrm{i}$	1/5	$0.2263378581\mathrm{i}$	$Q + m$	0	$\mathcal{O}(0,0)$
	$-1.107886516 - 1.057104151\mathrm{i}$	$-0.207 - 0.157\mathrm{i}$	$0.3827232997 - 0.1962048569\mathrm{i}$	$Q + m$	$3Q + 3m - \frac{1}{2}$	$\mathcal{O}(1,1)$
	$-1.107886516 + 1.057104151\mathrm{i}$	$-0.207 + 0.157\mathrm{i}$	$0.3827232997 + 0.1962048569\mathrm{i}$	$Q - m$	$3Q - 3m - \frac{1}{2}$	$\mathcal{O}(-1,-1)$
-1	$-0.2575549702 - 0.2778334856\mathrm{i}$	$-0.512 - 0.195\mathrm{i}$	$-0.5570091734 - 0.1033985032\mathrm{i}$	$Q + m - 1$	$-2Q - 3m + 2$	$\mathcal{O}(-1,0)$
	$-0.2575549702 + 0.2778334856\mathrm{i}$	$-0.512 + 0.195\mathrm{i}$	$-0.5570091734 + 0.1033985032\mathrm{i}$	$-Q + m + 1$	$-5Q + 3m + 4$	$\mathcal{O}(2,1)$
	$-0.6006581337 - 0.5900126542\mathrm{i}$	$0.094 + 0.262\mathrm{i}$	$-0.1891167048 - 0.1775197647\mathrm{i}$	$Q + m$	$3Q$	$\mathcal{O}(1,1)$
	$-0.6006581337 + 0.5900126542\mathrm{i}$	$0.094 - 0.262\mathrm{i}$	$-0.1891167048 + 0.1775197647\mathrm{i}$	$-Q + m$	0	$\mathcal{O}(0,0)$
$-\frac{27}{256}$	$-0.5459669299 - 0.6836214670i$	$0.261 + 0.592\mathrm{i}$	$-0.1802984704 - 0.0463640951\mathrm{i}$	$Q + m$	0	$\mathcal{O}(0,0)$
	$-0.5459669299 + 0.6836214670i$	$0.261 - 0.592\mathrm{i}$	$-0.1802984704 + 0.0463640951\mathrm{i}$	$-Q + m$	$3Q - 3m - \frac{1}{2}$	$\mathcal{O}(-1,-1)$

Table 5.3: Periods at conifold points.

Now, applying the formula (5.185) with $\alpha_j = (1,1,-1,-1), \beta_k = (2,-1,-1)$, and using

functional identities satisfied by the dilogarithm function, we arrive at

$$\begin{aligned}\mathcal{Q}(b) =& \frac{1}{4\pi^2}\left[\mathrm{Li}_2(b^3) - 4\,\mathrm{Li}_2(b^2) + 5\,\mathrm{Li}_2(b)\right] + \frac{1}{8\pi^2}(\log b)^2 \\ &+ \frac{3}{4\pi^2}\log b\,\log(b^2+b+1) - \frac{2}{\pi^2}\log b\,\log(b+1) - \frac{1}{12} \\ &+ \frac{3\mathrm{i}}{2\pi}\Theta(-b_1-\tfrac{1}{2})\,\mathrm{sign}(b_2)\,\left(1-\Theta(b_2-\sqrt{3}b_1)\,\Theta(-b_2-\sqrt{3}b_1)\,\Theta(b_2)\right)\log b \\ &- \frac{1}{2}\Theta(-b_1)\left[2\Theta(|b|-1)\Theta(b_2-\sqrt{3}b_1)\,\Theta(-b_2-\sqrt{3}b_1) + \mathrm{sign}(1-|b|)\right]\end{aligned} \tag{5.198}$$

where $b = b_1 + \mathrm{i}b_2$ and $\Theta(x)$ is the Heaviside function. Note that the last two lines vanish when $\mathrm{Re}(b) > 0$, and $\mathcal{Q}(b) = -\tilde{G}_0(b)/(2\pi)^2$ where $\tilde{G}_0$ was defined in (5.139). One may check that this expression is a continuous function of b, except at the singular points $b = \pm e^{\mathrm{i}\pi/6}$ and along the negative semi-axis $(-\infty, 0)$. Moreover, we observe that $\mathcal{Q}$ is an odd function under $b \mapsto 1/b$,

$$\mathcal{Q}(b) + \mathcal{Q}(1/b) = 0 \tag{5.199}$$

and that the imaginary part is given by a much simpler formula[12]

$$\mathrm{Im}\,\mathcal{Q}(b) = \frac{1}{4\pi^2}\left[\mathcal{D}_2(b^3) - 4\mathcal{D}_2(b^2) + 5\mathcal{D}_2(b)\right] + \frac{1}{4\pi^2}\arg(b)\times\log\left|\frac{b\left(b^2+b+1\right)^3}{(b+1)^8}\right| \tag{5.200}$$

where $\mathcal{D}_2(z) = \mathrm{Im}(\mathrm{Li}_2(z)) + \log|z|\arg(1-z)$ is the Bloch-Wigner dilogarithm. Using the identities

$$\mathcal{D}_2(z^2) = 2(\mathcal{D}_2(z) + \mathcal{D}_2(-z)), \quad \mathcal{D}_2(z^3) = 3(\mathcal{D}_2(z) + \mathcal{D}_2(\omega z) + \mathcal{D}_2(\omega^2 z)) \tag{5.201}$$

where $\omega = e^{2\pi\mathrm{i}/3}$, we can also write

$$\mathrm{Im}\,\mathcal{Q}(b) = \frac{1}{4\pi^2}\left[3\mathcal{D}_2(\omega b) + 3\mathcal{D}_2(\omega^2 b) - 8\mathcal{D}_2(-b)\right] + \frac{1}{4\pi^2}\arg(b)\times\log\left|\frac{b\left(b^2+b+1\right)^3}{(b+1)^8}\right| \tag{5.202}$$

We have checked numerically that these formulae correctly reproduce the values of the periods at the conifold point, up to an additive constant and multiple of m (see Table 5.3).

[12]The last term proportional to $\log|\ell|$ was predicted by M. Kerr, in private communication with M. Marino.

6

Black Hole Quantum Mechanics and Generalized Error Functions

This chapter is based entirely on the paper *Black Hole Quantum Mechanics and Generalized Error Functions* [167], written in collaboration with Boris Pioline, and is reproduced here with only minor editorial changes. Its main goal is to explain the origin of the non-holomorphic modular completion of generating series of BPS indices for D4-D2-D0 black holes on Calabi–Yau threefolds. More precisely, the chapter shows how the generalized error functions that appear in the modular completion arise naturally from the supersymmetric quantum mechanics of multi-centered BPS black holes. This is achieved by evaluating the refined Witten index by localization, which reduces the problem to a finite-dimensional integral over relative positions and leads to the expected generalized error functions after separating the contribution of the phase space of BPS ground states from the transverse fluctuations.

6.1 Introduction

In string vacua with extended supersymmetry, an important challenge is to count BPS states with given electromagnetic charge γ, and match its logarithm with the Bekenstein-Hawking entropy of the corresponding supersymmetric black hole in the large charge regime. While this is usually a formidable task, it becomes feasible when suitable generating series of BPS indices possess modular properties, since the asymptotic growth of Fourier coefficients of modular forms is then under excellent analytic control. Such modular properties are guaranteed when the BPS black holes arise as BPS black strings wound on a circle, as the generating series of indices can be identified with the elliptic genus of a superconformal field theory (SCFT) on the string worldsheet [175].

This applies in particular to D4-D2-D0 black holes in Type IIA strings compactified on a Calabi-Yau (CY) threefold, as they arise from the M-theory viewpoint as M5-branes wrapped on a divisor $\mathcal{D}$ determined by the D4-charge, leading to a black string in 5 dimensions, further wrapped on the eleven-dimensional circle. If the divisor $\mathcal{D}$ is very ample and irreducible, the black string SCFT has a discrete spectrum (after factoring out the center of mass degrees of freedom) and the growth of the Fourier coefficients of the elliptic genus precisely matches the Bekenstein-Hawking-Wald prediction [140]. In general, however, if the divisor class $[\mathcal{D}]$ is reducible into a sum $\sum_{i=1}^{n}[\mathcal{D}_i]$ of irreducible classes, the black string can split into n constituents, depending on the values of the moduli at infinity. The elliptic genus in a suitable chamber (or rather, the vector-valued modular form arising from its theta series decomposition) then becomes mock modular of depth $n-1$, with a specific modular anomaly which has been characterized in a series of recent works [8, 10, 14, 17] (see [7] for a review).

This modular anomaly (or mock modular behavior) was first observed in the context of $\mathcal{N}=4$ string vacua, such as Type II strings on $K3\times T^2$ or heterotic strings on T^6, where the only possible

splittings involve only $n = 2$ constituents, and the BPS indices in the attractor chamber are given by Fourier coefficients of mock modular forms of depth one [68], similar to Ramanujan's famous mock theta series. As discovered in [189] (see also [187] for a broader historical account), their non-holomorphic completion is given by a certain indefinite theta series of signature $(1, 1)$, with a kernel expressed as a linear combination of error functions of the lattice vector coordinates, decaying exponentially outside the positive light-cone. The fact that the error function satisfies a specific, second-order partial differential equation known as Vignéras' equation, along with the decay property of the kernel, ensures the convergence and modularity of the completed theta series [183]. Physically, the non-holomorphic completion can be traced to the contribution of the spectral asymmetry of the continuum of scattering states in the quantum mechanics of two BPS black holes [166], or equivalently in the SCFT of two BPS black strings [158] (see [26, 27, 85, 97, 104, 106, 130, 157, 180] for other examples of superconformal field theories with continuous spectrum where the elliptic genus turns out to be non-holomorphic). Indeed, the two-body quantum mechanics is simple enough that the density of bosonic and fermionic states can be computed separately — their difference leads to a complementary error function of the Fayet-Iliopoulos (FI) stability parameter (namely, $M_1(x)$ defined in (6.2) below), which combines with the step function $\mathrm{sign}(x)$ in the bound state contribution to produce a smooth error function ($E_1(x)$ defined in (6.1) below) across the wall of marginal stability [166].

For a general CY threefold X with $SU(3)$ holonomy, the number n of bound state constituents can be arbitrarily large, and the modular completion of the generating series of BPS indices in general involves an indefinite theta series of signature $(n-1, (n-1)(b_2(X)-1))$, whose kernel is expressed as a specific combination of so-called generalized error functions $E_n(\mathcal{M}, x)$, $M_n(\mathcal{M}, x)$ of the lattice vector coordinates. These special functions were introduced in [9] for the purpose of constructing indefinite theta series satisfying Vignéras' criteria [183] for convergence and modularity. They are natural generalizations of the standard and complementary error functions[1]

$$E_1(x) = \int_{\mathbb{R}} e^{-\pi(x-x')^2}\,\mathrm{sign}(x')\,\mathrm{d}x' = \mathrm{Erf}(x\sqrt{\pi}), \tag{6.1}$$

$$M_1(x) = \frac{\mathrm{i}}{\pi}\int_{\mathbb{R}-\mathrm{i}x} e^{-\pi z^2-2\pi \mathrm{i}z}\frac{\mathrm{d}z}{z} = -\,\mathrm{sign}(x)\,\mathrm{Erfc}(|x|\sqrt{\pi}), \tag{6.2}$$

now involving a $(n-1)$-dimensional Gaussian integral, a product of $n-1$ factors $\mathrm{sign}(C_i, x)$ in the case of E_n, or a product of $n-1$ poles $1/(C_i^\star, z)$ in the case of M_n, where the vectors C_i and $C_i^\star$ are determined by the matrix $\mathcal{M}$. While $E_n(\mathcal{M}, x)$ is a smooth C^∞ function of x, $M_n(\mathcal{M}, x)$ is discontinuous on hyperplanes $(C_i^\star, x) = 0$ but the two can be expressed in terms of each other through analogues of the relation $E_1(x) = M_1(x) + \mathrm{sign}(x)$ [160]. Our goal in this chapter is to show how these non-holomorphic completion terms arise from the Witten index of the supersymmetric quantum mechanics of n BPS dyons.

More specifically, we shall compute the Witten index $\mathcal{I}_n = \mathrm{Tr}(-1)^F e^{-\beta H}$ by localization, reducing the functional integral to a finite-dimensional integral over time-independent configurations. We will see that the integral over the relative locations of the n centers in $\mathbb{R}^3$, along with their fermionic partners, can be rewritten as an integral over the $2n-2$-dimensional phase space $\mathcal{M}_n(\{\gamma_i, u_i\})$ of supersymmetric multi-centered black holes with charges $\{\gamma_i\}$ for fixed values of the (dynamical) FI parameters $\{u_i\}$, times an integral over the $n-1$ transverse directions corresponding to varying the u_i's, with a Gaussian measure factor depending on the (fixed,

[1] The latter can also be expressed in terms of the incomplete Gamma functions, $E_1(x) = \gamma(\frac{1}{2}, \pi x^2)/\sqrt{\pi}$, $M_1(x) = -\,\mathrm{sign}(x)\Gamma(\frac{1}{2}, \pi x^2)/\sqrt{\pi}$, but the representations (6.1), (6.2) are the ones which generalize most directly.

physical) FI parameters c_i. The former integral being locally constant in the u_i's, the latter leads to a linear superposition of generalized error functions, as required for the modular completion.

The remainder of this chapter is organized as follows. In Section 6.2, we review the prescription for the non-holomorphic modular completion of generating series of D4-D2-D0 indices, and define the generalized error functions from the title. In Section 6.3, after recalling basic aspects of the supersymmetric quantum mechanics of n dyons, we compute the refined Witten index using localization (see Section 6.3.3 and Appendix 6.6 for the actual computation). In Section 6.4, we compare this result to the modular prediction for $n = 3$ and $n = 4$ centers in the special case $X = K_{\mathbb{P}^2}$, and find perfect agreement with the results of [14], at least when the fugacity y is a pure phase. We give further evidence that the supersymmetric quantum mechanics reproduces the instanton generating potential for an arbitrary CY threefold.

6.2 Modular completions and generalized error functions

In this section we briefly review the mock modular properties of generating series of D4-D2-D0 indices in Type IIA strings compactified on a general smooth Calabi-Yau threefold X, and their non-holomorphic completion in terms of generalized error functions.

In this context, BPS states are identified mathematically as semi-stable objects E in the derived category of coherent sheaves $D^b\mathrm{Coh}(X)$. They carry the 'electromagnetic' charge $\gamma(E) = \mathrm{ch}\, E\sqrt{\mathrm{Todd}(X)} \in H^{\mathrm{even}}(X,\mathbb{Q})$, with components $\gamma = (p^0, p^a, q_a, q_0)$ on a basis $(1, \omega_a, \omega^a, \mathrm{Vol}\, X) \in H^0 \oplus H^2 \oplus H^4 \oplus H^6$ corresponding respectively to the D6-, D4-, D2- and D0-brane charges (here $\omega_a, a = 1 \ldots b_2(X)$ denotes a basis of the Kähler cone in $H^2(X,\mathbb{Z})$, and ω^a is the Poincaré dual basis in $H^4(X,\mathbb{Z})$, such that $\omega_a\omega^b = \delta_a^b\, \mathrm{Vol}\, X$). The mass of a BPS state of charge γ is given (in Planck units) by the absolute value of the central charge $Z(\gamma)$, which in the large volume limit takes the form

$$Z_{\mathrm{LV}}(\gamma) = q_0 + q_a z^a + \frac{1}{2}\kappa_{abc}p^a z^b z^c - \frac{1}{6}p^0\kappa_{abc}z^a z^b z^c. \tag{6.3}$$

Here $z^a = b^a + \mathrm{i}t^a$ parametrize the complexified Kähler moduli space $\mathcal{M}_K$ and $\kappa_{abc} = \int_X \omega_a\omega_b\omega_c$ is the cubic intersection form. The Dirac-Schwinger-Zwanziger (DSZ) product is given by the antisymmetrized Euler form $\langle\gamma,\gamma'\rangle = p'^0 q_0 + p'^a q_a - p^a q'_a - p^0 q'_0$. Wall-crossing for a fixed charge γ may occur along real codimension-one loci in $\mathcal{M}_K$ where the central charges $Z(\gamma_i)$ of two charge vectors γ_1, γ_2 with $\gamma = N_1\gamma_1 + N_2\gamma_2$ become aligned, with $N_1, N_2 \geq 1$ and $\langle\gamma_1,\gamma_2\rangle \neq 0$.

When the D6-brane charge p^0 vanishes (the main case of interest in this chapter), the central charge at leading order $Z_{\mathrm{LV}}(\gamma) \simeq -\frac{1}{2}(pt^2) + i(q_a + (pb)_a)t^a$ and the DSZ product $\langle\gamma_1,\gamma_2\rangle$ depend only on the reduced charge vector $\check{\gamma} = (p^a, q_a)$. In the large volume limit, wall-crossing may occur when the following quantity vanishes,

$$\mathcal{I}_{\gamma_1,\gamma_2} = \frac{\mathrm{Im}(\bar{Z}_{\mathrm{LV}}(\gamma_1)Z_{\mathrm{LV}}(\gamma_2))}{\sqrt{2|Z_{\mathrm{LV}}(\gamma_1)Z_{\mathrm{LV}}(\gamma_2)Z_{\mathrm{LV}}(\gamma)|}} = \frac{(p_2t^2)(q_{1,a} + (bp_1)_a)t^a - (p_1t^2)(q_{2,a} + (bp_2)_a)t^a}{\sqrt{(p_1t^2)(p_2t^2)(pt^2)}}, \tag{6.4}$$

where we use the shorthand notations $(pt^2) = \kappa_{abc}p^a t^b t^c$, $(bp)_a = \kappa_{abc}b^b p^c$. The factors in the denominator ensure that $\mathcal{I}_{\gamma_1,\gamma_2}$ is invariant under rescaling $t^a \to \lambda t^a$ with $\lambda > 0$, and are recognized as products of the masses $m_i = \frac{1}{2}(p_i t^2)$ in the large-volume limit.

6.2.1 Mock modularity of D4-D2-D0 invariants

Let $\bar\Omega(\gamma, z^a, y)$ be the refined, rational Donaldson-Thomas (DT) invariant counting semi-stable BPS states of charge γ with respect to the stability condition associated to the point $z^a = b^a + \mathrm{i}t^a$. $\bar\Omega(\gamma, z^a, y)$ is in general a rational function of y, but it is expected that the 'integer DT invariant'

$$\Omega(\gamma, z^a, y) := \sum_{d|\gamma} \mu(d) \frac{y - 1/y}{y^d - 1/y^d} \bar\Omega(\gamma/d, z^a, y^d), \tag{6.5}$$

is a symmetric Laurent polynomial in y with integer coefficients, corresponding to the physical refined BPS index (here $\mu(d)$ is the multiplicative Möbius function). This refined index in general depends on the complex structure moduli (except for toric threefolds, in which case it is protected), but its 'unrefined' limit as $y \to 1$ depends only on the Kähler moduli (or more generally, on the choice of Bridgeland stability condition). As explained in [14], even if one is only interested in unrefined indices, it is advantageous to introduce the refinement at intermediate stages, as it allows to express the modular completion in a much more concise way.

We now focus on the so-called MSW invariants, counting objects with vanishing D6-brane charge p^0 and fixed D4-brane charge supported on an ample divisor $p^a \in \Lambda^* = H^2(X, \mathbb{Z})$ in the 'large volume attractor chamber' $t^a = \lambda p^a$, $b^a = -\kappa^{ab} q_b$ where κ^{ab} is the inverse of the quadratic form $\kappa_{ab} := \kappa_{abc} p^c$ and λ is taken arbitrarily large and positive. By spectral flow invariance (i.e.tensoring by a flat line bundle), the index $\bar\Omega(\gamma, z^a, y)$ only depends on the 'invariant D0-brane charge' $\hat q_0 \in \mathbb{Q}$ and 'discrete flux' $\mu_a \in \Lambda^*/\Lambda$ defined by

$$\hat q_0 = q_0 - \frac{1}{2}\kappa^{ab} q_a q_b, \quad q_a = \mu_a + \frac{1}{2}\kappa_{ab} p^b + \kappa_{ab}\epsilon^b, \tag{6.6}$$

where $\epsilon^a \in \mathbb{Z}$ are the spectral flow parameters. We define the MSW invariants as

$$\bar\Omega_{p^a,\mu^a}(\hat q_0) := \lim_{\lambda\to+\infty} \bar\Omega((0, p^a, q_a, q_0), -\kappa^{ab} q_b + \mathrm{i}\lambda p^a, y). \tag{6.7}$$

Since $\hat q_0$ is bounded from above by the Bogomolov bound, we can define the generating series

$$h_{p,\mu}(\tau, y) = \frac{1}{y - 1/y} \sum_{\hat q_0 \le \hat q_0^{\max}} \bar\Omega_{p^a,\mu^a}(\hat q_0)\, e^{-2\pi \mathrm{i} \hat q_0 \tau}, \tag{6.8}$$

where τ lives in the Poincaré upper half-plane, $\tau_2 := \mathrm{Im}\,\tau > 0$. The S-duality symmetry of string theory (which is manifest from the viewpoint of M-theory compactified on $X \times T^2$) then implies that the generating series $h_{p,\mu}(\tau, y)$, $\mu \in \Lambda^*/\Lambda$ should in general transform under $(\tau, w) \mapsto (\frac{a\tau+b}{c\tau+d}, \frac{w}{c\tau+d})$ (with $y := e^{2\pi \mathrm{i} w}$) as a vector-valued mock Jacobi form[2] of depth $n-1$, where n is the maximal number of irreducible constituents in the divisor class p. This means that they admit a non-holomorphic completion of the form

$$\widehat{h}_{p,\mu}(\tau, y) := h_{p,\mu}(\tau, y) + \sum_{n\ge 2} \sum_{\substack{p=\sum_{i=1}^n p_i \\ \mu=\sum_{i=1}^n \mu_i \mod \Lambda}} \Theta_\mu(\{p_i, \mu_i\}, \tau, y) \prod_{i=1}^n h_{p_i,\mu_i}(\tau, y)\,, \tag{6.9}$$

[2] To be precise, as currently understood, S-duality only implies that the unrefined limit $h_{p,\mu}(\tau) := \lim_{y\to 1}(y - 1/y) h_{p,\mu}(\tau, y)$ transforms as a vector-valued mock modular form of depth $n-1$. For non-compact CY threefolds of the form $X = K_S$ where S is a Fano surface, such that MSW invariants supported on $r[S]$ coincide with rank r Vafa-Witten invariants [182], it is expected that the generating series of refined VW invariants are mock Jacobi form of depth $r-1$ [101, 177], and it was checked in [14] that the prescription below for constructing the modular completion reproduces known results for $S = \mathbb{P}^2$ and rank $r \le 3$ [54, 143], and further used in [5, 6] to predict VW invariants for arbitrary del Pezzo surfaces and rank. Conservatively, the modularity conjecture only applies to the unrefined limit.

where $\Theta_\mu(\{p_i,\mu_i\},\tau,y)$ are universal indefinite theta series such that $\widehat{h}_{p,\mu}(\tau,y)$ transforms as a (ordinary, but non-holomorphic) vector-valued Jacobi form of fixed weight, index and multiplier system. The indefinite theta series are neither holomorphic in w nor modular covariant, but they are constructed such that their modular anomaly cancels that of $h_{p,\mu}$. Moreover, $\Theta_\mu(\{p_i,\mu_i\},\tau,y)$ has a zero of order $n-1$ at $y=1$, such that (6.9) reduces in the unrefined limit to

$$\widehat{h}_{p,\mu}(\tau) := h_{p,\mu}(\tau) + \sum_{n\geq 2} \sum_{\substack{p=\sum_{i=1}^n p_i \\ \mu=\sum_{i=1}^n \mu_i \mod \Lambda}} \Theta_\mu(\{p_i,\mu_i\},\tau) \prod_{i=1}^n h_{p_i,\mu_i}(\tau)\,, \tag{6.10}$$

with $\Theta_\mu(\{p_i,\mu_i\},\tau) = \lim_{y\to 1}(y-1/y)^{1-n}\Theta_\mu(\{p_i,\mu_i\},\tau,y)$. The theta series, $\Theta_\mu(\{p_i,\mu_i\},\tau,y)$, are considerably simpler than their unrefined counterparts, and given by an indefinite theta series

$$\Theta_\mu(\{p_i,\mu_i\},\tau,y) = \sum_{\substack{q_{a,i}\in\Lambda+\mu_a+\frac{1}{2}\kappa_{ab,i}p_i^b \\ \sum_{i=1}^n q_{a,i}=\mu_a+\frac{1}{2}\kappa_{ab}p^b}} R_n\left(\{p_i,q_i\},\tau_2,y\right) e^{i\pi\tau Q_n(\{p_i,q_i\})}, \tag{6.11}$$

where $\kappa_{ab,i}=\kappa_{abc}p_i^c$, κ_i^{ab} is its inverse and Q_n is the quadratic form

$$Q_n\left(\{p_i,q_i\}\right) := \kappa^{ab}q_aq_b - \sum_{i=1}^n \kappa_i^{ab}q_{i,a}q_{i,b}, \tag{6.12}$$

of signature $(n-1)(b_2(X)-1,1)$ on the lattice specified in the summation range in (6.11). The kernel $R_n\left(\{p_i,q_i\},\tau_2,y\right)$ is given by a sum of generalized error functions multiplied by step functions of the q_i's, determined as follows:[3]

$$R_n(\{p_i,q_i\},\tau_2,y) = \mathrm{Sym}\left\{\frac{(-y)^{\sum_{i<j}\langle\alpha_i,\alpha_j\rangle}}{2^{n-1}}\sum_{T\in\mathbb{T}_n^{\mathrm{S}}}(-1)^{|V_T|-1}(\mathcal{E}_{v_0}-\mathcal{E}_{v_0}^{(0)})\prod_{v\in V_T\setminus\{v_0\}}\mathcal{E}_v^{(0)}\right\}. \tag{6.13}$$

Here, T runs over all rooted planar trees and valency ≥ 3 (also called Schröder trees) with n leaves; V_T denotes the set of vertices (excluding the leaves) and v_0 the root vertex; one then associates a reduced charge vector $\check{\gamma}_v=(p_v,q_v)$ to each vertex such that the leaves carry charges $\check{\gamma}_i=(p_i^a,q_{a,i})$ and the charges add up at each vertex. For each vertex, $\mathcal{E}_v^{(0)}$ is a product of $m-1$ sign factors (m being the number of descendants of the vertex v, and $\{\alpha_i\}$ being the corresponding reduced charges)[4]

$$\mathcal{E}_v^{(0)} = \prod_{k=1}^{m-1}\mathrm{sign}\,\Gamma_k, \quad \Gamma_k := \left(\sum_{i=1}^k\sum_{j=k+1}^m\langle\alpha_i,\alpha_j\rangle\right). \tag{6.14}$$

Finally, the factor $\mathcal{E}_{v_0}$ attached to the root vertex is a depth $m-1$ generalized boosted error function (defined in the next subsection, Eq. (6.27))

$$\mathcal{E}_{v_0} = \Phi_{m-1}^E(\mathcal{Q},\{\boldsymbol{v}_k\},\mathbf{x}). \tag{6.15}$$

[3] We follow the conventions in [7, 12]. The symbol Sym indicates that one should sum over all permutations of $\{(p_i,q_i)\}$ with weight $1/n!$.

[4] There is a subtlety in interpreting the formula in (6.14) when some of the Γ_k's vanish. If the subset $\mathcal{I}\subset\{1,\dots,m-1\}$ such that $\Gamma_k=0$ has even cardinality, then the product $\prod_{k=1}^{m-1}\mathrm{sign}\,\Gamma_k$ should be replaced by $\frac{1}{|\mathcal{I}|+1}\prod_{k\notin\mathcal{I}}\mathrm{sign}\,\Gamma_k$. If the set $\mathcal{I}$ has odd cardinality, then $\mathcal{E}_v^{(0)}$ should be taken to vanish.

Here bold letters denote elements of a vector space which is n copies of $\mathbb{R}^{1,b_2(X)-1}$ (a vector $\boldsymbol{x}$ has components x_i^a) endowed with a quadratic form Q given by $\boldsymbol{x}\cdot\boldsymbol{y}=\sum_{i=1}^n(p_ix_iy_i)$. The vectors $\{\boldsymbol{v}_k, k=1,\dots m\}$ in (6.15) are chosen such that

$$\boldsymbol{v}_k\cdot\boldsymbol{x}=\sum_{i=1}^{k}\sum_{j=k+1}^{m}\kappa_{abc}p_i^a p_j^b(x_i^c-x_j^c). \tag{6.16}$$

The vector $\boldsymbol{x}=(x_1^a,\dots,x_n^a)$ is in turn related to the electric charges $q_{a,i}$ by

$$x_i^a=\sqrt{2\tau_2}\left(\kappa_i^{ab}q_{b,i}+\eta\rho_i^a\right), \tag{6.17}$$

where $\eta:=\frac{\mathrm{Re}(\log y)}{2\pi\tau_2}$ and $\rho_i^a:=-\sum_{j<i}p_j^a+\sum_{j>i}p_j^a$. The η-dependent shift appears whenever the refinement parameter $y=e^{2\pi\mathrm{i}w}$ is not a pure phase, and is necessary to resolve ambiguities in defining $\mathrm{sign}(x)$ for $x=0$. Note that in the limit $\tau_2\to+\infty$ (after setting $\eta=0$), $\mathcal{E}_{v_0}$ reduces to the same product of sign functions as $\mathcal{E}_{v_0}^{(0)}$, so the factor $(\mathcal{E}_{v_0}-\mathcal{E}_{v_0}^{(0)})$ associated to the root vertex in (6.13) is actually a generalized complementary error function, denoted by $\mathcal{E}_{v_0}^{\mathrm{ref}(+)}$ in [14, (3.13)].

Finally, we mention that the completed generating series $\widehat{h}_{p,\mu}$ enter in the 'instanton generating potential' $\mathcal{G}$, whose refined version was introduced in [14, Section 3.3],

$$\mathcal{G}=\sum_{n=1}^{\infty}\frac{1}{2\pi\sqrt{\tau_2}}\,e^{-\sum_i S_{p_i}^{\mathrm{cl}}}\vartheta_{p,\mu}(\Phi_n^{\mathrm{tot}},-1)\left[\prod_{i=1}^{n}\sum_{p_i,\mu_i}\sigma_{p_i}h_{p_i,\mu_i}\right]. \tag{6.18}$$

Here $S_p^{\mathrm{cl}}=\pi\tau_2(pt^2)-2\pi\mathrm{i}p^a\tilde{c}_a$ is the 'classical action', $\tilde{c}_a$ being a chemical potential conjugate to the magnetic charge p^a, σ_{p_i} are 'quadratic refinement' factors defined in [17, (D.5)], and we have set $\eta=0$ for simplicity. The kernel Φ_n^{tot} in the indefinite theta series is again obtained as a sum over Schröder trees [14, (C.17)]

$$\Phi_n^{\mathrm{tot}}=\frac{(-y)^{\sum_{i<j}\langle\alpha_i,\alpha_j\rangle}}{2^{n-1}}\Phi_1^{\int}\sum_{T\in\mathbb{T}_n^{\mathrm{S}}}(-1)^{|V_T|-1}(\widetilde{\mathcal{E}}_{v_0}-\mathcal{E}_{v_0}^{(0)})\prod_{v\in V_T\setminus\{v_0\}}\mathcal{E}_v^{(0)}, \tag{6.19}$$

where $\Phi_1^{\int}$ is a Gaussian factor ensuring convergence for the total D2-brane charge $x=\sum\mathbf{x}_i$,

$$\Phi_1^{\int}(x)=\frac{e^{-\frac{\pi(pxt)^2}{(pt^2)}}}{2\pi\sqrt{2\tau_2(pt^2)}}, \tag{6.20}$$

and $\widetilde{\Phi}_v$ is given for a vertex with m descendants by

$$\widetilde{\mathcal{E}}_v=\Phi_{m-1}^{E}(Q,\{\boldsymbol{u}_k\},\mathbf{x}). \tag{6.21}$$

Here, $\boldsymbol{u}_k, k=1\dots m-1$ are moduli-dependent vectors chosen such that (compare with (6.16))

$$\boldsymbol{u}_k\cdot\boldsymbol{x}=\sum_{i=1}^{k}\sum_{j=k+1}^{m}\left[(p_jt^2)(p_ix_it)-(p_it^2)(p_jx_jt)\right]. \tag{6.22}$$

We note that $\mathcal{G}$ can be just as well represented as a sum over monomials in the completed generating series $\widehat{h}_{p_i,\mu_i}$, at the expense of replacing the locally constant $\mathcal{E}_v^{(0)}$ in (6.19) by the full error function $\mathcal{E}_v$ [14, (3.31)]. These definitions ensure that $\mathcal{G}$ is a completely smooth function of the moduli (away from conifold singularities), transforming as a Jacobi form of weight $(-\frac{1}{2},\frac{1}{2})$ under $SL(2,\mathbb{Z})$. Its residue at $y=1$ is closely related to the contact potential on the moduli space after compactification on a circle, and plays the role of the Witten index for the full 4D supergravity theory on $\mathbb{R}^3\times S^1$ [15].

While the prescriptions summarized above appear to be complicated, it is straightforward to implement them on a symbolic computation system. For $n=2$, the theta series (6.11) entering the modular completion of the refined partition function $\widehat{h}_{p,\mu}$ reduces to the simple result

$$\Theta_\mu(\{p_1,\mu_1,p_2,\mu_2\};\tau,y)=\sum_{q_1+q_2=\mu+\frac{1}{2}p}\frac{(-y)^{\gamma_{12}}}{2}\left(E_1\left(\frac{\sqrt{2\tau_2}(\gamma_{12}+\eta(pp_1p_2))}{\sqrt{(pp_1p_2)}}\right)-\mathrm{sign}(\gamma_{12})\right)e^{\mathrm{i}\pi\tau Q_2}, \tag{6.23}$$

where $\gamma_{12}=p_2q_1-p_1q_2$ and $(pp_1p_2):=\kappa_{abc}p^ap_1^bp_2^c$. In the unrefined limit[5], symmetrizing under the exchange of q_1,q_2 and using the identities $E_1(x)-\mathrm{sign}(x)=M_1(x)$, $\partial_xE_1(x)=e^{-\pi x^2}$, one arrives at

$$\Theta_\mu(\{p_1,\mu_1,p_2,\mu_2\};\tau)=\sum_{q_1+q_2=\mu+\frac{1}{2}p}\frac{(-1)^{\gamma_{12}}}{4}\left(\gamma_{12}\,M_1\left(\frac{\sqrt{2\tau_2}\gamma_{12}}{\sqrt{(pp_1p_2)}}\right)+\frac{\sqrt{(pp_1p_2)}}{\pi\sqrt{2\tau_2}}e^{-\frac{2\pi\tau_2\gamma_{12}^2}{(pp_1p_2)}}\right)e^{\mathrm{i}\pi\tau Q_2}. \tag{6.24}$$

Analogous results for $n=3$ and $n=4$ will be discussed in Section 6.4.

For later reference, we also recall the two-body contribution to the (refined) instanton generating potential (first found in [141], rederived in [8, Section 2.2], and refined in [17, (G.8)]),

$$\mathcal{G}_2=\sum_{p_1,p_2,q_1,q_2}\frac{e^{2\pi\tau_2\mathcal{I}^2_{\gamma_1,\gamma_2}}}{8\pi^2\sqrt{2\tau_2(pt^2)}}\left[E_1\left(\sqrt{2\tau_2}\mathcal{I}_{\gamma_1,\gamma_2}\right)-\mathrm{sign}\,\gamma_{12}\right]e^{\mathrm{i}\pi\tau Q_2}\,h_{p_1,q_1}\,h_{p_2,q_2}. \tag{6.25}$$

It is worth stressing that the argument of the error function in (6.25) in general does *not* reduce to the argument of the error function in the modular completion (6.23) in the large volume attractor chamber, even for $\eta=0$. Indeed, $\mathcal{I}_{\gamma_1,\gamma_2}$ evaluates at that point to

$$\mathcal{I}^*_{\gamma_1,\gamma_2}=\gamma_{12}\sqrt{\frac{(p^3)}{(p_1p^2)(p_2p^2)}}, \tag{6.26}$$

such that the arguments of the two E_1 functions differ by a rescaling by $\sqrt{\frac{(p^3)(p_1p_2p)}{(p_1p^2)(p_2p^2)}}$. In the special case where the D4-brane charges p_1,p_2 are collinear, this ratio evaluates to one and the two arguments are then identical.

6.2.2 Generalized error functions

Here we briefly review the definitions of the generalized error functions introduced in [9] and further developed in [160]. For any invertible, $r\times r$ matrix $\mathcal{M}$ with real entries, and vector

[5] Following the prescription in [14], the unrefined limit is obtained by setting $\eta=\frac{w}{2\mathrm{i}\tau_2}$, $\bar{w}=0$ and taking the limit $w=\frac{\log y}{2\pi\mathrm{i}}\to 0$.

$\mathbf{x} \in \mathbb{R}^r$ we define the generalized error function E_r and complementary error function M_r by

$$E_r(\mathcal{M}, \mathbf{x}) = \int_{\mathbb{R}^r} \mathrm{d}[r]\mathbf{z} e^{-\pi(\mathbf{x}-\mathbf{z})^T(\mathbf{x}-\mathbf{z})} \prod_{i=1}^{r} \mathrm{sign}(\mathcal{M}^T\mathbf{z})_i, \tag{6.27}$$

$$M_r(\mathcal{M}; \mathbf{x}) = \left(\frac{\mathrm{i}}{\pi}\right)^r |\det \mathcal{M}|^{-1} \int_{\mathbb{R}^r - \mathrm{i}\mathbf{x}} \mathrm{d}[r]\mathbf{z} \frac{e^{-\pi\mathbf{z}^T\mathbf{z} - 2\pi\mathrm{i}\mathbf{z}^T\mathbf{x}}}{\prod_{i=1}^{r} \left(\mathcal{M}^{-1}\mathbf{z}\right)_i}. \tag{6.28}$$

We refer to the index r as the 'depth'. The function $E_r(\mathcal{M}, \mathbf{x})$ is a C^∞ function of $\mathbf{x}$, which asymptotes to $\prod_{i=1}^r \mathrm{sign}(\mathcal{M}^T\mathbf{x})_i$ in the limit where $\mathbf{x}$ is scaled by an arbitrarily large positive factor. Similarly $M_r(\mathcal{M}, \mathbf{x})$ is a C^∞ function away from the hyperplanes $(\mathcal{M}^{-1}\mathbf{x})_i = 0$, exponentially suppressed if $\mathbf{x}$ is scaled by an arbitrarily large positive factor. Moreover, both E_r and M_r are invariant (up to a sign $(-1)^r$) under $\mathbf{x} \mapsto -\mathbf{x}$, as well as under rescaling the columns of $\mathcal{M}$ by arbitrary positive factors or permuting them, and under rotating $(\mathcal{M}, \mathbf{x}) \mapsto (O\,\mathcal{M}, O\,\mathbf{x})$ by an arbitrary orthogonal transformation $O \in O(r)$. For $r = 1$, this allows to set $\mathcal{M} = 1$, recovering the functions in (6.1),(6.2). More generally, we can always reach a standard form such that $\mathcal{M}$ is lower-triangular with unit diagonal. For displaying results with $r \leq 3$ we shall use the shorthand notations

$$E_2(\alpha; x_1, x_2) = E_2\left(\begin{pmatrix} 1 & 0 \\ \alpha & 1 \end{pmatrix}, \begin{pmatrix} x_1 \\ x_2 \end{pmatrix}\right), \quad E_3(\alpha, \beta, \gamma; x_1, x_2, x_3) = E_3\left(\begin{pmatrix} 1 & 0 & 0 \\ \alpha & 1 & 0 \\ \beta & \gamma & 1 \end{pmatrix}, \begin{pmatrix} x_1 \\ x_2 \\ x_3 \end{pmatrix}\right), \tag{6.29}$$

and similarly for M_r. The symmetry under permutations of the columns implies functional relations, for example [9, Cor. 3.10]

$$E_2(\alpha; x_1, x_2) = E_2\left(\alpha; \frac{x_2 - \alpha x_1}{\sqrt{1+\alpha^2}}, \frac{x_1 + \alpha x_2}{\sqrt{1+\alpha^2}}\right) = -E_2(-\alpha; -x_1, x_2), \tag{6.30}$$

and similar relations for M_2. In addition, every identity among products of sign functions implies a corresponding identity among the generalized error functions $E_r(\mathcal{M}, \mathbf{x})$, where the matrices $\mathcal{M}$ are related by specific linear transformations [17, Eq. (D.13)]. For example, the identity valid away from the loci where x_1, x_2 or $x_1 + x_2$ vanish

$$\mathrm{sign}(x_1)\,\mathrm{sign}(x_2) = (\mathrm{sign}(x_1) + \mathrm{sign}(x_2))\,\mathrm{sign}(x_1 + x_2) - 1, \tag{6.31}$$

implies the functional relation[6]

$$E_2(\mathcal{M}, \mathbf{x}) = E_2(\mathcal{M}_1, \mathbf{x}) + E_2(\mathcal{M}_2, \mathbf{x}) - 1, \tag{6.32}$$

where the matrices $\mathcal{M}, \mathcal{M}_1, \mathcal{M}_2 \in \mathbb{R}^{2\times 2}$ satisfy

$$\mathcal{M} = \begin{pmatrix} \mathcal{M}_{11} & \mathcal{M}_{12} \\ \mathcal{M}_{21} & \mathcal{M}_{22} \end{pmatrix}, \quad \mathcal{M}_1 = \begin{pmatrix} \mathcal{M}_{11} & \mathcal{M}_{12} + \mathcal{M}_{11} \\ \mathcal{M}_{21} & \mathcal{M}_{22} + \mathcal{M}_{21} \end{pmatrix}, \quad \mathcal{M}_2 = \begin{pmatrix} \mathcal{M}_{11} + \mathcal{M}_{12} & \mathcal{M}_{12} \\ \mathcal{M}_{21} + \mathcal{M}_{22} & \mathcal{M}_{22} \end{pmatrix}. \tag{6.33}$$

In terms of the standard form defined in (6.29), the identity can be expressed as in a manifestly $\mathbb{Z}_3$-symmetric form, which will be relevant in the three-body case discussed in Section 6.3.3 below,

$$E_2(\alpha_1; x_1, y_1) + E_2(\alpha_2; x_2, y_2) + E_2(\alpha_3; x_3, y_3) = 1, \tag{6.34}$$

[6] See [12, Appendix A.2] for more general functional relations.

under the constraint

$$\alpha_1\alpha_2 + \alpha_2\alpha_3 + \alpha_3\alpha_1 = 1, \tag{6.35}$$

provided the variables (x_i, y_i) are related by

$$(x_{i+1}, y_{i+1}) = \left(\frac{y_i + \alpha_{i+1}x_i}{\sqrt{1+\alpha_{i+1}^2}}, \frac{\alpha_{i+1}y_i - x_i}{\sqrt{1+\alpha_{i+1}^2}}\right), \tag{6.36}$$

where $\alpha_4 := \alpha_1$ and $(x_4, y_4) = \pm(x_1, y_1)$.

More generally, we need boosted versions of the generalized error functions, where the vector $\mathbf{x}$ lives in $\mathbb{R}^d$ with fixed quadratic form Q of signature $(r, d-r)$, and the arguments of the sign functions are given by a collection of r vectors $(\boldsymbol{v}_1, \ldots, \boldsymbol{v}_r)$, corresponding to the columns of a $d \times r$ matrix $\mathcal{V}$, spanning a positive definite subspace in $\mathbb{R}^d$, i.e.such that the Gram matrix $\mathcal{V}^T Q \mathcal{V}$ is positive definite. Choosing $\mathcal{B}$ to be any $r \times d$ matrix whose rows define an orthonormal basis for this subspace (hence $\mathcal{B}Q\mathcal{B}^T = 1$), we define the boosted generalized error functions as

$$\Phi_r^E(Q, \{\boldsymbol{v}_i\}, \mathbf{x}) = E_r(\mathcal{B}Q\mathcal{V}, \mathcal{B}Q\mathbf{x}), \quad \Phi_r^M(Q, \{\boldsymbol{v}_i\}, \mathbf{x}) = M_r(\mathcal{B}Q\mathcal{V}, \mathcal{B}Q\mathbf{x}). \tag{6.37}$$

Independence of the choice of basis follows from the $O(r)$ invariance of E_r, M_r. Similar to E_r and M_r, $\Phi_r^E(Q, \mathcal{V}, \mathbf{x})$ is a C^∞ function of $\mathbf{x}$ which asymptotes to[7] $\operatorname{sign}(\mathcal{V}^T Q\mathbf{x})$ as $\mathbf{x}$ is scaled to infinity, while $\Phi_r^M(Q, \mathcal{V}, \mathbf{x})$ is C^∞ away from a set of r hyperplanes and exponentially suppressed as $\mathbf{x}$ is scaled to infinity. In fact, Φ_r^E can be expressed in terms of Φ_r^M through the identity [160, Prop. 1], generalizing similar identities obtained in [9] for $r = 2, 3$)

$$\Phi_r^E(Q, \{\boldsymbol{v}_i\}, \mathbf{x}) = \sum_{\mathcal{I} \subset \{1,\ldots r\}} \Phi_{|\mathcal{I}|}^M(Q, \{\boldsymbol{v}_i\}_{i\in\mathcal{I}}, \mathbf{x}) \prod_{j\notin\mathcal{I}} \operatorname{sign}(\boldsymbol{v}_{j\perp\mathcal{I}} Q\mathbf{x}), \tag{6.38}$$

where $\boldsymbol{v}_{j\perp\mathcal{I}}$ is the projection of $\boldsymbol{v}_j$ orthogonal to the vectors $\boldsymbol{v}_i$ with $i \in \mathcal{I}$, such that all discontinuities on the r.h.s. cancel, leaving a C^∞ function of $\mathbf{x}$. For $n \le 3$, this identity specializes to

$$E_1(x) \;=\; M_1(x) + \operatorname{sign}(x), \tag{6.39}$$

$$\begin{aligned} E_2(\alpha, x_1, x_2) \;=\; & M_2(\alpha; x_1, x_2) + M_1\left(\frac{\alpha x_2 + x_1}{\sqrt{\alpha^2+1}}\right) \operatorname{sign}(x_2 - \alpha x_1) + M_1(x_2) \operatorname{sign}(x_1) \\ & + \operatorname{sign}(x_2) \operatorname{sign}(x_1 + \alpha x_2), \end{aligned} \tag{6.40}$$

$$\begin{aligned} E_3(\alpha, \beta, \gamma;\, x_1, x_2, x_3) \;=\; & M_3(\alpha, \beta, \gamma;\, x_1, x_2, x_3) + M_2(\gamma;\, x_2, x_3)\, \operatorname{sign}(x_1) \\ & + M_2\Big(\tfrac{\beta}{\sqrt{1+\alpha^2}};\, \tfrac{x_1+\alpha x_2}{\sqrt{1+\alpha^2}},\, x_3\Big)\, \operatorname{sign}(-\alpha x_1 + x_2) \\ & + M_2\Big(\tfrac{\alpha+\beta\gamma}{\sqrt{1+\beta^2-2\alpha\beta\gamma+(1+\alpha^2)\gamma^2}};\, \tfrac{(1+\gamma^2)x_1-(\beta-\alpha\gamma)(\gamma x_2-x_3)}{\sqrt{(1+\gamma^2)\left(1+\beta^2-2\alpha\beta\gamma+(1+\alpha^2)\gamma^2\right)}},\, \tfrac{x_2+\gamma x_3}{\sqrt{1+\gamma^2}}\Big) \\ & \quad \times \operatorname{sign}\big((\alpha\gamma - \beta)x_1 - \gamma x_2 + x_3\big) \\ & + M_1(x_3)\, \operatorname{sign}(x_2)\, \operatorname{sign}(x_1 + \alpha x_2) \\ & + M_1\Big(\tfrac{x_2+\gamma x_3}{\sqrt{1+\gamma^2}}\Big)\, \operatorname{sign}\big((1+\gamma^2)x_1 - (\beta - \alpha\gamma)(\gamma x_2 - x_3)\big)\, \operatorname{sign}(-\gamma x_2 + x_3) \\ & + M_1\Big(\tfrac{x_1+\alpha x_2+\beta x_3}{\sqrt{1+\alpha^2+\beta^2}}\Big)\, \operatorname{sign}\big((1+\alpha^2)x_3 - \beta(x_1 + \alpha x_2)\big) \\ & \quad \times \operatorname{sign}\big((1 + \beta^2 - \alpha\beta\gamma)\, x_2 + (\gamma + \alpha^2\gamma - \alpha\beta)\, x_3 - (\alpha + \beta\gamma)\, x_1\big) \\ & + \operatorname{sign}(x_3)\, \operatorname{sign}(x_1 + \alpha x_2 + \beta x_3)\, \operatorname{sign}(x_2 + \gamma x_3)\,. \end{aligned} \tag{6.41}$$

[7] Here we denote $\operatorname{sign} v := \prod_{i=1}^r \operatorname{sign} v_i$ for a vector $v = (v_i)_{i=1}^r$.

Functional relations originating from sign identities take a simple form in terms of boosted error functions, for example (6.34) is equivalent to

$$\Phi_2^E(Q,\{\boldsymbol{v}_1+\boldsymbol{v}_2,\boldsymbol{v}_2\},\mathbf{x})+\Phi_2^E(Q,\{\boldsymbol{v}_1,\boldsymbol{v}_1+\boldsymbol{v}_2\},\mathbf{x})=1+\Phi_2^E(Q,\{\boldsymbol{v}_1,\boldsymbol{v}_2\},\mathbf{x}). \tag{6.42}$$

6.3 Witten index from localization

In this section, we evaluate the Witten index of the supersymmetric quantum mechanics of n dyonic black holes using localization. We start by recalling the Lagrangian, and the structure of the supersymmetric ground states, both at the semiclassical and quantum level. Readers familiar with this may skip to the localization computation in Section 6.3.3.

6.3.1 Supersymmetric quantum mechanics of n dyons

Following [73] (see also [126, 133]), the quantum mechanics of n BPS dyons of charge $\{\gamma_i\}_{i=1}^n$ in 3+1-dimensional theories with $\mathcal{N}=2$ supersymmetry is given by the Lagrangian

$$L=\sum_{i=1}^n\frac{m_i}{2}\left(\dot{\vec{x}}_i^2+D_i^2+2\mathrm{i}\bar{\lambda}_i\dot{\lambda}_i\right)+\sum_{i=1}^n(-U_iD_i+\vec{A}_i\cdot\dot{\vec{x}}_i)+\sum_{i,j=1}^n\vec{\nabla}_iU_j\cdot\bar{\lambda}_i\vec{\sigma}\lambda_j, \tag{6.43}$$

where $\vec{x}_i$ denotes the location of the i-th dyon of mass m_i in $\mathbb{R}^3$, λ_i are the associated fermionic zero-modes, D_i are auxiliary fields and $\vec{\sigma}$ are the standard Pauli matrices. The functions $U_i(\vec{x})$ and 3-vectors $\vec{A}_i(\vec{x})$ are determined from the DSZ pairings $\gamma_{ij}=\langle\gamma_i,\gamma_j\rangle$ and FI parameters c_i (subject to the constraint $\sum_i c_i=0$) via

$$U_i=-\frac{1}{2}\left(\sum_{j\neq i}\frac{\gamma_{ij}}{|\vec{x}_i-\vec{x}_j|}-c_i\right),\quad \vec{\nabla}_iU_j=\vec{\nabla}_jU_i=\frac{1}{2}(\vec{\nabla}_i\times\vec{A}_j+\vec{\nabla}_j\times\vec{A}_i). \tag{6.44}$$

This Lagrangian admits 4 real supersymmetries (corresponding to the unbroken supercharges in four dimensions), and follows from the supersymmetric quiver quantum mechanics with n Abelian vector multiplets and $|\gamma_{ij}|$ bifundamental chiral multiplets for each pair (i,j), after integrating out the chiral multiplets [73]. Integrating out the auxiliary fields D_i leads to a scalar potential

$$V=\sum_{i=1}^n\frac{U_i^2}{2m_i}. \tag{6.45}$$

We denote by $\mathcal{M}_n(\{\gamma_i,c_i\})$ the space of classical supersymmetric ground states up to overall translations,

$$\mathcal{M}_n(\{\gamma_i,c_i\})=\left\{(\vec{x}_i)\in\mathbb{R}^{3n},\ \forall i\ \sum_{j\neq i}\frac{\gamma_{ij}}{|\vec{x}_i-\vec{x}_j|}=c_i\right\}\Big/\mathbb{R}^3. \tag{6.46}$$

As observed in [73], this is exactly the space of multi-centered BPS black hole solutions in $\mathcal{N}=2$, four-dimensional supergravity if one identifies

$$c_i=2\,\mathrm{Im}(e^{-i\phi}Z(\gamma_i)),\quad m_i=|Z(\gamma_i)|,\quad \phi=\arg(Z(\gamma)), \tag{6.47}$$

with all central charges evaluated at spatial infinity. With these identifications, the asymptotic value of the potential $V_\infty=\sum_{i=1}^n\frac{c_i^2}{8m}$ coincides with the binding energy $\sum_{i=1}^n|Z_i|-|Z|$, in the limit where all central charges Z_i are nearly aligned. This is indeed the case for D4-branes in the large volume limit, where $Z_i\simeq-\frac{1}{2}(p_it^2)\in\mathbb{R}^-$.

6.3.2 Phase space of multicentered BPS black holes and Dirac index

Since the n constraints $U_i = 0$ sum up to zero, the space of multicentered BPS black holes defined in (6.46) has even real dimension $2n-2$. As noted in [42], it carries a natural symplectic form

$$\omega = \frac{1}{2}\sum_{i,j=1}^{n} \epsilon_{abc}\, \nabla_j^a U_i \, \mathrm{dx}_i^b \wedge \mathrm{dx}_j^c = \frac{1}{4}\sum_{i<j} \epsilon_{abc} \frac{\gamma_{ij}}{r_{ij}^3}\, \mathrm{x}_{ij}^a \, \mathrm{dx}_{ij}^b \wedge \mathrm{dx}_{ij}^c, \tag{6.48}$$

and a Hamiltonian action of $SO(3)$ with moment map

$$\vec{J} = \frac{1}{2}\sum_{i<j} \gamma_{ij}\, \frac{\vec{x}_{ij}}{r_{ij}}, \tag{6.49}$$

which coincides with the total angular momentum carried by the multi-centered black hole solution.

When the phase space $\mathcal{M}_n(\{\gamma_i, c_i\})$ is compact[8], its equivariant volume

$$\mathrm{Vol}(\{\gamma, c\};\, y) = \frac{(-1)^{\sum_{i<j}\gamma_{ij}-n+1}}{(2\pi)^{n-1}(n-1)!}\int_{\mathcal{M}_n} y^{2\mathrm{J}_3}\omega^{n-1}, \tag{6.50}$$

can be computed using the Duistermaat-Heckmann formula [146]: the fixed points with respect to rotations along the z axis (or equivalently, the critical points of J_3) are collinear configurations $\vec{x}_i = (0,0,z_i)$ subject to the one dimensional reduction of the equations $U_i = 0$. They are in general isolated, and characterized by the order of the centers along the z axis. We denote by $F_{C,n}(\{\gamma_i, c_i\})$ the number of solutions with the standard ordering $z_1 < z_2 < \cdots < z_n$, weighted by the sign of the determinant of the Hessian matrix of the 'superpotential' $W = -\sum_{i<j}\gamma_{ij}\log|z_j - z_i| - \sum_i c_i z_i$. The equivariant volume is then given by a sum over all permutations,

$$\mathrm{Vol}(\{\gamma, c\};\, y) = \frac{(-1)^{\sum_{i<j}\gamma_{ij}-n+1}}{(2\log y)^{n-1}}\sum_{\sigma\in S_n} F_{C,n}(\{\gamma_{\sigma(i)}, c_{\sigma(i)}\})\, y^{\sum_{i<j}\gamma_{\sigma(i)\sigma(j)}}. \tag{6.51}$$

Quantum mechanically, the index counting normalizable BPS states is expected to coincide[9] with the equivariant index of the Dirac operator twisted by a line bundle whose first Chern class is equal to the symplectic form ω [42]. The latter can be computed by replacing the volume form in (6.50) by a suitable equivariant cohomology class

$$\frac{\omega^{n-1}}{(2\pi)^{n-1}} \to \left[e^{\frac{\omega}{2\pi}}\widehat{A}(\mathcal{M}_n, y)\right]_{n-1}, \tag{6.52}$$

where $\widehat{A}(\mathcal{M}_n, y)$ is the equivariant A-roof genus of $\mathcal{M}_n$, and $[A]_{n-1}$ denotes the degree $2n-2$ part of the multiform A (see [145, Section 2.5] for more details). This integral can in turn be computed using the Atiyah-Bott Lefschetz fixed point theorem [145], and (because the fixed

[8] This is the case when the corresponding quiver has no closed loops, or more generally when scaling solutions are absent, which depends on certain linear inequalities on the γ_{ij}'s [39, 77].

[9] Possibly up to an overall sign, depending whether the harmonic spinors are supported on positive or negative chirality [145, Section 2.5].

points are isolated) it coincides with the equivariant volume up to a simple rescaling, arising from the A-roof genus at the fixed points,

$$\begin{aligned}\mathrm{Ind}_C(\{\gamma, c\};\, y) &= \left(\frac{2\log y}{y-1/y}\right)^{n-1} \mathrm{Vol}(\{\gamma, c\};\, y) \\ &= \frac{(-1)^{\sum_{i<j}\gamma_{ij}-n+1}}{(y-1/y)^{n-1}} \sum_{\sigma\in S_n} F_{C,n}(\{\gamma_{\sigma(i)}, c_{\sigma(i)}\})\, y^{\sum_{i<j}\gamma_{\sigma(i)\sigma(j)}}.\end{aligned} \tag{6.53}$$

Now, if the phase space $\mathcal{M}_n$ is compact, the r.h.s. of (6.53) is guaranteed to be a symmetric Laurent polynomial in y, and correctly computes the character of the $SO(3)$ action on the space of harmonic spinors. In the presence of scaling solutions, however, $\mathcal{M}_n$ is no longer compact, and the r.h.s. of (6.53) is in general a rational function of y, which cannot be understood as a $SO(3)$ character. A possible remedy, advocated in [145], is to include suitable boundary contributions such that the final result is a symmetric Laurent polynomial with integer coefficients. This procedure was designed to extract single-centered black hole indices, whose mathematical definition has remained elusive.

Instead, for the purposes of extracting attractor indices (of which MSW indices are a special case), the correct procedure is to use the flow tree formula, which relies on a partition of the phase space of multi-centered black holes into components labeled by attractor flow trees. As shown in [16], this prescription leads to a similar formula as in (6.53),

$$\mathrm{Ind}_{\mathrm{tree}}(\{\gamma, c\};\, y) = \frac{(-1)^{\sum_{i<j}\gamma_{ij}-n+1}}{(y-1/y)^{n-1}} \sum_{\sigma\in S_n} F_{\mathrm{tree},n}(\{\gamma_{\sigma(i)}, c_{\sigma(i)}\})\, y^{\sum_{i<j}\gamma_{\sigma(i)\sigma(j)}}, \tag{6.54}$$

where the coefficients $F_{\mathrm{tree},n}(\{\gamma_i, c_i\})$ (sometimes called 'partial tree indices') now count planar attractor flow trees. Those can be computed recursively as follows [16]:

$$F_{\mathrm{tree},n}(\{\gamma, c\}) = F_n^{(0)}(c_1, \ldots, c_n) - \sum_{\substack{n_1+\cdots+n_m=n \\ n_k\geq 1,\, m<n}} F_{\mathrm{tree},m}(\{\gamma', c'\}) \prod_{k=1}^{m} F_{n_k}^{(0)}(c_1^\star, \ldots, c_{n_k}^\star), \tag{6.55}$$

where $F^{(0)}$ is given by

$$F_n^{(0)}(c_1, \ldots, c_n) = \frac{1}{2^{n-1}} \prod_{i=1}^{n-1} \mathrm{sign}(S_i), \qquad S_i = c_1 + c_2 + \ldots + c_i. \tag{6.56}$$

The sum in (6.55) runs over all *compositions* (ordered partitions) of n with length $m < n$[10]. For a particular composition $(n_1, \ldots, n_m)$, we define the list of m charges and FI parameters

$$\gamma'_k = \sum_{\ell=1}^{n_k} \gamma_{s_{k-1}+\ell}, \qquad c'_k = \sum_{\ell=1}^{n_k} c_{s_{k-1}+\ell}, \qquad k = 1, \ldots, m. \tag{6.57}$$

[10]One can compute the number of compositions, $p_{\mathrm{C}}(n)$ as follows: write n as a row of n ones and make an independent binary choice in each of the $n-1$ interstices: either insert a separator (starting a new part) or leave the gap open. This produces 2^{n-1} compositions; the single pattern that inserts separators everywhere gives the length-n composition $(1, \ldots, 1)$, which is excluded. Hence $p_{\mathrm{C}}(n) = 2^{n-1} - 1$.

where $s_k = n_1 + \cdots + n_k$ and $s_0 = 0$. For a particular charge $\gamma'_k = \sum_{\ell=1}^{n_k} \gamma_{s_{k-1}+\ell}$, we further define the n_k numbers $c^\star_\ell$ as the attractor value of the FI parameters for this subset, i.e.$c^\star_\ell = \langle \gamma'_k, \gamma_{s_{k-1}+\ell} \rangle$. The initial value for the recursion is set by $F_{\text{tree},1}(\{\gamma_1, c_1\}) = 1$.

As an illustration of this recursion relation, consider the partial tree index for two charges (γ_1, γ_2) for FI parameters (c_1, c_2) such that $c_1 + c_2 = 0$. There is only one composition (2) and for this composition $\gamma' = \gamma_1 + \gamma_2$ and $c^\star_1 = -\gamma_{12}$. Thus,

$$F_{\text{tree},2} = \frac{1}{2}\,\text{sign}(c_1) - \frac{1}{2}\,\text{sign}(c^\star_1) = \frac{1}{2}[\text{sign}(c_1) + \text{sign}(\gamma_{12})]. \tag{6.58}$$

For three centers, there are 3 compositions $(1,2)$, $(2,1)$, and (3) and we get

$$\begin{aligned} F_{\text{tree},3} = {} & F^{(0)}_3(c_1, c_2, c_3) - F_{\text{tree},2}\,(\gamma_1, \gamma_{2+3})\, F^{(0)}_2(-\gamma_{23}, \gamma_{23}) - F_{\text{tree},2}\,(\gamma_{1+2}, \gamma_3)\, F^{(0)}_2(-\gamma_{12}, \gamma_{12}) \\ & - F^{(0)}_3(\gamma_{2+3,1}, \gamma_{1+3,2}, \gamma_{1+2,3}), \end{aligned} \tag{6.59}$$

where $\gamma_{2+3,1} := \gamma_{21} + \gamma_{31}$, and similarly for $\gamma_{1+3,2}$. The full result for up to four centers was given in [16, Section C.1], and will be recalled when we need it in Section 6.3.3 below.

6.3.3 Computing the Witten index by localization

In the remainder of this section, our goal is to evaluate the refined Witten index of this supersymmetric quantum mechanics, which includes the contribution from the whole spectrum, rather than just normalizable bound states. The key observation is that, for non-linear sigma models with potential[11], the functional integral computing the Witten index reduces to an integral over constant modes [99, 117]. Thus, we are left to evaluate the following integral,[12]

$$\mathcal{I}_n(\{\gamma, c\}, \beta) = \int \prod_{i=1}^n \frac{\mathrm{d}[3]\vec{x}_i\, \mathrm{d}\bar{\lambda}_i\, \mathrm{d}\lambda_i\, \mathrm{d}D_i}{4\pi^2\beta}\, \exp\left(-\beta\left(\sum_{i=1}^n \left(\mathrm{i}U_i D_i + \frac{m_i}{2}D_i^2\right) + \sum_{i,j=1}^n \vec{\nabla}_j U_i \bar{\lambda}_i \vec{\sigma} \lambda_j\right)\right). \tag{6.60}$$

Formally this integral is infinite due to the flat directions corresponding to overall translations of the position multiplet: $(\vec{x}_i, \lambda_i, \bar{\lambda}_i, D_i) \to (\vec{x}_i + \vec{d}, \lambda_i + \chi, \bar{\lambda}_i + \bar{\chi}, D_i + t)$. To remove these *center of mass* degrees of freedom, we can do the following change of variables

$$\{\vec{x}_i\}_{i=1}^n \;\longrightarrow\; \{\tilde{\vec{x}}_i = \vec{x}_i - \vec{x}_n\}_{i=1}^{n-1}, \quad \tilde{\vec{x}}_0 = \frac{\sum_i m_i \vec{x}_i}{\sum_i m_i}, \tag{6.61}$$

and similarly for $\tilde{\lambda}_i$, $\tilde{\bar{\lambda}}_i$, and $\tilde{D}_i$. We immediately see the following relations

$$\sum_{i=1}^n U_i D_i = \sum_{i=1}^{n-1} U_i \tilde{D}_i, \quad \sum_{i,j=1}^n \vec{\nabla}_j U_i(\vec{x})\, \bar{\lambda}_i \vec{\sigma} \lambda_j = \sum_{i,j=1}^{n-1} \vec{\nabla}_j U_i(\tilde{\vec{x}})\, \tilde{\bar{\lambda}}_i \vec{\sigma} \tilde{\lambda}_j. \tag{6.62}$$

using $\sum_i U_i = 0$ and the fact that $U_i(\vec{x})$ is translation invariant. The quadratic term for the auxiliary fields becomes

$$\sum_{i=1}^n \frac{m_i}{2} D_i^2 = \frac{m_{\text{tot}}}{2}\tilde{D}_0^2 + \frac{1}{2}\sum_{i,j=1}^{n-1} \mathsf{M}_{ij} \tilde{D}_i \tilde{D}_j, \quad \text{where} \quad \mathsf{M}_{ij} = m_i \delta_{ij} - \frac{m_i m_j}{m_{\text{tot}}}. \tag{6.63}$$

[11] The occurrence of terms at first-order in time derivatives does not affect this conclusion.

[12] The factor of i in the exponent arises due to Wick rotation $D \to -\mathrm{i}D$. The normalization factor $(4\pi^2\beta)^n$ will be justified a posteriori by matching the contribution of normalizable bound states.

We shall refer to the $(n-1)\times(n-1)$ matrix M as the reduced mass matrix. For example, for $n=2$ bodies, $M_{11}=\frac{m_1m_2}{m_1+m_2}$ is the usual reduced mass. Thus, the integral along the flat direction in (6.60) can be isolated as $\frac{1}{(2\pi)^2\beta}\int \mathrm{d}[3]\tilde{\vec{x}}_0\mathrm{d}\tilde{\lambda}_0\mathrm{d}\bar{\tilde{\lambda}}_0\mathrm{d}\tilde{D}_0 e^{-\beta\frac{m_{\rm tot}}{2}\tilde{D}_0^2}$. Having removed the center of mass direction, let us rewrite (6.60). For brevity, we will not put tilde's to denote the relative coordinates but instead use the same notation as the original coordinates,

$$\mathcal{I}_n(\{\gamma,c\},\beta)=\int\prod_{i=1}^{n-1}\frac{\mathrm{d}[3]\vec{x}_i\,\mathrm{d}\bar{\lambda}_i\,\mathrm{d}\lambda_i\,\mathrm{d}D_i}{4\pi^2\beta}\,\exp\left(-\beta\left(\sum_{i=1}^{n-1}\mathrm{i}U_iD_i+\sum_{i,j=1}^{n-1}\left(\frac{\mathsf{M}_{ij}}{2}D_iD_j+\vec{\nabla}_jU_i\bar{\lambda}_i\vec{\sigma}\lambda_j\right)\right)\right). \tag{6.64}$$

Similarly, the refined index is expected to be computed by the integral

$$\begin{aligned}\mathcal{I}_n(\{\gamma,c\},\beta,y)=&\left(\frac{2\log y}{y-1/y}\right)^{n-1}\int\prod_{i=1}^{n-1}\frac{\mathrm{d}[3]\vec{x}_i\,\mathrm{d}\bar{\lambda}_i\,\mathrm{d}\lambda_i\,\mathrm{d}D_i}{4\pi^2\beta}\\&y^{2J_3}\exp\left(-\beta\left(\sum_{i=1}^{n-1}\mathrm{i}U_iD_i+\sum_{i,j=1}^{n-1}\left(\frac{1}{2}\mathsf{M}_{ij}D_iD_j+\vec{\nabla}_jU_i\bar{\lambda}_i\vec{\sigma}\lambda_j\right)\right)\right),\end{aligned} \tag{6.65}$$

where J_3 is the z-component of the angular momentum defined in (6.49), and the power of $2\log y/(y-1/y)$ is motivated by the relation (6.53) between equivariant volume and equivariant Dirac index.

Two-body case, revisited

As a warm-up, we consider the two-body case, which was already studied at length in [166]. For brevity, we denote $\vec{x}=\vec{x}_{12}$, $\kappa=\gamma_{12}$, $c_1=-c_2=c$ and define the reduced mass

$$m=m_{12}:=\frac{m_1m_2}{m_1+m_2}. \tag{6.66}$$

Focusing first on the unrefined index, we have to evaluate

$$\mathcal{I}_2=\frac{1}{4\pi^2\beta}\int \mathrm{d}^3\vec{x}\,\mathrm{d}D\,\mathrm{d}^2\lambda\,\mathrm{d}^2\bar{\lambda}\,e^{-\beta\left(\mathrm{i}UD+\frac{m}{2}D^2+\vec{\nabla}U\cdot\bar{\lambda}\vec{\sigma}\lambda\right)}, \tag{6.67}$$

where $U=-\frac{1}{2}\,(\kappa/|\vec{x}|-c)$. The fermion contribution readily evaluates to

$$\int \mathrm{d}^2\lambda\,\mathrm{d}^2\bar{\lambda}\,e^{-\beta\vec{\nabla}U\cdot\bar{\lambda}\vec{\sigma}\lambda}=-\beta^2(\vec{\nabla}U)^2=-\frac{\beta^2\kappa^2}{4|\vec{x}|^4}. \tag{6.68}$$

Going to spherical coordinates, the integral becomes

$$\begin{aligned}\mathcal{I}_2&=-\frac{\beta\kappa^2}{4\pi}\int_0^\infty\frac{r^2\mathrm{d}r}{r^4}\int_{-\infty}^\infty\mathrm{d}D\;e^{-\beta\left(-\frac{\mathrm{i}}{2}D\left(\frac{\kappa}{r}-c\right)+\frac{m}{2}D^2\right)}\\&=-\frac{\beta\kappa^2}{4\pi}\left(\frac{\beta m}{2\pi}\right)^{-\frac{1}{2}}\int_0^\infty\mathrm{d}\rho\;e^{-\frac{\beta}{8m}(\kappa\rho-c)^2},\end{aligned} \tag{6.69}$$

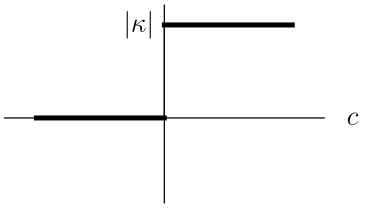
where we defined $\rho = 1/r$ and integrated over D in the second line. We can compute the integral by extending its range to the full real axis by inserting the step function $\frac{\text{sign}\,\rho+1}{2}$:

$$\begin{aligned}\int_0^\infty \mathrm{d}\rho\; e^{-\frac{\beta}{8m}(\kappa\rho-c)^2} &= \frac{1}{2}\int_{-\infty}^{\infty}\mathrm{d}\rho\; e^{-\frac{\beta}{8m}(\kappa\rho-c)^2} + \frac{1}{2}\int_{-\infty}^{\infty}\mathrm{d}\rho\;\,\text{sign}(\rho)\; e^{-\frac{\beta}{8m}(\kappa\rho-c)^2}\\ &= \frac{1}{2}\left(\frac{\beta\kappa^2}{8\pi m}\right)^{-\frac{1}{2}} + \frac{1}{2}\left(\frac{\beta\kappa^2}{8\pi m}\right)^{-\frac{1}{2}}\int_{-\infty}^{\infty}\mathrm{d}u\;\,\text{sign}(u)\; e^{-\pi\left(u-\sqrt{\frac{\beta}{8\pi m}}\,\text{sign}(\kappa)c\right)^2}\\ &= \frac{1}{2}\left(\frac{\beta\kappa^2}{8\pi m}\right)^{-\frac{1}{2}}\left[1+\text{sign}(\kappa)\,E_1\left(c\sqrt{\frac{\beta}{8\pi m}}\right)\right],\end{aligned} \tag{6.70}$$

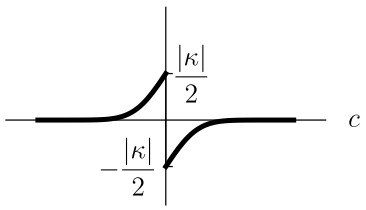
where we changed variable to $u = \sqrt{\frac{\beta}{8\pi m}}|\kappa|\rho$ in the second line and used the definition (6.1) of the error function. Substituting in (6.69), we arrive at

$$\begin{aligned}\mathcal{I}_2 &= -\frac{\kappa}{2}\left[\text{sign}(\kappa) + E_1\left(c\sqrt{\frac{\beta}{8\pi m}}\right)\right]\\ &= -\frac{\kappa}{2}\left[\text{sign}(c)+\text{sign}(\kappa)+M_1\left(c\sqrt{\frac{\beta}{8\pi m}}\right)\right].\end{aligned} \tag{6.71}$$

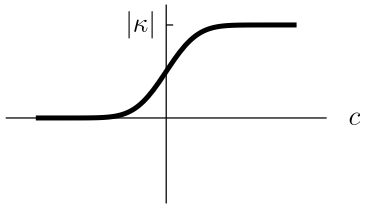
The expression in the first line shows that the Witten index is a smooth function of the stability



(a) Contribution from supersymmetric bound states, proportional to the step function $\text{sign}(c)$ and equal to $|\kappa|$ when c and κ have the same sign.



(b) Contribution from the continuum of scattering states, given by the complementary error function $M_1(c)$ and interpolating discontinuously between $\pm|\kappa|/2$.



(c) Total two-body Witten index $\mathcal{I}_2 = \mathcal{I}_2^{(\text{bound})} + \mathcal{I}_2^{(\text{scatt})}$, a smooth error function completion across the wall of marginal stability.

Figure 6.1: Decomposition of the two-body Witten index into contributions from bound states (a) and scattering states (b). Their sum (c) produces a smooth interpolation described by the error function $E_1(c)$, consistent with the modular completion of the BPS index.

parameter c, as emphasized in [166]. The second line expresses it, as the sum of the contributions of the $|\kappa|$ supersymmetric bound states, which exist whenever c and κ have the same sign, and the contribution of the continuum of scattering states, proportional to the complementary error function M_1. Indeed, the latter can be rewritten as

$$M_1\left(c\sqrt{\frac{\beta}{8\pi m}}\right) = -\frac{2c}{\pi}\int_{2|c|}^{\infty}\frac{\mathrm{d}k}{k\sqrt{4k^2-c^2}}e^{-\frac{\beta k^2}{2m}}, \tag{6.72}$$

consistent with the spectral asymmetry computed in [166, (3.36)] (where k is the norm of the momentum in $\mathbb{R}^3$). This decomposition is illustrated in Fig. 6.1. In terms of the combination

$\mathcal{I}_{\gamma_1,\gamma_2}$ defined in (6.4) and of the modular parameter $\tau_2 = \beta/(2\pi)$, the result (6.71) may be rewritten as

$$\mathcal{I}_2 = -\frac{\gamma_{12}}{2}\left[\mathrm{sign}(\gamma_{12}) - E_1\left(\sqrt{2\tau_2}\mathcal{I}_{\gamma_1,\gamma_2}\right)\right]. \tag{6.73}$$

Comparing with two-body contribution to the instanton generating potential (6.25), we find perfect agreement up to overall normalization factors. However, if one specializes to the large volume attractor chamber $c = 2\lambda\gamma_{12}$, leading to the λ-independent ratio $\mathcal{I}^*_{\gamma_1,\gamma_2}$ in (6.26), we find agreement with the modular completion (6.24) only up to a rescaling of the argument of the complementary error function by a factor $\sqrt{\frac{(pp_1p_2)(p^3)}{(p_1p^2)(p_2p^2)}}$. At present we do not understand the physical origin of this rescaling. Nevertheless, we proceed since it disappears when the D4-brane charges are collinear, which covers the case of one-parameter compact CY threefolds as well as non-compact CY threefolds of the form $X = K_S$ for S a complex surface.

A second puzzle is that the localization computation does not reproduce the Gaussian term in (6.24). This term is necessary for modular invariance, and arises by differentiation from the refined completion (6.24), due to the η-dependence in the argument. One may attempt instead to compute the refined modular completion (6.23) directly by inserting the factor y^{2J_3} in the integral, as in (6.65). The computation proceeds as before, except that the integral over the angular coordinates now includes a factor $y^{\kappa\cos\theta}$, which replaces the 4π solid angle by

$$4\pi \mapsto \int_0^{2\pi} \mathrm{d}\phi \int_{-\pi}^{\pi} \sin\theta\,\mathrm{d}\theta\, y^{\kappa\cos\theta} = \frac{2\pi}{\kappa\log y}\left(y^\kappa - y^{-\kappa}\right). \tag{6.74}$$

We thus obtain

$$\mathcal{I}_2(y) = -\frac{1}{2}\left(\frac{y^\kappa - y^{-\kappa}}{y - 1/y}\right)\left[\mathrm{sign}(\kappa) + E_1\left(c\sqrt{\frac{\beta}{8\pi m}}\right)\right], \tag{6.75}$$

in precise agreement with the refined modular completion (6.23) under the same identifications as above, provided $\eta = 0$, i.e.y is a pure phase. The microscopic effect of the parameter η, which is connected to the Gaussian term in (6.24), unfortunately remains mysterious at this point.

Finally, it is instructive to compute the same integral without eliminating the auxiliary fields. For this, we must be more specific about the contour of integration. We claim that the correct choice is to shift $D \mapsto D - \mathrm{i}\epsilon\ \mathrm{sign}\,\kappa$, where $\epsilon > 0$ is an infinitesimal positive parameter. This ensures that the integral over $\rho = 1/r$ in the first line of (6.69) is convergent and becomes

$$\mathcal{I}_2 = \frac{\mathrm{i}\kappa}{2\pi}\int_{-\infty}^{\infty}\frac{\mathrm{d}D}{D - \mathrm{i}\epsilon\,\mathrm{sign}\,\kappa}\, e^{-\frac{\beta}{2}\left(\mathrm{i}cD + mD^2\right)}. \tag{6.76}$$

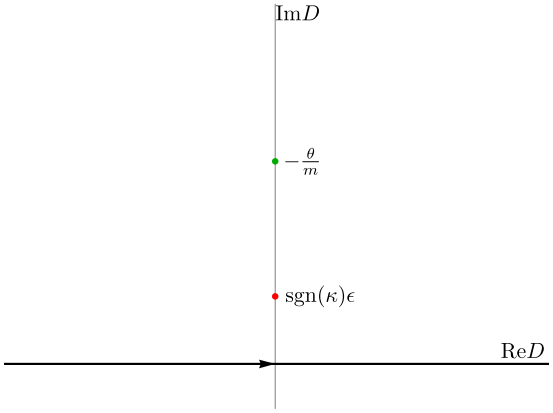
Upon shifting the contour of D integration to run across the saddle point $D_* = -\frac{\mathrm{i}c}{2m}$, we recognize the integral representation (6.2) of the complementary error function,

$$\mathcal{I}_2^{\mathrm{saddle}} = \frac{\kappa}{2}\, M_1\left(c\sqrt{\frac{\beta}{8\pi m}}\right). \tag{6.77}$$

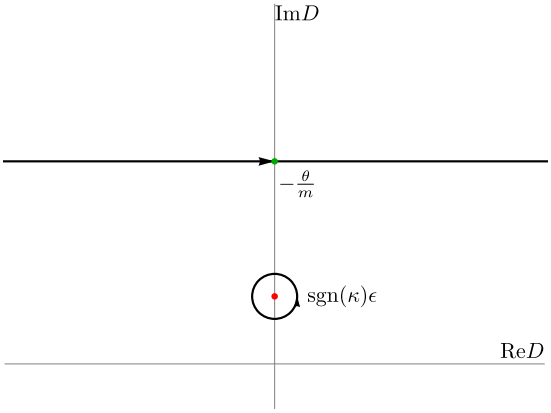
However, we have to take into account the pole at $D = \mathrm{i}\epsilon\,\mathrm{sign}\,\kappa$. Clearly, in shifting the contour we encounter the pole only if κ has the same sign as c (see Fig. 6.2). If this is the case, we pick up an additional pole contribution

$$\mathcal{I}_2^{\mathrm{pole}} = -\kappa\ \mathrm{sign}(\kappa)\,\mathrm{Res}_{D=\mathrm{i}\epsilon\,\mathrm{sign}\,\kappa}\left(\frac{e^{-\frac{\beta}{2}\left(\mathrm{i}cD + mD^2\right)}}{D - \mathrm{i}\,\mathrm{sign}(\kappa)\epsilon}\right) = -|\kappa|, \tag{6.78}$$

where the factor of $\text{sign}(\kappa)$ before the residue comes from the fact that the contour closes counterclockwise if $\kappa > 0$ and clockwise if $\kappa < 0$. It is easy to see that the sum of (6.77) and (6.78) reproduces (6.71).



(a) The original contour integral in the auxiliary field D along with the pole at $D = i\,\text{sign}(\kappa)\epsilon$ (in red) and the saddle point of the integrand, $D = -i\frac{\theta}{m}$ (in green). This figure is for the case when $\kappa\theta < 0$.



(b) After shifting the contour to pass through the saddle, $D = -i\theta/m$, we pick up the contribution from the pole at $D = i\,\text{sign}(\kappa)\epsilon$ coming from the bound state in this case.

Figure 6.2: Contour integral in the D plane

General case

We now turn to the general n-body Witten index defined in (6.64). The fermion integral gives the determinant

$$\int \prod_{i=1}^{n-1} \mathrm{d}\bar{\lambda}_i\, \mathrm{d}\lambda_i\, \exp\left(-\beta \sum_{i,j=1}^{n-1} \vec{\nabla}_j U_i\, \bar{\lambda}_i \vec{\sigma} \lambda_j\right) = (\beta^2)^{n-1} \det(\vec{\nabla}_j U_i \otimes \vec{\sigma}), \tag{6.79}$$

The key observation is that the space of relative positions $\mathbb{R}^{3n-3}$ is foliated by the phase spaces $\mathcal{M}_n(\{\gamma_i, u_i\})$ introduced in (6.46), with arbitrary FI parameters $u_i \in \mathbb{R}^n$ (with $\sum_i u_i = 0$), such that the flat measure on $\mathbb{R}^{3n-3}$ times the fermion determinant equals the flat measure on $\mathbb{R}^{n-1}$ times the symplectic volume form ω^{n-1} on each leaf:

$$\boxed{\prod_{i=1}^{n-1} \mathrm{d}^3\vec{x}_i \det(\vec{\nabla}_i U_j \otimes \vec{\sigma}) = \frac{(-1)^{n-1}}{2^{n-1}(n-1)!} \left(\prod_{i=1}^{n-1} \mathrm{d}u_i\right) \omega^{n-1},} \tag{6.80}$$

where ω was defined in (6.48). In particular for $n = 2$, where $u = \frac{\kappa}{r} = \kappa\rho$ and $\omega = \frac{\kappa}{2} \sin\theta\, \mathrm{d}\theta\, \mathrm{d}\phi$, this formula boils down to

$$r^2 \mathrm{d}r \sin\theta\, \mathrm{d}\theta\, \mathrm{d}\phi \times -\frac{\kappa^2}{4r^4} = \frac{1}{2}\kappa \mathrm{d}\rho \times \frac{1}{2}\kappa \sin\theta\, \mathrm{d}\theta\, \mathrm{d}\phi\,, \tag{6.81}$$

see Appendix 6.6 for a proof for arbitrary n.

Inserting the identity (6.80) in (6.64), we can trade the integral over $\vec{x}_i$ into an integral over $\mathcal{M}_n(\{\gamma_i, u_i\})$ at fixed values of u_i, further integrated over $\mathbb{R}^{n-1}$. The integral over $\mathcal{M}_n(\{\gamma_i, u_i\})$

produces the symplectic volume (6.50), leading to

$$\begin{aligned}\mathcal{I}_n(\{\gamma_i, c_i\}, \beta) &= \left(\frac{\beta}{4\pi}\right)^{n-1} \int \prod_{i=1}^{n-1} \mathrm{d}u_i \, \mathrm{d}D_i \ \mathrm{Vol}(\{\gamma_i, u_i\}) \, e^{-\frac{\beta}{2}\left(\sum_{i=1}^{n-1}(c_i-u_i)D_i + \sum_{i,j=1}^{n-1} \mathsf{M}_{ij} D_i D_j\right)} \\ &= \left(\frac{\beta}{4\pi}\right)^{n-1} \left(\det \frac{\beta \mathsf{M}}{2\pi}\right)^{-1/2} \int \prod_{i=1}^{n-1} \mathrm{d}u_i \ \mathrm{Vol}(\{\gamma_i, u_i\}) \, e^{-\frac{\beta}{8}\sum_{i,j=1}^{n-1}(u_i-c_i)\mathsf{M}^{-1}_{ij}(u_j-c_j)},\end{aligned} \tag{6.82}$$

where in the second line we integrated over $D_i \in \mathbb{R}^{n-1} - \mathrm{i}\epsilon$. It is convenient to change variables

$$u_i \to z_i = \sqrt{\frac{\beta}{8\pi}} u_j \mathsf{E}^{-1}_{ji}, \tag{6.83}$$

where E is defined as a Cholesky-type factor for M through the relation $\mathsf{E}^T\mathsf{E} = \mathsf{M}$. Since there is an $\mathrm{O}(n-1)$ arbitrariness in E, we choose it for definiteness so that it is lower-triangular with a positive diagonal. The transformation above makes the quadratic form inside the exponent in (6.82) diagonal,

$$-\frac{\beta}{8}\sum_{i,j=1}^{n-1}(u_i - c_i)\,\mathsf{M}^{-1}_{ij}\,(u_j - c_j) = -\pi \sum_{i=1}^{n-1}(z_i - \xi_i)^2, \quad \xi_i = \sqrt{\frac{\beta}{8\pi}} c_i E^{-1}_{ji}. \tag{6.84}$$

Further, the measure $\prod_{i=1}^{n-1} \mathrm{d}u_i$ becomes

$$\prod_{i=1}^{n-1} \mathrm{d}u_i = \det\left(\sqrt{\frac{8\pi}{\beta}}\mathsf{E}^T\right) \prod_{i=1}^{n-1} \mathrm{d}z_i = \left(\frac{8\pi}{\beta}\right)^{\frac{n-1}{2}} \sqrt{\det \mathsf{M}} \prod_{i=1}^{n-1} \mathrm{d}z_i, \tag{6.85}$$

such that the factor in front of the integral over z_i becomes unity,

$$\left(\frac{\beta}{4\pi}\right)^{n-1} \left(\det \frac{\beta \mathsf{M}}{2\pi}\right)^{-1/2} \left(\frac{8\pi}{\beta}\right)^{\frac{n-1}{2}} \sqrt{\det \mathsf{M}} = 1, \tag{6.86}$$

justifying *a posteriori* the choice of normalization of the integral in (6.60). The remaining integral can be written as

$$\boxed{\mathcal{I}_n(\{\gamma_i, c_i\}, \beta) = \int \prod_{i=1}^{n-1} \mathrm{d}z_i \, e^{-\pi \sum_{i=1}^{n-1}(z_i-\xi_i)^2} \ \mathrm{Vol}(\{\gamma_i, \mathsf{E}^T z\}).} \tag{6.87}$$

Similarly for the refined index, assuming that switching on the chemical potential y has the effect of performing the same replacement (6.52) on the r.h.s. of (6.80), we obtain

$$\boxed{\mathcal{I}_n(\{\gamma_i, c_i\}, \beta, y) = \int \prod_{i=1}^{n-1} \mathrm{d}z_i \, e^{-\pi \sum_{i=1}^{n-1}(z_i-\xi_i)^2} \ \mathrm{Ind}_{\mathrm{tree}}(\{\gamma_i, \mathsf{E}^T z\}, y).} \tag{6.88}$$

We shall refer to the contribution of a particular permutation σ in (6.54) as a 'partial Witten index'.

In particular, for any term of the form $\prod_{\alpha=1}^{r} \text{sign}\left(\sum_{i=1}^{n-1} c_i \mathsf{H}_{i\alpha}\right)$ in $\text{Vol}(\{\gamma_i, c_i\})$ or $\text{Ind}_{\text{tree}}(\{\gamma_i, c_i\})$, the integral yields a term

$$\int \prod_{i=1}^{n-1} \mathrm{d}z_i \, e^{-\pi \sum_{i=1}^{n-1}(z_i-\xi_i)^2} \prod_{\alpha=1}^{r} \text{sign}\left(\sum_{i,j=1}^{n-1} z_j \mathsf{E}_{ji} \mathsf{H}_{i\alpha}\right), \tag{6.89}$$

which is clearly a generalized error function of depth r. To obtain its explicit form, we have to rotate the z_i's such that the r linear forms $\sum_{i,j=1}^{n-1} z_j \mathsf{E}_{ji} \mathsf{H}_{i\alpha}$ labeled by α only involve z_1 through z_r. This ensures that the integration over the remaining $z_{r+1}, \ldots z_{n-1}$ will be trivial and yield 1. This rotation can be done by an orthogonalization procedure for the columns of EH. The result is a certain lower-triangular $r \times r$ matrix L and a row-orthonormal $r \times (n-1)$ matrix O such that $\mathsf{EH} = O^T \mathsf{L}$. Noting that the generalized error functions are invariant under arbitrary orthogonal transformations, and recalling the definition of ξ in (6.84), the integral can finally be written as

$$\boxed{\int \prod_{i=1}^{n-1} \mathrm{d}z_i \, e^{-\pi \sum_{i=1}^{n-1}(z_i-\xi_i)^2} \prod_{\alpha=1}^{r} \text{sign}\left(\sum_{i,j=1}^{n-1} z_j \mathsf{E}_{ji} \mathsf{H}_{i\alpha}\right) = E_r\left(\mathsf{L}, \sqrt{\frac{\beta}{8\pi}}\, O\, \mathsf{E}^{-T} c\right).} \tag{6.90}$$

Since $O^T \mathsf{L} = \mathsf{EH}$, the result can also be written as

$$E_r\left(\mathsf{L}, \sqrt{\frac{\beta}{8\pi}}\, O\, \mathsf{E}^{-T} c\right) = E_r\left(\tilde{\mathsf{L}}, \sqrt{\frac{\beta}{8\pi}}\, \mathsf{L}^{-T}\, (\mathsf{H}^T c\right), \tag{6.91}$$

where $\tilde{\mathsf{L}}$ is a lower triangular matrix with 1s on the diagonal obtained by scaling the columns of L by the corresponding diagonal element (which we are allowed to do because of the scaling properties of the generalized error functions given in Section 6.2.2). Thus, for any number n of centers, the refined Witten index can be expressed as a sum of generalized error functions of depth $\leq n-1$, weighted by products of sign functions of the γ_{ij}'s and by factors of $y^{\gamma_{ij}}$.

Explicit results for up to 4 centers

We can now compute the Witten index for up to 4 centers using the prescription just outlined. The starting point is the formula for the partial tree index, computed by applying the recursion relation from Section 6.3.2 (or by reading off the result from [16, Section C.1]):

$$F_{\text{tree},2} = \frac{1}{2}[\text{sign}(c_1) + \text{sign}(\gamma_{12})], \tag{6.92}$$

$$\begin{aligned} F_{\text{tree},3} = \frac{1}{4} \big[&(\text{sign}(c_1) + \text{sign}(\gamma_{12}))\,(\text{sign}(c_1 + c_2) + \text{sign}(\gamma_{23})) \\ &- \big(\text{sign}(\gamma_{2+3,1}) + \text{sign}(\gamma_{12})\big)\,\big(\text{sign}(\gamma_{3,1+2}) + \text{sign}(\gamma_{23})\big)\big], \end{aligned} \tag{6.93}$$

$$\begin{aligned} F_{\text{tree},4} = \frac{1}{8}\Big[&(\text{sign}(c_1) + \text{sign}(\gamma_{12}))(\text{sign}(c_1 + c_2) + \text{sign}(\gamma_{23}))(\text{sign}(c_1 + c_2 + c_3) + \text{sign}(\gamma_{34})) \\ &- (\text{sign}(\gamma_{2+3+4,1}) + \text{sign}(\gamma_{12}))(\text{sign}(\gamma_{3+4,1+2}) + \text{sign}(\gamma_{23}))(\text{sign}(\gamma_{4,1+2+3}) + \text{sign}(\gamma_{34})) \\ &- (\text{sign}(c_1) - \text{sign}(\gamma_{2+3+4,1}))(\text{sign}(\gamma_{3+4,2}) + \text{sign}(\gamma_{23}))(\text{sign}(\gamma_{4,2+3}) + \text{sign}(\gamma_{34})) \\ &- (\text{sign}(c_1 + c_2 + c_3) - \text{sign}(\gamma_{4,1+2+3}))(\text{sign}(\gamma_{2+3,1}) + \text{sign}(\gamma_{12}))(\text{sign}(\gamma_{3,1+2}) + \text{sign}(\gamma_{23}))\Big], \end{aligned} \tag{6.94}$$

where we recall that the FI parameters c_i are related to the central charges of the constituents via (6.47). Using these partial tree indices as the starting point, one can compute the index (6.65). We already know the result for two centers but now we can see it even more explicitly: inserting (6.92) into our general formula (6.87), and noting that $\mathsf{E} = \sqrt{m} = \sqrt{\frac{m_1 m_2}{m_1+m_2}}$ for two centers, we see that the effect of the integration over u is to replace

$$\text{sign}(c_1) \to E_1\left(\sqrt{\frac{\beta}{8\pi m}}c_1\right), \tag{6.95}$$

leading to the partial Witten index

$$\mathcal{J}_2 = \frac{1}{2}[\text{sign}(\gamma_{12}) + E_1\left(\sqrt{\frac{\beta}{8\pi m}}c_1\right)]. \tag{6.96}$$

Using the fact that $\mathcal{J}_1$ is odd under the permutation $\gamma_1 \leftrightarrow \gamma_2$, the sum over permutations gives the refined index for two centers,

$$\mathcal{I}_2(\{\gamma_1,\gamma_2,c_1\},\beta,y) = -\frac{(-1)^{\gamma_{12}}}{2}\left(E_1\left(\sqrt{\frac{\beta}{8\pi m}}c_1\right) + \text{sign}(\gamma_{12})\right)\left(\frac{y^{\gamma_{12}} - y^{-\gamma_{12}}}{y - y^{-1}}\right), \tag{6.97}$$

which agrees with (6.75) up to an overall sign. In the presence of a non-vanishing η parameter, we expect that the argument of the E_1 will be shifted in opposite directions for the two permutations, such that the dependence in y no longer factorizes, leading to the additional Gaussian term in the unrefined limit $y \to 1$. At the attractor point $c_1 = -2\lambda\gamma_{12}$, the partial Witten index simplifies to

$$\mathcal{J}_2^* = -\frac{1}{2}M_1\left(\sqrt{\frac{\lambda^2\tau_2}{m}}\gamma_{12}\right), \tag{6.98}$$

where we have set $\beta = 2\pi\tau_2$.

Three Centers

For three centers, starting with the partial tree index (6.93), the u–integration implements the following replacements: [13]

$$\begin{aligned}
\text{sign}(c_1)\ \text{sign}(c_1+c_2) &\longrightarrow E_2\Big(\sqrt{\frac{m_1 m_3}{m_2\,(m_1+m_2+m_3)}};\ \frac{c_1 m_2 - c_2 m_1}{\sqrt{m_1 m_2 (m_1+m_2)}},\ \frac{c_1+c_2}{\sqrt{m_{1+2,3}}}\Big),\\
\text{sign}(c_1+c_2) &\longrightarrow E_1\Big(\tfrac{c_1+c_2}{\sqrt{m_{1+2,3}}}\Big),\\
\text{sign}(c_1) &\longrightarrow E_1\Big(\tfrac{c_1}{\sqrt{m_{1,2+3}}}\Big).
\end{aligned} \tag{6.99}$$

[13] To avoid cluttering, we set $\beta = 8\pi$. The parameter β can be easily reinstated by rescaling $m \mapsto 8\pi m/\beta$ in the arguments x_i of E_n, keeping the parameters $\mathcal{M}$ fixed.

The contribution from the trivial permutation leads to the following 'partial Witten index',

$$\begin{aligned}\mathcal{J}_3 = \frac{1}{4}\Big[& E_2\Big(\sqrt{\frac{m_1m_3}{m_2(m_1+m_2+m_3)}};\ \frac{c_2m_1-c_1m_2}{\sqrt{m_1m_2(m_1+m_2)}},\ \frac{c_3}{\sqrt{m_{1+2,3}}}\Big) - \operatorname{sign}(\gamma_{1,2+3})\ \operatorname{sign}(\gamma_{1+2,3}) \\ & - \Big[E_1\big(\tfrac{c_3}{\sqrt{m_{1+2,3}}}\big) - \operatorname{sign}(\gamma_{1+2,3})\Big]\ \operatorname{sign}(\gamma_{12}) + \Big[E_1\big(\tfrac{c_1}{\sqrt{m_{1,2+3}}}\big) - \operatorname{sign}(\gamma_{2+3,1})\Big]\ \operatorname{sign}(\gamma_{23})\Big].\end{aligned} \tag{6.100}$$

where $m_{1+2,3} = \frac{m_3(m_1+m_2)}{(m_1+m_2+m_3)}$ denotes the reduced mass for the two-body problem $(\gamma_1+\gamma_2, \gamma_3)$, and similarly for $m_{1,2+3}$. Similarly, we denote $\gamma_{1+2,3} = \langle \gamma_1+\gamma_2, \gamma_3\rangle = \gamma_{12}+\gamma_{13}$. Multiplying by $y^{\sum_{i<j}\gamma_{ij}}/(y-1/y)^2$ and summing over all permutations (for vanishing η), we can recombine the terms as follows:

$$\begin{aligned}\mathcal{I}_3 = -\frac{1}{4}\Big[& E_2\Big(\sqrt{\tfrac{m_2m_3}{m_1(m_1+m_2+m_3)}};\ \tfrac{-c_2m_1+c_1m_2}{\sqrt{m_1m_2(m_1+m_2)}},\ \tfrac{c_3}{\sqrt{m_{1+2,3}}}\Big)\,\kappa(\gamma_{13})\,\kappa(\gamma_{1+3,2}) \\ & - E_2\Big(\sqrt{\tfrac{m_1m_3}{m_2(m_1+m_2+m_3)}};\ \tfrac{c_2m_1-c_1m_2}{\sqrt{m_1m_2(m_1+m_2)}},\ \tfrac{c_3}{\sqrt{m_{1+2,3}}}\Big)\,\kappa(\gamma_{23})\,\kappa(\gamma_{2+3,1}) \\ & - E_1\Big(\tfrac{c_3}{\sqrt{m_{1+2,3}}}\Big)\,\kappa(\gamma_{12})\,\kappa(\gamma_{1+2,3})\ \operatorname{sign}(\gamma_{12}) - E_1\Big(\tfrac{c_2}{\sqrt{m_{1+3,2}}}\Big)\,\kappa(\gamma_{13})\,\kappa(\gamma_{1+3,2})\ \operatorname{sign}(\gamma_{13}) \\ & - E_1\Big(\tfrac{c_1}{\sqrt{m_{2+3,1}}}\Big)\,\kappa(\gamma_{23})\,\kappa(\gamma_{2+3,1})\ \operatorname{sign}(\gamma_{23}) + \kappa(\gamma_{2+3,1})\,\kappa(\gamma_{23}) \\ & + \kappa(\gamma_{13})\,\kappa(\gamma_{1+3,2})\ \operatorname{sign}(\gamma_{13})\ \operatorname{sign}(\gamma_{1+3,2}) + \kappa(\gamma_{2+3,1})\,\kappa(\gamma_{23})\ \operatorname{sign}(\gamma_{2+3,1})\ \operatorname{sign}(\gamma_{1+3,2}) \\ & + \kappa(\gamma_{2+3,1})\,\kappa(\gamma_{23})\ \operatorname{sign}(\gamma_{2+3,1})\ \operatorname{sign}(\gamma_{23}) + \kappa(\gamma_{12})\,\kappa(\gamma_{1+2,3})\ \operatorname{sign}(\gamma_{12})\ \operatorname{sign}(\gamma_{1+2,3}) \\ & - \kappa(\gamma_{12})\,\kappa(\gamma_{1+2,3})\ \operatorname{sign}(\gamma_{1+3,2})\ \operatorname{sign}(\gamma_{1+2,3})\Big].\end{aligned} \tag{6.101}$$

where we denoted by $\kappa(p) = (-1)^p \frac{y^p-y^{-p}}{y-1/y}$ the character of a spin $(|p|-1)/2$ representation of $SO(3)$, and used the functional equation (6.34) to eliminate one of the three E_2 functions. At the attractor point $c_1 = 2\lambda\gamma_{2+3,1}$, $c_2 = 2\lambda\gamma_{1+3,2}$, using the identities (6.39)–(6.40), the partial Witten index reduces to

$$\begin{aligned}\mathcal{J}_3^* = \frac{1}{4}\Bigg(& M_2\left(\sqrt{\frac{m_1m_3}{m_2\,(m_1+m_2+m_3)}};-\frac{\sqrt{\lambda^2\tau_2}\,\big(m_2\gamma_{1,2+3}-m_1\gamma_{2,1+3}\big)}{\sqrt{m_1m_2\,(m_1+m_2)}},-\frac{\sqrt{\lambda^2\tau_2}\gamma_{1+2,3}}{\sqrt{m_{1+2,3}}}\right) \\ & + M_1\left(\frac{\sqrt{\lambda^2\tau_2}\gamma_{1+2,3}}{\sqrt{m_{1+2,3}}}\right)\Big(\operatorname{sign}\big(m_2\gamma_{1,2+3}-m_1\gamma_{2,1+3}\big)-\operatorname{sign}\left(\gamma_{12}\right)\Big) \\ & + M_1\left(\frac{\sqrt{\lambda^2\tau_2}\gamma_{1,2+3}}{\sqrt{m_{1,2+3}}}\right)\Big(\operatorname{sign}\big(m_2\gamma_{1+2,3}-m_3\gamma_{1+3,2}\big)-\operatorname{sign}\left(\gamma_{23}\right)\Big)\Bigg).\end{aligned} \tag{6.102}$$

The terms proportional to M_2 are identified as the contribution to the Witten index from the continuum of scattering states for the 3-body supersymmetric quantum mechanics. The terms proportional to M_1 arise instead from scattering states in the 2-body problem, where one of the bodies is a two-particle bound state. In the special case where all D4-brane charges are collinear, we observe that the coefficients of M_1 vanish,[14] i.e.two-particle bound states are absent in the attractor chamber, leaving only the contribution from the 3-body continuum of scattering states.

[14]For example, setting $p_i = N_i p_0$ with $N_i > 0$ and $(p_0)^3 > 0$, $m_2\gamma_{1,2+3} - m_1\gamma_{2,1+3} = (p_0^3)(N_1+N_2+N_3)\gamma_{12}$.

Four Centers

For four centers, it is convenient to introduce

$$\begin{aligned}
\alpha &= \sqrt{\frac{m_1 m_3}{m_2(m_1+m_2+m_3)}}, \quad \beta = \sqrt{\frac{m_1(m_1+m_2)m_4}{m_2(m_1+m_2+m_3)(m_1+m_2+m_3+m_4)}}, \\
\gamma &= \sqrt{\frac{(m_1+m_2)m_4}{m_3(m_1+m_2+m_3+m_4)}}.
\end{aligned} \tag{6.103}$$

We then define the building blocks

$$\begin{aligned}
\Phi_3 &= E_3\Big(\alpha,\ \beta,\ \gamma;\ \tfrac{c_1 m_2 - c_2 m_1}{\sqrt{m_1 m_2 (m_1+m_2)}},\ \tfrac{(c_1+c_2)m_3 - c_3(m_1+m_2)}{\sqrt{(m_1+m_2)m_3(m_1+m_2+m_3)}},\ \tfrac{-c_4}{\sqrt{m_{1+2+3,4}}}\Big), \\
\Phi_2^{(12)} &= E_2\Big(\sqrt{\tfrac{(m_1+m_2)m_4}{m_3(m_1+m_2+m_3+m_4)}};\ \tfrac{c_3(m_1+m_2)-(c_1+c_2)m_3}{\sqrt{(m_1+m_2)m_3(m_1+m_2+m_3)}},\ \tfrac{c_4}{\sqrt{m_{1+2+3,4}}}\Big), \\
\Phi_2^{(23)} &= E_2\Big(\sqrt{\tfrac{m_1 m_4}{(m_2+m_3)(m_1+m_2+m_3+m_4)}};\ \tfrac{(c_2+c_3)m_1 - c_1(m_2+m_3)}{\sqrt{m_1(m_2+m_3)(m_1+m_2+m_3)}},\ \tfrac{c_4}{\sqrt{m_{1+2+3,4}}}\Big), \\
\Phi_2^{(34)} &= E_2\Big(\sqrt{\tfrac{m_1(m_3+m_4)}{m_2(m_1+m_2+m_3+m_4)}};\ \tfrac{c_1 m_2 - c_2 m_1}{\sqrt{m_1 m_2(m_1+m_2)}},\ \tfrac{c_1+c_2}{\sqrt{m_{1+2,3+4}}}\Big).
\end{aligned} \tag{6.104}$$

The partial Witten index then takes the form

$$\begin{aligned}
\mathcal{J}_4 = \frac{1}{8}\Big[&\Phi_3 + \Phi_2^{(12)}\,\mathrm{sign}(\gamma_{12}) + \Phi_2^{(23)}\,\mathrm{sign}(\gamma_{23}) + \Phi_2^{(34)}\,\mathrm{sign}(\gamma_{34}) \\
&+ E_1\left(\frac{c_1}{\sqrt{m_{1,2+3+4}}}\right)\Big[\mathrm{sign}(\gamma_{2,3+4})\,\mathrm{sign}(\gamma_{34}) + \mathrm{sign}(\gamma_{23})\,\mathrm{sign}(\gamma_{2+3,4}) \\
&\qquad - \mathrm{sign}(\gamma_{2,3+4})\,\mathrm{sign}(\gamma_{2+3,4})\Big] \\
&+ E_1\left(\frac{c_1+c_2}{\sqrt{m_{1+2,3+4}}}\right)\mathrm{sign}(\gamma_{12})\,\mathrm{sign}(\gamma_{34}) \\
&+ E_1\left(\frac{c_1+c_2+c_3}{\sqrt{m_{1+2+3,4}}}\right)\Big[\mathrm{sign}(\gamma_{1,2+3})\,\mathrm{sign}(\gamma_{23}) + \mathrm{sign}(\gamma_{12})\,\mathrm{sign}(\gamma_{1+2,3}) \\
&\qquad - \mathrm{sign}(\gamma_{1,2+3})\,\mathrm{sign}(\gamma_{1+2,3})\Big] \\
&+ \Big[\mathrm{sign}(\gamma_{1,2+3+4})\,\mathrm{sign}(\gamma_{2,3+4})\,\mathrm{sign}(\gamma_{34}) + \mathrm{sign}(\gamma_{12})\,\mathrm{sign}(\gamma_{1+2,3+4})\,\mathrm{sign}(\gamma_{34}) \\
&\quad - \mathrm{sign}(\gamma_{1,2+3+4})\,\mathrm{sign}(\gamma_{1+2,3+4})\,\mathrm{sign}(\gamma_{34}) + \mathrm{sign}(\gamma_{1,2+3+4})\,\mathrm{sign}(\gamma_{23})\,\mathrm{sign}(\gamma_{2,3+4}) \\
&\quad - \mathrm{sign}(\gamma_{1,2+3+4})\,\mathrm{sign}(\gamma_{2,3+4})\,\mathrm{sign}(\gamma_{2+3,4}) + \mathrm{sign}(\gamma_{1,2+3})\,\mathrm{sign}(\gamma_{23})\,\mathrm{sign}(\gamma_{1+2+3,4}) \\
&\quad - \mathrm{sign}(\gamma_{1,2+3+4})\,\mathrm{sign}(\gamma_{23})\,\mathrm{sign}(\gamma_{1+2+3,4}) + \mathrm{sign}(\gamma_{12})\,\mathrm{sign}(\gamma_{1+2,3})\,\mathrm{sign}(\gamma_{1+2+3,4}) \\
&\quad - \mathrm{sign}(\gamma_{1,2+3})\,\mathrm{sign}(\gamma_{1+2,3})\,\mathrm{sign}(\gamma_{1+2+3,4}) - \mathrm{sign}(\gamma_{12})\,\mathrm{sign}(\gamma_{1+2,3+4})\,\mathrm{sign}(\gamma_{1+2+3,4}) \\
&\quad + \mathrm{sign}(\gamma_{1,2+3+4})\,\mathrm{sign}(\gamma_{1+2,3+4})\,\mathrm{sign}(\gamma_{1+2+3,4})\Big]\Big].
\end{aligned} \tag{6.105}$$

The full index is obtained by multiplying by $y^{\sum_{i<j}\gamma_{ij}}/(y-1/y)^3$ and summing over all permutations. At the attractor point, using (6.39)–(6.41) this reduces to

$$\begin{aligned}
\mathcal{J}_4^* = \frac{1}{8}\Big\{ & H_3 + H_2^{(12)}\Big[\mathrm{sign}(\gamma_{12}) - \mathrm{sign}\big(\gamma_{1+3+4,2}\,m_1 - \gamma_{2+3+4,1}\,m_2\big)\Big] \\
& + H_2^{(23)}\Big[\mathrm{sign}(\gamma_{23}) - \mathrm{sign}\big(\gamma_{1+2+4,3}\,m_2 - \gamma_{1+3+4,2}\,m_3\big)\Big] \\
& + H_2^{(34)}\Big[\mathrm{sign}(\gamma_{34}) - \mathrm{sign}\big(\gamma_{1+2+3,4}\,m_3 - \gamma_{1+2+4,3}\,m_4\big)\Big] \\
& + M_1\Big(\tfrac{c_1}{\sqrt{m_{1,2+3+4}}}\Big)\Big[\mathrm{sign}(\gamma_{2,3+4})\big(\mathrm{sign}(\gamma_{34}) - \mathrm{sign}(\gamma_{2+3,4})\big) \\
& \quad - \mathrm{sign}\big(\gamma_{1,2+3+4}\,m_2 + \gamma_{2,1+3+4}\,m_{2+3+4}\big)\big(\mathrm{sign}(\gamma_{34}) - \mathrm{sign}\big(\gamma_{1,2+3+4}\,m_{2+3} - \gamma_{1+4,2+3}\,m_{2+3+4}\big)\big) \\
& \quad + \mathrm{sign}(\gamma_{23})\big(\mathrm{sign}(\gamma_{2,3+4}) - \mathrm{sign}\big(\gamma_{1,2+3+4}\,m_{2+3} - \gamma_{1+4,2+3}\,m_{2+3+4}\big)\big)\Big] \\
& + M_1\Big(\tfrac{c_1+c_2}{\sqrt{m_{1+2,3+4}}}\Big)\Big[\mathrm{sign}(\gamma_{12})\ \mathrm{sign}(\gamma_{34}) - \mathrm{sign}(\gamma_{34})\ \mathrm{sign}\big(-\gamma_{2,3+4}\,m_1 + \gamma_{1,3+4}\,m_2 + \gamma_{12}(m_1+m_2)\big) \\
& \quad - \mathrm{sign}(\gamma_{12})\ \mathrm{sign}\big(\gamma_{1+2+3,4}\,m_3 - \gamma_{1+2,3}\,m_4 + \gamma_{34}\,m_4\big) \\
& \quad + \mathrm{sign}\big(-\gamma_{2,3+4}\,m_1 + \gamma_{1,3+4}\,m_2 + \gamma_{12}(m_1+m_2)\big)\ \mathrm{sign}\big(\gamma_{1+2+3,4}\,m_3 - \gamma_{1+2,3}\,m_4 + \gamma_{34}\,m_4\big)\Big] \\
& + M_1\Big(\tfrac{c_1+c_2+c_3}{\sqrt{m_{1+2+3,4}}}\Big)\Big[\mathrm{sign}(\gamma_{1,2+3})\ \mathrm{sign}(\gamma_{23}) + \mathrm{sign}(\gamma_{12})\ \mathrm{sign}(\gamma_{1+2,3}) \\
& \quad - \mathrm{sign}(\gamma_{1,2+3})\ \mathrm{sign}(\gamma_{1+2,3}) + \mathrm{sign}(\gamma_{12})\ \mathrm{sign}\big(-2(\gamma_{1+2,3}-\gamma_{34})(m_1+m_2) - 2\,\gamma_{1,3+4}\,m_3\big) \\
& \quad + \mathrm{sign}(\gamma_{23})\ \mathrm{sign}\big(-2(\gamma_{1,2+3}-\gamma_{2+3,4})\,m_1 - 2\,\gamma_{1,2+3+4}(m_2+m_3)\big) \\
& \quad - \mathrm{sign}\big(-2(\gamma_{1+2,3}-\gamma_{34})(m_1+m_2) - 2\,\gamma_{1,3+4}\,m_3\big) \\
& \quad \mathrm{sign}\big(-\gamma_{2+3,4}\,m_1 - \gamma_{34}\,m_1 + \gamma_{14}(m_2+m_3) + \gamma_{12}(m_1+m_2+m_3) + \gamma_{13}(m_1+m_2+m_3)\big)\Big]\Big\}.
\end{aligned} \tag{6.106}$$

where as in Eq. (6.104), we define

$$\begin{aligned}
H_3 &= M_3\Big(\alpha,\ \beta,\ \gamma;\ \tfrac{2\,\gamma_{2+3+4,1}\,m_2 - 2\,\gamma_{1+3+4,2}\,m_1}{\sqrt{m_1\,m_2\,(m_1+m_2)}},\ \tfrac{2\,\gamma_{3+4,1+2}\,m_3 - 2\,\gamma_{1+2+4,3}\,(m_1+m_2)}{\sqrt{(m_1+m_2)\,m_3\,(m_1+m_2+m_3)}},\ \tfrac{-2\,\gamma_{1+2+3,4}}{\sqrt{m_{1+2+3,4}}}\Big), \\
H_2^{(12)} &= M_2\Big(\sqrt{\tfrac{(m_1+m_2)\,m_4}{m_3\,(m_1+m_2+m_3+m_4)}};\ \tfrac{2\,\gamma_{3+4,1+2}\,m_3 - 2\,\gamma_{1+2+4,3}\,(m_1+m_2)}{\sqrt{(m_1+m_2)\,m_3\,(m_1+m_2+m_3)}},\ \tfrac{-2\,\gamma_{1+2+3,4}}{\sqrt{m_{1+2+3,4}}}\Big), \\
H_2^{(23)} &= M_2\Big(\sqrt{\tfrac{m_1\,m_4}{(m_2+m_3)\,(m_1+m_2+m_3+m_4)}};\ -2\tfrac{\gamma_{1+4,2+3}\,m_1 + \gamma_{1,2+3+4}\,(m_2+m_3)}{\sqrt{m_1\,(m_2+m_3)\,(m_1+m_2+m_3)}}, \\
&\qquad\qquad - 2\tfrac{\gamma_{1+4,2+3}\,m_1 + \gamma_{1,2+3+4}\,(m_2+m_3)}{\sqrt{m_1\,(m_2+m_3)\,(m_1+m_2+m_3)}}\Big), \\
H_2^{(34)} &= M_2\Big(\sqrt{\tfrac{m_1\,(m_3+m_4)}{m_2\,(m_1+m_2+m_3+m_4)}};\ -2\tfrac{\gamma_{1+3+4,2}\,m_1 + \gamma_{1,2+3+4}\,m_2}{\sqrt{m_1\,m_2\,(m_1+m_2)}},\ -2\,\gamma_{1+2,3+4}\,\sqrt{\tfrac{m_1+m_2+m_3+m_4}{(m_1+m_2)\,(m_3+m_4)}}\Big).
\end{aligned} \tag{6.107}$$

The coefficient of M_3 is identified as the contribution from the continuum of scattering states for the 4-body supersymmetric quantum mechanics. The terms proportional to M_2 arise instead from scattering states in the 3-body problem, where one of the bodies is a two-particle bound state, and those proportional to M_1 arise from scattering states in the 2-body problem, where each of the two bodies is a two-particle bound state, or one is a three-particle bound state and the other is the remaining center. Again, in cases where magnetic charges are collinear, we observe that the coefficients of M_2 and M_1 vanish, leaving only the contribution from the continuum of 4-body scattering states.

6.4 Comparison with modular predictions

In this section, we compare the results of the localization computation in Section 6.3.3 with the prescription for the modular completion reviewed in Section 6.2.1. We first consider the special case of local $\mathbb{P}^2$, which was treated in detail in [14, Section 4]. Returning to the case of a generic CY threefold, we then compare the Witten index of the supersymmetric quantum mechanics with the instanton generating potential.

6.4.1 Vafa-Witten invariants on $\mathbb{P}^2$

As explained in [14, Section 4], the non-compact CY threefold $X = K_{\mathbb{P}^2} = \mathcal{O}_{\mathbb{P}^2}(-3)$ (i.e.the total space of the canonical bundle over the complex projective plane) arises in the large fiber limit of a smooth elliptic fibration $\mathcal{E} \to \tilde{X} \to \mathbb{P}^2$. The D4-D2-D0 indices counting D4-branes wrapped on N times the section $S \simeq \mathbb{P}^2$ coincide with rank N Vafa-Witten (VW) invariants of $\mathbb{P}^2$, which have been computed by various methods (see [37] for a review). Even though the section S itself is not an ample divisor, it was conjectured in [14] that the modular anomaly equations continue to hold, predicting the modular completion of generating series of VW invariants at arbitrary rank. For rank 2 and 3, it was shown to reproduce the known modular completions obtained in [54, 143]. The modular anomaly was subsequently derived in [69] by studying the elliptic genus of the superconformal field theory obtained by reducing the (0,2) six-dimensional SCFT of type A_{N-1} on $\mathbb{P}^2$. Our goal is to reproduce the modular completions for rank $N \leq 4$ from the Witten index of the supersymmetric quantum mechanics of n dyons computed in the previous subsection.

Following [14, Appendix F], we define the normalized generating series of rank N refined Vafa-Witten invariants on $\mathbb{P}^2$ as

$$g_{N,\mu}(\tau, w) := \frac{h_{N,\mu+\frac{1}{2}N(N-1)}(\tau, w+\frac{1}{2})}{\left(h_{1,0}(\tau, w+\frac{1}{2})\right)^N}, \qquad h_{1,0}(\tau, w) = \frac{\mathrm{i}}{\theta_1(\tau, 2w)}, \tag{6.108}$$

where μ denotes the D2-brane charge (or 't Hooft flux) along the hyperplane class of $\mathbb{P}^2$, and the rank one result $h_{1,0}(\tau, w)$ follows from Göttsche's formula [100]. Similarly, we define the normalized completed series $\widehat{g}_{N,\mu}$ as the ratio $\widehat{h}_{N,\mu+\frac{1}{2}N(N-1)}(\tau, w+\frac{1}{2})/(h_{1,0}(\tau, w+\frac{1}{2}))^N$.

In order to compare to the explicit formulae for $\widehat{g}_{N,\mu}$ in [14, Appendix F], we need to evaluate the masses m_i and FI parameters c_i for the relevant constituents. The total D4-brane charge $N[S]$ can a priori split into any number $n \leq N$ of constituents with charge $N_i[S]$, such that $N = \sum_{i=1}^n N_i$. Correspondingly, the D2-brane charge $q[H]$ along the hyperplane class H in $\mathbb{P}^2$ splits into $q = \sum_{i=1}^n q_i$, such that each constituent carries reduced charge $\check{\gamma}_i = (N_i, q_i)$. The DSZ pairing is given by

$$\langle \gamma_i, \gamma_j \rangle = 3(N_i q_j - N_j q_i), \tag{6.109}$$

where the factor 3 comes from the intersection $[S] \cap [H] = -3$. The mass and FI parameters of each constituent at the large volume attractor point are given by

$$c_i = 2\lambda \, \langle \gamma, \gamma_i \rangle = 6\lambda \, (N \, q_i - N_i \, q), \qquad m_i = \tfrac{1}{2} \, \lambda^2 \, (p_i \, p^2) = \tfrac{9}{2} \, \lambda^2 \, N^2 \, N_i, \tag{6.110}$$

where we used the fact that $[S]^3 = c_1(\mathbb{P}^2)^2 = 9$.

Rank 2

For $N = 2$, the only contributing partition has two constituents, with $N_1 = N_2 = 1$. The modular completion is given by [14, (F.4)]

$$\widehat{g}_{2,\mu} = g_{2,\mu} + \frac{1}{2}\sum_{\ell\in\mathbb{Z}+\mu/2}\left[E_1(\sqrt{\tau_2}(2\ell+6\eta)) - \operatorname{sign}\ell\right] q^{-\ell^2} y^{6\ell}. \tag{6.111}$$

Upon identifying $\gamma_{12} = 6\ell = 3(q_2 - q_1)$, we compute

$$c_1 = 6\lambda\,(q_1 - q_2) = -12\lambda\,\ell, \qquad m_1 = m_2 = 18\lambda^2\,. \tag{6.112}$$

The result from our index computation (6.97) thus reads (after identifying $\beta = 2\pi\tau_2$)

$$\mathcal{I}_2 = \frac{(-1)^{\gamma_{12}}}{2}\left(E_1\left(\sqrt{\tau_2}2\ell\right) - \operatorname{sign}(\ell)\right) y^{6\ell} = \frac{(-1)^{\gamma_{12}}}{2} M_1\left(\sqrt{\tau_2}2\ell\right), \tag{6.113}$$

which matches with (6.111) up to an overall sign in the limit $\eta \to 0$.

Rank 3

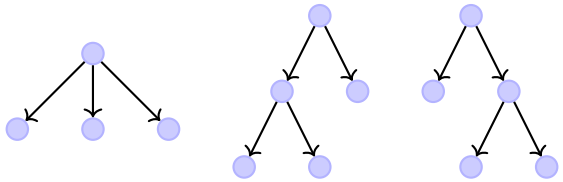


Figure 6.3: Schröder trees contributing to the modular completion for $N = 3, N_i = 1$

For $N = 3$, two possible partitions contribute to the total result shown in [14, (F.10)], namely $3 = 2 + 1$ and $3 = 1 + 1 + 1$. The contribution from the partition matches the Witten index for 2-body quantum mechanics, exactly as in the rank 2 case above. We focus on the contribution of the second partition which arises from the three Schröder trees shown in Fig. 6.3:

$$\begin{aligned}\Delta\widehat{g}_{3,\mu} = \frac{1}{4}\sum_{q_1+q_2+q_3=\mu+\frac{3}{2}} (-y)^{6(q_3-q_1)} \exp\Big[-\tfrac{\tau}{6}\big((q_2-q_1)^2+(q_3-q_2)^2+(q_3-q_1)^2\big)\Big] \\ \times\Big[E_2\Big(\tfrac{1}{\sqrt{3}};\,\sqrt{\tau_2}(q_2-q_1+6\eta),\,\sqrt{\tfrac{\tau_2}{3}}(2q_3-q_1-q_2+18\eta)\Big) \\ -\ \operatorname{sign}(q_2+q_3-2q_1)\,\operatorname{sign}(2q_3-q_1-q_2)\ -\ \tfrac{1}{3}\,\delta_{q_1=q_2=q_3} \\ -\ \big(E_1(\sqrt{\tfrac{\tau_2}{3}}\,(2q_3-q_1-q_2+18\eta)) - \operatorname{sign}(2q_3-q_1-q_2)\big)\,\operatorname{sign}(q_2-q_1) \\ -\ \big(E_1(\sqrt{\tfrac{\tau_2}{3}}\,(q_2+q_3-2q_1+18\eta)) - \operatorname{sign}(q_2+q_3-2q_1)\big)\,\operatorname{sign}(q_3-q_2)\Big].\end{aligned} \tag{6.114}$$

One verifies that under the substitutions

$$c_i \;=\; 6\lambda^2\,(3\,q_i - (q_1+q_2+q_3)), \qquad m_i \;=\; \tfrac{81}{2}\lambda^2, \tag{6.115}$$

the partial Witten index (6.100) reduces exactly to the modular-completion (6.114) above, up to the η-shifts and the Kronecker-delta term $\frac{1}{3}\,\delta_{q_1=q_2=q_3}$. In fact, up to the same terms, (6.114) can be rewritten in terms of the M_2 function only,

$$\begin{aligned}\Delta\widehat{g}_{3,\mu} = \frac{1}{4} \sum_{q_1+q_2+q_3=\mu+\frac{3}{2}} (-y)^{6(q_3-q_1)} \exp\Big[-\tfrac{\tau}{6}\big((q_2-q_1)^2+(q_3-q_2)^2+(q_3-q_1)^2\big)\Big] \\ \times M_2\Big(\tfrac{1}{\sqrt{3}};\, \sqrt{\tau_2}(q_2-q_1+6\eta),\, \sqrt{\tfrac{\tau_2}{3}}(2q_3-q_1-q_2+18\eta)\Big).\end{aligned} \tag{6.116}$$

Rank 4

For $N = 4$, the modular completion shown in [14, (F.10)] involves contributions from the partitions $N = 3+1 = 2+2 = 2+1+1 = 1+1+1+1$. The contributions from the 2-body and 3-body partitions match our prescription exactly as in the rank 2 and rank 3 cases. The remaining partition with $N_i = 4$ involves the contribution of the 11 Schröder trees shown in Fig. 6.4 (omitting Kronecker delta contributions):

$$\begin{aligned}\Delta\widehat{g}_{4,\mu} \;=\; & \frac{1}{8} \sum_{\substack{q_1+q_2+q_3+q_4\\=\mu+2}} q^{-\frac{1}{8}\,\sum_{i<j}(q_i-q_j)^2}\; y^{-9q_1-3q_2+3q_3+9q_4} \\ & \times \Big\{ E_3\Big(\tfrac{1}{\sqrt{3}},\, \tfrac{1}{\sqrt{6}},\, \tfrac{1}{\sqrt{2}};\, \sqrt{\tau_2}\,\big(-q_1+q_2+6\eta\big),\, \sqrt{\tfrac{\tau_2}{3}}\,\big(2q_3-q_1-q_2+18\eta\big),\, \sqrt{\tfrac{\tau_2}{6}}\,\big(-q_1-q_2-q_3+3q_4+36\eta\big)\Big) \\ & \quad + E_2\Big(\tfrac{1}{\sqrt{2}};\, \sqrt{\tfrac{\tau_2}{3}}\,\big(-q_1-q_2+2q_3+18\eta\big),\, \sqrt{\tfrac{\tau_2}{6}}\,\big(-q_1-q_2-q_3+3q_4+36\eta\big)\Big)\; \operatorname{sign}(q_1-q_2) \\ & \quad + E_2\Big(\tfrac{1}{2\sqrt{2}};\, \sqrt{\tfrac{\tau_2}{3}}\,\big(-2q_1+q_2+q_3+18\eta\big),\, \sqrt{\tfrac{\tau_2}{6}}\,\big(-q_1-q_2-q_3+3q_4+36\eta\big)\Big)\; \operatorname{sign}(q_2-q_3) \\ & \quad + E_2\Big(\tfrac{1}{\sqrt{2}};\, \sqrt{\tau_2}\,\big(-q_1+q_2+6\eta\big),\, \sqrt{\tfrac{\tau_2}{2}}\,\big(-q_1-q_2+q_3+q_4+24\eta\big)\Big)\; \operatorname{sign}(q_3-q_4) \\ & \quad + E_1\Big(\sqrt{\tfrac{\tau_2}{6}}\,\big(-q_1-q_2-q_3+3q_4+36\eta\big)\Big)\; \operatorname{sign}(q_2-q_1)\operatorname{sign}(q_3-q_2) \\ & \quad + E_1\Big(\sqrt{\tfrac{\tau_2}{6}}\,\big(-3q_1+q_2+q_3+q_4+36\eta\big)\Big)\; \operatorname{sign}(q_3-q_2)\operatorname{sign}(q_4-q_3) \\ & \quad + E_1\Big(\sqrt{\tfrac{\tau_2}{2}}\,\big(-q_1-q_2+q_3+q_4+24\eta\big)\Big)\; \operatorname{sign}(q_2-q_1)\operatorname{sign}(q_4-q_3) \\ & \quad - \operatorname{sign}(q_2-q_1)\operatorname{sign}(q_3-q_2)\operatorname{sign}(q_4-q_3)\Big\}.\end{aligned} \tag{6.117}$$

Disregarding η-shifts, this result can again be written in terms of a single maximum depth complementary error function,

$$\begin{aligned}\Delta\widehat{g}_{4,\mu} \;=\; & \frac{1}{8} \sum_{\substack{q_1+q_2+q_3+q_4\\=\mu+2}} q^{-\frac{1}{8}\,\sum_{i<j}(q_i-q_j)^2}\; y^{-9q_1-3q_2+3q_3+9q_4} \\ & \times M_3\Big(\tfrac{1}{\sqrt{3}},\, \tfrac{1}{\sqrt{6}},\, \tfrac{1}{\sqrt{2}};\, \sqrt{\tau_2}\,\big(-q_1+q_2+6\eta\big),\, \sqrt{\tfrac{\tau_2}{3}}\,\big(2q_3-q_1-q_2+18\eta\big),\, \sqrt{\tfrac{\tau_2}{6}}\,\big(-q_1-q_2-q_3+3q_4+36\eta\big)\Big).\end{aligned} \tag{6.118}$$

The observation that all complementary error functions but the one of maximal depth cancel was the basis for [7, Conjecture 6.1], where an exact formula was put forward the modular

completion in one-modulus models (or more accurately, collinear D4-brane charges) at arbitrary rank, which also reproduces the Kronecker-delta terms. Mathematically, this implies that the modular completion can be written as an iterated Eichler integral, as was observed for $N = 3$ in [143]. Unfortunately we do not yet understand the physical origin of the Kronecker delta contributions.

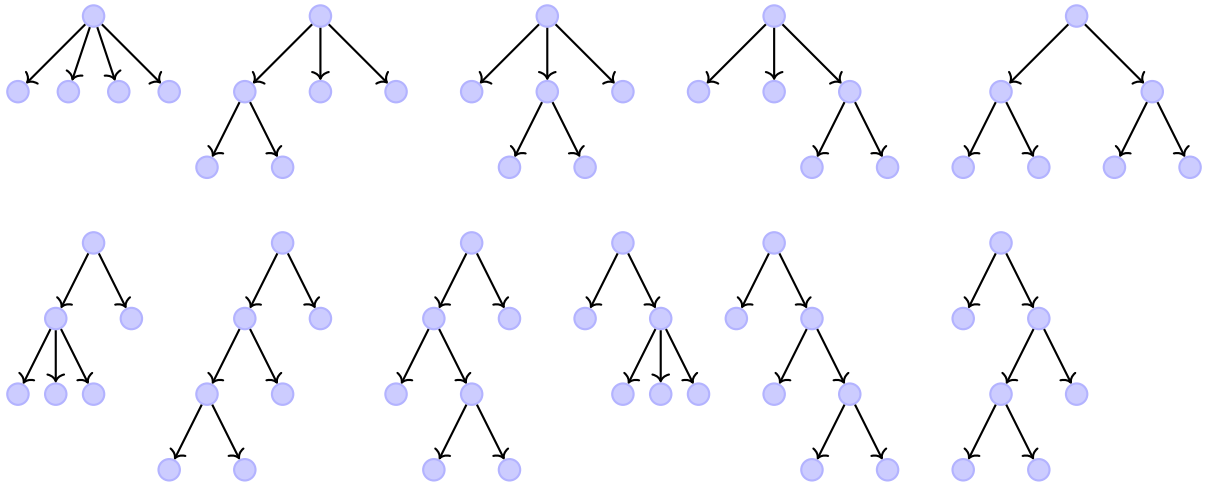


Figure 6.4: Schröder trees contributing to the modular completion for $N = 4, N_i = 1$

6.4.2 Comparison to the instanton generating potential

In view of the interpretation of the instanton generating potential (or its close cousin the contact potential) as the Witten index of the $\mathcal{N} = 2$ effective supergravity on $\mathbb{R}^3$ [15], it is natural to ask if the localization computation in the supersymmetric quantum mechanics reproduces more generally the coefficient of the monomial $\prod_i h_{p_i,\mu_i}$ in the expansion (6.18). In fact, up to the Gaussian factor $\Phi_1^{\int}$ which depends only on the total charge, the kernel of the theta series is identical to the one appearing in the modular completion (6.13), after replacing the moduli-independent vectors $\boldsymbol{v}_k$ with their moduli-dependent counterpart $\boldsymbol{u}_k$. We claim that the Witten index of the supersymmetric quantum mechanics correctly reproduces the sum over Schröder trees in (6.19), even for non-collinear D4-brane charges. In particular, the contribution for the 'purely moduli-dependent term' $\mathrm{sign}(c_1)\,\mathrm{sign}(c_1+c_2)\cdots\mathrm{sign}(c_1+\cdots+c_{n-1})$ in the partial tree index reproduces the contribution $\widetilde{\mathcal{E}}_{v_0}$ from the simplest Schröder tree with a single node. To see this, it suffices to i) compare the Gram matrix of the vectors $\boldsymbol{u}_k$ with respect to the quadratic form Q defined below (6.15), with the Gram matrix of the vectors $\mathsf{H}_{i\alpha} = 1$ if $\alpha \geq i$, and zero otherwise, with respect to the quadratic form M defined in (6.63), and ii) compare the inner products $\boldsymbol{u}_k \cdot \mathbf{x}$ with the products $\mathsf{H}^T c$. A straightforward computation shows that the Gram matrices agree, up to a simple rescaling,

$$\boldsymbol{u}_k^T\, Q\, \boldsymbol{u}_l = 8\, m_{\rm tot}^2\, (\mathsf{H}^T \mathsf{M} \mathsf{H})_{kl} = 8\, m_{\rm tot} \left(\sum_{i=1}^{\min(k,l)} m_i\right)\left(\sum_{i=\max(k,l)}^{n} m_i\right), \tag{6.119}$$

where $m_{\rm tot} = \sum_i m_i$, while the inner products agree (up to a factor of $-m_{\rm tot}$), by construction,

$$\boldsymbol{u}_k \cdot \boldsymbol{x} = -m_{\rm tot}\,(c_1 + \cdots + c_k). \tag{6.120}$$

Thus, the error function E_{n-1} of maximal depth is correctly reproduced, even for non-collinear D4-brane charges. Evidence that the supersymmetric quantum mechanics correctly reproduces the contributions from all Schröder trees in (6.19) comes from the matching of the modular completions in the previous subsection, although that evidence is restricted to the collinear case so far. We leave it as an open problem to prove agreement in general.

6.5 Discussion

In this chapter, we have computed the Witten index of the supersymmetric quantum mechanics of n dyons for any $n \geq 2$ by localizing to time-independent configurations, following [99, 117]. The key observation is that the remaining integral over the positions of the constituents (and their fermionic partners) naturally splits into an integral over the phase space of n-centered supersymmetric ground states $\mathcal{M}_n(\{\gamma_i, u_i\})$ at fixed values of the stability parameters $\{u_i\}$, with its standard Liouville measure ω^{n-1}, times an integral over these parameters with a Gaussian weight centered around the physical FI parameters $\{c_i\}$. The integral over $\mathcal{M}_n(\{\gamma_i, u_i\})$ is a locally constant function of the u_i's, computable by localization with respect to rotations along a fixed axis [145] or by applying the attractor flow tree decomposition [16]. The resulting convolution with the Gaussian integral along the u_i's then produces a linear superposition of generalized error functions E_r of depth $r \leq n-1$, multiplied by $n-1-r$ sign functions of the FI parameters c_i and DSZ products γ_{ij}. Upon expressing the E_r's in terms of complementary error functions $M_{r'}$ with $r' \leq r$, we identified the terms proportional to M_r with the contribution of the spectral asymmetry of the continuum of scattering states with $r+1$ constituents, which are in general themselves bound states of the fundamental constituents with charges γ_i. As an application, we reproduced the non-holomorphic terms appearing in the modular completion of the generating series of Vafa-Witten invariants on $\mathbb{P}^2$, which count D4-D2-D0 bound states in the local CY geometry $K_{\mathbb{P}^2}$, as well as the contributions to the so-called instanton generating potential. We expect that this agreement carries over to generating series of MSW indices in more general CY geometries, in particular arbitrary del Pezzo local surfaces, and gives a direct physical derivation of the modular completion, which was previously derived through indirect arguments in the series of papers culminating with [14, 17]. It would be interesting to see if one can also derive the modular completion of the generating series of single-centered indices [59] by replacing the partial flow tree indices by the partial Coulomb indices [148] counting collinear solutions.

While the agreement with the modular completion prescription holds to a remarkable level of detail, there are some intriguing discrepancies that indicate that our localization analysis may be too naive. In particular, in the two-body case, our result correctly captures the complementary error function M_1 in (6.24), but misses the extra Gaussian term, which is crucial for modular invariance [141]. As understood in [14][15], this term can be traced to an η-dependent shift in the refined index (where η is proportional to $\mathrm{Re}\log y$), which is also absent in our computation of the refined Witten index. In fact, our refined index computation also misses the contribution of the A-roof genus in the reduction to the symplectic leaves $\mathcal{M}_n(\{\gamma_i, u_i\})$, which is necessary to produce the equivariant Dirac index which is supposed to count BPS states. Fortunately, under localization

[15]The Gaussian term was reproduced in [158] by a localization computation in a gauged linear sigma model, where it also followed from an η-dependent shift in the refined index. It would be interesting to perform a similar computation in the quiver quantum mechanics reducing to our supersymmetric quantum mechanics on the Coulomb branch, along the lines of [110].

with respect to rotations, the A-roof genus only contributes powers of $(\log y)/(y-1/y)$ at isolated fixed points, powers which we have fixed by a suitable choice of normalization. These issues are likely related, and it would be desirable to develop a more rigorous treatment of localization in this system.

Another noteworthy issue is that our computation correctly reproduces the moduli-dependent error functions appearing in the instanton generating potential (which plays the role of the Witten index for the 4D effective supergravity on $\mathbb{R}^3$), but not the moduli-independent error functions appearing in the modular completion, which in general differ by a rescaling of their arguments (for example in the two-body case, a rescaling by $\sqrt{\frac{(p^3)(p_1p_2p)}{(p_1p^2)(p_2p^2)}}$). Fortunately, these rescalings disappear when the D4-brane charge vectors are aligned, which is automatic in local CY geometries of the form $X = K_S$ where S is a complex surface, or in compact CY geometries with $b_2(X) = 1$. It would certainly be desirable to have a better understanding of this apparent discrepancy.

Finally, we have not attempted to match the 'exceptional' contributions to the modular completion which originate when the arguments of certain sign functions vanish. At such loci, the attractor point lies on a wall of marginal stability, and the dynamics is complicated by the existence of marginal bound states. It would be very interesting to have a physical derivation of these contributions, which are necessary to ensure a smooth unrefined limit.

6.6 Appendix: The master integral identity

In this section, we prove the key identity (6.80), which we copy for the reader's convenience:

$$\prod_{i=1}^{n-1} \mathrm{d}^3\vec{x}_i \det(\vec{\nabla}_i U_j \otimes \vec{\sigma}) = k_n \left(\prod_{i=1}^{n-1} \mathrm{d}u_i\right) \omega^{n-1}, \tag{6.121}$$

where ω is the symplectic form defined in (6.48) on the space $\mathcal{M}_n(\{\gamma_i, u_i\})$ of multi-centered solutions with stability parameters $u_i = \sum_{j\neq i} \frac{\gamma_{ij}}{|\vec{x}_i - \vec{x}_j|}$ (we do not enforce the constraint $i < j$ in the sum, even though it is antisymmetric in (ij)),

$$\omega = \frac{1}{2} \sum_{i,j} \epsilon_{abc} \nabla_i^a U_j \mathrm{d}\mathrm{x}_i^b \wedge \mathrm{d}\mathrm{x}_j^c. \tag{6.122}$$

In (6.121), $\vec{\nabla}_i U_j \otimes \vec{\sigma}$ is a $(2n-2)\times(2n-2)$ matrix with components $\sum_a \nabla_i^a U_j \, (\sigma^a)_{\alpha\beta}$ with $U_i = -\frac{1}{2}\left(\sum_{j\neq i} \frac{\gamma_{ij}}{|\vec{x}_i - \vec{x}_j|} - c_i\right)$, and k_n is a proportionality constant which will be fixed momentarily.

Let us write $\vec{x}_i = (x_i, y_i, z_i)$ and define $(n-1)\times(n-1)$ matrices $\mathsf{U}_x = \left(\frac{\partial U_i}{\partial x_j}\right)$, $\mathsf{U}_y = \left(\frac{\partial U_i}{\partial y_j}\right)$, $\mathsf{U}_z = \left(\frac{\partial U_i}{\partial z_j}\right)$. The left hand side of (6.121) can be written as the block matrix determinant

$$\det(\vec{\nabla} U \otimes \vec{\sigma}) = \det \begin{bmatrix} \mathsf{U}_z & \mathsf{U}_x - i\mathsf{U}_y \\ \mathsf{U}_x + i\mathsf{U}_y & -\mathsf{U}_z \end{bmatrix} = (-1)^{n-1} \det(\mathsf{U}_z) \det(\mathsf{Q} + i\mathsf{M}), \tag{6.123}$$

where $\mathsf{Q} = \mathsf{U}_z + \mathsf{U}_x\mathsf{U}_z^{-1}\mathsf{U}_x + \mathsf{U}_y\mathsf{U}_z^{-1}\mathsf{U}_y$, and $\mathsf{M} = \mathsf{U}_y\mathsf{U}_z^{-1}\mathsf{U}_x - \mathsf{U}_x\mathsf{U}_z^{-1}\mathsf{U}_y$ are symmetric and anti-symmetric matrices respectively, such that $\mathsf{Q} + i\mathsf{M}$ is Hermitian. Here we have used the identity for the determinant of block matrices

$$\det \begin{bmatrix} \mathsf{A} & \mathsf{B} \\ \mathsf{C} & \mathsf{D} \end{bmatrix} = \det(\mathsf{A}) \det(\mathsf{D} - \mathsf{C}\mathsf{A}^{-1}\mathsf{B}), \quad \text{if } \mathsf{A} \text{ is invertible.} \tag{6.124}$$

The right hand side of (6.121) can be evaluated by noting that at constant $u_i(\mathbf{x}) = u_i$ (or equivalently constant $U_i = -\frac{1}{2}(u_i - c_i)$), z_i can be expressed locally as a function of x_j and y_j: $z_i = z_i(x, y; u)$. In other words, we can use (x_i, y_i) as local coordinates on the phase space $\mathcal{M}_n(\{\gamma_i, u_i\})$. Thus, variations of z can be traded for variations of x and y,

$$0 = \mathrm{d}U_i = \frac{\partial U_i}{\partial x_j}\mathrm{d}x_j + \frac{\partial U_i}{\partial y_j}\mathrm{d}y_j + \frac{\partial U_i}{\partial z_j}\mathrm{d}z_j \implies \frac{\partial z_i}{\partial x_j} = -\frac{\partial z_i}{\partial U_k}\frac{\partial U_k}{\partial x_j}, \quad \frac{\partial z_i}{\partial y_j} = -\frac{\partial z_i}{\partial U_k}\frac{\partial U_k}{\partial y_j}, \tag{6.125}$$

or, as matrices, $\left(\frac{\partial z_i}{\partial x_j}\right) = -\mathsf{U}_z^{-1}\mathsf{U}_x$, $\left(\frac{\partial z_i}{\partial y_j}\right) = -\mathsf{U}_z^{-1}\mathsf{U}_y$. We can now write the r.h.s. of (6.121) as (here, summation convention is implied for $i, j = 1, \ldots, n-1$),

$$\begin{aligned}
\omega &= \frac{\partial U_i}{\partial z_j}\mathrm{d}x_i \wedge \mathrm{d}y_j + \frac{\partial U_i}{\partial x_j}\mathrm{d}y_i \wedge \mathrm{d}z_j + \frac{\partial U_i}{\partial y_j}\mathrm{d}z_i \wedge \mathrm{d}x_j, \qquad \mathrm{d}z_i = \frac{\partial z_i}{\partial x_k}\mathrm{d}x_k + \frac{\partial z_i}{\partial y_k}\mathrm{d}y_k, \\
&= \frac{\partial U_i}{\partial z_j}\mathrm{d}x_i \wedge \mathrm{d}y_j + \left(\frac{\partial U_i}{\partial x_j}\frac{\partial z_j}{\partial y_k}\mathrm{d}y_i \wedge \mathrm{d}y_k + \frac{\partial U_i}{\partial x_j}\frac{\partial z_j}{\partial x_k}\mathrm{d}y_i \wedge \mathrm{d}x_k\right) \\
&\quad + \left(\frac{\partial U_i}{\partial y_j}\frac{\partial z_i}{\partial x_r}\mathrm{d}x_r \wedge \mathrm{d}x_j + \frac{\partial U_i}{\partial y_j}\frac{\partial z_i}{\partial y_k}\mathrm{d}y_k \wedge \mathrm{d}x_j\right) \\
&= \mathsf{A}_{ij}\,\mathrm{d}x_i \wedge \mathrm{d}y_j \;+\; \mathsf{B}_{ij}\,\mathrm{d}x_i \wedge \mathrm{d}x_j \;+\; \mathsf{C}_{ij}\,\mathrm{d}y_i \wedge \mathrm{d}y_j,
\end{aligned} \tag{6.126}$$

where

$$\mathsf{A}_{ij} = \frac{\partial U_i}{\partial z_j} - \frac{\partial U_j}{\partial x_l}\frac{\partial z_l}{\partial x_i} - \frac{\partial U_l}{\partial y_i}\frac{\partial z_l}{\partial y_j}, \quad \mathsf{B}_{ij} = \frac{\partial U_l}{\partial y_j}\frac{\partial z_l}{\partial x_i}, \quad \mathsf{C}_{ij} = \frac{\partial U_i}{\partial x_l}\frac{\partial z_l}{\partial y_j}. \tag{6.127}$$

Using (6.125), and the symmetry $\nabla_i^a U_j = \nabla_j^a U_i$, etc, we get $\mathsf{A} = \mathsf{Q}$, and $\mathsf{B} = \mathsf{C} = -\mathsf{U}_x\mathsf{U}_z^{-1}\mathsf{U}_y$. From (6.126), only the antisymmetric part of B and C are relevant, but $\mathsf{B} - \mathsf{B}^T = \mathsf{C} - \mathsf{C}^T = \mathsf{U}_y\mathsf{U}_z^{-1}\mathsf{U}_x - \mathsf{U}_x\mathsf{U}_z^{-1}\mathsf{U}_y = \mathsf{M}$. Thus we can write,

$$\omega = \frac{1}{2}\sum_{i,j,\alpha,\beta} \mathfrak{M}_{i\alpha,j\beta}\,\mathrm{d}\xi_i^\alpha \wedge \mathrm{d}\xi_j^\beta, \quad (\xi_i^1, \xi_i^2) = (x_i, y_i), \tag{6.128}$$

where $\mathfrak{M}$ is a $(2n-2)\times(2n-2)$ block matrix $\mathfrak{M} = \begin{bmatrix} \mathsf{M} & \mathsf{Q} \\ -\mathsf{Q} & \mathsf{M} \end{bmatrix}$. We can now compute the symplectic volume form as

$$\omega^{n-1} = 2^{n-1}(n-1)! \times \frac{1}{2^{n-1}}\,\mathrm{pf}\,(\mathfrak{M})\;\mathrm{d}x_1 \wedge \mathrm{d}y_1 \wedge \ldots \wedge \mathrm{d}x_{n-1} \wedge \mathrm{d}y_{n-1}. \tag{6.129}$$

Using (6.125), and noting that $\mathrm{d}U_i = -\frac{1}{2}\mathrm{d}u_i$, we have

$$\mathrm{d}u_1 \wedge \ldots \wedge \mathrm{d}u_{n-1} = 2^{n-1}\det(\mathsf{U}_z)\mathrm{d}z_1 \wedge \ldots \wedge \mathrm{d}z_{n-1} + \ldots\,, \tag{6.130}$$

where the dots include terms that have at least one factor of $\mathrm{d}x_i$ or $\mathrm{d}y_i$ which are annihilated when multiplied by ω^{n-1}. Putting everything together, we obtain the r.h.s. of (6.121),

$$\left(\prod_{i=1}^{n-1}\mathrm{d}u_i\right)\;\omega^{n-1} = 2^{n-1}(n-1)!\;\det(\mathsf{U}_z)\;\mathrm{pf}\,(\mathfrak{M})\;\mathrm{d}^3\mathbf{x}_1 \ldots \mathrm{d}^3\mathbf{x}_{n-1}. \tag{6.131}$$

The equality (6.121) then follows from the identity for the Pfaffian of antisymmetric block matrices

$$\mathrm{pf}\begin{bmatrix} \mathsf{M} & \mathsf{Q} \\ -\mathsf{Q} & \mathsf{M} \end{bmatrix} = \det(\mathsf{Q} + i\mathsf{M}). \tag{6.132}$$

provided the proportionality constant is set to

$$k_n = \frac{(-1)^{n-1}}{2^{n-1}(n-1)!}. \tag{6.133}$$

7

Conclusions and Outlook

7.1 Summary of the thesis

The central question addressed in this thesis is: what is the global structure of protected BPS spectra in type IIA string theory compactified on a non-compact toric Calabi–Yau threefold $X = K_S$? The Donaldson–Thomas invariants $\Omega_\sigma(\gamma)$, counting semistable objects of charge γ in the derived category $\mathcal{C} = D^b \operatorname{Coh}_c X$ for a given Bridgeland stability condition $\sigma \in \operatorname{Stab} \mathcal{C}$, are locally computable in favourable chambers, but their organisation across full stability space is a far subtler matter. This thesis addresses this question along two independent but complementary lines. The first, developed in Chapters 4 and 5, is the explicit construction of stability scattering diagrams for local $\mathbb{F}_0$ and local $\mathbb{F}_1$ via the dendroscopy programme. The second, developed in Chapter 6, concerns the physical origin of the non-holomorphic modular completions of D4-D2-D0 generating series, a question that is largely independent of the toric or non-compact specialisation and applies equally to compact Calabi–Yau threefolds.

The proof of principle for the dendroscopy programme was established in [47] for local $\mathbb{P}^2$. With $b_2(\mathbb{P}^2) = 1$ and modular group $\Gamma_1(3)$, this geometry offers a single complex Kähler parameter and a clean modular structure with no ramification in the fundamental domain, and the scattering diagram was constructed explicitly both along the large-volume slice Λ and the physical Π-stability slice, establishing the validity of the Split Attractor Flow Conjecture (SAFC) on the physical slice. The local $\mathbb{P}^2$ result served as the founding example of the programme while leaving open whether the construction could be extended to genuinely multi-parameter geometries with richer modular presentations, or to cases admitting no modular presentation at all.

The first major contribution of this thesis is the study of local $\mathbb{F}_0 = K_{\mathbb{F}_0}$, where $\mathbb{F}_0 = \mathbb{P}^1 \times \mathbb{P}^1$. This geometry, with $b_2(\mathbb{F}_0) = 2$, is the first genuinely two-parameter case in the programme and engineers a five-dimensional $\mathcal{N} = 1$ pure $SU(2)$ gauge theory with vanishing discrete theta angle upon M-theory compactification. The scattering diagram $\mathcal{D}_{\psi,m}$ is constructed explicitly along three complementary slices: the large-volume slice Λ, the orbifold quiver region, and the physical Π-stability slice, with modular symmetry group $\Gamma_0(4)$ acting on the Coulomb branch parameter τ. The key structural finding is that the infinite tower of initial rays in the large-volume slice descends entirely from a geometric helix of just two pairs of D4 and anti-D4 branes with Dirac product $\langle \gamma_1, \gamma_2 \rangle = \pm 2$ and attractor invariants $\Omega_\star(\gamma_i) = 1$, confirming that the boundary data are minimal and dictated by the canonical class of the surface. For generic mass parameter m, the physical slice is a multi-sheeted cover of $\mathbb{H}$, ramified above a point $\tau_B(m)$ determined by the $\Gamma_0(4)$ Hauptmodul; for integer m, the branch cuts close and $\Gamma_0(4)$ acts cleanly on $\mathbb{H}$, in direct analogy with local $\mathbb{P}^2$.

The second major contribution is the extension of BPS dendroscopy to local $\mathbb{F}_1 = K_{\mathbb{F}_1}$, which provides the UV completion of five-dimensional $\mathcal{N} = 1$ $SU(2)$ super-Yang–Mills theory with half-unit theta angle and deforms to local $\mathbb{P}^2$ as the exceptional curve shrinks. Local $\mathbb{F}_1$

is the decisive stress test of the framework. The exceptional curve B with $B^2 = -1$ introduces supplementary spherical D2-brane initial rays absent from the $\mathbb{F}_0$ case; the mirror curve does not generically admit a Hauptmodul for any congruence subgroup of $PSL(2,\mathbb{Z})$; and at the Argyres–Douglas locus $\ell = -27/256$, two conifold points collide and the monodromy group reduces to a non-congruence subgroup $\Gamma \subset PSL(2,\mathbb{Z})$ of index 10. Despite these complications, the geometric-helix structure of the initial data persists and global reconstruction proceeds. At the Argyres–Douglas point, the Hauptmodul of Γ furnishes a branch-cut-free modular presentation of the Coulomb branch; and the conifold periods are derived in closed form as linear combinations of Bloch–Wigner dilogarithms via a rational parametrisation of the discriminant locus.

The third contribution, Chapter 6, addresses a separate question: the microscopic origin of the non-holomorphic completions of D4-D2-D0 generating series. These series transform as vector-valued mock modular forms, and their completions involve generalised error functions whose presence is required by modular covariance. Prior to this work, these terms had been obtained only through indirect modular bootstrap arguments, with no derivation from the underlying quantum mechanics. By localising the supersymmetric quantum mechanics of n dyons to time-independent configurations, the Witten index factorises into an integral over the Denef phase space of multi-centred solutions, convolved with a Gaussian integral over the Fayet–Iliopoulos parameters. The former yields Coulomb-branch sign functions and the latter yields generalised error functions E_r of depth $r \leq n-1$. Re-expressing these in terms of complementary error functions $M_{r'}$ identifies each term as the contribution of the spectral asymmetry between bosonic and fermionic scattering states with $r+1$ constituent centres. The non-holomorphic completion is therefore an infrared datum of the quantum mechanics: it encodes the contribution of multi-particle scattering states that are integrated out in the holomorphic generating series, and is required by the spectral asymmetry of the system rather than imposed by hand. For $n = 2, 3, 4$, this correctly reproduces the non-holomorphic error-function contribution to the modular completion of the Vafa–Witten generating series on $\mathbb{P}^2$.

Both strands share the broader conviction that BPS generating series carry more structure than is visible locally: in the dendroscopy chapters, global reconstruction of the spectrum from sparse canonical seed data is possible because wall-crossing consistency is highly constraining; in the modularity chapter, the non-holomorphic terms in the generating series are fixed by the infrared dynamics of the quantum mechanics. The remainder of this chapter examines each strand in turn and the directions each opens up.

7.2 Lessons from dendroscopy

The main lesson of the dendroscopy programme is that global reconstruction of the BPS spectrum requires remarkably sparse initial data. For local $\mathbb{F}_0$, the initial rays of the large-volume scattering diagram are generated by a geometric helix of invertible sheaves: pairs of D4-branes $\mathcal{O}(k_1,k_2)$ and their homological shifts $\mathcal{O}(k_1,k_2)[1]$, with Dirac product $\langle\gamma_1,\gamma_2\rangle = \pm 2$ and attractor invariants $\Omega^\star(\gamma_i) = 1$. Extending the diagram slightly below the boundary parabola in affine coordinates reveals that the entire infinite tower of initial rays pair-produces from these two rays. For local $\mathbb{F}_1$, the initial rays are again of the form $\mathcal{O}(k_1,k_2)$ and $\mathcal{O}(k_1,k_2)[1]$, but the Dirac products between consecutive rays in the helix follow the more intricate pattern $2,1,2,3,\ldots$ reflecting the more complex intersection geometry of $\mathbb{F}_1$. The exceptional curve B with $B^2 = -1$ introduces a spherical D2-brane state into the spectrum. In the open neighbourhood of $\psi = 0$ where Π-stability coincides with large-volume stability, this state is produced from the $\mathcal{O}(k_1,k_2)$

initial rays rather than appearing as an independent seed; however, for parameter values at which this coincidence breaks down, the spherical D2-brane can itself become an initial ray, a phenomenon that is not specific to $\mathbb{F}_1$ and occurs for $\mathbb{P}^2$ and $\mathbb{F}_0$ as well. The Attractor Conjecture is shown to hold for both $\mathbb{F}_0$ and $\mathbb{F}_1$: the only non-vanishing attractor invariants are those of the simple dimension vectors γ_i and of D0-branes.

The reconstruction is achieved by probing Stab $\mathcal{C}$ through three complementary regions. The large-volume slice Λ connects to classical sheaf-theoretic stability: the central charge reduces to the Kähler volume and BPS stability reduces to Gieseker stability for coherent sheaves. The quiver region admits a finite-dimensional description of the BPS spectrum in terms of the representation theory of a quiver with potential, and attractor invariants are computable there by equivariant localisation. For local $\mathbb{F}_0$, this region is associated with a $\mathbb{Z}_2$ orbifold of the resolved conifold at generic m, enhanced to a $\mathbb{Z}_4$ orbifold at $m = 0$. For local $\mathbb{F}_1$, there is no analogous orbifold interpretation; a quiver description exists, but the quiver does not inherit the cyclic symmetry present in the $\mathbb{F}_0$ case. The physical Π-stability slice, parametrised by the mirror complex structure modulus τ, carries the full action of the monodromy group and exposes the global structure through exact period central charges and the complete group of autoequivalences. The non-trivial content of the programme is mutual consistency across all three regions: Gieseker indices extracted from the large-volume diagram agree with known results, the quiver wall-crossing matches independent localisation computations, and the Π-stability diagram reduces to both in the appropriate limits. A direct consequence appears at the attractor phase $\psi = \pi/2$: the diagram simplifies to rays that are level sets of the slope function $s(\tau) = \operatorname{Im} T_D / \operatorname{Im} T$, intersecting only at the ramification points τ_B and their images, which explains directly the equality between quiver and Gieseker indices noted in the literature.

Local $\mathbb{F}_0$ is the controlled instance of this programme. The two Kähler parameters are coupled by a single real mass parameter m, the Coulomb branch is a double cover of $\mathbb{H}/\Gamma_0(4)$ ramified above a single point $\tau_B(m)$, and for integer m the branch cuts close and $\Gamma_0(4)$ acts cleanly, in direct analogy with local $\mathbb{P}^2$. As ψ increases from 0 to $\pi/2$, the diagram undergoes a structured sequence of rearrangements, with two critical values ψ_{cr} and $\tilde{\psi}_{\mathrm{cr}}$ (coinciding at $m = 1/2$) marking qualitative changes in the ray structure. The SAFC is formulated precisely for local $\mathbb{F}_0$ and proved for ψ in a convexity interval $\mathcal{I}_{\mathrm{cvx}}$ around $\psi = 0$: in this range, every attractor flow tree decomposes either into a shrub (a subtree rooted at an element of the exceptional collection and supported entirely within the corresponding quiver region) or a lone branch emanating from a conifold point at $\tau \in \mathbb{Z}$ or $\tau \in \mathbb{Z} + \frac{1}{2}$. A further observation is the coincidence between the large-volume scattering diagram and the tropical geometry controlling Gromov–Witten invariants of the log Calabi–Yau pair $(\mathbb{F}_0, D)$, where D is the smooth anticanonical divisor. This is not accidental: the Gross–Hacking–Keel mirror construction for log Calabi–Yau surfaces produces a scattering diagram from the same initial ray data as the large-volume BPS diagram, and the identification should hold uniformly across the del Pezzo series, placing the large-volume BPS scattering diagram as the natural combinatorial realisation of mirror symmetry for these geometries.

Local $\mathbb{F}_1$ was the decisive stress test of the programme. Three features make the reconstruction substantially more intricate than for $\mathbb{F}_0$ or $\mathbb{P}^2$. The negative self-intersection $B^2 = -1$ complicates the large-volume stability analysis and modifies the pattern of Dirac products between initial rays as described above. The mirror curve does not generically admit a Hauptmodul for any congruence subgroup of $PSL(2, \mathbb{Z})$, so no global unfolding to $\mathbb{H}$ is available. The absence of an Atkin–Lehner–Fricke involution, which for $\mathbb{F}_0$ conveniently exchanges conifold points with the large-volume cusp, means the conifold periods must be obtained by independent calculations at each cusp. At the Argyres–Douglas locus $\ell = -27/256$, two conifold points collide and the

monodromy group reduces to a non-congruence subgroup $\Gamma \subset PSL(2,\mathbb{Z})$ of index 10 with genus zero and three cusps; the Argyres–Douglas point is a $\mathbb{Z}_6$ point of Γ, consistent with its $\mathbb{Z}_6$ local monodromy. The conifold periods are derived in closed form as linear combinations of Bloch–Wigner dilogarithms in a rational parametrisation of the discriminant locus, a result required as initial data by the programme. Throughout all of this, the geometric-helix structure of the initial data persists and global reconstruction proceeds exactly as in the simpler cases. The robustness of the programme under these complications is strong evidence that BPS dendroscopy extends uniformly to all local del Pezzo geometries.

Several directions follow directly from these results. The most immediate is the completion of the global scattering diagram for local $\mathbb{F}_1$ at generic ℓ, extending the Π-stability analysis from the Argyres–Douglas locus to a systematic treatment of the multi-sheet structure for all four conifold points. A precise dictionary between stability scattering diagrams and the exponential spectral networks of [34, 84] would also be valuable: both constructions encode the same BPS spectra and should be related by a change of coordinates in Stab $\mathcal{C}$, but the precise map has not been established. Finally, framed BPS indices jump along the rays of $\mathcal{D}_{\psi,m}$, and their generating series are expected to interpolate between the crystal-melting partition function near the orbifold point and the topological string amplitude near large volume, generalising the correspondence of [61, 119]; the scattering diagram is the natural candidate for the interpolating object between these two regimes, and making this precise is a concrete open problem.

7.3 Lessons from quantum mechanics and modularity

The generating series of D4-D2-D0 BPS indices, known as Vafa–Witten partition functions in the context of twisted $\mathcal{N} = 4$ Yang–Mills theory on a del Pezzo surface S, transform as vector-valued mock modular forms. Their non-holomorphic modular completions involve generalised error functions whose presence is required for modular covariance, but whose physical origin had, prior to the work presented in this thesis, remained obscure. The standard derivation of these completions proceeds by indirect modular bootstrap arguments, which determine the non-holomorphic terms by the requirement of transformation properties under the modular group without identifying their microscopic origin. The physical setting is clear: a single D4-brane wrapped on $S \subset K_S$, with D2 and D0 charge dissolved in its worldvolume flux, is described at low energies by the supersymmetric quantum mechanics on the moduli space of multi-centred BPS black hole configurations, i.e. the Denef phase space. The precise question addressed in this thesis is whether the generalised error functions can be derived directly from a localisation computation in this quantum mechanics, without assuming modularity as an input.

The Witten index of the supersymmetric quantum mechanics of n dyons with charges $\{\gamma_i\}$ is computed by localising to time-independent configurations, following [99, 117]. The resulting integral over positions and their superpartners exhibits a natural factorisation. The first factor is an integral over the phase space $\mathcal{M}_n(\{\gamma_i, u_i\})$ of n-centred supersymmetric ground states at fixed Fayet-Iliopoulos parameters $\{u_i\}$, equipped with the standard Liouville measure ω^{n-1}. The second factor is an integral over the stability parameters $\{u_i\}$ themselves, with a Gaussian weight centred around the physical FI parameters $\{c_i\}$. The integral over $\mathcal{M}_n$ is a locally constant function of the u_i, computable either by equivariant localisation with respect to rotations [145] or by the attractor flow tree decomposition [16], and yields products of sign functions of DSZ pairings $\langle\gamma_i, \gamma_j\rangle$ weighted by Coulomb-branch indices. The subsequent Gaussian convolution over the u_i then produces a linear superposition of generalised error functions E_r of depth

$r \leq n-1$, each multiplied by $(n-1-r)$ sign functions of the physical FI parameters.

The conceptual core of this analysis lies in the physical interpretation of the resulting non-holomorphic terms. Upon re-expressing the error functions E_r in terms of complementary error functions $M_{r'}$ with $r' \leq r$, each term proportional to M_r captures the contribution of the spectral asymmetry between bosonic and fermionic scattering states with $r+1$ constituent centres. These scattering states populate the continuum of non-normalizable modes above threshold and contribute to the Witten index at finite temperature, as anticipated on general grounds in [17]. The localisation thus makes manifest that the modular completion is an infrared datum: it encodes the contribution of multi-particle scattering states that are systematically integrated out when attention is restricted to the holomorphic generating series of single-centred BPS indices. The non-holomorphic terms are not anomalies or artefacts of a poorly defined index; they are required by the spectral asymmetry of the open quantum mechanical system.

As a concrete application, the formula for $n = 2, 3, 4$ reproduces the complementary error functions M_r appearing in the modular completion of the Vafa–Witten generating series on $\mathbb{P}^2$, as well as the moduli-dependent contributions to the instanton generating potential. To the best of our knowledge, this gives the first direct physical derivation, for an arbitrary number of centres, of these non-holomorphic terms from the supersymmetric quantum mechanics. Nonetheless, the analysis also reveals several intriguing open questions. In the two-body case, the computation correctly captures M_1 but is missing a Gaussian term required by full modular invariance [141]. As discussed in [14], this term can be traced to an η-dependent shift in the refined index, suggesting that the $\hat{A}$-roof genus correction and the equivariant Dirac index have not been fully accounted for in the symplectic-leaf reduction. Furthermore, for non-collinear D4-charge vectors, the arguments of the error functions are rescaled relative to the modular completion by factors depending on triple intersection numbers, a discrepancy that vanishes automatically for local Calabi–Yau geometries of the form K_S but must be understood more generally. Several directions for future work follow naturally. One is to prove agreement with the modular completion for general non-collinear charges. Another is to determine whether replacing the partial flow-tree index by the partial Coulomb branch index of [148] reproduces the modular completion for single-centred black holes. Finally, the localisation prescription developed here requires only a supersymmetric quantum mechanics description and should be applicable to more exotic models in other physical contexts.

7.4 Broader perspective

This thesis contributes to a broader programme at the intersection of mathematical physics and enumerative geometry, whose aspiration is to understand the generating series of sheaf-counting invariants on complex surfaces as mock modular or automorphic objects, and to derive their symmetry properties from the geometry and physics of the underlying string compactification rather than imposing them by hand. The scattering diagrams constructed in this thesis provide explicit and algorithmic access to Donaldson–Thomas invariants across the stability slices considered here. Crucially, the modularity of their generating series is not imposed as an assumption: it is reflected in the symmetry of the Π-stability slice under the group of autoequivalences, which acts as the relevant congruence or non-congruence subgroup of $PSL(2,\mathbb{Z})$. In this way, the work serves as a bridge between the physics of BPS black holes and the mathematics of Bridgeland stability conditions. Results that had previously been established by independent methods, such as the Attractor Conjecture, the Split Attractor Flow Conjecture,

and the modular completion formula, acquire a unified geometric interpretation within a single framework.

Two connections to other areas of mathematical physics deserve particular emphasis. The first concerns the relationship between BPS dendroscopy and the mirror symmetry of open topological string theory. The large-volume scattering diagram constructed in this thesis coincides with the tropical scattering geometry that controls Gromov–Witten invariants of the corresponding log Calabi–Yau surface (S, D), where D is the anticanonical divisor. This places BPS dendroscopy in direct correspondence with the mirror symmetry of open topological strings and suggests that the scattering diagram is the natural object through which the various enumerative theories on S communicate. The second connection concerns the orbifold and crystal-melting descriptions near the large-radius degeneration limit. Near the orbifold point, the BPS spectrum is governed by quiver quantum mechanics whose partition functions reproduce crystal-melting generating series and their refinements. The full scattering diagram in stability space then provides the interpolating structure between this combinatorial description and the topological string amplitude at large volume. These observations together suggest that the stability scattering diagram, viewed as a global object over Stab C, encodes in a single geometric structure the multiple enumerative theories associated to a Calabi–Yau geometry: Gromov–Witten theory, Donaldson–Thomas theory, and crystal melting.

The results of this thesis establish that global reconstruction of BPS spectra is tractable for two-parameter toric geometries with non-trivial, and in some cases non-congruence, modular symmetry. Several natural milestones present themselves for future work. The most immediate is the systematic extension of BPS dendroscopy to all rank-one local del Pezzo geometries, K_{dP_n} with $dP_n = \mathrm{Bl}_n\mathbb{P}^2$ for $n = 2, \ldots, 8$, including a classification of the non-congruence subgroups and Argyres–Douglas loci that appear in each case. A second milestone is the extension of the black hole quantum mechanics localisation to n-body systems with general non-collinear charges, resolving the discrepancies with the modular completion identified in this thesis. More broadly, recent progress on mock modularity for compact Calabi–Yau threefolds and on dualities and trialities in one-dimensional supersymmetric gauged quantum mechanics suggests that the localization methods used here may extend to more general quiver quantum-mechanical systems, including models with chiral and Fermi multiplets and non-trivial duality frames [11, 66]. A third is a mathematically rigorous proof of the SAFC for local $\mathbb{F}_0$ and local $\mathbb{F}_1$ for all values of the phase ψ, building on the convexity arguments developed here.

A mathematically well-posed but physically less developed direction is to ask whether an analogue of the present local-surface story exists for local Calabi–Yau fourfolds. If Y is a Fano threefold, then $X = K_Y$ is a non-compact Calabi–Yau fourfold with compact zero section Y, providing a direct higher-dimensional analogue of the geometries K_S studied in this thesis. The relevant enumerative theory is not Donaldson–Thomas theory on Calabi–Yau threefolds, but DT_4 theory, whose virtual classes are constructed from the (-2)-shifted symplectic structure on moduli spaces of sheaves and depend on a choice of orientation data [44, 57, 161]. This makes local fourfolds K_Y, and in particular those associated with smooth toric Fano threefolds, natural testing grounds for higher-dimensional analogues of the stability and wall-crossing questions considered here. On the algebraic side, the technology of exceptional collections and semiorthogonal decompositions of $D^b(Y)$ remains available for many Fano threefolds, including toric examples [19, 123, 131, 181]. On the quiver gauge-theory side, the role of brane tilings for toric Calabi–Yau threefold singularities is taken over, for toric Calabi–Yau fourfold singularities, by brane brick models and the associated 2-graded quivers with J- and E-terms, which encode two-dimensional $\mathcal{N} = (0, 2)$ quiver gauge theories on the worldvolume

of D1-branes probing such singularities [63, 64, 96]. Recent work on four-dimensional crystal melting for toric Calabi–Yau fourfolds establishes that a combinatorial chamber description also exists in this setting [95]. The physical interpretation of DT_4 invariants is, however, less direct than in the threefold case. Type IIA string theory compactified on a Calabi–Yau fourfold yields a two-dimensional effective theory, in which D-branes wrapping holomorphic cycles appear as BPS kinks or solitons rather than as four-dimensional black holes, and the counting problem is no longer naturally tied to an attractor mechanism in four-dimensional $\mathcal{N} = 2$ supergravity. M-theory compactified on a Calabi–Yau fourfold instead yields a three-dimensional $\mathcal{N} = 2$ effective theory, in which M2-branes wrapping holomorphic 2-cycles give rise to BPS particles and M5-branes wrapping holomorphic 4-cycles give rise to BPS domain walls; this setting may provide a more natural arena for a physical interpretation of the wrapped-brane BPS states counted by DT_4 invariants [159, 170]. It would be interesting to determine whether scattering diagrams, attractor-type decompositions, or crystal-melting models admit a coherent DT_4 counterpart.

The methods developed here, combining large-volume, orbifold, and Π-stability data via monodromy and consistency, should extend beyond toric geometries to compact Calabi–Yau threefolds and to four-dimensional $\mathcal{N} = 2$ theories arising from non-toric compactifications, where the global perspective of stability scattering diagrams becomes especially valuable. In each setting studied here, wall-crossing structure, modular completions, and attractor flow trees are revealed as different expressions of the same data over stability space, reconstructible from sparse geometric input. Extending this to a wider class of geometries is the natural next step.

A

Modular Forms and Theta Series

This appendix reviews the modular background used in the thesis. The aim is not to give a complete treatment, but to introduce the main ideas and conventions needed for the modular, mock modular, Jacobi, and theta-series structures that appear in the study of BPS generating functions. The discussion is based primarily on [9, 41, 79, 86, 122, 183, 186, 189].

We begin with classical modular forms for the full modular group, including Eisenstein series, cusp forms, the discriminant, and the modular invariant. We then discuss congruence subgroups and modular forms of level, including cusp expansions and characters. Next, we review quasimodular forms, Jacobi forms, and positive-definite theta series, emphasizing how differentiation, elliptic variables, and lattice sums enter the theory.

The final part of the appendix turns to structures where holomorphicity and modularity no longer coexist in the simplest way. Mock modular forms are introduced through their non-holomorphic completions and shadows, while noncongruence subgroups are included to indicate the broader class of modular curves beyond the congruence setting. We conclude with Vignéras' theorem and indefinite theta series, where modularity is controlled by suitable kernels, often involving error functions or their generalizations.

A.1 Classical modular forms for $SL(2,\mathbb{Z})$

We first recall the basic theory of modular forms for the full modular group. Let

$$\gamma = \begin{pmatrix} a & b \\ c & d \end{pmatrix} \in SL(2,\mathbb{Z}), \qquad ad - bc = 1.$$

The group $SL(2,\mathbb{Z})$ acts on the upper half-plane

$$\mathcal{H} = \{\tau \in \mathbb{C} \mid \operatorname{Im}\tau > 0\}$$

by fractional linear transformations,

$$\gamma\tau = \frac{a\tau + b}{c\tau + d}.$$

This action preserves $\mathcal{H}$, since

$$\operatorname{Im}(\gamma\tau) = \frac{\operatorname{Im}\tau}{|c\tau + d|^2}.$$

The transformations

$$T : \tau \mapsto \tau + 1, \qquad S : \tau \mapsto -\frac{1}{\tau}$$

generate the action of $SL(2,\mathbb{Z})$ on $\mathcal{H}$. At the level of matrices one may take

$$T = \begin{pmatrix} 1 & 1 \\ 0 & 1 \end{pmatrix}, \qquad S = \begin{pmatrix} 0 & -1 \\ 1 & 0 \end{pmatrix}.$$

They satisfy

$$S^2 = (ST)^3 = -I,$$

and since the central element $-I$ acts trivially on $\mathcal{H}$, the induced action of $PSL(2,\mathbb{Z}) = SL(2,\mathbb{Z})/\{\pm I\}$ satisfies $S^2 = (ST)^3 = 1$.

Let $k \in \mathbb{Z}$. A meromorphic function $f : \mathcal{H} \to \mathbb{C}$ is said to transform with weight k under $SL(2,\mathbb{Z})$ if

$$f(\gamma\tau) = (c\tau + d)^k f(\tau) \qquad \text{for all } \gamma = \begin{pmatrix} a & b \\ c & d \end{pmatrix} \in SL(2,\mathbb{Z}).$$

This condition expresses the fact that f is not quite an ordinary function on the quotient $SL(2,\mathbb{Z})\backslash\mathcal{H}$, but rather a section of a natural line bundle over it. Since $-I \in SL(2,\mathbb{Z})$ acts trivially on $\mathcal{H}$, the transformation law also implies

$$f(\tau) = (-1)^k f(\tau).$$

Thus, for the full modular group and trivial multiplier system, nonzero modular forms occur only in even weight.

The transformation $T : \tau \mapsto \tau + 1$ is particularly important near the cusp at infinity. If f has weight k, then the relation $f(\tau + 1) = f(\tau)$ implies that f admits a Fourier expansion in the local parameter

$$q = e^{2\pi i\tau}.$$

The point $\tau = i\infty$ corresponds to $q = 0$. One says that f is holomorphic at the cusp if its q-expansion contains no negative powers of q. Thus a holomorphic modular form of weight k for $SL(2,\mathbb{Z})$ is a holomorphic function on $\mathcal{H}$ satisfying the above transformation law and admitting an expansion

$$f(\tau) = \sum_{n \geq 0} a_n q^n$$

near $q = 0$. If moreover $a_0 = 0$, then f is called a cusp form. A meromorphic modular function is the corresponding notion in weight zero, allowing poles; in particular, poles at the cusp are visible as negative powers of q.

A convenient fundamental domain for the action of $SL(2,\mathbb{Z})$ on $\mathcal{H}$ is

$$\mathcal{F} = \left\{ \tau \in \mathcal{H} \;\middle|\; |\operatorname{Re}(\tau)| \leq \frac{1}{2},\ |\tau| \geq 1 \right\},$$

with the boundary identifications induced by S and T. The quotient becomes compact after adjoining the cusp at infinity; the resulting compact modular curve is denoted

$$X(1) = SL(2,\mathbb{Z})\backslash\mathcal{H}^*,$$

where $\mathcal{H}^*$ denotes the upper half-plane together with the cusp.

The most important holomorphic modular forms for the full modular group are the Eisenstein series. For even $k \geq 4$, the normalized Eisenstein series of weight k is

$$E_k(\tau) = 1 - \frac{2k}{B_k} \sum_{n=1}^{\infty} \sigma_{k-1}(n)\, q^n,$$

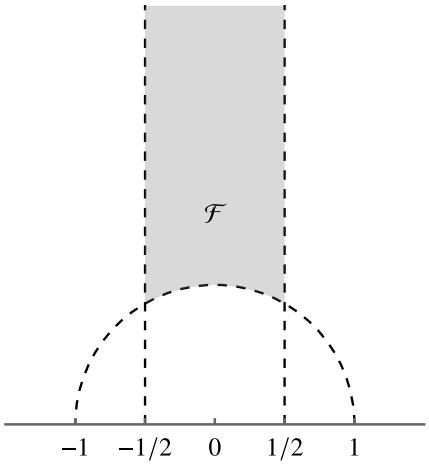


Figure A.1: A fundamental domain for the action of $SL(2,\mathbb{Z})$ on $\mathcal{H}$.

where B_k is the k-th Bernoulli number and

$$\sigma_r(n) := \sum_{d|n} d^r$$

is the divisor sum. The normalization is chosen so that the constant term is equal to one. The first two nontrivial examples are

$$E_4(\tau) = 1 + 240 \sum_{n=1}^{\infty} \sigma_3(n)\, q^n, \qquad E_6(\tau) = 1 - 504 \sum_{n=1}^{\infty} \sigma_5(n)\, q^n.$$

These are holomorphic modular forms of weights 4 and 6, respectively. They are fundamental because every holomorphic modular form for $SL(2,\mathbb{Z})$ can be written as a polynomial in E_4 and E_6.

The first cusp form occurs in weight 12. It is the modular discriminant

$$\Delta(\tau) = \frac{E_4(\tau)^3 - E_6(\tau)^2}{1728}.$$

Equivalently,

$$\Delta(\tau) = q \prod_{n=1}^{\infty} (1 - q^n)^{24}.$$

This expression shows that Δ vanishes to first order at the cusp and has no zeros on $\mathcal{H}$. It is the unique normalized cusp form of weight 12.

The discriminant also gives the basic modular function for the full modular group. Define

$$j(\tau) = \frac{E_4(\tau)^3}{\Delta(\tau)}.$$

Since both E_4^3 and Δ have weight 12, the quotient has weight zero. It is therefore invariant under $SL(2,\mathbb{Z})$, holomorphic on $\mathcal{H}$, and meromorphic at the cusp. Its Fourier expansion begins

$$j(\tau) = q^{-1} + 744 + 196884\, q + \cdots .$$

Thus j has a simple pole at the cusp and no other poles. It gives a coordinate on the compact modular curve $X(1)$; equivalently, j is a Hauptmodul for the genus-zero curve $X(1)$. This example will serve as the basic model for analogous constructions at higher level and, in a different sense, for modular parametrizations of genus-zero noncongruence modular curves [40, 186].

The preceding examples are summarized by the structure theorem

$$M_*(SL(2,\mathbb{Z})) = \mathbb{C}[E_4, E_6],$$

where $M_*(SL(2,\mathbb{Z}))$ denotes the graded ring of holomorphic modular forms for the full modular group. In weight k, this statement means that any holomorphic modular form of weight k is a finite linear combination of monomials

$$E_4^a E_6^b, \qquad 4a + 6b = k.$$

Similarly, the graded ideal of cusp forms is

$$S_*(SL(2,\mathbb{Z})) = \Delta\, \mathbb{C}[E_4, E_6].$$

Thus a cusp form for the full modular group is precisely a modular form divisible by Δ. Consequently, whenever a modular form for $SL(2,\mathbb{Z})$ appears, it can be expressed algebraically in terms of E_4 and E_6, while cusp forms carry an additional overall factor of the discriminant.

A.2 Congruence subgroups and modular forms of level N

The full modular group is often too large for the modular objects that arise in applications. One is then led to subgroups of $SL(2,\mathbb{Z})$ defined by congruence conditions on the matrix entries. Let $N \geq 1$ be an integer. The principal congruence subgroup of level N is

$$\Gamma(N) = \left\{ \gamma = \begin{pmatrix} a & b \\ c & d \end{pmatrix} \in SL(2,\mathbb{Z}) \;\middle|\; \gamma \equiv \begin{pmatrix} 1 & 0 \\ 0 & 1 \end{pmatrix} \pmod{N} \right\}.$$

Two related congruence subgroups, used especially frequently, are

$$\Gamma_0(N) = \left\{ \gamma = \begin{pmatrix} a & b \\ c & d \end{pmatrix} \in SL(2,\mathbb{Z}) \;\middle|\; c \equiv 0 \pmod{N} \right\},$$

and

$$\Gamma_1(N) = \left\{ \gamma = \begin{pmatrix} a & b \\ c & d \end{pmatrix} \in SL(2,\mathbb{Z}) \;\middle|\; c \equiv 0 \pmod{N},\ a \equiv d \equiv 1 \pmod{N} \right\}.$$

They satisfy the inclusions

$$\Gamma(N) \subset \Gamma_1(N) \subset \Gamma_0(N) \subset SL(2,\mathbb{Z}).$$

Thus passing from $SL(2,\mathbb{Z})$ to one of these subgroups weakens the modular transformation law: the function is required to transform in a controlled way only under matrices satisfying the chosen congruence condition.

It is useful to express this transformation law through the slash operator. For a function $f : \mathcal{H} \to \mathbb{C}$, an integer k, and

$$\gamma = \begin{pmatrix} a & b \\ c & d \end{pmatrix} \in SL(2,\mathbb{Z}),$$

define

$$(f[\gamma]_k)(\tau) := (c\tau + d)^{-k} f\left(\frac{a\tau + b}{c\tau + d}\right).$$

The function f transforms with weight k under a subgroup $G \subset SL(2,\mathbb{Z})$ if

$$f[\gamma]_k = f \qquad \text{for all } \gamma \in G.$$

A holomorphic modular form of weight k for G is a holomorphic function on $\mathcal{H}$ satisfying this transformation law and satisfying a holomorphy condition at each cusp of G.

Let us spell out the cusp condition, since it is one of the points where modular forms of higher level differ from forms for the full modular group. The cusps are the G-equivalence classes in

$$\mathbb{P}^1(\mathbb{Q}) = \mathbb{Q} \cup \{\infty\}.$$

For a cusp $\mathfrak{a}$, choose a matrix $\sigma \in SL(2,\mathbb{Z})$ such that $\sigma(\infty) = \mathfrak{a}$. Then f is holomorphic at $\mathfrak{a}$ if the transformed function

$$f[\sigma]_k$$

has a Fourier expansion at infinity with no negative powers of the corresponding local parameter. More explicitly, because the stabilizer of the cusp may have width $w_{\mathfrak{a}}$, the local parameter is

$$q_{\mathfrak{a}} = e^{2\pi i\tau/w_{\mathfrak{a}}},$$

and holomorphy at $\mathfrak{a}$ means that

$$(f[\sigma]_k)(\tau) = \sum_{n\geq 0} a_n q_{\mathfrak{a}}^n.$$

If the expansion has vanishing constant term at every cusp, then f is a cusp form.

One can slightly generalize the transformation law by allowing a finite multiplicative factor. This factor is encoded by a Dirichlet character modulo N. Concretely, a Dirichlet character modulo N is a function

$$\chi : \mathbb{Z} \to \mathbb{C}$$

which depends only on the residue class of its argument modulo N, is multiplicative,

$$\chi(mn) = \chi(m)\chi(n),$$

and vanishes on integers not coprime to N. Equivalently, it is a group homomorphism

$$\chi : (\mathbb{Z}/N\mathbb{Z})^\times \longrightarrow \mathbb{C}^\times$$

extended to all integers by setting $\chi(n) = 0$ when $(n, N) > 1$.

Now let

$$\gamma = \begin{pmatrix} a & b \\ c & d \end{pmatrix} \in \Gamma_0(N).$$

By definition of $\Gamma_0(N)$, one has $c \equiv 0 \pmod N$. Since $\gamma \in SL(2,\mathbb{Z})$, one also has $ad - bc = 1$. Reducing this relation modulo N gives

$$ad \equiv 1 \pmod N.$$

Thus d is invertible modulo N, so it makes sense to evaluate the character on d. In particular, $\chi(d)$ is a nonzero complex number, in fact a root of unity.

A modular form of weight k and character χ for $\Gamma_0(N)$ is then a holomorphic function

$$f : \mathcal{H} \to \mathbb{C}$$

which satisfies

$$f[\gamma]_k = \chi(d)\, f \qquad \text{for all } \gamma = \begin{pmatrix} a & b \\ c & d \end{pmatrix} \in \Gamma_0(N),$$

and is holomorphic at all cusps. Thus the usual weight-k modular transformation law is modified by the extra factor $\chi(d)$, which depends only on the lower-right entry of the matrix modulo N. The character χ is called the nebentypus character. The corresponding space of modular forms is denoted

$$M_k(\Gamma_0(N), \chi),$$

and its subspace of cusp forms is denoted

$$S_k(\Gamma_0(N), \chi).$$

There is one immediate constraint on the possible pair (k, χ). The matrix $-I$ belongs to $\Gamma_0(N)$ and acts trivially on $\mathcal{H}$. Applying the transformation law to $-I$ gives

$$f(\tau) = \chi(-1)(-1)^k f(\tau).$$

Therefore

$$M_k(\Gamma_0(N), \chi) = \{0\} \qquad \text{unless} \qquad \chi(-1) = (-1)^k.$$

For the trivial character this reduces to the familiar parity condition: nonzero modular forms for groups containing $-I$ have even weight.

The case $N = 1$ recovers the full modular group. Indeed,

$$\Gamma_0(1) = \Gamma_1(1) = \Gamma(1) = SL(2, \mathbb{Z}),$$

and the only Dirichlet character modulo 1 is trivial. Thus the definitions above reduce to the modular forms for $SL(2, \mathbb{Z})$ discussed in the previous section. For $N > 1$, the same formalism allows one to describe functions transforming under a smaller modular group, with additional cusps and, when present, a character in the transformation law [79].

A.3 Quasimodular forms

The ring of holomorphic modular forms for the full modular group is generated by E_4 and E_6. There is, however, an important holomorphic function of weight 2 whose transformation law is close to modular but contains an anomaly. It is the Eisenstein series

$$E_2(\tau) = 1 - 24 \sum_{n=1}^{\infty} \sigma_1(n)\, q^n.$$

Unlike E_4 and E_6, this function is not a modular form. Its transformation law contains an additional term:

$$E_2\left(\frac{a\tau + b}{c\tau + d}\right) = (c\tau + d)^2 E_2(\tau) + \frac{12c(c\tau + d)}{2\pi \mathrm{i}}.$$

Thus E_2 transforms as a weight-2 modular form only up to an explicit correction term depending on c and $c\tau + d$. This is the simplest example of a quasimodular form. The failure of modularity is not arbitrary: it is controlled by a polynomial expression in the entries of the modular transformation. [122]

There is a useful way to restore modularity at the cost of holomorphicity. Define

$$E_2^*(\tau) := E_2(\tau) - \frac{3}{\pi\ \mathrm{Im}\,\tau}.$$

Then one checks that

$$E_2^*(\gamma\tau) = (c\tau + d)^2 E_2^*(\tau) \qquad \text{for all } \gamma = \begin{pmatrix} a & b \\ c & d \end{pmatrix} \in SL(2,\mathbb{Z}).$$

The function E_2^* is therefore a genuine modular object of weight 2, but it is no longer holomorphic because it depends explicitly on $\mathrm{Im}\,\tau$. This distinction is important. The holomorphic function E_2 is quasimodular, while its real-analytic completion E_2^* is modular. This is the basic mechanism behind many non-holomorphic completions: a holomorphic function has an anomalous modular transformation law, and a genuinely modular object is obtained only after adding a suitable real-analytic correction. [122, 186]

For the full modular group, the ring of holomorphic quasimodular forms is

$$\widetilde{M}_*(SL(2,\mathbb{Z})) = \mathbb{C}[E_2, E_4, E_6].$$

The weight grading is determined by assigning weights 2, 4, and 6 to E_2, E_4 and E_6 respectively, as usual. Equivalently, a quasimodular form for $SL(2,\mathbb{Z})$ is a polynomial in E_2, E_4, and E_6. Its failure to be modular is entirely due to the occurrences of E_2. Replacing E_2 by E_2^* gives the corresponding almost holomorphic modular form. In this sense, quasimodular forms may be viewed as the holomorphic parts of almost holomorphic modular forms. [122]

A central reason quasimodular forms occur so naturally is that they are stable under differentiation. Introduce

$$D := \frac{1}{2\pi\mathrm{i}}\frac{\mathrm{d}}{\mathrm{d}\tau} = q\frac{\mathrm{d}}{\mathrm{d}q}.$$

Differentiating an ordinary modular form does not usually produce another modular form, because the derivative also acts on the factor $(c\tau + d)^k$ in the transformation law. The resulting correction is precisely of the same type as the anomaly of E_2. For the Eisenstein series, this structure is expressed by the Ramanujan identities

$$DE_2 = \frac{E_2^2 - E_4}{12}, \qquad DE_4 = \frac{E_2E_4 - E_6}{3}, \qquad DE_6 = \frac{E_2E_6 - E_4^2}{2}.$$

These equations show that applying D to any polynomial in E_2, E_4, E_6 again gives a polynomial in E_2, E_4, E_6. Thus

$$D\widetilde{M}_*(SL(2,\mathbb{Z})) \subset \widetilde{M}_*(SL(2,\mathbb{Z})).$$

The ring of quasimodular forms is therefore a differential ring. This simple fact is one of the reasons quasimodular forms are well adapted to recursive structures such as holomorphic anomaly equations. [103, 122, 185]

It is sometimes useful to separate the non-modular part of the derivative from the modular part. If f is a modular form of weight k, the Serre derivative is defined by

$$D_k f := Df - \frac{k}{12}E_2 f.$$

Although E_2 itself is only quasimodular, the combination $D_k f$ transforms as a modular form of weight $k+2$. Thus the appearance of E_2 precisely compensates for the anomalous transformation of the ordinary derivative.

A.4 Jacobi forms and positive-definite theta series

We now turn to Jacobi forms. These are functions of two complex variables: the modular parameter $\tau \in \mathcal{H}$ and an elliptic variable $z \in \mathbb{C}$. It is convenient to write

$$q = e^{2\pi i \tau}, \qquad y = e^{2\pi i z}.$$

A holomorphic Jacobi form of weight k and index m for the full modular group is a holomorphic function

$$\phi : \mathcal{H} \times \mathbb{C} \to \mathbb{C}$$

satisfying two transformation laws. The first describes the behavior under modular transformations:

$$\phi\left(\frac{a\tau + b}{c\tau + d}, \frac{z}{c\tau + d}\right) = (c\tau + d)^k \exp\left(\frac{2\pi i m c z^2}{c\tau + d}\right) \phi(\tau, z),$$

for all

$$\begin{pmatrix} a & b \\ c & d \end{pmatrix} \in SL(2, \mathbb{Z}).$$

The second describes the behavior under translations by the lattice generated by 1 and τ:

$$\phi(\tau, z + \lambda\tau + \mu) = \exp\Big(-2\pi i m(\lambda^2 \tau + 2\lambda z)\Big)\, \phi(\tau, z), \qquad \lambda, \mu \in \mathbb{Z}.$$

The first condition says that ϕ transforms modularly in τ, with a correction involving z^2. The second condition says that, for fixed τ, the dependence on z is compatible with the elliptic curve

$$\mathbb{C}/(\mathbb{Z}\tau + \mathbb{Z}).$$

The integer m is called the index. It controls the exponential factor in the elliptic transformation law and plays the role of a quadratic coefficient for the elliptic variable. [86]

The translation $z \mapsto z + 1$ implies periodicity in z, so a Jacobi form has a Fourier expansion in powers of y. The translation $\tau \mapsto \tau + 1$ similarly gives an expansion in powers of q. Thus one writes

$$\phi(\tau, z) = \sum_{n,r} c(n, r)\, q^n y^r.$$

For a holomorphic Jacobi form of index m, the Fourier coefficients satisfy

$$c(n, r) = 0 \qquad \text{unless} \qquad 4mn - r^2 \geq 0.$$

Equivalently,

$$\phi(\tau, z) = \sum_{n=0}^{\infty} \sum_{\substack{r \in \mathbb{Z} \\ r^2 \leq 4mn}} c(n, r)\, q^n y^r.$$

The quantity $4mn - r^2$ is the discriminant associated with the Fourier monomial $q^n y^r$. The inequality above is the Jacobi analogue of holomorphy at the cusp. It prevents arbitrarily

negative growth as $\operatorname{Im}\tau \to \infty$ and is one of the main differences between holomorphic, weak, and meromorphic Jacobi forms. A weak Jacobi form allows all terms with $n \geq 0$, even when $4mn - r^2 < 0$, while a meromorphic Jacobi form may have poles in the elliptic variable z.

The elliptic transformation law also implies that the coefficients are not independent for all $r \in \mathbb{Z}$. They are organized by the residue class of r modulo $2m$ and by the discriminant $4mn - r^2$. This leads to the theta decomposition. For $\ell \in \mathbb{Z}/2m\mathbb{Z}$, define the unary theta series

$$\theta_{m,\ell}(\tau, z) = \sum_{\substack{r \in \mathbb{Z} \\ r \equiv \ell \pmod{2m}}} q^{r^2/4m} y^r.$$

Then every holomorphic Jacobi form of weight k and index m admits a decomposition

$$\phi(\tau, z) = \sum_{\ell \bmod 2m} h_\ell(\tau)\, \theta_{m,\ell}(\tau, z).$$

The functions $h_\ell(\tau)$ are not independent scalar modular forms in general. Rather, the vector

$$(h_\ell)_{\ell \bmod 2m}$$

transforms as a vector-valued modular form of weight $k - \frac{1}{2}$. Thus a Jacobi form can be viewed as a finite combination of theta functions in the elliptic variable, with modular coefficients in τ. This decomposition is often the most practical way to connect Jacobi forms with lattice theta series. [86]

Theta series provide the basic examples behind this structure. Let L be a positive-definite lattice with quadratic form $Q(\lambda) = \frac{1}{2}(\lambda, \lambda)$. The associated theta series is

$$\Theta_L(\tau) = \sum_{\lambda \in L} q^{Q(\lambda)}.$$

Positive-definiteness ensures convergence for $\tau \in \mathcal{H}$. Under suitable integrality assumptions on L, this theta series transforms as a modular form, or more generally as a component of a vector-valued modular form. If one also keeps an elliptic variable z paired with the lattice vector, one obtains

$$\Theta_L(\tau, z) = \sum_{\lambda \in L} q^{Q(\lambda)} e^{2\pi \mathrm{i}(\lambda, z)}.$$

This is the prototype of a Jacobi theta series: the variable τ records the value of the quadratic form, while the variable z records the lattice vector itself.

The restriction to positive-definite lattices is essential in this elementary construction. If the quadratic form is indefinite, the naive theta series generally fails to converge and does not transform modularly without further modification. Indefinite theta series therefore require additional choices, such as kernels imposing convergence, and often acquire non-holomorphic completions. This is the point at which the structures reviewed here connect with the discussion of mock modularity, Vafa–Witten invariants, and generalized error functions.

A.5 Mock modular forms and harmonic Maass forms

Mock modular forms arise from a basic phenomenon: a holomorphic q-series may have coefficients and asymptotic behaviour strongly suggestive of modularity, while nevertheless

failing to satisfy an honest modular transformation law. The modern way to understand this failure is not to treat it as accidental, but to enlarge the object. One asks whether the given holomorphic function can be completed by adding a non-holomorphic term so that the sum transforms modularly.

The historical examples are Ramanujan's mock theta functions. A classical third-order mock theta function is

$$f(q) = 1 + \sum_{n=1}^{\infty} \frac{q^{n^2}}{(1+q)^2(1+q^2)^2\cdots(1+q^n)^2}.$$

This is a holomorphic q-series for $|q| < 1$, but it is not a modular form in the classical sense. Its modular behaviour is recovered only after adjoining a suitable non-holomorphic correction. In this sense, mock modular forms should be regarded as holomorphic parts of real-analytic modular objects [187, 189].

The natural ambient objects are harmonic Maass forms. Write

$$\tau = \tau_1 + \mathrm{i}\tau_2, \qquad \tau_2 = \operatorname{Im}\tau > 0.$$

A harmonic Maass form of weight k for a subgroup $\Gamma \subset SL(2,\mathbb{Z})$ is a real-analytic function

$$F : \mathcal{H} \to \mathbb{C}$$

which satisfies three conditions. First, it transforms with weight k:

$$F(\gamma\tau) = (c\tau + d)^k F(\tau) \qquad \text{for all } \gamma = \begin{pmatrix} a & b \\ c & d \end{pmatrix} \in \Gamma.$$

Second, it has prescribed growth at the cusps. Third, it is annihilated by the weight-k hyperbolic Laplacian,

$$\Delta_k F = 0,$$

where

$$\Delta_k = -\tau_2^2\left(\frac{\partial^2}{\partial\tau_1^2} + \frac{\partial^2}{\partial\tau_2^2}\right) + \mathrm{i}k\tau_2\left(\frac{\partial}{\partial\tau_1} + \mathrm{i}\frac{\partial}{\partial\tau_2}\right).$$

Thus a harmonic Maass form is modular, but it is not required to be holomorphic. It may depend on both τ and $\bar{\tau}$.

A harmonic Maass form often decomposes naturally into two parts,

$$F(\tau) = F^+(\tau) + F^-(\tau).$$

The first part, $F^+(\tau)$, is holomorphic in τ and is usually given by a q-series. This is the mock modular form. The second part, $F^-(\tau)$, is non-holomorphic and is responsible for restoring modularity. The completed function

$$\widehat{F^+}(\tau) := F^+(\tau) + F^-(\tau)$$

is modular in the real-analytic sense, whereas $F^+(\tau)$ alone is not.

The failure of F^+ to be modular is measured by the shadow. This is described by the antilinear differential operator

$$\xi_k(F)(\tau) = 2\mathrm{i}\,\tau_2^k \overline{\frac{\partial F}{\partial\bar{\tau}}}.$$

If F is a harmonic Maass form of weight k, then $\xi_k(F)$ transforms with weight $2-k$. In many important examples, $\xi_k(F)$ is a holomorphic modular form, often a cusp form. This modular form is called the shadow of the mock modular form F^+, up to conventional normalizations [53, 189]. The terminology reflects the fact that the shadow determines the non-holomorphic term needed to complete the mock modular form.

The simplest analogy is the Eisenstein series E_2. The holomorphic function E_2 is not modular, while

$$E_2^*(\tau) = E_2(\tau) - \frac{3}{\pi \operatorname{Im}\tau}$$

is modular but non-holomorphic. Mock modular forms follow the same general pattern, but their non-holomorphic completions are more intricate. Instead of a simple rational function of $\operatorname{Im}\tau$, the correction term is typically expressed using incomplete gamma functions or error functions.

A particularly important source of mock modular behaviour is given by Appell–Lerch sums. Following Zwegers, consider

$$\mu(u,v;\tau) = \frac{e^{\pi i u}}{\vartheta(v;\tau)} \sum_{n\in\mathbb{Z}} \frac{(-1)^n e^{\pi i (n^2+n)\tau + 2\pi i n v}}{1 - e^{2\pi i n\tau + 2\pi i u}},$$

where $\vartheta(v;\tau)$ denotes the odd Jacobi theta function. The variables u and v are elliptic variables, while τ is the modular parameter. The denominator

$$1 - e^{2\pi i n\tau + 2\pi i u}$$

is the characteristic feature of an Appell–Lerch sum. It introduces poles in the elliptic variable and prevents the holomorphic function $\mu(u,v;\tau)$ from transforming as an ordinary Jacobi form [189].

Zwegers showed that this defect can be corrected explicitly. Define

$$\widetilde{\mu}(u,v;\tau) = \mu(u,v;\tau) + \frac{i}{2} R(u-v;\tau),$$

where

$$R(u;\tau) = \sum_{\nu\in\frac{1}{2}+\mathbb{Z}} \Big\{ \operatorname{sign}(\nu) - E\big((\nu+a)\sqrt{2\,\operatorname{Im}\tau}\big) \Big\} (-1)^{\nu-\frac{1}{2}} e^{-\pi i \nu^2 \tau - 2\pi i \nu u},$$

with

$$a = \frac{\operatorname{Im}(u)}{\operatorname{Im}(\tau)}$$

and

$$E(x) = 2\int_0^x e^{-\pi t^2}\, dt.$$

The function $E(x)$ is a rescaled error function. It is smooth, odd, and satisfies

$$E(x) \longrightarrow \operatorname{sign}(x) \qquad \text{as } |x| \to \infty.$$

Thus the term

$$\operatorname{sign}(\nu) - E\big((\nu+a)\sqrt{2\,\operatorname{Im}\tau}\big)$$

measures the difference between a discontinuous sign function and its smooth error-function regularization.

This formula displays the essential mechanism very clearly. The holomorphic Appell–Lerch sum contains a sign-like discontinuity hidden in its transformation behaviour. Such discontinuous kernels are poorly behaved under modular transformations. The non-holomorphic correction replaces the discontinuous sign by a smooth real-analytic approximation built from the error function. After this correction, the completed function $\widehat{\mu}(u, v; \tau)$ has the appropriate modular and elliptic transformation properties. The original holomorphic function $\mu(u, v; \tau)$ is therefore a mock Jacobi form, and $R(u - v; \tau)$ supplies its completion.

This example is useful because it makes mock modularity concrete. A mock modular form is not simply a function that "almost" transforms modularly. Rather, it is the holomorphic part of a larger real-analytic object that does transform modularly. The obstruction to modularity is controlled by the shadow, and the correction term is often expressible through special functions such as error functions or incomplete gamma functions. This point of view connects mock modularity with theta series of indefinite signature: in positive-definite theta series, convergence and modularity are compatible with a purely holomorphic sum, whereas in indefinite signature one must regularize the summation kernel. Error-function completions provide precisely such regularizations [9, 189].

A.6 Modular forms on noncongruence subgroups

The congruence subgroups introduced above form the most familiar class of finite-index subgroups of $SL(2, \mathbb{Z})$, but they do not exhaust all possibilities. One may consider modular forms for any finite-index subgroup

$$G \subset SL(2, \mathbb{Z}).$$

Such a subgroup acts properly discontinuously on the upper half-plane, and the quotient

$$G \backslash \mathcal{H}$$

can be compactified by adjoining finitely many cusps. The resulting compact Riemann surface is the modular curve associated with G, usually denoted by

$$X_G.$$

A finite-index subgroup $G \subset SL(2, \mathbb{Z})$ is called a congruence subgroup if it contains the principal congruence subgroup $\Gamma(N)$ for some integer $N \geq 1$. Equivalently, the condition defining G can be detected at some finite level modulo N. A finite-index subgroup which does not contain any $\Gamma(N)$ is called a noncongruence subgroup. Thus a noncongruence subgroup still gives a perfectly good modular curve, but it is not obtained by imposing one of the usual congruence conditions on the entries of matrices in $SL(2, \mathbb{Z})$ [33, 41].

The inclusion

$$G \subset SL(2, \mathbb{Z})$$

induces a natural holomorphic map

$$X_G \longrightarrow X(1),$$

where $X(1)$ is the compact modular curve for the full modular group. Since

$$X(1) \simeq \mathbb{P}^1$$

with coordinate given by the classical j-invariant, this map may be viewed as a finite covering of the j-line, ramified only over the elliptic points and the cusp. In this sense, noncongruence modular curves are still part of the same geometric theory of modular curves, even though their defining groups are not described by congruence conditions.

The definition of modular forms extends without difficulty to such subgroups. A holomorphic modular form of weight k for G is a holomorphic function

$$f : \mathcal{H} \to \mathbb{C}$$

satisfying

$$f(\gamma\tau) = (c\tau + d)^k f(\tau) \qquad \text{for all } \gamma = \begin{pmatrix} a & b \\ c & d \end{pmatrix} \in G,$$

together with holomorphy at all cusps of G. Equivalently, one requires

$$f[\gamma]_k = f \qquad \text{for all } \gamma \in G,$$

using the slash operator introduced earlier. The difference from the congruence case is therefore not in the formal definition of a modular form, but in the arithmetic nature of the group G.

This difference becomes visible in the Fourier expansions. For congruence subgroups, modular forms with algebraic Fourier coefficients often have strong integrality properties after a suitable normalization. By contrast, modular forms on genuinely noncongruence subgroups frequently display Fourier coefficients with unbounded denominators. This phenomenon was already observed in the work of Atkin and Swinnerton-Dyer and is one of the characteristic arithmetic features of the noncongruence setting [33, 41, 87]. It should not be interpreted as saying that every coefficient is badly behaved. Rather, the point is that the denominators cannot, in general, be cleared once and for all by multiplying the whole q-series by a fixed algebraic number.

Another distinction concerns Hecke operators. For congruence subgroups, Hecke operators are central to the structure of spaces of modular forms: they organize eigenforms, impose arithmetic recursion relations on Fourier coefficients, and connect modular forms to Galois representations. For noncongruence subgroups, there is no comparable Hecke theory available in the same general form. Instead, one often encounters Atkin–Swinnerton-Dyer congruences: p-adic congruence relations between Fourier coefficients of noncongruence modular forms and those of suitable congruence modular forms. These congruences provide a substitute for Hecke-type arithmetic structure, but they are subtler and less uniform than in the congruence case.

The algebraic description is especially transparent when the modular curve X_G has genus zero. In that case its function field is generated by a single meromorphic function,

$$\mathbb{C}(X_G) = \mathbb{C}(j_G),$$

where j_G is called a Hauptmodul for G. Since the natural map

$$X_G \longrightarrow X(1)$$

is a map to the j-line, the classical modular invariant j becomes a rational function of the Hauptmodul:

$$j = R(j_G),$$

for some rational function R. The function R records the covering map

$$X_G \simeq \mathbb{P}^1 \longrightarrow X(1) \simeq \mathbb{P}^1.$$

Its ramification behaviour is determined by the elliptic points and cusps of the subgroup. This gives an effective way to describe genus-zero noncongruence modular curves explicitly [40, 179].

The genus-zero case should not be mistaken for the general situation. If X_G has positive genus, its function field is no longer generated by one Hauptmodul. Instead, one must describe X_G by an algebraic curve together with the map to the j-line. In such examples, modular functions on X_G are rational functions on this algebraic curve, rather than rational functions of a single Hauptmodul [40, 41].

The conceptual point is the following. Congruence subgroups are distinguished by their arithmetic definition modulo N, and they support a particularly rich theory of Hecke operators and Fourier-coefficient arithmetic. Noncongruence subgroups are still finite-index subgroups of $SL(2,\mathbb{Z})$ and therefore still define modular curves and modular forms, but their arithmetic properties can be substantially different. In geometric problems where a modular curve appears through monodromy, periods, or a covering of the j-line, the resulting subgroup need not be congruence. It is therefore useful to keep the noncongruence case conceptually separate from the higher-level congruence case, even though the analytic definition of a modular form is formally the same.

A.7 Vignéras' theorem and indefinite theta series

Theta series attached to positive-definite lattices are among the basic examples of modular forms. Let L be a lattice equipped with an integral quadratic form Q. If Q is positive definite, the series

$$\Theta_L(\tau) = \sum_{x \in L} q^{Q(x)}, \qquad q = e^{2\pi i \tau},$$

converges for $\tau \in \mathcal{H}$, because

$$|q^{Q(x)}| = e^{-2\pi \operatorname{Im}(\tau) Q(x)}$$

decays rapidly as x goes to infinity in L. This exponential damping is the analytic reason that positive-definite theta series are well behaved.

The situation changes fundamentally when the quadratic form is indefinite. Let

$$L$$

have rank

$$n = s + t$$

and let Q have signature (s,t), with both s and t allowed to be nonzero. In this case $Q(x)$ can be arbitrarily large and positive, but also arbitrarily large and negative. Therefore the naive theta series

$$\sum_{x \in L} q^{Q(x)}$$

no longer has uniform exponential decay. Along directions where $Q(x) < 0$, the factor $q^{Q(x)}$ grows rather than decays. Consequently, the direct analogue of the positive-definite theta series is usually divergent. This is the basic analytic obstruction in the theory of indefinite theta series.

The remedy is to insert a kernel into the lattice sum. Instead of summing $q^{Q(x)}$ alone, one considers a weighted theta series in which each lattice point is multiplied by a function of x. Schematic examples have the form

$$\Theta_\Phi(\tau) = \sum_{x \in L+\mu} \Phi\big(\sqrt{2\,\mathrm{Im}\,\tau}\,x\big)\, e^{2\pi i \tau Q(x)},$$

where μ is a possible shift of the lattice and Φ is a function on

$$L \otimes_{\mathbb{Z}} \mathbb{R}.$$

The factor $\sqrt{2\,\mathrm{Im}\,\tau}$ is a conventional scaling which is useful for modular transformations. Different authors distribute Gaussian factors and powers of $\mathrm{Im}\,\tau$ differently between the definition of the theta series and the definition of the kernel. The essential point is: the kernel must do two jobs simultaneously. It must make the lattice sum convergent, and it must be compatible with modular transformations.

Vignéras' theorem gives a precise criterion for this compatibility. We now describe the criterion in one common normalization, after the relevant Gaussian factors have been distributed as in the theta series above. Let

$$V = L \otimes_{\mathbb{Z}} \mathbb{R}$$

and choose linear coordinates

$$x = (x_1, \ldots, x_n)$$

in which the quadratic form has signature (s, t). Thus, up to an orthogonal change of coordinates,

$$Q(x) = \frac{1}{2}\left(x_1^2 + \cdots + x_s^2 - x_{s+1}^2 - \cdots - x_{s+t}^2\right).$$

Let

$$E = \sum_{i=1}^{n} x_i \frac{\partial}{\partial x_i}$$

be the Euler operator. It measures homogeneity: if $p(x)$ is homogeneous of degree r, then $Ep = rp$. Let

$$\Delta_Q = \sum_{i=1}^{s} \frac{\partial^2}{\partial x_i^2} - \sum_{j=s+1}^{s+t} \frac{\partial^2}{\partial x_j^2}$$

be the Laplacian associated with the quadratic form. The minus signs in the second sum reflect the negative directions of Q.

In this normalization, a Vignéras-type differential equation for a kernel Φ is

$$\big(\Delta_Q + 2\pi E\big)\,\Phi = 2\pi\lambda\,\Phi,$$

or equivalently

$$\big(\Delta_Q + 2\pi E - 2\pi\lambda\big)\,\Phi = 0.$$

The real number λ is a parameter which contributes to the modular weight of the resulting theta series. Since the precise numerical factors depend on where the Gaussian and $\mathrm{Im}\,\tau$-dependent factors are placed, this formula should be read together with the convention for the theta kernel. What is invariant is the structure of the condition: the signature Laplacian and the Euler operator must combine in a prescribed way.

Vignéras' theorem states, roughly, that if Φ satisfies this differential equation and has sufficient decay, together with corresponding decay for its first and second derivatives, then the theta series built from Φ transforms as a modular object. More precisely, the different cosets

$$\mu \in L^\vee/L$$

usually assemble into a vector-valued theta series, and Vignéras' theorem gives its modular transformation law under $SL(2,\mathbb{Z})$, with weight determined by n and λ and with multiplier determined by the discriminant form of the lattice. Thus the theorem is not merely a convergence statement. It identifies a differential equation on the kernel which guarantees that the lattice sum is compatible with modular transformation.

In the positive-definite case, the constant kernel $\Phi(x) = 1$ is already sufficient: convergence is supplied by the quadratic form itself. In indefinite signature, the quadratic form no longer supplies convergence in all directions. One must choose a kernel which suppresses the bad directions, but an arbitrary suppressing function will not transform modularly. Vignéras' equation singles out kernels for which convergence and modularity are simultaneously preserved.

The most important examples of such kernels are built from sign functions and error functions. A sign function is natural in indefinite problems because it selects a cone or chamber in the real vector space V. For instance, in signature $(1,1)$, a difference of signs can restrict the sum to a region where the quadratic form behaves effectively like a positive-definite form. Such kernels often produce convergent holomorphic theta series, but the discontinuity of the sign function obstructs clean modular behaviour.

Error functions provide the corresponding smooth replacements. The one-dimensional function

$$E(x) = 2\int_0^x e^{-\pi u^2}\,\mathrm{d}u$$

is a smooth approximation to $\operatorname{sign}(x)$, since

$$E(x) \longrightarrow \operatorname{sign}(x) \qquad \text{as } |x| \to \infty.$$

Replacing sign functions by error functions changes the kernel from a discontinuous, piecewise-constant object into a real-analytic one. In favourable cases, the smoothed kernel satisfies Vignéras' differential equation. The resulting theta series then has a modular completion: its holomorphic or piecewise-holomorphic part is corrected by explicitly non-holomorphic error-function terms.

This is the indefinite-theta analogue of the completion phenomena encountered earlier. For E_2, modularity is restored by adding the non-holomorphic term

$$-\frac{3}{\pi\,\operatorname{Im}\tau}.$$

For mock modular forms, modularity is restored by adjoining a non-holomorphic part controlled by the shadow. For indefinite theta series, modularity is restored by replacing discontinuous or insufficiently regular kernels with kernels satisfying Vignéras' equation, often built from error functions or their higher-dimensional generalizations.

The theorem therefore supplies the analytic bridge between indefinite lattice sums and modular forms. Starting from an indefinite lattice, one cannot simply write down the naive theta series and expect modularity. One must specify a kernel. The kernel must ensure convergence, encode the relevant chamber or cone, and satisfy the Euler–Laplacian equation required by Vignéras' theorem. When these conditions are met, the resulting theta series becomes a controlled modular object rather than a divergent or anomalous lattice sum [9, 54, 183].

Bibliography

[1] M Aganagic, V Bouchard, and A Klemm. "Topological Strings and (Almost) Modular Forms". In: *Commun. Math. Phys.* 277 (2008), pp. 771–819. DOI: 10.1007/s00220-007-0383-3. arXiv: hep-th/0607100.

[2] M Aganagic, A Klemm, M Marino, and C Vafa. "Matrix model as a mirror of Chern-Simons theory". In: *JHEP* 02 (2004), p. 010. DOI: 10.1088/1126-6708/2004/02/010. arXiv: hep-th/0211098.

[3] M Aganagic, M Marino, and C Vafa. "All loop topological string amplitudes from Chern-Simons theory". In: *Commun. Math. Phys.* 247 (2004), pp. 467–512. DOI: 10.1007/s00220-004-1067-x. arXiv: hep-th/0206164.

[4] O Aharony, A Hanany, and B Kol. "Webs of (p,q) five-branes, five-dimensional field theories and grid diagrams". In: *JHEP* 01 (1998), p. 002. DOI: 10.1088/1126-6708/1998/01/002. arXiv: hep-th/9710116.

[5] S Alexandrov. "Rank N Vafa–Witten invariants, modularity and blow-up". In: *Adv. Theor. Math. Phys.* 25.2 (2021), pp. 275–308. DOI: 10.4310/ATMP.2021.v25.n2.a1. arXiv: 2006.10074 [hep-th].

[6] S Alexandrov. "Vafa–Witten invariants from modular anomaly". In: *Commun. Num. Theor. Phys.* 15.1 (2021), pp. 149–219. DOI: 10.4310/CNTP.2021.v15.n1.a4. arXiv: 2005.03680 [hep-th].

[7] S Alexandrov. "Mock Modularity at Work, or Black Holes in a Forest". In: *Entropy* 27.7 (2025), p. 719. DOI: 10.3390/e27070719. arXiv: 2505.02572 [hep-th].

[8] S Alexandrov, S Banerjee, J Manschot, and B Pioline. "Multiple D3-instantons and mock modular forms I". In: *Commun. Math. Phys.* 353.1 (2017), pp. 379–411. DOI: 10.1007/s00220-016-2799-0. arXiv: 1605.05945 [hep-th].

[9] S Alexandrov, S Banerjee, J Manschot, and B Pioline. "Indefinite theta series and generalized error functions". In: *Selecta Mathematica* 24 (2018), pp. 3927–3972. arXiv: 1606.05495 [math.NT].

[10] S Alexandrov, S Banerjee, J Manschot, and B Pioline. "Multiple D3-instantons and mock modular forms II". In: *Commun. Math. Phys.* 359.1 (2018), pp. 297–346. DOI: 10.1007/s00220-018-3114-z. arXiv: 1702.05497 [hep-th].

[11] S Alexandrov and K Bendriss. "Mock modularity of Calabi-Yau threefolds". In: (2024). arXiv: 2411.17699 [hep-th].

[12] S Alexandrov and K Bendriss. "Modular anomaly of BPS black holes". In: *JHEP* 12 (2024), p. 180. DOI: 10.1007/JHEP12(2024)180. arXiv: 2408.16819 [hep-th].

[13] S Alexandrov, S Feyzbakhsh, A Klemm, B Pioline, and T Schimannek. "Quantum geometry, stability and modularity". In: *Commun. Num. Theor. Phys.* 18.1 (2024), pp. 49–151. DOI: 10.4310/CNTP.2024.v18.n1.a2. arXiv: 2301.08066 [hep-th].

[14] S Alexandrov, J Manschot, and B Pioline. "S-duality and refined BPS indices". In: *Commun. Math. Phys.* 380.2 (2020), pp. 755–810. DOI: 10.1007/s00220-020-03854-6. arXiv: 1910.03098 [hep-th].

[15] S Alexandrov, GW Moore, A Neitzke, and B Pioline. "$\mathbb{R}^3$ Index for Four-Dimensional $N = 2$ Field Theories". In: *Phys. Rev. Lett.* 114 (2015), p. 121601. DOI: 10.1103/PhysRevLett.114.121601. arXiv: 1406.2360 [hep-th].

[16] S Alexandrov and B Pioline. "Attractor flow trees, BPS indices and quivers". In: *Adv. Theor. Math. Phys.* 23.3 (2019), pp. 627–699. DOI: 10.4310/ATMP.2019.v23.n3.a2. arXiv: 1804.06928 [hep-th].

[17] S Alexandrov and B Pioline. "Black holes and higher depth mock modular forms". In: *Commun. Math. Phys.* 374.2 (2019), pp. 549–625. DOI: 10.1007/s00220-019-03609-y. arXiv: 1808.08479 [hep-th].

[18] M Alim, F Beck, A Biggs, and D Bryan. "Special geometry, quasi-modularity and attractor flow for BPS structures". In: (2023). arXiv: 2308.16854 [hep-th].

[19] R Anderson. "Exceptional Collections of Line Bundles for Smooth Toric Fano Surfaces and Threefolds". In: (2024). arXiv: 2403.09663 [math.AG].

[20] E Andriyash, F Denef, DL Jafferis, and GW Moore. "Bound state transformation walls". In: *JHEP* 03 (2012), p. 007. DOI: 10.1007/JHEP03(2012)007. arXiv: 1008.3555 [hep-th].

[21] E Andriyash, F Denef, DL Jafferis, and GW Moore. "Wall-crossing from supersymmetric galaxies". In: *JHEP* 1201 (2012), p. 115. DOI: 10.1007/JHEP01(2012)115. arXiv: 1008.0030 [hep-th].

[22] D Arcara, A Bertram, and M Lieblich. "Bridgeland-stable moduli spaces for K-trivial surfaces". In: *J. Eur. Math. Soc.(JEMS)* 15.1 (2013), pp. 1–38.

[23] D Arcara and E Miles. "Bridgeland Stability of Line Bundles on Surfaces". In: *Journal of Pure and Applied Algebra* 220.4 (2016), pp. 1655–1677. arXiv: 1401.6149 [math.AG].

[24] D Arcara and E Miles. "Projectivity of Bridgeland moduli spaces on del Pezzo surfaces of Picard rank 2". In: *International Mathematics Research Notices* 2017.11 (2017), pp. 3426–3462.

[25] H Argüz and P Bousseau. "The flow tree formula for Donaldson-Thomas invariants of quivers with potentials". In: *Compositio Mathematica* 158.12 (2022), pp. 2206–2249. arXiv: 2102.11200 [math.RT].

[26] SK Ashok, N Doroud, and J Troost. "Localization and real Jacobi forms". In: *JHEP* 04 (2014), p. 119. DOI: 10.1007/JHEP04(2014)119. arXiv: 1311.1110 [hep-th].

[27] SK Ashok and J Troost. "A Twisted Non-compact Elliptic Genus". In: *JHEP* 03 (2011), p. 067. DOI: 10.1007/JHEP03(2011)067. arXiv: 1101.1059 [hep-th].

[28] PS Aspinwall. "D-branes on Calabi-Yau manifolds". In: *Theoretical Advanced Study Institute in Elementary Particle Physics (TASI 2003): Recent Trends in String Theory*. 2004, pp. 1–152. DOI: 10.1142/9789812775108_0001. arXiv: hep-th/0403166.

[29] PS Aspinwall. "D-Branes on Toric Calabi-Yau Varieties". In: (2008). arXiv: 0806.2612 [hep-th].

[30] PS Aspinwall and LM Fidkowski. "Superpotentials for quiver gauge theories". In: *JHEP* 10 (2006), p. 047. DOI: 10.1088/1126-6708/2006/10/047. arXiv: hep-th/0506041.

[31] PS Aspinwall and SH Katz. "Computation of superpotentials for D-branes". In: *Commun. Math. Phys.* 264 (2006), pp. 227–253. DOI: 10.1007/s00220-006-1527-6. arXiv: hep-th/0412209.

[32] J Aspman, E Furrer, and J Manschot. "Cutting and gluing with running couplings in N=2 QCD". In: *Phys. Rev. D* 105.2 (2022), p. 025021. DOI: 10.1103/PhysRevD.105.025021. arXiv: 2107.04600 [hep-th].

[33] AOL Atkin and HPF Swinnerton-Dyer. "Modular forms on noncongruence subgroups". In: *Combinatorics* 19 (1971), pp. 1–25.

[34] S Banerjee, P Longhi, and M Romo. "Exponential BPS graphs and D-brane counting on toric Calabi-Yau threefolds: Part II". In: (2020). arXiv: 2012.09769 [hep-th].

[35] B Bates and F Denef. "Exact solutions for supersymmetric stationary black hole composites". In: *JHEP* 11 (2011), p. 127. DOI: 10.1007/JHEP11(2011)127. arXiv: hep-th/0304094.

[36] A Bayer and E Macri. "The space of stability conditions on the local projective plane". In: *Duke Math. J.* 160 (2011), pp. 263–322. DOI: 10.1215/00127094-1444249. arXiv: 0912.0043 [math.AG].

[37] G Beaujard, J Manschot, and B Pioline. "Vafa–Witten Invariants from Exceptional Collections". In: *Commun. Math. Phys.* 385.1 (2021), pp. 101–226. DOI: 10.1007/s00220-021-04074-2. arXiv: 2004.14466 [hep-th].

[38] K Behrend. *Donaldson-Thomas invariants via microlocal geometry*. 2005. arXiv: math/0507523 [math.AG].

[39] I Bena, M Berkooz, J de Boer, S El-Showk, and D Van den Bleeken. "Scaling BPS Solutions and pure-Higgs States". In: *JHEP* 1211 (2012), p. 171. DOI: 10.1007/JHEP11(2012)171. arXiv: 1205.5023 [hep-th].

[40] D Berghaus, H Monien, and D Radchenko. "A database of modular forms on noncongruence subgroups". In: (2023). arXiv: 2301.02135.

[41] D Berghaus, H Monien, and D Radchenko. "On the computation of modular forms on noncongruence subgroups". In: *Mathematics of Computation* 93.347 (2024), pp. 1399–1425. arXiv: 2207.13365.

[42] J de Boer, S El-Showk, I Messamah, and D Van den Bleeken. "Quantizing N=2 Multicenter Solutions". In: *JHEP* 05 (2009), p. 002. DOI: 10.1088/1126-6708/2009/05/002. arXiv: 0807.4556 [hep-th].

[43] AI Bondal. "REPRESENTATION OF ASSOCIATIVE ALGEBRAS AND COHERENT SHEAVES". In: *Mathematics of the USSR-Izvestiya* 34.1 (1990), p. 23. DOI: 10.1070/IM1990v034n01ABEH000583.

[44] D Borisov and D Joyce. "Virtual fundamental classes for moduli spaces of sheaves on Calabi-Yau four-folds". In: (2015). arXiv: 1504.00690 [math.AG].

[45] P Bousseau. "Scattering diagrams, stability conditions, and coherent sheaves on $\mathbb{P}^2$". In: *J. Algebraic Geom.* 31 (2022), pp. 593–686. arXiv: 1909.02985 [math.AG].

[46] P Bousseau. “Geometric helices on del Pezzo surfaces from tilting”. In: (2026). arXiv: 2603.22065 [math.AG].

[47] P Bousseau, P Descombes, B Le Floch, and B Pioline. “BPS Dendroscopy on Local $\mathbb{P}^2$”. In: *Commun. Math. Phys.* 405.4 (2024), p. 108. DOI: 10.1007/s00220-024-04938-3. arXiv: 2210.10712 [hep-th].

[48] T Bridgeland. “Stability conditions on a non-compact Calabi-Yau threefold”. In: *Commun. Math. Phys.* 266 (2006), pp. 715–733. DOI: 10.1007/s00220-006-0048-7. arXiv: math/0509048.

[49] T Bridgeland. “Stability conditions on triangulated categories”. In: *Annals Math.* 166.2 (2007), pp. 317–345. DOI: 10.4007/annals.2007.166.317. arXiv: math/0212237 [math.AG].

[50] T Bridgeland. “Scattering diagrams, Hall algebras and stability conditions”. In: *Alg. Geo.* 4 (2017), pp. 523–561. arXiv: 1603.00416 [math.AG].

[51] T Bridgeland, F Del Monte, and L Giovenzana. “Invariant Stability Conditions on Certain Calabi-Yau Threefolds”. In: (2024). arXiv: 2412.08531 [math.AG].

[52] T Bridgeland and D Stern. “Helices on del Pezzo surfaces and tilting Calabi–Yau algebras”. In: *Advances in Mathematics* 224.4 (2010), pp. 1672–1716.

[53] K Bringmann, A Folsom, K Ono, and L Rolen. “Harmonic Maass Forms and Mock Modular Forms: Theory and Applications”. In: *AMS Colloquium Publications* 64 (2017).

[54] K Bringmann and J Manschot. “From sheaves on $\mathbb{P}^2$ to a generalization of the Rademacher expansion”. In: *Am. J. of Math.* 135 (2013), pp. 1039–1065. arXiv: 1006.0915 [math.NT].

[55] A Brini and A Tanzini. “Exact results for topological strings on resolved $Y^{p,q}$ singularities”. In: *Commun. Math. Phys.* 289 (2009), pp. 205–252. DOI: 10.1007/s00220-009-0814-4. arXiv: 0804.2598 [hep-th].

[56] P Candelas, X De La Ossa, A Font, SH Katz, and DR Morrison. “Mirror symmetry for two parameter models. 1.” In: *Nucl. Phys. B* 416 (1994). Ed. by B Greene and ST Yau, pp. 481–538. DOI: 10.1016/0550-3213(94)90322-0. arXiv: hep-th/9308083.

[57] Y Cao and NC Leung. “Donaldson-Thomas theory for Calabi-Yau 4-folds”. In: (2014). arXiv: 1407.7659 [math.AG].

[58] A Ceresole and S Ferrara. “Black Holes and Attractors in Supergravity”. In: *Conference in Honor of Murray Gell-Mann’s 80th Birthday: Quantum Mechanics, Elementary Particles, Quantum Cosmology & Complexity*. 2010, pp. 316–328. DOI: 10.1142/9789814335614_0028. arXiv: 1009.4175 [hep-th].

[59] A Chattopadhyaya, J Manschot, and S Mondal. “Scaling black holes and modularity”. In: *JHEP* 03 (2022), p. 001. DOI: 10.1007/JHEP03(2022)001. arXiv: 2110.05504 [hep-th].

[60] TM Chiang, A Klemm, ST Yau, and E Zaslow. “Local mirror symmetry: Calculations and interpretations”. In: *Adv. Theor. Math. Phys.* 3 (1999), pp. 495–565. DOI: 10.4310/ATMP.1999.v3.n3.a3. arXiv: hep-th/9903053 [hep-th].

[61] Wy Chuang and DL Jafferis. "Wall Crossing of BPS States on the Conifold from Seiberg Duality and Pyramid Partitions". In: *Commun. Math. Phys.* 292 (2009), pp. 285–301. DOI: 10.1007/s00220-009-0832-2. arXiv: 0810.5072 [hep-th].

[62] C Closset and M Del Zotto. "On 5D SCFTs and their BPS quivers. Part I: B-branes and brane tilings". In: *Adv. Theor. Math. Phys.* 26.1 (2022), pp. 37–142. DOI: 10.4310/ATMP.2022.v26.n1.a2. arXiv: 1912.13502 [hep-th].

[63] C Closset, S Franco, J Guo, and A Hasan. "Graded quivers and B-branes at Calabi-Yau singularities". In: *JHEP* 03 (2019), p. 053. DOI: 10.1007/JHEP03(2019)053. arXiv: 1811.07016 [hep-th].

[64] C Closset, J Guo, and E Sharpe. "B-branes and supersymmetric quivers in 2d". In: *JHEP* 02 (2018), p. 051. DOI: 10.1007/JHEP02(2018)051. arXiv: 1711.10195 [hep-th].

[65] C Closset and H Magureanu. "The U-plane of rank-one 4d $\mathcal{N} = 2$ KK theories". In: *SciPost Phys.* 12 (2022), p. 065. DOI: 10.21468/SciPostPhys.12.2.065. arXiv: 2107.03509 [hep-th].

[66] C Closset and J Wynne. "Dualities and trialities in $\mathcal{N} = 2$ supersymmetric gauged quantum mechanics". In: (2025). arXiv: 2512.02984 [hep-th].

[67] I Coskun and J Huizenga. "Existence of semistable sheaves on Hirzebruch surfaces". In: *Advances in Mathematics* 381 (2021), p. 107636.

[68] A Dabholkar, S Murthy, and D Zagier. "Quantum Black Holes, Wall Crossing, and Mock Modular Forms". In: (2012). arXiv: 1208.4074 [hep-th].

[69] A Dabholkar, P Putrov, and E Witten. "Duality and Mock Modularity". In: *SciPost Phys.* 9.5 (2020), p. 072. DOI: 10.21468/SciPostPhys.9.5.072. arXiv: 2004.14387 [hep-th].

[70] F Del Monte and P Longhi. "Quiver Symmetries and Wall-Crossing Invariance". In: *Commun. Math. Phys.* 398.1 (2023), pp. 89–132. DOI: 10.1007/s00220-022-04515-6. arXiv: 2107.14255 [hep-th].

[71] F Del Monte and P Longhi. "The threefold way to quantum periods: WKB, TBA equations and q-Painlevé". In: *SciPost Phys.* 15.3 (2023), p. 112. DOI: 10.21468/SciPostPhys.15.3.112. arXiv: 2207.07135 [hep-th].

[72] F Denef. "Supergravity flows and D-brane stability". In: *JHEP* 08 (2000), p. 050. DOI: 10.1088/1126-6708/2000/08/050. arXiv: hep-th/0005049.

[73] F Denef. "Quantum quivers and Hall/hole halos". In: *JHEP* 10 (2002), p. 023. arXiv: hep-th/0206072.

[74] F Denef, BR Greene, and M Raugas. "Split attractor flows and the spectrum of BPS D-branes on the quintic". In: *JHEP* 05 (2001), p. 012. arXiv: hep-th/0101135.

[75] F Denef and GW Moore. "Split states, entropy enigmas, holes and halos". In: *JHEP* 1111 (2011), p. 129. DOI: 10.1007/JHEP11(2011)129. arXiv: hep-th/0702146 [HEP-TH].

[76] P Descombes. "Cohomological DT invariants from localization". In: *J. Lond. Math. Soc.* 106.4 (2022), pp. 2959–3007. DOI: 10.1112/jlms.12653. arXiv: 2106.02518 [math.AG].

[77] P Descombes and B Pioline. "On the Existence of Scaling Multi-Centered Black Holes". In: *Annales Henri Poincare* 23.10 (2022), pp. 3633–3665. DOI: 10.1007/s00023-022-01185-x. arXiv: 2110.06652 [hep-th].

[78] E Diaconescu and GW Moore. "Crossing the wall: Branes versus bundles". In: *Adv. Theor. Math. Phys.* 14.6 (2010), pp. 1621–1650. DOI: 10.4310/ATMP.2010.v14.n6.a2. arXiv: 0706.3193 [hep-th].

[79] F Diamond and J Shurman. *A First Course in Modular Forms*. Graduate Texts in Mathematics, Springer, 2005. DOI: 10.1007/978-0-387-27226-9.

[80] CF Doran and M Kerr. "Algebraic K-theory of toric hypersurfaces". In: *Communications in Number Theory and Physics* 5.2 (2011), pp. 397–600. arXiv: 0809.4669 [math.AG].

[81] MR Douglas. "D-branes, categories and N=1 supersymmetry". In: *J. Math. Phys.* 42 (2001), pp. 2818–2843. DOI: 10.1063/1.1374448. arXiv: hep-th/0011017.

[82] MR Douglas and GW Moore. "D-branes, quivers, and ALE instantons". In: (1996). arXiv: hep-th/9603167.

[83] JM Drézet and J Le Potier. "Fibrés stables et fibrés exceptionnels sur $\mathbb{P}_2$". In: *Annales scientifiques de l'École Normale Supérieure*. Vol. 18. 2. 1985, pp. 193–243.

[84] R Eager, SA Selmani, and J Walcher. "Exponential Networks and Representations of Quivers". In: *JHEP* 08 (2017), p. 063. DOI: 10.1007/JHEP08(2017)063. arXiv: 1611.06177 [hep-th].

[85] T Eguchi and Y Sugawara. "Non-holomorphic Modular Forms and SL(2,R)/U(1) Superconformal Field Theory". In: *JHEP* 03 (2011), p. 107. DOI: 10.1007/JHEP03(2011)107. arXiv: 1012.5721 [hep-th].

[86] M Eichler and D Zagier. *The Theory of Jacobi Forms*. Progress in Mathematics, 1985. DOI: 10.1007/978-1-4684-9162-3.

[87] L Fang, JW Hoffman, B Linowitz, A Rupinski, and H Verrill. "Modular Forms on Noncongruence Subgroups and Atkin–Swinnerton-Dyer Relations". In: *Experimental Mathematics* 19.1 (2010), pp. 1–27. DOI: 10.48550/arXiv.0805.2144. arXiv: 0805.2144 [math.NT].

[88] B Feng, A Hanany, and YH He. "D-brane gauge theories from toric singularities and toric duality". In: *Nucl. Phys.* B595 (2001), pp. 165–200. DOI: 10.1016/S0550-3213(00)00699-4. arXiv: hep-th/0003085 [hep-th].

[89] B Feng, A Hanany, and YH He. "Phase structure of D-brane gauge theories and toric duality". In: *JHEP* 08 (2001), p. 040. DOI: 10.1088/1126-6708/2001/08/040. arXiv: hep-th/0104259 [hep-th].

[90] S Ferrara and R Kallosh. "Supersymmetry and attractors". In: *Phys. Rev. D* 54 (1996), pp. 1514–1524. DOI: 10.1103/PhysRevD.54.1514. arXiv: hep-th/9602136.

[91] S Ferrara, R Kallosh, and A Strominger. "N=2 extremal black holes". In: *Phys. Rev. D* 52 (1995), R5412–R5416. DOI: 10.1103/PhysRevD.52.R5412. arXiv: hep-th/9508072.

[92] S Feyzbakhsh. "Explicit formulae for rank zero DT invariants and the OSV conjecture". In: (2022). arXiv: 2203.10617 [math.AG].

[93] S Feyzbakhsh and RP Thomas. "Curve counting and S-duality". In: *Épijournal de Géométrie Algébrique* 7, 15 (2023). DOI: 10.46298/epiga.2023.volume7.9818.

[94] S Feyzbakhsh and RP Thomas. "Rank r DT theory from rank 0". In: *Duke Math. J.* 173.11 (2024), pp. 2063–2116. DOI: 10.1215/00127094-2023-0050. arXiv: 2103.02915 [math.AG].

[95] S Franco. "4d crystal melting, toric Calabi-Yau 4-folds and brane brick models". In: *JHEP* 03 (2024), p. 091. DOI: 10.1007/JHEP03(2024)091. arXiv: 2311.04404 [hep-th].

[96] S Franco, S Lee, and RK Seong. "Brane Brick Models, Toric Calabi-Yau 4-Folds and 2d (0,2) Quivers". In: *JHEP* 02 (2016), p. 047. DOI: 10.1007/JHEP02(2016)047. arXiv: 1510.01744 [hep-th].

[97] D Gaiotto and T Johnson-Freyd. "Mock modularity and a secondary elliptic genus". In: *JHEP* 08 (2023), p. 094. DOI: 10.1007/JHEP08(2023)094. arXiv: 1904.05788 [hep-th].

[98] D Gaiotto, GW Moore, and A Neitzke. "Framed BPS States". In: *Adv. Theor. Math. Phys.* 17.2 (2013), pp. 241–397. DOI: 10.4310/ATMP.2013.v17.n2.a1. arXiv: 1006.0146 [hep-th].

[99] L Girardello, C Imbimbo, and S Mukhi. "On Constant Configurations and the Evaluation of the Witten Index". In: *Phys. Lett. B* 132 (1983), pp. 69–74. DOI: 10.1016/0370-2693(83)90224-1.

[100] L Göttsche. "The Betti numbers of the Hilbert scheme of points on a smooth projective surface". In: *Math. Ann.* 286 (1990), pp. 193–207.

[101] L Göttsche and M Kool. "Refined $SU(3)$ Vafa-Witten invariants and modularity". In: *Pure and Applied Mathematics Quarterly* 14.3-4 (2019), pp. 467–513. arXiv: 1808.03245 [math.AG].

[102] T Graefnitz. "Tropical correspondence for smooth del Pezzo log Calabi-Yau pairs". In: *J. Alg. Geom.* 31.4 (2022), pp. 687–749. DOI: 10.1090/jag/794. arXiv: 2005.14018 [math.AG].

[103] TW Grimm, A Klemm, M Marino, and M Weiss. "Direct Integration of the Topological String". In: *JHEP* 08 (2007), p. 058. DOI: 10.1088/1126-6708/2007/08/058. arXiv: hep-th/0702187.

[104] RK Gupta and S Murthy. "Squashed toric sigma models and mock modular forms". In: (2017). DOI: 10.1007/s00220-017-3069-5. arXiv: 1705.00649 [hep-th].

[105] B Haghighat, A Klemm, and M Rauch. "Integrability of the holomorphic anomaly equations". In: *JHEP* 10 (2008), p. 097. DOI: 10.1088/1126-6708/2008/10/097. arXiv: 0809.1674 [hep-th].

[106] JA Harvey, S Lee, and S Murthy. "Elliptic genera of ALE and ALF manifolds from gauged linear sigma models". In: *JHEP* 02 (2015), p. 110. DOI: 10.1007/JHEP02(2015)110. arXiv: 1406.6342 [hep-th].

[107] CP Herzog and RL Karp. "Exceptional collections and D-branes probing toric singularities". In: *JHEP* 02 (2006), p. 061. DOI: 10.1088/1126-6708/2006/02/061. arXiv: hep-th/0507175 [hep-th].

[108] CP Herzog and RL Karp. "On the geometry of quiver gauge theories (Stacking exceptional collections)". In: *Adv. Theor. Math. Phys.* 13.3 (2009), pp. 599–636. DOI: 10.4310/ATMP.2009.v13.n3.a1. arXiv: hep-th/0605177.

[109] L Hille and M Perling. “Exceptional sequences of invertible sheaves on rational surfaces”. In: *Compositio Mathematica* 147.4 (2011), pp. 1230–1280.

[110] K Hori, H Kim, and P Yi. “Witten Index and Wall Crossing”. In: *JHEP* 01 (2015), p. 124. DOI: 10.1007/JHEP01(2015)124. arXiv: 1407.2567 [hep-th].

[111] K Hori and C Vafa. “Mirror symmetry”. In: (2000). arXiv: hep-th/0002222.

[112] S Hosono. “Local mirror symmetry and type IIA monodromy of Calabi-Yau manifolds”. In: *Adv. Theor. Math. Phys.* 4 (2000), pp. 335–376. DOI: 10.4310/ATMP.2000.v4.n2.a5. arXiv: hep-th/0007071.

[113] S Hosono. “Central charges, symplectic forms, and hypergeometric series in local mirror symmetry”. In: (2004). arXiv: hep-th/0404043.

[114] Mx Huang, AK Kashani-Poor, and A Klemm. “The Ω deformed B-model for rigid $\mathcal{N} = 2$ theories”. In: *Annales Henri Poincare* 14 (2013), pp. 425–497. DOI: 10.1007/s00023-012-0192-x. arXiv: 1109.5728 [hep-th].

[115] Mx Huang and A Klemm. “Direct integration for general Ω backgrounds”. In: *Adv. Theor. Math. Phys.* 16.3 (2012), pp. 805–849. DOI: 10.4310/ATMP.2012.v16.n3.a2. arXiv: 1009.1126 [hep-th].

[116] MX Huang, A Klemm, and M Poretschkin. “Refined stable pair invariants for E-, M- and $[p, q]$-strings”. In: *JHEP* 11 (2013), p. 112. DOI: 10.1007/JHEP11(2013)112. arXiv: 1308.0619 [hep-th].

[117] C Imbimbo and S Mukhi. “Topological Invariance in Supersymmetric Theories With a Continuous Spectrum”. In: *Nucl. Phys. B* 242 (1984), pp. 81–92. DOI: 10.1016/0550-3213(84)90135-4.

[118] A Iqbal, C Kozcaz, and C Vafa. “The Refined topological vertex”. In: *JHEP* 10 (2009), p. 069. DOI: 10.1088/1126-6708/2009/10/069. arXiv: hep-th/0701156 [hep-th].

[119] DL Jafferis and GW Moore. “Wall crossing in local Calabi Yau manifolds”. In: (2008). arXiv: 0810.4909 [hep-th].

[120] V Jejjala, S Mondkar, A Mukhopadhyay, and R Raj. “Learning holographic horizons”. In: *Phys. Rev. D* 111.2 (2025), p. 026016. DOI: 10.1103/PhysRevD.111.026016. arXiv: 2312.08442 [hep-th].

[121] D Joyce and Y Song. *A theory of generalized Donaldson–Thomas invariants*. Vol. 217. 1020. American Mathematical Society, 2012.

[122] M Kaneko and D Zagier. “A generalized Jacobi theta function and quasimodular forms”. In: *The Moduli Space of Curves, Progress in Mathematics* 129 (1995), pp. 165–172. DOI: 10.1007/978-1-4612-4264-2_6.

[123] AM Kasprzyk. “Canonical toric Fano threefolds”. In: (2008). arXiv: 0806.2604 [math.AG].

[124] SH Katz, A Klemm, and C Vafa. “Geometric engineering of quantum field theories”. In: *Nucl. Phys. B* 497 (1997), pp. 173–195. DOI: 10.1016/S0550-3213(97)00282-4. arXiv: hep-th/9609239.

[125] H Kim, J Manschot, GW Moore, R Tao, and X Zhang. “Path Integral Derivations Of K-Theoretic Donaldson Invariants”. In: (2025). arXiv: 2509.23042 [hep-th].

[126] H Kim, J Park, Z Wang, and P Yi. "Ab Initio Wall-Crossing". In: *JHEP* 09 (2011), p. 079. DOI: 10.1007/JHEP09(2011)079. arXiv: 1107.0723 [hep-th].

[127] M Kontsevich and Y Soibelman. "Stability structures, motivic Donaldson-Thomas invariants and cluster transformations". In: (). arXiv: 0811.2435 [math.AG].

[128] M Kontsevich and Y Soibelman. "Motivic Donaldson-Thomas invariants: summary of results". In: *Mirror Symmetry and Tropical Geometry* (2009), pp. 55–89. arXiv: 0910.4315 [math.AG].

[129] M Kontsevich and Y Soibelman. "Wall-crossing structures in Donaldson-Thomas invariants, integrable systems and Mirror Symmetry". In: *Lect. Notes Union. Mat. Ital.* 15 (2014). Ed. by R Castano-Bernard, F Catanese, M Kontsevich, T Pantev, Y Soibelman, and I Zharkov, pp. 197–308. DOI: 10.1007/978-3-319-06514-4_6. arXiv: 1303.3253 [math.AG].

[130] R Kumar Gupta, S Murthy, and C Nazaroglu. "Squashed Toric Manifolds and Higher Depth Mock Modular Forms". In: *JHEP* 02 (2019), p. 064. DOI: 10.1007/JHEP02(2019)064. arXiv: 1808.00012 [hep-th].

[131] A Kuznetsov. "Derived categories of Fano threefolds". In: (2008). arXiv: 0809.0225 [math.AG].

[132] B Le Floch, B Pioline, and R Raj. "BPS Dendroscopy on Local $\mathbb{P}^1 \times \mathbb{P}^1$". In: *Annales Henri Poincaré* (2026). DOI: 10.1007/s00023-026-01666-3. arXiv: 2412.07680 [hep-th].

[133] S Lee and P Yi. "Framed BPS States, Moduli Dynamics, and Wall-Crossing". In: *JHEP* 04 (2011), p. 098. DOI: 10.1007/JHEP04(2011)098. arXiv: 1102.1729 [hep-th].

[134] W Lerche. "Introduction to Seiberg-Witten theory and its stringy origin". In: *Nucl. Phys. B Proc. Suppl.* 55 (1997). Ed. by A Connes, K Gawedzki, and J Zinn-Justin, pp. 83–117. DOI: 10.1016/S0920-5632(97)00073-X. arXiv: hep-th/9611190.

[135] D Levine and S Zhang. "Brill-Noether and existence of semistable sheaves on del Pezzo surfaces". In: *arXiv preprint arXiv:1910.14060* (2019).

[136] P Longhi. "Instanton Particles and Monopole Strings in 5D SU(2) Supersymmetric Yang-Mills Theory". In: *Phys. Rev. Lett.* 126.21 (2021), p. 211601. DOI: 10.1103/PhysRevLett.126.211601. arXiv: 2101.01681 [hep-th].

[137] A Maciocia. "Computing the walls associated to Bridgeland stability conditions on projective surfaces". In: *Asian Journal of Mathematics* 18.2 (2014), pp. 263–280. arXiv: 1202.4587.

[138] E Macrì and B Schmidt. "Lectures on Bridgeland Stability". In: *Moduli of Curves: CIMAT Guanajuato, Mexico 2016*. Springer, 2017, pp. 139–211. arXiv: 1607.01262 [math.AG].

[139] H Magureanu. "Seiberg-Witten geometry, modular rational elliptic surfaces and BPS quivers". In: *JHEP* 05 (2022), p. 163. DOI: 10.1007/JHEP05(2022)163. arXiv: 2203.03755 [hep-th].

[140] JM Maldacena, A Strominger, and E Witten. "Black hole entropy in M-theory". In: *JHEP* 12 (1997), p. 002. eprint: hep-th/9711053.

[141] J Manschot. "Stability and duality in N=2 supergravity". In: *Commun. Math. Phys.* 299 (2010), pp. 651–676. DOI: 10.1007/s00220-010-1104-x. arXiv: 0906.1767 [hep-th].

[142] J Manschot. "BPS invariants of semi-stable sheaves on rational surfaces". In: *Lett. Math. Phys.* 103 (2013), pp. 895–918. DOI: 10.1007/s11005-013-0624-7. arXiv: 1109.4861 [math-ph].

[143] J Manschot. "Vafa-Witten Theory and Iterated Integrals of Modular Forms". In: *Commun. Math. Phys.* 371.2 (2019), pp. 787–831. DOI: 10.1007/s00220-019-03389-5. arXiv: 1709.10098 [hep-th].

[144] J Manschot and S Mozgovoy. "Intersection cohomology of moduli spaces of sheaves on surfaces". In: (2016). DOI: 10.1007/s00029-018-0431-1. arXiv: 1612.07620 [math.AG].

[145] J Manschot, B Pioline, and A Sen. "A Fixed point formula for the index of multi-centered N=2 black holes". In: *JHEP* 1105 (2011), p. 057. DOI: 10.1007/JHEP05(2011)057. arXiv: 1103.1887 [hep-th].

[146] J Manschot, B Pioline, and A Sen. "Wall Crossing from Boltzmann Black Hole Halos". In: *JHEP* 07 (2011), p. 059. DOI: 10.1007/JHEP07(2011)059. arXiv: 1011.1258 [hep-th].

[147] J Manschot, B Pioline, and A Sen. "From Black Holes to Quivers". In: *JHEP* 11 (2012), p. 023. DOI: 10.1007/JHEP11(2012)023. arXiv: 1207.2230 [hep-th].

[148] J Manschot, B Pioline, and A Sen. "On the Coulomb and Higgs branch formulae for multi-centered black holes and quiver invariants". In: *JHEP* 05 (2013), p. 166. DOI: 10.1007/JHEP05(2013)166. arXiv: 1302.5498 [hep-th].

[149] D Maulik and J Shen. "Cohomological χ–independence for moduli of one-dimensional sheaves and moduli of Higgs bundles". In: *Geometry & Topology* 27.4 (2023), pp. 1539–1586.

[150] M Mezzarobba. "Rigorous Multiple-Precision Evaluation of D-Finite Functions in SageMath". In: *CoRR* abs/1607.01967 (2016). arXiv: 1607.01967.

[151] K Mohri, Y Onjo, and SK Yang. "Closed submonodromy problems, local mirror symmetry and branes on orbifolds". In: *Rev. Math. Phys.* 13 (2001), pp. 675–715. DOI: 10.1142/S0129055X01000867. arXiv: hep-th/0009072.

[152] L Mou. "Scattering diagrams of quivers with potentials and mutations". In: (2019). arXiv: 1910.13714 [math.AG].

[153] S Mozgovoy. "Invariants of moduli spaces of stable sheaves on ruled surfaces". In: (2013). arXiv: 1302.4134 [math.AG].

[154] S Mozgovoy. "Operadic approach to wall-crossing". In: *J. Algebra* 596 (2022), pp. 53–88. DOI: 10.1016/j.jalgebra.2021.12.032. arXiv: 2101.07636 [math.AG].

[155] S Mozgovoy and B Pioline. "Attractor invariants, brane tilings and crystals". In: *Annales Inst. Fourier* 75 (2025), p. 1331. arXiv: 2012.14358 [hep-th].

[156] S Mozgovoy and M Reineke. "On the noncommutative Donaldson-Thomas invariants arising from brane tilings". In: *Advances in mathematics* 223.5 (2010), pp. 1521–1544. arXiv: 0809.0117 [math.AG].

[157] S Murthy. "A holomorphic anomaly in the elliptic genus". In: *JHEP* 06 (2014), p. 165. DOI: 10.1007/JHEP06(2014)165. arXiv: 1311.0918 [hep-th].

[158] S Murthy and B Pioline. "Mock modularity from black hole scattering states". In: *JHEP* 12 (2018), p. 119. DOI: 10.1007/JHEP12(2018)119. arXiv: 1808.05606 [hep-th].

[159] M Najjar, J Tian, and YN Wang. "3d $\mathcal{N} = 2$ theories from M-theory on CY4 and IIB brane box". In: *JHEP* 05 (2024), p. 038. DOI: 10.1007/JHEP05(2024)038. arXiv: 2312.17082 [hep-th].

[160] C Nazaroglu. "r-Tuple Error Functions and Indefinite Theta Series of Higher-Depth". In: *Commun. Num. Theor. Phys.* 12 (2018), pp. 581–608. DOI: 10.4310/CNTP.2018.v12.n3.a4. arXiv: 1609.01224 [math.NT].

[161] J Oh and RP Thomas. "Counting sheaves on Calabi–Yau 4-folds, I". In: *Duke Math. J.* 172.7 (2023), pp. 1333–1409. DOI: 10.1215/00127094-2022-0059. arXiv: 2009.05542 [math.AG].

[162] A Okounkov, N Reshetikhin, and C Vafa. "Quantum Calabi-Yau and classical crystals". In: *Prog. Math.* 244 (2006), p. 597. DOI: 10.1007/0-8176-4467-9_16. arXiv: hep-th/0309208.

[163] R Pandharipande and RP Thomas. "Curve counting via stable pairs in the derived category". In: *Invent. Math.* 178 (2009), pp. 407–447. DOI: 10.1007/s00222-009-0203-9. arXiv: 0707.2348 [math.AG].

[164] M Perling. *Some quivers describing the derived categories of the toric del Pezzos*. 2003.

[165] B Pioline. "Corfu lectures on wall-crossing, multi-centered black holes, and quiver invariants". In: *PoS* Corfu2012 (2013). Ed. by K Anagnostopoulos, I Bakas, N Irges, J Kalinowski, A Kehagias, R Pittau, MN Rebelo, G Wolschin, and G Zoupanos, p. 085. DOI: 10.22323/1.177.0085. arXiv: 1304.7159 [hep-th].

[166] B Pioline. "Wall-crossing made smooth". In: *JHEP* 04 (2015), p. 092. DOI: 10.1007/JHEP04(2015)092. arXiv: 1501.01643 [hep-th].

[167] B Pioline and R Raj. "Black hole quantum mechanics and generalized error functions". In: *JHEP* 03 (2026), p. 179. DOI: 10.1007/JHEP03(2026)179. arXiv: 2507.08551 [hep-th].

[168] B Pioline and R Raj. "BPS Dendroscopy on local $\mathbb{F}_1$". 2026.

[169] AN Rudakov, A Bondal, A Gorodentsev, B Karpov, M Kapranov, S Kuleshov, A Kvichansky, DY Nogin, and S Zube. *Helices and vector bundles: Seminaire Rudakov*. Vol. 148. Cambridge University Press, 1990.

[170] A Sangiovanni and R Valandro. "M-theory geometric engineering for rank-0 3d $\mathcal{N} = 2$ theories". In: *JHEP* 03 (2025), p. 160. DOI: 10.1007/JHEP03(2025)160. arXiv: 2410.13943 [hep-th].

[171] N Seiberg and E Witten. "Electric - magnetic duality, monopole condensation, and confinement in N=2 supersymmetric Yang-Mills theory". In: *Nucl. Phys. B* 426 (1994), pp. 19–52. DOI: 10.1016/0550-3213(94)90124-4. arXiv: hep-th/9407087.

[172] T Shioda. "On elliptic modular surfaces". In: *J. Math. Soc. Japan* 24 (1972), pp. 20–59. DOI: 10.2969/jmsj/02410020.

[173] F Strömberg. “Noncongruence subgroups and Maass waveforms”. In: *Journal of Number Theory* 199 (2019), pp. 436–493.

[174] A Strominger. “Macroscopic entropy of N=2 extremal black holes”. In: *Phys. Lett. B* 383 (1996), pp. 39–43. DOI: 10.1016/0370-2693(96)00711-3. arXiv: hep-th/9602111.

[175] A Strominger and C Vafa. “Microscopic origin of the Bekenstein-Hawking entropy”. In: *Phys. Lett.* B379 (1996), pp. 99–104. eprint: hep-th/9601029.

[176] RP Thomas. “A Holomorphic Casson invariant for Calabi-Yau three folds, and bundles on K3 fibrations”. In: *J. Diff. Geom.* 54.2 (2000), pp. 367–438. arXiv: math/9806111.

[177] RP Thomas. “Equivariant K-Theory and Refined Vafa-Witten Invariants”. In: *Commun. Math. Phys.* 378.2 (2020), pp. 1451–1500. DOI: 10.1007/s00220-020-03821-1. arXiv: 1810.00078 [math.AG].

[178] Y Toda. “Bogomolov-Gieseker type inequality and counting invariants”. In: (2011). DOI: 10.1112/jtopol/jts037. arXiv: 1112.3411 [math.AG].

[179] J Top and N Yui. “Explicit equations of some elliptic modular surfaces”. In: *The Rocky Mountain Journal of Mathematics* 37 (2007), pp. 663–687.

[180] J Troost. “The non-compact elliptic genus: mock or modular”. In: *JHEP* 06 (2010), p. 104. DOI: 10.1007/JHEP06(2010)104. arXiv: 1004.3649 [hep-th].

[181] H Uehara. “Exceptional collections on toric Fano threefolds and birational geometry”. In: (2010). arXiv: 1012.4086 [math.AG].

[182] C Vafa and E Witten. “A Strong coupling test of S duality”. In: *Nucl.Phys.* B431 (1994), pp. 3–77. DOI: 10.1016/0550-3213(94)90097-3. arXiv: hep-th/9408074 [hep-th].

[183] MF Vignéras. “Séries thêta des formes quadratiques indéfinies”. In: *Springer Lecture Notes* 627 (1977), pp. 227–239.

[184] Y Xiong. “Invariant stability conditions on local $\mathbb{P}^1 \times \mathbb{P}^1$ (after Del Monte-Longhi)”. In: (2025). arXiv: 2404.05232 [math.AG].

[185] S Yamaguchi and ST Yau. “Topological string partition functions as polynomials”. In: *JHEP* 07 (2004), p. 047. DOI: 10.1088/1126-6708/2004/07/047. arXiv: hep-th/0406078.

[186] D Zagier. “Elliptic Modular Forms and Their Applications”. In: *The 1-2-3 of Modular Forms, Springer* (2008), pp. 1–103.

[187] D Zagier. “Ramanujan’s mock theta functions and their applications (after Zwegers and Ono-Bringmann)”. In: *Astérisque* 326 (2009), Exp. No. 986, vii–viii, 143–164 (2010).

[188] J Zhao. “Moduli Spaces of Sheaves on General Blow-ups of $\mathbb{P}^2$”. In: *arXiv preprint arXiv:2208.03619* (2022).

[189] S Zwegers. *Mock Theta Functions*. PhD dissertation, Utrecht University. 2002.

List of Figures

2.1 Elementary split attractor flow for a decomposition $\Gamma \to \Gamma_1 + \Gamma_2$. Taken from [16, Figure 1]. 22
2.2 Discrete attractor flow data along a branch of a rooted tree. Taken from [16, Figure 5] 23
2.3 True walls and fake walls in the three-center stability plane. Taken from [16, Figure 4] 25
2.4 A three-leaf split attractor flow tree. Taken from [16, Figure 3]. 26
2.5 Schematic relation between Coulomb and Higgs descriptions of a quiver bound state. Taken from [73, Figure 6]. 34

3.1 Reflexive Polyhedra Δ_B in two dimensions. $\hat{\Delta}_p = \Delta_{17-p}$ for $p = 1, \ldots, 6$. $\Delta_{7,8,9,10}$ are self-dual. Case 1 is the polyhedron representing $\mathbb{P}^2$; Cases 2, 3, and 4 are the Hirzebruch surfaces $\mathbb{F}_0 = \mathbb{P}^1 \times \mathbb{P}^1$, $\mathbb{F}_1$, $\mathbb{F}_2$, and the others are various blow-ups of these cases. Taken from [60, Figure 1]. 59
3.2 Three-node quiver for local $\mathbb{P}^2$, with fractional branes $\mathcal{E}_i^\vee$ at the nodes and three arrows along each edge corresponding to the relevant Ext-group generators. . . 68
3.3 Phase-I quiver for local $\mathbb{F}_0$, associated with the fractional brane basis (3.57). The multiplicities of the arrows are determined by the antisymmetrized Euler form (3.61). 68
3.4 Examples of two-dimensional scattering diagrams. Left: the A_2 quiver, with walls corresponding to the three indecomposable representations. Right: the Kronecker quiver, with walls corresponding to the dimension vectors of indecomposable representations. Adapted from [50, Figures 1 and 2]. 72
3.5 Contractible loop and reordering of central-charge rays in the derivation of the KS product formula. Taken from [21, Figures 1 and 2]. 75
3.6 One-dimensional moduli space of local $K_{\mathbb{P}^2}$, showing the large-radius point $z = 0$, the conifold point $z = -1/27$, and the orbifold point $1/z = 0$, together with generators of the corresponding monodromies. Taken from [105, Figure 1]. 79
3.7 Placeholder: resolved moduli space of local $K_{\mathbb{F}_0}$, showing the large-radius divisors L_1, L_2, the conifold divisors E, C, and the additional components F_1, F_2. [105] 80
3.8 Placeholder: local geometry of the conifold coordinates $z_c^1 = 0$ and $z_c^2 = 0$ for local $K_{\mathbb{F}_0}$, showing their intersection with the discriminant locus $\Delta = 0$. [105] . 81
3.9 Paths γ_v generating the fundamental group of the U-plane. The path around infinity is equal to minus the sum of all the other paths, $\gamma_\infty = -(\gamma_1 + \cdots + \gamma_k)$. Taken from [65, Figure 1]. 83
3.10 Fundamental domains for $\Gamma^0(4)$ governing the modular parametrization of the pure $SU(2)$ Coulomb branch. The left panel shows a standard choice of fundamental domain, with width-one cusps at $\tau = 0$ and $\tau = 2$ and the width-four cusp at $\tau = i\infty$. The right panel shows an equivalent presentation in which the cusp at $\tau = \pm 2$ is split, with the branch cut of the periods indicated by the dashed line. Adapted from [65, Figure 4]. 84

4.1 Initial rays for the large volume scattering diagram of local $\mathbb{F}_0$ in the (s,t) plane at $m = 1/2$. 88
4.2 Quiver associated to the Ext-exceptional collection (4.3), sometimes known as phase II or orbifold quiver. This is accompanied by the quartic superpotential W in (4.65). 90
4.3 Scattering diagram of the orbifold quiver for $m = 1/2$, keeping rays with height $\sum_i N_i \leq 8$. 91
4.4 Fundamental domain $\mathcal{F}$ (in blue) for the action of $\Gamma_0(4)$ on the upper half-plane, and its images under $\tau \mapsto \frac{\tau-1}{4\tau-3}$ and $\tau \mapsto \frac{3\tau-1}{4\tau-1}$. The cusps at $\tau = (\mathrm{i}\infty, 0, \frac{1}{2})$ correspond to the large volume limit $z = 0$, conifold point $z = \frac{1}{4(1+\sqrt{\lambda})^2}$ and dual conifold point $z = \frac{1}{4(1-\sqrt{\lambda})^2}$, while the branch point τ_B corresponds to $z = \infty$. The dotted lines show the cuts joining τ_B and its images to $\tau = \frac{1}{2}$ along geodesic circles. 91
4.5 (Putative) boundary of the space of geometric stability conditions, for $m = 0.4 + 0.3\mathrm{i}$. The red solid line is the locus $\mathrm{Im}\, T = 0$. Along the blue, yellow, green and orange lines, the central charge associated to $\mathcal{O}(0,0), \mathcal{O}(1,0), \mathcal{O}(0,1)$ (or rather its image $\mathcal{O}(1,0)$ through the cut) and $\mathcal{O}(1,1)$ become real and negative, destabilizing skyscraper sheaves. The green and orange lines intersect at a point τ_b where $\mathrm{Im}\, T = \mathrm{Im}\, T_D = 0$, and similarly the blue and yellow lines intersect at $\tilde{\tau}_b$ where where $\mathrm{Im}\, T = \mathrm{Im}\, T_D = 0$. Along the segment of the locus $\mathrm{Im}\, T = 0$ joining τ_b to τ_B, skyscraper sheaves are instead destabilized by D2-branes. The fundamental domain $\widehat{\mathcal{F}}$ is defined as the region above the blue, yellow, green, orange lines with the red segment from τ_b to τ_B excised. 92
4.6 Initial rays emitted from $\tau = 0$ (left) and $\tau = \frac{1}{2}$ (right), for $m = 1/2$ and $\psi = 0$. Rays with positive and negative rank r are shown in magenta and blue, respectively. 93
4.7 Scattering diagram $\mathcal{D}^{\Pi}_{m,\psi}$ along the Π-stability slice for $m = 0.4$, $\psi = 0$. For clarity, only primary scatterings are shown. 94
4.8 Scattering diagram $\mathcal{D}^{\Pi}_{m,\psi}$ for $m = 0.4$, $\psi = 0.4$ below the first critical value $\psi_{cr} \simeq 0.545$. 95
4.9 Scattering diagram $\mathcal{D}^{\Pi}_{m,\psi}$ for $m = 0.4$, $\psi = 0.68$ between the first two critical values $\psi_{cr} \simeq 0.545$ and $\tilde{\psi}_{cr} \simeq 0.832$. 95
4.10 Scattering diagram $\mathcal{D}^{\Pi}_{m,\psi}$ for $m = 0.4$, $\psi = 0.98$ above $\tilde{\psi}_{cr} \simeq 0.832$. 96
4.11 Embedding of the orbifold scattering diagram into the Π-stability scattering diagram around $\tau_B - 1 = \frac{\mathrm{i}-1}{4}$, for $m = 1/2$ and $\psi = 0.72$. The initial rays $\mathcal{R}(\gamma_i)$ for the exceptional collection (4.117) are shown in green, blue, red and orange. The scatterings of $\{\gamma_1, \gamma_2\}$ and $\{\gamma_2, \gamma_3\}$ take place on one sheet, and those of $\{\gamma_3, \gamma_4\}$ and $\{\gamma_4, \gamma_1\}$ on another sheet, glued along the branch cut (shown in red dashed line). 97
4.12 Contour lines of $s = \frac{\mathrm{Im}\, T_D}{\mathrm{Im}\, T}$ for $m = 1/2$. 98
4.13 Lower bound $\delta_{\mathrm{DLP}}(\eta, a, b)$ on the discriminant of non-exceptional H-stable sheaves for $\eta = 1$, obtained by retaining exceptional sheaves with rank up to 19. Figure adapted from [67, Fig. 5]. 99
4.14 Approximate shape of $\delta(s, \eta, M_1)$ for $\eta = 1, M_1 = 1/4$. The red dots indicate the corresponding lowest values arising from exceptional stable bundles. . . . 106

4.15 For $m = 0$ (hence $\lambda = 1$), the contours with fixed $s = \frac{\mathrm{Im}\, T_D}{\mathrm{Im}\, T}$ in the strip $\tau_1 \in (0,1)$, shown in orange, all converge to $\tau = \frac{1}{2}$. The contours with fixed (and real) $t = \sqrt{2w - s^2}$ approach $\tau = 0$ and $\tau = 1$ when $t \to 0$ (shown in dashed line), but stay away from $\tau = \frac{1}{2}$. In the region above the dashed line, Π stability is related to large volume stability by $GL(2,\mathbb{R})^+$. 107

4.16 Image of the fundamental domain $\mathcal{F}$ and its translates into the (s,w) plane for $m = 0$. The dashed line is the parabola $w = \frac{1}{2}s^2$, the red vertical segments are the images of the half-circles on the boundary of the fundamental domain and its translates and the segments in magenta correspond to the values of (s,w) around the dual conifolds $\tau \in \frac{1}{2} + \mathbb{Z}$. The blue curve denotes the (continuous part of the) lower bound $\frac{1}{2}s^2 - \frac{1}{2}\delta(s,1,0)$ of w in the geometric domain (4.49), and the red dots are the discontinuous values occurring at slopes of exceptional stable bundles. The circled ones are those which are massless at the conifold points $\tau = k$ and $\tau = k + \frac{1}{2}$. 108

4.17 For $m = \frac{1}{2}$, the contours with fixed $s = \frac{\mathrm{Im}\, T_D}{\mathrm{Im}\, T}$ in the strip $\tau_1 \in (0,1)$, shown in orange, converge either to $\tau = \frac{1+\mathrm{i}}{4}$ or $\tau = \frac{3+\mathrm{i}}{4}$. The contours with fixed (and real) $t = \sqrt{2w - (s - \frac{1}{4})^2}$ stay well above the conifold and branch points In the region above the dashed line $t = 0$, Π stability is related to large volume stability by $GL(2,\mathbb{R})^+$. 109

4.18 Image of the fundamental domain $\mathcal{F}$ and its translates into the (s,w) plane, shown for $m = 1/4$. The dashed line is the parabola $w = \frac{1}{2}(s - \frac{m}{2})^2$, the red vertical segments are the images of the half-circles on the boundary of the fundamental domain and its translates and the segments in magenta correspond to the values of (s,w) on an infinitesimal circle around the branch points. The blue curve denotes the (continuous part of the) lower bound $\frac{1}{2}(s - \frac{m}{2})^2 - \frac{1}{2}\delta(s,1,m)$ on w in the geometric domain (4.49), and the red dots are the discontinuous values occurring at slopes of exceptional stable bundles. The circled ones are those which are massless at the conifold points $\tau = k$ and $\tau = k + \frac{1}{2}$, lying along the shifted parabolas $w - \frac{1}{2}(s - \frac{m}{2})^2 = -\frac{m^2}{8}$ and $-\frac{(1-m)^2}{8}$, respectively. 110

4.19 Contours with fixed s (orange) or fixed $t = \sqrt{2w_1}$ (black) in the τ half-plane, for $m = 0.4 + 0.3\mathrm{i}$. In the region above the dashed line, corresponding to $t = 0$, Π stability is related to large volume stability by $GL(2,\mathbb{R})^+$. The blue, yellow, green, dark orange and red lines delimit (putatively) the domain of geometric stability conditions, as in Fig. 4.5. 112

4.20 Values of w_1 (defined in (4.41)) along the various components of the boundary of the space of geometric stability conditions, including either side of the locus $\mathrm{Im}\, T = 0$, compared to the sufficient lower bound $-2/(9\eta)$ (dashed line) following from $\delta(s,\eta,M_1) > \frac{4}{9}$. The value of m and the color coding for the boundary components is the same as in Figs. 4.5 and 4.19. 113

4.21 Scattering diagram $\mathcal{D}^o_\mu$ for the orbifold quiver at $\mu = 1/4$. The shaded area corresponds to the generalized 'collimation chamber' (4.75). 118

4.22 Quiver associated to the Ext-exceptional collection (4.82), sometimes known as phase I quiver. This is accompanied by the cubic superpotential W in (4.84). . 119

4.23 Scattering diagram $\mathcal{D}^I_\mu$ for the phase I quiver at $\mu = 1/2$, keeping rays with height $\sum_i N'_i \leq 8$, with $\max(n_1, n_2) \leq 4$ at each intersection. Up to truncation effects, it coincides with the scattering diagram for the orbifold quiver in Fig. 4.3 when $\zeta_4 < 0$, i.e. outside the shaded region. 121
4.24 Scattering diagram in the (x, y) plane at $m = \frac{1}{2}$, including only primary scattering of initial rays. 122
4.25 Initial rays for the large volume scattering diagram in the (x, t) plane at $m = 1/4$. The shaded blue and red regions correspond to the validity of the Ext-exceptional collection (4.82) tensored with $\mathcal{O}(k, k)$ and $\mathcal{O}(k, k-1)$, respectively. 123
4.26 Images of the phase I quiver under mutations μ_1 and $\mu_2\mu_3$. 127
4.27 Initial rays in the (x, t) plane for $m = 0$. The orange rays are obtained from the phase I collection by iterating the mutations μ_1 and $\mu_2\mu_3$. The dense yellow rays arise from the scattering of $\mathcal{R}(\mathcal{O}(1,0))$ and $\mathcal{R}(\mathcal{O}(0,-1)[1])$ with $|\langle\gamma_1, \gamma_2\rangle| = 4$. 128
4.28 Initial rays for the large volume scattering diagram $\mathcal{D}^\Lambda_{m,0}$ for fixed $m = 0.4 + 0.3\mathrm{i}$, and their primary scatterings. The red and magenta lines denote the walls of marginal stability for the binary trees $\{\mathcal{O}(1,0), \mathcal{O}(0,-1)[1]\}$ and $\{\mathcal{O}(1,1), \mathcal{O}(0,-1)[1]\}$. 128
4.29 Scattering diagram $\mathcal{D}^\Pi_{m,\psi}$ for $m = 0$, $\psi = 0.01$, keeping only primary scatterings. Note that rays related by fiber-based duality are indistinguishable, with further degeneracies when $r = 0$. As $\psi \to 0$, the intersection point between $\mathcal{O}(0,-1)[1], \mathcal{O}(-1,0)[1]$ and $\mathcal{O}(0,0)$ coalesces with $\tau = 0$, similar to Fig. 4.27. 130
4.30 $\mathcal{V}_\psi$ and $\tilde{\mathcal{V}}_\psi$ as a function of ψ, for $m = 1/4$. The values ψ^+_{cr} and $\tilde{\psi}^+_{\mathrm{cr}}$ correspond to the transitions where $\mathcal{V}_\psi = 0$ and $\tilde{\mathcal{V}}_\psi = 1 - \mu$, respectively. For $m = 1/2$, $\tilde{\mathcal{V}}_\psi = \mathcal{V}_\psi + \frac{1}{2}$ and the two critical values coincide. 132
4.31 Left: Domain of validity of the quiver descriptions based on the collections (4.117), (4.120), for $m = 0.3$. The solid green and red lines are the boundaries of Δ_ψ and $\tilde{\Delta}_\psi$ and correspond to straight lines in the (x, y) plane. Right: the same regions in the (x, y) plane, together with some of their translates; the overlaps correspond to different stability conditions that map to the same values of x, y coordinates. The region above all of these translates is W_ψ. 133
4.32 Top: Trees contributing to the structure sheaf index $\Omega([1,0,0,0])$ as function of m (real) and ψ. Bottom: Trees in τ-plane for $m = 0.35$, varying ψ. Note that the tree $\mathcal{T}_4$ does not arise for this value. 138
4.33 Top: Trees contributing to the D2 index $\Omega([0,1,0,0])$ as function of m (real) and ψ. Bottom: Trees in τ-plane for $m = 0.5$, varying ψ. 139
4.34 Convergence regions of the expansions around $\tau = \mathrm{i}\infty, 0, 1, \frac{1}{2}$ (halfplane and disks intersected with the fundamental domain, shaded in blue, orange, green, red, respectively), and domains where each of these expansions are used, as well as expansion around images of the branch point τ_B (black dot, connected to $\tau = \frac{1}{2}$ by the cut). Different values of m require different subsets of the expansions. Left: $m = 0.4$, involving the first six expansions. Right: $m = 0.4 + 0.3\mathrm{i}$, involving the first seven expansions (the last two would become relevant for other values of m). 158

5.1 Lower bound $\delta_{\mathrm{DLP}}(M, a, b)$ on the discriminant of non-exceptional H_M-stable sheaves for $M = 0$, obtained by retaining exceptional sheaves with rank up to 19. Figure adapted from [67, Fig. 6]. 166

5.2 Approximate shape of $\delta(s,m)$ for $m = 1/4$. The red dots indicate the corresponding lowest values arising from exceptional stable bundles. 168
5.3 Quivers corresponding to the exceptional collections C, C', C''. Observe that the usual quiver for $S = \mathbb{P}^2$ arises by merging the nodes 2 and 3 in the first quiver (a procedure called Higgsing). This is possible because there is only one arrow from 2 to 3, ... 170
5.4 Domains of validy of the quiver descriptions covering the real axis, assuming that $-\frac{1}{3} < m < 0$ (plotted here for $m = -\frac{1}{10}$). Quivers obtain by tensoring the Ext-exceptional collections C (5.32), C' (5.40) and C'' (5.43) with a suitable line bundle $\mathcal{O}(m_F, m_B)$ are plotted in blue, red and green, respectively. Grey lines correspond to the geometric rays for $\mathcal{O}(d_F, d_B)$ and $\mathcal{O}(d_F, d_B)[1]$. Those which lie inside quiver domains must necessarily decay before reaching this domain. Initial rays coming from below the parabola are plotted in thick black lines. . . 175
5.5 Similar as Figure 5.4, now assuming $0 < m < \frac{1}{3}$ (plotted for $m = \frac{1}{10}$). 175
5.6 Similar as Figure 5.4, now assuming $\frac{1}{3} < m < \frac{2}{3}$ (plotted for $m = \frac{2}{5}$). 176
5.7 Initial and secondary rays in affine coordinates (x, y) for $-\frac{1}{3} < m < 0$ (here drawn for $m = -\frac{1}{6}$). Secondary rays originating from collisions with Dirac product $\kappa = 1, 2, 3$ are shown in blue, green, red, respectively. Collisions with $\kappa = 1, 2, 3$ occur below, at and above the parabola, respectively. 176
5.8 Initial rays in the (m, s) plane at the boundary $t = 0$ of the large volume slice. The structure sheaf tensored with $\mathcal{O}(1, 1)$ is stable only for $m > -\frac{1}{3}$ (thick blue line), while the correspond anti-brane is stable only for $m < 1$ (in red). In the range $-\frac{1}{3} < m < 1$, both objects are initial rays of the scattering diagram below the parabola; outside this range, they are level-k bound states of the Kronecker quiver K_2 associated to the same initial rays, shown in light blue in plot on the left and labelled in the magnified plot on the right. The remaining initial rays are shown in orange and green. 178
5.9 Real slice of the discriminant locus for local $\mathbb{F}_1$. The slices $|\lambda| = cte$ correspond to lines of fixed $\mathrm{Im}(T_F - 2T_B)$. The Kähler cone of $\mathbb{F}_1$ corresponds to the first quadrant $\mathrm{Im}\, T_F > 0, \mathrm{Im}\, T_B > 0$. The Kähler cone of the flopped geometry corresponds to $\mathrm{Im}\, T_B < 0, \mathrm{Im}(T_F + T_B) > 0$ i.e. $\mathrm{Im}\, T_C > 0, \mathrm{Im}\, T_H > 0$. The dashed and dotted lines correspond to loci with fixed λ equal to $(-27/256)^{1/3}$ and 1, respectively. 183
5.10 A fundamental domain for the non-congruence subgroup Γ. The blue dots correspond to elliptic points of order 3. 198

6.1 Decomposition of the two-body Witten index into contributions from bound states (a) and scattering states (b). Their sum (c) produces a smooth interpolation described by the error function $E_1(c)$, consistent with the modular completion of the BPS index. 217
6.2 Contour integral in the D plane 219
6.3 Schröder trees contributing to the modular completion for $N = 3, N_i = 1$ 227
6.4 Schröder trees contributing to the modular completion for $N = 4, N_i = 1$ 229

A.1 A fundamental domain for the action of $SL(2,\mathbb{Z})$ on $\mathcal{H}$. 245

List of Tables

3.1 Kodaira singular fibers for rank-one Seiberg–Witten geometries. Monodromy entries are representatives of conjugacy classes in $SL(2,\mathbb{Z})$. 83

4.1 Trees contributing to the index $\Omega_{s,t}(\gamma)$ at $t \to \infty$, for m in the range specified in the third column. As m reaches the ends of the interval, the last wall of marginal stability shrinks to zero radius. 125

5.1 Quiver descriptions at $t = 0$, obtained by tensoring one of the Ext-collections C (5.32), C' (5.40) and C'' (5.43) with a suitable line bundle $\mathcal{O}(m_F, m_B)$. When both a D4-brane $\mathcal{O}(d_F, d_B)$ and an anti D4-brane $\mathcal{O}(d'_F, d'_B)[1]$ with $|\langle\gamma, \gamma'\rangle| = 2$ enter the boundary at the same point, they produce an infinite set of rays, indexed by $k \in \mathbb{N}$. Quiver descriptions outside the range $s_{\min} < s < s_{\min} + 1$ covered in the table can be obtained by tensoring with $\mathcal{O}(3k, 2k)$. 174

5.2 Charges, contributing trees for $m = -\frac{1}{10}$, and the nonnegative-power part of the refined index $\Omega_H(y)$ (the full Laurent polynomial is symmetric under $y \leftrightarrow y^{-1}$). The rank 0 entries are consistent with the refined D2-D0 indices in (5.15). . . . 177

5.3 Periods at conifold points. 200

Résumé en français

Dans la théorie des cordes de type II sur des variétés de Calabi–Yau de dimension trois, les trous noirs BPS se réalisent, à faible couplage, comme des états liés de D-branes. Leur dénombrement est régi par des indices BPS protégés, ou invariants de Donaldson–Thomas (DT) généralisés. Ces invariants, ainsi que leurs versions raffinées, dépendent d'une condition de stabilité de Bridgeland et subissent des sauts à travers les murs de stabilité marginale. Pour déterminer les spectres BPS dans des exemples concrets et leur réorganisation dans l'espace des stabilités, cette thèse utilise le cadre de la « dendroscopie BPS », qui reconstruit les invariants DT à partir de rayons initiaux associés à des objets sphériques sans masse au bord de l'espace des stabilités.

La première partie développe cette méthode pour les fibrés canoniques au-dessus de $\mathbb{F}_0 = \mathbb{P}^1 \times \mathbb{P}^1$ et de $\mathbb{F}_1$. Pour la géométrie locale de $\mathbb{F}_0$, elle construit des diagrammes de diffusion près du point orbifold, sur la tranche de grand volume et sur la tranche physique de Π-stabilité. Après prolongement du diagramme de grand volume sous la parabole naturelle, les familles infinies de rayons de bord proviennent de la diffusion d'un nombre fini de paires pures D4–anti-D4, de couplage de Dirac ± 2. Sur la tranche physique, des points de ramification et des coupures apparaissent pour des valeurs génériques du paramètre de masse, c'est-à-dire du couplage de jauge en dimension cinq, si bien que l'espace des stabilités devient un revêtement infini du demi-plan supérieur, à feuillets étiquetés par $\mathbb{Z}^4$. Le diagramme est alors déterminé par ses limites de grand volume et d'orbifold, ainsi que par l'invariance de monodromie, et porte une action d'une extension de $\Gamma_0(4)$ par $\mathbb{Z}^4$.

Pour la géométrie locale de $\mathbb{F}_1$, l'existence d'une courbe effective de self-intersection négative empêche les fibrés en droites d'être stables partout sur la tranche de grand volume. Après prolongement du diagramme sous la parabole, les rayons initiaux se réorganisent en paires pures D4–anti-D4 associées à une hélice géométrique de faisceaux inversibles. Du côté miroir, la famille de courbes elliptiques possède génériquement un type de ramification $I_8 + 4I_1$ et n'admet pas, en général, de paramétrisation modulaire par un sous-groupe de $\mathrm{PSL}(2,\mathbb{Z})$. À la valeur spéciale $\ell = -27/256$, deux fibres I_1 entrent en collision et produisent un point d'Argyres–Douglas de type H_0 ; le groupe de monodromie se réduit alors à une extension d'un sous-groupe non congruent de genre zéro $\Gamma \subset \mathrm{PSL}(2,\mathbb{Z})$, d'indice 10, donnant une paramétrisation modulaire de la branche de Coulomb et un diagramme de diffusion Γ-invariant sans coupures.

La seconde partie étudie la complétion modulaire des séries génératrices des invariants D4-D2-D0. Lorsque la charge D4 se décompose en n constituants irréductibles, la S-dualité prédit des formes modulaires mock de profondeur $n-1$, dont la complétion non holomorphe est gouvernée par des fonctions d'erreur généralisées. La thèse dérive ces termes à partir de la mécanique quantique supersymétrique des trous noirs BPS multicentrés. Par localisation, l'indice de Witten raffiné total se ramène à une intégrale finie qui se factorise en une intégrale sur l'espace des phases des solutions multicentrées et une intégrale sur les directions transverses associées aux paramètres de Fayet–Iliopoulos dynamiques. Cette dernière produit les fonctions d'erreur généralisées et identifie l'anomalie modulaire à l'asymétrie spectrale du continuum des états de diffusion.

Ces résultats fournissent de nouveaux outils pour l'analyse des spectres BPS en théorie des cordes et clarifient le rôle du franchissement de murs, de la dynamique multicentrée et de la modularité dans la description des trous noirs supersymétriques et des états liés de D-branes.